Titre: Title:	An investigation of the model for mass, momentum and energy interchange between interconnected subshannels as applied in the ASSERT computer code
Auteur: Author:	Peter Frederick Tye
Date:	1991
Type:	Mémoire ou thèse / Dissertation or Thesis
Référence: Citation:	Tye, P. F. (1991). An investigation of the model for mass, momentum and energy interchange between interconnected subshannels as applied in the ASSERT computer code [Master's thesis, Polytechnique Montréal]. PolyPublie. https://publications.polymtl.ca/57016/

Université de Montréal

An Investigation of the Model for Mass, Momentum and Energy Interchange Between Interconnected Subchannels as Applied in the ASSERT Computer Code

par

Peter F. Tye
Institut de Génie Énergétique École Polytechnique de Montréal
ÉCOLE POLYTECHNIQUE

MÉMOIRE PRÉSENTÉ EN VUE DE L'OBTENTION
DU GRADE DE MAÎTRE ÈS SCIENCES APPLIQUÉES (M.Sc.A.)
Nucléaire
Novembre 1991

INCOMPLET
correction
impossible

UNIVERSITÉ DE MONTRÉAL
ÉCOLE POLYTECHNIQUE

Ce mémoire intitulé:

An Investigation of the Model for Mass, Momentum and Energy Interchange Between Interconnected Subchannels as Applied in the ASSERT Computer Code

présenté par: Peter F. Tye
en vue de l'obtention du grade de: Maître ès science appliquées (M.Sc.A.)
a été dûment accepté par le jury d'examen constitué de:

Zikovsky, Lubomir, Ph.D., président
Tapucu , Altan, D.Sc.A., membre et directeur de recherche
Carver, M.B., Ph.D., Membre

To my mother.

and

To the memory of my father, who beleived that the greatest gift a parent could give a child was an education. Thanks dad I wish you'd been here to see this...

ABSTRACT

The objective of this research project is to compare the predictions of the ASSERT–4 subchannel code developed by Atomic Energy of Canada Limited against the experimental results on two–interconnected subchannels obtained at the Institut de Génie Énergétique.

As an integral part of the comparison between the predicted and the experimental results an analysis of the basic equations of two–phase flow is carried out. This involves the formal derivation of a space–time averaged set of conservation equations for mass, momentum, and energy. From this general model the equations actually used in the ASSERT–4 subchannel code are derived. To do this a number of simplifying assumptions are introduced and the physical implications of these simplifications are assessed.

The numerical solution scheme employed to solve the set of equations used in the ASSERT–4 subchannel code is then analyzed. The limitations that the choice of the particular solution scheme places on the code are then examined.

The correlations and constitutive equations used to supply the information required to model the intersubchannel transfer mechanisms and the impact of the choices made for these models on the code predictions are then examined in detail.

Two versions of the ASSERT – 4 subchannel code, ASSERT – 4 Version 1.5 and ASSERT – 4 Version 2.2B are used to simulate a large number of experiments carried out on two interconnected subchannels at I.G.E. for both vertical and horizontal flows. For the horizontal flows a number of different subchannel arrangements are studied, these are: the two subchannels at the same elevation, the high void subchannel above the low void subchannel and the high void subchannel below the low void subchannel. For all these simulations the effects of

varying certain parameters in the correlations and constitutive equations for the intersubchannel transfer mechanisms are examined.

Using one of the versions of ASSERT–4, version 2.2B, a model for one of the intersubchannel transfer mechanisms, the buoyancy drift, taken from the literature is tested.

A comparison of the simulations against the experimental results showed that by adequately choosing the parameters used in the correlations and constitutive equations for the intersubchannel transfer mechanisms reasonably good predictions can be obtained for all the experiments analyzed.

Recommendations are made for the values of the parameters used in the correlations and constitutive equations for the intersubchannel transfer mechanisms which seem to improve the predictions on the whole range of experiments analyzed.

On the whole it is found that ASSERT–4 version 2.2B is a great improvement over the earlier version.

SOMMAIRE

Dans les réacteurs à eau lourde pressurisée de type CANDU, les grappes de combustible se trouvent dans des tubes de force qui traversent le coeur du réacteur. Ces grappes sont composées de crayons de combustible distribués de façon à former des sous–canaux à travers lesquels s'écoule le caloporteur (eau lourde). Dans certaines conditions, le caloporteur peut bouillir, et crée ainsi un écoulement horizontal diphasique. Pour mieux concevoir et mieux évaluer la performance des grappes de combustible, la connaissance de certains paramètres thermohydraulique comme le titre, la fraction de vide, la pression, la température et le débit a l'intérieur des sous–canaux des grappes de combustible est de très grande importance. Ces informations sont fournies par l'entremise des codes de sous–canaux. Le code de sous–canaux utilisé dans l'industrie nucléaire canadienne est ASSERT – 4. Lorsqu'un code de sous–canaux a été développé, il est nécessaire de valider sa performance en comparant ses prédictions avec des résultats expérimentaux.

L'objet de cette recherche est de comparer les prédictions du code de sous–canaux ASSERT – 4 développé par l'Énergie Atomique du Canada Ltée et les résultats expérimentaux sur les sous–canaux interconnectés obtenus à l'Institut de Génie Énergétique.

La section de test à l'I.G.E. représente deux sous–canaux interconnectés dans une grappe de combustible à réseaux carré. La section de test peut être orientée à la fois verticalement et horizontalement. Pour les expériences en horizontal, trois orientations possibles des deux canaux ont été examinées: les deux canaux à la même hauteur, le canal à basse fraction de vide en–dessous du canal à haute fraction de vide et le canal à basse fraction de vide au–dessus du canal à haute fraction de vide. L'écoulement diphasique est un mélange d'air et d'eau à une

pression proche de la pression atmosphérique. La fraction de vide était déterminée en mesurant l'admittance entre deux électrodes en argent, la pression était mesurée avec des capteurs de pression, les débits d'eau à l'entrée de la section sont mesurés avec des débitmètres à turbine et les débits d'air sont mesurés avec des rotamètres.

Faisant partie intégrante de la comparaison entre les prédiction et les données expérimentales, une analyse détaillée des équations de base pour les écoulements à deux fluides est présentée. Ceci implique le développement de la forme moyennée dans l'espace et dans le temps de l'ensemble des équations de conservation de masse, de quantité de mouvement et d'énergie. Les équations actuellement utilisées dans le code de sous–canaux ASSERT – 4 sont ensuite dérivées de cette forme générale en tenant compte des différant mécanismes d'échange de masse entre les sous–canaux. Ces mécanismes d'échange sont:

Écoulement latéral forcé qui est un mécanisme d'écoulement latéral dû au gradient de pression entre les sous–canaux.

Échange turbulent qui est un mécanisme dû aux fluctuations aléatoires des vitesses et des pressions qui entraînent un échange de masse (dû à la différence de fraction de vide entre les deux canaux), de quantité de mouvement et d'énergie entre les sous–canaux.

Dérive du taux de vide vers les régions à haute vitesse: ce mécanisme tient compte de la tendance de la phase gazeuse de se déplacer vers le sous–canal dont la vitesse est plus élevée.

Dérive du taux de vide par gravité qui est le mécanisme qui force les phases à se séparer dans les écoulements horizontaux.

Pour faire cette dérivation, un nombre d'hypothèses simplificatrices est nécessaire. Les implications physiques qui découlent de ces hypothèses sont analysées en détail.

Le schéma numérique servant à solutionner cette série d'équations est décrit et les limitations intrinsèques induites par le choix particulier de cette méthode de solution sont examinées. Les corrélations et les équations constitutives, utilisées pour fournir les informations requises pour décrire les mécanismes d'échange de masse entre les sous-canaux sont étudiées ainsi que l'impact du choix particulier qu'ont ces corrélations et ces équations constitutives sur les prédictions du code.

Deux versions du code de sous-canaux ASSERT - 4, version 1.5 et version 2.2B ont été utilisées pour simuler un grand nombre d'expériences sur des sous-canaux interconnectés faites à l'I.G.E.. Les effets produits par la variation de certains paramètres à l'intérieur des corrélations et des équations constitutives servant à décrire l'échange turbulent et la dérive du taux de vide par gravité sont montrés. Un modèle pris de la littérature et décrivant l'effet de la dérive du taux de vide par gravité est testé en utilisant ASSERT - 4 version 2.2B. On a pu démontrer qu'en choisissant adéquatement la valeur des paramètres dans les corrélations et les équations constitutives, utilisées pour fournir les informations requises pour décrire l'échange turbulent et la dérive du taux de vide par gravité entre les sous-canaux, il est possible d'obtenir des prédictions raisonnablement bonnes pour toutes les expériences analysées.

Dans l'ensemble, la version 2.2B du code de sous-canaux ASSERT - 4 a été considérée comme une grande amélioration de sa version précédente.

ACKNOWLEDGMENTS

I would like to thank my thesis director Dr. Altan Tapucu and Dr. Alberto Teyssedou for the invaluable help and advice they have given me throught the course of this work.

The contributions of Dr. Guy Marleau the resident TEXpert who wrote the LATEX thesis style format and fixed all of my typesetting problems, Mr. Marcel Davidson who did the experiments to determine the single, and two–phase fraction factors and Mr. François Aubé who proof read the french sections of this text for me are all greatfully acknowledged.

Thanks also go to my mother for her continued financial and moral support and my girlfriend Johanne for her love and understanding during the last two years.

I would also like to thank Dr. M.B. Carver and Mr. J.C. Kiteley of the Advanced Reactor Development Division, Thermal Hydraulics Development Branch of Chalk River Nuclear Laboratories for the help they have given me in the course of this work.

ASSERT was made available to Ecole Polytechnique by agreement with the CANDU OWNERS GROUP (COG) Fuel Channel Critical Power Working Party.

I also wish to the thank the electrons in the CPU of my computer who did all the real work.

TABLE OF CONTENTS

LIST OF FIGURES

LIST OF TABLES

NOMENCLATURE

a	area,	$[m^2]$
C	crossflow resistance coefficient,	$[-]$
C	tracer concentration,	$[mg/\ell]$
C_0	void distribution parameter,	$[-]$
D	lateral matrix operator which takes care of donor assignment and indicates a summation of the crossflow over all the gaps communicating with the current subchannel	$[-]$
D_h	hydraulic diameter,	$[m]$
$\mathcal{E}$	represents equation of conservation of enthalpy,	$[-]$
f	friction factor,	$[-]$
F	axial mass flow rate of the mixture	$[kg/s]$
$\mathcal{F}$	represents equation of conservation of mass,	$[-]$
g	acceleration due to gravity	$[m/s^2]$
G	mass flux,	$[kg/m^2s]$
h	enthalpy,	$[kJ/kg]$
h	height (used in chapter 5 for experiments),	$[m]$
$\overline{\overline{I}}$	identity matrix,	$[-]$
j	superficial velocity,	$[m/s]$
K_G	loss coefficient and is of the order of 0.5,	$[-]$
K_1	leading coefficient for v_∞,	$[-]$
m	axial mass flow rate (used in chapter 5),	$[kg/s]$
$\mathcal{M}$	represents equation of conservation of axial momentum,	$[-]$
$\hat{n}_k$	outwardly directed unit vector, normal to the interface,	$[-]$
p	pressure,	$[kg/ms^2]$
Pe	Peclet number,	$[-]$
q	heat flux,	$[kw/m^2]$
Q	volumetric flow rate,	$[m^3/s]$

$\vec{r}$	spacial position vector,	$[m]$
$\vec{R}$	material position vector,	$[m]$
Re	Reynolds number,	$[-]$
s	actual subchannel gap,	$[m]$
$\bar{s}$	effective subchannel gap clearence	$[m]$
u	axial velocity,	$[m/s]$
u^*	average axial velocity in the gap region,	$[m/s]$
t	time,	$[s]$
$\vec{v}$	velocity vector,	$[m/s]$
v	transverse velocity,	$[m/s]$
v_∞	terminal rise velocity,	$[m/s]$
V	volume	$[m^3]$
$\mathcal{V}$	material volume,	$[m^3]$
W	crossflow per unit lenght,	$[kg/s]$
W'	turbulent crossflow per unit lenght,	$[kg/s]$
$\mathcal{W}$	represents equation of conservation of transverse momentum,	$[-]$
X	accepted to mean $X = (x, y, z)$	
Δx	axial node lenght	$[m]$

Superscripts:

$*$	used to denote donour assignment ie. quantity is associated with the value of that quantity in the donour subchannel	[–]
m	denotes mass weighting	[–]
n	denotes previous time step value	[–]
T	denotes transpose of a matrix	[–]

Subscripts:

1	refers to the liquid phase	[–]
2	refers to the gas phase	[–]
d	drag	[–]
eq	equilibrium	[–]
g	gravitational	[–]
i	refers to the interface.	[–]
ij	means between subchannels i and j,	[–]
ik	refers to interface with the k^{th} phase	[–]
k	refers to the k^{th} phase,	[–]
kw	refers to the interaction of the k^{th} phase and the wall	[–]
m	refers to the mixture	[–]
ni	refers to the normal component at the interface	[–]
p	pressure	[–]
r	relative	[–]
ref	reference	[–]

Greek Characters:

α	void fraction,	$[-]$
β	volumetric flow quality,	$[-]$
β_{ij}	turbulent mixing parameter which is supplied by a number of optional correlations (used in COBRA),	$[-]$
ε	void diffusivity,	$[m^2/s]$
Γ	net vapour volumetric production rate resulting from phase change,	$[kg/m^2s]$
ℓ	centroid to centroid distance between adjacent subchannels,	$[m]$
ρ	density	$[kg/m^3]$
Ψ	conserved quantity per unit of mass,	$[-]$
ϕ	centroid to centroid angle,	$[Deg.]$
$\vec{\phi}$	represents the influx of the quantity Ψ per unit of mass,	$[-]$
Φ^2_{fo}	two phase friction multiplier,	$[-]$
$\dot{\Psi}$	body source term of the quantity Ψ per unit of mass,	$[-]$
$\bar{\Psi}$	steady component of the quantity Ψ	$[-]$
Ψ'	fluctuating component of the quantity Ψ	$[-]$
τ	wall shear stress,	$[kg/ms^2]$
θ	axial orientation of the bundle measured from the vertical	$[Deg.]$
$\Delta\tau$	sampling time interval	$[s]$

Special Characters:

$\overline{\quad}$	is used to denote a temporal or time average
$\langle\langle\langle\ \rangle\rangle\rangle$	is used to denote a volume average
$\langle\langle\ \rangle\rangle$	is used to denote an area average
$\langle\ \rangle$	is used to denote a line average
$\overline{\quad}^{s}$	is used to denote a statistical average
$\sum_{k=1}^{n}$	summation over all the k subchannel gaps
$\pm$	the side from which the boundary approaches the observation point
$\iiint$	represents a volume integration
$\iint$	represents an area integration
$\int$	represents a surface integration

LIST OF APPENDICES

CHAPTER 1

INTRODUCTION

The channel of a nuclear reactor contains the fuel bundles, which are made up of fuel elements distributed in a manner that creates a series of interconnected subchannels through which the coolant flows. The continued safe and efficient day to day operation of a nuclear reactor, as well as a realistic assessment of its behaviour under abnormal conditions, depends greatly on our ability to accurately predict its thermalhydraulic behaviour. Of particular importance is the ability to accurately predict the "Critical Heat Flux" (CHF), which limits the maximum rate at which heat can be removed from a nuclear fuel bundle. CHF defines the point at which the heat transfer mechanism from the fuel element to the coolant deteriorates and results in temperature rises which may endanger the fuel integrity. During the last three decades a considerable amount of work has been devoted to the study of CHF for a wide range of geometries, from a simple round tube to complex multirod fuel bundles. For a given geometry, the experimental results have usually been presented as a correlation between the CHF and the average values of quality and mass flow over the flow section, this approach is even used for complex geometries such as multirod fuel bundles. Correlations are only applicable to the conditions and geometries for which they are established and their extrapolation beyond these conditions may lead to erroneous results. Possibly a better approach to determining CHF in complex geometries is its characterization by local conditions such as: mass flow rate, enthalpy, void fraction and pressure. Therefore, in complex geometry experiments, the determination of the local conditions is of prime importance. Unfortunately, the experiments aimed at obtaining detailed information on mass flow, enthalpy, void fraction and pressure distribution throughout a rod bundle are

very difficult to carry out. To circumvent this difficulty, another approach to the problem, which consists of developing more sophisticated analysis techniques, has been employed. In these techniques, the complex geometry (rod bundle) is divided into smaller sections called "subchannels" (Figure 1.1). Using a lumped parameter approach, the equations of mass, momentum and energy are written for each subchannel and solved numerically while taking into account possible mixing mechanisms between adjacent subchannels. These mechanisms, as identified by various authors [Tahir and Carver, 1984a] are: diversion crossflow, turbulent interchange, void drift and, buoyancy drift.

The computer programs performing the numerical solution of the conservation equations for the geometry discribed above are known as "subchannel codes". Most of the codes found in the open literature are limited to vertical flow [Rowe, 1973, Stewart, et al., 1977, Sha et al., 1977] and their application to horizontal flow may yield erroneous results. Among the codes capable of handling interconnected subchannels in horizontal two-phase flow Aly and Ahmad [1980], Tahir and Carver [1982], Judd et al. [1984] the code ASSERT-4 [Judd et al., 1984], developed by Atomic Energy of Canada Limited, is the one used in the Canadian Nuclear Industry. The end product of these codes is a "map" of mass flow rates, enthalpies, void fractions, etc., throughout the rod bundle. The experimentally determined critical heat flux can then be correlated with the local conditions in the bundle. The resulting correlations may, therefore, be extrapolated to other rod bundles having a geometrical configuration different from the one on which the correlation was obtained by means of a subchannel analysis of each bundle.

Once a subchannel code is developed, its ability to predict the thermalhydraulic behaviour must be checked against experimental data. Very limited detailed data including void fractions, liquid and gas mass flow rates, and pressures throughout the rod bundles are available. Due to the difficulties in carrying out the experi-

ments, most of the data available on the important flow parameters in subchannels are for adiabatic cases only. Tsuge et al.[1979] gave data on the transverse void distribution in two rectangular subchannels with different flow sections. The channels were interconnected over the entire width of the narrower channel. Tapucu et al. [1982, 1984a, 1984b, 1988a, 1988b, 1990] obtained data on void fractions, liquid and gas flow rates, and pressures on two laterally interconnected subchannels under both horizontal and vertical flow conditions. The redistribution of the two-phase flow in two horizontal interconnected subchannels has also been studied by, among others, Shoukri et al. [1984] and data on the axial distribution of void fraction and liquid and gas flow rates have been reported.

For cases of steam water flows with heat addition there is a limited amount of data available. This includes the work of Bosio and Imset [1970] in which the void fractions in two typical subchannels of a 7 rod bundle at 3 different elevations were presented. In this latter case only the central rod was heated.

1.1 Purpose and Outline of Present Research

The principle objective of this research project is to carry out an extensive comparison between the predictions of both ASSERT–4 Version 1.5 and ASSERT–4 Version 2.2B and the experimental results of Tapucu et al. [1988a and 1988b] on two interconnected subchannels.

It is important to point out, that this is not merely an academic exercise, as the experimental facility has almost the exact subchannel dimensions as seen in the fuel bundle of a CANDU reactor. This can be seen by examining figures 1.2 and 1.3 which show the cross-sectional views of both the test section and a CANDU type fuel bundle.

An integral part of the comparison between the experimental and the computed results is understanding how the various models and modelling assumptions used

to pass from the basic equations of conservation of mass, momentum and energy to the actual subchannel code affect the predictions. To this end the following steps will be carried out:

1. A literature survey will be done reviewing the different theoretical models used to obtain the basic equations that describe two–phase flows. A review of the various methods used for rod bundle thermalhydraulics analysis in the nuclear industry will also be done.

2. Starting from the local instant formulation of the basic conservation equations, the three dimensional volume and time averaged formulation will be derived. Using the three dimensional averaged equations as a starting point, a formal derivation of the equations used in ASSERT–4 will be carried out. A detailed examination of the assumptions necessary in carrying out this development as well as the physical implications of these assumptions. The discretized form of the equations and the numerical solution scheme used in ASSERT–4 will then be presented.

3. Using the data from interconnected subchannel experiments conducted by Tapucu et al. [1984a, 1984b], a comparison of the predictions of both ASSERT–4 Version 1.5 and ASSERT–4 Version 2.2B will be made against the experimental results. A sensitivity analysis will be carried out to determine the effect of certain coefficients used in ASSERT–4 on its predictions. As the experimental results cover a wide range of cases for both horizontal and vertical single and two-phase flows, it should be possible to fully test the predictive capabilities of the ASSERT–4 subchannel code and determine whether modelling defficiencies, if any, exist, and to recommend any improvements that this analysis shows may be required. To the best of the authors knowledge this thesis presents the most extensive comparison between the experiments

of Tapucu et al. and the predictions of the ASSERT–4 subchannel code yet to be carried out.

1.2 Organization of this Thesis

Chapter One is an introduction and outline of the work that has been done.

Chapter Two reviews the techniques available for developing theoretical models of two–phase flows and averaging techniques. The general domain of two–phase flow modelling is also reviewed. Special attention is paid to the area of rod bundle thermalhydraulics analysis.

Chapter Three presents the basic mathematical tools required to develop a set of equations describing two–phase flow. These basic mathematical tools are then used to formulate a set of space–time averaged equations which form the basis of a model for three dimensional transient two–phase flow. Starting from the model that has been developed, the equations of the ASSERT–4 subchannel code are derived. The necessary assumptions, that must be made to pass from the full three dimensional model, to the equations used in ASSERT–4 are detailed. The implications these assumptions have on the model are also discussed.

Chapter Four presents the discretized equations and the numerical solution scheme used in ASSERT–4.

Chapter Five describes the experimental air–water test facility at the Institut de Génie Énergétique as well as the experimental procedure. While no experimental work was done as part of this thesis a description of the experimental apparatus and procedures used to obtain the data required for the comparisons with the ASSERT–4 predictions presented in chapters 6 and 7 is included for completeness. Also included is an analysis of the expected experimental accuracy of this data. This chapter is taken in large part directly from Tapucu et al. [1990].

Chapter Six gives a comparison between the predictions of both ASSERT–4

Version 1.5 and ASSERT–4 Version 2.2B and the vertical experiments of Tapucu et al. [1984a].

Chapter Seven gives a comparison between the predictions of both ASSERT–4 Version 1.5 and ASSERT–4 Version 2.2B and the horizontal experiments of Tapucu et al. [1984b].

Chapter Eight is the conclusions.

A discussion of certain minor modifications made in ASSERT – 4 to model the two subchannel experiments and the values of important parameters used for the comparisons given in chapters 6 and 7 are presented in the appendix.

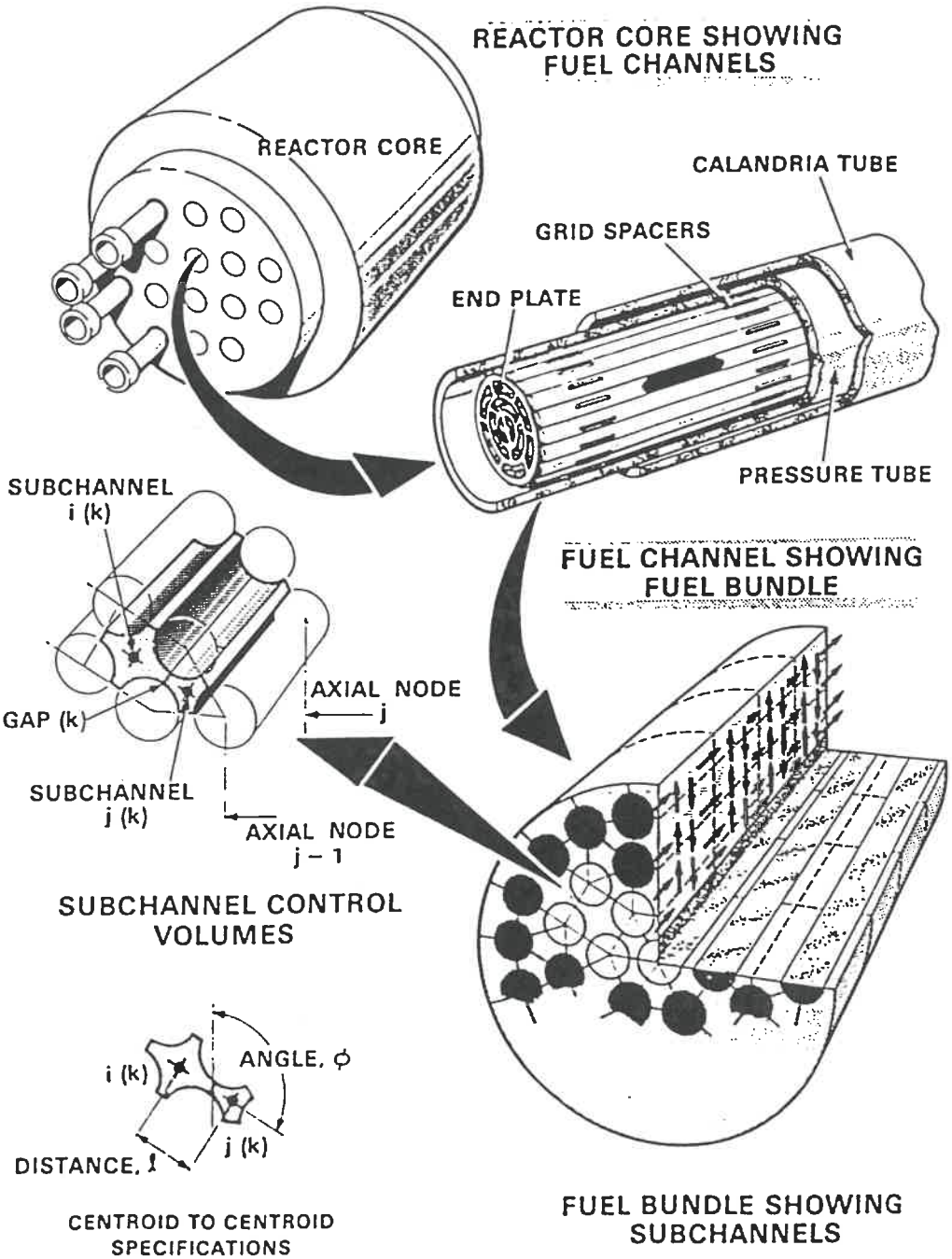

Figure 1.1: Rod Bundle Subchannels

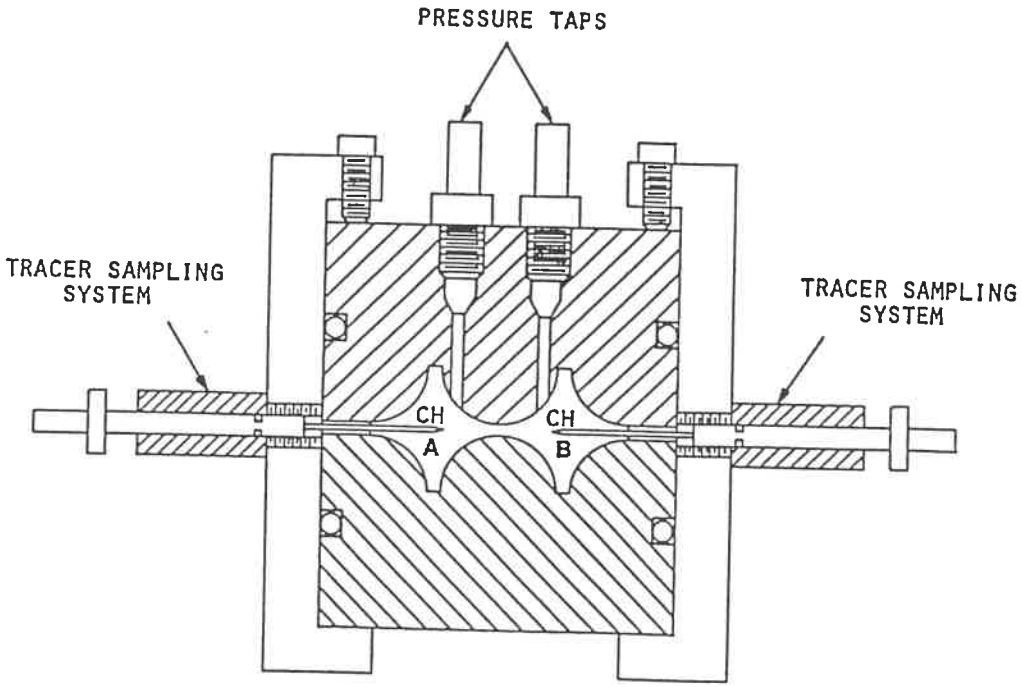

Figure 1.2: Cross Sectional View of Test Section

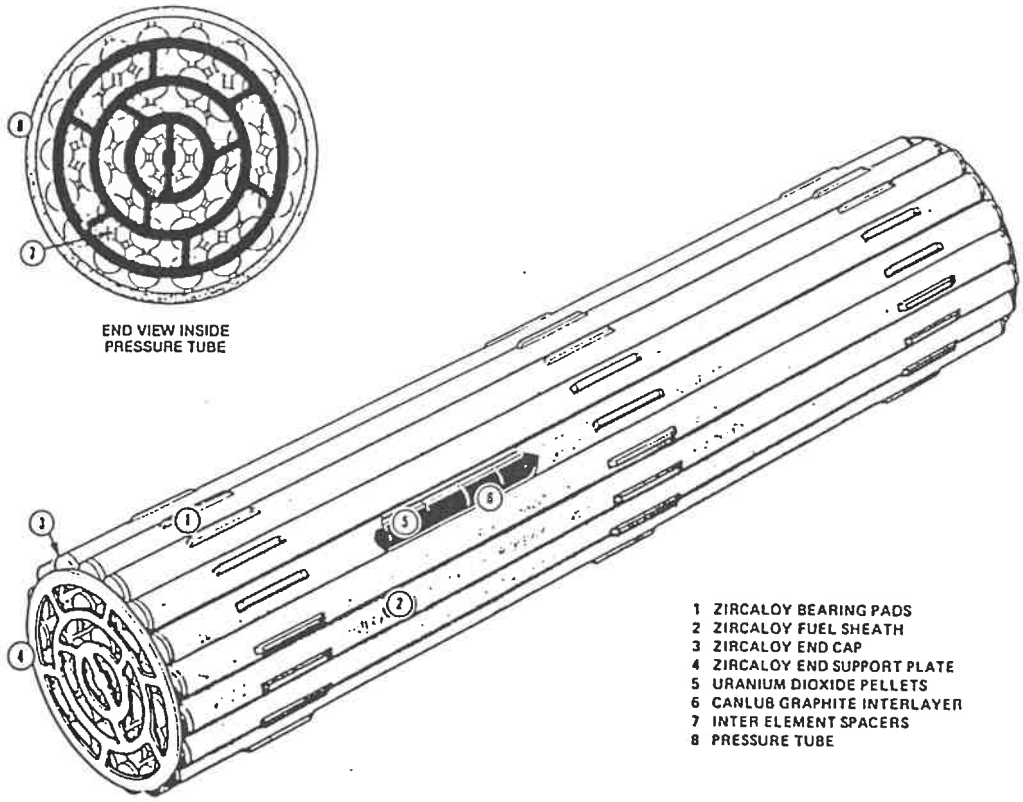

Figure 1.3: CANDU Reactor Fuel Bundle

CHAPTER 2

MODELS AND METHODS FOR TWO–PHASE FLOW

Many authors have described methods that can be used to develop the local instant formulation of the conservation equations of mass, momentum, and energy as they are applied in the various mathematical models used in both single– and two–phase flows. A large body of work also exists in the area of averaging techniques, be it, temporal, spatial, or statistical averaging, or some combination thereof, that can be applied to the microscopic form of the conservation equations to transform them into an averaged form that takes into account, in a simplified manner, the interfacial phenomena. The averaged equations can then be used to develop computational tools for two–phase flow calculations.

2.1 Theoretical Models

2.1.1 Local Instant Formulation

Thorough mathematical treatment of the derivation of the local instant formulation of the conservation equations for single– Bird et al. [1960] and Aris [1962], and two–phase flows Vernier and Delhaye [1968] Kocamustafaogullari [1971], and Ishii [1975] have been firmly established for about 15 to 20 years.

As far as the local instant formulation for two-phase flow is concerned there is good agreement between various authors (nomenclature aside) as to the form of the general local instant conservation equation, which is:

$$\frac{\partial}{\partial t}\rho_k\Psi_k + \nabla\cdot\rho_k\vec{v}_k\Psi_k = -\nabla\cdot\vec{\phi}_k + \rho_k\dot{\Psi}_k \quad , \tag{2.1}$$

the general form of the equation describing the local instantaneous interfacial "jump" conditions is:

$$\sum_{k=1,2} \left(\Psi_k \rho_k \left(\vec{v}_k - \vec{v}_i \right) \cdot \hat{n}_k + \hat{n}_k \cdot \vec{\phi}_k + \dot{\Psi}_k \right) = 0 \quad , \tag{2.2}$$

where:

ρ_k	is the density of the k^{th} phase,	$[kg/m^3]$
Ψ_k	is the conserved quantity per unit of mass,	$[-]$
$\vec{\phi}_k$	represents the flux of the quantity Ψ_k per unit of mass,	$[-]$
$\dot{\Psi}_k$	is the body source term per unit of mass,	$[-]$
$\hat{n}_k$	is an outwardly directed unit vector, normal to the interface,	$[-]$
$\vec{v}_k$	is the velocity of the k^{th} phase,	$[m/s]$
$\vec{v}_i$	is the velocity of the interface.	$[m/s]$

The conservation equations for mass, momentum, and energy may then be obtained by substitutions of the appropriate values for the terms Ψ_k, $\vec{\phi}_k$, and $\dot{\Psi}_k$ into the general form of the equation. Table 2.1 gives the various terms required to obtain the different conservation equations:

Table 2.1: Terms To Generate Conservation Equations

CONSERVATION EQUATION	Ψ_k	$\vec{\phi}_k$	$\dot{\Psi}_k$
MASS	1	0	0
MOMENTUM	$\vec{v}$	$-\bar{\bar{\pi}}$	$\vec{g}$
ENERGY	$u_k + \frac{v_k^2}{2}$	$\vec{q}_k - \bar{\bar{\pi}}_k \cdot \vec{v}_k$	$\vec{g} \cdot \vec{v}_k$

where:

$\vec{v}_k$	is the k^{th} phase velocity,	$[m/s]$
$\overline{\overline{\pi}}$	represents a combination of both the pressure forces and the viscous stress forces $\tau_k + p_k\overline{\overline{I}}$,	$[kg/ms^2]$
u_k	is the internal energy	$[kJ/kg]$
$\vec{q}_k$	is the heat flux	$[J/m^2]$
$\vec{g}$	is the gravitational acceleration.	$[m/s^2]$

2.1.2 Averaged Equations and Averaging Techniques

Banerjee [1980] has stated that in principle, a system of equations may be obtained by writing the local instantaneous conservation equations for each phase, together with appropriate molecular transport properties, as well as, initial, interfacial and wall, boundary conditions. He also states that while in theory, this system of equations may be solvable, it is in practice, intractable for all but the most simplified cases. Further, for cases of engineering interest averaged values of the quantities is quite sufficient. Thus it is reasonable to average the local instantaneous equations. The type of averaging used may be temporal, statistical (or ensemble), spatial or some combination thereof. For temporal or statistical averaging the resulting equations are commonly refered to as local time (or ensemble) averaged equations and the spatialy averaged equations are refered to as instantaneous space averaged equations. For a given function $\Psi = \Psi(t, X)$ the various averaging techniques are defined by Ishii1 [1975] as:

LOCAL TIME (OR ENSEMBLE) AVERAGE

TEMPORAL

$$\overline{\Psi} = \frac{1}{\Delta t}\int_{\Delta t} \Psi(t, X)dt \tag{2.3}$$

STATISTICAL

$$\overline{\Psi}^N = \frac{1}{N}\sum_{n=1}^{N} \Psi(t, X) \tag{2.4}$$

INSTANTANEOUS SPACE AVERAGE

VOLUME

$$\langle\langle\langle\Psi\rangle\rangle\rangle = \frac{1}{V}\int_V \Psi(t,X)dv \tag{2.5}$$

AREA

$$\langle\langle\Psi\rangle\rangle = \frac{1}{A}\int_A \Psi(t,X)da \tag{2.6}$$

LINE

$$\langle\Psi\rangle = \frac{1}{C}\int_C \Psi(t,X)dc \tag{2.7}$$

where:

Δt	is averaging time,	$[s]$
N	is the number of samples,	$[-]$
V	is the averaging volume,	$[m^3]$
A	is the averaging area,	$[m^2]$
C	is the averaging line,	$[m]$
X	is accepted to mean $X = \left(x\hat{i}, y\hat{j}, z\hat{k}\right)$,	$[-]$
$\overline{\ }$	is used to denote a temporal or time average	$[-]$
$\langle\langle\langle\ \rangle\rangle\rangle$	is used to denote a volume average,	$[-]$
$\langle\langle\ \rangle\rangle$	is used to denote an area average,	$[-]$
$\langle\ \rangle$	is used to denote a line average,	$[-]$
$\overline{\ }^N$	is used to denote a statistical average over N observations.	$[-]$

The use of both single and double time averages has been discussed by Vernier and Delhaye [1968]. However, the standard reference on the use of time averages as a means of obtaining practical models for two–phase flow calculations is Ishii [1975], in which the mathematical formulation for the equations of two–phase flow based on Eulerian time averaging are developped. In Ishii's work the development of the averaged conservation equations of mass, momentum and energy, as well as the two–phase jump (or interfacial) conditions is clearly laid out. The development of the two fluid and diffusion formulation of a three dimensional model for two–phase flow systems is also presented.

Spatial averaging techniques for the equations of two-phase flow have also been discussed in [Vernier and Delhaye, 1968]. A thorough study of the use both area

and line averaging techniques, as applied to the area of falling film flow has been presented in [Kocamustafaogullari, 1971]. The use volume averaging to develop the average form of the two-phase flow, neglecting surface tension was presented in [Nigmatulin, 1979]. Articles by Dorbran [1984, 1985] have given a solid mathematical foundation to the development of the macroscopic form of the conservation equations for two–phase flow based on volume averaging.

The use of multiple averages time–space or ensemble–space are discussed in Vernier and Delhaye [1968], Drew [1971], and Banerjee and Chan [1980]. There are two very good reasons to develop a multiply averaged form of the basic equations of two–phase flow. The first, due to Banerjee and Chan [1980], is that under certain conditions difficulties arise with the continuity of flow parameters and their first derivatives if they are time or cross–sectional area averaged. An example of this would be, if a cross–sectional area average is done, the first derivative is discontinuous each time an interface becomes tangent to the cross sectional plane. In time averaging, the derivative of a point void fraction measurement is also discontinuous, since at any time the result is either that the vapour or liquid phase is or is not present. The second reason to develop a multiply averaged form of the conservation equations for two–phase flow is of a less theoretical but much more practical nature, mainly, that it is the only form of the equations that is programmable. The process of casting the continuous differential equations into a discretized, and hence numerically solvable form, inherently involves both a temporal, i.e., the time step, and spatial, i.e., the mesh size, discretization. Thus it would appear reasonable to forsee this and develop a set of averaged equations that are guarantied to be valid after discretization.

2.2 Two-Phase Flow Modelling

2.2.1 General Models

A nuclear reactor is a very complex system, containing many different components, boilers, heat exchangers, fuel assemblies, pumps, and many miles of piping, just to name a few. Due to this complexity, its behaviour can be predicted only by using large computer codes, and even then only a simplified approximation of the real system can be represented. Many codes have been developed for use in nuclear reactor design and safety analysis. Due to the complicated nature of the two-phase flow phenomena in a nuclear reactor, a mathematical model must be formulated that describes, in a simplified manner, though as accurately as possible, the actual physical system and the physical processes that it carries out.

Depending on the various assumptions that are made, about the nature of the two-phase flow, and the averaging techniques used, different levels of complexity may be considered by the resulting models.

The simplest description of the two-phase flow phenomena is the one dimensional homogeneous equilibrium model (HEM). Models are described using the nomenclature, 1V1T One Velocity One Temperature, One Velocity Drift Flux Two Temperature 1VDF2T, One Velocity Slip Two Temperature 1VS2T or 2V2T Two Velocity Two Temperature or some combination thereof. Table 2.2 [Delhaye, 1981] gives a list of models, the restrictions imposed on them and the number of additional constitutive relations required for each model. Table 2.3 [Delhaye, 1981] gives the characteristics of each of the models and the remaining dependent variables to be computed.

Table 2.2: Two Phase Flow Models

Model Designation	Restriction		Number of field equations			No. of interface transfer equations	External Constitutive Relations	
	No.	Imposed on	Mass	Momentum	Energy		No.	type
1V1T	3	$v_2 = v_1, h_1, h_2$	1	1	1	0	2	$\bar{\tau}, \bar{q}$
1VS1T	3	$v_2/v_1, h_1, h_2$	1	1	1	0	3	$\bar{\tau}, \bar{q}, v_2/v_1 = slip$
1VDF1T	3	$v_2 - v_1, h_1, h_2$	1	1	1	0	3	$\bar{\tau}, \bar{q}, v_r = v_2 - v_1$
$1VT_kT_{SAT}$	2	$v_2 = v_1, h_1$	1	1	2	1	3	$\bar{\tau}, \bar{q}, q_2$,E
$1VST_kT_{SAT}$	2	v_2/v_1,or	1	1	2	1	4	$\bar{\tau}, \bar{q}, v_2/v_1$,E
$1VDFT_kT_{SAT}$	2	$v_2 - v_1, h_2$	2	1	1	1	4	$\bar{\tau}, \bar{q}, \Gamma, v_r$
2V1T	2	h_1, h_2	1	2	1	1	4	$\tau_1, \tau_2, \bar{q}$,M
1V2T	1	$v_2 = v_1$	2	1	2	2	5	$\bar{\tau}, q_1, q_2, \Gamma$,E
1VDF2T	1	v_2/v_1	2	1	2	2	6	$\bar{\tau}, q_1, q_2, v_r$,E
$2VT_kT_{SAT}$	1	h_1 or h_2	2	2	1	2	5	$\tau_1, \tau_2, \bar{q}, \Gamma$,M
$2VT_kT_{SAT}$	1	h_1 or h_2	1	2	2	2	6	$\tau_1, \tau_2, \bar{q}, q_k$,M,E
2V2T	0	*None*	2	2	2	3	7	$\tau_1, \tau_2, q_1, q_2, \Gamma$,M,E

Table 2.3: Characteristics of Two Phase Flow Models

MODEL Designation	Characteristics	Remaining computed dependent variables
1V1T	Homogeneous, equilibrium (HEM)	p,$\underset{\sim}{\tilde{v}}$,$\alpha$
1VS1T	Slip, equilibrium	p,$\underset{\sim}{v}$,α
1VDF1T	Drift Flux, equilibrium	p,v,α
$1VT_kT_{SAT}$	Homogeneous,partial nonequilibrium	p,$\underset{\sim}{\tilde{v}}$,$\alpha$,$h_1$ or h_2
$1VST_kT_{SAT}$	Slip, partial nonequilibrium	p,$\underset{\sim}{v}$,α,h_1 or h_2
$1VDFT_kT_{SAT}$	Drift Flux, partial nonequilibrium	p,v,α,h_1 or h_2
2V1T	Two-Fluid,equilibrium	p,v_1,v_2,α
1V2T	Homogeneous,full nonequilibrium	p,$\underset{\sim}{\tilde{v}}$,$\alpha$,$h_1$,$h_2$
1VDF2T	Drift Flux,full nonequilibrium	p,v,α,h_1,h_2
$2VT_kT_{SAT}$	Two-Fliud,partial nonequilibrium	p,v_1,v_2,α,h_1 or h_2
2V2T	Two-Fliud,Full nonequilibrium	p,v_1,v_2,α,h_1,h_2

where:

v	is the velocity,	$[m/s]$
h	is the enthalpy,	$[kJ/kg]$
τ	is the wall shear stress,	$[kg/ms^2]$
$\tilde{q}$	is the heat flux between the two–phase mixture and the wall,	
q	is the heat flux,	$[J/m^2]$
E	is the energy transfer between the phases,	$[J]$
Γ	is the net vapour volumetric production rate resulting from phase change per unit volume,	$[kg/m^3]$
M	is the momentum transfer between the phases,	$[kgm^2/s^2]$
p	is the pressure,	$[kg/ms^2]$
α	is the void fraction,	$[-]$
$\sim$	refers to mixture quantities,	$[-]$
1	refers to liquid phase,	$[-]$
2	refers to gas phase,	$[-]$
k	is the phase index.	$[-]$

In the HEM model the steam-water mixture is treated as a single pseudo-fluid with averaged properties determined by the mass fraction of steam in the mixture, having, one velocity, and one temperature (saturation). Using the above nomenclature its designation would thus be 1V1T.

Depending on the respective flow rates of the gas and liquid phases, various flow patterns will develop. These patterns are shown in figure 2.1 and 2.2 for vertical and horizontal flows respectively. These flows may be broken down into three broad classes. These classes are known as: separated flows, which include both annular and stratified flows, mixed or transitional flows, which include slug flow and bubbly annular flows, and finally dispersed flows which include such patterns as bubbly and droplet flows.

In reality, the only flow regime where the assumptions, of the fluid having one velocity and one temperature would hold, or even come close to holding, would be homogeneous flow having a very high mass flux such that the relative velocity is a

small fraction of the phasic velocities [Webb and Rowe, 1986].

In most cases the two–phases are not well mixed and each phase tends to flow at its own velocity and the two–phases may not be at equilibrium, thus the liquid and vapour phases would not be at the same temperature, for example subcooled boiling, or the flow of superheated steam. Further, the flow phenomena will, most likely be, in some way multi–dimensional, and the problem will most likely be transient in nature. Thus, due to the nature of the two–phase flow phenomena, the only model capable of completely describing the physical phenomena is the two–fluid model.

This model can be written using either local time averages [Ishii, 1975] or space averages [Kocamustafaogullari, 1971]. If the spatial average is carried out over the entire cross–sectional flow area of the pipe the resulting model is only capable of representing one dimensional transient two–phase flow problems. If, however, the spatial average is carried out over an elemental control volume containing a sufficient number of molecules such that their properties can be accurately represented by an average property, then the model is capable of treating problems of a three dimensional nature.

The complete description of the two–phase flow phenomena requires the conservation equations for mass, momentum, and energy to be written for each phase along with appropriate constitutive equations to relate interfacial transport between phases. Such a complete system of equations is very large and both quite difficult and costly to solve. Thus, codes of varying degrees of complexity from 1V1T to 2V2T, both transient and steady state, are used in the nuclear industry depending on the physical nature of the problem being analyzed. Most of the codes, however, are still one dimensional in nature. The most basic model, 1V1T, is only applicable in a very limited number of cases and was found to be unsuitable for modelling many postulated accident scenarios. Even if thermal equilibrium exists

between the phases it is quite rare to find cases when mechanical equilibrium exists,

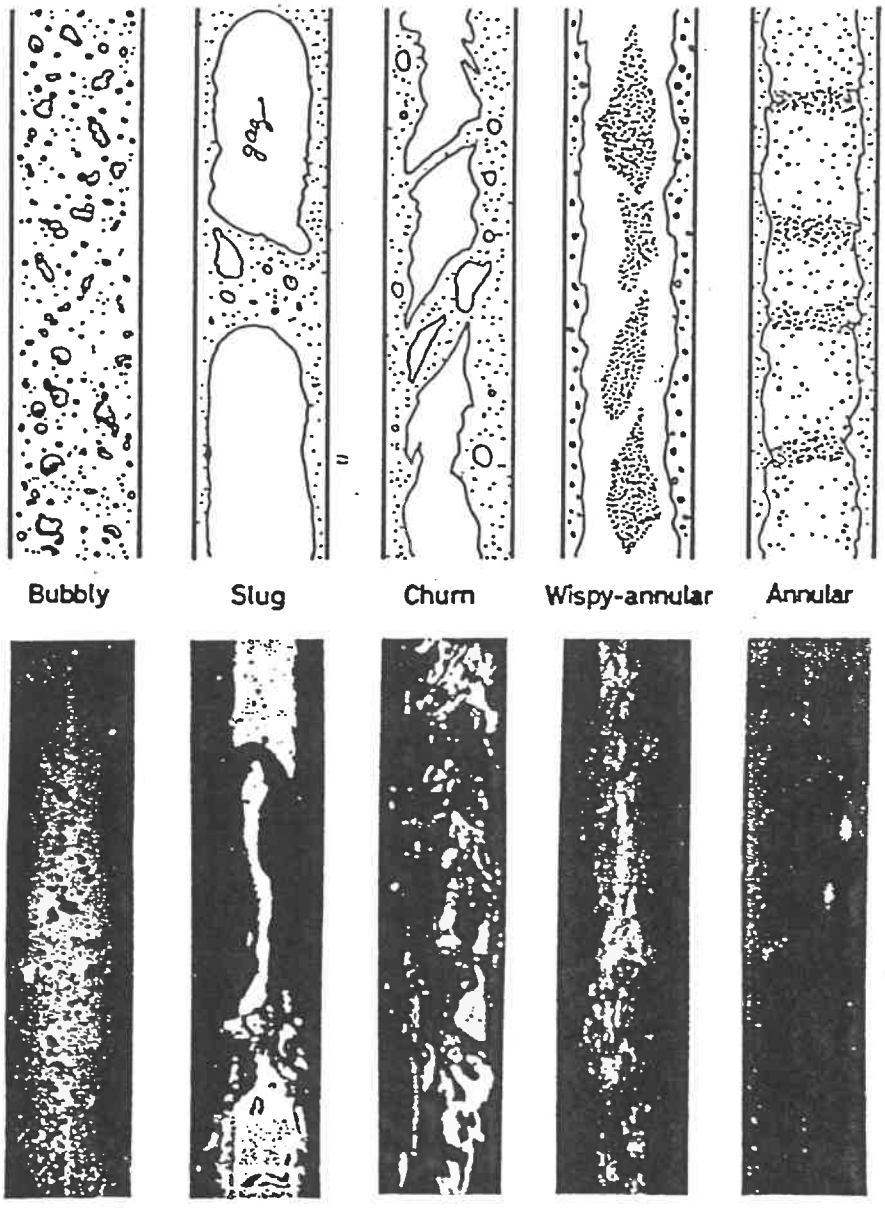

Figure 2.1: Flow Regimes in Vertical Flow

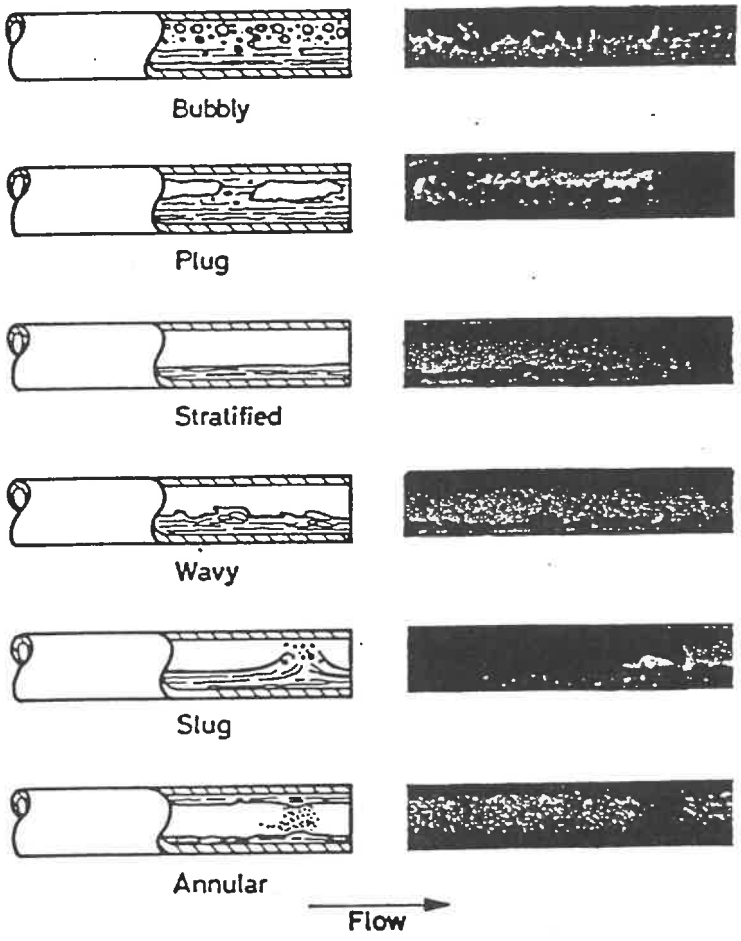

Figure 2.2: Flow Regimes in Horizontal Flow

as the vapour phase tends to always travel faster than the liquid phase. This can be due to acceleration or gravitational influences in vertical flow or due to the effect of acceleration in horizontal flow. Various approaches used to take the difference of the phase velocities into account as described in [Carver, 1987] include an approach based on a slip between the two phases where the slip ratio was given by a correlation with the void fraction; a much better approach was later developed using the concept of a relative velocity between the phases [Wallis, 1969]. The relative velocity is supplied by a semi-analytical correlation such as the ones developed by Ohkawa and Lahey [1980] or Chexal and Lellouche [1986]. The 1VDF1T model requires that the same number of field equations be solved as for the 1V1T model but requires the solution of an extra (relative velocity) constitutive equation (see Table 2.2). An example of a computer code based on the use of a 1VDF1T model is SOPHT, developed by Ontario Hydro, a detailed description is given by Chang and Skears [1977]. It should be noted, that one of the underlying assumptions of the drift flux model, and hence limitations, is that there must be a strong coupling between the two phases. Thus, modelling cases having low mass fluxes and hence stratified flow (see Figure 2.2), where there is little coupling between the phases is not possible, or at best questionable, using the drift flux model.

A true separated flow model, capable of treating cases with little coupling between the two–phases, requires the solution of the momentum equation for both phases. An example of a one dimensional six equation, 2V2T, code is CATHENA, developed by WNRE [Mallory and Ingham, 1986]. An example of a three dimensional 2V2T code is TRAC, developed by Los Alamos National Labs [Delhaye, 1981], which is one dimensional in the components and three dimensional in the reactor vessel.

Codes such as SOPHT and CATHENA treat the fuel channels which contain the fuel bundles simply as a pipe, although SOPHT does a hot pin calculation for

fuel temperature prediction and CATHENA can treat up to ten fuel pins for purposes of fuel temperature calculations. Such codes do not supply any information about the detailed flow structure in the reactor fuel assembly. However, this detailed information such as mass flow rate, enthalpy, void fraction, pressure, and fuel temperature are needed for reasons of both safety and economy. These details are provided by codes which perform what is known as rod–bunble thermalhydraulic analysis.

2.3 Review of Rod–Bundle Thermalhydraulic Analysis

There are four main methods used for rod-bundle thermalhydraulics analysis, these are [Van Doormal, 1980]: 1) the finite element method, 2) the boundary fitted curvilinear coordinate method, 3) the porosity and distributed resistance method, and, 4) subchannel analysis. Excellent reviews of the computational methods used for rod-bundle thermalhydraulics analysis are given in both [Sha, 1980] and [Van Doormal, 1980], however for completeness a brief review will be included here.

2.3.1 The Finite Element Method

The finite element method is a piecewise application of a variational method. There are two basic steps in the variational solution of a set of differential equations:

1. To cast a given differential equation in variational form.

2. To determine the approximate solution using a variational method, such as the Ritz method, the Galerkin method or some other method.

The term "variational formulation" is used to mean the weak formulation in which a given differential equation is recast in an equivalent integral form by

trading the differentiation between a test function and the dependent variable [Reddy, 1984].

The test function is used to describe how the dependent variable varies over an element. Determination of a suitable test function in two–phase flow is a very difficult task. Further, the use of the finite element technique in thermalhydraulics suffers from certain problems [Patankar, 1980]. These problems include spurious pressure field oscillations and the need for a suitable way to determine upstream weighting.

Nonetheless, two dimensional finite element models for the treatment of the non linear, transient response of fluids and structures have been developed [Sha, 1980]. However, the use of the finite element method in rod–bundle thermal–hydraulics analysis is quite limited.

2.3.2 The Boundary Fitted Curvilinear Coordinate Method

The concept of boundary fitted coordinates, involves the generation of coordinate lines that are coincident with all boundaries including the fuel rods in a rod bundle. The advantage of this method is that the fine structure of both the velocity and the temperature in a rod-bundle can be represented.

An example of a rod–bundle thermal–hydraulics analysis code using the technique of boundary fitted curvilinear coordinates is the Bodyfit–1 code, that is described in [Vanka, et al., 1980]. The main drawback of this method is the large amount of computer storage required and the long running time required to obtain a solution. While yielding excellent results, this method remains at present too computationally expensive to have a widespread use in the area of nuclear reactor safety analysis.

2.3.3 The Porosity and Distributed Resistance Method

The basic concept of the porosity and distributed resistance approach is that over a given control volume, which includes both solid and fluid regions, the solid objects have two effects on the fluid flow: (1) the geometrical effect, and (2) the physical effect.

The geometrical effect, due to the reduction in available space by the presence of the solid, is taken into account by including volume porosity, which is defined as the ratio of the fluid volume to the total control volume, and surface porosity, which is defined as being the ratio of the surface area occupied by the fluid to the total surface area over a control volume. The physical effects, due to the influence of the solid objects on the momentum and heat transfer to the fluid flow, are taken into account by introducing distributed resistances in the momentum transfer and distributed sources for heat transfer.

The basic assumptions made in developing the porosity and distributed resistance method include:

1. the fine structure of both the velocity and temperature within a control volume are ignored.

2. the distributed resistance represents the sum of drag forces of the solid on the fluid and the difference between the fine structure and cell averaged velocity distribution in the computational cell.

3. In the general quasi-continuum (with solid present) differential balance equations, the fluid and solid are considered to coexist, at any given location, in the fraction determined by the local volume and surface porosity values, as if the fluid and solid where evenly distributed.

One of the major problems in the porosity and distributed resistance method is the determination of the distributed resistances and heat sources. Since the rod-

bundle is discretized in a simple manner without regard for the flow, the physical effect of the solid on the local character of the flow, which is not known a priori, must be included in the distributed resistance and source terms. Thus the evaluation of these terms becomes rather difficult and is a major source of uncertainty. Correlations based on experiments and extensions of other analytic solutions must be introduced in order to obtain approximate distributed resistance and heat source terms.

This method was been used as the basis for the development of rod-bundle thermal-hydraulics analysis codes. An example of such a code is COMMIX–1 [Sha, 1980]. The porosity and distributed resistance method has however not gained widespread popularity in the area of rod-bundle thermal-hydraulics analysis.

2.3.4 The Subchannel Method

The subchannel method is the most widely used approach currently applied in the area of rod–bundle thermalhydraulics analysis. As this is the method used in the code ASSERT–4 [Judd et al., 1984], which is used in the remainder of this work; the history of the development of this method, and the basic assumptions that it entails, will be treated in some detail.

In explaining the concept of subchannel analysis it is first important to define what is meant by the term subchannel, as "subchannels" do not actually exist, they are, for all practical purposes, artificial constructs used to discretize a rod bundle of a nuclear fuel assembly in the transverse direction in a fairly natural way. The result was the concept of the subchannel which is created by drawing imaginary lines between the centres of adjacent rods in the fuel bundle, the resulting control volumes described by these imaginary lines are known as subchannels. The computer codes used in the area or rod bundle thermalhydraulics analysis that use

the subchannel approach are known, not surprisingly, as subchannel codes. In order to derive the equations used by such codes one writes the one dimensional form of the equations of conservation of mass, momentum and, energy for a control volume as if the subchannel where a simple pipe having the same hydraulic diameter as the subchannel. Additional terms are then added to describe, in a simplified manner, the mechanisms that produce the crossflow between adjacent subchannels. In all cases however, the flow is assumed to be predominantly one dimensional, that is to say that the crossflow is assumed to be much smaller than the axial flow, which is in most cases a completely justified and reasonable assumption. The mechanisms that produce the crossflow as they have been described by various authors such as [Tahir and Carver, 1984a] are:

1. Diversion CrossFlow

Diversion crossflow is the directed flow caused by pressure gradients between the channels. These gradients may be induced by differences in subchannel geometries, the variation of heat flux from one subchannel to the other, incipient boiling in one of the subchannels or by flow section variations caused by blockages.

2. Turbulent Interchange

In turbulent flow, the velocity and pressure at a fixed point do not remain constant but display random fluctuations. These fluctuations promote the exchange of mass, momentum and energy between the subchannels. In single phase flows, there is momentum and energy transfer between the subchannels but there is no net mass transfer. However, in two-phase flows, in addition to momentum and energy transfer there is usually a substantial net mass transfer. In the discussion of the void fraction data, this mechanism will be identified as "turbulent void diffusion".

3. Void Drift

This mechanism accounts for the tendency of the vapor phase to shift to higher velocity channels. It has been clearly identified, however, it is not yet fully under-

stood.

4. Buoyancy Drift

In horizontal channels, the void is pushed upwardly normal to the major flow direction due to the difference in specific masses between the two phases. The significance of this mechanism should diminish at high mass fluxes.

The subchannel code ASSERT–4 [Judd et al., 1984] used for this investigation is the culmination of over 20 years of code development which began with the COBRA family of subchannel codes Rowe [1970], Rowe [1973] and Stewart et al. [1977]. Early subchannel codes such as COBRA–II [Rowe, 1970] treated the transverse momentum equation in an extremely simplified manner which is unable to account for the temporal and spatial acceleration of the crossflow.

2.3.4.1 COBRA–II Transverse Momentum Equation

The transverse momentum equation used the COBRA–II subchannel code is:

$$[C\,|W|\,W] = p_i - p_j \quad , \tag{2.8}$$

where:

C	is the crossflow resistance coefficient,	$[-]$
W	is the crossflow,	$[kg/ms]$
p	is the subchannel pressure.	$[kPa]$

COBRA–II has the ability to account for certain inter–subchannel mixing mechanisms such as both single– and two–phase turbulent and diversion crossflow. It is assumed that the turbulent crossflow between subchannels can cause an exchange of axial momentum and energy between the two subchannels communicating through a given gap, but that it causes no net mass transfer. The single–phase turbulent crossflow W' is defined by an emperical correlation given by:

$$W'_{ij} = \beta_{ij} s_{ij} \frac{m_i + m_j}{A_i + A_j} \quad , \tag{2.9}$$

where:

W'	is the turbulent crossflow,	$[kg/ms]$
β_{ij}	is the turbulent mixing parameter which is supplied by a number of optional correlations,	$[-]$
s_{ij}	is the subchannel gap between subchannels i and j,	$[m]$
m	is the axial mass flow rate,	$[kg/s]$
A	is the subchannel area.	$[m^2]$

The effects of two–phase flow on the turbulent crossflow are taken into account by allowing the turbulent mixing parameter β_{ij} to be a function of the flow quality.

2.3.4.2 COBRA–IIIC Transverse Momentum Equation

The idea of using a complete momentum equation which was capable of accounting for the temporal and spatial acceleration of the crossflow between adjacent subchannels was first introduced by Rowe in the implementation of COBRA–IIIC Rowe [1973]. He developed a separate transverse momentum equation for a control volume located in the region of the gap between two adjacent subchannels (see Figure 2.3). The form of the transverse momentum equation used in COBRA–IIIC is:

$$\frac{\partial W_{ij}}{\partial t} + \frac{\partial \left(U^* W_{ij}\right)}{\partial x} = \frac{s_{ij}}{\ell} \left(p_i - p_j\right) - F_{ij} \quad , \tag{2.10}$$

where:

W_{ij}	is the crossflow,	$[kg/ms]$
U^*	is the average axial velocity in the gap region,	$[m/s]$
s_{ij}	is the subchannel gap,	$[m]$
ℓ	is the centroid to centroid distance,	$[m]$
F_{ij}	is the transverse pressure loss term,	$[kPa]$
p	is the pressure.	$[kg/ms]$

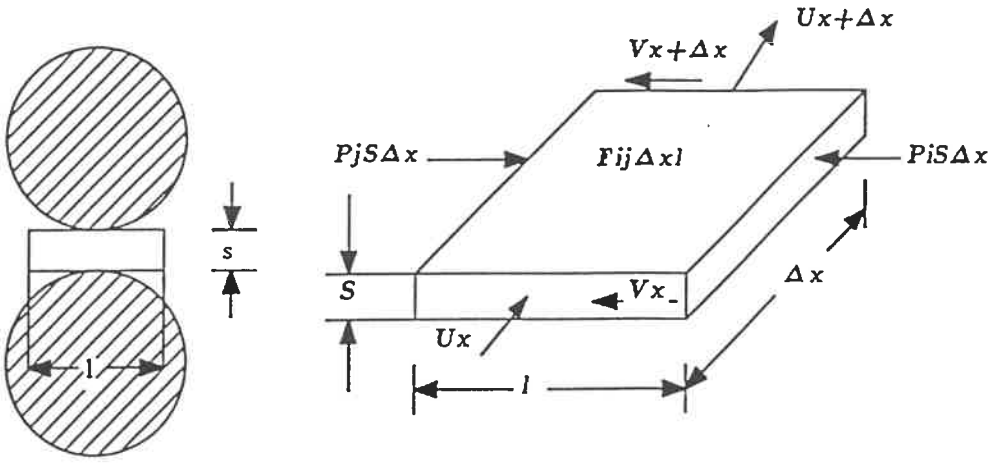

Figure 2.3: COBRA-IIIC Transverse Momentum Equation Control Volume

As in COBRA–II Rowe [1970], the assumption is made in COBRA–IIIC Rowe [1973] that the turbulent crossflow between subchannels can cause an exchange of momentum and energy between the two subchannels communicating through a given gap, but that it causes no net mass transfer. This is known as the equal mass transfer assumption. The mass exchange between adjacent subchannels is due to the diversion crossflow that results from the pressure gradients between adjacent subchannels. The diversion crossflow may also be forced to occur due to the presence of obstructions such as grid spacers redirecting the flow.

2.3.4.3 COBRA–IV Transverse Momentum Equation

In COBRA–IV, for the calculation of the transverse momentum component it is assumed, as explained in [Stewart, et al., 1977], that the flow direction is determined by the orientation of the gap. The control volume for the transverse momentum component denoted, V' has flow area A' as seen in Figure 2.4.

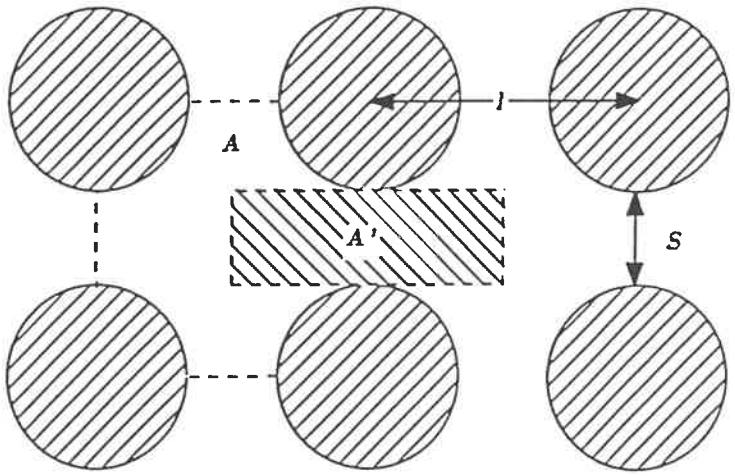

Figure 2.4: COBRA-IV Transverse Momentum Equation Control Volume

The control volume has dimensions of s by ℓ by Δx where ℓ is usually taken to be the centroid to centroid distance between adjacent subchannels i and j. The transverse momentum control volume is assumed to have a volume equal to the average of the two subchannels that communicate through the transverse control volume in question. The dimensions of the transverse control volume are given by:

$$s \times \ell \Delta x = A' \Delta x = \frac{1}{2}[A_i + A_j]\Delta x \quad . \tag{2.11}$$

where:

s	is the subchannel gap between adjacent subchannels,	$[m]$
ℓ	is approximately equal to the centroid to centroid distance between adjacent subchannels,	$[m]$
A'	is the area of the transverse momentum control volume,	$[m^2]$
A	is the flow area in the axial direction.	$[m^2]$

The complex geometry of the gap in the direction of the crossflow precludes the exact calculation of the wall friction and drag forces, the lateral momentum flux and the lateral pressure forces. These quantities must be determined from empirical correlations or approximated by various means. The definitions of the components of the transverse momentum equation are based on the rod bundle configuration. The general form of the transverse momentum equation in COBRA–IV is:

$$s\ell\Delta x\frac{\partial}{\partial t}\langle\langle\langle\rho v\rangle\rangle\rangle + s\ell\Delta x\frac{\partial}{\partial x}\langle\langle\langle\rho vu\rangle\rangle\rangle + Gs = -F_d + F_p - F_g \quad , \qquad (2.12)$$

where:

ρ	is the density of the mixture,	$[kg/m^3]$
v	is the transverse velocity,	$[m/s]$
u	is the axial velocity,	$[m/s]$
G_s	is the transverse momentum flux,	$[kgm/s^2]$
F_d	is the drag force,	$[kgm/s^2]$
F_p	is the inter–subchannel pressure force,	$[kgm/s^2]$
F_g	is the gravitational components of the transverse momentum,	$[kgm/s^2]$
Δx	is the axial node length,	$[m]$
ℓ	is the centroid to centroid distance,	$[m]$
s	is the inter–subchannel gap width.	$[m]$

The first term in equation 2.12 accounts for the temporal acceleration of the crossflow, the second term in equation 2.12 accounts for the spatial acceleration of the crossflow. The remaining individual terms will now be treated in more detail.

The pressure loss through the gap is modeled by an overal loss coefficient, K_G,

which accounts for friction as well as the form drag caused by the area change. The total drag force, F_d, acting on the transverse control volume is given by:

$$F_d = \tfrac{1}{2} K_G \left\langle \left\langle \left\langle \rho v^2 \right\rangle \right\rangle \right\rangle s \Delta x \quad , \tag{2.13}$$

where:

F_d	is the drag force,	$[kgm/s^2]$
K_G	is the loss coefficient and is of the order of 0.5,	$[-]$
ρ	is the density of the mixture,	$[kg/m^3]$
v	is the velocity in the lateral direction,	$[m/s]$
s	is the gap width,	$[m]$
Δx	is the axial node length,	$[m]$

The driving force for the crossflow is assumed to be the pressure difference between adjacent subchannels. Given two subchannels i and j communicating through a gap of width s and of length Δx, the total pressure force, F_p, on the transverse control volume is:

$$F_p = [p_i - p_j]\, s \Delta x \quad , \tag{2.14}$$

Although it is assumed that the crossflow is only defined in or near its gap region, it is more realistic to assume that the crossflows are not entirely independent of each other. This results in a term in the transverse momentum equation to account for the transverse momentum flux. The need for this term can be seen by examining Figure 2.3, it is clear that in some existing rod bundle configurations the crossflow through a given gap, denoted as A, in this case, could influence the crossflow through an adjacent gap, denoted as B. The transverse momentum flux term is written by assigning an angle β to each gap, with respect to a given reference angle. The net lateral momentum flux, G_s out of the control volume V' can be written as:

$$G_s = \sum_{k=1}^{n} C_s \left\{ \left\langle \left\langle \rho v^2 \right\rangle \right\rangle s \Delta x \cos \Delta\beta \right\} \quad , \tag{2.15}$$

where:

G_s	is the transverse momentum flux	$[kgm/s^2]$
C_s	is a factor to account for the incomplete coupling between subchannels	$[-]$
ρ	is the density of the mixture	$[kg/m^3]$
v	is the velocity in the lateral direction	$[m/s]$
s	is the gap width	$[m]$
Δx	is the axial node length	$[m]$
$\sum_{k=1}^{n}$	represents a summation over all the subchannel gaps	$[-]$
$\Delta\beta$	is the angle between two gaps	$[Deg.]$

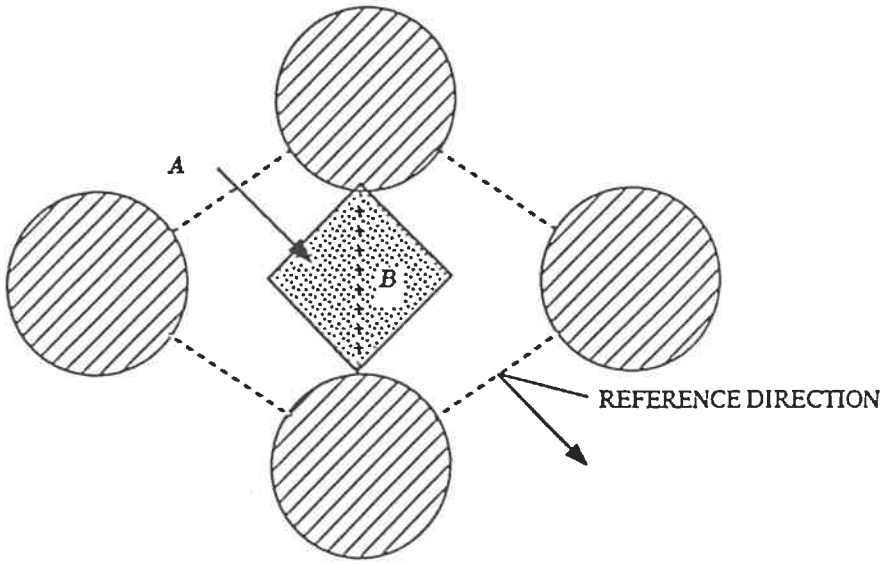

Figure 2.5: COBRA-IV Transverse Momentum Flux

The attempt to model the lateral momentum flux in COBRA-IV was not entirely succesful, and this term was left as an option the user could use or turn off at will. The angle β is also used to calculate a gravitational component, F_g of the

transverse momentum. By choosing the reference angle for β as being parallel to the bundle axis, the gravitational force acting on the transverse momentum control volume V' can be written as:

$$F_g = -g \langle\langle\langle \rho \rangle\rangle\rangle s\ell\Delta x \sin\Theta \cos\beta \quad , \tag{2.16}$$

where:

Θ	is the axial orientation of the bundle measured from the vertical	$[Deg.]$
g	is the acceleration due to gravity	$[m/s^2]$

This term is included in the derivation of the transverse momentum equation but is not programmed in the code. It is however useful, as COBRA–IV was the code used as the basis of the ASSERT–4 subchannel code, which required this term as the fuel bundles in Canadian reactors are oriented horizontally and thus subject to the influence of gravitational forces.

The subchannel code ASSERT–4, written by Atomic Energy of Canada Limited, that was used in the present research work was based on COBRA–IV. Additional terms were used in the transverse momentum equation to account for the effect of gravity induced phase seperation, buoyancy drift which is unique to the CANDU reactor design. The other major difference between COBRA–IV and ASSERT–4 is that the turbulent crossflow W'_{ij} component in COBRA–IV is assumed to transfer momentum and energy between suchannels i and j but not mass, which is known as the equal mass assumption. ASSERT–4 on the other hand assumes that the turbulent crossflow does transfer mass, and this mass is the result of the fact that the densities of the flows in the two subchannels are different and that an equal volume is transfered from one subchannel to the other, this is known as the equal volume assumption. Tahir and Carver [1984b] have compared ASSERT–4 and COBRA–IV for the simulation of a number of vertical mixing experiments and

found that ASSERT–4 successfully simulated the experiments while COBRA–IV significantly underpredicted the mixing between subchannels. It would thus appear that the equal volume assumption used in ASSERT–4 is an improvement over the equal mass assumption used in COBRA–IV. The development of the equations used in ASSERT–4 is presented in detail in the following chapters.

CHAPTER 3

DERIVATION OF THE BASIC EQUATIONS OF TWO–PHASE FLOW

The objective of this chapter is to present the derivation of the basic equations used in the ASSERT-4 [Judd et al., 1984] subchannel code. The approach taken will be the following:

1. present the basic mathematical tools required for the derivation and define the averaging process to be used,
2. develop the local instant form of the general differential balance equation,
3. develop the multiply averaged (space–time) form of the three–dimensional conservation equations, and
4. starting from the general three–dimensional averaged conservation equations previously derived, introduce the assumptions required to simplify the equations to arrive at the form of the basic equations used in the ASSERT-4 subchannel code.

In this derivation we will attempt to follow a set of guiding principles, as was done by [Patankar, 1980] for single phase flow. The guiding principles of this development will be the following:

1. to develop a physically meaningfull representation of the equations of two–phase flow,
2. to keep the formulation of the equations, as much as possible, intuitively obvious, and

3. to develop a set of equations that lend themselves easily to being discretized and thus applied in a computer code.

3.1 Basic Mathematical Concepts

The basic mathematical concepts that will be used in the derivations to follow will in most cases simply be stated as their proofs may be found in numerous reference texts such as [Aris, 1962].

3.1.1 Material and Spatial Coordinates

In this section we will examine the meaning of the terms: material coordinates and spatial coordinates. These terms, and the concepts they represent, will permit us to describe the motion of a fluid [Whitaker, 1960]. Following the method outlined in [Aris, 1962] we will also examine the link, or transformation, that exists between these two coordinate representations. The concepts of a material or a spatial coordinate system give us two alternative methods of locating the position of a given fluid particle, or group of particles.

Let $\mathcal{V}_m$ be a small volume element, that is assumed to contain a sufficient number of particles such that the velocity of the volume element can be described by an average of the velocities of the particles it contains. We will further assume that it always contains the same material, i.e., the same fluid particles. We may at any time, t, describe the position of this material volume, $\mathcal{V}_m$, by its spatial coordinates x, y, and z. Further, we may at some given time, designated as $t = 0$, fix the particle(s) contained by the material volume, that is to say:

$$x = X, \quad y = Y, \quad z = Z, \quad at \quad t = 0 \quad ,$$

where X,Y,Z are the material coordinates of the elemental volume $\mathcal{V}_m$. At any later time, $t > 0$, the position of the volume element is given by [Whitaker, 1960]:

$$x = X + \int_0^t \left(\frac{dx(X)}{dt} \right) dt \quad , \tag{3.1}$$

$$y = Y + \int_0^t \left(\frac{dy(Y)}{dt} \right) dt \quad , \tag{3.2}$$

$$z = Z + \int_0^t \left(\frac{dz(Z)}{dt} \right) dt \quad . \tag{3.3}$$

If we now multiply equations 3.1, 3.2, and 3.3 by $\hat{\imath}$, $\hat{\jmath}$, and $\hat{k}$ respectively, we may express these equations in vector form as:

$$\vec{r} = \vec{R} + \int_0^t \left(\frac{d\vec{r}\left(\vec{R}\right)}{dt} \right) dt \quad , \tag{3.4}$$

where we let

$$\vec{r} = \hat{\imath}x + \hat{\jmath}y + \hat{k}z \quad ,$$

and

$$\vec{R} = \hat{\imath}X + \hat{\jmath}Y + \hat{k}Z \quad .$$

Equation 3.4 states that the spatial position, $\vec{r}$, at any time, t, is a function of the initial position, which is the material coordinate, $\vec{R}$, and the time, t. We will refer to $\vec{r}$ as the spatial position vector, because it locates the elemental volume $\mathcal{V}_m$ in space, and refer to $\vec{R}$ as the material position vector, because it uniquely identifies the particular elemental volume to which we are refering [Aris, 1962].

3.1.2 Material and Spatial Derivatives

This section will examine both the material and spatial derivatives and the link between them.

Material Derivative

The rate of change of some property represented by a scalar, vector or tensor field function, Ψ, as observed when moving with the particle, i.e., keeping $\vec{R}$ constant, is $\frac{d\Psi}{dt}$, and is known as the material derivative.

Spatial Derivative

The rate of change of Ψ as seen by an observer located at a fixed position, i.e. keeping $\vec{r}$ constant, is $\frac{\partial \Psi}{\partial t}$ and is known as the spatial derivative of the function Ψ.

Link Between the Material and Spatial Derivatives

If the Jacobian, which is defined as:

$$J = \frac{\partial \vec{r}}{\partial \vec{R}} \neq 0 \quad , \tag{3.5}$$

is not equal to zero, then a transformation between the material and spatial description is possible [Aris, 1962]. That is to say, given a material description of some property represented by a scalar, vector or tensor field function, $\Psi(\vec{R}, t)$, it can be changed, with the use of a suitable transformation, into a spatial description $\Psi(\vec{r}, t)$.

$$\Psi\left(\vec{r}, t\right) \equiv \Psi\left[\vec{R}\left(\vec{r}, t\right), t\right] \quad . \tag{3.6}$$

The inverse is also possible, given a spatial description of some property $\Psi(\vec{r}, t)$, the use of the inverse transformation permits a material description, $\Psi(\vec{R}, t)$, to be obtained:

$$\Psi\left(\vec{R}, t\right) \equiv \Psi\left[\vec{r}\left(\vec{R}, t\right), t\right] \quad . \tag{3.7}$$

We may establish a relation between the material and spatial derivatives. Realizing that position, $\vec{r}$, itself may be considered a property [Aris, 1962] we may set $\Psi = \vec{r}$. Noting that the material derivative of a particles position is its velocity yields:

$$v_i = \frac{dx_i}{dt} = \frac{\partial x_i\left(X, Y, Z, t\right)}{\partial t} \quad , \tag{3.8}$$

in vector form, this can be expressed as:

$$\vec{v} = \frac{d\vec{r}}{dt} = \frac{\partial \vec{r}\left(\vec{R}, t\right)}{\partial t} \quad . \tag{3.9}$$

Using equation 3.9 we may establish the following relation between the material and spatial derivatives [Aris, 1962]:

$$\begin{aligned} \frac{d\Psi}{dt} = \frac{\partial}{\partial t}\Psi(\vec{R}, t) &= \frac{\partial}{\partial t}\Psi\left(\vec{r}\left(\vec{R}, t\right), t\right) \\ &= \frac{\partial \Psi}{\partial x_i}\left(\frac{\partial x_i}{\partial t}\right)_R + \left(\frac{\partial \Psi}{\partial t}\right)_r \\ &= v_i \frac{\partial \Psi}{\partial x_i} + \frac{\partial \Psi}{\partial t} \quad . \end{aligned} \tag{3.10}$$

For convenience this can be rewritten in vector form as:

$$\frac{d\Psi}{dt} = \frac{\partial \Psi}{\partial t} + \left(\vec{v} \cdot \vec{\nabla}\right)\Psi \quad . \tag{3.11}$$

Equation 3.11 mathematically represents the concept that, given a property, described by a function, Ψ, that can vary in both time and space, of a given material volume which moves with the fluid velocity, $\vec{v}$, the first term on the right hand side, $\frac{\partial \Psi}{\partial t}$, describes the local temporal variation of Ψ, while the second term on the right hand side, $\left(\vec{v} \cdot \vec{\nabla}\right)\Psi$, describes the spatial variation of Ψ.

3.2 Divergence Theorem

The divergence theorem provide a relation between the surface integral of a vector field $\vec{\Psi}$ and the volume integral of the divergence of that vector field [Aris, 1962]. Two versions of the divergence theorem will be presented in this section, the first

will be the standard form of the divergence theorem, the second will be the divergence theorem for a volume containing discontinuities.

3.2.1 Divergence Theorem: Standard Form

Suppose V is an elemental control volume with a closed surface A, having an outwardly directed unit vector normal, $\hat{n}$, and $\vec{\Psi}$ any vector field defined in V and on A. If A is piecewise smooth, and $\vec{\Psi}$ as well as its first derivative are continuous in the region of interest, we may then relate the total flux of $\vec{\Psi}$ out of the volume V, (expressed as $\nabla \cdot \vec{\Psi}$) to the outwardly directed portion of that flux, i.e., $\vec{\Psi} \cdot \hat{n}$ over the entire surface A. This leads to the following relation:

$$\iiint_V \nabla \cdot \vec{\Psi} dV = \iint_A \vec{\Psi} \cdot \hat{n} dA \quad . \tag{3.12}$$

3.2.2 Divergence Theorem: For a Volume Containing Discontinuities

If V contains k phases of the field $\vec{\Psi}$, where each of the sub–fields $\vec{\Psi}_k$ takes up a sub–volume V_k in the volume V, such that:

$$V = \sum_k V_k \quad , \tag{3.13}$$

a slightly modified form of the divergence theorem will be required. This is due to the fact that the standard form of the divergence theorem is normally only defined for a continuous vector field which, in this instance, is not the case. The derivation of this modified form of the divergence theorem will now be presented following the ideas of Banerjee[1980], Delhaye[1981], and Dorbran[1985].

If we consider an averaging volume, V, as being a parallelepiped having opposing faces on x_1 and x_2, y_1 and y_2, and z_1 and z_2 where these faces may or may not be coincident with the duct wall, and if we further consider that the phase k

occupies a volume element V_k in V, the integral over the volume element V_k of the divergence of a vector field $\vec{\Psi}_k$, can be written as:

$$\begin{aligned}\iiint_{V_k} \nabla \cdot \vec{\Psi}_k dV &= \iint_{A_k(x_2,t)} \vec{\Psi}_k \cdot \hat{n}_k dA - \iint_{A_k(x_1,t)} \vec{\Psi}_k \cdot \hat{n}_k dA \\ &+ \iint_{A_k(y_2,t)} \vec{\Psi}_k \cdot \hat{n}_k dA - \iint_{A_k(y_1,t)} \vec{\Psi}_k \cdot \hat{n}_k dA \\ &+ \iint_{A_k(z_2,t)} \vec{\Psi}_k \cdot \hat{n}_k dA - \iint_{A_k(z_1,t)} \vec{\Psi}_k \cdot \hat{n}_k dA \\ &+ \iint_{A_i} \vec{\Psi}_k \cdot \hat{n}_k dA + \iint_{A_{kw}} \vec{\Psi}_k \cdot \hat{n}_{kw} dA \quad . \end{aligned} \tag{3.14}$$

Assuming that $x_2 = x_1 + \Delta x$, $y_2 = y_1 + \Delta y$, and $z_2 = z_1 + \Delta z$ we can use the fundamental theorem of integral calculus, to write:

$$\iint_{A_k(x_2,t)} \vec{\Psi}_k \cdot \hat{n}_x dA - \iint_{A_k(x_1,t)} \vec{\Psi}_k \cdot \hat{n}_x dA = \frac{\partial}{\partial x} \iiint_{V_k} \vec{\Psi}_k \cdot \hat{n}_x dV \quad , \tag{3.15}$$

$$\iint_{A_k(y_2,t)} \vec{\Psi}_k \cdot \hat{n}_y dA - \iint_{A_k(y_1,t)} \vec{\Psi}_k \cdot \hat{n}_y dA = \frac{\partial}{\partial y} \iiint_{V_k} \vec{\Psi}_k \cdot \hat{n}_y dV \quad , \tag{3.16}$$

$$\iint_{A_k(z_2,t)} \vec{\Psi}_k \cdot \hat{n}_z dA - \iint_{A_k(z_1,t)} \vec{\Psi}_k \cdot \hat{n}_z dA = \frac{\partial}{\partial z} \iiint_{V_k} \vec{\Psi}_k \cdot \hat{n}_z dV \quad . \tag{3.17}$$

We may express the volume average of a vector field, $\vec{\Psi}_k$, as:

$$\langle\langle\langle \vec{\Psi}_k \rangle\rangle\rangle = \frac{1}{V_k} \iiint_{V_k} \vec{\Psi}_k dV \quad . \tag{3.18}$$

Thus, for the volume V_k, the volume average of the divergence of a field, $\vec{\Psi}_k$, can be expressed in terms of the divergence of an averaged field as:

$$\iiint_{V_k} \nabla \cdot \vec{\Psi}_k dV = \nabla \cdot V_k \langle\langle\langle \vec{\Psi}_k \rangle\rangle\rangle + \iint_{A_i} \vec{\Psi}_k \cdot \hat{n}_k dA + \iint_{A_{kw}} \vec{\Psi}_k \cdot \hat{n}_{kw} dA \quad . \tag{3.19}$$

Introducing the definition of the volume fraction as being the fraction of the volume, V, taken up by the phase k, $\alpha_k = \frac{V_k}{V}$. We may replace V_k by $\alpha_k V$ in equation 3.19. It is important to note that, while the control volume, V, is fixed in space, it may vary in shape in each coordinate direction. This can be accounted for, by having V appear inside the divergence term, as has been suggested in [Lahey, Jr. and Drew, 1988]. We may now rewrite equation 3.19 as:

$$\iiint_V \vec{\nabla} \cdot \vec{\Psi}_k dV = \vec{\nabla} \cdot \alpha_k V \langle\langle\langle \vec{\Psi}_k \rangle\rangle\rangle + \iint_{A_i} \vec{\Psi}_k \cdot \hat{n}_k dA + \iint_{A_{kw}} \vec{\Psi}_k \cdot \hat{n}_{kw} dA \quad . \tag{3.20}$$

Equation 3.20 is the divergence theorem expressed for a volume containing discontinuities. The first term on the right hand side of equation 3.20 represents the divergence term, the second term is the phasic interface and the last term represents the interactions of the k^{th} phase and the wall.

3.3 Transport Theorems

Transport theorems provide us with relations between the rate of change of the volume integral of a given scalar, vector or tensor quantity, Ψ, and the volume integral of the rate of change of the same quantity. A number of different formulations of various transport theorems that could be useful in the analysis of two-phase flows are given by [Truesdell and Toupin, 1960].

3.3.1 Stationary Volume

For a stationary control volume, V, the rate of change of the volume integral of the quantity, Ψ, and the volume integral of the rate of change of the same quantity, are related by the following:

$$\frac{\partial}{\partial t} \iiint_V \Psi dV = \iiint_V \frac{\partial \Psi}{\partial t} dV \quad , \tag{3.21}$$

which of course is the simplest limiting case of any possible transport theorem.

3.3.2 Reynold's and Leibnitz's Theorems

Reynold's and Leibnitz's theorems provide a relationship between rate of change of a volume integral of a continuously differentiable scalar, vector or tensor field, Ψ, over a moving material or geometric volume, $V(t)$, and the volume integral of the same field over a fixed spatial volume, V.

3.3.3 Reynold's and Leibnitz's Theorems: Standard Form

Let $V(t)$ be a geometric volume having a bounding surface, $A(t)$, moving with a velocity $\vec{w}$ which is not equal to the velocity of the fluid. Further, let $\hat{n}$ be an outwardly directed unit vector normal to the surface $A(t)$. By choosing a fixed spatial volume, V, having a surface, A, which at a given time, t, is coincident with the geometric volume, $V(t)$, we may relate the rate of change of the integral of a quantity, Ψ, over the geometric volume, $V(t)$, to the rate of change of the same quantity over the fixed volume, V, plus the flux of Ψ through its bounding surface A. This is given by:

$$\frac{d}{dt}\iiint_{V(t)} \Psi dV = \frac{\partial}{\partial t}\iiint_{V} \Psi dV + \iint_{A} \Psi \vec{w}\cdot\hat{n} dA \quad . \tag{3.22}$$

Remembering (eqn. 3.21) which relates the rate of change of the volume integral of a quantity to the volume integral of the rate of change of the same quantity, for a fixed volume, V, we may write:

$$\frac{d}{dt}\iiint_{V(t)} \Psi dV = \iiint_{V} \frac{\partial \Psi}{\partial t} dV + \iint_{A} \Psi \vec{w}\cdot\hat{n} dA \quad , \tag{3.23}$$

which is known as Leibnitz's theorem. If the volume, $V(t)$, is a material volume having a velocity, $\vec{v}$, which is the velocity of the fluid, equations 3.22 and 3.23

become:

$$\frac{d}{dt}\iiint_{V(t)} \Psi dV = \frac{\partial}{\partial t}\iiint_{V} \Psi dV + \iint_{A} \Psi \vec{v}\cdot\hat{n}dA \quad , \tag{3.24}$$

and

$$\frac{d}{dt}\iiint_{V(t)} \Psi dV = \iiint_{V} \frac{\partial \Psi}{\partial t} dV + \iint_{A} \Psi \vec{v}\cdot\hat{n}dA \quad , \tag{3.25}$$

respectively. Equations 3.24 and 3.25 are known as Reynolds' Transport Theorem.

A further point of some importance is that if we set the velocity, $\vec{w}$, equal to zero equations 3.22 and 3.23 both reduce to equation 3.21.

3.3.4 Leibnitz's Theorem: For a Volume Containing Discontinuities

In the derivation of the Reynolds and Leibnitz theorems that have just been presented, an important point was that the field, Ψ, was continuously differentiable in the volume, V. In two-phase flows a given volume, V, may be filled with part of both phases such that each individual field, Ψ_k, may be continuous in a sub-volume, V_k, but not in, V, as a whole. In this case a modified form of the transport theorem will be needed.

Let us assume that the volume, V, is a fixed control volume, containing k phases each of which occupies a sub-volume, V_k, such that:

$$V = \sum_{k} V_k \quad . \tag{3.26}$$

Further assume that each of the sub-volumes is bounded by a moving interface, A_i, and that the k^{th} phase has an area of interaction with the wall, A_{kw}. We will also assume that the interfaces have outwardly directed unit vector normals, $\hat{n}_k$, and velocities, $\vec{v}_i$, and that the wall interface has an outwardly directed unit vector

normal, $\hat{n}_{kw}$, and velocity, $\vec{v}_{iw}$. Applying, Leibnitz's theorem equation 3.23 to the volume V_k yields:

$$\frac{d}{dt}\iiint_{V_k}\Psi_k dV = \iiint_{V_k}\frac{\partial\Psi_k}{\partial t}dV + \iint_{A_i}\Psi_k\left(\vec{v}_i\cdot\hat{n}_k\right)dA + \iint_{A_{kw}}\Psi_k\left(\vec{v}_{iw}\cdot\hat{n}_{kw}\right)dA \quad . \quad (3.27)$$

In the case of the fixed volume, V, where the sub–volume taken up by the k^{th} phase, V_k, of the volume, V, is equal to $\alpha_k V$. Assuming that the volume, V, contains the two phases $k = 1$ and 2 and remembering that for the quantity Ψ_1:

$$\iiint_{V}\Psi_1 dV = \iiint_{V_1}\Psi_1 dV + \overbrace{\iiint_{V_2}\Psi_1 dV}^{0} \quad (3.28)$$

and similarly for the quantity Ψ_2:

$$\iiint_{V}\Psi_2 dV = \overbrace{\iiint_{V_1}\Psi_2 dV}^{0} + \iiint_{V_2}\Psi_2 dV \quad (3.29)$$

Using equation 3.18, which is the definition of the volume average of a field function, Ψ_k, equation 3.27 may be re–written for the fixed volume, V, as:

$$\iiint_{V}\frac{\partial\Psi_k}{\partial t}dV = \frac{\partial}{\partial t}\alpha_k V\left\langle\left\langle\Psi_k\right\rangle\right\rangle - \iint_{A_i}\Psi_k\left(\vec{v}_i\cdot\hat{n}_k\right)dA - \iint_{A_{kw}}\Psi_k\left(\vec{v}_{iw}\cdot\hat{n}_{kw}\right)dA \quad (3.30)$$

which is the form of Leibnitz's theorem for a volume containing discontinuities that is normally seen in the literature [Banergee and Chan, 1980].

3.4 Time Average of Derivatives

In order to develop the combined volume and time averaged conservation equations the time average of certain derivatives is needed. This work has already been done in [Ishii, 1975] and will simply be presented here. A relation between the time

average of the derivative and the derivative of the time average is also needed. It is important to first point out that, for a two–phase flow the time average of a scalar, vector or tensor quantity, Ψ_k, at a given point represents the fraction of the averaging period, $\Delta\tau$, that the phase k occupies the point. Further, a quantity known as the time fraction of the k^{th} phase, analogous to the volume fraction represents the probability of finding the k^{th} phase present at the point in question during the time interval $\Delta\tau$. This quantity for k^{th} phase is given by, $\overline{\alpha_k{}^t} = \frac{\sum \Delta\tau_k}{\Delta\tau}$. It should however be noted that for some fraction of the averaging time, $\Delta\tau$, the interface between the phases will be present at the averaging point. Therefore a time average of any phase of the quantity, Ψ, is defined while assuming that the thickness of the interface, δ, approaches zero. Thus the time average of, Ψ_k, is defined as:

$$\overline{\Psi_k(X_0,t_0)} = \lim_{\delta\to 0}\frac{1}{\Delta\tau}\int_{\Delta\tau}\Psi_k(X_0,\tau)d\tau \quad . \tag{3.31}$$

We will now examine some time average relations as defined in [Ishii, 1975] remembering that in all cases the assumption, $\delta \to 0$, holds. The time average of the derivative is defined as being:

$$\frac{1}{\Delta\tau}\int_{\Delta\tau}\frac{\partial}{\partial t}\Psi_k(X_0,\tau)\,d\tau = \overline{\frac{\partial\Psi_k(X_0,t_0)}{\partial t}} \quad , \tag{3.32}$$

while the derivative of the time average is defined as being:

$$\frac{\partial}{\partial t}\frac{1}{\Delta\tau}\int_{\Delta\tau}\Psi_k(X_0,\tau)\,d\tau = \frac{\partial\overline{\Psi_k(X_0,t_0)}}{\partial t} \quad . \tag{3.33}$$

The relation between these two averages is given by in [Ishii, 1975] as being:

$$\begin{aligned}\frac{1}{\Delta\tau}\int_{\Delta\tau}\frac{\partial}{\partial t}\Psi_k(X_0,\tau)d\tau &= \frac{\partial}{\partial t}\frac{1}{\Delta\tau}\int_{\Delta\tau}\Psi_k(X_0,\tau)d\tau \\ &- \frac{1}{\Delta\tau}\sum_j\frac{1}{v_{ni}}\left\{\Psi^+\hat{n}^+\cdot\vec{v}_i+\Psi^-\hat{n}^-\cdot\vec{v}_i\right\}_j \quad .\end{aligned} \tag{3.34}$$

Using the definitions given in equations 3.32 and 3.33 we may write:

$$\overline{\frac{\partial \Psi_k(X_0,t_0)}{\partial t}} = \frac{\partial \overline{\Psi_k(X_0,t_0)}}{\partial t} - \frac{1}{\Delta\tau}\sum_j \frac{1}{v_{ni}}\left\{\Psi_k^+ \hat{n}^+ \cdot \vec{v}_i + \Psi_k^- \hat{n}^- \cdot \vec{v}_i\right\}_j \quad , \qquad (3.35)$$

where:

Ψ	is a scalar or vector field function,	$[-]$
v_{ni}	is the normal conponent of the velocity of the interface $(= \vec{v}_{ik} \cdot \hat{n})$,	$[m/s]$
$\vec{v}_i$	is the velocity of the interface,	$[m/s]$
$\Delta\tau$	is the sampling time interval about time, t_0	$[s]$
$\hat{n}^{\pm}$	is a unit vector normal to the interface	$[-]$
$\sum_j$	represents a summation over all the elemental time intervals,	$[-]$
$\pm$	the side from which the boundary approaches the observation point,	$[-]$
τ	is a dummy variable for integration.	$[s]$

An other relation is needed between the time average of a divergence given by:

$$\frac{1}{\Delta\tau}\int_{\Delta\tau} \nabla \cdot \vec{\Psi}_k(X_0,\tau)\, d\tau = \overline{\nabla \cdot \vec{\Psi}_k(X_0,t_0)} \quad , \qquad (3.36)$$

and the divergence of a time average which is given by:

$$\nabla \cdot \frac{1}{\Delta\tau}\int_{\Delta\tau} \vec{\Psi}_k(X_0,\tau)\, d\tau = \nabla \cdot \overline{\vec{\Psi}_k(X_0,t_0)} \quad . \qquad (3.37)$$

The relation between these two averages is given in [Ishii, 1975] as being:

$$\begin{aligned}\frac{1}{\Delta\tau}\int_{\Delta\tau} \nabla\cdot\vec{\Psi}_k(X_0,\tau)\, d\tau &= \nabla \cdot \frac{1}{\Delta\tau}\int_{\Delta\tau} \vec{\Psi}_k(X_0,\tau)\, d\tau \\ &+ \frac{1}{\Delta\tau}\sum_j \frac{1}{\vec{v}_{ni}}\left\{\hat{n}^+ \cdot \vec{\Psi}_k^+ - \hat{n}^- \cdot \vec{\Psi}_k^-\right\} \quad . \qquad (3.38)\end{aligned}$$

Using the definitions given in equations 3.36 and 3.37 we may write:

$$\overline{\nabla \cdot \vec{\Psi}_k(X_0,t_0)} = \nabla \cdot \overline{\vec{\Psi}_k(X_0,t_0)} + \frac{1}{\Delta\tau}\sum_j \frac{1}{\vec{v}_{ni}}\left\{\hat{n}^+ \cdot \vec{\Psi}_k^+ - \hat{n}^- \cdot \vec{\Psi}_k^-\right\} \quad . \tag{3.39}$$

3.4.1 Time Average of Volume Averages

If the phenomena under consideration follows a *stationary-ergodic process*, which is defined as a process in which the *time average*, as defined by equation 3.31, and the *statistical average* defined by:

$$\overline{\Psi_k(X_0,t_0)}^N = \lim_{N\to\infty}\frac{1}{N}\sum_{n=1}^{N}\Psi(X,\tau) \quad , \tag{3.40}$$

are equal, which can be expressed as:

$$\overline{\Psi_k(X_0,t_0)}^N = \overline{\Psi_k(X_0,t_0)} \quad , \tag{3.41}$$

then the rate of change of time average, about a given time t_0, of a volume averaged scalar, vector, or tensor field, denoted as $\langle\langle\langle\Psi_k\rangle\rangle\rangle$, where the volume average has been taken over a volume that is assumed to be constant over the time interval of the time average, would be [Lahey, Jr. and Drew, 1988]:

$$\left.\frac{\partial\overline{\langle\langle\langle\Psi_k(X_0,t_0)\rangle\rangle\rangle}}{\partial t}\right|_{X=const.} = \left.\overline{\frac{\partial\langle\langle\langle\Psi_k(X_0,t_0)\rangle\rangle\rangle}{\partial t}}\right|_{X=const.} \quad . \tag{3.42}$$

where

$$X = \left(x\hat{i}, y\hat{j}, z\hat{k}\right) \quad .$$

The relationship given by equation 3.42 states that the rate of change of the time average of a volume averaged field is equal to the time average of the rate of change of a volume averaged field.

A relationship similar to equation 3.42 between the divergence of the time average of a volume averaged vector field and time average of the divergence of a volume

averaged vector field also exists. It has been given in [Lahey, Jr. and Drew, 1988] as:

$$\nabla \cdot \overline{\left\langle\left\langle\left\langle \vec{\Psi}_k\left(X_0, t_0\right)\right\rangle\right\rangle\right\rangle}\Big|_{X=const.} = \overline{\nabla \cdot \left\langle\left\langle\left\langle \vec{\Psi}_k\left(X_0, t_0\right)\right\rangle\right\rangle\right\rangle}\Big|_{X=const.} \quad . \tag{3.43}$$

Thus the divergence of the time average of a volume averaged vector field is equal to the time average of the divergence of a volume averaged vector field. It is important to note that for equations 3.42 and 3.43 the size of the control volume is not permitted to change during the interval of the time average about a given time t_0, i.e., during the time interval $t_0 - \frac{\Delta\tau}{2}$ to $t_0 + \frac{\Delta\tau}{2}$. The control volume is, however permitted to change size from one averaging time interval to the next, i.e., from time t_1 (defined as: $t_0 - \frac{\Delta\tau}{2}$ to $t_0 + \frac{\Delta\tau}{2}$) to time t_2 (defined as: $t_0 + \frac{\Delta\tau}{2}$ to $t_0 + \frac{3\Delta\tau}{2}$).

3.5 Averaged Properties

In the derivation of the volume and time averages presented in sections 3.2, 3.3 and 3.4 the averaged properties where described in terms of a volume weighting. This results in the averaged values of the k^{th} phase properties being related to the center of volume. It has been pointed out in [Kocamustafaogullari, 1971] that a more correct form of weighting is with respect to the center of mass. This is due to the fact that the quantities represented by Ψ are an additive set function of mass [Ishii, 1975]. Thus, appropriate forms of mass-weighted volume and time averages of a field function, Ψ_k, will now be presented.

Mass Weighted Form of a Volume Average

$$\left\langle\left\langle\left\langle \Psi_k^m \right\rangle\right\rangle\right\rangle = \frac{\iiint_{V_k} \rho_k \Psi_k dV}{\iiint_{V_k} \rho_k dV} = \frac{\left\langle\left\langle\left\langle \rho_k \Psi_k \right\rangle\right\rangle\right\rangle}{\left\langle\left\langle\left\langle \rho_k \right\rangle\right\rangle\right\rangle} \quad . \tag{3.44}$$

Mass Weighted Form of a Time Average

$$\overline{\Psi_k^m} = \frac{\int_{\Delta\tau} \rho_k \Psi_k d\tau}{\int_{\Delta\tau} \rho_k d\tau} = \frac{\overline{\rho_k \Psi_k}}{\overline{\rho_k}} \quad , \tag{3.45}$$

where the superscript m is used to denote mass weighting and ρ_k is the density of the k^{th} phase.

3.6 Static and Flowing Quantities

The mixture properties in two–phase flow can be defined in terms of both static and flowing parameters [Ishii, 1975]. In a detailed explanation of the differences between static and flowing quantities Kocamustafaogullari, [1971], explains that static parameters such as the void fraction, α, and the static quality, $X_{stat.}$, defined as the ratio of the mass of the gas phase to the total mass, are determined by examining a region of the flow field and observing the fraction of the static volume (or mass) which is occupied at any instant by a given phase, or in the case of mass, the fraction of the mass in the volume due to a given phase. In the case of flowing quantities such as the flow quality, X, defined as the ratio of the mass flow rate of the gas phase to the total mass flow rate, the parameter is determined examining a surface in the flow field and then measuring the fraction of the total flow across the surface area due to a given phase. Kocamustafaogullari [1971], also examines the errors that can arise due to the use of flowing quantities to define mixture quantities.

3.7 Mixture Properties

In two–phase flow calculations the two largest classes of models involve either separated flow models, in which case two separate phasic densities, enthalpies, velocities, etc. are needed, or mixture models, in which case appropriate methods of weighting the average are needed. Kocamustafaogullari [1971], has pointed out

that it is important to present mixture quantities in terms of static parameters only. This means that mixture properties should be presented in terms of the void fraction which is a static parameter, not in terms of the quality which is a flowing quantity. A simple illustrative example of why this is important would be a case in which the flow stagnates, the quality which is defined as being the mass flow rate of the vapor divided by the total mass flow rate no longer has any meaning. We will now present the mixture properties in terms of static parameters, namely the volume fraction of the k^{th} phase, which is defined as:

$$\alpha_k = \frac{V_k}{V} \quad , \tag{3.46}$$

for a steam–water mixture the volume fraction is known as the void fraction, and represents the volume fraction taken up by the vapour phase compared to the total volume. The volume fraction satisfies the following condition:

$$\sum_{k=1}^{n} \alpha_k = 1 \quad , \tag{3.47}$$

where n is the total number of phases. Using the standard convention that k=1 represents the liquid phase while k=2 represents the vapour phase, and that the void fraction, α, will represent the volume fraction of the vapour phase, α_2, while, $1 - \alpha$, will be used to represent the volume fraction of the liquid phase, α_1. The correct form of the mixture density can be expressed as:

$$\langle\langle\langle \rho_m \rangle\rangle\rangle = \frac{1}{V} \sum_{k=1}^{2} \langle\langle\langle \rho_k \rangle\rangle\rangle V_k \quad , \tag{3.48}$$

where:

ρ_m	is the density of the mixture,	$[kg/m^3]$
ρ_k	is the density of the k^{th} phase,	$[kg/m^3]$
V	is the total averaging volume,	$[m^3]$
V_k	is the volume taken up by the k^{th} phase,	$[m^3]$

using the definition of the void fraction we may now write:

$$\langle\langle\langle \rho_m \rangle\rangle\rangle = (1-\alpha)\,\langle\langle\langle \rho_1 \rangle\rangle\rangle + \alpha\,\langle\langle\langle \rho_2 \rangle\rangle\rangle \quad . \tag{3.49}$$

We can now use the mixture density, $\langle\langle\langle \rho_m \rangle\rangle\rangle$, to develop the correct form of the other mixture properties. Let Ψ_m be a quantity associated with the mixture, and let Ψ_k be the same quantity associated with the k^{th} phase, we may now express the averaged properties as:

$$\iiint_V \rho_m \Psi_m dV = \sum_{k=1}^{2} \iiint_{V_k} \rho_k \Psi_k dV \quad , \tag{3.50}$$

using the definition of the void fraction we can write:

$$\langle\langle\langle \rho_m \Psi_m \rangle\rangle\rangle = (1-\alpha)\langle\langle\langle \rho_1 \Psi_1 \rangle\rangle\rangle + \alpha\langle\langle\langle \rho_2 \Psi_2 \rangle\rangle\rangle \quad , \tag{3.51}$$

which is the volume averaged form of the quantity $\rho_m \Psi_m$. Using the definition of the mass weighted average presented in equation 3.44 we can express the volume average of the mixture property, $\langle\langle\langle \Psi_m^m \rangle\rangle\rangle$, in terms of mass weighted averages as:

$$\langle\langle\langle \Psi_m^m \rangle\rangle\rangle = (1-\alpha)\frac{\langle\langle\langle \rho_1 \rangle\rangle\rangle}{\langle\langle\langle \rho_m \rangle\rangle\rangle}\,\langle\langle\langle \Psi_1^m \rangle\rangle\rangle + \alpha\frac{\langle\langle\langle \rho_2 \rangle\rangle\rangle}{\langle\langle\langle \rho_m \rangle\rangle\rangle}\,\langle\langle\langle \Psi_2^m \rangle\rangle\rangle \quad , \tag{3.52}$$

where:

^{m}	superscript m represents mass weighting,	$[-]$
$_m$	subscript m denotes a mixture property,	$[-]$
α	void fraction,	$[-]$
ρ_k	is the density of the k^{th} phase,	$[kg/m^3]$
ρ_m	is the density of the mixture.	$[kg/m^3]$

3.8 Velocity Fields

In general two–phase flows are characterized by the two different density and velocity fields, which are never equal. Thus for problems in two–phase flow it is necessary to formulate two properly defined mean velocity fields which accurately represent the effects of the relative motion between the two phases. There are, however, a number of different velocity fields which are useful for analyzing different aspects of two–phase flow systems. The choice between these different flow fields for use in solving a particular problem in two–phase flow depends on the character of the flow and on the information available for use in constitutive relations. The following will present a number of the most common velocity fields used in solving problems in two–phase flow. In a two–phase flow system, the flow field can be formulated in terms of the individual phasic velocities or in terms of a mixture velocity for the entire flow field. For simplicity only the volume averaged form of the velocity fields will be presented, it should, however, be noted that analogous forms based on time averaging exist for all the velocity fields presented. Interested readers should consult [Ishii, 1975] for the time averaged formulations.

3.8.1 Phasic Center of Mass Velocities

By substituting $\vec{v}$ for Ψ in equation 3.44 we obtain the mass weighted volume averaged velocity of the k^{th} phase.

$$\langle\langle\langle \vec{v}_k^m \rangle\rangle\rangle = \frac{\iiint_{V_k} \rho_k \vec{v}_k dV}{\iiint_{V_k} \rho_k dV} = \frac{\langle\langle\langle \rho_k \vec{v}_k \rangle\rangle\rangle}{\langle\langle\langle \rho_k \rangle\rangle\rangle} \quad , \tag{3.53}$$

where the superscript m is used to denote mass weighting and ρ_k is the density of the k^{th} phase.

3.8.2 Relative Velocity

The relative velocity between the two phases $\langle\langle\langle \vec{v}_r^{\,m} \rangle\rangle\rangle$ is given by:

$$\langle\langle\langle \vec{v}_r^{\,m} \rangle\rangle\rangle = \langle\langle\langle \vec{v}_2^{\,m} \rangle\rangle\rangle - \langle\langle\langle \vec{v}_1^{\,m} \rangle\rangle\rangle \quad . \tag{3.54}$$

The relative velocity between the two individual phases is one of the most important velocity fields in the study of two–phase flows. Judicious use of the relative velocity allows the motion of the individual phases to be adequately represented by the use of a single mixture momentum equation. In this method, the motion of the mixture center of mass is described by the mixture momentum equation and the motion of the individual phases are described in terms of the relative velocity with respect to the mixture velocity. This representation eliminates many problems of numerical instability associated with the full two–fluid model [Webb and Rowe, 1986]. It should be noted, that the use of the concept of a relative velocity between the phases does impose some restrictions on the nature of the flow to which it is applied, the main restriction is essentially that a strong coupling must exist between the two phases.

3.8.3 Mixture Center of Mass Velocity

The definition of the center of mass velocity of a two–phase mixture is based on the principle of additivity of functions, which is applied to the linear momentum. It is important to note that linear momentum of the mixture is an additive function of the mass of its constituent phases. That is to say that, the directional components of the linear momentum of the mixture is the sum of the directional components of the linear momentum of its constituents. This is represented mathematically as:

$$\iiint_V \rho_m \vec{v}_m dV = \sum_{k=1}^{2} \iiint_{V_k} \rho_k \vec{v}_k dV \quad . \tag{3.55}$$

Equation 3.55 leads to the definition of the mixture velocity, for the center of mass, using the definition of the mass weighted volume averaged phasic velocity as seen in equation 3.53 we can write:

$$\langle\langle\langle \vec{v}_m^{\,m} \rangle\rangle\rangle = (1-\alpha)\frac{\langle\langle\langle \rho_1 \rangle\rangle\rangle}{\langle\langle\langle \rho_m \rangle\rangle\rangle}\langle\langle\langle \vec{v}_1^{\,m} \rangle\rangle\rangle + \alpha\frac{\langle\langle\langle \rho_2 \rangle\rangle\rangle}{\langle\langle\langle \rho_m \rangle\rangle\rangle}\langle\langle\langle \vec{v}_2^{\,m} \rangle\rangle\rangle \quad , \tag{3.56}$$

which is the definition of the mass weighted volume averaged form of the mixture velocity.

3.8.4 Diffusion Velocity

In two–phase flow an important and frequently used quantity is the velocity of a given phase with respect to the center of mass of the mixture. This quantity is known as the diffusion velocity, $\langle\langle\langle \vec{v}_{km}^{\,m} \rangle\rangle\rangle$, of the k^{th} phase. The diffusion velocity is defined as being:

$$\langle\langle\langle \vec{v}_{km}^{\,m} \rangle\rangle\rangle = \langle\langle\langle \vec{v}_k^{\,m} \rangle\rangle\rangle - \langle\langle\langle \vec{v}_m^{\,m} \rangle\rangle\rangle \quad . \tag{3.57}$$

The diffusion velocities of phase 1, $\langle\langle\langle \vec{v}_{1m} \rangle\rangle\rangle$, and phase 2, $\langle\langle\langle \vec{v}_{2m} \rangle\rangle\rangle$, can also be expressed in terms of the relative velocity as defined by equation 3.54 and are given by:

$$\langle\langle\langle \vec{v}_{1m}^{\,m} \rangle\rangle\rangle = -\frac{\langle\langle\langle \rho_2 \rangle\rangle\rangle}{\langle\langle\langle \rho_m \rangle\rangle\rangle}\alpha\,\langle\langle\langle \vec{v}_r^{\,m} \rangle\rangle\rangle \quad , \tag{3.58}$$

for the liquid phase, and

$$\langle\langle\langle \vec{v}_{2m}^{\,m} \rangle\rangle\rangle = \frac{\langle\langle\langle \rho_1 \rangle\rangle\rangle}{\langle\langle\langle \rho_m \rangle\rangle\rangle}(1-\alpha)\,\langle\langle\langle \vec{v}_r^{\,m} \rangle\rangle\rangle \quad , \tag{3.59}$$

for the vapour phase.

3.8.5 Volumetric Flux

In certain cases another useful velocity field is the velocity of the center of volume denoted by $\langle\langle\langle \vec{j} \rangle\rangle\rangle$. This quantity, known as the volumetric flux, can be considered to be the velocity that the k^{th} phase would have if it occupied the entire volume V. The velocity of the center of volume is defined for the two phases as:

$$\langle\langle\langle \vec{j}_1^{\,m} \rangle\rangle\rangle = (1-\alpha)\,\langle\langle\langle \vec{v}_1^{\,m} \rangle\rangle\rangle \quad , \tag{3.60}$$

for the liquid phase, and

$$\langle\langle\langle \vec{j}_2^{\,m} \rangle\rangle\rangle = \alpha\,\langle\langle\langle \vec{v}_2^{\,m} \rangle\rangle\rangle \quad , \tag{3.61}$$

for the vapour phase. The volumetric flux of the mixture is given by:

$$\langle\langle\langle \vec{j}_m^{\,m} \rangle\rangle\rangle = \langle\langle\langle \vec{j}_1^{\,m} \rangle\rangle\rangle + \langle\langle\langle \vec{j}_2^{\,m} \rangle\rangle\rangle \quad , \tag{3.62}$$

or in terms of the mass weighted averaged velocities, the volumetric flux of the mixture can be written as:

$$\langle\langle\langle \vec{j}_m^{\,m} \rangle\rangle\rangle = (1-\alpha)\,\langle\langle\langle \vec{v}_1^{\,m} \rangle\rangle\rangle + \alpha\,\langle\langle\langle \vec{v}_2^{\,m} \rangle\rangle\rangle \quad . \tag{3.63}$$

3.8.6 Drift Velocity

In two–phase flow, the quantity known as the drift velocity of the k^{th} phase is also of importance and is defined as being the velocity of the phase–k with respect to the center of volume of the mixture. The drift velocity, $\left\langle\left\langle\left\langle \vec{v}_{kj}^{\,m} \right\rangle\right\rangle\right\rangle$, of the k^{th} phase is given by:

$$\left\langle\left\langle\left\langle \vec{v}_{kj}^{\,m} \right\rangle\right\rangle\right\rangle = \langle\langle\langle \vec{v}_k^{\,m} \rangle\rangle\rangle - \langle\langle\langle \vec{j}_m^{\,m} \rangle\rangle\rangle \quad . \tag{3.64}$$

Using the results of equation 3.63 and the definition of the relative velocity, $\langle\langle\langle\vec{v}_r^{\,m}\rangle\rangle\rangle$, defined by equation 3.54 it is possible to show that the drift velocities of the two phases can be written as:

$$\left\langle\left\langle\left\langle\vec{v}_{1j}^{\,m}\right\rangle\right\rangle\right\rangle = -\alpha\langle\langle\langle\vec{v}_r^{\,m}\rangle\rangle\rangle \quad , \tag{3.65}$$

for the liquid phase, and

$$\left\langle\left\langle\left\langle\vec{v}_{2j}^{\,m}\right\rangle\right\rangle\right\rangle = (1-\alpha)\langle\langle\langle\vec{v}_r^{\,m}\rangle\rangle\rangle \quad , \tag{3.66}$$

for the vapour phase, finally we can see that this also yields an alternative definition of the relative velocity, $\langle\langle\langle\vec{v}_r^{\,m}\rangle\rangle\rangle$:

$$\langle\langle\langle\vec{v}_r^{\,m}\rangle\rangle\rangle = \left\langle\left\langle\left\langle\vec{v}_{2j}^{\,m}\right\rangle\right\rangle\right\rangle - \left\langle\left\langle\left\langle\vec{v}_{1j}^{\,m}\right\rangle\right\rangle\right\rangle \quad . \tag{3.67}$$

3.9 Covariance and Spatial Distribution Coefficients

The basic conservation equations of two–phase flow are non–linear in nature. The process of introducing averaged system variables in these equations creates difficulties due to the fact the average of the product of two functions, say Ψ_k and Φ_k, is usually not equal to the product of the average of the two functions.

$$\langle\langle\langle\Psi_k \cdot \Phi_k\rangle\rangle\rangle \neq \langle\langle\langle\Psi_k\rangle\rangle\rangle \cdot \langle\langle\langle\Phi_k\rangle\rangle\rangle \quad . \tag{3.68}$$

Consequently,

$$\left\langle\left\langle\left\langle\Psi_k^2\right\rangle\right\rangle\right\rangle \neq \langle\langle\langle\Psi_k\rangle\rangle\rangle^2 \quad , \tag{3.69}$$

unless Ψ_k is constant in the volume V, over which the average is taken.

It is, however, possible to relate the average of the product of Ψ_k and Φ_k to the product of their averages by the use of the covariance between the two functions. The covariance is defined as:

$$Cov\left(\Psi_k, \Phi_k\right) = \left\langle\left\langle\left\langle \Psi_k \cdot \Phi_k \right\rangle\right\rangle\right\rangle - \left\langle\left\langle\left\langle \Psi_k \right\rangle\right\rangle\right\rangle \cdot \left\langle\left\langle\left\langle \Phi_k \right\rangle\right\rangle\right\rangle \quad . \tag{3.70}$$

It is also possible to split the average of a product into the product of averaged values by means of a spatial distribution coefficient, C_k, as has been done in [Zuber and Findlay, 1965].

$$\left\langle\left\langle\left\langle \Psi_k \cdot \Phi_k \right\rangle\right\rangle\right\rangle = C_k \left\langle\left\langle\left\langle \Psi_k \right\rangle\right\rangle\right\rangle \cdot \left\langle\left\langle\left\langle \Phi_k \right\rangle\right\rangle\right\rangle \quad . \tag{3.71}$$

The covariance and the spatial distribution coefficient are related by:

$$Cov\left(\Psi_k, \Phi_k\right) = \left(C_k - 1\right) \left\langle\left\langle\left\langle \Psi_k \right\rangle\right\rangle\right\rangle \cdot \left\langle\left\langle\left\langle \Phi_k \right\rangle\right\rangle\right\rangle \quad . \tag{3.72}$$

It has been shown [Ishii, 1977] that, for all practical applications in turbulent two–phase flows, the covariance terms are of negligeble importance. Thus, for most practical two–phase flow applications the covariance is equal to, or almost equal to, zero and in view of equation 3.72 the spatial distribution coefficient, C_k, is equal, or approximately equal, to 1.

3.10 Fundamental Identity

The important, relation and question, which arises out of a consideration of the mixture properties of a two–phase flow system is "what is the relationship between the mean convective flux denoted by, $\left\langle\left\langle\left\langle \rho_m \vec{v}_m \Psi_m \right\rangle\right\rangle\right\rangle$, with respect to the center of mass of the mixture and the average fluxes of the individual phases, $\left(1-\alpha\right)\left\langle\left\langle\left\langle \rho_1 \vec{v}_1 \Psi_1 \right\rangle\right\rangle\right\rangle$ and $\alpha\left\langle\left\langle\left\langle \rho_2 \vec{v}_2 \Psi_2 \right\rangle\right\rangle\right\rangle$, with respect to their individual centers of mass ?" [Kocamustafaogullari, 1971]. This question results in what is known

as the "fundamental identity," a term introduced in [Kocamustafaogullari, 1971]. This relation is of prime importance in the area of two–phase flow analysis when mixture properties are used to describe the flow phenomenon since it accounts for the behaviour of the mixture even when it differs from the ideal case of a perfectly homogeneous two–phase flow by taking into account the effects that the relative velocity between the phases has on the flow. Writing the term $\langle\langle\langle\Psi_m^m\rangle\rangle\rangle$ as defined in equation 3.52 and the term $\langle\langle\langle\vec{v}_m^m\rangle\rangle\rangle$ as defined in equation 3.56 we obtain:

$$\begin{aligned}
&\langle\langle\langle\rho_m\rangle\rangle\rangle\,\langle\langle\langle\vec{v}_m^m\rangle\rangle\rangle\,\langle\langle\langle\Psi_m^m\rangle\rangle\rangle = \\
&\langle\langle\langle\rho_m\rangle\rangle\rangle\left[(1-\alpha)\,\frac{\langle\langle\langle\rho_1\rangle\rangle\rangle}{\langle\langle\langle\rho_m\rangle\rangle\rangle}\,\langle\langle\langle\vec{v}_1^m\rangle\rangle\rangle + \alpha\frac{\langle\langle\langle\rho_2\rangle\rangle\rangle}{\langle\langle\langle\rho_m\rangle\rangle\rangle}\,\langle\langle\langle\vec{v}_2^m\rangle\rangle\rangle\right] \\
&\times\left[(1-\alpha)\,\frac{\langle\langle\langle\rho_1\rangle\rangle\rangle}{\langle\langle\langle\rho_m\rangle\rangle\rangle}\,\langle\langle\langle\Psi_1^m\rangle\rangle\rangle + \alpha\frac{\langle\langle\langle\rho_2\rangle\rangle\rangle}{\langle\langle\langle\rho_m\rangle\rangle\rangle}\,\langle\langle\langle\Psi_2^m\rangle\rangle\rangle\right] \quad . \qquad (3.73)
\end{aligned}$$

Canceling the ρ_m top and bottom on the right hand side of equation 3.73 we can write:

$$\begin{aligned}
&\langle\langle\langle\rho_m\rangle\rangle\rangle\,\langle\langle\langle\vec{v}_m^m\rangle\rangle\rangle\,\langle\langle\langle\Psi_m^m\rangle\rangle\rangle = [(1-\alpha)\,\langle\langle\langle\rho_1\rangle\rangle\rangle\,\langle\langle\langle\vec{v}_1^m\rangle\rangle\rangle + \alpha\langle\langle\langle\rho_2\rangle\rangle\rangle\,\langle\langle\langle\vec{v}_2^m\rangle\rangle\rangle] \\
&\times\left[(1-\alpha)\,\frac{\langle\langle\langle\rho_1\rangle\rangle\rangle}{\langle\langle\langle\rho_m\rangle\rangle\rangle}\,\langle\langle\langle\Psi_1^m\rangle\rangle\rangle + \alpha\frac{\langle\langle\langle\rho_2\rangle\rangle\rangle}{\langle\langle\langle\rho_m\rangle\rangle\rangle}\,\langle\langle\langle\Psi_2^m\rangle\rangle\rangle\right] \quad . \qquad (3.74)
\end{aligned}$$

Expanding the right hand side of equation 3.74 and introducing the definition of the mixture density (eqn. 3.49) we get:

$$\begin{aligned}
&\langle\langle\langle\rho_m\rangle\rangle\rangle\,\langle\langle\langle\vec{v}_m^m\rangle\rangle\rangle\,\langle\langle\langle\Psi_m^m\rangle\rangle\rangle = (1-\alpha)\,\langle\langle\langle\rho_1\rangle\rangle\rangle\,\langle\langle\langle\vec{v}_1^m\rangle\rangle\rangle\,\langle\langle\langle\Psi_1^m\rangle\rangle\rangle \\
+\;&\alpha\,\langle\langle\langle\rho_2\rangle\rangle\rangle\,\langle\langle\langle\vec{v}_2^m\rangle\rangle\rangle\langle\langle\langle\Psi_2^m\rangle\rangle\rangle - \frac{1}{\langle\langle\langle\rho_m\rangle\rangle\rangle}\alpha\,(1-\alpha)\,\langle\langle\langle\rho_1\rangle\rangle\rangle\langle\langle\langle\rho_2\rangle\rangle\rangle \\
&[(\langle\langle\langle\Psi_2^m\rangle\rangle\rangle - \langle\langle\langle\Psi_1^m\rangle\rangle\rangle)\,(\langle\langle\langle\vec{v}_2^m\rangle\rangle\rangle - \langle\langle\langle\vec{v}_1^m\rangle\rangle\rangle)] \quad . \qquad (3.75)
\end{aligned}$$

Using the definitions of the covariance given by equation 3.70, the relative velocity given by equation 3.54, and of the mass weighted form of a volume av-

erage given by equation3.44 the first and second terms on the right hand side of equation 3.75 can be rewritten as the products of the averages. Thus:

$$\langle\langle\langle\rho_m\rangle\rangle\rangle\langle\langle\langle\vec{v}_m^m\rangle\rangle\rangle\langle\langle\langle\Psi_m^m\rangle\rangle\rangle = (1-\alpha)\langle\langle\langle\rho_1\vec{v}_1\Psi_1\rangle\rangle\rangle + \alpha\langle\langle\langle\rho_2\vec{v}_2\Psi_2\rangle\rangle\rangle$$
$$-\frac{1}{\langle\langle\langle\rho_m\rangle\rangle\rangle}\alpha(1-\alpha)\langle\langle\langle\rho_1\rangle\rangle\rangle\langle\langle\langle\rho_2\rangle\rangle\rangle\langle\langle\langle\vec{v}_r^m\rangle\rangle\rangle[\langle\langle\langle\Psi_2^m\rangle\rangle\rangle - \langle\langle\langle\Psi_1^m\rangle\rangle\rangle]$$
$$-(1-\alpha)\langle\langle\langle\rho_1\rangle\rangle\rangle Cov(\vec{v}_1,\Psi_1) - \alpha\langle\langle\langle\rho_2\rangle\rangle\rangle Cov(\vec{v}_2,\Psi_2) \quad . \tag{3.76}$$

Equation 3.76 is the fundamental identity of two–phase flow. It has been shown [Ishii, 1977] that, for most practical two–phase flow applications, the covariance term may be neglected, however the third term on the right hand side of equation 3.76 which takes into account the effects of the relative velocty between the phases is of great importance. Recognizing that the sum of the first and second terms on the right hand side are the average mixture flux of $\langle\langle\langle\Psi_m\rangle\rangle\rangle$, i.e.:

$$\langle\langle\langle\rho_m\vec{v}_m\Psi_m\rangle\rangle\rangle = (1-\alpha)\langle\langle\langle\rho_1\vec{v}_1\Psi_1\rangle\rangle\rangle + \alpha\langle\langle\langle\rho_2\vec{v}_2\Psi_2\rangle\rangle\rangle \quad , \tag{3.77}$$

and, since the covariance terms are in most cases negligeable [Ishii, 1977] equation 3.76 may be rewritten as:

$$\langle\langle\langle\rho_m\vec{v}_m\Psi_m\rangle\rangle\rangle = \langle\langle\langle\rho_m\rangle\rangle\rangle\langle\langle\langle\vec{v}_m^m\rangle\rangle\rangle\langle\langle\langle\Psi_m^m\rangle\rangle\rangle$$
$$+\alpha(1-\alpha)\frac{\langle\langle\langle\rho_1\rangle\rangle\rangle\langle\langle\langle\rho_2\rangle\rangle\rangle}{\langle\langle\langle\rho_m\rangle\rangle\rangle}\langle\langle\langle\vec{v}_r^m\rangle\rangle\rangle[\langle\langle\langle\Psi_2^m\rangle\rangle\rangle - \langle\langle\langle\Psi_1^m\rangle\rangle\rangle] \quad . \tag{3.78}$$

3.11 Local Instant Formulation of the Differential Balance Equations

The complete derivation of the local instant differential balance equations and their associated interfacial "jump" conditions will not be presented as this has already been presented by a number of authors, interested readers may see these

derivations in [Ishii, 1975, Truesdell and Toupin, 1960, Delhaye, 1981] among others. The general form of local instantaneous differential balance equation is:

$$\frac{\partial}{\partial t}\rho_k\Psi_k + \nabla\cdot\rho_k\vec{v}_k\Psi_k = -\nabla\cdot\vec{\phi}_k + \rho_k\dot{\Psi}_k \quad , \tag{3.79}$$

the general form of the equation describing the local instantaneous interfacial "jump" conditions is:

$$\sum_{k=1,2}\left(\Psi_k\rho_k\left(\vec{v}_k - \vec{v}_i\right)\cdot\hat{n}_k + \hat{n}_k\cdot\vec{\phi}_k + \dot{\Psi}_k\right) = 0 \quad , \tag{3.80}$$

where:

ρ_k	is the density of the k^{th} phase,	$[kg/m^3]$
Ψ_k	is the conserved quantity per unit of mass,	$[-]$
$\vec{\phi}_k$	represents the flux of the quantity Ψ_k per unit of mass,	$[-]$
$\dot{\Psi}_k$	is the body source term per unit of mass,	$[-]$
$\hat{n}_k$	is an outwardly directed unit vector, normal to the interface,	$[-]$
$\vec{v}_k$	is the velocity of the k^{th} phase,	$[m/s]$
$\vec{v}_i$	is the velocity of the interface.	$[m/s]$

By substituting the appropriate values for the terms Ψ_k, $\vec{\phi}_k$, and $\dot{\Psi}_k$ as given in Table 2.1 into the general form of the equations, we will develop the appropriate forms of the local instant conservation and interfacial equations for mass, momentum and energy.

3.11.1 Conservation of Mass: Local Instant Form

Setting the conserved quantity, $\Psi_k = 1$, the flux, $\vec{\phi}_k = 0$, and the body source, $\dot{\Psi}_k = 0$, in equation 3.79 we get the local instant form of the equation of conservation of mass:

$$\frac{\partial}{\partial t}\rho_k + \nabla\cdot\rho_k\vec{v}_k = 0 \quad , \tag{3.81}$$

where:

ρ_k	is the density of the k^{th} phase,	$[kg/m^3]$
$\vec{v}_k$	is the k^{th} phase velocity.	$[m/s]$

In the same manner the interfacial jump condition for mass can be obtained by the appropriate substitutions in equation 3.80. This yields:

$$\rho_1 (\vec{v}_1 - \vec{v}_i) \cdot \hat{n}_1 + \rho_2 (\vec{v}_2 - \vec{v}_i) \cdot \hat{n}_2 = 0 \quad . \tag{3.82}$$

For simplicity equation 3.82 is sometimes written as:

$$\Gamma_1 + \Gamma_2 = 0 \quad , \tag{3.83}$$

where

$$\Gamma_k = \rho_k (\vec{v}_k - \vec{v}_i) \cdot \hat{n}_k \quad . \tag{3.84}$$

where the term, Γ_k, is known as the interfacial mass source term.

3.11.2 Conservation of Momentum: Local Instant Form

Setting the conserved quantity, $\Psi_k = \vec{v}_k$, the flux, $\vec{\phi_k} = -\bar{\bar{\pi}}_k$, and the body source, $\dot{\Psi}_k = \vec{g}$, in equation 3.79 we get the local instant form of the equation of conservation of momentum:

$$\frac{\partial}{\partial t}\rho_k \vec{v}_k + \nabla \cdot \rho_k \vec{v}_k \vec{v}_k = -\nabla \cdot -\bar{\bar{\pi}}_k + \rho_k \vec{g} \quad , \tag{3.85}$$

where:

ρ_k	is the density of the k^{th} phase,	$[kg/m^3]$
$\vec{v}_k$	is the k^{th} phase velocity,	$[m/s]$
$-\bar{\bar{\pi}}$	represents a combination of both the pressure forces and the viscous stress forces, and can be expanded as: $-p\bar{\bar{I}} + \bar{\bar{\tau}}$,	$[kg/ms^2]$
$\vec{g}$	is the gravitational acceleration.	$[m/s^2]$

The interfacial jump condition for momentum may be obtained by appropriate substitution into eqaution 3.80, it should however be noted that the body source term, $\dot{\Psi}_k$, for the interface is not used to account for gravity as in the conservation equation 3.85 but represents the forces due to surface tension, σ. The interfacial momentum jump condition as given by [Delhaye, 1981] is:

$$\Gamma_1 \vec{v}_1 + \Gamma_2 \vec{v}_2 - \hat{n}_1 \tilde{\tilde{\pi}}_1 - \hat{n}_2 \tilde{\tilde{\pi}}_2 + \frac{d\sigma}{d\ell}\hat{\tau} - \frac{\sigma}{R}\hat{n}_1 = 0 \quad , \tag{3.86}$$

where:

R	is the radius of curvature of the interface,	$[m]$
$\hat{\tau}$	is the unit vector tangent to the interface,	$[-]$
ℓ	is the curvilinear abscissa along the interface.	$[-]$

3.11.3 Conservation of Total Energy: Local Instant Form

Setting the conserved quantity, $\Psi_k = \mathrm{u}_k + \frac{\vec{v}_k^2}{2}$, the flux, $\vec{\phi_k} = \vec{q}_k - \tilde{\tilde{\pi}}_k \cdot \vec{v}_k$, and the body source, $\dot{\Psi}_k = \vec{g} \cdot \vec{v}_k$, in equation 3.79 we get the local instant form of the equation of conservation of total energy:

$$\frac{\partial}{\partial t}\rho_k(\mathrm{u} + \frac{\vec{v}^2}{2})_k + \nabla \cdot \rho_k \vec{v}_k(\mathrm{u} + \frac{\vec{v}^2}{2})_k = -\nabla \cdot (\vec{q} - \tilde{\tilde{\pi}} \cdot \vec{v})_k + \rho_k \vec{g} \cdot \vec{v}_k \quad , \tag{3.87}$$

where:

ρ_k	is the density of the k^{th} phase,	$[kg/m^3]$
u	is the internal energy,	$[J]$
$v^2/2$	is the kinetic energy,	$[J]$
$-\tilde{\tilde{\pi}}$	represents a combination of both the pressure forces and the viscous stress forces, and can be expanded as: $-p\overline{\overline{I}} + \tilde{\tilde{\tau}}$,	$[kg/ms^2]$
$\vec{g}$	is the gravitational acceleration.	$[m/s^2]$

Neglecting the surface tension terms the interfacial jump condition for total energy can be written as:

$$\Gamma_1 \left(u_1 + \frac{v_1^2}{2}\right) + \Gamma_2 \left(u_2 + \frac{v_2^2}{2}\right) + \hat{n}_1 \cdot \vec{q}_1 + \hat{n}_2 \cdot \vec{q}_2 - \left(\hat{n}_1 \cdot \tilde{\tilde{\pi}}_1\right) \cdot \vec{v}_1 - \left(\hat{n}_2 \cdot \tilde{\tilde{\pi}}_2\right) \cdot \vec{v}_2 = 0 \quad . \tag{3.88}$$

3.11.4 Conservation of Mechanical Energy: Local Instant Form

Using the local instantaneous equation of conservation of momentum and taking its scalar product with, $\vec{v}_k$, we get the local instant equations of conservation of mechanical energy which is given by:

$$\frac{\partial}{\partial t}\left(\rho_k \frac{v_k^2}{2}\right) + \nabla \cdot \left(\rho_k \frac{v_k^2}{2} \vec{v}_k\right) = \nabla \cdot \left(\tilde{\tilde{\pi}}_k \cdot \vec{v}_k\right) - \tilde{\tilde{\pi}}_k : \nabla \vec{v}_k + \rho_k \vec{g} \cdot \vec{v}_k \quad . \tag{3.89}$$

The mechanical energy jump condition may be obtained by multiplying the interfacial momentum jump condition 3.86 by the velocity of the interface particles $\vec{v}_p$. The velocity of the interface particles as given in [Delhaye, 1981] is:

$$\vec{v}_p = \left(\vec{v}_i \cdot \hat{n}_k\right) \hat{n}_k + \vec{v}^t \quad , \tag{3.90}$$

where $\vec{v}^t$ is the tangential component of $\vec{v}_p$. Neglecting the surface tension terms equation 3.86 becomes [Delhaye, 1981]:

$$\Gamma_1 \vec{v}_1 \cdot \vec{v}_p + \Gamma_2 \vec{v}_2 \cdot \vec{v}_p - \left(\tilde{\tilde{\pi}}_1 \cdot \hat{n}_1\right) \cdot \vec{v}_p - \left(\tilde{\tilde{\pi}}_2 \cdot \hat{n}_2\right) \cdot \vec{v}_p = 0 \quad . \tag{3.91}$$

3.11.5 Conservation of Internal Energy: Local Instant Form

By subtracting the mechanical energy, equation 3.89, from the total energy, equation 3.87, we obtain the local instantaneous form of the internal energy equation:

$$\frac{\partial}{\partial t} \rho_k u_k + \nabla \cdot \rho_k u_k \vec{v}_k = -\nabla \cdot \vec{q}_k - \tilde{\tilde{\pi}}_k : \nabla \vec{v}_k \quad . \tag{3.92}$$

Following the procedure described in [Delhaye, 1981] the equation describing the internal energy interfacial jump condition may be obtained by subtracting the mechanical energy interfacial jump condition, equation 3.91, from the total energy interfacial jump condition, equation 3.88, yielding:

$$\Gamma_1\left[u_1+\frac{(\vec{v}_1-\vec{v}_p)^2}{2}\right]+\Gamma_2\left[u_2+\frac{(\vec{v}_2-\vec{v}_p)^2}{2}\right]+\hat{n}_1\cdot\vec{q}_1+\hat{n}_2\cdot\vec{q}_2$$
$$-\left(\hat{n}_1\cdot\tilde{\tilde{\pi}}_1\right)\cdot(\vec{v}_1-\vec{v}_p)-\left(\hat{n}_2\cdot\tilde{\tilde{\pi}}_2\right)\cdot(\vec{v}_2-\vec{v}_p)=0 \quad . \tag{3.93}$$

3.11.6 Conservation of Enthalpy: Local Instant Form

By using the definition of enthalpy as being:

$$h_k=u_k+\frac{p_k}{\rho_k} \quad , \tag{3.94}$$

and defining $\tilde{\tilde{\pi}}_k$ as:

$$\tilde{\tilde{\pi}}_k=p_k\bar{\bar{I}}-\bar{\bar{\tau}}_k \tag{3.95}$$

the internal energy equation becomes [Ishii, 1975]:

$$\frac{\partial\rho_k h_k}{\partial t}+\nabla\cdot(\rho_k h_k\vec{v}_k)=-\nabla\cdot\vec{q}_k+\frac{dp_k}{dt}+\bar{\bar{\tau}}_k:\nabla\vec{v}_k \quad , \tag{3.96}$$

where $\frac{d}{dt}$ has the same definition as in equation 3.11.

Using:

$$(\vec{v}_k-\vec{v}_p)^2=\frac{\Gamma_k}{\rho_k}\hat{n}_k+\left(\vec{v}_k^{\,t}-\vec{v}^{\,t}\right) \quad . \tag{3.97}$$

The interfacial jump condition for the enthalpy is [Delhaye, 1981]:

$$\Gamma_1\left[h_1+\frac{(\vec{v}_1-\vec{v}_p)^2}{2}-\frac{1}{\rho_1}(\hat{n}_1\cdot\bar{\bar{\tau}}_1)\cdot\hat{n}_1\right]+\Gamma_2\left[h_2+\frac{(\vec{v}_2-\vec{v}_p)^2}{2}-\frac{1}{\rho_2}(\hat{n}_2\cdot\bar{\bar{\tau}}_2)\cdot\hat{n}_2\right]$$
$$+\quad\hat{n}_1\cdot\vec{q}_1+\hat{n}_2\cdot\vec{q}_2-(\hat{n}_1\cdot\bar{\bar{\tau}}_1)\cdot\left(\vec{v}_1^{\,t}-\vec{v}^{\,t}\right)-(\hat{n}_2\cdot\bar{\bar{\tau}}_2)\cdot\left(\vec{v}_2^{\,t}-\vec{v}^{\,t}\right)=0 \quad . \tag{3.98}$$

3.12 Derivation of Multiply Averaged Conservation Equations

We will now develop the multiply averaged conservation equations for three dimensional two–phase flows. As any implementation in a computer code must, by the simple nature of the discretization process, create both a volume average, created by the computational mesh, and a time average, created by the time step, it would seem reasonable to develop a multiply averaged form of the conservation equations. The spatial averging created by the discretization is due to the fact that spatial information of a level of detail finer than the mesh size is not available. Similarly, the inherent temporal averaging is a result of the fact that any information on phenomena having a time scale smaller than the time step is also unavailable.

We will use the divergence (eq. 3.20) and Leibnitz's (eq. 3.30) theorems for volumes containing discontinuities and the definition of the void fraction (eq. 3.46) to average the local instant form of the differential balance equation (eq. 3.79) over a control volume, V. We will then integrate the resulting equations over a time interval, $\Delta\tau$, that is assumed to be long enough to smooth out the small temporal variations in properties yet small compared to the macroscopic time constant of the unsteadiness of the bulk fluid [Ishii, 1975], to arrive at the final form of the equations that we will use in our model.

3.12.1 Volume Average

The first step is to integrate the local instant form of the general integral balance equation 3.79 over an arbitrary control volume, V, containing discontinuities. This leads to:

$$\iiint_V \frac{\partial}{\partial t}\rho_k\Psi_k dV + \iiint_V \nabla\cdot\rho_k\Psi_k\vec{v}_k dV = -\iiint_V \nabla\cdot\vec{\phi}_k dV + \iiint_V \rho_k\dot{\Psi}_k dV \quad , \quad (3.99)$$

where:

ρ_k	is the density of the k^{th} phase,	$[kg/m^3]$
$\vec{v}_k$	is the k^{th} phase velocity,	$[m/s]$
Ψ_k	is the conserved quantity,	$[-]$
$\vec{\phi}_k$	is the flux of the conserved quantity,	$[-]$
$\dot{\Psi}_k$	is the volume source of Ψ,	$[-]$
V	is the volume of integration,	$[m^3]$

Applying Leibnitz's theorem for volumes containing discontinuities (eq. 3.30) to the first term in equation 3.99 we get the following:

$$\iiint_V \frac{\partial}{\partial t}\rho_k\Psi_k dV = \frac{\partial}{\partial t}\alpha_k V \langle\langle\langle \rho_k\Psi_k\rangle\rangle\rangle - \iint_{A_i} \rho_k\Psi_k\left(\vec{v}_i\cdot\hat{n}_k\right)dA - \iint_{A_{kw}} \rho_k\Psi_k\left(\vec{v}_{iw}\cdot\hat{n}_{kw}\right)dA \quad . \tag{3.100}$$

Making the usual assumption of no slip at the wall, which has the effect of making $\vec{v}_{iw} = 0$, the last term of equation 3.100 disappears. This yields:

$$\iiint_V \frac{\partial}{\partial t}\rho_k\Psi_k dV = \frac{\partial}{\partial t}\alpha_k V \langle\langle\langle \rho_k\Psi_k\rangle\rangle\rangle - \iint_{A_i} \rho_k\Psi_k\left(\vec{v}_i\cdot\hat{n}_k\right)dA \quad . \tag{3.101}$$

Next, we apply the divergence theorem for volumes containing discontinuities (eq. 3.20) to the second and third terms of equation 3.99. For the second term we obtain:

$$\iiint_V \nabla\cdot\rho_k\Psi_k\vec{v}_k dV = \nabla\cdot\alpha_k V\langle\langle\langle\rho_k\Psi_k\vec{v}_k\rangle\rangle\rangle + \iint_{A_i}\rho_k\Psi_k\vec{v}_k\cdot\hat{n}_k dA + \iint_{A_{kw}}\rho_k\Psi_k\vec{v}_k\cdot\hat{n}_k dA \quad . \tag{3.102}$$

Again, making the usual assumption of no slip at the wall, which has the effect of making $\vec{v}_k = 0$ on the wall, A_{kw}, the last term of equation 3.102 disappears which yields:

$$\iiint_V \nabla \cdot \rho_k \Psi_k \vec{v}_k dV = \nabla \cdot \alpha_k V \langle\langle \langle \rho_k \Psi_k \vec{v}_k \rangle\rangle\rangle + \iint_{A_i} \rho_k \Psi_k \left(\vec{v}_k \cdot \hat{n}_{ki}\right) dA \quad . \tag{3.103}$$

Similarly, for the third term of equation 3.99 we obtain:

$$\begin{aligned} \iiint_V \nabla \cdot \vec{\phi}_k dV &= \nabla \cdot \alpha_k V \langle\langle \langle \vec{\phi}_k \rangle\rangle\rangle \\ &+ \iint_{A_i} \vec{\phi}_{ki} \cdot \hat{n}_{ki} dA + \iint_{A_{kw}} \vec{\phi}_{kw} \cdot \hat{n}_{kw} dA \quad . \end{aligned} \tag{3.104}$$

For the fourth term it is simply necessary to volume average the term and introduce the void fraction given by equation 3.46, this yields:

$$\iiint_V \rho_k \dot{\Psi}_k dV = \alpha_k V \langle\langle \langle \rho_k \dot{\Psi}_k \rangle\rangle\rangle \quad . \tag{3.105}$$

Bringing together the right hand sides of equations 3.101, 3.103, 3.104 and 3.105 we get:

$$\begin{aligned} \frac{\partial}{\partial t} \alpha_k V \langle\langle \langle \rho_k \Psi_k \rangle\rangle\rangle + \nabla \cdot \alpha_k V \langle\langle \langle \rho_k \Psi_k \vec{v}_k \rangle\rangle\rangle \; &= \\ -\nabla \cdot \alpha_k V \langle\langle \langle \vec{\phi}_k \rangle\rangle\rangle + \iint_{A_i} \rho_k \Psi_k \left(\vec{v}_i \cdot \hat{n}_{ki}\right) dA - \iint_{A_i} \rho_k \Psi_k \left(\vec{v}_k \cdot \hat{n}_{ki}\right) dA \; &- \\ \iint_{A_{kw}} \hat{n}_{kw} \cdot \vec{\phi}_{kw} dA - \iint_{A_i} \hat{n}_{ki} \cdot \vec{\phi}_{ki} dA + \alpha_k V \langle\langle \langle \rho_k \dot{\Psi}_k \rangle\rangle\rangle \quad . \end{aligned} \tag{3.106}$$

where:

ρ_k	is the density of the k^{th} phase,	$[kg/m^3]$
$\vec{v}_k$	is the k^{th} phase velocity,	$[m/s]$
Ψ_k	is the conserved quantity,	$[-]$
$\vec{\phi}_k$	is the flux of the conserved quantity,	$[-]$
$\dot{\Psi}_k$	is the volume source of Ψ,	$[-]$
V	is the volume of integration,	$[m^3]$
$\hat{n}_k$	is an outwardly directed unit vector normal on the interface of the k^{th} phase,	$[-]$
A_i	is the interfacial area,	$[m^2]$
A_{kw}	is the area of interaction between the k^{th} phase and the wall.	$[m^2]$

The second and third terms on the right hand side of equation 3.106 can be grouped together, this yields:

$$\begin{aligned} \iint_{A_i} \rho_k \Psi_k \left(\vec{v}_i \cdot \hat{n}_k\right) dA \; - \; & \iint_{A_i} \rho_k \Psi_k \left(\vec{v}_k \cdot \hat{n}_k\right) dA \\ = \; & - \iint_{A_i} \rho_k \Psi_k \hat{n}_k \cdot \left(\vec{v}_k - \vec{v}_i\right) dA \end{aligned} \tag{3.107}$$

Introducing equation 3.107 in equation 3.106 yields:

$$\begin{aligned} \frac{\partial}{\partial t} \alpha_k V \langle\langle\langle \rho_k \Psi_k \rangle\rangle\rangle + \nabla \cdot \alpha_k V \langle\langle\langle \rho_k \Psi_k \vec{v}_k \rangle\rangle\rangle \; = \\ -\nabla \cdot \alpha_k V \langle\langle\langle \vec{\phi}_k \rangle\rangle\rangle - \iint_{A_i} \rho_k \Psi_k \hat{n}_k \cdot \left(\vec{v}_k - \vec{v}_i\right) dA \; - \\ \iint_{A_{kw}} \hat{n}_{kw} \cdot \vec{\phi}_{kw} dA - \iint_{A_i} \hat{n}_{ki} \cdot \vec{\phi}_{ki} dA + \alpha_k V \langle\langle\langle \rho_k \dot{\Psi}_k \rangle\rangle\rangle \quad , \end{aligned} \tag{3.108}$$

which is the volume averaged form of the general instantaneous marcoscopic conservation equation where $\vec{\phi}$ is the flux of the conserved quantity Ψ and $\dot{\Psi}$ is the volume source.

3.12.2 Time Average

Using the Reynolds decomposition we can split the conserved quantity and the velocity into two parts, a steady component and a time fluctuating component, in

the following manner:

$$\Psi_k = \overline{\Psi}_k + \Psi'_k \quad , \tag{3.109}$$

$$\vec{v}_k = \overline{\vec{v}}_k + \vec{v}'_k \quad , \tag{3.110}$$

where:

$\overline{\Psi}_k$	is the steady component of the conserved quantity,	$[-]$
Ψ'_k	is the fluctuating component of the conserved quantity,	$[-]$
$\overline{\vec{v}}_k$	is the steady component of the velocity,	$[m/s]$
$\vec{v}'_k$	is the fluctuating component of the velocity.	$[m/s]$

Introducing this decomposition into equation 3.108 we get the following:

$$\begin{aligned}
&\frac{\partial}{\partial t}\alpha_k V\langle\langle\langle\rho_k\left(\overline{\Psi}_k+\Psi'_k\right)\rangle\rangle\rangle + \nabla\cdot\alpha_k V\langle\langle\langle\rho_k\left(\overline{\Psi}_k+\Psi'_k\right)\left(\overline{\vec{v}}_k+\vec{v}'_k\right)\rangle\rangle\rangle = \\
&-\nabla\cdot\alpha_k V\langle\langle\langle\vec{\phi}_k\rangle\rangle\rangle - \iint\limits_{A_i}\rho_k\left(\overline{\Psi}_k+\Psi'_k\right)\left(\left(\overline{\vec{v}}_k+\vec{v}'_k\right)-\left(\overline{\vec{v}}_i+\vec{v}'_i\right)\right)\cdot\hat{n}_k dA \\
&-\iint\limits_{A_{kw}}\hat{n}_{kw}\cdot\vec{\phi}_{kw}dA - \iint\limits_{A_i}\hat{n}_{ki}\cdot\vec{\phi}_{ki}dA + \alpha_k V\langle\langle\langle\rho_k\dot{\Psi}_k\rangle\rangle\rangle \quad ,
\end{aligned} \tag{3.111}$$

Using the fact that for a stationary–ergodic process the time average of the rate of change of a volume averaged field is equal to the rate of change of the time average of a volume averaged field as given by equation 3.42 and remembering the fact that the time average of the divergence of a volume averaged field is equal to the divergence of the time average of a volume averaged field, as given by equation 3.43, we will time average equation 3.111. Before doing this however, it will first be necessary to state some of the assumptions that will be made regarding the time averaging of fluctuating quantities.

Rules For Time Averaging Fluctuating Quantities

- We will assume that the time average of the fluctuating quantities, $\overline{\Psi'_k}$, are zero [Teyssedou, 1987].

$$\overline{\Psi'_k} = \lim_{\delta \to 0} \frac{1}{\Delta\tau} \int_{\Delta\tau} \Psi'_k dt = 0 \quad . \tag{3.112}$$

- We will also assume that the time average of the highly correlated property fluctuations such as $\overline{\Psi'_k \vec{v}'_k}$ are not zero [Bird, et al., 1960].

$$\overline{\Psi'_k \vec{v}'_k} = \lim_{\delta \to 0} \frac{1}{\Delta\tau} \int_{\Delta\tau} \Psi'_k \vec{v}'_k dt \neq 0 \quad . \tag{3.113}$$

Thus, keeping in mind the above assumptions, the time average of equation 3.111 can be written as:

$$\begin{aligned}
&\frac{\partial}{\partial t}\alpha_k V\overline{\langle\langle\langle\rho_k\overline{\Psi}_k\rangle\rangle\rangle} + \nabla\cdot\alpha_k V\overline{\langle\langle\langle\rho_k\overline{\Psi}_k\overline{\vec{v}}_k\rangle\rangle\rangle} + \nabla\cdot\alpha_k V\overline{\langle\langle\langle\rho_k\Psi'_k\vec{v}'_k\rangle\rangle\rangle} = \\
&-\nabla\cdot\alpha_k V\overline{\langle\langle\langle\vec{\phi}_k\rangle\rangle\rangle} - \overline{\iint\limits_{A_i}\rho_k\overline{\Psi}_k\hat{n}_k\cdot\left(\overline{\vec{v}}_k-\overline{\vec{v}}_i\right)dA} - \overline{\iint\limits_{A_i}\rho_k\Psi'_k\hat{n}_k\cdot\left(\vec{v}'_k-\vec{v}'_i\right)dA} \\
&-\overline{\iint\limits_{A_{kw}}\hat{n}_{kw}\cdot\vec{\phi}_{kw}dA} - \overline{\iint\limits_{A_i}\hat{n}_{ki}\cdot\vec{\phi}_{ki}dA} + \alpha_k V\overline{\langle\langle\langle\rho_k\dot{\Psi}_k\rangle\rangle\rangle} \quad ,
\end{aligned} \tag{3.114}$$

we now have the final form of the multiply (space–time) averaged general macroscopic conservation equation for three dimensional transient two phase flow. We may now obtain any of the multiply averaged conservation equations for mass, momentum and enthalpy by substituting the appropriate values of the terms Ψ_k, $\vec{\phi}_k$ and $\dot{\Psi}_k$ as given in table 2.1 into equation3.114.

3.12.3 Averaged Mass Conservation Equation

Setting the conserved quantity $\Psi_k = 1$, the flux $\vec{\phi}_k = 0$ and the body source $\dot{\Psi}_k = 0$ in equation 3.114, we get the macroscopic form of the equation of conservation of mass.

$$\frac{\partial}{\partial t}\alpha_k V\overline{\langle\langle\langle\rho_k\rangle\rangle\rangle} + \nabla\cdot\alpha_k V\overline{\langle\langle\langle\rho_k\overline{\vec{v}}_k\rangle\rangle\rangle} = -\overline{\iint\limits_{A_i}\rho_k\left(\overline{\vec{v}}_k - \overline{\vec{v}}_i\right)\cdot\hat{n}_k dA} \quad . \quad (3.115)$$

where the term on the right hand side is the interfacial vapour source term, and is generally defined as:

$$\overline{\Gamma}_{ki} = \overline{\iint\limits_{A_i}\rho_k\left(\overline{\vec{v}}_k - \overline{\vec{v}}_i\right)\cdot\hat{n}_k dA} \quad . \quad (3.116)$$

where:

ρ_k	is the density of the k^{th} phase,	$[kg/m^3]$
$\vec{v}_k$	is the k^{th} phase velocity,	$[m/s]$
$\vec{v}_i$	is the velocity of the interface.	$[m/s]$

3.12.4 Averaged Momentum Conservation Equation

Setting the conserved quantity $\Psi_k = \vec{v}_k$, the flux $\vec{\phi}_k = -\overline{\overline{\pi}}_k$ and the body source $\dot{\Psi}_k = \vec{g}$ in equation 3.114 we get the macroscopic form of the equation of conservation of momentum.

$$\begin{aligned}
&\frac{\partial}{\partial t}\alpha_k V\overline{\langle\langle\langle\rho_k\overline{\vec{v}}_k\rangle\rangle\rangle} + \nabla\cdot\alpha_k V\overline{\langle\langle\langle\rho_k\overline{\vec{v}}_k : \overline{\vec{v}}_k\rangle\rangle\rangle} + \nabla\cdot\alpha_k V\overline{\langle\langle\langle\rho_k\vec{v}'_k : \vec{v}'_k\rangle\rangle\rangle} \;=\\
&-\nabla\cdot\alpha_k V\overline{\langle\langle\langle p_k\rangle\rangle\rangle}\,\overline{\overline{I}} + \nabla\cdot\alpha_k V\overline{\langle\langle\langle\overline{\overline{\tau}}_k\rangle\rangle\rangle} - \overline{\iint\limits_{A_i}\rho_k\overline{\vec{v}}_k\left(\overline{\vec{v}}_k - \overline{\vec{v}}_i\right)\cdot\hat{n}_k dA} \;-\\
&\overline{\iint\limits_{A_i}\rho_k\vec{v}'_k\left(\vec{v}'_k - \vec{v}'_i\right)\cdot\hat{n}_k dA} - \overline{\iint\limits_{A_{kw}}\hat{n}_{kw}\cdot p_{kw}\overline{\overline{I}}dA} + \overline{\iint\limits_{A_{kw}}\hat{n}_{kw}\cdot\overline{\overline{\tau}}_{kw}dA} \;-\\
&\overline{\iint\limits_{A_i}\hat{n}_k\cdot p_{ki}\overline{\overline{I}}dA} + \overline{\iint\limits_{A_i}\hat{n}_k\cdot\overline{\overline{\tau}}_{ki}dA} + \alpha_k V\,\overline{\langle\langle\langle\rho_k\rangle\rangle\rangle}\vec{g} \quad . \quad (3.117)
\end{aligned}$$

where:

ρ_k	is the density of the k^{th} phase,	$[kg/m^3]$
$\vec{v}_k$	is the k^{th} phase velocity,	$[m/s]$
$-\bar{\bar{\pi}}$	represents a combination of both the pressure forces and the viscous stress forces, and can be expanded as: $-p\bar{\bar{I}} + \bar{\bar{\tau}}$,	$[kg/ms^2]$
$\vec{g}$	is the gravitational acceleration.	$[m/s^2]$

3.12.5 Averaged Total Energy Conservation Equation

Setting the conserved quantity $\Psi_k = \mathrm{u}_k + \frac{\vec{v}_k^2}{2}$, the flux $\vec{\phi_k} = \vec{q}_k - \bar{\bar{\pi}}_k \cdot \vec{v}_k$ and the body source $\dot{\Psi}_k = \vec{g} \cdot \vec{v}_k$ in equation 3.79 we get the macroscopic form of the equation of conservation of total energy.

$$\frac{\partial}{\partial t}\alpha_k V\overline{\left\langle\left\langle\left\langle \rho_k(\overline{\mathrm{u}}_k + \frac{\overline{\vec{v}}_k^2}{2})\right\rangle\right\rangle\right\rangle} + \nabla\cdot\alpha_k V\overline{\left\langle\left\langle\left\langle \rho_k\overline{\vec{v}}_k(\overline{\mathrm{u}}_k + \frac{\overline{\vec{v}}_k^2}{2})\right\rangle\right\rangle\right\rangle} +$$
$$\nabla\cdot\alpha_k V\overline{\left\langle\left\langle\left\langle \rho_k\vec{v}_k'(\mathrm{u}_k' + \frac{\vec{v}_k'^2}{2})\right\rangle\right\rangle\right\rangle} = -\nabla\cdot\alpha_k V\overline{\left\langle\left\langle\left\langle\left(\vec{q}_k - \bar{\bar{\pi}}_k\cdot\overline{\vec{v}}_k\right)\right\rangle\right\rangle\right\rangle} -$$
$$\overline{\iint\limits_{A_i}\rho_k(\overline{\mathrm{u}}_k + \frac{\overline{\vec{v}}_k^2}{2})(\overline{\vec{v}}_k - \overline{\vec{v}}_i)\cdot\hat{n}_k dA} - \overline{\iint\limits_{A_i}\rho_k(u_k' + \frac{\vec{v}_k'^2}{2})(\vec{v}_k' - \vec{v}_i')\cdot\hat{n}_k dA} -$$
$$\overline{\iint\limits_{A_{kw}}\hat{n}_{kw}\cdot\left(\vec{q}_{kw} - \bar{\bar{\pi}}_{kw}\cdot\overline{\vec{v}}_k\right)dA} - \overline{\iint\limits_{A_i}\hat{n}_k\cdot\left(\vec{q}_{ki} - \bar{\bar{\pi}}_{ki}\cdot\overline{\vec{v}}_k\right)dA} -$$
$$\nabla\cdot\alpha_k V\overline{\left\langle\left\langle\left\langle\rho_k\left(\vec{g}\cdot\overline{\vec{v}}_k\right)\right\rangle\right\rangle\right\rangle} \quad . \qquad (3.118)$$

where:

ρ_k	is the density of the k^{th} phase,	$[kg/m^3]$
u	is the internal energy,	$[J]$
$\bar{\bar{\pi}}$	represents a combination of both the pressure forces and the viscous stress forces,	$[kg/ms^2]$
$\vec{g}$	is the gravitational acceleration.	$[m/s^2]$

3.12.6 Averaged Mechanical Energy Conservation Equation

Using the macroscopic form of the equation of conservation of momentum 3.117 and taking its scalar product with, $\vec{v}_k$, we get the macroscopic form of the equation of conservation of mechanical energy, which is given by:

$$\frac{\partial}{\partial t}\alpha_k V\overline{\left\langle\left\langle\left\langle \rho_k \frac{\vec{\overline{v}}_k^2}{2}\right\rangle\right\rangle\right\rangle} + \nabla\cdot\alpha_k V\overline{\left\langle\left\langle\left\langle \rho_k \vec{\overline{v}}_k \frac{\vec{\overline{v}}_k^2}{2}\right\rangle\right\rangle\right\rangle} + \nabla\cdot\alpha_k V\overline{\left\langle\left\langle\left\langle \rho_k \vec{v}'_k \frac{\vec{v}'^2_k}{2}\right\rangle\right\rangle\right\rangle} =$$
$$+\nabla\cdot\alpha_k V\overline{\langle\langle\langle\bar{\bar{\pi}}_k\cdot\vec{\overline{v}}_k\rangle\rangle\rangle} - \overline{\langle\langle\langle\bar{\bar{\pi}}_k\rangle\rangle\rangle} : \nabla\cdot\alpha_k V\overline{\langle\langle\langle\vec{\overline{v}}_k\rangle\rangle\rangle} - \overline{\iint\limits_{A_i}\rho_k\frac{\vec{\overline{v}}_k^2}{2}\left(\vec{\overline{v}}_k-\vec{\overline{v}}_i\right)\cdot\hat{n}_k dA}$$
$$-\overline{\iint\limits_{A_i}\rho_k\frac{\vec{v}'^2_k}{2}{}_k\,(\vec{v}'_k-\vec{v}'_i)\cdot\hat{n}_k dA} + \overline{\iint\limits_{A_{kw}}\hat{n}_{kw}\cdot(\bar{\bar{\pi}}_{kw}\cdot\vec{\overline{v}}_{kw})dA} + \overline{\iint\limits_{A_{ki}}\hat{n}_{ki}\cdot(\bar{\bar{\pi}}_{ki}\cdot\vec{\overline{v}}_{ki})dA}$$
$$+\alpha_k V\,\overline{\langle\langle\langle\rho_k(\vec{g}\cdot\vec{\overline{v}}_k)\rangle\rangle\rangle}\quad . \tag{3.119}$$

3.12.7 Averaged Internal Energy Conservation Equation

By subtracting the mechanical energy equation 3.119 from the total energy equation 3.118 we obtain the macroscopic form of the equation of conservation of internal energy:

$$\frac{\partial}{\partial t}\alpha_k V\overline{\langle\langle\langle\rho_k\overline{\mathrm{u}}_k\rangle\rangle\rangle} + \nabla\cdot\alpha_k V\overline{\left\langle\left\langle\left\langle\rho_k\vec{\overline{v}}_k\overline{\mathrm{u}}_k\right\rangle\right\rangle\right\rangle} + \nabla\cdot\alpha_k V\overline{\langle\langle\langle\rho_k\vec{v}'_k\mathrm{u}'_k\rangle\rangle\rangle} =$$
$$-\nabla\cdot\alpha_k V\overline{\langle\langle\langle\vec{q}_k\rangle\rangle\rangle} + \overline{\langle\langle\langle\bar{\bar{\pi}}_k\rangle\rangle\rangle} : \nabla\cdot\alpha_k V\overline{\left\langle\left\langle\left\langle\vec{\overline{v}}_k\right\rangle\right\rangle\right\rangle} - \overline{\iint\limits_{A_i}\rho_k\overline{\mathrm{u}}_k(\vec{\overline{v}}_k-\vec{\overline{v}}_i)\cdot\hat{n}_k dA}$$
$$-\overline{\iint\limits_{A_i}\rho_k\mathrm{u}'_k\,(\vec{v}'_k-\vec{v}'_i)\cdot\hat{n}_k dA} - \overline{\iint\limits_{A_{kw}}\hat{n}_{kw}\cdot\vec{q}_k dA} - \overline{\iint\limits_{A_i}\hat{n}_k\cdot\vec{q}_k dA}\quad . \tag{3.120}$$

3.12.8 Averaged Enthalpy Conservation Equation

By using the definition of enthalpy as being:

$$h_k = u_k + \frac{p_k}{\rho_k} \quad , \tag{3.121}$$

and defining $\tilde{\tilde{\pi}}_k$ as:

$$\tilde{\tilde{\pi}}_k = p_k \bar{\bar{I}} - \bar{\bar{\tau}}_k \tag{3.122}$$

we get the macroscopic form of the equation of conservation of enthaply. However, before proceding with the derivation of the equation of conservation of enthalpy we will make the standard assumption [Ishii, 1975] that the mechanical energy term $\tilde{\tilde{\tau}}_k : \nabla \vec{v}_k$ which represents the contribution due to the frictional heating of the fluid and the work done by the pressure forces is negligeable compared to the heat flux terms $\vec{q}$. We will also assume that the interfacial pressure terms are negligeable [Todreas and Kazimi, 1989]. The macroscopic form of the equation of conservation of enthaply can therefore be written as:

$$\begin{aligned}
&\frac{\partial}{\partial t}\alpha_k V\overline{\left\langle\left\langle\left\langle \rho_k \bar{h}_k \right\rangle\right\rangle\right\rangle} - \frac{\partial}{\partial t}\alpha_k V\overline{\langle\langle\langle p_k \rangle\rangle\rangle} + \nabla \cdot \alpha_k V\overline{\left\langle\left\langle\left\langle \rho_k \bar{\vec{v}}_k \bar{h}_k \right\rangle\right\rangle\right\rangle} \\
&+\nabla \cdot \alpha_k V\overline{\langle\langle\langle \rho_k \vec{v}'_k h'_k \rangle\rangle\rangle} = -\nabla \cdot \alpha_k V\overline{\langle\langle\langle \vec{q}_k \rangle\rangle\rangle} - \overline{\iint\limits_{A_i} \rho_k \bar{h}_k (\bar{\vec{v}}_k - \bar{\vec{v}}_i) \cdot \hat{n}_k dA} \\
&- \overline{\iint\limits_{A_i} \rho_k h'_k (\vec{v}'_k - \vec{v}'_i) \cdot \hat{n}_k dA} - \overline{\iint\limits_{A_{kw}} \hat{n}_{kw} \cdot \vec{q}_k dA} - \overline{\iint\limits_{A_i} \hat{n}_k \cdot \vec{q}_k dA} \quad .
\end{aligned} \tag{3.123}$$

3.13 Derivation of the Equations Used in ASSERT–4

We will now develop the equations used in the ASSERT–4 subchannel code as described in [Tahir and Carver, 1984a]. In doing so, we will examine the assumptions necessary to pass from the full three–dimensional two fluid model which consists of two equations for conservation of mass, six equations for conservation of momentum and two equations for conservation of energy, to the model used in ASSERT–4. The model in ASSERT–4 consists of four mixture conservation equations one each for conservation of mass, axial and transverse momentum and

energy as well as two phasic equations for conservation of energy to allow problems involving thermal non-equilibrium to be considered. We will also examine the constitutive equations used in ASSERT–4 to close the set of equations used to describe the two–phase flow. ASSERT–4 uses a drift flux model which does not explicitly treat the two fluids as distinct entities, thus in the development of the equations used in ASSERT–4 the first step will be to develop the mixture conservation equations starting from the set of phasic conservation equations given by equation 3.115 for mass, equation 3.117 for momentum and equation 3.123 for enthalpy. The mixture properties used in ASSERT–4 are of the mass weighted volume averaged form as shown in section 3.6.

Since ASSERT–4 uses the drift flux model we will review the basic assumptions or conditions under which this model is applicable. It is only reasonable to apply the drift flux model to the analysis of two–phase flow when the behaviour of the two components are strongly coupled. This occures in the case of dispersed flows, such as would be seen in the bubbly or slug flow regimes. From this fact it would be reasonable to conclude that it would be inappropriate to use ASSERT–4 for the analysis of cases where the flow is separated such as in the case of stratified flow.

After having obtained the mixture conservation equations by adding the phasic conservation equations a few more simplifying assumptions will be required to obtain the form of the equation used in ASSERT–4. The ASSERT–4 subchannel code is actually only quasi multidimensional at the level of the fuel bundle, more correctly it treats one dimensional flow in the individual subchannels with extra terms included to account for the crossflow between adjacent subchannels. We must therefore reduce the set of three–dimensional mixture equations to a one dimensional form and then write the crossflow contribution to the mass, momentum and energy balance as source terms much like the interfacial vapour source term.

To simplify the notation, all the space and time averaging notation will be

dropped, although it should be understood that the variables are to be interpreted in terms of their rigorous definitions. It should also be noted that the multiple (space–time) average of a product of two or more variables will be kept inside of a single bracket, $\langle\rangle$, to show that they are averaged together. Special procedures are required to separate the average of a product into the product of averages. These will be dealt with in the appropriate sections.

3.13.1 Conservation of Mass

The first step of this derivation will be to define the subchannel control volumes for the axial and transverse directions. Figure 3.1 shows both the axial subchannel control volume, and the transverse inter–subchannel control volume.

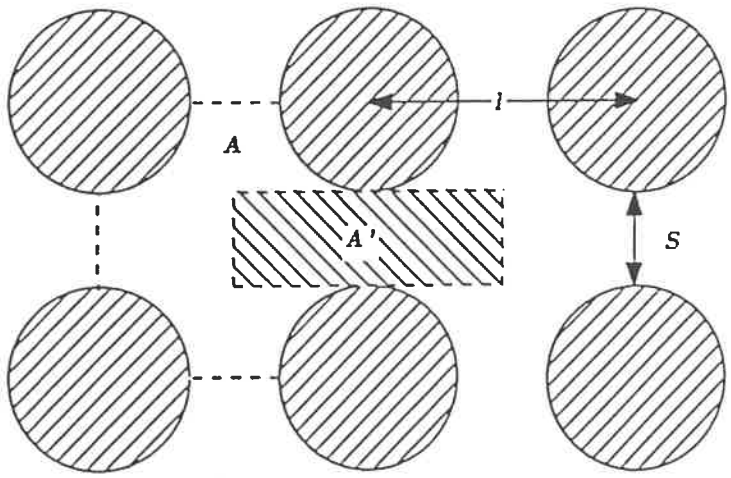

Figure 3.1: Subchannel Axial and Transverse Control Volumes

In the axial direction the control volume is defined by the flow area A of the subchannel created by the fuel rods, and axially by an arbitrary axial node lenght Δx. In the transverse direction the control volume has dimensions of $\bar{s}$ by ℓ by Δx where $\bar{s}$ is the effective gap clearence between two adjacent fuel rods and ℓ is usually taken to be the centroid to centroid distance between adjacent subchannels

i and j. The effective gap clearence is not neccesarily equal to the actual gap clearence, s, between the two fuel rods which create the gap, but is defined so as to preserve the volume of the lateral momentum cell [Carver, et al. 1983]. The volume of the lateral momentum cell is taken to be the average of the volume of the two subchannels communicating through this cell. The volume of the transverse cell is thus defined as:

$$\bar{s} \times \ell \Delta x = A' \Delta x = \frac{1}{2}[A_i + A_j]\Delta x \quad . \tag{3.124}$$

The effective gap clearence, $\bar{s}$, is therefore defined as:

$$\bar{s} = \frac{[A_i + A_j]}{2\ell} \quad . \tag{3.125}$$

The effective gap clearence $\bar{s}$ is used in the calculation of the equation of conservation of momentum, while the actual gap clearence is used for the calculation of the equation of conservation of mass.
where:

$\bar{s}$	is the effective subchannel gap ,
s	is the actual subchannel gap between adjacent subchannels,
ℓ	is approximately equal to the centroid to centroid distance between adjacent subchannels i and j,
Δx	is the axial node lenght,
A'	is the area of the transverse momentum control volume,
A_i	is the flow area in the axial direction for subchannel i,
A_j	is the flow area in the axial direction for subchannel j.

Equation 3.115, is the macroscopic space–time averaged equation of conservation of mass. In equation 3.115 the velocity $\vec{v}_k$ is defined as:

$$\vec{\overline{v}}_k = \left(\overline{u}_k\hat{\imath} + \overline{v}_k\hat{\jmath} + \overline{w}_k\hat{k}\right) \quad , \tag{3.126}$$

where the overbar denotes the steady component of the velocity.

Since ASSERT–4 treats only one dimensional flow at the level of the individual subchannels we will assume that both the y and z components of the divergence term in the equation of conservation of mass are zero, ie.:

$$\frac{\partial}{\partial y}\alpha_k V\langle\rho_k\overline{v}_k\rangle = 0 \quad . \tag{3.127}$$

$$\frac{\partial}{\partial z}\alpha_k V\langle\rho_k\overline{w}_k\rangle = 0 \quad . \tag{3.128}$$

Since the the derivation of the averaged conservation equations presented in the previous section was done for a completely arbitrary control volume they can be considered to apply to any geometry. We will thus apply the equation of conservation of mass to the subchannel geometry shown in figure 3.1, where the volume V is equal to the flow area A times the lenght Δx. We will also split the interface terms A_i into two parts one representing the interphase interface A_{phase} and another representing the area of interaction between the k^{th} phase and the intersubchannel interface A_{kgap}. In doing so we will make the following assumption:

- The intersubchannel interface in stationary, thus: $\overline{v_i}|_{kgap} = 0$,

Applying the above assumption to equation 3.115 yields:

$$\frac{\partial}{\partial t}\alpha_k A\Delta x\rho_k + \frac{\partial}{\partial x}\alpha_k A\Delta x\langle\rho_k\overline{u}_k\rangle = -\iint\limits_{A_{phase}} \rho_k\hat{n}_k\cdot\left(\overline{u}_k - \overline{u}_i\right)dA$$
$$-\sum_K \iint\limits_{A_{kgap}} \rho_k\hat{n}_k\cdot\overline{v}_k dA \quad . \tag{3.129}$$

equation 3.129 is the one dimensional equation of conservation of mass for the k^{th} phase including the intersubchannel contribution to the mass balance in a given subchannel. The term $\sum_K$ represents a summation over all the K gaps communicating with the subchannel under consideration. By writing the individual phasic equations for both the gas and liquid phases and adding them, using the definition of mixture properties given by equation 3.51, we get the equation of conservation of mixture mass for a subchannel. This is given by:

$$\frac{\partial}{\partial t} A\Delta x \rho_m + \frac{\partial}{\partial x} A\Delta x \langle \rho_m \overline{u}_m \rangle = -\sum_K \iint_{s\Delta x} \rho_m^* \overline{v}_m dA \quad , \tag{3.130}$$

where the intersubchannel flow area A_{gap} is defined as the gap width s times the axial node lenght Δx. The star $(*)$ denotes donor assignment of a quantity. That is to say, given two subchannels i and j where the crossflow is from subchannel i to subchannel j, and assuming that we are calculating the mass balance of subchannel j the density used for the crossflow contribution to this mass balance would be that of fluid in subchannel i, known as the donor subchannel.

3.13.1.1 Axial Mass Flow

Equation 3.130 is the equation of conservation of mass for a single subchannel with a source term added to account for the effects of an in or out flow due to communication with an adjacent subchannel. It however uses variables such as axial and transverse velocities which are not explicitely known in ASSERT-4. We must therefore replace them by known quantities. One of these known quantities is the mixture axial mass flow rate which can be written as:

$$F_m = F_1 + F_2 = A\langle \rho_m \overline{u}_m \rangle \quad , \tag{3.131}$$

where the phasic axial mass flow rates can be written as:

$$F_1 = (1-\alpha)A\langle\rho_1\overline{u}_1\rangle \quad , \tag{3.132}$$

for the liquid phase, and

$$F_2 = \alpha A\langle\rho_2\overline{u}_2\rangle \quad , \tag{3.133}$$

for the vapour phase.

Since ASSERT–4 only uses the equation of conservation of mixture momentum, in the axial and transverse directions, the velocities of the individual phases are not explicitly computed variables. In fact the mixture velocity is not even an explicitly computed variable. The calculated flow variables are actually the axial and transverse mixture mass flow rates F_m and W_m respectively. The axial mixture velocity is obtained by dividing the axial mixture mass flow rate by the mixture density and the subchannel flow area. This results in the mass weighted form of the mixture axial velocity as given by equation 3.56. Thus, the axial mixture velocity as defined in ASSERT–4 is given by:

$$\overline{u}_m^m = \frac{F_m}{A\rho_m} \tag{3.134}$$

To obtain the individual phasic velocities it is necessary to use the definition of the diffusion velocity given by equation 3.57, which gives the velocity of each phase with respect to the center of mass of the mixture. The diffusion velocities of phases 1 and 2 are given by equations 3.58 and 3.59 respectively. Using the definition of the diffusion velocities for phases 1 and 2 the axial phasic velocities can be written in terms of the mass weighted forms of the mixture velocity $\overline{u}_m^m$, and the relative velocity between the two phases, $\overline{u}_r^m$. The individual phasic axial mass flow rates can be written as:

$$F_1 = (1-\alpha)A\rho_1\left[\overline{u}_m^m - \frac{\alpha\rho_2}{\rho_m}\overline{u}_r^m\right] \quad , \tag{3.135}$$

for the liquid phase, and:

$$F_2 = \alpha A\rho_2\left[\overline{u}_m^m + \frac{(1-\alpha)\rho_1}{\rho_m}\overline{u}_r^m\right] \quad , \tag{3.136}$$

for the vapour phase.

where:

$\overline{u}_m^m$	is the axial velocity of the mixture,	$[m/s]$
$\overline{u}_r^m$	is the axial relative velocity.	$[m/s]$

3.13.1.2 Transverse Mass Flow

The transverse mass flow rate (crossflow), per unit lenght, into the control volume through the interconnecting gap of width, s, can be written as:

$$W_m = W_1 + W_2 = s\langle\rho_m^*\overline{v}_m\rangle \quad , \tag{3.137}$$

where the phasic transverse mass flow rates, per unit lenght, can be written as:

$$W_1 = (1-\alpha)s\langle\rho_1^*\overline{v}_1\rangle \quad , \tag{3.138}$$

for the liquid phase, and

$$W_2 = \alpha s\langle\rho_2^*\overline{v}_2\rangle \quad , \tag{3.139}$$

for the vapour phase.

As in the case of the axial velocity the transverse mixture velocity is obtained by dividing the transverse mixture mass flow rate, per unit lenght, by the mixture density and the inter-subchannel gap spacing s. This results in the mass weighted

form of transverse velocity as given by equation 3.56. The transverse mixture velocity is given by:

$$\overline{v}_m^m = \frac{W_m}{s\rho_m^*} \quad . \tag{3.140}$$

Again, as in the case of the axial phasic velocities, the definition of the diffusion velocity given by equation 3.57 is used to compute the individual transverse phasic velocities. Using the definition of the diffusion velocities for phases 1 and 2 the transverse phasic velocities can be written in terms of the mass weighted forms of the transverse mixture velocity $\overline{v}_m^m$, and the relative velocity between the two phases, $\overline{v}_r^m$. The individual phasic transverse mass flow rates can be written as:

$$W_1 = (1-\alpha)^* s\rho_1^* \left[\overline{v}_m^m - \frac{\alpha^*\rho_2^*}{\rho_m^*}\overline{v}_r^m\right] \quad , \tag{3.141}$$

for the liquid phase, and

$$W_2 = \alpha^* s\rho_2^* \left[\overline{v}_m^m + \frac{(1-\alpha)^*\rho_1^*}{\rho_m^*}\overline{v}_r^m\right] \quad , \tag{3.142}$$

where:

$\overline{v}_m^m$	is the transverse velocity of the mixture,	$[m/s]$
$\overline{v}_r^m$	is the transverse relative velocity,	$[m/s]$
$*$	is used to denote donor assignment i.e. quantity is associated with the value of that quantity in the donor subchannel.	$[-]$

We can now rewrite the equation of conservation of mass given by equation 3.130 as:

$$A\Delta x\frac{\partial}{\partial t}\rho_m + \Delta x\frac{\partial}{\partial x}F_m + \sum_{K_{\Delta x}}\int W_m dx = 0 \quad , \tag{3.143}$$

Since the crossflow W_m has no dependence on x the integration simply results in:

$$A\Delta x\frac{\partial}{\partial t}\rho_m + \Delta x\frac{\partial}{\partial x}F_m + \sum_K \Delta x W_m = 0 \quad , \tag{3.144}$$

which is the form of the equation of conservation of mixture mass used in ASSERT–4.

where:

ρ_m	density of the mixture,	$[kg/m^3]$
F_m	is the axial mass flow rate of the mixture,	$[kg/s]$
W_m	is the mixture crossflow,	$[kg/ms]$
$\sum_K$	represents a summation over all the K gaps communicating with the subchannel under consideration.	$[-]$

3.13.2 Conservation of Momentum

The three dimensional form of the equation of conservation of phasic momentum is given by equation 3.117. To obtain the form of the equations of conservation of momentum used in ASSERT–4, from this equation, a number of simplifying assumption are required. This development will be done separately for the equation of conservation of momentum in the axial and transverse directions.

3.13.2.1 Axial Momentum

Before starting to simplify equation 3.117 to obtain the equation of conservation of momentum in the axial direction it is necessary to split the interface terms A_i into two parts one representing the interphase interface A_{phase} and another representing the area of interaction between the k^{th} phase and the intersubchannel interface A_{kgap}. So as to obtain the additional terms used to account for the crossflow. In doing so we will use the same assumption as in the case of the equation of conservation of mass namely that:

- The intersubchannel interface in stationary, thus: $\overline{v}_i|_{kgap} = 0$.

- as well as: $v'_i|_{kgap} = 0$

We will also replace the general control volume V by the control volume for the subchannel as shown in figure 3.1, having flow area A and lenght Δx. Thus equation 3.117 becomes:

$$\frac{\partial}{\partial t}\alpha_k A\Delta x\langle\rho_k\overline{\vec{v}}_k\rangle + \nabla\cdot\alpha_k A\Delta x\langle\rho_k\overline{\vec{v}}_k:\overline{\vec{v}}_k\rangle + \nabla\cdot\alpha_k A\Delta x\langle\rho_k\vec{v}'_k:\vec{v}'_k\rangle =$$
$$-\nabla\cdot\alpha_k A\Delta x p_k\overline{\overline{I}} + \nabla\cdot\alpha_k A\Delta x\overline{\overline{\tau}}_k - \iint\limits_{A_{phase}}\langle\rho_k\overline{\vec{v}}_k\left(\overline{\vec{v}}_k-\overline{\vec{v}}_i\right)\rangle\cdot\hat{n}_k dA$$
$$-\iint\limits_{A_{phase}}\langle\rho_k\vec{v}'_k\left(\vec{v}'_k-\vec{v}'_i\right)\rangle\cdot\hat{n}_k dA - \sum_K\iint\limits_{A_{kgap}}\langle\rho_k\overline{\vec{v}}_k\overline{\vec{v}}_k\rangle\cdot\hat{n}_{kgap}dA - \sum_K\iint\limits_{A_{kgap}}\langle\rho_k\vec{v}'_k\vec{v}'_k\rangle\cdot\hat{n}_{kgap}dA$$
$$-\iint\limits_{A_{kw}}\hat{n}_{kw}\cdot p_{kw}\overline{\overline{I}}dA + \iint\limits_{A_{kw}}\hat{n}_{kw}\cdot\overline{\overline{\tau}}_{kw}dA - \iint\limits_{A_{phase}}\hat{n}_k\cdot p_{ki}\overline{\overline{I}}dA - \sum_K\iint\limits_{A_{kgap}}\hat{n}_{kgap}\cdot p_{ki}\overline{\overline{I}}dA$$
$$\iint\limits_{A_{phase}}\hat{n}_k\cdot\overline{\overline{\tau}}_{ki}dA + \sum_K\iint\limits_{A_{kgap}}\hat{n}_{kgap}\cdot\overline{\overline{\tau}}_{ki}dA + \alpha_k A\Delta x\rho_k\vec{g} \quad . \tag{3.145}$$

The first simplifiying assumption is due to the fact that ASSERT–4 only treats the fluid as a mixture. We will thus add the two phasic conservation equations to obtain the equation of conservation of mixture momentum. The next simplification to be made is due to the fact that ASSERT–4, as has already been stated is only a quasi multidimensional code, and is more correctly a one dimensional code with additional terms to account for the crossflow.

We will let the coordinate of the axial direction be x, having unit vector $\hat{\imath}$. We may thus obtain the equation of conservation of mixture momentum in the axial direction by dotting the equation resulting from the addition of the two phasic equations 3.145 with the unit vector $\hat{\imath}$. We may also simplify the resulting equation by eliminating the terms in $\frac{\partial}{\partial y}$ and $\frac{\partial}{\partial z}$ appearing in it. Applying all of the above to equation 3.145 results in:

$$\frac{\partial}{\partial t}A\Delta x\langle\rho_m\overline{u}_m\rangle + \frac{\partial}{\partial x}A\Delta x\langle\rho_m\overline{u}_m\overline{u}_m\rangle + \frac{\partial}{\partial x}A\Delta x\langle\rho_m u'_m u'_m\rangle =$$

$$-\frac{\partial}{\partial x}A\Delta x p_m + \frac{\partial}{\partial x}A\Delta x\overline{\overline{\tau}}_{mxx} - \sum_K \iint_{A_{gap}} \langle \rho_m \overline{u}_m \overline{v}_m \rangle dA$$
$$-\sum_K \iint_{A_{gap}} \langle \rho_m u'_m v'_m \rangle dA - \iint_{A_{mw}} \left(\hat{n}_{mw} \cdot p_{mw}\overline{\overline{I}}\right) \cdot \hat{\imath} dA + \iint_{A_{mw}} (\hat{n}_{mw} \cdot \overline{\overline{\tau}}_{mw}) \cdot \hat{\imath} dA$$
$$-\iint_{A_{gap}} \left(\hat{n}_{gap} \cdot p_m \overline{\overline{I}}\right) \cdot \hat{\imath} dA + \sum_K \iint_{A_{gap}} \hat{n}_{gap} \cdot \overline{\overline{\tau}}_{m_{gap}} dA - A\Delta x \rho_m g_x \quad . \tag{3.146}$$

Equation 3.146 is now one–dimensional but not yet in the form used in ASSERT–4. We will now examine some of the individual terms in more detail, and develop some of the simplifications required to obtain the form of the equation of conservation of axial momentum as applied in ASSERT–4. The first term we will look at will be:

$$-\iint_{A_{mw}} (\hat{n}_{mw} \cdot p_{mw}\overline{\overline{I}}) \cdot \hat{\imath} dA \quad . \tag{3.147}$$

If we imagine the control volume V as having lenght Δx and a wall surface area A_{mw} equation 3.147 represents the average phase pressure at the bounding wall. The term dA can be expressed as $\frac{dV}{dx}$, if there is no change in the volume of the control volume, V, with respect to the x direction then $\frac{dV}{dx}$ is equal to zero. Thus:

$$(\hat{n}_{mw} \cdot p_{mw}\overline{\overline{I}}) \cdot \hat{\imath}\frac{dV}{dx} = 0 \quad . \tag{3.148}$$

The next term we will examine is the turbulent component of the axial momentum balance. ASSERT–4 does not treat the turbulent fluctuations in the velocity, thus u'_m is not known, and thus:

$$\frac{\partial}{\partial x}A\Delta x\langle \rho_m u'_m u'_m \rangle = 0 \quad . \tag{3.149}$$

This is also true for the turbulent component of the transverse velocity v'_m, thus:

$$\iint_{A_{gap}} \langle \rho_m u'_m v'_m \rangle dA = 0 \quad . \tag{3.150}$$

Next, we will look at the term representing the axial gradient of the viscous stress tensor. It has been shown [Vernier and Delhaye, 1968] that this term is negligeable, thus:

$$\frac{\partial}{\partial x} A \Delta x \overline{\overline{\tau}}_{mxx} \approx 0 \quad . \tag{3.151}$$

The interfacial pressure term can be cancelled due to the fact that $\hat{n}_{kgap}$ and $\hat{\imath}$ are perpendicular to each other. Thus:

$$\iint_{A_{gap}} \left(\hat{n}_{gap} \cdot p_m \overline{\overline{I}} \right) \cdot \hat{\imath} dA = 0 \quad . \tag{3.152}$$

The last term that needs to be looked at is the axial component of the viscous shear stress at the intersubchannel interface. When compared to the viscous shear stresses on the solid wall interface this term is of negligeable importance. Thus:

$$\iint_{A_{kgap}} \hat{n}_{kgap} \cdot \overline{\overline{\tau}}_{m_{kgap}} dA \approx 0 \quad . \tag{3.153}$$

Applying all of the above simplifications to equation 3.146 yields:

$$\begin{aligned} \frac{\partial}{\partial t} A \Delta x \langle \rho_m \overline{u}_m \rangle + \frac{\partial}{\partial x} A \Delta x \langle \rho_m \overline{u}_m \overline{u}_m \rangle \; = \\ -\frac{\partial}{\partial x} A \Delta x p_m - \sum_K \iint_{A_{gap}} \langle \rho_m \overline{u}_m \overline{v}_m \rangle dA + \iint_{A_{mw}} (\hat{n}_{mw} \cdot \overline{\overline{\tau}}_{mw}) \cdot \hat{\imath} dA \; - \\ + A \Delta x \rho_m g_x \quad . \end{aligned} \tag{3.154}$$

where:

ρ_m	density of the mixture,	$[kg/m^3]$
$\overline{u}_m$	is the axial velocity of the mixture,	$[m/s]$
$\overline{v}_m$	is the transverse velocity of the mixture,	$[m/s]$
p_m	is the pressure,	$[Pa]$
$\overline{\overline{\tau}}$	is the viscous stress tensor of the bulk mixture,	$[kg/ms^2]$
$_m$	subscript $_m$ refers to the mixture properties,	$[-]$
$\sum_K$	represents a summation over all the gaps communicating with the subchannel under concideration,	$[-]$
g	is the acceleration due to gravity,	$[m/s^2]$

The conserved quantity of the first term of the axial momentum equation 3.154 is identical to the axial mass flow rate as defined by equation 3.131. We may thus write:

$$\frac{\partial}{\partial t} A\Delta x \langle \rho_m \overline{u}_m \rangle = \Delta x \frac{\partial}{\partial t} F_m \quad . \tag{3.155}$$

The next term we will look at is the momentum flux in the axial direction which is represented by:

$$\frac{\partial}{\partial x} A\Delta x \langle \rho_m \overline{u}_m \overline{u}_m \rangle \tag{3.156}$$

Remembering the definition of the axial mixture mass flow rate given by equation 3.131, equation 3.156 could be expressed as:

$$\frac{\partial}{\partial x} A\Delta x \langle \rho_m \overline{u}_m \overline{u}_m \rangle = \frac{\partial}{\partial x} \Delta x \langle F_m \overline{u}_m \rangle \quad . \tag{3.157}$$

Remembering that the axial velocity is not a directly calculated property, and is in fact defined as the axial mass flow rate divided by the flow area times the density as given by equation 3.134, it is clear that in order to calculate the conserved quantity representing the axial momentum flux, namely $\langle F_m \overline{u}_m \rangle$ it will be necessary to split the volume average of the product of the axial mass flow rate times the velocity into the product of the volume averaged quantities. This can be done

using the fundamental identity as given by equation 3.78, with the mass weighted axial velocity $\overline{u}_m^m$ being the quantity Ψ_m^m and the quantities $\overline{u}_1^m$ being Ψ_1^m and $\overline{u}_2^m$ being Ψ_2^m respectively. For convenience, we will drop the leading $\frac{\partial}{\partial x}\Delta x$ and the conserved quantity in equation 3.157 could be rewritten as:

$$\langle F_m \overline{u}_m \rangle = F_m \overline{u}_m^m + A\frac{\alpha(1-\alpha)\rho_1\rho_2}{\rho_m}\overline{u}_r^m\left[\overline{u}_2^m - \overline{u}_1^m\right] \quad . \tag{3.158}$$

Noting that the term in the square brackets is the axial relative velocity, and replacing the mass weighted axial velocity by its definition as given by equation 3.134, equation 3.158 can be rewritten as:

$$\langle F_m \overline{u}_m \rangle = \frac{F_m^2}{A\rho_m} + A\frac{\alpha(1-\alpha)\rho_1\rho_2}{\rho_m}\overline{u}_r^{m\,2} \quad . \tag{3.159}$$

Using the results of this development the momentum flux in the axial direction, given by equation 3.156 can be written as:

$$\frac{\partial}{\partial x}A\Delta x\langle \rho_m \overline{u}_m \overline{u}_m \rangle = \Delta x\frac{\partial}{\partial x}\frac{F_m^2}{A\rho_m} + A\frac{\alpha(1-\alpha)\rho_1\rho_2}{\rho_m}\overline{u}_r^{m\,2} \quad . \tag{3.160}$$

We now have the final form of the axial flux term of the axial momentum conservation equation.

The next term we will look at is the transverse flow contribution to the axial momentum. This term is:

$$\iint_{A_{gap}} \langle \rho_m \overline{u}_m \overline{v}_m \rangle dA \quad . \tag{3.161}$$

If we consider to subchannels, i and j, that are communicating with each other, and if we will further suppose that the crossflow W_m is from i to j, thus i is the

donor subchannel and j is the recipient subchannel. The contribution to the axial momentum balance in subchannel j, would be the crossflow W_m , having the axial velocity of the donor subchannel. As before we will denote the donor quantities by *. Introducing donor assignment of the appropriate quantities, and replacing the area A_{gap} by its definition as given by figure 3.1, which is $s\Delta x$ equation 3.161 becomes:

$$\iint_{s\Delta x} \langle \rho_m^* \overline{u}_m^* \overline{v}_m \rangle dA \quad . \tag{3.162}$$

Carrying out the first integration results in:

$$\int_{\Delta x} s \langle \rho_m^* \overline{u}_m^* \overline{v}_m \rangle dx \quad . \tag{3.163}$$

The terms $s\rho_m^* \overline{v}_m$ are identical to the definition of the crossflow given by equation 3.137. Thus:

$$\int_{\Delta x} s \langle \rho_m^* \overline{u}_m^* \overline{v}_m \rangle dx = \int_{\Delta x} \langle W_m \overline{u}_m^* \rangle dx \quad . \tag{3.164}$$

In order to open the average of the product $\langle W_m \overline{u}_m^* \rangle$ in equation 3.164 it is necessary to use the fundamental identity 3.78 with the conserved quantities Ψ_1^m, and Ψ_2^m being the axial velocities of the two phases in the donor channel $\overline{u}_1^{*m}$, and $\overline{u}_2^{*m}$, respectively. This results in:

$$\langle W_m \overline{u}_m^* \rangle = W_m \overline{u}_m^{*m} + s \frac{\alpha (1-\alpha) \rho_1 \rho_2}{\rho_m^*} \overline{v}_r^m \left[\overline{u}_2^{*m} - \overline{u}_1^{*m} \right] \quad . \tag{3.165}$$

Noting that the last term of equation 3.165 is the donor relative velocity $\overline{u}_r^{*m}$, we may now use the above development to rewrite the transverse flow contribution to the conservation of axial momentum 3.161 as:

$$\iint_{s\Delta x} (\rho_m^* \overline{m}_m \overline{u}_m^*) \cdot \hat{n}_{gap} dA = \Delta x \left[W_m \overline{u}_m^{*m} + s \frac{\alpha(1-\alpha)\rho_1\rho_2}{\rho_m^*} \overline{v}_r^m \overline{u}_r^{*m} \right] \tag{3.166}$$

We will next examine the term which accounts for the wall friction which is given by the third term on the right hand side of equation 3.154 Expressing the frictional loss component as being a function of the cross–sectional flow area, A, the axial mass flow rate F, and a resistance coefficient K, which includes the two phase friction multiplier, $\phi_{\ell 0}^2$, we may write this term as:

$$\iint_{A_{mw}} (\hat{n}_{mw} \cdot \overline{\overline{\tau}}_{mw}) \cdot \hat{\imath} dA = -\mathcal{F}(A, K, |F|, F) \quad . \tag{3.167}$$

Using the all of the above we may now write the axial momentum equation as:

$$\begin{aligned} \Delta x \frac{\partial}{\partial t} F_m + \Delta x \frac{\partial}{\partial x} \frac{F_m^2}{A\rho_m} + \Delta x \frac{\partial}{\partial x} A \frac{\alpha(1-\alpha)\rho_1\rho_2}{\rho_m} \overline{u}_r^{m2} \quad + \\ \sum_K \Delta x W_m \overline{u}_m^{*m} + \sum_K \Delta x s \frac{\alpha(1-\alpha)\rho_1\rho_2}{\rho_m^*} \overline{v}_r^m \overline{u}_r^{*m} \quad = \\ -A\Delta x \frac{\partial}{\partial x} p_m - \mathcal{F}(A, K, |F|, F) - A\Delta x \rho_m g_x \quad . \end{aligned} \tag{3.168}$$

3.13.2.2 Transverse Momentum

Since the derivation of the multiply average equation of conservation of momentum was carried out for an arbitrary control volume it is completely general and may thus be applied to any control volume we choose. We will therefore apply it to the transverse control volume shown in figure 3.1 having the volume $\bar{s}\ell\Delta x$.

To arrive at the transverse momentum equation used in ASSERT–4 certain simplifiying assumptions are needed. The first simplifiying assumption is due to the fact that ASSERT–4 only treats the fluid as a mixture. We will thus add the two phasic conservation equations to obtain the equation of conservation of

mixture momentum. The next simplification to be made is due to the fact that ASSERT–4, as has already been stated is only a quasi multidimensional code, and is more correctly a one dimensional code with additional terms to account for the crossflow.

We will let the coordinate of the transverse direction be y, having unit vector $\hat{\jmath}$. We may thus obtain the equation of conservation of mixture momentum in the transverse direction by dotting the equation resulting from the addition of the two phasic equations with the unit vector $\hat{\jmath}$. We may further simplify the resulting equation by using the following argument. If we consider the partial transverse momentum equation given below, where we use the x direction as the direction of the axial flow, and the y direction to be the direction of the crossflow. We will also consider that, u, the axial velocity is of order 1 and, v, the transverse velocity to be of order δ by retaining terms of order 1 and δ only and discarding terms of order δ^2 the transverse momentum equation can be greatly simplified.

$$\frac{\partial \rho \overbrace{v}^{\delta}}{\partial t} + \frac{\partial \rho \overbrace{u \cdot v}^{1 \cdot \delta}}{\partial x} + \frac{\partial \rho \overbrace{v \cdot v}^{\delta \cdot \delta}}{\partial y} + \frac{\partial P}{\partial y} = \ldots \tag{3.169}$$

Doing this is not only useful as a means of simplifying the transverse momentum equation but is actually an essential part of the basic assumptions of the subchannel method. This is due to the fact that if a term involving $\frac{\partial}{\partial y}$ were to be retained in the transverse momentum equation it would be necesary to define a full transverse grid, instead of the simplified transverse momentum control volume that is currently used. Further it would be necessary to define the upwind and down wind directions for the discretization scheme, which is not possible as it is assumed that the crossflow looses its identity after it leaves the gap region.

Before actually developing the equation of conservation of transverse momentum we will examine the terms representing the rate of change of transverse momentum and the flux of the transverse momentum in more detail. The rate of

change of transverse momentum is given by:

$$\frac{\partial}{\partial t}\alpha_k \bar{s}\ell\Delta x\langle\rho_k\overline{v}_k\rangle \tag{3.170}$$

The term can be split into two parts, as follows:

$$\frac{\partial}{\partial t}\alpha_k \bar{s}\ell\Delta x\langle\rho_k\overline{v}_k\rangle = \frac{\partial}{\partial t}\alpha_k s\ell\Delta x\langle\rho_k\overline{v}_k\rangle + \overbrace{\frac{\partial}{\partial t}\alpha_k(\bar{s}-s)\ell\Delta x\langle\rho_k\overline{v}_k\rangle}^{0} \tag{3.171}$$

Given the rate of change of transverse momentum in a control volume $\bar{s}\ell\Delta x$ where $\bar{s}$ is the effective gap clearence as defined in equation 3.125, the first term on the right hand side of equation 3.171 represents the contribution to the rate of change term of the transverse momentum that passes through the actual gap spacing s. The second term on the right hand side of equation 3.171 is the contribution to the rate of change term of the transverse momentum due to the portion that passes through the ficticious part of the effective gap $\bar{s}$ which could be defined as $\bar{s}-s$. Since in reality this is solid no flow can pass through the section $\bar{s}-s$ and the rate of change of transverse momentum in the control volume $\bar{s}\ell\Delta x$ can be written as:

$$\frac{\partial}{\partial t}\alpha_k \bar{s}\ell\Delta x\langle\rho_k\overline{v}_k\rangle = \frac{\partial}{\partial t}\alpha_k s\ell\Delta x\langle\rho_k\overline{v}_k\rangle \tag{3.172}$$

A similar argument can be made for the momentum flux terms in the transverse momentum equation, thus:

$$\begin{aligned}\nabla\cdot\alpha_k\bar{s}\ell\Delta x\langle\rho_k\overline{v_k}\overline{u}_k\rangle &= \nabla\cdot\alpha_k s\ell\Delta x\langle\rho_k\overline{v}_k\overline{u}_k\rangle \\ &+ \overbrace{\nabla\cdot\alpha_k(\bar{s}-s)\ell\Delta x\langle\rho_k\overline{v}_k\overline{u}_k\rangle}^{0}\end{aligned} \tag{3.173}$$

Using the arguments presented above and equation 3.169 as a guide to which terms to keep and which to discard we can write the equation of conservation of transverse mixture momentum in a simplified form as:

$$\begin{aligned}\frac{\partial}{\partial t}s\ell\Delta x\langle\rho_m\overline{v}_m\rangle + \frac{\partial}{\partial x}s\ell\Delta x\langle\rho_m\overline{v}_m\overline{u}_m\rangle + \frac{\partial}{\partial x}s\ell\Delta x\langle\rho_m v'_m u'_m\rangle &= \\ -\frac{\partial}{\partial y}\bar{s}\ell\Delta x p_m + \frac{\partial}{\partial y}\bar{s}\ell\Delta x\overline{\overline{\tau}}_{myy} - \iint\limits_{\bar{s}\Delta x}\left(\hat{n}_{mw}\cdot p_{mw}\overline{\overline{I}}\right)\cdot\hat{j}dA &+ \\ \iint\limits_{\bar{s}\Delta x}(\hat{n}_{mw}\cdot\overline{\overline{\tau}}_{mw})\cdot\hat{j}dA - \bar{s}\ell\Delta x\rho_m g_y \quad . &\end{aligned} \tag{3.174}$$

Equation 3.174 is now one dimensional but it is not yet in the final form of the equation of conservation of transverse momentum as it is applied in ASSERT–4. In order to further simplify equation 3.174 we will now examine some of the terms individualy.

The first term we will look at is the turbulent component of the transverse momentum balance. Since ASSERT–4 does not treat the turbulent fluctuations in the velocity both v'_m and u'_m are not known, thus:

$$\frac{\partial}{\partial x}s\ell\Delta x\langle\rho_m v'_m u'_m\rangle = 0 \tag{3.175}$$

Next, we will look at the term representing the transverse gradient of the viscous stress tensor. It has been shown by Vernier and Delhaye [Vernier and Delhaye, 1968] that this term is negligeable, thus:

$$\frac{\partial}{\partial y}\bar{s}\ell\Delta x\overline{\overline{\tau}}_{myy} \approx 0 \quad . \tag{3.176}$$

The last term we will look at represents the pressure forces on the solid wall interface. Since $\hat{n}_{mw}$ and $\hat{j}$ are perpendicular to each other their dot product is zero. Thus:

$$-\iint_{s\Delta x}\left(\hat{n}_{mw}\cdot p_{mw}\overline{\overline{I}}\right)\cdot\hat{j}dA=0 \tag{3.177}$$

Applying the above simplifications to equation 3.174 and introducing donor assignment and subchannel average assignment of the appropriate quantities yields:

$$\begin{aligned}&\frac{\partial}{\partial t}s\ell\Delta x\langle\rho_m^*\overline{v}_m\rangle+\frac{\partial}{\partial x}s\ell\Delta x\langle(\rho_m\overline{u}_m)_{ave}\overline{v}_m\rangle=\\&-\frac{\partial}{\partial y}\bar{s}\ell\Delta x p_m+\iint_{\bar{s}\Delta x}(\hat{n}_{mw}\cdot\overline{\overline{\tau}}_{mw})\cdot\hat{j}dA-\bar{s}\ell\Delta x\rho_{m_{ave}}g_y\end{aligned}\quad . \tag{3.178}$$

We will now examine equation 3.178 term by term. The first term we will look at is the rate of change term given by:

$$\frac{\partial}{\partial t}s\ell\Delta x\langle\rho_m^*\overline{v}_m\rangle \quad . \tag{3.179}$$

It can be seen that the quantity $s\langle\rho_m^*\overline{v}_m\rangle$ in equation 3.179 is identical to the definition of the crossflow W_m as defined by equation 3.137. We may thus rewrite the rate of change term as:

$$\frac{\partial}{\partial t}s\ell\Delta x\langle\rho_m^*\overline{v}_m\rangle=\ell\Delta x\frac{\partial}{\partial t}W_m \quad . \tag{3.180}$$

The next term we will look at in the transverse momentum flux convected downstream by the axial flow. This term is represented by:

$$\frac{\partial}{\partial x}s\ell\Delta x\langle(\rho_m\overline{u}_m)_{ave}\overline{v}_m\rangle \tag{3.181}$$

Since the transverse momentum control volume straddles the two adjacent axial control volumes, as can be seen in figure 3.1, and since the axial velocities are only defined in the axial control volumes an appropriate method of defining the

axial velocity that is used to convect the transverse momentum downstream is required. Since the two adjacent subchannels connected by the transverse control volume in question "share" the "job" of providing this down stream velocity an appropriate method of defining the axial velocity of the transverse momentum convected downstream would be an area weighted average of the two subchannel velocities.

We look at the definitions of the average quantities over two subchannels which for the moment we will denote as subchannel i and subchannel j. The subchannel average mixture density is given by:

$$\rho_{m_{ave}} = \frac{\rho_{mi}A_i + \rho_{mj}A_j}{A_i + A_j} \tag{3.182}$$

The average phasic mass fluxes in the axial direction are given by:

$$(\alpha\rho\overline{u})_{2_{ave}} = \frac{\alpha_i\rho_{2i}\overline{u}_{2i}A_i + \alpha_j\rho_{2j}\overline{u}_{2j}A_j}{A_i + A_j} \tag{3.183}$$

for the vapour phase, and

$$((1-\alpha)\rho\overline{u})_{1_{ave}} = \frac{(1-\alpha_i)\rho_{1i}\overline{u}_{1i}A_i + (1-\alpha_j)\rho_{1j}\overline{u}_{1j}A_j}{A_i + A_j} \tag{3.184}$$

for the liquid phase.

The mass weighted form of the subchannel average axial mixture velocity is given by:

$$\overline{u}^m_{m_{ave}} = \frac{(\alpha\rho\overline{u})_{2_{ave}} + ((1-\alpha)\rho\overline{u})_{1_{ave}}}{\rho^*} \tag{3.185}$$

and mass weighted form of the subchannel average axial relative velocity is given by:

$$\overline{u}^m_{r_{ave}} = \frac{(\alpha\rho\overline{u})_{2_{ave}} - ((1-\alpha)\rho\overline{u})_{1_{ave}}}{\rho^*} \tag{3.186}$$

The transverse momentum flux can be defined as:

$$\langle W\overline{u}\rangle_{m_{ave}} = \left[(\alpha\rho\overline{u})_{2_{ave}}\,\overline{v}_2 + ((1-\alpha)\,\rho\overline{u})_{1_{ave}}\,\overline{v}_1\right] s \tag{3.187}$$

Using the fundamental identity 3.78 this can be written in terms of the mass weighted forms of the average axial mixture velocity $\overline{u}^m_{m_{ave}}$ which is given by equation 3.185, the average axial relative velocity $\overline{u}^m_{r_{ave}}$ which is given by equation 3.186 and the mass weighted transverse relative velocity $\overline{v}^m_r$ which will not be defined here as it is not calculated in terms of other variables calculated in ASSERT–4, but is supplied by a correlation using the drift flux model.

$$\langle W\overline{u}\rangle_{m_{ave}} = W_m\overline{u}^m_{m_{ave}} + s\left[\frac{\alpha^*(1-\alpha)^*\rho^*_1\rho^*_2}{\rho^*_m}\right]\overline{u}^m_{r_{ave}}\overline{v}^m_r \tag{3.188}$$

Using the above the term representing transverse momentum flux convected downstream by the axial flow could be rewritten as:

$$\begin{aligned}\frac{\partial}{\partial x}s\ell\Delta x\langle(\rho_m\overline{u}_m)_{ave}\overline{v}_m\rangle &= \ell\Delta x\frac{\partial}{\partial x}W_m\overline{u}^m_{m_{ave}} \\ &+ s\ell\Delta x\frac{\partial}{\partial x}\left[\frac{\alpha^*(1-\alpha)^*\rho^*_1\rho^*_2}{\rho^*_m}\right]\overline{u}^m_{r\ ave}\overline{v}^m_r\end{aligned} \tag{3.189}$$

The next term that we will examine is the one representing the frictional loss component of the momentum balance. Which is given by:

$$\iint_{\bar{s}\Delta x}(\hat{n}_{mw}\cdot\overline{\overline{\tau}}_{mw}\cdot\hat{j})\,dA \tag{3.190}$$

It can be expressed as being a function of the transverse mass flow rate (cross-flow) W, and a resistance coefficient C, which includes the two phase friction multiplier, $\phi^2_{\ell 0}$, we may rewrite 3.190 as

$$\iint_{\bar{s}\Delta x}(\hat{n}_{mw}\cdot\overline{\overline{\tau}}_{mw})\cdot\hat{j}dA = -\Delta x\bar{s}\mathcal{F}(C,|W|,W) \quad . \tag{3.191}$$

Using the results of the developments of equation3.180, equation 3.189 and equation 3.191 we may rewrite the equation of conservation of transverse momentum 3.178 as:

$$\ell\Delta x\frac{\partial}{\partial t}W_m + \ell\Delta x\frac{\partial}{\partial x}W_m\overline{u}^m_{mave} + \ell\Delta x\frac{\partial}{\partial x}s\left[\frac{\alpha^*(1-\alpha)^*\rho_1^*\rho_2^*}{\rho_m^*}\right]\overline{u}^m_{r\ ave}\overline{v}^m_r =$$
$$-\bar{s}\ell\Delta x\frac{\partial}{\partial y}p_m - \Delta x\bar{s}\mathcal{F}(C,|W|,W) - \bar{s}\ell\Delta x\rho_{m_{ave}}g_y \quad . \tag{3.192}$$

Since we want the final form of the equation of transverse momentum to be expressed in terms of the rate of change of momentum flux we will divide equation 3.192 by $\ell\Delta x$. This yields:

$$\frac{\partial}{\partial t}W_m + \frac{\partial}{\partial x}W_m\overline{u}^m_{mave} + \frac{\partial}{\partial x}s\left[\frac{\alpha^*(1-\alpha)^*\rho_1^*\rho_2^*}{\rho_m^*}\right]\overline{u}^m_{r\ ave}\overline{u}^m_r =$$
$$-\bar{s}\frac{\partial}{\partial y}p_m - \frac{\bar{s}}{\ell}\mathcal{F}(C,|W|,W) - \bar{s}\rho_{m_{ave}}g_y \quad . \tag{3.193}$$

Which is the final form of the equation of conservation of transverse momentum as applied in ASSERT-4.

where:

W_m	is the crossflow,	$[kg/ms]$
$\rho_{m_{ave}}$	is the average density of the mixture in the two adjacent subchannel under consideration,	$[kg/m^3]$
$*$	is used to denote donour assignment i.e. quantity is associated with the value of that quantity in the donour subchannel,	$[-]$
$\bar{s}$	is effective gap clearence,	$[m]$
s	is real gap clearence,	$[m]$
$\overline{u}_{m_{ave}}$	is the average axial velocity of the flow in the two adjacent subchannel under consideration.	$[m/s]$

3.13.3 Conservation of Energy

ASSERT–4 uses three equations of conservation of enthalpy, one for the mixture and one each for the vapour and liquid phases, thus making it possible to consider cases of thermal non–equilibrium. The first part of this derivation will be carried out with the general k^{th} phase conservation equation, afterwards specific attention will be given to the equations used in ASSERT–4.

The three dimensional form of the equation of conservation of phasic enthalpy is given by equation 3.123. To obtain the form of the thermal energy equations used in ASSERT–4 certain simplifying assumptions must be made. However, before simplifying equation 3.123 it is necessary to split the interface terms, A_i, into two parts one representing the interphase interface, A_{phase}, and another representing the intersubchannel interface, A_{kgap}. So as to obtain the additional terms used to account for the crossflow conribution to the overall energy balance. In doing so we will use the same assumption as in the case of the equation of conservation of mass namely that:

- The intersubchannel interface in stationary, thus: $\overline{v_i}|_{kgap} = 0$.
- as well as: $v'_i|_{kgap} = 0$

Since the the derivation of the averaged conservation equations presented in the previous section was done for a completely arbitrary control volume they can be considered to apply to any geometry. We will thus apply the equation of conservation of enthalpy to the subchannel geometry shown in figure 3.1, where the volume V is equal to the flow area A times the lenght Δx. Introducing donor assignment of appropriate quantities and the above assumptions equation 3.123 can be rewritten as:

$$\frac{\partial}{\partial t}\alpha_k A\Delta x\langle\rho_k\overline{h}_k\rangle + \nabla\cdot\alpha_k A\Delta x\langle\rho_k\overline{\vec{v}}_k\overline{h}_k\rangle - \frac{\partial}{\partial t}\alpha_k A\Delta x p_k + \nabla\cdot\alpha_k A\Delta x\langle\rho_k\vec{v}'_k h'_k\rangle$$

$$= -\nabla \cdot \alpha_k A \Delta x \vec{q}_k - \iint_{A_{phase}} \rho_k \bar{h}_k (\bar{\vec{v}}_k - \bar{\vec{v}}_i) \cdot \hat{n}_k dA - \iint_{A_{phase}} \rho_k h'_k (\vec{v}'_k - \vec{v}'_i) \cdot \hat{n}_k dA$$
$$- \sum_K \iint_{A_{kgap}} \langle \rho^*_k \overline{h^*_k} \bar{\vec{v}}_k \rangle \cdot \hat{n}_{kgap} dA - \iint_{A_{kgap}} \langle \rho^*_k h'^*_k \vec{v}'_k \rangle \cdot \hat{n}_{kgap} dA - \iint_{A_{kw}} \hat{n}_{kw} \cdot \vec{q}_k dA$$
$$- \iint_{A_{phase}} \hat{n}_k \cdot \vec{q}_k dA - \sum_K \iint_{A_{kgap}} \hat{n}_{kgap} \cdot \vec{q}_k dA \quad . \tag{3.194}$$

Since ASSERT-4 treats only one dimensional flow at the level of the individual subchannels we will assume that both the y and z components of the divergence term in the equation of conservation of enthalpy are zero, ie.:

$$\frac{\partial}{\partial y} \alpha_k A \Delta x \langle \rho_k \bar{v}_k \bar{h}_k \rangle = 0 \quad . \tag{3.195}$$

$$\frac{\partial}{\partial z} \alpha_k A \Delta x \langle \rho_k \bar{w}_k \bar{h}_k \rangle = 0 \quad . \tag{3.196}$$

$$\frac{\partial}{\partial y} \alpha_k A \Delta x \langle \rho_k v'_k h'_k \rangle = 0 \quad . \tag{3.197}$$

$$\frac{\partial}{\partial z} \alpha_k A \Delta x \langle \rho_k w'_k h'_k \rangle = 0 \quad . \tag{3.198}$$

$$\frac{\partial}{\partial y} \alpha_k A \Delta x q_{ky} = 0 \quad . \tag{3.199}$$

$$\frac{\partial}{\partial z} \alpha_k A \Delta x q_{kz} = 0 \quad . \tag{3.200}$$

Applying the above to equation 3.194 yields.

$$\frac{\partial}{\partial t} \alpha_k A \Delta x \langle \rho_k \bar{h}_k \rangle - \frac{\partial}{\partial t} \alpha_k A \Delta x p_k + \frac{\partial}{\partial x} \alpha_k A \Delta x \langle \rho_k \bar{u}_k \bar{h}_k \rangle + \frac{\partial}{\partial x} \alpha_k A \Delta x \langle \rho_k u'_k h'_k \rangle$$
$$= -\frac{\partial}{\partial x} \alpha_k A \Delta x q_{kx} - \iint_{A_{phase}} \langle \rho_k \bar{h}_k (\bar{\vec{v}}_k - \bar{\vec{v}}_i) \rangle \cdot \hat{n}_k dA - \iint_{A_{phase}} \langle \rho_k h'_k (\vec{v}'_k - \vec{v}'_i) \rangle \cdot \hat{n}_k dA$$

$$-\sum_K \iint_{s\Delta x} \langle \rho_k^* \overline{h}_k^* \overline{u}_k \rangle dA - \sum_K \iint_{s\Delta x} \langle \rho_k^* h'^*_k v'_k \rangle dA - \iint_{A_{kw}} \hat{n}_{kw} \cdot \vec{q}_k dA$$
$$- \iint_{A_{phase}} \hat{n}_k \cdot \vec{q}_k dA - \sum_K \iint_{s\Delta x} \hat{n}_{kgap} \cdot \vec{q}_k dA \quad , \tag{3.201}$$

where the intersubchannel flow area A_{kgap} is defined as the gap width s times the axial node lenght Δx.

Before developing the individual phasic and mixture conservation equations we will look at some of the terms in equation 3.201 in more detail. The first term that we will look at is the turbulent component of the energy transport in the x–direction. Since ASSERT–4 does not calculate the turbulent fluctuations in velocity, u'_k, or the turbulent fluctuations in the enthalpy, h'_k, these terms are not known. Thus:

$$\frac{\partial}{\partial x} \alpha_k A \Delta x \langle \rho_k u'_k h'_k \rangle = 0 \quad . \tag{3.202}$$

This is also true of the turbulent component of the interfacial heat transfer.

$$- \iint_{A_{phase}} \langle \rho_k h'_k \left(\vec{v}'_k - \vec{v}'_i \right) \rangle \cdot \hat{n}_k dA = 0 \tag{3.203}$$

The last term that contains turbulent quantities is the turbulent crossflow contribution to the energy balance. The turbulent crossflow is not calculated using the momentum equation as ASSERT–4 does not treat the turbulent fluctuations in the velocity. However the turbulent crossflow is supplied by means of a correlation between the Reynold's number and the inverse turbulent Peclet number, $\frac{\epsilon}{uD}$. This correlation will be examined in more detail in chapter 4. For the time being we will simply represent the turbulent energy interchange between two subchannels i and j as:

$$-\sum_K \iint_{s\Delta x} \langle \rho_k^* h'^*_k v'_k \rangle dA = -\sum_K \Delta x W'_k \left[\bar{h}_k(j) - \bar{h}_k(i) \right] \tag{3.204}$$

where:

W'_k	is the turbulent crossflow between subchannels i and j,	$[kg/ms]$
$\bar{h}_k(i)$	is the k^{th} phase enthalpy in subchannel i,	$[kJ/kg]$
$\bar{h}_k(j)$	is the k^{th} phase enthalpy in subchannel j,	$[kJ/kg]$
$\sum_K$	represents a summation over all the K gaps communicating with the subchannel under study.	$[-]$

The term which represents the crossflow contribution to the energy balance is given by:

$$-\sum_K \iint_{s\Delta x} \langle \rho_k^* \bar{h}_k^* \bar{v}_k \rangle dA \tag{3.205}$$

Using the definition of the crossflows W_k given by equations 3.138 for the liquid phase and 3.139 for the vapour phase. Equation 3.205 can be rewritten as:

$$-\sum_K \iint_{s\Delta x} \langle \rho_k^* \overline{h}_k^* \overline{v}_k \rangle dA = -\sum_K \Delta x \langle W_k \overline{h}_k^* \rangle \quad . \tag{3.206}$$

The next term we will look at is the axial gradient of the k^{th} phase heat flux. This term represents axial heat conduction in the k^{th} phase. This term is only significant in cases where the working fluid has a very high conductivity such as in the case of a liquid metals. In our case we will consider this term to be zero. Thus:

$$-A\Delta x \frac{\partial}{\partial x} \alpha_k q_{kx} = 0 \quad . \tag{3.207}$$

The next term we will examine is the heat flux in the transverse direction. Like the case of the axial gradient of the k^{th} phase heat flux, this term is normaly only important for liquids with a very high conductivity such as liquid metals. Thus:

$$-\iint_{s\Delta x} \hat{n}_{kgap} \cdot \vec{q}_k dA = 0 \quad . \tag{3.208}$$

Applying all of the above to equation 3.201 yields:

$$\begin{aligned}\frac{\partial}{\partial t}\alpha_k A\Delta x\langle\rho_k\overline{h}_k\rangle - \frac{\partial}{\partial t}\alpha_k A\Delta x p_k + \frac{\partial}{\partial x}\alpha_k A\Delta x\langle\rho_k\overline{u}_k\overline{h}_k\rangle &= \\ -\iint_{A_{phase}}\langle\rho_k\overline{h}_k(\overline{\vec{v}}_k-\overline{\vec{v}}_i)\rangle\cdot\hat{n}_k dA - \sum_K \Delta x\langle W_k\overline{h}_k^*\rangle &- \\ \sum_K \Delta x W_k'\left[\overline{h}_k(j)-\overline{h}_k(i)\right] - \iint_{A_{kw}}\hat{n}_{kw}\cdot\vec{q}_k dA - \iint_{A_{phase}}\hat{n}_k\cdot\vec{q}_k dA &\quad , \qquad (3.209)\end{aligned}$$

We will now develop the specific forms of the phasic and mixture equations.

3.13.3.1 Conservation of Energy: Liquid Phase

The equation of conservation of enthalpy for the liquid phase is given by:

$$\begin{aligned}\frac{\partial}{\partial t}(1-\alpha)A\Delta x\langle\rho_1\overline{h}_1\rangle - \frac{\partial}{\partial t}(1-\alpha)A\Delta x p_1 + \frac{\partial}{\partial x}(1-\alpha)A\Delta x\langle\rho_1\overline{u}_1\overline{h}_1\rangle &= \\ -\iint_{A_{phase}}\langle\rho_1\overline{h}_1(\overline{\vec{v}}_1-\overline{\vec{v}}_i)\rangle\cdot\hat{n}_1 dA - \sum_K \Delta x\langle W_1\overline{h}_1^*\rangle &- \\ \sum_K \Delta x W_1'\left[\overline{h}_1(j)-\overline{h}_1(i)\right] - \iint_{A_{1w}}\hat{n}_{1w}\cdot\vec{q}_1 dA - \iint_{A_{phase}}\hat{n}_1\cdot\vec{q}_1 dA &\quad . \qquad (3.210)\end{aligned}$$

Using the definition of the axial mass flow rate of the liquid phase as given by equation 3.132 we can rewrite equation 3.210 as:

$$\begin{aligned}\frac{\partial}{\partial t}(1-\alpha)A\Delta x\langle\rho_1\overline{h}_1\rangle - \frac{\partial}{\partial t}(1-\alpha)A\Delta x p_1 + \frac{\partial}{\partial x}\Delta x\langle F_1\overline{h}_1\rangle &= \\ -\iint_{A_{phase}}\langle\rho_1\overline{h}_1(\overline{\vec{v}}_1-\overline{\vec{v}}_i)\rangle\cdot\hat{n}_1 dA - \sum_K \Delta x\langle W_1\overline{h}_1^*\rangle &- \\ \sum_K \Delta x W_1'\left[\overline{h}_1(j)-\overline{h}_1(i)\right] - \iint_{A_{1w}}\hat{n}_{1w}\cdot\vec{q}_1 dA - \iint_{A_{phase}}\hat{n}_1\cdot\vec{q}_1 dA &\quad . \qquad (3.211)\end{aligned}$$

Equation 3.211 is the conservative form of the equation of conservation of enthalpy for the liquid phase. By factoring the first two terms of equation 3.211 we obtain the following:

$$(1-\alpha)A\Delta x\rho_1\frac{\partial\overline{h}_1^m}{\partial t}+\overbrace{(1-\alpha)A\Delta x\overline{h}_1^m\frac{\partial\rho_1}{\partial t}}^{A}-\frac{\partial}{\partial t}(1-\alpha)A\Delta xp_1 \quad +$$

$$\Delta xF_1\frac{\partial\overline{h}_1^m}{\partial x}+\overbrace{\Delta x\overline{h}_1^m\frac{\partial F_1}{\partial x}}^{B} \quad =$$

$$-\iint_{A_{phase}}\langle\rho_1\overline{h}_1^m(\overline{\vec{v}}_1-\overline{\vec{v}}_i)\rangle\cdot\hat{n}_1dA-\sum_K\Delta x\langle W_1\overline{h}_1^*\rangle \quad -$$

$$\sum_K\Delta xW_1'\left[\overline{h}_1^m(j)-\overline{h}_1^m(i)\right]-\iint_{A_{1w}}\hat{n}_{1w}\cdot\vec{q}_1dA-\iint_{A_{phase}}\hat{n}_1\cdot\vec{q}_1dA \quad . \qquad (3.212)$$

Using the equation of conservation of mass for the liquid phase which is given by:

$$(1-\alpha)A\Delta x\frac{\partial\rho_1}{\partial t}+\Delta x\frac{\partial F_1}{\partial x}=-\iint_{A_{phase}}\langle\rho_1(\overline{\vec{v}}_1-\overline{\vec{v}}_i)\rangle\cdot\hat{n}_1dA-\sum_K\Delta xW_1 \quad , \quad (3.213)$$

and multiplying both sides of equation 3.213 by the mass weighted form of the enthalpy of the liquid phase h_1^m we can replace the terms A and B in equation 3.212 by the right hand side of equation 3.213. Equation 3.212 can then be written in transportive form. This results in:

$$(1-\alpha)A\Delta x\rho_1\frac{\partial}{\partial t}\overline{h}_1^m-(1-\alpha)A\Delta x\frac{\partial}{\partial t}p_1+F_1\Delta x\frac{\partial}{\partial x}\overline{h}_1^m-\sum_K\overline{h}_1^m\Delta xW_1 \quad +$$

$$\sum_K\Delta x\langle W_1\overline{h}_1^{*m}\rangle=-\sum_K\Delta xW_1'\left[\overline{h}_1^m(j)-\overline{h}_1^m(i)\right]-\iint_{A_{1w}}\hat{n}_{1w}\cdot\vec{q}_1dA \quad -$$

$$\iint_{A_{phase}}\hat{n}_1\cdot\vec{q}_1dA \quad . \quad (3.214)$$

Equation 3.214 is known as the transportive form of the equation of conservation of enthalpy for the liquid phase due to the fact that it discribes the transport of enthalpy along a streamline. The advantage of the transportive form of the equation

of conservation of enthalpy over the conservative form is that it is more tolerant of mass imbalances at early stages of the iterative solution [Webb and Rowe, 1986]. This is the form of the equation of conservation of liquid enthalpy that is used for computation in ASSERT-4. The last two terms on the right hand side of equation 3.214 discribe the heat transfer from the wall to the liquid and from the interface to the liquid respectively.

3.13.3.2 Conservation of Energy: Vapour Phase

The equation of conservation of enthalpy for the vapour phase is given by:

$$\begin{aligned}\frac{\partial}{\partial t}\alpha A\Delta x\langle\rho_2\overline{h}_2\rangle - \frac{\partial}{\partial t}\alpha A\Delta x p_2 + \frac{\partial}{\partial x}\alpha A\Delta x\langle\rho_2\overline{u}_2\overline{h}_2\rangle &= \\ -\iint_{A_{phase}}\langle\rho_2\overline{h}_2(\overline{\vec{v}}_2-\overline{\vec{v}}_i)\rangle\cdot\hat{n}_2 dA - \sum_K \Delta x\langle W_2\overline{h}_2^*\rangle &- \\ \sum_K \Delta x W_2'\left[\overline{h}_2(j)-\overline{h}_2(i)\right] - \iint_{A_{1w}}\hat{n}_{1w}\cdot\vec{q}_2 dA - \iint_{A_{phase}}\hat{n}_2\cdot\vec{q}_2 dA \quad . \qquad (3.215)\end{aligned}$$

Following the same procedure as was used for the equation of conservation of enthalpy for the liquid phase equation 3.215 can be rewritten in transportive form as:

$$\begin{aligned}\alpha A\Delta x\rho_2\frac{\partial}{\partial t}\overline{h}_2^m - \alpha A\Delta x\frac{\partial}{\partial t}p_2 + F_2\Delta x\frac{\partial}{\partial x}\overline{h}_2^m - \sum_K \overline{h}_2^m\Delta x W_2 + \sum_K \Delta x\langle W_2\overline{h}_2^{*m}\rangle = \\ -\sum_K \Delta x W_2'\left[\overline{h}_2^m(j)-\overline{h}_2^m(i)\right] - \iint_{A_{2w}}\hat{n}_{2w}\cdot\vec{q}_2 dA - \iint_{A_{phase}}\hat{n}_2\cdot\vec{q}_2 dA \quad . \qquad (3.216)\end{aligned}$$

Equation 3.216 is the transportive form of the equation of conservation of enthalpy for the vapour phase that is used for computation in ASSERT-4.

3.13.3.3 Conservation of Energy: Mixture

The equation of conservation of enthalpy for the liquid and vapour phases can be added giving:

$$\frac{\partial}{\partial t}A\Delta x\langle\rho_m\overline{h}_m\rangle - \frac{\partial}{\partial t}A\Delta x p_m + \frac{\partial}{\partial x}A\Delta x\langle\rho_m\overline{u}_m\overline{h}_m\rangle + \sum_K \Delta x\langle W_m\overline{h}^*_m\rangle =$$
$$-\sum_K \Delta x W_1'\left[\overline{h}_1(j) - \overline{h}_1(i)\right] - \sum_K \Delta x W_2'\left[\overline{h}_2(j) - \overline{h}_2(i)\right]$$
$$-\iint_{A_{mw}} \hat{n}_{mw}\cdot\vec{q}_m dA \quad . \tag{3.217}$$

Where the interfacial energy transfer terms for the liquid and vapour phases have cancelled each other out. The reason that there are two terms for the phasic turbulent crossflow contributions to the mixture energy balance is that the correlations that supply the terms W_1' and W_2' are not defined for the mixture, therefore the two individual phasic contributions are used.

Using the fundamental identity 3.78 with the conserved quantities, Ψ_1^m and Ψ_2^m being , $\overline{h}_1^m$ and $\overline{h}_2^m$ respectively, and the definition of the mass weighted form of the mixture enthaply given by:

$$\overline{h}_m^m = \frac{\langle\rho_m\overline{h}_m\rangle}{\rho_m} \quad . \tag{3.218}$$

the mixture axial enthalpy flux term can be rewritten as:

$$A\langle\rho_m\overline{u}_m\overline{h}_m\rangle = F_m\overline{h}_m^m + \frac{(1-\alpha)\rho_1\alpha\rho_2}{\rho_m}(\overline{h}_2^m - \overline{h}_1^m)A\overline{u}_r^m \quad , \tag{3.219}$$

where equation 3.219 is only defined for the axial relative velocity.

As was done for the phasic conservation equations, the equation of conservation of enthalpy for the mixture may be written in transportive form. Taking into account the results of equation 3.219 we may write the transportive form of the equation of mixture enthalpy 3.217 as:

$$A\Delta x\rho_m\frac{\partial}{\partial t}\overline{h}_m^m - A\Delta x\frac{\partial}{\partial t}p_m + F_m\Delta x\frac{\partial}{\partial x}\overline{h}_m^m +$$
$$\Delta x\frac{\partial}{\partial x}\frac{\alpha(1-\alpha)\rho_1\rho_2}{\rho_m}(\overline{h}_2^m - \overline{h}_1^m)A\overline{u}_r^m - \sum_K \overline{h}_m^m\Delta x W_m + \sum_K \Delta x(W_m\overline{h}_m^{*m}) =$$
$$-\sum_K \Delta x W_1'\left[\overline{h}_1^m(j) - \overline{h}_1^m(i)\right] - \sum_K \Delta x W_2'\left[\overline{h}_2^m(j) - \overline{h}_2^m(i)\right]$$
$$-\iint_{A_{mw}} \hat{n}_{mw}\cdot\vec{q}_m dA \qquad (3.220)$$

Equation 3.220 is the final form of the equation of conservation of mixture enthalpy used in ASSERT–4.

The set of equations given by equation 3.144 for the conservation of mass, equation 3.168 for the conservation of axial momentum, equation 3.193 for the conservation of transverse momentum, equation 3.214 for the conservation of enthalpy for the liquid phase, equation 3.216 for the conservation of enthalpy for the vapour phase, and equation 3.220 for the conservation of mixture enthalpy are the equations used for computation in the ASSERT–4 subchannel code.

CHAPTER 4

DISCRETIZED EQUATIONS AND SOLUTION SCHEME

The ASSERT–4 subchannel code Tahir and Carver [1984a], Judd et al. [1984] has been developed to model single– and two–phase flows through vertical and horizontal rod bundles; the latter being the type seen in CANDU fuel channels. ASSERT–4 uses a 5 equation advanced drift flux model to account for the effect of thermal non–equilibrium as well as unequal phasic velocities. The relative velocity model has been used to account not only for the different velocities between the phases in the axial direction but also to model some of the transverse transport phenomena which are important in subchannel flows. These being: gravity driven phase separation which is unique to the horizontal geometry of a CANDU fuel channel, turbulent void diffusion, and void drift.

4.1 Conservation Equations

Using the equations developed in section 3.12, which are the differential forms of the equations used for computation in ASSERT–4, we will develop the discretized forms of these equations.

ASSERT–4 uses a fully implicit first order finite difference solution. The advantage of a fully implicit discretization is that it can greatly reduce or eliminate time step restrictions that exist in explicit methods [Webb and Rowe, 1986]. The disadvantage of a fully implicit scheme is that all the variables must be solved for simultaneously. For arbitrary flow directions this can result in a solution that becomes too complex for practical application [Webb and Rowe, 1986]. If however

the flows are limited to one direction, the solution is sufficiently simplified that fully implicit solution schemes become practical.

This argument gives us the first restricition that we will place on the numerical solution used in ASSERT-4: *The axial flow in ASSERT-4 is restricted to the positive direction only.*

The spatial discretization scheme used in ASSERT-4 is known as a first order, upwind donor finite difference scheme. A first order finite difference scheme has, by definition, a truncation error of order Δx. The upwind difference method however produces results superior to many higher order schemes. This is due to the fact that the upwind donor assignment inherently reflects the physics of the flow. It is, however, of prime importance for the succesfull application of this method that correct upwind differencing be used at all times. This implies that the logic for determining the upwind side in a given flow be included in the computer code, or that the flow be restricted to one direction, as is the case for the axial flow in ASSERT-4.

The discretization process involves replacing the differential operators in a given equation by their finite difference analogs. The upwind form of the finite difference analog of $\frac{\partial}{\partial x}$ for an arbitrary function, f, that is known at a given point i, can be obtained by a backward Taylor series expansion about f_i. This leads to:

$$f_{i-1} = f_i - \left.\frac{\partial f}{\partial x}\right|_i \Delta x + \tfrac{1}{2} \left.\frac{\partial^2 f}{\partial x^2}\right|_i \Delta x^2 - \ldots \quad . \tag{4.1}$$

Solving for $\frac{\partial f}{\partial x}$ gives:

$$\frac{\partial f}{\partial x} = \frac{f_i - f_{i-1}}{\Delta x} + \tfrac{1}{2} \left.\frac{\partial^2 f}{\partial x^2}\right|_i \Delta x - \ldots \quad . \tag{4.2}$$

Discarding terms of order Δx and higher leaves:

$$\frac{\partial f}{\partial x} = \frac{f_i - f_{i-1}}{\Delta x} + O(\Delta x) \quad , \tag{4.3}$$

where $O(\Delta x)$ means plus terms of order Δx. The finite difference analog to $\frac{\partial f}{\partial x}$ given by equation 4.3 is the finite difference form of the spatial discretization used in ASSERT–4.

Similarly a finite difference analog to the rate of change given by, $\frac{\partial f}{\partial t}$, can be developed. It can be written as:

$$\frac{\partial f}{\partial t} = \frac{f - f^n}{\Delta t} + O(\Delta t) \quad . \tag{4.4}$$

Where the superscipt n is used to denote values at the previous time, i.e. time t, while variables without the superscript refer to the present time, i.e. time $t + \Delta t$.

4.1.1 Mixture Mass Conservation

In the previous chapter we developed the differential equation describing the conservation of mass as it is applied in ASSERT–4 which is given by equation 3.144.

$$A\Delta x \frac{\partial}{\partial t}\rho_m + \Delta x \frac{\partial}{\partial x} F_m + \sum_K \Delta x W_m = 0 \quad , \tag{4.5}$$

where:

ρ_m	density of the mixture,	$[kg/m^3]$
F_m	is the axial mass flow rate of the mixture,	$[kg/s]$
W_m	is the mixture crossflow,	$[kg/ms]$
$\sum_K$	represents a summation over all the K gaps communicating with the subchannel under consideration.	$[-]$

To pass from the differential form of the equation of conservation of mass 4.5 to the discretized form of the equation used by ASSERT–4, it will be necessary to introduce some of the simplifications used in ASSERT–4 to treat the crossflow. If we look at the crossflow term of equation 4.5 which is given by:

$$+\sum_{K}\Delta x W_m \quad , \tag{4.6}$$

we can see that equation 4.6 is simply a source term to the overall mass balance. As it is written in equation 4.5 nothing is said about the direction of the crossflow. In the discretized mass balance equation this directional information is required. In discretized form this information is supplied by what is known as the transverse matrix operator. This matrix operator has the effect of performing a differencing operation between two adjacent subchannels.

For example, given two subchannels i and j having pressures, p_i and p_j respectively, which communicate through a given gap, k, the intersubchannel pressure difference can be expressed using the transverse matrix operator as:

$$p_i - p_j = -D_{ki} p_i \quad . \tag{4.7}$$

The transpose of the transverse matrix operator $D_{ki}^T = D_{ik}$ performs an operation that is equivalent to a dimensionless divergence in the transverse direction [Judd et al., 1984], where the sign of D_{ki} accounts for flow into or out of the control volume. Thus we may use the transpose of the transverse matrix operator to supply the directional information to the crossflow term of equation 4.5. This could be expressed as:

$$+\sum_{K}\Delta x W_m \equiv +\sum_{K}\Delta x D_{ik} W_m \quad . \tag{4.8}$$

Using equation 4.3 to finite difference the spatial terms and 4.4 to finite difference the rate of change terms in equation 4.5, and using the results of equation 4.8 to supply the directional information in the transverse direction. We may write the finite difference form of the equation of conservation of mass as:

$$A_{i,j}\Delta x_j \frac{\rho_{mi,j} - \rho^n_{mi,j}}{\Delta t} + \Delta x_j \frac{F_{mi,j} - F_{mi,j-1}}{\Delta x_j} + \sum_K \Delta x_j D_{ik} W_{mk,j} = 0 \quad , \qquad (4.9)$$

It should be noted that while the Δx_j is required so that the proper quantity is conserved it is not necessary for the solution of the mass balance at any but the final step. Thus the equation for conservation of mass as it is actually solved is:

$$A_{i,j} \frac{\rho_{mi,j} - \rho^n_{mi,j}}{\Delta t} + \frac{F_{mi,j} - F_{mi,j-1}}{\Delta x_j} + \sum_K D_{ik} W_{mk,j} = 0 \quad , \qquad (4.10)$$

where:

Δt	is the time step,	$[s]$
Δx_j	is the axial step size,	$[m]$
$A_{i,j}$	is the area of subchannel i at axial position j,	$[m^2]$
$\rho_{mi,j}$	is the mixture density in subchannel i at axial position j,	$[kg/m^3]$
^{n}	superscript n is used to denote the previous time step values,	$[-]$
$F_{mi,j}$	is the axial flow in subchannel i at axial position j,	$[kg/s]$
$W_{mk,j}$	is the crossflow through gap k at axial position j,	$[kg/ms]$
D_{ik}	is transverse matrix operator which takes care of donor assignment and indicates a differencing of the quantity upon which it operates between the two subchannels under consideration.	$[-]$

4.1.2 Mixture Momentum Conservation

Starting from the differential forms of the equations of conservation of axial momentum, given by equation 3.168, and of conservation of transverse momentum, given by equation 3.193, we will develop the discretized forms of these equation as they are applied in ASSERT-4.

4.1.2.1 Mixture Momentum Conservation: Axial Direction

Using equation 3.159 to combine the second and third terms of equation 3.168 and equation 3.166 to combine the fourth and fifth terms on the right hand side of equation 3.168, the differential form of the equation of conservation of axial momentum can be rewritten as:

$$\Delta x \frac{\partial}{\partial t} F_m + \Delta x \frac{\partial}{\partial x} \langle F_m \bar{u}_m \rangle + \sum_K \Delta x \langle W_m \bar{u}_m^* \rangle = -A \Delta x \frac{\partial}{\partial x} p_m - \mathcal{F}(A, K, |F|, F) - A \Delta x \rho_m g_x \quad . \tag{4.11}$$

where:

$\bar{u}_m$	is the axial velocity of the mixture,	$[m/s]$
$*$	is used to denote donour assignment ie. quantity is associated with the value of that quantity in the donour subchannel,	$[-]$
ρ_m	is the mixture density,	$[kg.m^3]$
F_m	is the axial flow,	$[kg/s]$
W_m	is the crossflow.	$[kg/ms]$

We will now proceed term by term to develop the finite difference analogs to the terms of equation 4.11. The first term we will look at represents the rate of change of axial momentum. We will finite difference this term using equation and 4.4. This results in:

$$\Delta x \frac{\partial}{\partial t} F_m = \Delta x \frac{F_{m\,i,j} - F^n_{m\,i,j}}{\Delta t} \quad , \tag{4.12}$$

We will next use the results of equation 4.3 to discretize the axial momentum flux and pressure drop terms of equation 4.11. This results in:

$$\Delta x \frac{\partial}{\partial x} \langle F_m \bar{u}_m \rangle = \Delta x_j \frac{\langle F_m \bar{u}_m \rangle_{i,j} - \langle F_m \bar{u}_m \rangle_{i,j-1}}{\Delta x} \quad , \tag{4.13}$$

for the axial momentum flux term, and

$$-A\Delta x\frac{\partial}{\partial x}p_m = -\bar{A}_{i,j}\Delta x_j\frac{p_{mi,j} - p_{mi,j-1}}{\Delta x_j} \quad , \tag{4.14}$$

for the term representing the axial pressure gradient.

The next term we will look at represents the crossflow contribution to the axial momentum balance. This term will be represented in discretized form by the use of the transpose of transverse matrix operator, D_{ik}, as given in equation 4.8. This results in:

$$\sum_K \Delta x\langle W_m\bar{u}^*_m\rangle = \sum_K \Delta x_j D_{ik}\langle W_m\bar{u}^*_m\rangle_k \tag{4.15}$$

where the subcsript $_k$ is used to refer to the crossflow through the gap k.

The term representing the gravitational effects will simply be multiplied by a term representing the channel orientation, where θ is defined as being zero vertically upwards.

$$-A\Delta x\rho_m g_x = -\bar{A}_{i,j}\Delta x_j\rho_m g\cos\theta \quad . \tag{4.16}$$

The term representing the frictional component of the axial momentum balance, $-\mathcal{F}(\bar{A}_{i,j}, K, |F|, F)$, is supplied by a correlation which is dependent on the flow, the void fraction and the flow area. It will be left in its current form in the discretized equation.

The term $\bar{A}_{i,j}$ represents the average area of the two axial nodes used in the spatial discretization. It is given by:

$$\bar{A}_{i,j} = \frac{1}{\frac{1}{2}\left[\frac{1}{A_{i,j}} + \frac{1}{A_{i,j-1}}\right]} \quad , \tag{4.17}$$

This definition of the average area of the two subchannels is required to ensure the proper pressure drop through area changes [Judd et al., 1984].

Grouping together the right hand sides of equations 4.12 to 4.16, we may write the finite difference form of the equation of conservation of axial momentum as:

$$\begin{aligned}\Delta x_j \frac{F_{mi,j} - F^n_{mi,j}}{\Delta t} + \Delta x_j \frac{\langle F_m \bar{u}_m \rangle_{i,j} - \langle F_m \bar{u}_m \rangle_{i,j-1}}{\Delta x} \quad + \\ \sum_K \Delta x_j D_{ik} \langle W_m \bar{u}^*_m \rangle_k - \bar{A}_{i,j} \Delta x_j \frac{p_{mi,j} - p_{mi,j-1}}{\Delta x_j} \quad = \\ -\Delta x_j \mathcal{F}(\bar{A}_{i,j}, K, |F|, F)_{i,j} - \bar{A}_{i,j} \Delta x_j \rho_m g \cos\theta \end{aligned} \tag{4.18}$$

As in the case of the mass balance equation 4.10 the Δx_j is only required so that the correct quantity is conserved, the equation of conservation of axial momentum as it is actually solved is:

$$\begin{aligned}\frac{F_{mi,j} - F^n_{mi,j}}{\Delta t} + \frac{\langle F_m \bar{u}_m \rangle_{i,j} - \langle F_m \bar{u}_m \rangle_{i,j-1}}{\Delta x} \quad + \\ \sum_K D_{ik} \langle W_m \bar{u}^*_m \rangle_k - \bar{A}_{i,j} \frac{p_{mi,j} - p_{mi,j-1}}{\Delta x_j} \quad = \\ -\mathcal{F}(\bar{A}_{i,j}, K, |F|, F)_{i,j} - \bar{A}_{i,j} \rho_m g \cos\theta \end{aligned} \tag{4.19}$$

where:

$\bar{u}_m^m$	is the axial velocity of the mixture,	$[m/s]$
$*$	is used to denote donour assignment ie. quantity is associated with the value of that quantity in the donour subchannel,	$[-]$
$\rho_{mi,j}$	is the mixture density in subchannel i at axial position j,	$[kg/m^3]$
^{n}	is used to denote the previous time step values,	$[-]$
$F_{mi,j}$	is the axial flow in subchannel i at axial position j,	$[kg/s]$
$W_{mk,j}$	is the crossflow through gap k at axial position j,	$[kg/ms]$
$p_{mi,j}$	is the pressure in subchannel i at axial position j,	$[kg/ms^2]$
K	is the axial pressure loss coefficient,	$[-]$
g	is the acceleration due to gravity.	$[m/s^2]$

4.1.2.2 Mixture Momentum Conservation: Transverse Direction

Using equation 3.188 to combine the second and third terms of equation 3.193, the differential form of the transverse momentum equation can be written as:

$$\frac{\partial}{\partial t}W_m + \frac{\partial}{\partial x}\langle W\bar{u}\rangle_{m_{ave}} = -\bar{s}\frac{\partial}{\partial y}p_m - \frac{\bar{s}}{\ell}\mathcal{F}(C,|W|,W) - \bar{s}\rho_{m_{ave}}g_y \quad . \qquad (4.20)$$

where:

W_m	is the crossflow,	$[kg/ms]$
$\rho_{m_{ave}}$	is the average density of the mixture in the two adjacent subchannel under consideration,	$[kg/m^3]$
$*$	is used to denote donour assignment i.e. quantity is associated with the value of that quantity in the donour subchannel,	$[-]$
$\bar{s}$	is the effective gap clearence,	$[m]$
s	is the real gap clearence,	$[m]$
$\bar{u}_{m_{ave}}$	is the average axial velocity of the flow in the two adjacent subchannel under consideration.	$[m/s]$

We will now proceed term by term to develop the finite difference analogs to the terms of equation 4.20. The first term we will look at represents the rate of change of transverse momentum. We will finite difference this term using equation 4.4. This results in:

$$\frac{\partial}{\partial t}W_m = \frac{W_{mk,j} - W^n_{mk,j}}{\Delta t} \quad . \tag{4.21}$$

We will now use equation 4.3 to discretize the term representing the component of the transverse momentum flux convected downstream by the axial flow. The result of this discretization is:

$$\frac{\partial}{\partial x}\langle W\bar{u}\rangle_{m_{ave}} = \frac{\langle W\bar{u}\rangle_{m_{ave}k,j} - \langle W\bar{u}\rangle_{m_{ave}k,j-1}}{\Delta x_j} \quad . \tag{4.22}$$

The next term we will look at is the intersubchannel pressure gradient. Since it is not possible to discretize this term in the normal manner it will be represented in discretized form by the use of the transverse matrix operator, D_{ki}, as given in equation 4.7. We will however replace the differential operator $\frac{\partial}{\partial y}$ by its finite difference form. This results in:

$$\frac{\partial}{\partial y} = \frac{1}{\ell} \tag{4.23}$$

Applying the above to the term representing the intersubchannel pressure gradient leads to:

$$-\bar{s}\frac{\partial}{\partial y}p_m = -\frac{\bar{s}}{\ell}D_{ki}p_{m_{i,j-1}} \tag{4.24}$$

The term representing the gravitational effects will simply be multiplied by a term representing the channel orientation, where θ is defined as being zero vertically

upwards, and ϕ represents the orientation of the intersubchannel gap, again with zero being vertically upwards.

$$-\bar{s}\rho_{m_{ave}}g_y = -\bar{s}\rho_{m_{ave}}g\cos\phi\sin\theta \quad , \tag{4.25}$$

The term representing the frictional component of the axial momentum balance, $-\frac{\bar{s}}{\ell}\mathcal{F}(C,|W|,W)$, is supplied by a correlation which is dependent on the flow, the void fraction and the flow area. It will be left in its current form in the discretized equation.

Grouping together the right hand sides of equations 4.21, 4.22, 4.24, and 4.25, we may write the finite difference form of the equation of conservation of transverse momentum as:

$$\frac{W_{mk,j}-W^n_{mk,j}}{\Delta t}+\frac{\langle W\bar{u}\rangle_{m_{ave}k,j}-\langle W\bar{u}\rangle_{m_{ave}k,j-1}}{\Delta x_j} \quad - \\ \frac{\bar{s}}{\ell}D_{ki}p_{mi,j-1} = -\frac{s}{\ell}\mathcal{F}(C,|W|,W)-\bar{s}\rho_{m_{ave}}g\cos\phi\sin\theta \tag{4.26}$$

4.1.3 Energy Conservation

Using the differential equations developed in section 3.12, where 3.220 is the mixture enthalpy conservation, 3.214 is the liquid enthalpy conservation, and 3.216 is the vapour enthalpy conservation, as a starting point we will develop the discretized forms of the enthalpy conservation equations used in ASSERT-4.

4.1.3.1 Mixture Energy Conservation

The transportive form of the differential equation for conservation of mixture energy is given by:

$$A\Delta x\rho_m\frac{\partial}{\partial t}\overline{h}^m_m - A\Delta x\frac{\partial}{\partial t}p_m + F_m\Delta x\frac{\partial}{\partial x}\overline{h}^m_m +$$

$$\Delta x \frac{\partial}{\partial x} \frac{\alpha(1-\alpha)\rho_1\rho_2}{\rho_m}(\overline{h}_2^m - \overline{h}_1^m)A\overline{u}_r^m - \sum_K \overline{h}_m^m \Delta x W_m + \sum_K \Delta x \langle W_m \overline{h}_m^{*m} \rangle =$$
$$-\sum_K \Delta x W_1' \left[\overline{h}_1^m(j) - \overline{h}_1^m(i)\right] - \sum_K \Delta x W_2' \left[\overline{h}_2^m(j) - \overline{h}_2^m(i)\right]$$
$$-\iint_{A_{mw}} \hat{n}_{mw} \cdot \vec{q}_m dA \quad . \tag{4.27}$$

As in the case of the equation of conservation of mass the leading Δx is only needed at the end of the calculation to ensure that the quantity is conserved in a volume, for the initial part of the calculation it is not needed. Thus equation 4.27 can be rewritten as:

$$A\rho_m \frac{\partial}{\partial t}\overline{h}_m^m - A\frac{\partial}{\partial t}p_m + F_m \frac{\partial}{\partial x}\overline{h}_m^m +$$
$$\frac{\partial}{\partial x}\frac{\alpha(1-\alpha)\rho_1\rho_2}{\rho_m}(\overline{h}_2^m - \overline{h}_1^m)A\overline{u}_r^m - \sum_K \overline{h}_m^m W_m + \sum_K \langle W_m \overline{h}_m^{*m} \rangle =$$
$$-\sum_K W_1' \left[\overline{h}_1^m(j) - \overline{h}_1^m(i)\right] - \sum_K W_2' \left[\overline{h}_2^m(j) - \overline{h}_2^m(i)\right]$$
$$-\iint_{A_{mw}} \hat{n}_{mw} \cdot \vec{q}_m dA \quad . \tag{4.28}$$

The term representing the effects of the relative velocity can be considered to be a function of the void fraction α and the axial mass flow rate F and can, for simpicity be rewritten as:

$$f(\alpha, F) = \frac{\alpha(1-\alpha)\rho_1\rho_2}{\rho_m}(\overline{h}_2^m - \overline{h}_1^m)A\overline{u}_r^m \quad . \tag{4.29}$$

Applying this simplification to equation 4.28 leads to:

$$A\rho_m \frac{\partial}{\partial t}\overline{h}_m^m - A\frac{\partial}{\partial t}p_m + F_m \frac{\partial}{\partial x}\overline{h}_m^m + \frac{\partial}{\partial x}f(\alpha, F) - \sum_K \overline{h}_m^m W_m + \sum_K \langle W_m \overline{h}_m^{*m} \rangle =$$
$$-\sum_K W_1' \left[\overline{h}_1^m(j) - \overline{h}_1^m(i)\right] - \sum_K W_2' \left[\overline{h}_2^m(j) - \overline{h}_2^m(i)\right]$$
$$-\iint_{A_{mw}} \hat{n}_{mw} \cdot \vec{q}_m dA \quad . \tag{4.30}$$

The transportive form of the equation of conservation of mixture enthalpy can be considered to include two types of terms; terms represening the storage and transport of enthalpy and source terms to the enthalpy transport. The source terms can be considered to include the terms represening crossflow contributions and heat flux contributions to the overall enthalpy balance in the subchannel. We will examine all of the source terms in equation 4.30 and write then in a simplified format.

The terms which represent the crossflow contribution to the enthalpy balance in the control volume can be written in discretized form by using the transpose of the transverse matrix operator to provide the directional information.

The first term we will look at is the transport of enthalpy out of the control volume due to the crossflow out of the subchannel. Using the transpose of the transverse matrix operator to define the direction of the crossflow we can write this term as:

$$-\sum_K \overline{h}_m^m W_m = -\sum_K \overline{h}_m^m D_{ik} W_m \tag{4.31}$$

similarly for the term representing the donor enthalpy transported into the subchannel by the crossflow, we get:

$$\sum_K (W_m \overline{h}_m^{*m}) = \sum_K D_{ik} (W_m \overline{h}_m^{*m}) \tag{4.32}$$

the terms representing the turbulent crossflow contributions can be rewritten as:

$$\sum_K W_1' [h_1^m(j) - h_1^m(i)] = \sum_K D_{ik} W_1' [h_1^m(j) - h_1^m(i)] \tag{4.33}$$

for the liquid phase, and:

$$\sum_K W_2' [h_2^m(j) - h_2^m(i)] = \sum_K D_{ik} W_2' [h_2^m(j) - h_2^m(i)] \tag{4.34}$$

for the vapour phase.

The heat flux from the wall to the fluid in the subchannel is a function of the wall temperature, the wall area, the fluid temperature and the heat transfer coefficients, for simpicity we will represent the heat flux as:

$$q_w' = \iint_{A_{mw}} \hat{n}_{mw} \cdot \vec{q}_m dA \tag{4.35}$$

Grouping the result of equations 4.31 to 4.35 we may express them as a single source term to equation 4.30 which we will call Q_m. This results in:

$$\begin{aligned} Q_m &= q_w' - \sum_K \overline{h}_m^m D_{ik} W_m - \sum_K D_{ik} \langle W_m \overline{h}_m^{*m} \rangle \\ &- \sum_K D_{ik} W_1' [h_1^m(j) - h_1^m(i)] - \sum_K D_{ik} W_2' [h_2^m(j) - h_2^m(i)] \end{aligned} \tag{4.36}$$

Applying the above to equation 4.30 yields:

$$A\rho_m \frac{\partial}{\partial t} \overline{h}_m^m - A \frac{\partial}{\partial t} p_m + F_m \frac{\partial}{\partial x} \overline{h}_m^m + \frac{\partial}{\partial x} f(\alpha, F) - Q_m = 0 \tag{4.37}$$

where the first term of equation 4.37 represents the rate of change of enthalpy in the control volume, the second represents the mechanical energy contribution to the enthalpy due to the pressure variations, the third represents the enthalpy flux and the fourth represents the contribution to the enthalpy flux due to the axial relative velocity.

We will now proceed term by term to develop the finite difference analogs to the terms of equation 4.37 . The first term we will look at represents the rate of

change of mixture enthaply in the control volume. We will finite difference this term using equation 4.4. This results in:

$$A\rho_m \frac{\partial}{\partial t}\overline{h}_m^m = A_{i,j}\rho_{mi,j}\frac{\overline{h}_{mi,j}^m - \overline{h}_{mi,j}^{mn}}{\Delta t} \quad . \tag{4.38}$$

Using equation 4.4 to discretive the term representing the pressure contribution to the enthalpy balance yields:

$$-A\frac{\partial}{\partial t}p_m = A_{i,j}\frac{p_{mref} - p_{mi,j}^n}{\Delta t} \quad . \tag{4.39}$$

We will now use equation 4.3 to discretize the term representing the enthalpy flux and the term representing the effects of the relative velocity on the enthalpy conservation. The result of this discretization is:

$$F_m \frac{\partial}{\partial x}\overline{h}_m^m = F_{mi,j}\frac{\overline{h}_{mi,j}^m - \overline{h}_{mi,j-1}^m}{\Delta x} \quad , \tag{4.40}$$

for the terms representing the enthalpy flux, and

$$\frac{\partial}{\partial x} f(\alpha, F) = \frac{f(\alpha, F)_{i,j} - f(\alpha, F)_{i,j-1}}{\Delta x} \quad , \tag{4.41}$$

for the term representing the effects of the relative velocity on the enthalpy conservation. The details regarding the derivation of the function $f(\alpha, F)_{i,j}$ are given in section 3.12.3.3.

Bringing together the right hand sides of equations 4.38, 4.39, 4.40 and 4.41, we get the discretized form of the equation of mixture enthalpy transport. Which is given by:

$$\begin{aligned} A_{i,j}\rho_{mi,j}\frac{\overline{h}_{mi,j}^m - \overline{h}_{mi,j}^{mn}}{\Delta t} \quad - \quad & A_{i,j}\frac{p_{ref} - p_{mi,j}^n}{\Delta t} + F_{mi,j}\frac{\overline{h}_{mi,j}^m - \overline{h}_{mi,j-1}^m}{\Delta x} \\ + \quad & \frac{f(\alpha, F)_{i,j} - f(\alpha, F)_{i,j-1}}{\Delta x} - Q_m = 0 \quad . \end{aligned} \tag{4.42}$$

4.1.3.2 Phasic Energy: Liquid

The transportive form of the differential equation for liquid energy is given by:

$$(1-\alpha)A\Delta x\rho_1\frac{\partial}{\partial t}\overline{h}_1^m - (1-\alpha)A\Delta x\frac{\partial}{\partial t}p_1 + F_1\Delta x\frac{\partial}{\partial x}\bar{h}_1^m - \sum_K \overline{h}_1^m\Delta x W_1 +$$
$$\sum_K \Delta x(W_1\overline{h}_1^{*m}\rangle = -\sum_K \Delta x W_1'\left[\overline{h}_1^m(j) - \overline{h}_1^m(i)\right] - \iint_{A_{1w}} \hat{n}_{1w}\cdot\vec{q}_1 dA$$
$$-\iint_{A_{phase}} \hat{n}_1\cdot\vec{q}_1 dA \qquad (4.43)$$

As was the previously case the additional Δx in all the terms of equation 4.43 is required to ensure that the proper quantity is conserved but it is not required for the solution. Equation 4.43 can be discretized in the same manner as was done for equation 4.37. Before doing so however we should point out that since ASSERT–4 only calculates one pressure per node and that $p_1 = p_2$ and both are assumed to be equal to p_m, the term representing the pressure change contribution to the phasic enthalpy balance for the liquid phase in discretized form will be represented by:

$$-(1-\alpha)A\frac{\partial}{\partial t}p_1 = -(1-\alpha)A_{i,j}\frac{p_{mref} - p^n_{mi,j}}{\Delta t} \quad . \qquad (4.44)$$

The discretized form of equation 4.43 can be written as:

$$(1-\alpha)A_{i,j}\rho_{1i,j}\frac{\overline{h}^m_{1\ i,j} - \overline{h}^{mn}_{1\ i,j}}{\Delta t} - (1-\alpha)A_{i,j}\frac{p_{mref} - p^n_{mi,j}}{\Delta t}$$
$$+ F_1\frac{\overline{h}^m_{1\ i,j} - \overline{h}^m_{1\ i,j-1}}{\Delta x_j} - Q_1 = 0 \quad . \qquad (4.45)$$

Equation 4.45 is the discretized form of the equation of the liquid phase enthalpy transport as it is solved in ASSERT–4.

4.1.3.3 Phasic Energy: Vapour

The transportive form of the differential equation for vapour energy is given by:

$$\alpha A\Delta x\rho_2\frac{\partial}{\partial t}\overline{h}_2^m - \alpha A\Delta x\rho_2\frac{\partial}{\partial t}p_2 + F_2\Delta x\frac{\partial}{\partial x}\bar{h}_2^m - \sum_K \overline{h}_2^m\Delta x W_2$$
$$+\sum_K \Delta x\langle W_2\overline{h}_2^{*m}\rangle = -\sum_K \Delta x W_2'\left[\overline{h}_2^m(j) - \overline{h}_2^m(i)\right] - \iint_{A_{2w}}\hat{n}_{2w}\cdot\vec{q}_2 dA$$
$$-\iint_{A_{phase}}\hat{n}_2\cdot\vec{q}_2 dA \qquad (4.46)$$

Equation 4.46 can be discretized in the same manner as was done for equation 4.37, making the same assumption about the pressure term, ie:

$$-\alpha A\frac{\partial}{\partial t}P_2 = -\alpha A_{i,j}\frac{p_{mref} - p_{mi,j}^n}{\Delta t} \quad . \qquad (4.47)$$

The discretized form of equation 4.46 can be written as:

$$\alpha A_{i,j}\rho_{2i,j}\frac{\overline{h}_{2\ i,j}^m - \overline{h}_{2\ i,j}^{mn}}{\Delta t} - \alpha A_{i,j}\frac{p_{mref} - p_{mi,j}^n}{\Delta t} + F_2\frac{\overline{h}_{2\ i,j}^m - \overline{h}_{2\ i,j-1}^m}{\Delta x_j} - Q_2 = 0 \quad (4.48)$$

Equation 4.48 is the discretized form of the equation for the vapour phase enthalpy transport as it is solved in ASSERT-4.

4.2 Constitutive Relations and Correlations

ASSERT-4 uses a number of constitutive relations and correlations to close the set of equations given by equations 4.10, 4.19, 4.26, 4.42, 4.45, and 4.48 used to describe the conservation of mass, momentum, mixture and phasic enthalpy. These constitutive relations and correlations supply a number of important relations that are needed such as:

1. Physical Properties, which are supplied by the phasic and mixture Equations of State.

2. The axial relative velocity, which is supplied by the Ohkawa–Lahey [1980] Full Range Drift Flux Model.

3. The transverse relative velocity which includes models to describe the effects of:

   Diversion Crossflow Diversion crossflow is the directed flow caused by pressure gradients between the channels. These gradients may be induced by flow section variations caused by differences in subchannel geometries, the variation of heat flux from one subchannel to the other, incipient boiling in one of the subchannels or by flow section variations caused by blockages.

   Buoyancy Drift The tendency of the lighter (vapour) phase to move upwards with respect to the heavier (liquid) phase due to the effects of gravity.

   Turbulent Void Diffusion In turbulent flow, the velocity and pressure at a fixed point do not remain constant but display random fluctuations. These fluctuations promote the exchange of mass, momentum and energy between the subchannels. In single phase flows, there is momentum and energy transfer between the subchannels but there is no net mass transfer. However, in two–phase flows, in addition to momentum and energy transfer there is usually a substantial net mass transfer due to the differences in the densities of the fluid mixture flowing in the two subchannels.

   Void Drift Which is the tendency of the vapour phase to redistribute itself to a prefered void distribution. This normaly implies that the void drifts

towards the higher velocity channels.

4. Axial and transverse frictional losses.

5. The liquid and vapour thermal mixing.

6. Heat transfer coefficients.

7. Interfacial area.

As this current study concentrated on the hydraulic models used in ASSERT-4, and all the experiments that have been used for comparison are adiabatic, we will not examine all of the above points in detail. Rather, we will focus our attention on the ones that were tested by this work, namely points 2, and 3, the axial and transverse relative velocity models and all of their inherent sub-models.

4.2.1 Drift Flux Model

The relative velocity $\vec{v}_r$ is modelled using the Ohkawa-Lahey [1980] Full Range Drift Flux Model, it is expressed in terms of the mixture volumetric flux $\vec{j}_m$:

According to Ishii [1975] the velocity of the vapour phase, $\vec{v}_2$, can be expressed as:

$$\vec{v}_2 = C_0 \vec{j}_m + \vec{v}_{2j} - \frac{\epsilon_\alpha}{\alpha} \nabla (\alpha - \alpha_{eq}) \quad . \tag{4.49}$$

Where the mixture volumetric flux, $\vec{j}_m$, is defined as:

$$\vec{j}_m = (1 - \alpha)\vec{v}_1 + \alpha \vec{v}_2 \quad , \tag{4.50}$$

and the liquid velocity, $\vec{v}_1$, can be expressed as:

$$\vec{v}_1 = \frac{\vec{j} - \alpha \vec{v}_2}{1 - \alpha} \quad . \tag{4.51}$$

Using the definition of the vapour phase velocity, $\vec{v}_2$, given by equation 4.49, the velocity of the liquid phase, $\vec{v}_1$, can be rewritten as:

$$\vec{v}_1 = \frac{1 - C_0}{1 - \alpha}\vec{j}_m - \frac{\alpha}{1 - \alpha}\vec{v}_{2j} - \frac{\varepsilon_\alpha}{\alpha(1 - \alpha)}\nabla(\alpha - \alpha_{eq}) \tag{4.52}$$

Using the above we may now write the relative velocity, $\vec{v}_r$, as:

$$\vec{v}_r = \frac{C_0 - 1}{1 - \alpha}\vec{j}_m + \frac{\vec{v}_{2j}}{1 - \alpha} - \frac{\varepsilon_\alpha}{\alpha(1 - \alpha)}\nabla(\alpha - \alpha_{eq}) \tag{4.53}$$

The first term on the right hand side accounts for the relative velocity due to cross sectional averaging. The phase distribution coefficient, C_0, is used as the correlating parameter. The second term represents the drift velocity between the liquid and vapour phases driven by gravity. The last term acconts for turbulent void diffusion and diffusion towards a prefered void distribution.

4.2.2 Axial Relative Velocity

In the axial direction the diffusion effects and the redistribution of the void towards a prefered void distribution need not be taken into account as they are phenomena that occur between subchannels. Therefore, the axial relative velocity is modelled using only the first two terms of equation 4.53. Remembering that we are using the x direction for axial flow equation 4.53 can be rewritten in the axial direction as:

$$u_r = \frac{C_0 - 1}{1 - \alpha}\vec{j}_m \cdot \hat{\imath} + \frac{u_{2j}}{1 - \alpha} \quad . \tag{4.54}$$

Looking at equation 4.50 we see that the mixture volumetric flux is calculated in terms of the liquid and vapour velocities, which are quantities that are:

1. Not explicitly known, and

2. Calculated in term of the diffusion velocity which uses the axial relative velocity and the mixture velocity as shown in section 3.7.4.

Thus if we wish to avoid an iterative solution to the relative velocity it would be practical to express it in terms of quantities that are already calculated. We will thus express the mixture volumetric flux, $\vec{j}_m \cdot \hat{\imath}$, in terms of the mixture mass flux, which is given by the axial mass flow rate devided by the flow area, $\frac{F_m}{A}$. Using the fundamental identity 3.78 to express the effects of the relative velocity on the mixture volumetric flux we may write:

$$\vec{j}_m \cdot \hat{\imath} = \frac{F_m}{A\rho_m} + \alpha(1-\alpha)\frac{(\rho_1 - \rho_2)}{\rho_m} u_r \quad . \tag{4.55}$$

Combining equation 4.54 and 4.55 we can express the mixture volumetric flux as:

$$\vec{j}_m \cdot \hat{\imath} = \frac{\left[(C_0 - 1)\frac{F_m}{A\rho_m} + \alpha\frac{(\rho_1-\rho_2)}{\rho_m} u_{2j}\right]}{\left[1 - \alpha\frac{(\rho_1-\rho_2)}{\rho_m}(C_0 - 1)\right]} \quad . \tag{4.56}$$

Combining equation 4.54 and 4.56 we can express the axial relative velocity as:

$$u_r = \frac{\left[\frac{(C_0-1)\frac{F_m}{A\rho_m} + u_{2j}}{\left[1-\alpha\frac{(\rho_1-\rho_2)}{\rho_m}(C_0-1)\right]}\right]}{(1-\alpha)} \tag{4.57}$$

Equation 4.57 is the axial relative velocity as used in ASSERT-4. The phase distribution coefficeint C_0 is given by the Ohkawa-Lahey [1980] Full Range Drift Flux Model, and u_{2j} is modelled in terms of a bubble rise velocity, thus for horizontal flow in the axial direction u_{2j} disappears and the axial relative velocity is only used to account for the effects of averaging non uniformly distributed quantities across the channel. For horizontal flow conditions equation 4.57 becomes:

$$u_r = \frac{\left[\frac{(C_0-1)\frac{F_m}{A\rho_m}}{\left[1-\alpha\frac{(\rho_1-\rho_2)}{\rho_m}(C_0-1)\right]}\right]}{(1-\alpha)} \tag{4.58}$$

4.2.3 Transverse Relative Velocity

In the transverse direction the value of C_0 is assumed to be 1. Thus, the first term of equation 4.53 is zero and only the last two terms are used to represent the transverse relative velocity.

$$v_r = \frac{v_{2j}}{1-\alpha} - \frac{\varepsilon_\alpha}{\alpha(1-\alpha)}\nabla(\alpha-\alpha_{eq}) \tag{4.59}$$

The first term of equation 6.1, which is the drift velocity v_{gj} represents the effect of gravity driving the vapour phase upwards with respect to the liquid phase. The second term of equation 6.1 represents the effects of both void diffusion and redistribution towards a preffered void distribution.

In chapters 6 and 7 of this work two different versions of ASSERT–4 are used for comparison against experimental results. The two versions of ASSERT–4 that are used in this work are ASSERT–4 Version 1.5 and ASSERT–4 Version 2.2B. Apart from differences and improvements in the fuel to coolant heat transfer models and CHF models, which are not tested in this report, the main differences between version 1.5 and version 2.2B are in the constitutive relations used to model the transverse relative velocity. Since a number of the various mechanisms that provoke a void transfer from one subchannel to another are modelled using the transverse relative velocity the differences in how these effects are represented in the two different versions of ASSERT–4 has a profound effect on the prediction of void distribution. Due to the importance of this particular model, the transverse relative model for the two versions of ASSERT–4 will be examined separately.

4.2.3.1 Transverse Relative Velocity: ASSERT–4 V1.5

The first term of equation 6.1, which is the drift velocity v_{2j} is expressed in terms of the terminal rise velocity of a bubble in an infinite medium v_∞,

$$v_{2j} = \bar{\alpha}(1-\bar{\alpha})^n v_\infty \tag{4.60}$$

The term $\bar{\alpha}(1-\bar{\alpha})^n$ is from the model due to Wallis [1969] and is used to account for the presence of other bubbles, in ASSERT–4 Version 1.5 the recommended value of n is 0 [Judd et al., 1984]. The terminal rise velocity, v_∞, also from the model due to Wallis [1969] model is given by:

$$v_\infty = 2K_1\left(\frac{(\rho_1-\rho_2)}{\rho_1^2}\sigma g\right)^{0.25}\cos\phi \tag{4.61}$$

where σ is the surface tension and ϕ is the angle of the centroid to centroid connection measuring the inclination from the vertical and the recommended value of K_1 is equal to 2 [Judd et al., 1984].

The second term of equation 6.1 accounts for both the turbulent void diffusion, $\frac{\varepsilon_\alpha}{\alpha(1-\alpha)}$, and the void redistribution to a preferred void distribution, $\nabla(\alpha-\alpha_{eq})$. The void diffusivity, ε_α, is calculated using a correlation with the Peclet number, which is a function of the void fraction. This correlation is given by:

$$P_e = \frac{\varepsilon}{\bar{U}\bar{D}h} = a\left(\frac{\alpha_m}{0.6}\right)^6 \tag{4.62}$$

where the recommended value of a is 0.075, $\bar{U}$ is the average mixture axial velocity of the adjacent subchannels i, and j $\bar{D}_h$ is the average hydraulic diameter of the adjacent subchannels, and α_m is the maximum of the void fraction in the two adjacent subchannels.

The void redistribution to a preferred void distribution, $\nabla(\alpha-\alpha_{eq})$ is calculated using Lahey's model [Lahey Jr. and Moody, 1977]. Given two subchannels i and j this term can be written as:

$$\begin{aligned}
\nabla(\alpha - \alpha_{eq})_{ij} &= [\alpha - \alpha_{eq}]_i - [\alpha - \alpha_{eq}]_j \\
&= [\alpha_j - \alpha_i] - [\alpha_j - \alpha_i]_{eq} \\
&= (\Delta\alpha - \Delta\alpha_{eq})_{ij} \\
&= \Delta(\alpha - \alpha_{eq})_{ij} \qquad (4.63)
\end{aligned}$$

α_{eq} is the prefered, or equilibrium, void distribution. The prefered void distribution is calculated using a weighting of the individual subchannel mass fluxes to the average mass flux in the two subchannel i, and j. The subchannel mass flux, G_m, can be defined as:

$$G_m = \frac{F_m}{A} \quad . \qquad (4.64)$$

The individual equilibrium, or prefered, void distributions can be calculated as:

$$\alpha_{ieq} = \left[\frac{\bar{\alpha}}{\bar{G}_m}\right] G_{mi} \quad , \qquad (4.65)$$

for subchannel i, and

$$\alpha_{jeq} = \left[\frac{\bar{\alpha}}{\bar{G}_m}\right] G_{mj} \quad , \qquad (4.66)$$

for subchannel j. For two subchannels i, and j, this is written as:

$$[\alpha_j - \alpha_i]_{eq} = \left[\frac{\bar{\alpha}}{\bar{G}_m}\right] \left[G_{mj} - G_{mi}\right] \qquad (4.67)$$

the average void fraction $\bar{\alpha}$ and the average mass flux $\bar{G}_m$ are calculated using:

$$\bar{\alpha} = \frac{(\alpha A)_i + (\alpha A)_j}{A_i + A_j} \qquad (4.68)$$

$$\bar{G}_m = \frac{F_{mi} + F_{mj}}{A_i + A_j} \tag{4.69}$$

Thus the transverse relative velocity is modelled using:

$$v_r = \frac{\left[4\bar{\alpha}\left(\frac{\rho_1-\rho_2}{\rho_1^2}\sigma g\right)^{0.25}\cos\phi - \frac{\varepsilon}{\bar{\alpha}\ell}\Delta\left(\alpha - \alpha_{eq}\right)_{ij}\right]}{(1-\bar{\alpha})} \tag{4.70}$$

It should be noted that in the case of the term, $\bar{\alpha}(1-\bar{\alpha})^n$, where ASSERT–4 Version 1.5 uses a value of $n = 0$, Wallis [1969] recommends a value of $n = 2$. Further, the leading coefficient in the correlation for the terminal rise velocity of a bubble in an infinite medium v_∞, is 4 in ASSERT–4 Version 1.5 while Wallis [1969] recommends a value in the range of $1.414 \rightarrow 1.56$.

There is one other consequence of using $n = 0$, in the term that accounts for the presence of other bubbles, $\bar{\alpha}(1-\bar{\alpha})^n$, this is that the first term in the expression for the relative velocity does not go to zero as $\alpha \rightarrow 1$. It is thus necessary to multiply the expression for the terminal rise velocity v_∞, given by the first term on the right hand side of equation 4.70 by an additional term that drives this term to zero as the void fraction tends towards one. The term used for this is the Ohkawa–Lahey correction factor F, which is given by:

$$F = \left[1 - \left(\frac{\alpha - \chi}{1 - \chi}\right)\right]^m \tag{4.71}$$

where:

$$\chi = 0.588 - 1.817\Psi + 2.0\Psi^2 - 3.343\Psi^3$$

and

$$\Psi = \sqrt[2]{\frac{\rho_2}{\rho_1}}$$

for $\alpha > \chi$, otherwise $F = 1$. The recommended value of m is 1.5.

4.2.3.2 Transverse Relative Velocity: ASSERT–4 V2.2B

As in the case of ASSERT–4 Version 1.5, in Version 2.2B the drift velocity v_{2j}, given by the first term of equation 6.1, is expressed in terms of the terminal rise velocity of a bubble in an infinite medium v_∞,

$$v_{2j} = \bar{\alpha}(1-\bar{\alpha})^n v_\infty \quad . \tag{4.72}$$

The term $\bar{\alpha}(1-\bar{\alpha})^n$ is from the model due to Wallis [1969] and is used to account for the presence of other bubbles, in ASSERT–4 Version 2.2B the recommended value of n is 0, and the remaining α is raised to the power of 0.1, thus the effects of other bubbles is represented as $\bar{\alpha}^{0.1}$ [Judd et al., 1984]. The terminal rise velocity, v_∞, also from Wallis [1969]. However ASSERT–4 Version 2.2B is more faithfull to the original model due to Wallis [1969] in its implementation of the terminal rise velocity than is ASSERT–4 Version 1.5. The terminal rise velocity is given by:

$$v_\infty = K_1 \left(\frac{(\rho_1 - \rho_2)}{\rho_1^2} \sigma g \right)^{0.25} \cos\phi \quad , \tag{4.73}$$

where σ is the surface tension and ϕ is the angle of the centroid to centroid connection measuring the inclination from the vertical and the recommended value of K_1 is equal to 1.4, [Judd et al., 1984], which is completely in line with the range of leading coefficients recommended by Wallis [1969].

The second term of equation 6.1 accounts for both the turbulent void diffusion, $\frac{\varepsilon_{Re}}{\alpha(1-\alpha)}$, and the void redistribution to a preferred void distribution, $\nabla(\alpha - \alpha_{eq})$. In ASSERT–4 Version 2.2B the void diffusivity, ε_{Re}, is calculated from a correlation with the Peclet number, which in this case is a function of the Reynolds number, hence the use of the subscript Re in Version 2.2B. This correlation is given by:

$$P_e = \frac{\varepsilon_{Re}}{\bar{U}\bar{D}h} = aRe^b \quad , \tag{4.74}$$

where the recommended value of a is 0.05 and the recommended value of b is 0, $\bar{U}$ is the average mixture axial velocity of the adjacent subchannels i and j, and $\bar{D}_h$ is the average hydraulic diameter of the adjacent subchannels. Thus in ASSERT–4 Version 2.2B the void diffusion coefficient is independent of the void fraction, and for that matter it is also independent of the Reynolds number as well, due to the fact that $b = 0$.

In ASSERT–4 Version 2.2B the void redistribution to a preferred void distribution, $\nabla(\alpha - \alpha_{eq})$ is calculated using the model proposed by Lahey and Moody [1977] using the same equations 4.67,4.68, and 4.69 as are used in ASSERT–4 Version 1.5.

Thus the transverse relative velocity in ASSERT–4 Version 2.2B is given by:

$$V_r = \frac{\left[1.4\bar{\alpha}^{0.1}\left(\frac{\rho_1-\rho_2}{\rho_1^2}\sigma g\right)^{0.25}\cos\phi - \frac{\varepsilon_{Re}}{\bar{\alpha}\ell}\Delta\left(\alpha-\alpha_{eq}\right)_{ij}\right]}{(1-\bar{\alpha})} \quad . \tag{4.75}$$

As in ASSERT–4 Version 1.5 the same problem exists for the terminal rise velocity as $\alpha \rightarrow 1$. ASSERT–4 Version 2.2B uses the same Ohkawa–Lahey [1980] correction factor, given by equation 7.3, as Version 1.5 to drive the terminal rise velocity to zero as the void fraction approaches one. The only difference being that the recommended value for the coefficient m in equation 7.3 is changed from $m = 1.5$ in ASSERT–4 Version 1.5 to $m = 3$ in ASSERT–4 Version 2.2B.

It is interesting to examine the difference in the calculation of the drift velocity, v_{gj} which is modelled using the terminal rise velocity of a bubble in an infinite medium, v_∞, as given by ASSERT–4 Version 1.5, ASSERT–4 Version 2.2B and that given by Wallis' model. Since the term which accounts for the buoyancy, ie:

$$\left(\frac{\rho_1-\rho_2}{\rho_1^2}\sigma g\right)^{0.25}\cos\phi$$

is identical in all three models we can drop this term and examine only the leading coefficients. These leading coefficients are:

$$Coef_{1.5} = 4\alpha F \quad , \tag{4.76}$$

for ASSERT–4 Version 1.5, where F is given by equation 7.3,

$$Coef_{2.2B} = 1.4\alpha^{0.1} F \quad , \tag{4.77}$$

for ASSERT–4 Version 2.2B, and

$$Coef_{Wallis} = 1.5\alpha(1-\alpha)^n \quad , \tag{4.78}$$

for Wallis' model, where values of $n = 2$ and $n = 1$ are tested.

For two different pressures, 150 kPa and 10 MPa, the relationship between the void fraction α and these leading coefficients are shown in figures 4.1 and 4.2 respectively.

It is clear from figures 4.1 and 4.2 that both versions of ASSERT–4 produce a leading coefficient for the drift velocity, v_{2j}, that is significantly larger than what results from the application of Wallis' model. The effects that these overpredictions have on the results, if any, will be discussed in chapter 7 where the comparison between experimental and computed results for horizontal flow cases will be presented.

It can also be seen that this overprediction is not as large at higher pressures. This is due to the fact that the Ohkawa–Lahey correction factor F which is a function of both the ratio of the vapour density to the liquid density, and the void fraction, has a greater effect at higher pressures. This can be seen from figure 4.3.

4.3 ASSERT–4 Solution Scheme

The solution scheme used in ASSERT–4 is based on a combination of the use of the Implicit Continuous Eulerian, I.C.E, algorithm developed by Amsden

and Harlow [1971] and Newton's method for solving nonlinear equations. The details of this method are clearly explained in both the ASSERT–4 theory manuel [Judd et al., 1984] and a paper written by Webb and Rowe [1986], and only the most important points will be reproduced here. The aim of this section is to describe the solution scheme, and the conditions, as described by Webb and Rowe [1986], under which it is applicable.

4.3.1 Newton's Method For Solving Problems in Two–Phase Flow

In ASSERT–4 Newton's method is used to solve the equations of two–phase flow. The method involves a successive correction procedure that updates a tentative solution thus driving the residual error to zero. The method will be illustrated using an arbitrary function $F(x)$. We will start with:

$$F(x) = 0 \quad , \tag{4.79}$$

where x is a solution to the equation. Let $\tilde{x}$ be an initial estimate close to the solution x and let δx be a correction to the initial estimate such that:

$$x = \tilde{x} + \delta x \quad , \tag{4.80}$$

equation 4.79 may then be written as:

$$F(\tilde{x} + \delta x) = 0 \quad , \tag{4.81}$$

this can be expanded as:

$$F(\tilde{x}) + \frac{\partial F}{\partial x}\delta x = 0 \quad , \tag{4.82}$$

rearranging equation 4.82 yields:

$$\frac{\partial F}{\partial x}\delta x = -F(\tilde{x}) \quad . \tag{4.83}$$

The right side is the residual error from the initial estimate and the left side contains the coefficient of δx. Solving for δx yields:

$$\delta x = -\left(\frac{\partial F}{\partial x}\right)^{-1} F(\tilde{x}) \quad . \tag{4.84}$$

When $\frac{\partial F}{\partial x}$ is a single valued function a simple division provides the solution for δx [Webb and Rowe, 1986]. Given the solution for δx, the tentative solution $\tilde{x}$ can be updated using equation 4.80, this value is then used as the new tentative solution. This process continues in an iterative manner until the residual shows that the desired degree of accuracy has been attained. If $\vec{F}(\vec{x})$ is a vector function then $\vec{x}$ becomes a solution vector and the term $\frac{\partial \vec{F}}{\partial x}$ becomes a Jacobian derivative matrix and the solution vector $\vec{\delta x}$ is obtained by solution of a set of simultaneous equations, which is the case in the ASSERT–4 subchannel code. Newton's method along with the basic ideas of the I.C.E. algorithm [Harlow and Amsden, 1971] are used to solve the conservation equations at each axial plane in ASSERT–4. The discretized form of the conservation equations 4.10,4.19,4.26,4.42,4.45, and 4.48 presented in section 1 are not the equations actually solved in ASSERT–4. Before the solution is attempted, the discretized equations 4.10,4.19,4.26,4.42,4.45, and 4.48 are transformed into their respective Newton solution forms. This is done by rearranging the equations in such a manner as to solve for the δ terms, which is the correction to the solution based on the initial, "guessed" values. Webb and Rowe [1986] have stated that for a wide class of problems it is both possible and convenient to decouple the solution of the energy equation from the solution of the mass and momentum equations. This is done by using the transportive form of the energy equation. Using the velocity defined at time $n+1$ the energy and flow solutions are coupled automatically through the iterative solution process. This is

exactly what is done in the ASSERT–4 subchannel code.

4.3.2 Application of Newton's Method In ASSERT–4

We will now examine Newton's method for solving problems in two–phase flow as it is implemented in ASSERT–4. This examination will focus on one iterative cycle occuring somewhere in the overall iterative process before convergence has been reached. This iterative cycle is shown graphically in figure 4.4. A brief description of this cycle for a given axial location is:

Using the flow and crossflow calculated at the end of the previous iteration, solve the energy equation for all the subchannels, under equilibrium or non-equilibrium conditions depending on the option that was chosen, and update the enthalpy(ies).

Use the newly calculated enthalpy values for each subchannel to calculate a new density for each subchannel.

Use the new densities and the existing estimates of the crossflows to solve the mass conservation equation for each of the subchannels individualy and update the axial flows for each subchannel.

Use the new densities, and flows along with the existing estimates of the crossflows to solve the axial momentum equation for each of the subchannels individualy and update the pressure drops for each subchannel.

Use the new pressure drops and the existing estimates of the crossflows to solve for all the new crossflows simultaneously for all the subchannels in a given axial plane.

Use the crossflows to correct the axial flows and pressures.

If converged, stop, if not repeat.

Since the energy and flow solutions are decoupled we will examine the Newton form of the energy and flow solutions separately.

4.3.2.1 Newton Form of Energy Solution

The phasic and mixture energy equations are solved simultaneously for all the subchannels at a given axial position. Each subchannel is solved for using a block iterative technique, where each block is a 4×4 matrix consisting of the three energy equations and a constraint equation. The coupling to the other subchannels is treated as a source term to the energy balance of the subchannel under consideration. This system of equations is solved seperately for each subchannel. The solution is done iteratively for each of the subchannels at a given axial position until the a sufficient degree of convergence is reached. The axial and transverse flows are normally variables in the solution of the energy equations. However, in this solution method, as has already been stated, the energy and flow solutions are decoupled. Thus the energy solution is performed for a set of fixed, tentative, values of the axial and transverse flows. The flows are then corrected as part of the flow solution and the corrected flows are used as part of the next energy iteration.

Thus, starting with a newly corrected but not yet correct crossflow $\widetilde{W}$, a just corrected flow, F, a just corrected pressure, P_x, and a just corrected density, ρ, solve the energy equations.

The energy equations can be written in vector functional form as:

$$\mathcal{E}_m\left(h_m, h_1, h_2, \alpha\right) = 0 \quad , \tag{4.85}$$

$$\mathcal{E}_1\left(h_m, h_1, h_2, \alpha\right) = 0 \quad , \tag{4.86}$$

$$\mathcal{E}_2\left(h_m, h_1, h_2, \alpha\right) = 0 \quad . \tag{4.87}$$

Since we have 3 equations and 4 unknowns, an extra equation is needed. This extra equation is supplied by the relationship between the enthalpy and the quality. This is given by:

$$\mathcal{H}(h_m, h_1, h_2, \alpha) = 0 \quad . \tag{4.88}$$

Where the void quality relationship is used to relate the constraint equation, $\mathcal{H}(h_m, h_1, h_2, \alpha)$ to the quality X.

Using Newton's solution method where the terms in equations 4.85, 4.86, 4.87, and 4.88 can be written as $h_m = \tilde{h}_m + \delta h_m$, $h_1 = \tilde{h}_1 + \delta h_1$, $h_2 = \tilde{h}_2 + \delta h_2$, and $\alpha = \tilde{\alpha} + \delta\alpha$. We may rewrite equations 4.85 to 4.88 as:

$$\frac{\partial \mathcal{E}_m}{\partial h_m}\delta h_m + \frac{\partial \mathcal{E}_m}{\partial h_1}\delta h_1 + \frac{\partial \mathcal{E}_m}{\partial h_2}\delta h_2 + \frac{\partial \mathcal{E}_m}{\partial \alpha}\delta\alpha = -\mathcal{E}_m\left(\tilde{h}_m, \tilde{h}_1, \tilde{h}_2, \tilde{\alpha}\right) \quad , \tag{4.89}$$

$$\frac{\partial \mathcal{E}_1}{\partial h_m}\delta h_m + \frac{\partial \mathcal{E}_1}{\partial h_1}\delta h_1 + \frac{\partial \mathcal{E}_1}{\partial h_2}\delta h_2 + \frac{\partial \mathcal{E}_1}{\partial \alpha}\delta\alpha = -\mathcal{E}_1\left(\tilde{h}_m, \tilde{h}_1, \tilde{h}_2, \tilde{\alpha}\right) \quad , \tag{4.90}$$

$$\frac{\partial \mathcal{E}_2}{\partial h_m}\delta h_m + \frac{\partial \mathcal{E}_2}{\partial h_1}\delta h_1 + \frac{\partial \mathcal{E}_2}{\partial h_2}\delta h_2 + \frac{\partial \mathcal{E}_2}{\partial \alpha}\delta\alpha = -\mathcal{E}_2\left(\tilde{h}_m, \tilde{h}_1, \tilde{h}_2, \tilde{\alpha}\right) \quad , \tag{4.91}$$

$$\frac{\partial \mathcal{H}}{\partial h_m}\delta h_m + \frac{\partial \mathcal{H}}{\partial h_1}\delta h_1 + \frac{\partial \mathcal{H}}{\partial h_2}\delta h_2 + \frac{\partial \mathcal{H}}{\partial \alpha}\delta\alpha = -\mathcal{H}\left(\tilde{h}_m, \tilde{h}_1, \tilde{h}_2, \tilde{\alpha}\right) \quad . \tag{4.92}$$

This system of equations is solved for each subchannel at a given axial plane. The process is repeated until convergence is reached for all the subchannels at the axial plane in question. The system of equations given by equations 4.89, 4.90, 4.91, and 4.92 can be written in matrix form as:

$$\begin{bmatrix} \frac{\partial \mathcal{E}_m}{\partial h_m} & \frac{\partial \mathcal{E}_m}{\partial h_1} & \frac{\partial \mathcal{E}_m}{\partial h_2} & \frac{\partial \mathcal{E}_m}{\partial \alpha} \\ \frac{\partial \mathcal{E}_1}{\partial h_m} & \frac{\partial \mathcal{E}_1}{\partial h_1} & \frac{\partial \mathcal{E}_1}{\partial h_2} & \frac{\partial \mathcal{E}_1}{\partial \alpha} \\ \frac{\partial \mathcal{E}_2}{\partial h_m} & \frac{\partial \mathcal{E}_2}{\partial h_1} & \frac{\partial \mathcal{E}_2}{\partial h_2} & \frac{\partial \mathcal{E}_2}{\partial \alpha} \\ \frac{\partial \mathcal{H}}{\partial h_m} & \frac{\partial \mathcal{H}}{\partial h_1} & \frac{\partial \mathcal{H}}{\partial h_2} & \frac{\partial \mathcal{H}}{\partial \alpha} \end{bmatrix} \begin{bmatrix} \delta h_m \\ \delta h_1 \\ \delta h_2 \\ \delta \alpha \end{bmatrix} = - \begin{bmatrix} \mathcal{E}_m \left(\tilde{h}_m, \tilde{h}_1, \tilde{h}_2, \tilde{\alpha} \right) \\ \mathcal{E}_1 \left(\tilde{h}_m, \tilde{h}_1, \tilde{h}_2, \tilde{\alpha} \right) \\ \mathcal{E}_2 \left(\tilde{h}_m, \tilde{h}_1, \tilde{h}_2, \tilde{\alpha} \right) \\ \mathcal{H} \left(\tilde{h}_m, \tilde{h}_1, \tilde{h}_2, \tilde{\alpha} \right) \end{bmatrix}$$

where:

$\mathcal{E}_m$	represents the equation of conservation of mixture enthalpy,	[–]
$\mathcal{E}_1$	represents the equation of conservation of liquid enthalpy,	[–]
$\mathcal{E}_2$	represents the equation of conservation of vapour enthalpy,	[–]
$\mathcal{H}$	represents the constraint equation.	[–]

The matrix is solved by gauss elimination for the incremental corrections δh_m, δh_1, δh_2, $\delta \alpha$. The variables are then updated by:

$$h_m = \tilde{h}_m + \delta h_m \quad , \tag{4.93}$$

$$h_1 = \tilde{h}_1 + \delta h_1 \quad , \tag{4.94}$$

$$h_2 = \tilde{h}_2 + \delta h_2 \quad , \tag{4.95}$$

$$\alpha = \tilde{\alpha} + \delta \alpha \quad . \tag{4.96}$$

Density Correction

Having obtained a new solution for the enthalpy, calculate a new density using:

$$\tilde{\rho}_m = \rho \left(h_m, p_x \right) \quad . \tag{4.97}$$

4.3.2.2 Newton Form of Flow Solution

Newtons method is used to solve the mass and momentum equations. In vector functional form, the equations of conservation of mass, axial and transverse momentum can be written as:

$$\mathcal{F}\left(\rho_m, F_m, W_m\right) = 0 \quad , \tag{4.98}$$

$$\mathcal{M}\left(\rho_m, F_m, W_m, p_x\right) = 0 \quad , \tag{4.99}$$

$$\mathcal{W}\left(W_m, p_x\right) = 0 \quad , \tag{4.100}$$

where the solution vectors at each axial location are ρ, F, W, p_x. It is also necessary to relate the effects that a change in crossflow has on the enthalpy and density. This is done using a reduced form of the mixture energy equation. In vector functional form this equation can be written as:

$$\mathcal{E}_m\left(h_m, W_m\right) = 0 \quad , \tag{4.101}$$

where:

$\mathcal{F}$	represents the equation of conservation of mass,	[–]
$\mathcal{M}$	represents the equation of conservation of axial momentum,	[–]
$\mathcal{W}$	represents the equation of conservation of transverse momentum,	[–]
$\mathcal{E}_m$	represents the equation of conservation of mixture enthalpy.	[–]

Using the fact that equations 4.98 to 4.101 can be expressed as:

$$\mathcal{F}\left(\rho_m, F_m, W_m\right) = \mathcal{F}\left(\tilde{\rho}_m + \delta\rho_m, \tilde{F}_m + \delta F_m, \widetilde{W}_m + \delta W_m\right) \quad , \tag{4.102}$$

$$\mathcal{M}\left(\rho, F, W, p_x\right) = \mathcal{M}\left(\tilde{\rho}_m + \delta\rho_m, \tilde{F}_m + \delta F_m, \widetilde{W}_m + \delta W_m, \tilde{p}_x + \delta p_x\right) \quad , \tag{4.103}$$

$$\mathcal{W}\left(W_m, p_x\right) = \mathcal{W}\left(\widetilde{W}_m + \delta W_m, \tilde{p}_x + \delta p_x\right) \quad , \tag{4.104}$$

$$\mathcal{E}_m\left(h, W\right) = \mathcal{E}_m\left(\tilde{h}_m + \delta h_m, \widetilde{W}_m + \delta W_m\right) \quad , \tag{4.105}$$

where $\tilde{\rho}_m$, $\tilde{F}_m$, $\widetilde{W}_m$ and $\tilde{p}_x$ are initial guesses close to the true solutions and $\delta\rho_m$, δF_m, δW_m and δP_x are corrections to these guesses.

Equations 4.98, 5.18, 4.100, and 4.101 can be rewritten as:

$$\begin{aligned}\mathcal{F}\left(\rho_m, F_m, W_m\right) &= \mathcal{F}\left(\tilde{\rho}_m, \tilde{F}_m, \widetilde{W}_m, 0\right) \\ &+ \frac{\partial\mathcal{F}}{\partial\rho_m}\frac{\partial\rho_m}{\partial h_m}\delta h_m + \frac{\partial\mathcal{F}}{\partial F_m}\delta F_m + \frac{\partial\mathcal{F}}{\partial W_m}\delta W_m \quad .\end{aligned} \tag{4.106}$$

$$\begin{aligned}\mathcal{M}\left(\rho_m, F_m, W_m, p_x\right) &= \mathcal{M}\left(\tilde{\rho}_m, \tilde{F}_m, \widetilde{W}_m, \tilde{p}_x\right) \\ &+ \frac{\partial\mathcal{M}}{\partial\rho_m}\frac{\partial\rho_m}{\partial h_m}\delta h_m + \frac{\partial\mathcal{M}}{\partial F_m}\delta F_m + \frac{\partial\mathcal{M}}{\partial W_m}\delta W_m + \frac{\partial\mathcal{M}}{\partial p_x}\delta p_x \quad .\end{aligned} \tag{4.107}$$

$$\mathcal{W}\left(W_m, p_x\right) = \mathcal{W}\left(\widetilde{W}_m, \tilde{p}_x\right) + \frac{\partial\mathcal{W}}{\partial W_m}\delta W_m + \frac{\partial\mathcal{W}}{\partial p_x}\delta p_x \quad . \tag{4.108}$$

$$\mathcal{E}_m\left(h_m, W_m\right) = \mathcal{E}_m\left(\tilde{h}_m, \widetilde{W}_m\right) + \frac{\partial\mathcal{E}_m}{\partial h_m}\delta h_m + \frac{\partial\mathcal{E}_m}{\partial W_m}\delta W_m \quad . \tag{4.109}$$

The Newton solution form of equations 4.98, 5.18, 4.100, and 4.101 can be written as:

$$\frac{\partial \mathcal{E}_m}{\partial h_m}\delta h_m + \frac{\partial \mathcal{E}_m}{\partial W_m}\delta W_m = -\mathcal{E}_m\left(\tilde{h}_m, \widetilde{W}_m\right) \quad . \tag{4.110}$$

$$\frac{\partial \mathcal{F}}{\partial \rho_m}\frac{\partial \rho_m}{\partial h_m}\delta h_m + \frac{\partial \mathcal{F}}{\partial F_m}\delta F_m + \frac{\partial \mathcal{F}}{\partial W_m}\delta W_m = -\mathcal{F}\left(\tilde{\rho}_m, \tilde{F}_m, \widetilde{W}_m\right) \quad . \tag{4.111}$$

$$\frac{\partial \mathcal{M}}{\partial \rho_m}\frac{\partial \rho_m}{\partial h_m}\delta h_m + \frac{\partial \mathcal{M}}{\partial F_m}\delta F_m + \frac{\partial \mathcal{M}}{\partial W_m}\delta W_m + \frac{\partial \mathcal{M}}{\partial p_x}\delta p_x = -\mathcal{M}\left(\tilde{\rho}_m, \tilde{F}_m, \widetilde{W}_m, \tilde{p}_x\right) \quad . \tag{4.112}$$

$$\frac{\partial \mathcal{W}}{\partial W}\delta W + \frac{\partial \mathcal{W}}{\partial p_x}\delta p_x = -\mathcal{W}\left(\widetilde{W}, \tilde{p}_x\right) \quad . \tag{4.113}$$

Conservation of Energy

Since the energy equation has already been solved using a tentative crossflow, $\widetilde{W}_m$, thus we may assume that:

$$\mathcal{E}_m\left(\tilde{h}_m, \widetilde{W}_m\right) \approx 0 \quad , \tag{4.114}$$

a good approximation of the effects of a change in the crossflow on the energy solution can be given by:

$$\frac{\partial \mathcal{E}_m}{\partial h_m}\delta h_m + \frac{\partial \mathcal{E}_m}{\partial W_m}\delta W_m = 0 \quad . \tag{4.115}$$

Which describes the way the mixture energy equation is effected by a change in the crossflow W. The derivative term $\frac{\partial \mathcal{E}_m}{\partial W_m}$ is obtained by differentiating the energy equation with respect to the crossflow. This yields:

$$\frac{\partial \mathcal{E}_m}{\partial W_m} = \left(D^T h_m^* - h_m D^T\right) \quad . \tag{4.116}$$

Solving equation 4.115 for the enthalpy correction we get:

$$\delta h_m = -\left[\frac{\partial \mathcal{E}_m}{\partial h_m}\right]^{-1} \left(D^T h_m^* - h_m D^T\right) \delta W_m \quad . \tag{4.117}$$

This result is not used in the iterative cycle to correct the enthalpy as this correction is made through the iteration between the flow and energy solutions, It is however needed to calculate the effect of a change in enthalpy on the axial pressure.

Newton Form of Conservation of Mass

Having obtained a new estimate of the density, we can now solve the mass balance for the flow $\tilde{F}_m$ using the new density $\tilde{\rho}_m$, the crossflow $\widetilde{W}_m$ and the old flow F_m. The is done using:

$$-\delta F_m = \Delta x \left(A_{i,j} \frac{\tilde{\rho}_{mi,j} - \rho^n_{mi,j}}{\Delta t} + \frac{F_{mi,j} - F_{mi,j-1}}{\Delta x_j} + D_{ik} \widetilde{W}_{mk,j} \right) \quad , \tag{4.118}$$

and:

$$\tilde{F}_m = F_m + \delta F_m \quad . \tag{4.119}$$

Where $\tilde{F}_m$ is a corrected value of the flow that satisfies:

$$\mathcal{F}\left(\tilde{\rho}_m, \tilde{F}_m, \widetilde{W}_m\right) = 0 \quad , \tag{4.120}$$

but is still subject to a further correction based on an anticipated change in the crossflow at the end of this iterative cycle.

Equation 4.120 permits us to write the Newton form of the equation of conservation of mass as:

$$\frac{\partial \mathcal{F}}{\partial \rho_m} \frac{\partial \rho_m}{\partial h_m} \delta h_m + \frac{\partial \mathcal{F}}{\partial F_m} \delta F_m + \frac{\partial \mathcal{F}}{\partial W_m} \delta W_m = 0 \quad . \tag{4.121}$$

Defining $\frac{\partial \mathcal{F}}{\partial F_m}$ as being equal to $\frac{1}{\Delta x}$, neglecting the term $\frac{\partial \mathcal{F}}{\partial \rho_m}$, and expressing the term $\frac{\partial \mathcal{F}}{\partial W_m}$ in terms of the transpose of the transverse matrix operator D^T equation 4.121 can be rewritten for the mass flow rate correction as:

$$\delta F_m = -\Delta x D^T \delta W_m \quad . \tag{4.122}$$

This represents a correction to the tentative flow solution $\tilde{F}_m$ based on a change in the crossflow.

Newton Form of Conservation of Axial Momentum

Using the just calculated tentative flow $\tilde{F}_m$, the crossflow $\widetilde{W}_m$, the density $\tilde{\rho}_m$ and the previous pressure p_x solve the axial momentum balance, im-balance for δp_x. This is done using:

$$\begin{aligned} \delta P_x &= \frac{\tilde{F}_{mi,j} - F^n_{mi,j}}{\Delta t} + \frac{\langle \widetilde{F_m \bar{u}_m} \rangle_{i,j} - \langle F_m \bar{u}_m \rangle_{i,j-1}}{\Delta x} \\ &+ D_{ik} \langle \widetilde{W_m \bar{u}^*_m} \rangle_k - \bar{A}_{i,j} \frac{p_{mi,j} - p_{mi,j-1}}{\Delta x_j} \\ &+ \mathcal{F}(\bar{A}, K, |F|, F)_{i,j} + \bar{A}_{i,j} \rho_m g \cos\theta \quad , \end{aligned} \tag{4.123}$$

and:

$$\tilde{p}_x = p_x + \delta p_x \quad . \tag{4.124}$$

Where $\tilde{p}_x$ is a corrected value of the pressure gradient which satisfies

$$\mathcal{M}\left(\tilde{\rho}_m, \tilde{F}_m, \widetilde{W}_m, \tilde{p}_x\right) = 0 \quad . \tag{4.125}$$

but is still subject to a further correction based on an anticipated change in the crossflow at the end of this iterative cycle.

Equation 4.125 permits us to write the Newton form of the equation of conservation of axial momentum as:

$$\frac{\partial \mathcal{M}}{\partial \rho_m}\frac{\partial \rho_m}{\partial h_m}\delta h_m + \frac{\partial \mathcal{M}}{\partial F_m}\delta F_m + \frac{\partial \mathcal{M}}{\partial W_m}\delta W_m + \frac{\partial \mathcal{M}}{\partial p_x}\delta p_x = 0 \quad . \tag{4.126}$$

Using the fact that:

$$\frac{\partial \mathcal{M}}{\partial \rho_m}\frac{\partial \rho_m}{\partial h_m} = \frac{\partial \mathcal{M}}{\partial v_m}\frac{\partial v_m}{\partial h_m} \quad . \tag{4.127}$$

Equation 4.126 can be rewritten in terms of the mixture specific volme v_m as:

$$\frac{\partial \mathcal{M}}{\partial v_m}\frac{\partial v_m}{\partial h_m}\delta h_m + \frac{\partial \mathcal{M}}{\partial F_m}\delta F_m + \frac{\partial \mathcal{M}}{\partial W_m}\delta W_m + \frac{\partial \mathcal{M}}{\partial p_x}\delta p_x = 0 \quad . \tag{4.128}$$

Due to the fact that $\frac{\partial \mathcal{M}}{\partial p_x} = \overline{\overline{I}}$, the identity matrix, equation 4.128 can be rearranged to yield an expression for the pressure correction term. This is:

$$\delta p_x = -\frac{\partial \mathcal{M}}{\partial v_m}\frac{\partial v_m}{\partial h_m}\delta h_m - \frac{\partial \mathcal{M}}{\partial F_m}\delta F_m - \frac{\partial \mathcal{M}}{\partial W_m}\delta W_m \quad . \tag{4.129}$$

Using equation 4.117 to replace the δh_m term and equation 4.122 to replace the δF_m term we may rewrite equation 4.129 as:

$$\delta p_x = \frac{\partial \mathcal{M}}{\partial v_m}\frac{\partial v_m}{\partial h_m}\left[\frac{\partial \mathcal{E}_m}{\partial h_m}\right]^{-1}\left(D^T h_m^* - h_m D^T\right)\delta W_m + \frac{\partial \mathcal{M}}{\partial F_m}\Delta x D^T \delta W_m - \frac{\partial \mathcal{M}}{\partial W_m}\delta W_m \quad . \tag{4.130}$$

In compact form this can be written as:

$$\delta p_x = \frac{\partial p_x}{\partial W_m}\delta W_m \quad . \tag{4.131}$$

This represents a correction to the tentative pressure solution $\tilde{p}_x$ as a function of the change in crossflow.

Newton Form of Conservation of Transverse Momentum

In vector form the transverse momentum equation can be written as:

$$\mathcal{W}(W_m, p_x) = 0 \quad . \tag{4.132}$$

which states that the transverse momentum solution is a function of the crossflow and the subchannel pressures. Using the basic ideas of Newton's solution we can rewrite the terms in equation 4.132 as: $W_m = \widetilde{W}_m + \delta W_m$ and $p_x = \tilde{p}_x + \delta p_x$. Applying this to equation 4.132 we get:

$$\mathcal{W}(W_m, P_x) = \mathcal{W}\left(\widetilde{W}_m + \delta W_m, \tilde{p}_x + \delta p_x\right) \quad . \tag{4.133}$$

The Newton form of the equation of conservation of transverse momentum can be written as:

$$\frac{\partial \mathcal{W}}{\partial W_m}\delta W_m + \frac{\partial \mathcal{W}}{\partial p_x}\delta p_x = -\mathcal{W}\left(\widetilde{W}_m, \tilde{p}_x\right) \quad . \tag{4.134}$$

Using the results of equation 4.131 which is an expression for p_x in terms of W_m equation 4.134 can be rewritten as:

$$\left[\frac{\partial \mathcal{W}}{\partial W_m} + \frac{\partial \mathcal{W}}{\partial p_x}\frac{\partial p_x}{\partial W_m}\right]\delta W_m = -\mathcal{W}\left(\widetilde{W}_m, \tilde{p}_x\right) \quad . \tag{4.135}$$

Equation 4.135 is solved for δW for all the gaps in a given axial plane simultaneously by Gauss elimination, using an LU decomposition and a back substitution solver.

The final step of the flow solution is to update all of the previous tentative solutions using the correction terms. This can be done by:

$$W_m = \widetilde{W}_m + \delta W_m \quad , \tag{4.136}$$

for the crossflow.

Using equation 4.122 the tentative flow $\tilde{F}_m$ is corrected by:

$$F_m = \tilde{F}_m + \delta F_m \quad . \tag{4.137}$$

Using equation 4.131 the tentative pressure $\tilde{p}_x$ is corrected by:

$$p_x = \tilde{p}_x + \delta p_x \quad . \tag{4.138}$$

This solution process can be expressed step by step as:

1. Given an initial tentative crossflow $\widetilde{W}$ solve the energy equation, or equations depending on whether the thermal equilibrium on non–equilibrium option is used, for the tentative enthalpies $\tilde{h}_m$, $\tilde{h}_l$, and $\tilde{h}_v$.

2. Using the tentative enthalpy $\tilde{h}_m$ and the pressure solve for the tentative density which is a function of pressure and enthalpy $\tilde{\rho}\left(\tilde{p}_x, \tilde{h}\right)$.

3. Using the tentative density $\tilde{\rho}$ and the initial tentative crossflow $\widetilde{W}$ solve the conservation of mass equation yielding a tentative axial mass flow $\tilde{F}$.

4. Using the tentative density $\tilde{\rho}$, axial flow $\tilde{F}$ and, crossflow $\widetilde{W}$ solve tha axial momentum equation for a tentative pressure gradient $\tilde{p}_x$.

5. Using the tentative crossflow $\widetilde{W}$ and the pressure gradient $\tilde{p}_x$ solve the transverse momentum equation for the crossflow correction δW.

6. Use the crossflow correction δW to calculate the axial flow correction δF and the pressure drop correction δp then update the axial flow F, the crossflow W and the axial pressure drop p_x.

7. Return once to step 3 to drive the residual to zero.

8. If convergence is reached stop, if not, return to step 2, and iterate until convergence is reached.

The enthalpy and density are not updated in the solution process, this is done through the iterative cycle between the energy and flow solutions. If the density is linear or invarient with pressure, the solution scheme presented above yields the correct pressure, velocity, and density without iteration. A second iteration would produce zero residuals. This fact is used in ASSERT–4 along with the use of the reference pressure concept, to reduce the number of iterations to two for the flow solution at each axial plane. The block diagram of the solution scheme is given in figure 4.5.

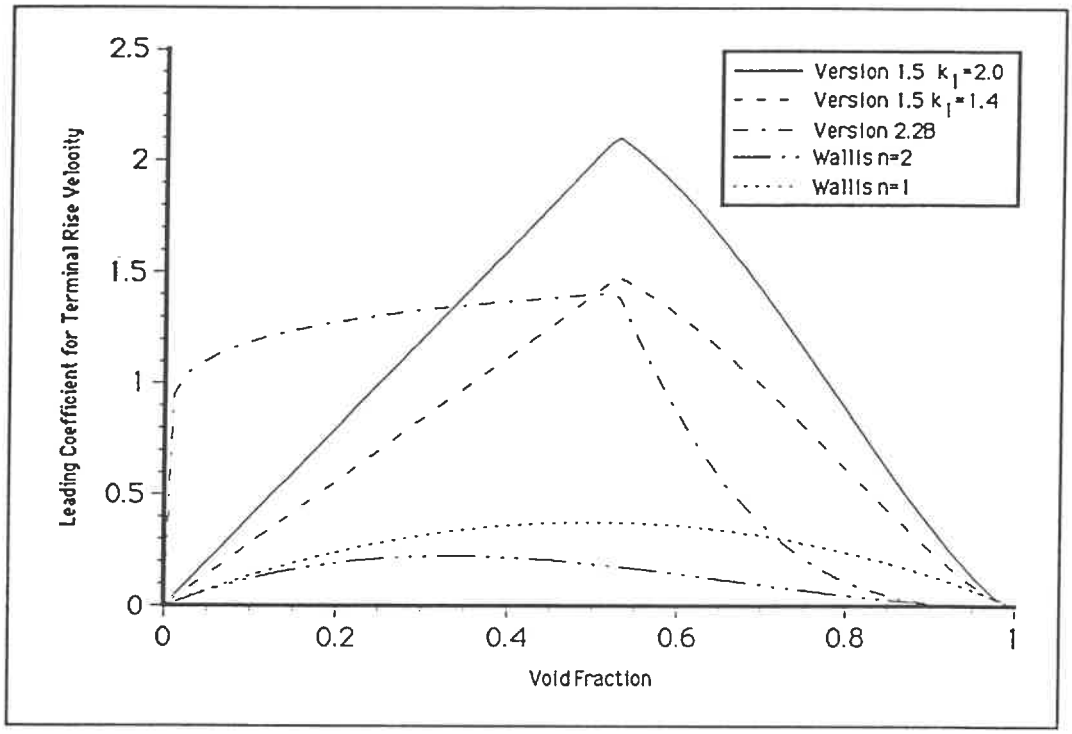

Figure 4.1: Comparison of Leading Coefficients for the Calculation of V_∞ 150 kPa

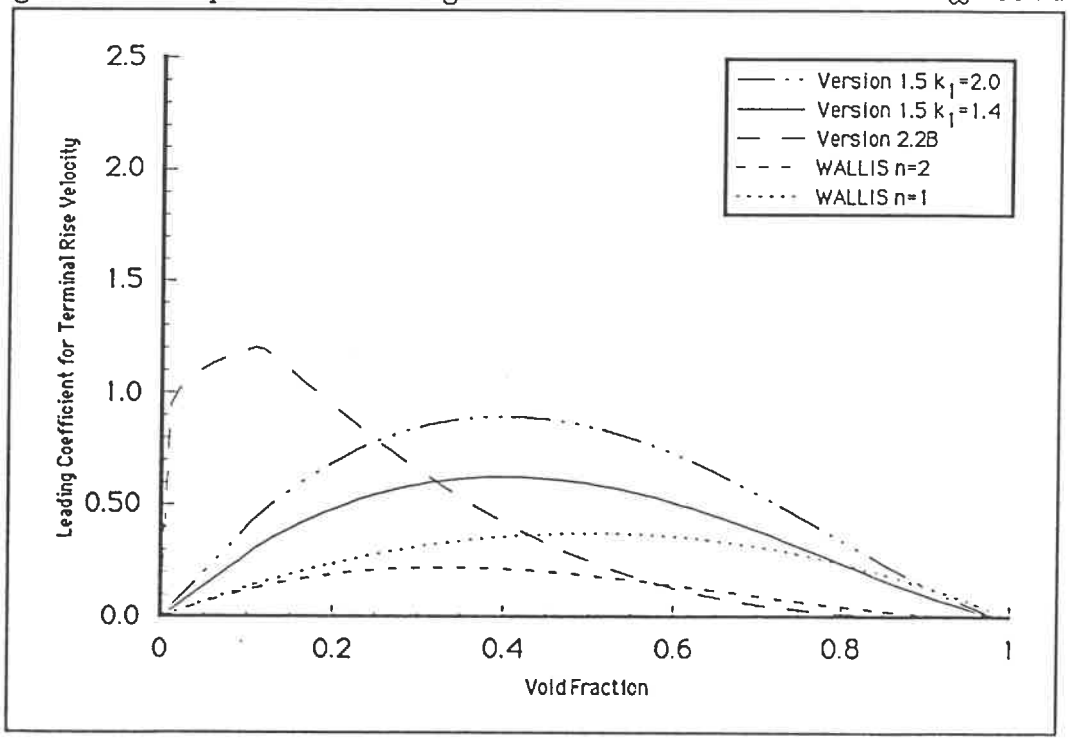

Figure 4.2: Comparison of Leading Coefficients for the Calculation of V_∞ 10 MPa

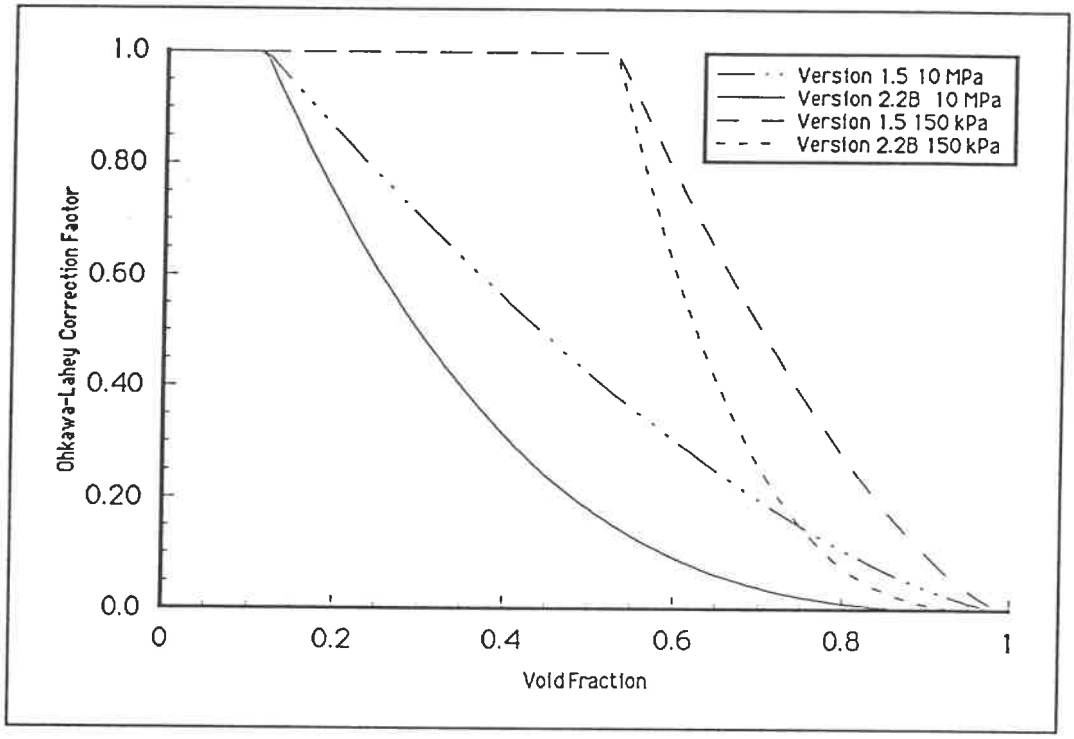

Figure 4.3: Ohkawa–Lahey Corrections Factor F for 150 kPa and 10 MPa

$$
\begin{array}{c}
\overbrace{\qquad\qquad}^{\widetilde{W}} \\
\underbrace{\mathcal{E}_m\left(h,h_\ell,h_v;\widetilde{W}\right),\mathcal{E}_\ell\left(h,h_l,h_v;\widetilde{W}\right),\mathcal{E}_v\left(h,h_\ell,h_v;\widetilde{W}\right)}_{\widetilde{h}_m,\widetilde{h}_\ell,\widetilde{h}_v} \\
\downarrow \widetilde{\rho} \\
\mathcal{F}\left(\widetilde{\rho},\widetilde{F},\widetilde{W}\right) \\
\downarrow \widetilde{F} \downarrow \\
\mathcal{M}\left(\widetilde{\rho},\widetilde{F},\widetilde{W},\widetilde{p}_x\right) \\
\downarrow \downarrow \\
\mathcal{W}\left(\widetilde{W},\widetilde{p}_x\right) \\
\downarrow \\
\overbrace{\delta F \quad \delta p_x}^{\delta W} \\
\downarrow \quad \downarrow \quad \downarrow \\
F \quad W \quad p
\end{array}
$$

Figure 4.4: Newton Solution Scheme

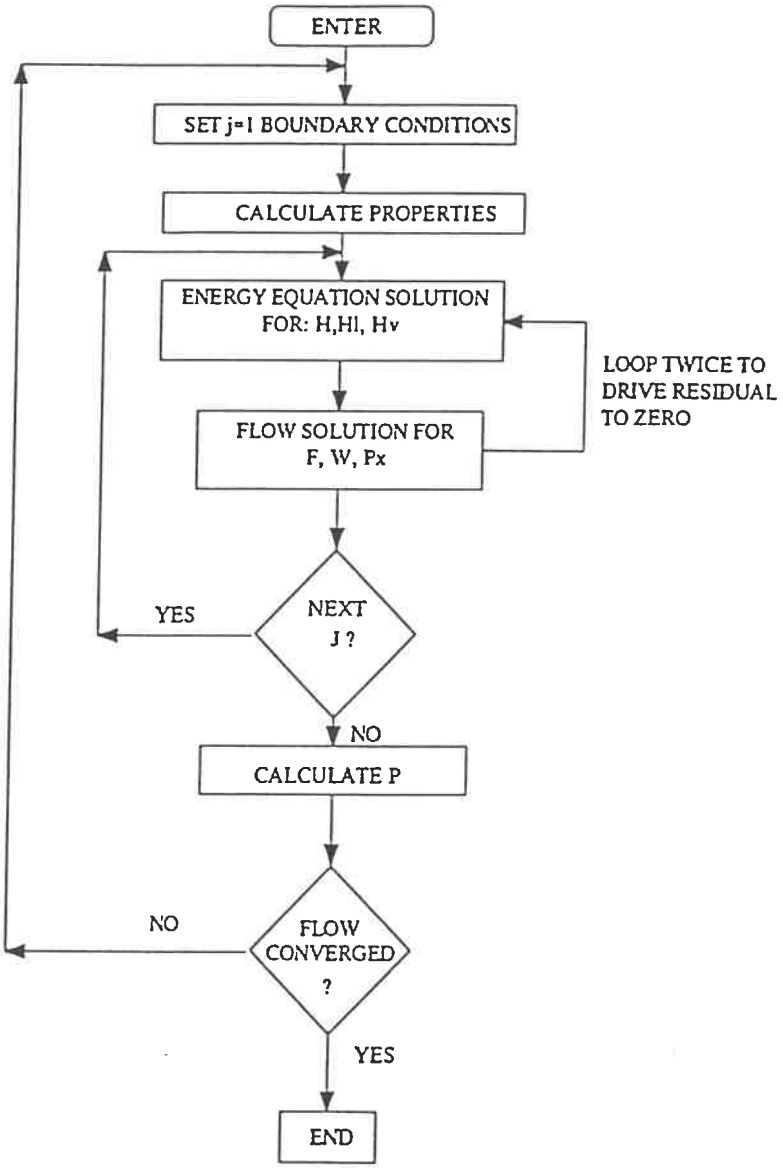

Figure 4.5: ASSERT Solution Scheme

CHAPTER 5

EXPERIMENTAL APPARATUS AND PROCEDURES

The details on the experimental apparatus and the procedures used to obtain the data which was used to compare against the predictions of ASSERT–4, as well as the experimental results are given by Tapucu et al. [1982], [1988a], [1988b] and [1990]. The descriptions of the experimental apparatus and procedures presented in this chapter are taken in large part from Tapucu [1990].

5.1 Experimental Apparatus

The apparatus enabling us to perform two interconnected channel experiments under two-phase flow conditions is shown in Figure 5.1. A cross-sectional view of the test section, representing two interconnected subchannels in a square-square rod bundle array is shown in Figure 5.2. Each half of the test section is machined from an acrylic block with a specially designed cutter, thus obtaining the desired profile with very high accuracy. The gap clearance between the rods can be varied at will. For the experiments analyzed the gap clearence was maintained constant at $1.6mm$. The relavent geometrical parameters of the test section are given in Table 5.1.

The water is supplied to the test section by a pump connected to a constant head water tank. The flow rate in each subchannel of the test section is adjusted with valves in each branch and in the corresponding bypass circuits. The air is supplied from the mains of the laboratory and regulated by a releiving type regulator.

The mixing of the liquid and the gas is acheived in a phase mixer. A cross

Table 5.1: Geometric Parameters of the Test Section–1.6 mm Gap

Rod radius	8.8 ± 0.1 mm
Gap clearence	1.6 ± 0.05 mm
CROSS-SECTIONAL AREA	
Subchannel A	116.6 ± 2 mm^2
Subchannel B	116.6 ± 2 mm^2
HYDRAULIC DIAMETERS	
Subchannel A	7.6 ± 0.2 mm
Subchannel B	7.6 ± 0.2 mm
Centroid–to–centroid distance	18.7 ± 0.1 mm
Interconnection lenght	1321 ± 5 mm

sectional view of the mixer is given in Figure 5.3. The incoming water is gradually accelerated by reducing the flow area with a solid cone mounted in the water line right at the inlet of the mixer. The conical element is followed by a cylindrical one to keep the velocity of the water high over a distance of 25.4 mm. The injection of the air through the sintered brass wall of the air chamber is done mainly in this high water velocity region. This set–up ensures an adequate mixing of the air–water mixture. Each branch of the supply system is equiped with its own phase mixer.

At the outlet of the test section, the two–phase mixture flows into an air–water seperator tank which consists of two compartments: one for each subchannel. The compartments are open to the atmosphere and their water levels are kept constant.

5.2 Instrumentation

5.2.1 Liquid and Gas Flow Rates

The water flow rates at the inlet of each of the subchannels and at the exit of subchannel A (high void channel) after the seperator tank are measured with "Flow Technology" flowmeters. According to the manufactures's specifications, the accuracy of the flowmeters is better than $\pm 1\%$ of the reading. This feature is also confirmed by our own calibration tests performed by weighing the water collected in a tank over a predetermined time interval. The flow rate of the air is measured with "Brooks" rotameters. To cover a wide range of flow rates, a set of three rotameters is used for each suchannel. For a given run, the pressure of the air at the outlet of the rotameter is kept constant. The accuracy of the rotameters is $\pm 2\%$ of full scale.

5.2.2 Void Fraction Measurement

In the past 20 years, several techniques have been developed for the measurement of the void fraction. However, the application of each technique is usually limited to a specific problem. All of the existing methods can be classified as providing either local or spatially averaged measurements.

The local methods, such as conductivity probes, film anemometers and optical fiber probes can give detailed information on the phase distribution. However, these probes have the drawback of introducing substantial perturbations in the flow patterns, especially when they are used in channels having a small flow area.

The average void fraction on a line or a surface is generally obtained by absoption of X–rays or γ–rays. The volume averaged void fraction is usually measured by quick closing valves or by impedence gauges. The neutron absorption or scattering technique becomes a sensitive and powerfull means of measuring the volume

averaged void fraction when the two–phase flow is in a steel pipe with thick walls.

One of the objectives of the present research is to obtain detailed information on the axial distribution of the average void fractions in the subchannels along the interconnection. To fulfill this requirement, the void fraction at several axial location should be measured quickly and simultaneously. Because of the simltaneous nature of the measurement, none of the above void fraction measuring techniques, with the exception of the impedence technique, is suitable for this research. Besides the advantages of simultaneous measurement, direct reading and the relatively low degree of uncertainty in the void fraction determination, the impedence technique has some disadvantages. It requires lenghty and complex calibration of the gauges, and has rather poor accuracy at high void fractions (80% or more) and finally, the response depends quite strongly on the temperature of the water and on the amount of disolved chemicals in the water supply.

As has been pointed out, the impedence technique is very suitable for the purpose of this research. With this technique, the values of the void fraction are obtained by measureing the admittance between two parallel silver electrodes (void gauges). The electrodes, cylindrical in shape and 4.75 mm in diameter, were imbedded in the acrylic blocks which form the test section and machined at the same time as the blocks to give the subchannel profile, see Figure 5.4. The sealing of the electrodes was ensured by glueing them to the acrylic block. Set–screws were used, as well as the glue, to ensure that the electrodes were held firmly in the block when flow pressure was applied on the wall of the subchannel. There are 10 pairs of electrodes in each subchannel: two pairs before the begining of the interconnected region and eight pairs in the interconnected region; they are connected to a void monitor. The positions of the electrodes are given in Figure 5.5.

The void monitor, manufactored by Auburn International Inc., was connected directly to a "Keithley DAS 500" data acquisition system. Figure 5.6 shows the

block diagram of the void fraction measurement system and its data acquistion unit. A software package was also developed to handle all the void channels simultaneously. The final results, which consist of a large amount of data (1000 points per channel and 50 ms of sampling time), were averaged and processed as graphics and output files.

A detailed block diagram of the electronic circuit associated with each electrode is given in Figure 5.7. Since all the electrodes are immersed in the same conductive media, special care should be taken to ensure that no cross conduction (resistive or reactive) occures between the measuring channels. The electric isolation of each measuring channel is acheived by coupling transformers excited from a common low impedence 5 kHz oscilator. Also, to avoid a possible current flow through the common power supply, a differential input stage with high common mode rejection and a very high input impedence is used. Since the voltage drop across the resistance R mounted between the secondaries of the coupling transformer Figure 5.7, is a direct function of the current through it, it may be assumed that this voltage is also proportional to the admittance between the electrodes, i.e., a function of the liquid fraction between them.

To correct for variations in the conductivity of the water due to temperature changes or impurities, a seperate reference channel is used to continuously monitor the admittance of the inlet water (see Figures 5.6 and 5.7). The responce of the main channels is then devided by the responce of the reference and the errors introduced by the changes mentioned above are substantially reduced.

5.2.3 Pressures

The pressure along channel B (low void channel) and pressure differences between the channels are measured with "Statham" pressure transducers located essentially every 50.8 mm over a region of 1473 mm. Figure 5.5 shows the locations

at which the pressures were measured. After conditioning, the electrical signals from the pressure transducers are sent to an integrating digital voltmeter. This allowed measurement of the pressure over a predetermined time interval (usually 50 seconds) and determination of its mean value. According to manufacturer specifications, the combined non linearity and hysteresis errors of the pressure transducer are less than 1% of the pressure excursion. They were checked periodically against "Meriam" manometers.

To prevent gas penetration into the connection line between the pressure taps and the pressure transducers, small bubble seperation pots were installed on the tubes which connect the taps to the main pressure line as shown in Figure 5.8. The tube coming from the pressure tap is connected to the top of the pot and the one going to the main pressure line is connected to the bottom of the same pot. This system limits the penetration of the bubbles to only the top of the pot when the toggle valve is opened to connect a given pressure tap to the main pressure line. The accumulation of air bubbles lowered the level of the water in the pot slightly. However, this level stabalized itself very quickly and an accurate measurement of the pressure was then possible.

The pressure in the high void subchannel, 76.2 mm upstream of the beginning of the interconnection, is measured relative to atmospheric pressure with a "Merian" manometer. Therefore, the absolute pressure along the subchannels can be determined.

5.2.4 Liquid Mass Exchange Between Subchannels

The liquid phase exchange between the channels is obtained by injecting a $NaCl$ solution into channel A (high void channel) upstream of the air–water mixer and determining the variation of salt concentration in both channels by sampling the liquid phase. A schematic diagram of the tracer sampling system is given in

Figure 5.2.

The sampling is carried out at 12 axial locations along the subchannels: two samplings before the beginning of the interconnection, 9 samplings in the interconnected region, and 1 sampling after the end of the interconnection. The position of the sampling stations are shown in Figure 5.5. In order to get a good idea of the average concentration at a given location, the sampling is also done at five different points in the transverse direction.

The sampling neddles are fully retractable, therefore they may be completely removed from the flow field when they are not in use. The salt concentration in the samples is determined by a conductivity meter with an accuracy of $\pm 1\%$. The average tracer concentration was 500 mg/l and it is assumed that the physical properties of the water, except its conductivity, are not affected.

5.3 Experimental Procedures

The interconnected subchannel experiments were carried out in two stages. The first consisted of single subchannel experiments where the impedance void gauges have been calibrated. Also in this stage the relationships between:

1. the average volumetric flux of the gas phase,
2. the volumetric flow quantity of the mixture,
3. the flow mass dryness fraction and,
4. the frictional pressure loss

with flow variables such as average void fractions and liquid phase mass fluxes have been determined. The second stage involved the two-subchannel experiments, where the information from the first stage has been used to determine the average void fraction and the net gas mass transfer in the the interconnected subchannels.

Knowledge of the frictional pressure losses is particularly important when the data is to be compared with the predictions of subchannel codes such as ASSERT.

This section will be devoted to the presentation of the experimental data obtained on single subchannel flow and to the procedures followed to determine the void fraction, the liquid phase mass exchange, the net gas mass transfer and the pressure drop in the two interconnected subchannel experiments.

5.3.1 Single Channel Calibration Experiments

5.3.1.1 Calibration of the Impedence Void Gauges

The impedence void gauges used in this research were calibrated by comparing their responce to the two-phase mixture flowing through the subchannel with the average void fraction in the whole subchannel. The average void fraction was determined by measuring the volume of water after having isolated the subchannel using quick closing valves. Because of the fluctuating nature of the flow and consequently the signals, the response of the ten impedence gauges were multiplexed for a sampling time of 50 ms, and a total of 1000 data points for each electrode were collected. The average of these values was taken as the mean value of the electrode responce. At the end of each data acquisition run the average void fraction in the test section was determined with the afore mentioned quick closing valve technique. Each subchannel was individually calibrated; during the calibration the temperature of the water was kept at 20 $\pm 1\,^{\circ}C$.

As typical examples, Figures 5.9 and 5.10 give the resulting calibration curves for void gauges A–6 and B–6 (single void gauge in subchannel A and B respectively). The liquid mass fluxes were ranged from 1000 kg/m^2s to 3000 kg/m^2s. From the calibration curves, it can be concluded that, for the subchannel geometry, void fractions up to 70 % can be measured with good accuracy. It should be pointed out that each void gauge was calibrated with its associated electronic circuit and

connection cables. The main assumption made in the calibration of the void gauges was that the changes in the void fraction along the subchannel caused by the expansion of the gas with decreasing absolute pressure could be ignored. In other words, the void fraction obtained by the quick closing valve technique adequately represents the void fraction seen by all impedance void gauges. This assumption may not be completely true when the gauges are distributed over a long distance (1422 mm in the present study) and when the pressure drop over this distance is not negligable compared to the operating pressure of the system. Therefore, the void fraction obtained from the calibration curve of each impedance gauge should be corrected to reflect the real void fraction at a given axial location. The procedure with which the correlation was done will be described later.

5.3.1.2 Frictional Pressure Losses

Because of the uncertainty involved in the calculation of frictional pressure losses in two–phase flow using correlations available in the literature, it was felt that for a better analysis of the pressure data obtained in these tests, the frictional loss charateristics of the test section should be determined experimentally. The experimental set–up for the determination of the frictional pressure losses is given in Figure 5.11. These pressure measurements were systematically taken between the pressure taps 9 and 13. The total pressure drop can be written in terms of its frictional, acceleration and gravity components, as follows:

$$\Delta p_T = \Delta p_{friction} + \Delta p_{accelaration} + \Delta p_{gravity} \quad . \tag{5.1}$$

Since the distance over which Δp is measure is small ($h_{9-13} = 203.2mm$), $\Delta p_{accelaration}$ can be neglected in comparison with $\Delta p_{friction}$. In fact, the two void gauges which are $101.6mm$ apart and located between pressure taps 9 and 13 gave no noticeable void fraction change. In the cases for horizontal flow, the gravity

component of the total pressure loss was zero; therefore the measured pressure drop was, equal to the frictional pressure loss. In the case of vertical flow, the gravitational component was subtracted from the total pressure drop to yield the frictional pressure drop.

$$\Delta p_{friction} \approx \Delta p_T - \Delta p_{gravity} \quad . \tag{5.2}$$

Where the gravitational componenent was given by:

$$\Delta p_{gravity} = h_{9-13} \left(\alpha \rho_2 + (1-\alpha)\, \rho_1\right) g \quad . \tag{5.3}$$

The frictional pressure gradient is then given by:

$$\left[\frac{dp}{dz}\right]_{friction} = \frac{\Delta p_{friction}}{h_{9-13}} \quad . \tag{5.4}$$

The pressure loss experiments were performed by keeping the liquid phase mass flow rate constant and by varying the void fraction. For each experiment, besides the pressures, the liquid flow rates, void fractions, the absolute pressure of the two-phase flow (almost half-way between the pressure taps 9 and 13), and gas flow rates have also been measured. The data on frictional pressure losses are presented in terms of the two-phase friction loss multiplier, Φ_L^2, which is defined by:

$$\Phi_L^2 = \frac{\left[\frac{dp}{dz}\right]_{TP,friction}}{\left[\frac{dp}{dz}\right]_{fo,friction}} \quad , \tag{5.5}$$

where $[dp/dz]_{fo,friction}$ is the pressure drop when the liquid phase flows alone in the subchannel. This pressure drop is given by:

$$\left[\frac{dp}{dz}\right]_{fo,friction} = f \frac{G_1^2}{2\rho_1 D_H} \quad . \tag{5.6}$$

For the friction factor, f, the following relation gives the best results (within 2-3 %) for the subchannel geometry used in this research and for Re numbers between 5000 and 50000:

$$f = 0.488 Re^{-0.3106} \quad , \tag{5.7}$$

for the channel when the gap is 1.6 mm.

Figure 5.12 shows the variation of the two-phase multiplier Φ_L^2 with mass fluxes between 1500 $kg/m^2s$and 3000 kg/m^2s for the 1.6 mm gap. This figure also includes a few points for a liquid mass flux of 1000 kg/m^2s at high void fractions.

5.3.1.3 Volumetric Flow Quality, Volumetric Flux of the Gas and Dryness Fraction

Figure 5.13 shows the relationship between the volumetric flow quality, β, and the volume averaged void fraction, $\langle\langle\langle\alpha\rangle\rangle\rangle$, for liquid mass fluxes from 1000 kg/m^2s to 3000 kg/m^2s. The data points are on or above the line $y = x$ showing that the slip ratio is equal to or greater than unity. The relationship between β and $\langle\langle\langle\alpha\rangle\rangle\rangle$ seems to be quite independant of the mass flux for void fractions up to 40 %. Beyond this limit, for a given void fraction, the volumetric flow quality decreases somewhat with increasing liquid mass flux.

Figures 5.14 and 5.15 give the relationship between the volumetric flux of the gas, $\langle j_2 \rangle$, and the void fraction, as well as the relationship between the void fraction and the flow mass dryness fraction respectively.

5.3.2 Interconnected Subchannels

The calibration curves for the responce of the electrodes and the β - $\langle\langle\langle\alpha\rangle\rangle\rangle$ relationship presented in the preceding section have been used in the interconnected

subchannel test section to determine parameters such as void fraction and gas flow rates along the interconnected region.

5.3.2.1 Void Fractions

The average responses of the void gauges located at ten points in the high and low void subchannels have been simultaneously measured. Subsequently, the void fraction corresponding to each gauge was determined by using its calibration curve which has a behaviour similar to those given in Figures 5.9 and 5.10. Each calibration curve was fitted by using Chebyshev polynomials and used by the void fraction data reduction software.

As was pointed out earlier, the calibration of the void gauges was carried out by comparing their response to the two–phase mixture flowing through the subchannel with the average void fraction in the whole subchannel as given by quick closing valves (QCV). In this procedure, the main assumption was that the variation of the void fraction along the subchannel due to the expansion of the gas could be ignored and a single value of void raction could be assigned to all the gauges. This assumption is not completely true when the probes are distributed over a long disctance and the pressure drop is substantial when compared to absolute pressure of the system. Therefore, the void fractions read from the calibration curves should be corrected with the procedure detailed below to take into account the expansion of the gas phase.

As can be seen from Figure 5.14, in both channels, void gauges A–5 and B–5 are located almost in the middle of the test section. Since the pressure variation along the subchannel is nearly linear (observed experimentally), it can be expected that the average void fraction determined by the QCV system in the whole subchannel closely reflects the void fraction existing at the level of these gauges and, their calibration curve is reasonably accurate. In addition, the relationship between

the volumetric flux of the gas ($\langle j_2 \rangle$), the liquid mass flux and the void fraction (Figure 5.15), and the absolute pressure at the level of these void gauges have been determined. Because of the expansion of the gas, the calibration curves for the gauges upstream of gauge #5 will overestimate the void fraction and those downstream of gauge #5 underestimate the void fraction. The degree of overestimation and underestimation increases with increasing distance from gauge #5.

Using the relationship $\langle j_2 \rangle = j_2 (\langle j_2 \rangle, m_1)$, the void fractions obtained using the responce and the calibration curves of the gauges upstream and downstream of gauges a–5 and B–5 can be corrected to obtain the real void fraction. This correction has been conducted as follows.

1. Under single subchannel flow conditions and using the void fraction measured by gauge #5, determine the total pressure drop gradient.

2. Assuming a linear pressure variation along the subchannel and knowing the absolute pressure at the level of the fifth void gauge determine the absolute pressures at the level of void gauges #1 and #10.

3. Knowing the volumetric flux density of the gas at the level of void gauge #5, determine this flux density at the level of void gauges #1 and #10.

4. Using the relationship $\langle j_2 \rangle - \langle \alpha \rangle$ for a liquid mass flux of 3000 $kg/m^2 s$ (Figure 5.15), determine the void fraction at the level of gauges #1 and #10.

Figure 5.16 gives the plot of $\varepsilon_{10} = \alpha'_{10}/\alpha_{10}$ and $\varepsilon_1 = \alpha'_1/\alpha_1$ (α is the void fraction obtained from the calibration curve and α' is the true void fraction) as a function of α_n. It should be pointed out that according to our void gauge calibration procedures, under single subchannel flow conditions, for a given mixture in the subchannel all gauges yield the same void fraction, i.e.: $\alpha_1 = \ldots = \alpha_n = \ldots = \alpha_{10} = \alpha_{QCV}$. For gauges between gauges #1 and #5, and gauges #5 and #10, $\varepsilon_n = \alpha'_n/\alpha_n$ are assumed to be given by:

$$\varepsilon_n = \frac{\alpha'_n}{\alpha_n} = 1 + (\varepsilon_1 - 1)\frac{z_{5-n}}{z_{5-1}} \quad n = 1,2,3,4,5 \quad , \tag{5.8}$$

for gauges between gauges #1 and #5, and by:

$$\varepsilon_n = \frac{\alpha'_n}{\alpha_n} = 1 + (\varepsilon_{10} - 1)\frac{z_{5-n}}{z_{5-10}} \quad n = 5,6,7,8,9,10 \quad , \tag{5.9}$$

for gauges between #5 and #10; where z_{5-n} distance of the n^{th} gauge from the fifth gauge. In interconnected subchannels, the value of the void fraction determined using the calibration curve of the n^{th} gauge (α_n) is therfore corrected by multiplying this by ε_n determined from relationships 5.8 or 5.9. The value ofε_1 or ε_{10} is determined from the void correction curve (Figure 5.16) by using the void α_n determined by the calibration curve.

5.3.2.2 Liquid Phase Mass Exchanges

In section 5.2.4, the method with which the liquid mass exchanges between the subchannels were determined, was outlined. This method consisted of injecting a salt solution into the high void subchannel and determining the variation of salt concentrations in both subchannels. To get a good idea of the average concentration at a given flow section, the sampling is done at five points in each subchannel on the line joining their centroids. The radial sampling positions are shown in Figure 5.17. This section deals with the determination of the average concentration over the flow section and with the derivation of the tracer mass conservation equations which allow us to determine the liquid masses exchanged between the subchannels when the axial variation of the average tracer concentration are known in both of them. The average tracer flux across the subchannel flow section is given by:

$$\frac{\iint \rho_1 j_1 C dA}{\iint dA} = \langle\langle \rho_1 j_1 C \rangle\rangle = \rho_1 \langle\langle j_1 C \rangle\rangle \quad , \tag{5.10}$$

where j_1 is the local superficial velocity of the liquid. Since no information is available on the local values of $\langle\langle j_1 C\rangle\rangle$ it is assumed that:

$$\langle\langle j_1 C\rangle\rangle \approx \langle\langle C\rangle\rangle \langle\langle j_1\rangle\rangle \quad , \tag{5.11}$$

and equation 5.10becomes:

$$\iint \rho_1 j_1 C dA = A\rho_1 \langle\langle j_1\rangle\rangle \langle\langle C\rangle\rangle = m_1 \langle\langle C\rangle\rangle \quad , \tag{5.12}$$

where $\langle\langle C\rangle\rangle$ is the cross–sectional average of the tracer concentration and is given by:

$$\frac{\iint C dA}{\iint dA} \quad . \tag{5.13}$$

In order to carry out the above integral, the cross–section of each subchannel is devided into four regions of 4.75 mm width (region I through region IV in Figure 5.18) accounting respectively for 10%, 40%, 40%, and 10% of the total subchannel area. It is also assumed that the average concentration in a region can be adequatly represented by the concentration obtained by a simple interpolation at the midpoint of this region. Two methods were used to determine the midpoint concentration.

METHOD I

In this method, the concentration at the midpoint of region I through III (C_{1A}, C_{2A}, and C_{3A} in Figure 5.18) are determined by interpolating the concentrations measured at the sampling positions preceeding and following this piont. The average concentration in region IV is obtained by extrapolating the measured concentration C_{3A} and C_{4A} to the midpoint of this region; this approach avoids using the information in the neighbouring channel. Obviously the same procedure is applied to the second channel.

METHOD II

In this method it is assumed that the average concentration in a region is best represented by an average of the concentrations at the boundary of the region (L_{1A}, L_{2A}, ... in Figure 5.19) determined by interpolation of the measured concentrations. This method uses interpolation between C_{4A} and C_{4B} to evaluate the concentration at the interface of the subchannels (point L in Figure 5.19). The cross–sectional average of the concentration is then given by:

$$\langle\langle C\rangle\rangle = \frac{\sum_{n=1}^{4} C_n \Delta A_n}{A} \quad , \tag{5.14}$$

C_n is the average of the tracer concentration in a region determined with the above methods, A_n is the area of the region and,

$$A = \sum_{n=1}^{4} \Delta A_n \quad . \tag{5.15}$$

A comparison of channel average concentration determined using the above methods with that determined by measuring the area under the concentration profile in each region with a planimeter has shown that Method I slightly overestimates the average concentration in the high void subchannel (also high concentration subchannel) and slightly underestimates it in the low void subchannel (also low concentration subchannel). The opposite situation has been observed with Method II. However, the arithmetic average between Method I and II agreed very satifactoraly with the planimeter results. Therefore, in reducing the data on liquid mass exchanges between the subchannels the arithmetic averages of the concentrations determined with the above methods have been used.

In order to derive the mass and tracer conservation equations, let us consider Figure 5.20 which shows the liquid mass flows entering and leaving the control volume as well as the tracer influx and efflux.

Applying the mass conservation principle to the control volumes and denoting by δw and $\delta w'$ respectively, the masses transfered from high void subchannel to

low void subchannel and vice versa, the following equations can be written:
High void channel (i),

$$\delta w - \delta w' = -\frac{m_i}{\Delta z} dz \quad , \tag{5.16}$$

Low void channel (j),

$$\delta w - \delta w' = \frac{m_j}{\Delta z} dz \quad . \tag{5.17}$$

In turn the mass conservation principle applied to the tracer yields: High void channel (i),

$$C_i \delta w - C_j \delta w' = -\frac{C_i m_i}{\Delta z} dz \quad , \tag{5.18}$$

Low void channel (j),

$$C_i \delta w - C_j \delta w' = \frac{C_j m_j}{\Delta z} dz \quad , \tag{5.19}$$

where m and C are the mass flow rate and the cross sectional average of the tracer concentration in the subchannel respectively.

Discretization of equation 5.16 through 5.19 gives:

Mass Conservation

High void subchannel (i),

$$m_{i,n+1} - m_{i,n} - \Delta w'_{n+1/2} + \Delta w_{n+1/2} = 0 \quad , \tag{5.20}$$

Low void subchannel (j),

$$m_{j,n+1} - m_{j,n} - \Delta w_{n+1/2} + \Delta w'_{n+1/2} = 0 \tag{5.21}$$

The addition of equations 5.20 and 5.21 gives:

$$m_{i,n} + m_{j,n} - m_{i,n+1} - m_{j,n+1} = 0 \tag{5.22}$$

Tracer Conservation

High void subchannel (i),

$$m_{i,n+1}C_{i,n+1} - m_{i,n}C_{i,n} + C_{i,n+1/2}\Delta w_{n+1/2} - C_{j,n+1/2}\Delta w'_{n+1/2} = 0 \tag{5.23}$$

Low void subchannel (j),

$$m_{j,n+1}C_{j,n+1} - m_{j,n}C_{j,n} - C_{i,n+1/2}\Delta w_{n+1/2} + C_{j,n+1/2}\Delta w'_{n+1/2} = 0 \tag{5.24}$$

Combining Equations 5.20,5.21,5.23, and 5.24 the values of $\Delta w_{n+1/2}$ and $\Delta w'_{n+1/2}$ can be written as:

$$\Delta w'_{n+1/2} = \frac{m_{i,n}\left(C_{i,n+1/2} - C_{i,n}\right)}{C_{j,n+1/2} - C_{i,n+1/2}} + \frac{m_{i,n+1}\left(C_{i,n+1} - C_{i,n+1/2}\right)}{C_{j,n+1/2} - C_{i,n+1/2}} \tag{5.25}$$

$$\Delta w_{n+1/2} = \frac{m_{j,n}\left(C_{j,n+1/2} - C_{j,n}\right)}{C_{i,n+1/2} - C_{j,n+1/2}} + \frac{m_{j,n+1}\left(C_{j,n+1} - C_{j,n+1/2}\right)}{C_{i,n+1/2} - C_{j,n+1/2}} \tag{5.26}$$

Substituting 5.25 and 5.26 into Equation 5.19 and taking into account Equation 5.21 for the mass flow rates in the high void channel (i), the following relationship results:

$$m_{i,n+1} = m_{i,n}\frac{C_{i,n} - C_{j,n+1}}{C_{i,n+1} - C_{j,n+1}} - m_{j,n}\frac{C_{j,n+1} - C_{j,n}}{C_{i,n+1} - C_{j,n+1}} \tag{5.27}$$

All concentrations appearing in Equation 5.27 have been determined experimentally. Moreover, the tracer concentration at the inlet of the high void subchannel ($C_{i,0}$) as well as the flow rates to the subchannels have also been determined.

5.3.2.3 Net Gas Mass Transfer

The net gas mass transfer from the high void subchannel to the low void subchannel and vise versa is determined by using the information on liquid phase volume flow rates (as determined by the tracer technique) and void fractions along the interconnected region in conjunction with the volumetric flow quality curve, $\beta = \beta(\langle\alpha\rangle, m_1)$, obtained under single subchannel flow conditions and given in Figure 5.20. The volumetric flow quality is defined as:

$$\beta = \frac{Q_2}{Q_2 + Q_1} \quad , \tag{5.28}$$

where Q_2 and Q_1 are the volume flow rates of the gas and liquid phases respectively. From the relation given by equation 5.28, Q_2 can be written as follows:

$$Q_2 = \frac{\beta Q_1}{1 - \beta} \quad . \tag{5.29}$$

Since the variation of the void fraction and liquid mass flow rate is known, the values of β in the high and low void subchannels can be determined from Figure 5.20. Equation 5.29 is the used to determine the gas flow rates in the subchannels.

It should be pointed out that the flow pressure in the single subchannel calibration experiments, where the relationship $\beta = \beta(\langle\alpha\rangle, m_1)$ is determined, may differ from the flow pressure in the interconnected subchannels. A set of experiments were conducted by Tapucu et al.[ref] to determine the effect of the varying pressure on the volumetric quality for a given liquid flow rate and void fraction. It is observed that, for liquid mass fluxes higher than $1800 kg/m^2 s$ and for the pressure range from 120 kPa to 120 kPa, the volumetric quality is independent of the flow pressure. Some effect of the pressure on the volumetric flow quality has been reported in the above reference for liquid mass fluxes less then $1400 kg/m^2 s$ and for void fractions higher than 55 %. It should be noted that in the two-subchannel

experiments used in for the comparison with ASSERT-4 that the liquid mass fluxes at the inlet of each subchannel were $3000 kg/m^2 s$.

An error analysis done in [Tapucu, et al., 1988b] showed that the uncertainty in this method depends on the void fraction and it is evaluated to be 6 % and 12 % for void fractions of 10 % and 60 % respectively. Therefore, for better accuracy, the gas mass flow rates were determined in the low void subchannel. The flow rates in the neighbouring subchannel were obtained by taking the difference between the total gas mass flow to the test section and the gas mass flow rates determined in the low void subchannel.

5.3.2.4 Pressures

In horizontal flow, the pressure differential measured by the axial pressure transducer between a given pressure tap and the reference pressure tap ($\Delta p_{a,measured}$) directly yields the total pressure loss. Therefore, contrary to vertical flow, no correction to the measured axial pressure losses is necessary to obtain the true pressure drop.

However, some correction to the measured pressure difference between the subchannels was necessary to take into account the water column in the pressure line corresponding to the difference of elevation between the two pressure taps in the same radial plane (Figure 5.21, 5.22, and 5.23). Furthermore, in the presentation of the data on the radial pressure differences, the gravity effect caused by the column of two-phase mixture between the taps is not included. Therefore, the radial pressure difference, Δp_r, caused by friction and acceleration components is given by:

$$\Delta p_r = (p_A = p_B) = \Delta p_{r,measured} \pm h \rho_1 g \cos(\Theta) \pm \Delta p_{gravity} \quad , \qquad (5.30)$$

where h is the distance between pressure taps in the same radial plane and Θ is

the angle of the centroid–to–centroid axis of the test section with the vertical. The term $h\rho_1 g\cos(\Theta)$ shows the correction for the water column in the pressure line is a added to or subtracted from $\Delta p_{r,measured}$ depending on whether the high void subchannel is below (Figure 5.21) or above (Figure 5.22) the low void subchannel. Also, the gravity component of the pressure loss is subtracted from or added to $\Delta P_{r,measured}$ depending on whether it is connected on the high side (Figure 5.21) or the low side (Figure 5.22) of the pressure transducer. Consequantly, the following relationships have been used to determine Δp_r:

1. High void subchannel below the low void subchannel $SH_{\frac{LV}{HV}}$ (Figure 5.21):

$$\Delta p_r = \Delta p_{r,measured} + h\rho_1 g - h\rho_1 g\left(1 - \frac{\alpha_{HV} + \alpha_{LV}}{2}\right) \quad . \tag{5.31}$$

2. High void subchannel above the low void subchannel $SH_{\frac{HV}{LV}}$ (Figure 5.22):

$$\Delta p_r = \Delta p_{r,measured} - h\rho_1 g + h\rho_1 g\left(1 - \frac{\alpha_{HV} + \alpha_{LV}}{2}\right) \quad . \tag{5.32}$$

3. High void subchannel at the same elevation as the low void subchannel $SH_{HV=LV}$ (Figure 5.23):

$$\Delta p_r = \Delta p_{r,measured} - d\rho_1 g\left(\alpha_{LV} - \alpha_{HV}\right) \quad . \tag{5.33}$$

The meaning of d and h are given in Figures 5.21, 5.22, and 5.23, and α_{HV} and α_{LV} are the void fraction in the high and low void subchannels respectively.

The errors in the directly measured quantites, the indirectly measured quantities and the gas mass exchange are given in tables 5.2, 5.3 and 5.4 respectively.

Table 5.2: Relative Error of Directly Measured Quantities

APPARATUS	ERROR(%)
Temperature	0.5
Hg–Manometer	1.0
Turbine Flow Meter	1.0
Rotameters (A1–B1)	3.0
Rotameters (A2–B2)	2.0
Rotameters (A3–B3)	4.0
Void Fraction	3.0
Conductivity	2.0
Pressure Transducers	1.0

Table 5.3: Relative Error of Indirectly Measured Quantities

PHYSICAL QUANTITY	ERROR (%)
Axial Pressure	1.2
Radial Pressure	1.0
Liquid Mass Transfer	4.0

Table 5.4: Errors on the Gas Mass Exchange (%)

VOID FRACTION (%)	$Q_1 = 1.2m^3/h$	$Q_1 = 1.8m^3/h$
10	6.0	6.0
20	6.0	6.0
40	7.0	7.0
50	8.0	8.0
60	12.0	10.0

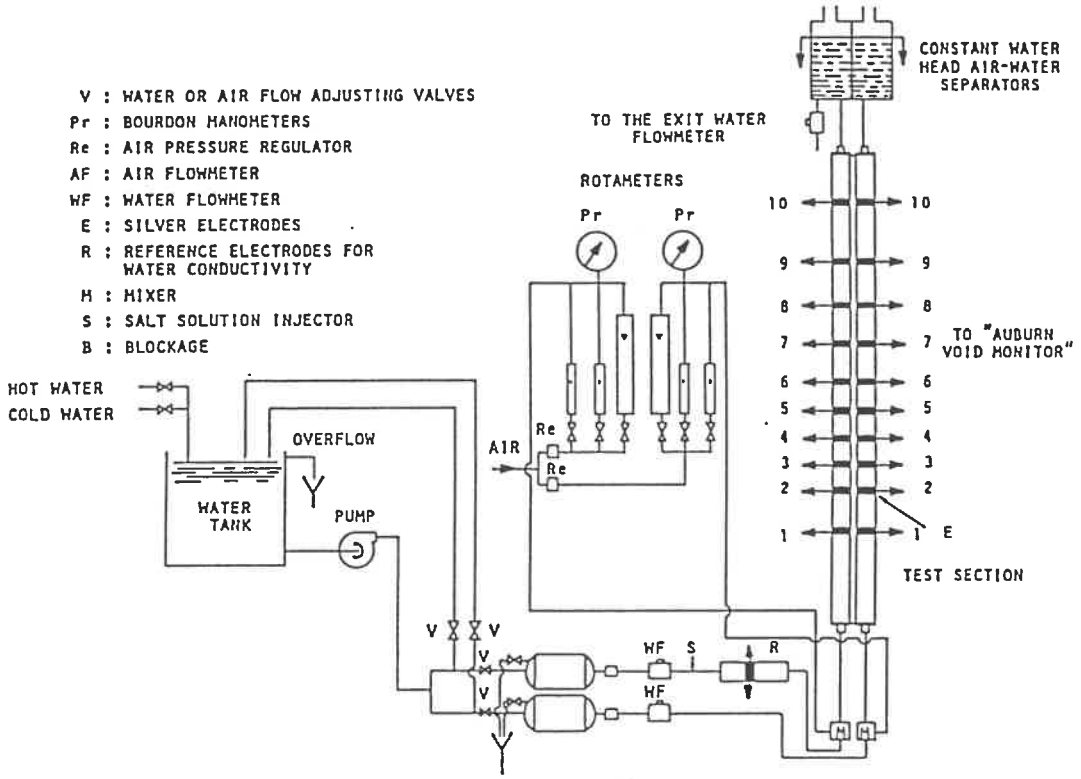

Figure 5.1: Two-Phase Flow Experimental Apparatus

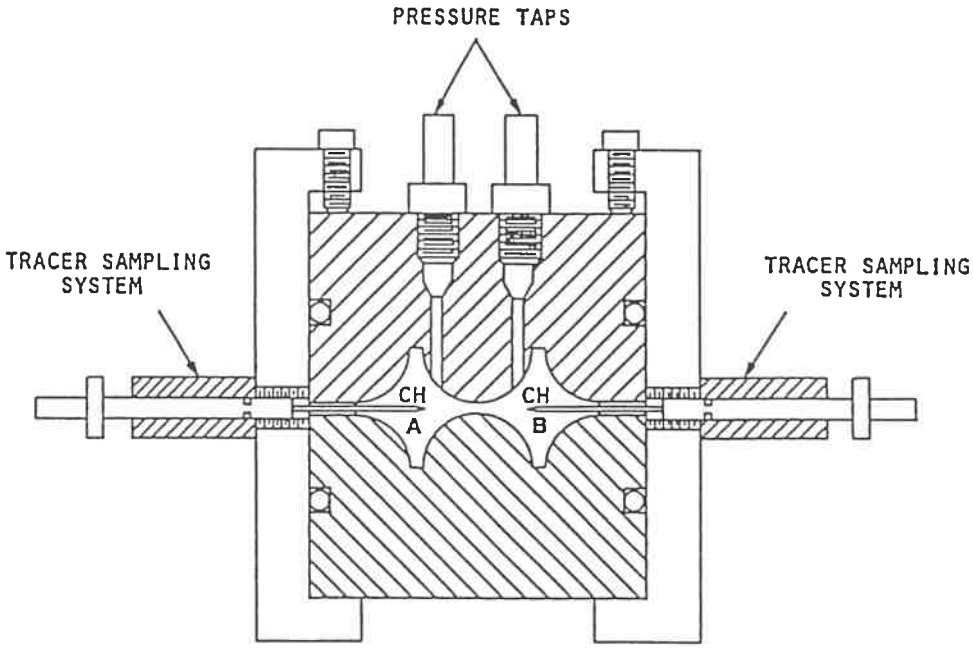

Figure 5.2: Cross-Sectional View of the Test Section

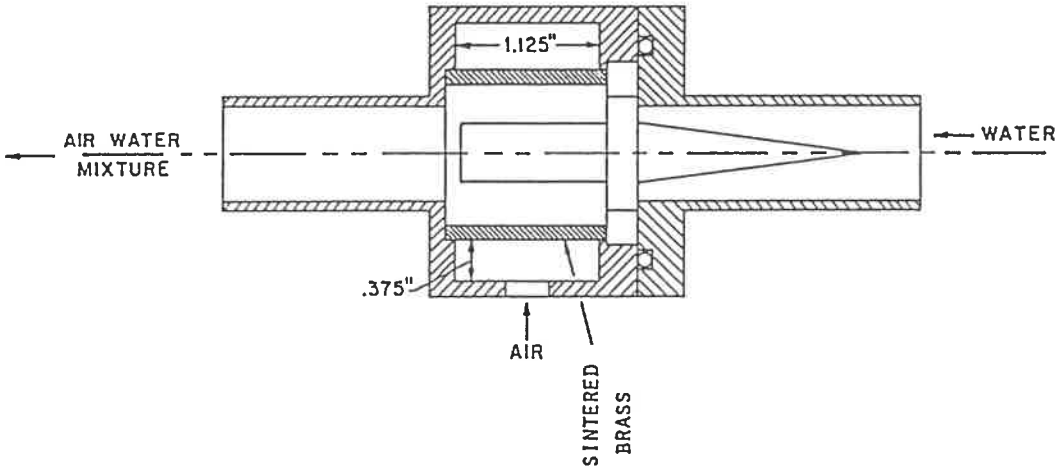

Figure 5.3: Air-Water Mixer

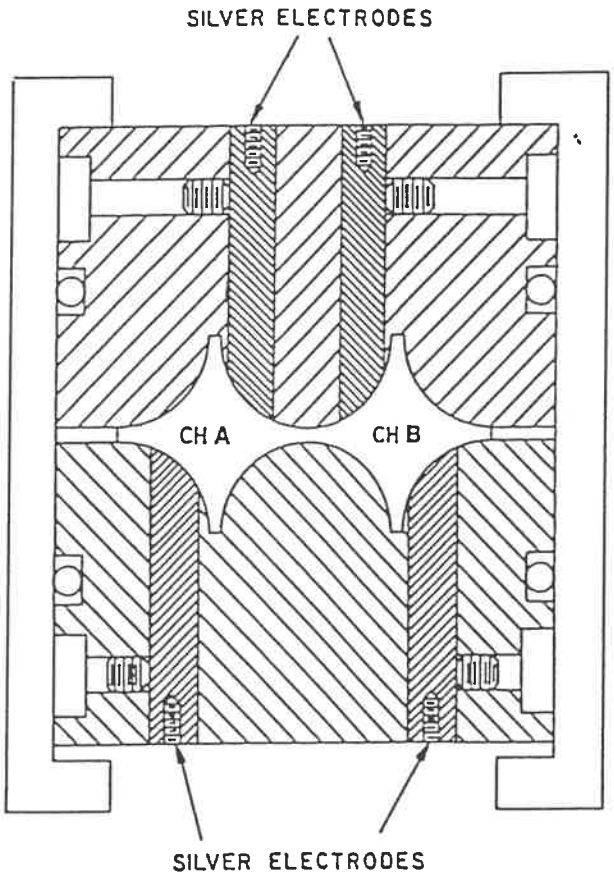

Figure 5.4: Impedance Gauges

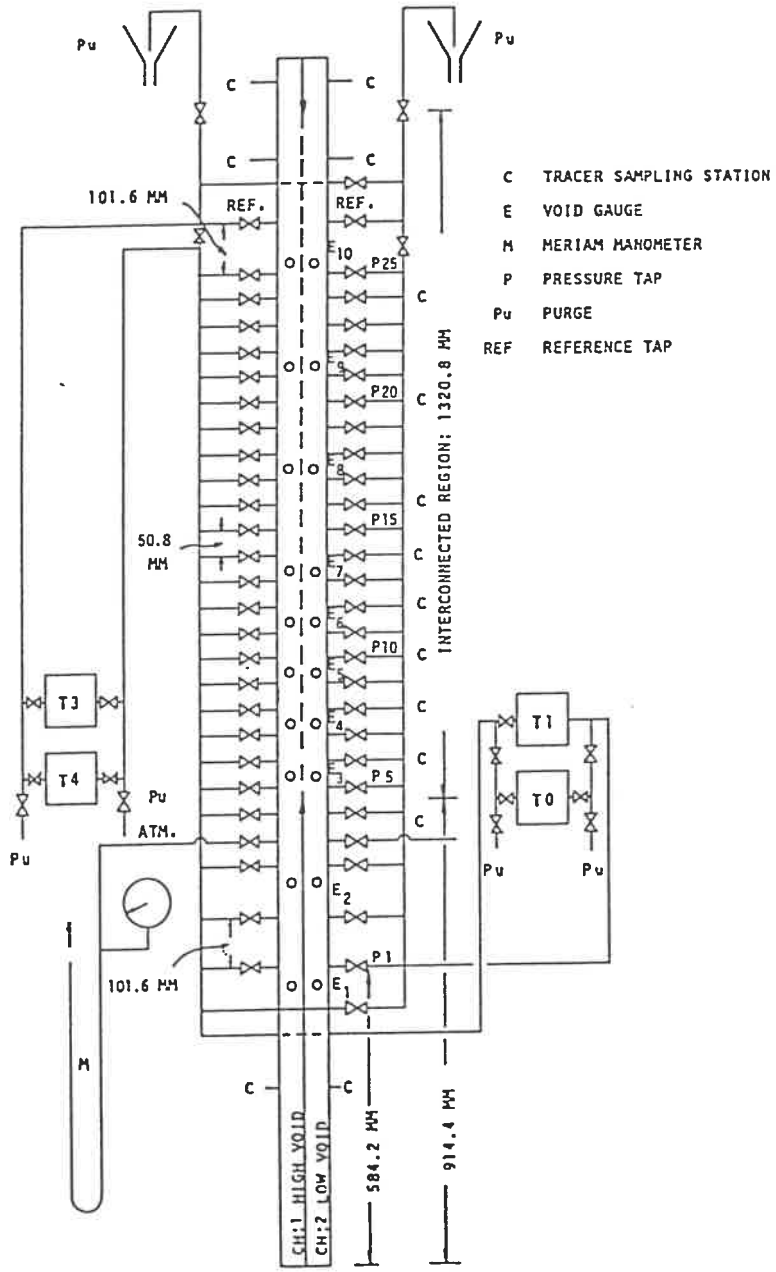

Figure 5.5: Location of the Void Gauges, Pressure Taps and Sampling Stations

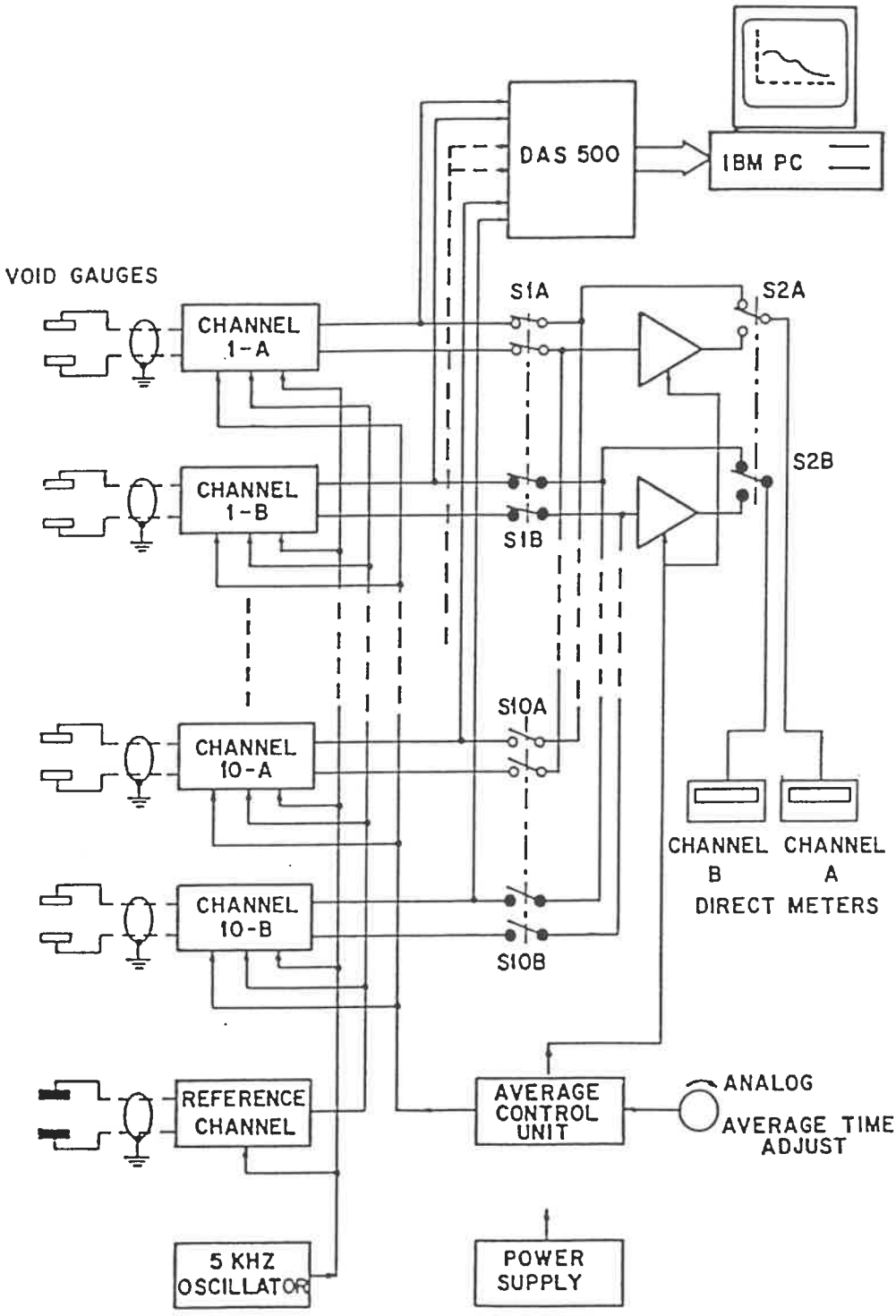

Figure 5.6: Block Diagram of the Void Measurement System

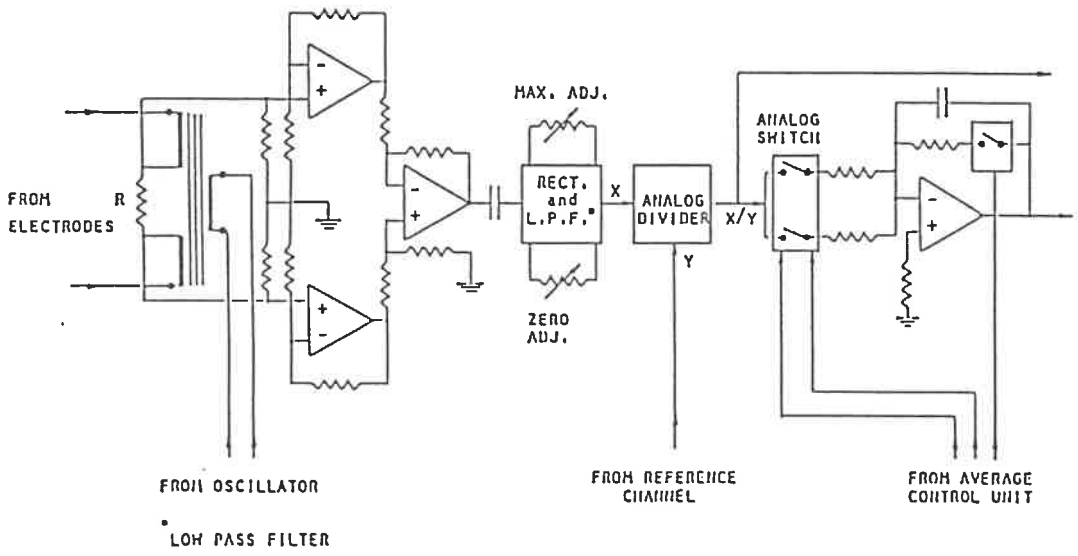

Figure 5.7: Block Diagram of the Electronics for the Void Measurement System

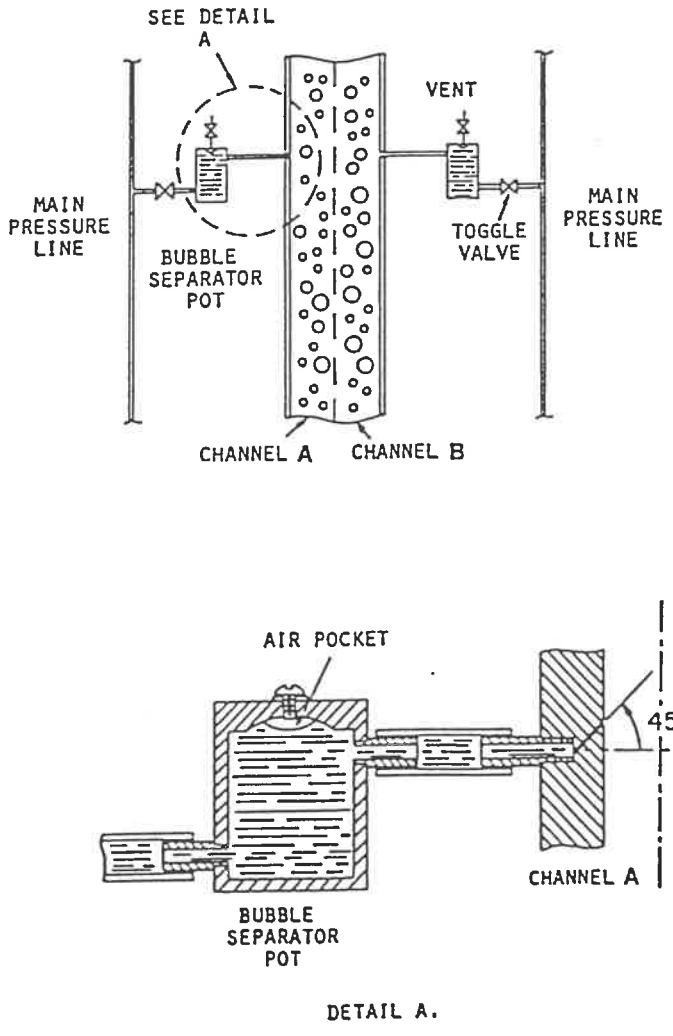

Figure 5.8: Gas Phase Seperation Pots

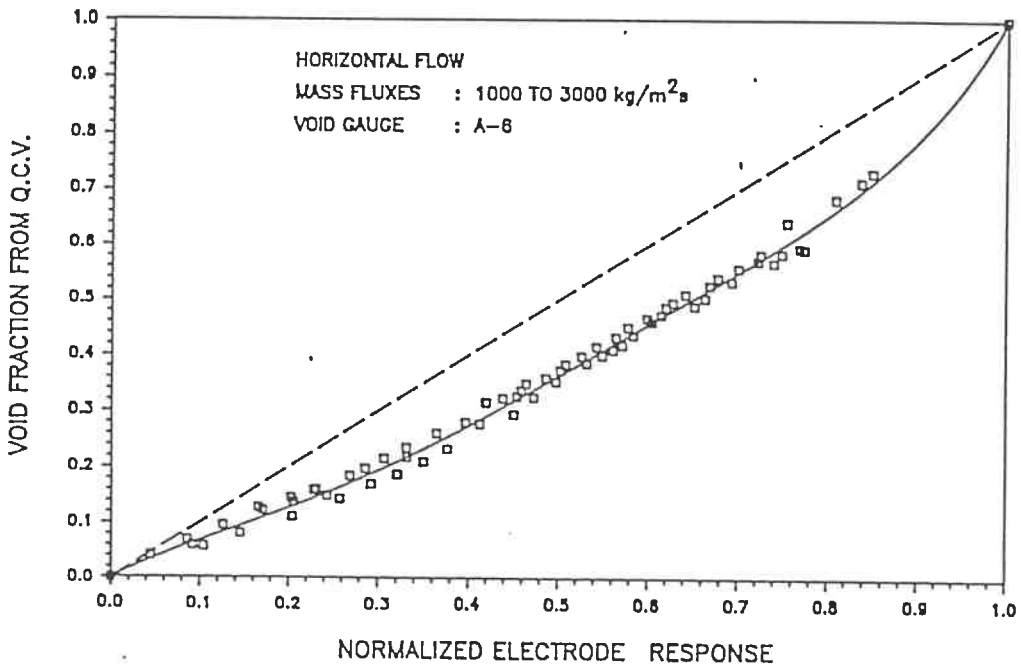

Figure 5.9: Typical Calibration Curve of a Void Gauge–Channel A

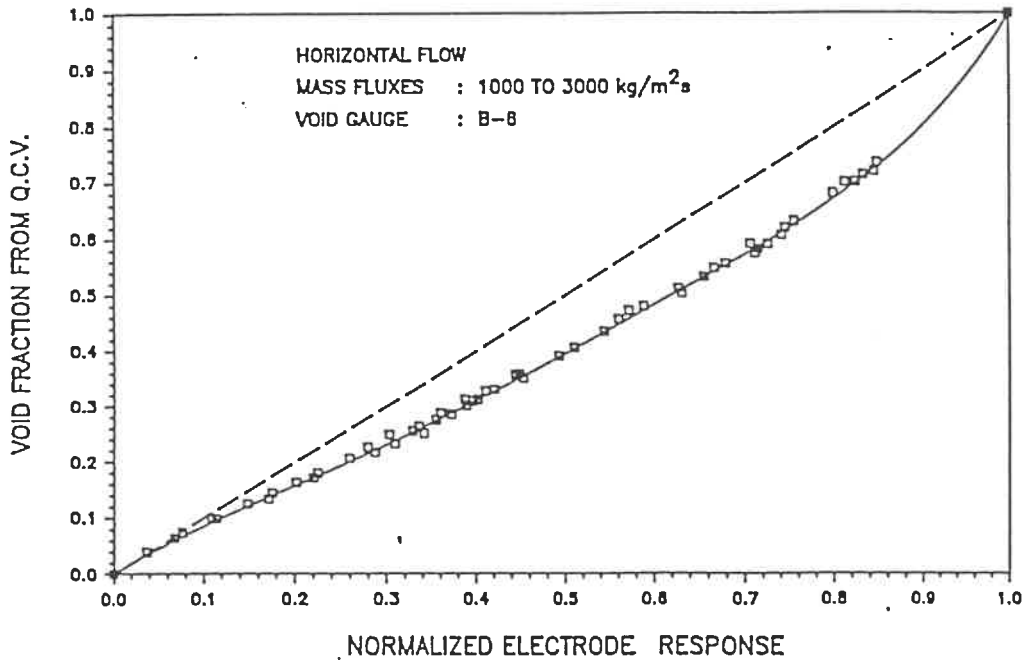

Figure 5.10: Typical Calibration Curve of a Void Gauge–Channel B

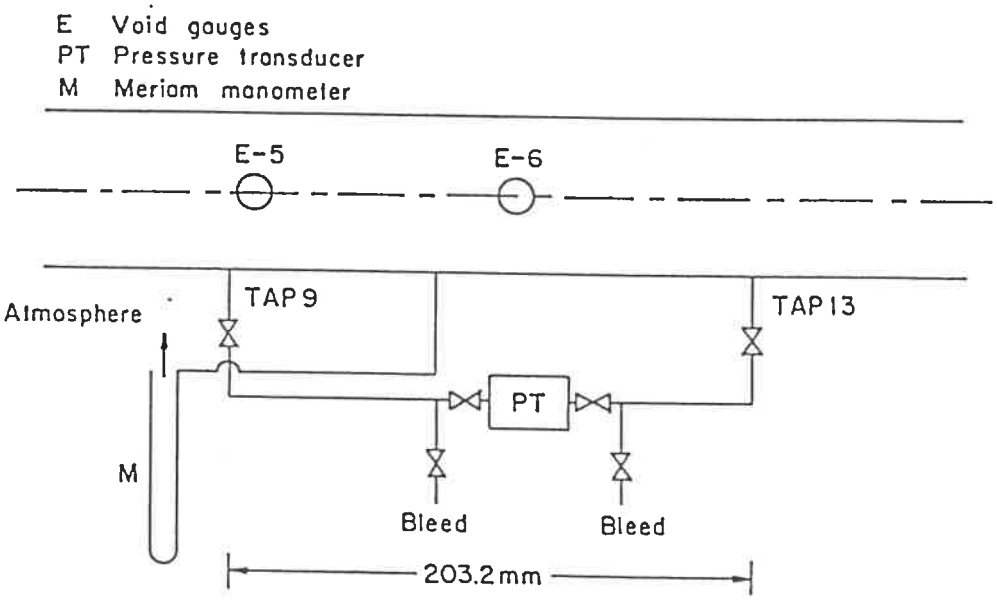

Figure 5.11: Set-Up for Frictional Pressure Loss

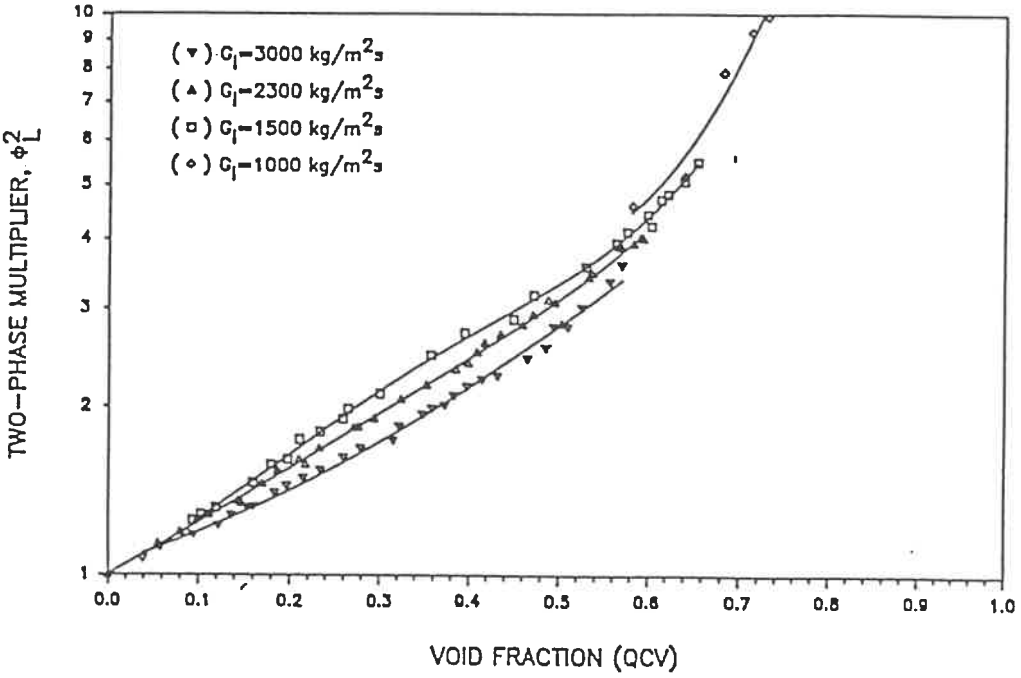

Figure 5.12: Variation of the Two-Phase Multiplier with Void Fraction-1.6 mm Gap

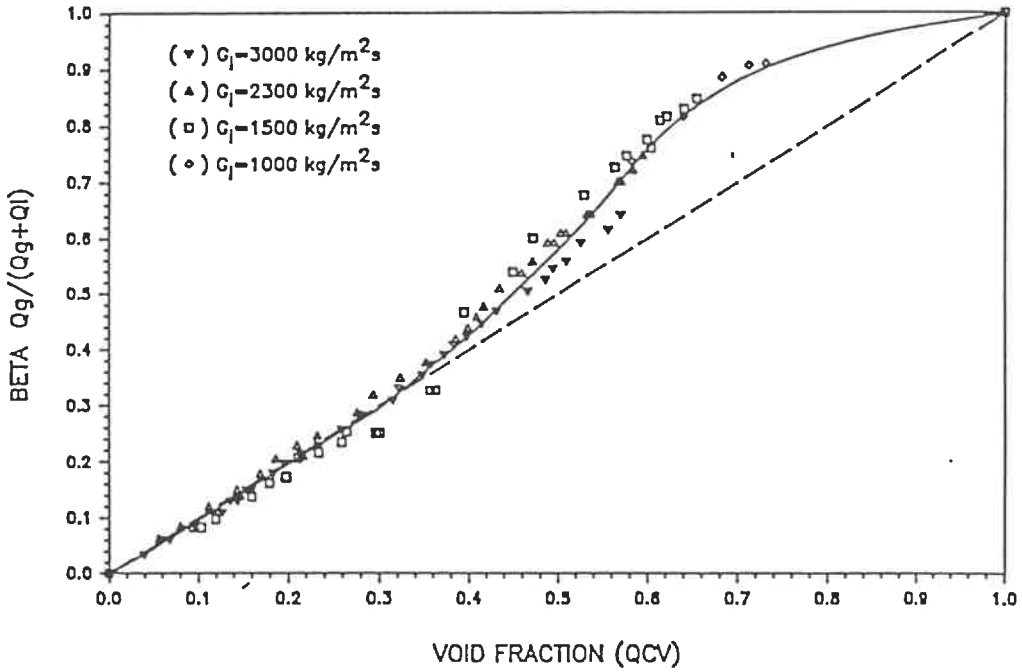

Figure 5.13: Relationship Between the Volumetric Flow Quality and Void Fraction

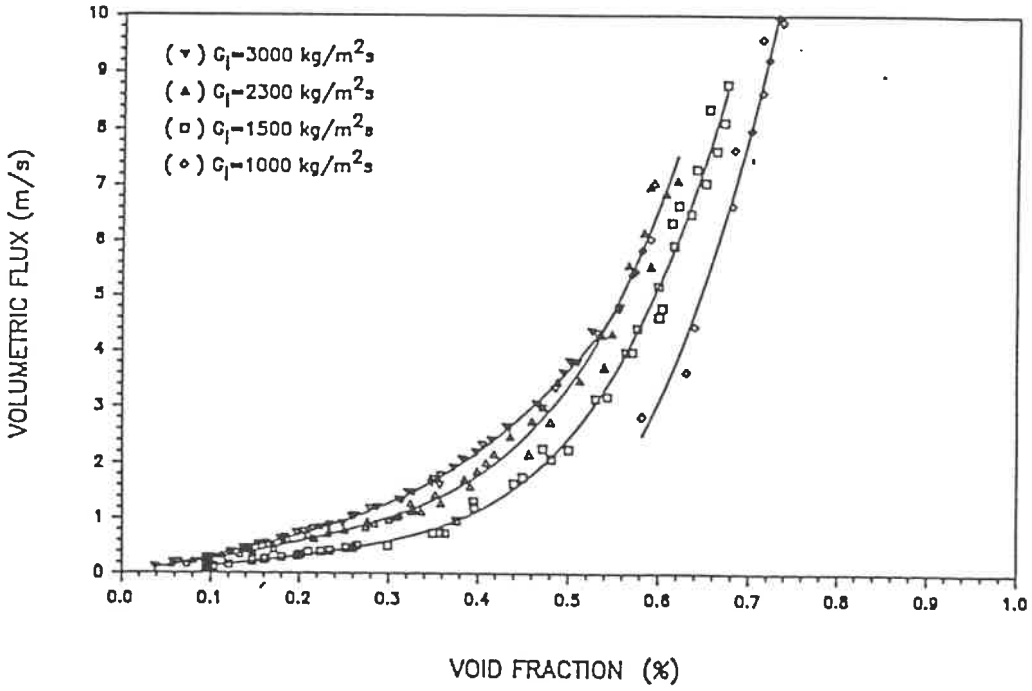

Figure 5.14: Relationship Between the Volumetric Flux of the Gas and Void Fraction

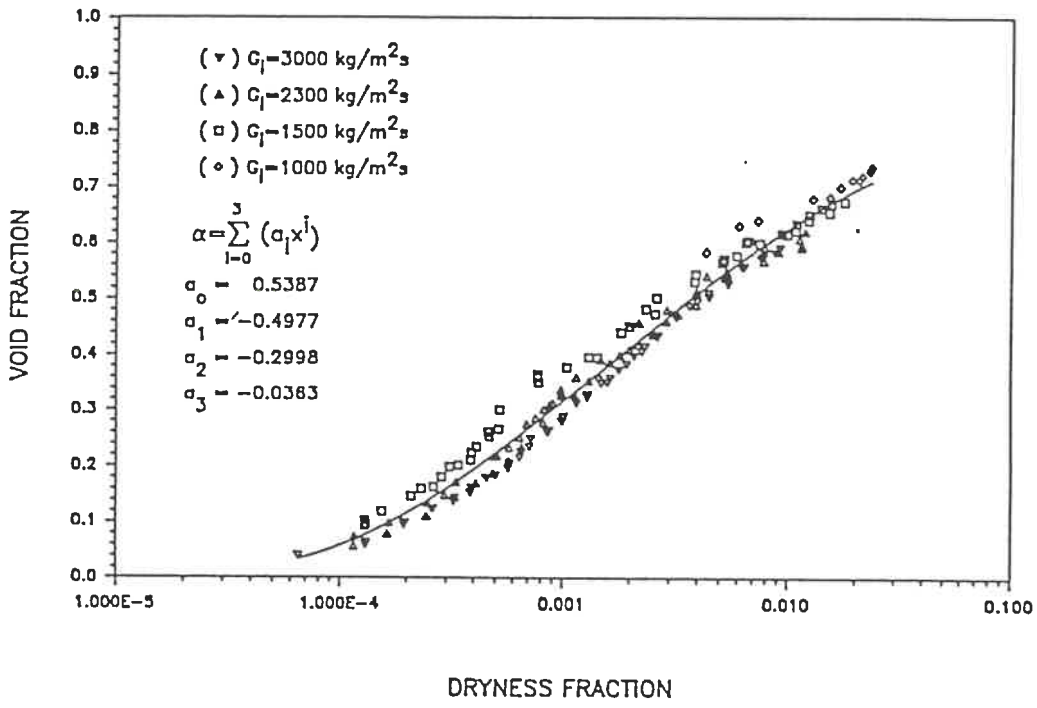

Figure 5.15: Relationship Between the Void Fraction and the Dryness Fraction

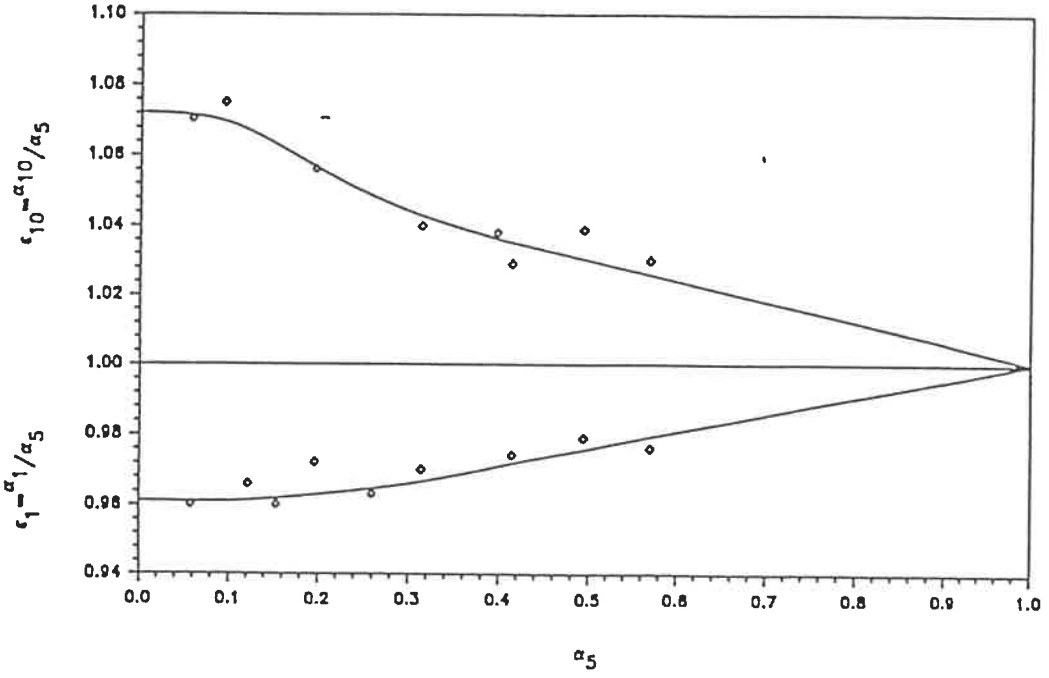

Figure 5.16: Void Fraction Correction Curve

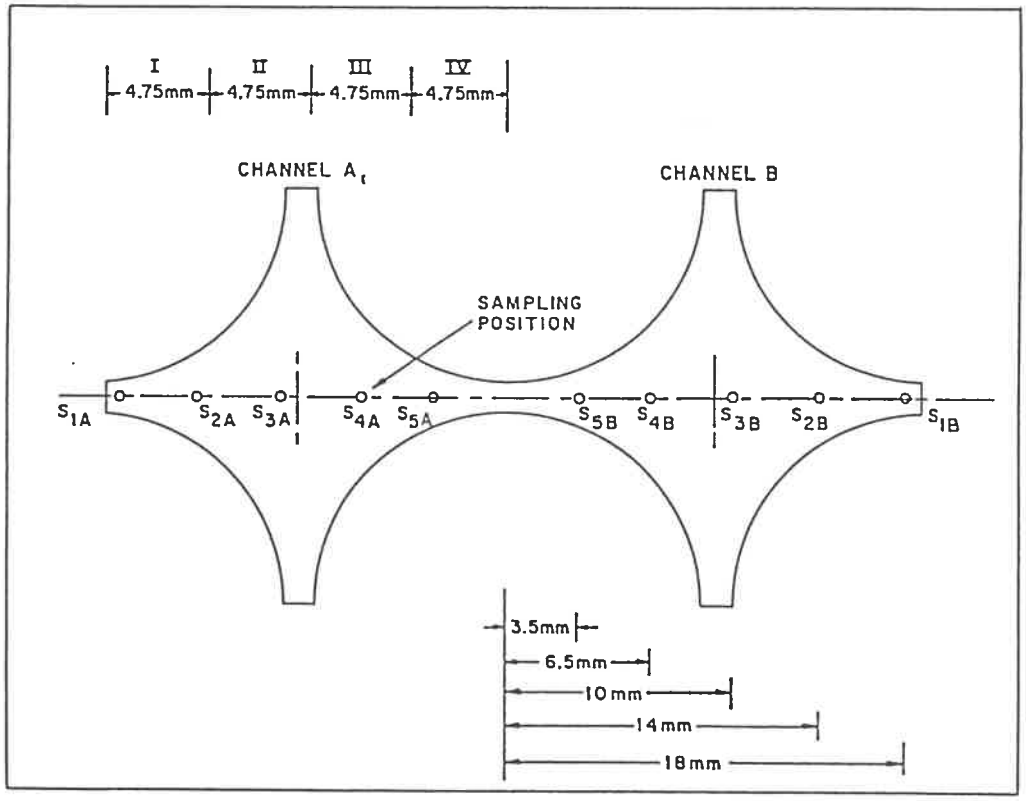

Figure 5.17: Radial Sampling Positions

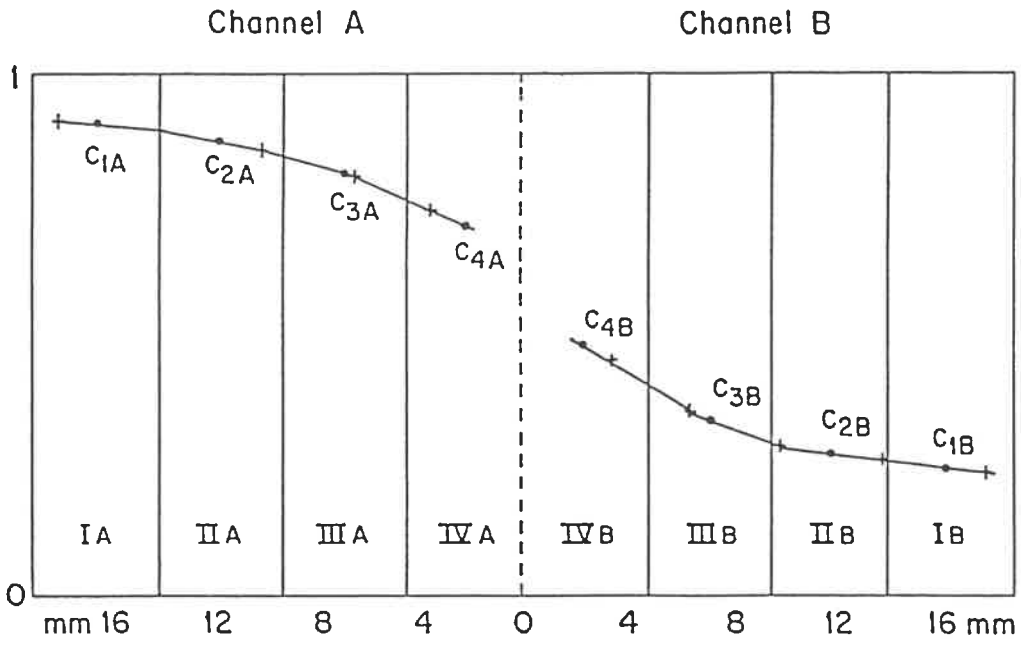

Figure 5.18: Determination of the Cross-Sectional Average of the Tracer Concentration, Method I

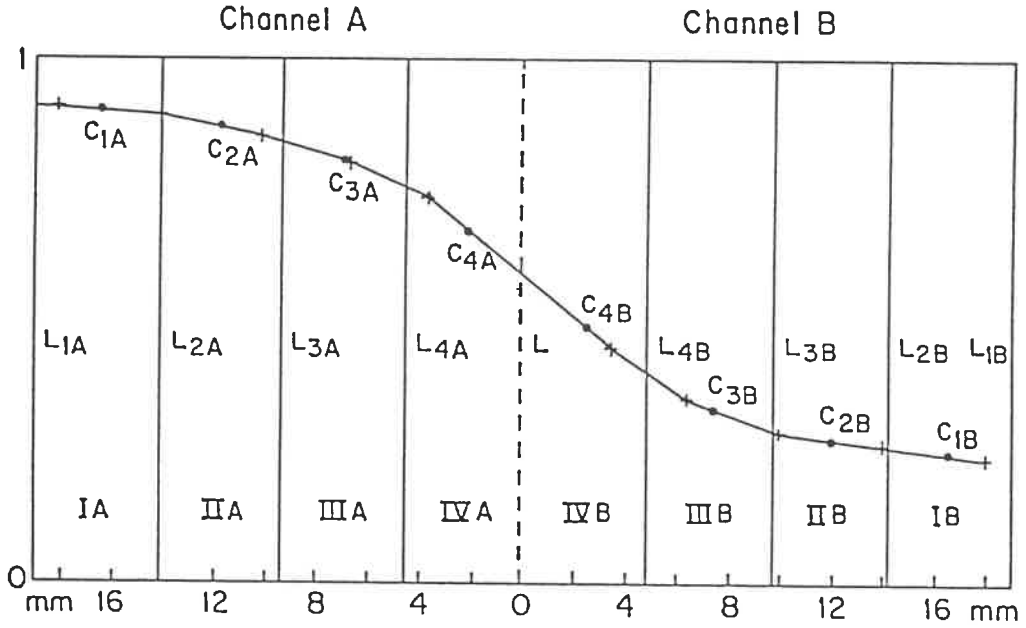

Figure 5.19: Determination of the Cross-Sectional Average of the Tracer Concentration, Method II

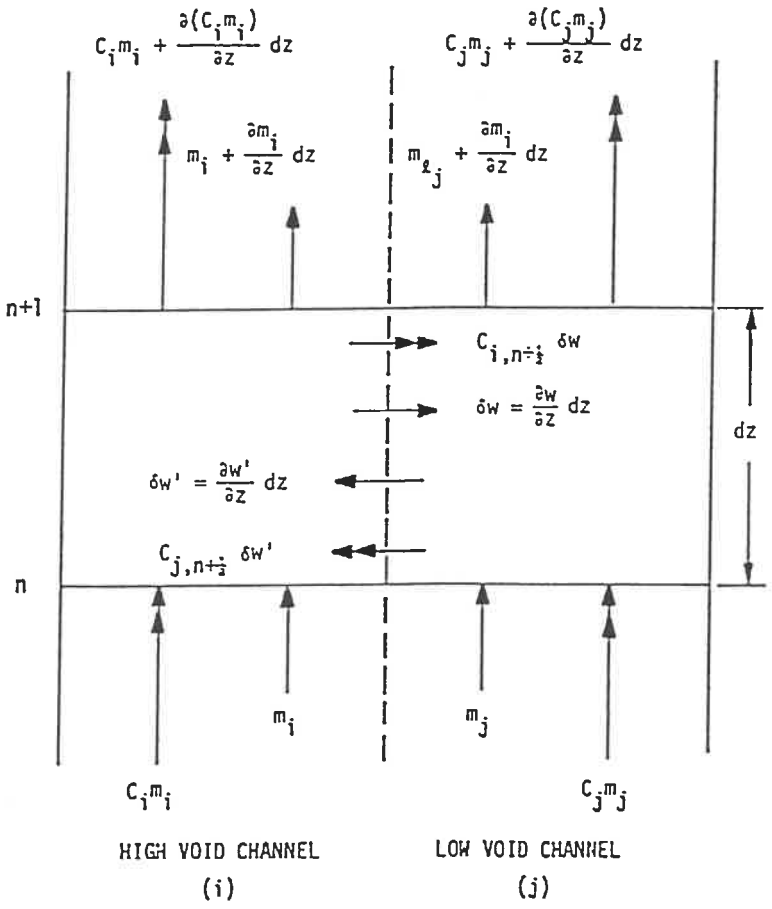

m Liquid Phase Flow Rate

C Tracer Concentration

Figure 5.20: Mass Conservation Liquid and Tracer

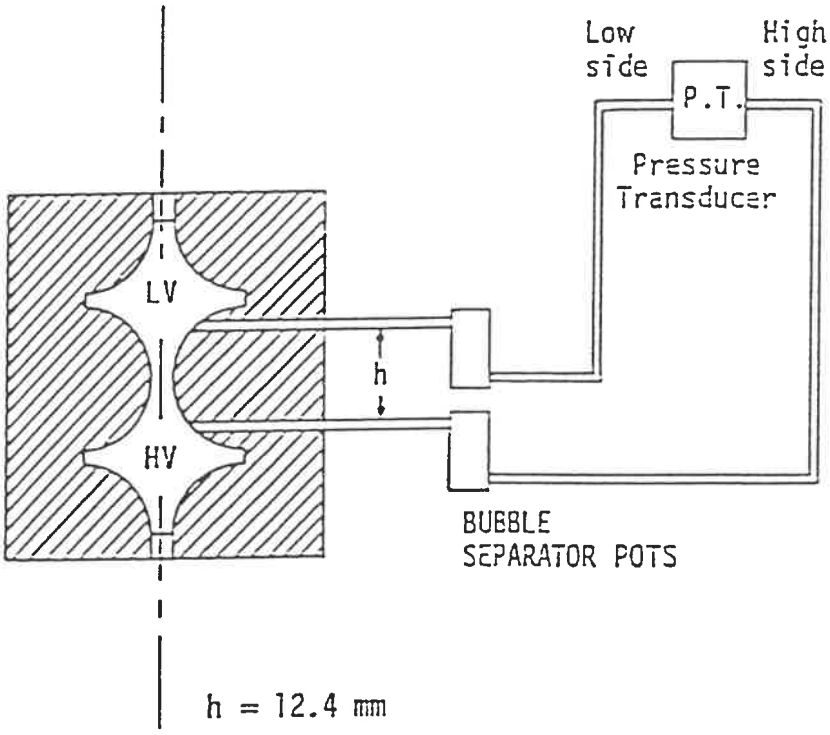

$$\Delta p_r = \Delta p_{r,measured} + h_{o_\ell} g - h_{o_\ell} g \, (1 - \bar{\alpha})$$

$$\bar{\alpha} = \frac{\alpha_{HV} \quad \alpha_{LV}}{2}$$

Figure 5.21: Radial Pressure Difference Measurement System LV/HV

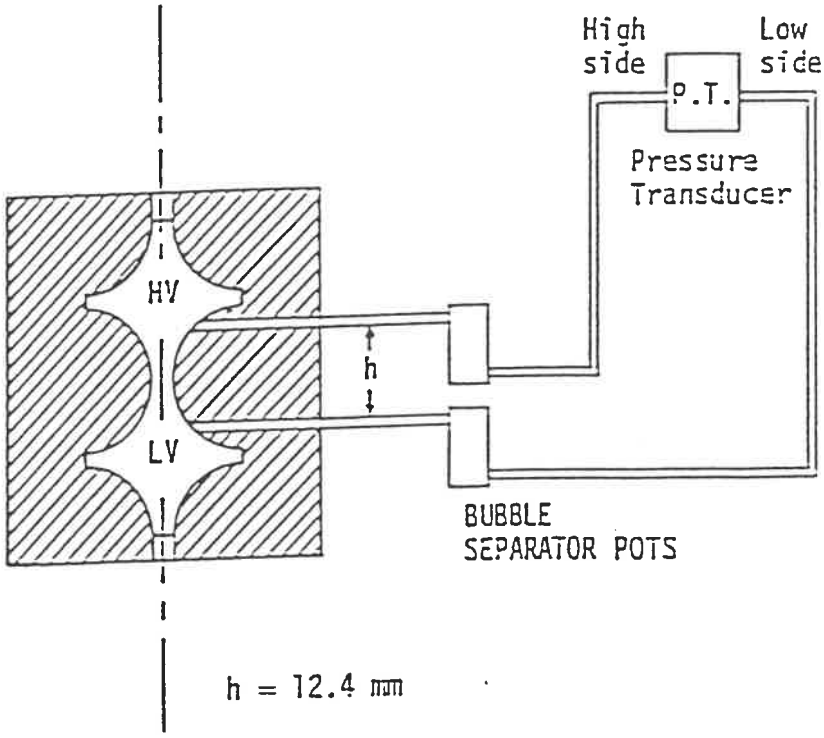

$$\Delta p_r = \Delta p_{r,measured} - h_{o_\ell} g + h_{o_2} g \, (1 - \bar{\alpha})$$

$$\bar{\alpha} = \frac{\alpha_{HV} + \alpha_{LV}}{2}$$

Figure 5.22: Radial Pressure Difference Measurement System HV/LV

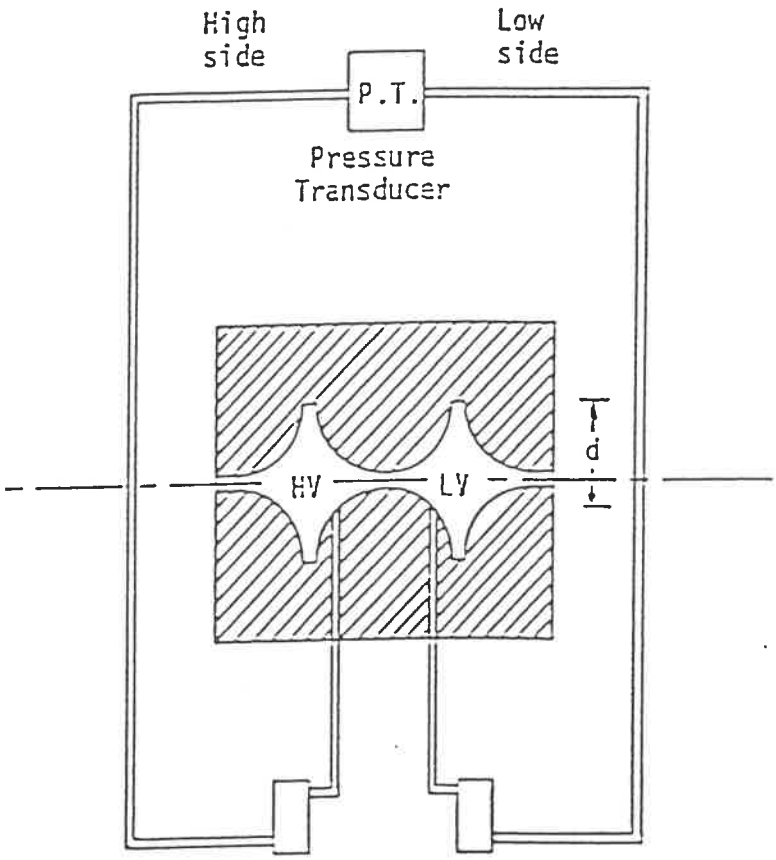

$$\Delta p_r = \Delta p_{r,measured} - d_{z,g} (c_{LV} - c_{HV})$$

Figure 5.23: Radial Pressure Difference Measurement System HV=LV

CHAPTER 6

COMPARISON OF COMPUTED AND MEASURED RESULTS–VERTICAL CASES

The vertical subchannel geometry experiments of Tapucu et al. [1984a] where simulated using both ASSERT – 4 Version 1.5 and Version 2.2B, the inlet conditions at the beginning of the interconnected region for both subchannels for all the experiments are shown in table 6.1.

As these experiments cover a wide range of void fractions for both the high void and low void subchannels an analysis of the correlation for the turbulent diffusion coefficient, ε, with respect to void fraction can be carried out. Before proceeding with the analysis of the comparisons between the results from the two versions of ASSERT – 4 and the experiments, we will first examine the mechanisms governing the lateral void and mass transfer. These mechanisms as described by Tahir and Carver [1984a] are:

1. Diversion Crossflow,
2. Buoyancy Drift,
3. Turbulent Void Diffusion,
4. Void Drift,

a more detailed description is given in section 4.2 of this thesis.

For the experiments analyzed the diversion crossflow is only significant in the first third of the interconnection region. In the remainder of the subchannel the other lateral transfer mechanisms dominate.

One of the advantages of having results for the same inlet conditions for both horizontal, (will be presented in chapter 7), and vertical conditions is that it permits us to at least partially isolate the effects of the various mechanisms which contribute to the crossflow. We may therefore break the experiments up into two broad classes, those dominated by diffusion and redistribution effects (i.e., vertical flow and the horizontal flow with channels at equal elevations), and those where gravity plays an important role (i.e., horizontal cases with one subchannel above the other). In the case of the vertical flows, in the region where the diversion crossflow is no longer significant, only two lateral transfer mechanisms exist. These are: turbulent void diffusion and void drift.

We will now look at the expression for the lateral relative velocity which is used to represent these effects in the ASSERT – 4 subchannel code. The lateral relative velocity is given by:

$$v_r = \frac{v_{2j}}{1-\alpha} - \frac{\varepsilon_\alpha}{\alpha(1-\alpha)}\nabla(\alpha - \alpha_{eq}) \quad , \tag{6.1}$$

in equation 6.1 the first term is used to represent the buoyancy drift mechanism while the second term represents the combined effects of turbulent void diffusion and void drift. The drift velocity v_{2j} is modelled in terms of the terminal rise velocity of a bubble in an infinite medium v_∞. In the case where the channels are oriented vertically the driving force for this effect disappears and the lateral relative velocity reduces to :

$$v_r = -\frac{\varepsilon_\alpha}{\alpha(1-\alpha)}\nabla(\alpha - \alpha_{eq}) \quad . \tag{6.2}$$

Due to the fact that we will be comparing the results of both ASSERT – 4 Version 1.5 and Version 2.2B predictions against the experimental results and since certain differences, although not major ones, do exist in the way the turbulent void diffusion and the redistribution to a preferred void distribution are modelled in the

two versions of the code we will examine the models as they are applied in both versions of ASSERT – 4 separatley.

6.1 ASSERT – 4 Version 1.5 Diffusion and Redistribution Models and Correlations

The difference in the diffusion and redistribution models in the two versions of ASSERT – 4 that are being used for this comparison are mainly due the differences in the recommended correlations for the void diffusion coefficient and the recommended model for the equilibrium distribution used in the void drift.

In ASSERT – 4 Version 1.5 two options for the correlation to determine the void diffusivity coefficient, ε, are available. The first involves a correlation with the Peclet number, which is a function of the void fraction. This correlation is given by:

$$P_e = \frac{\varepsilon}{\overline{u_m}\,\overline{D_h}} = a\left(\frac{\alpha_m}{0.6}\right)^6 \quad , \tag{6.3}$$

where the recommended value of a is 0.075, $\overline{u_m}$ is the average mixture axial velocity of the adjacent subchannels i and j, $\overline{D_h}$ is the average hydraulic diameter of the adjacent subchannels, and α_m is the maximum of the void fraction in the two adjacent subchannels. Thus the expression for the void diffusivity is given by:

$$\varepsilon = \overline{u_m}\,\overline{D_h}\,a\left(\frac{\alpha_m}{0.6}\right)^6 \quad . \tag{6.4}$$

The second option for ε is again based on a correlation with the Peclet number, but in this case it is represented as a function of the Reynolds number. This correlation is given by:

$$P_e = \frac{\varepsilon}{\overline{u_m}\,\overline{D_h}} = aRe^b \quad , \tag{6.5}$$

where the recommended value of a is 0.05 and the recommended value of b is 0. This correlation gives an expression for the void diffusivity which is essentially a constant times the average velocity and the average hydraulic diameter. The void diffusivity can be expressed as:

$$\varepsilon = 0.05\overline{u_m}\,\overline{D_h} \quad . \tag{6.6}$$

The void redistribution to a preferred void distribution, commonly refered to as void drift, $\nabla(\alpha - \alpha_{eq})$ is calculated using Lahey's model [Lahey Jr. and Moody, 1977]. Given two subchannels i and j this term can be written as:

$$\begin{aligned} \nabla(\alpha - \alpha_{eq})_{ij} &= [\alpha - \alpha_{eq}]_i - [\alpha - \alpha_{eq}]_j \\ &= \alpha_i - \alpha_{eqi} - \alpha_j + \alpha_{eqj} \\ &= [\alpha_i - \alpha_j] + [\alpha_{eqj} - \alpha_{eqi}] \quad , \end{aligned} \tag{6.7}$$

where α_{eq} is the prefered, or equilibrium, void distribution. In ASSERT – 4 Version 1.5 two options are available to calculate the prefered void distribution. The first uses a weighting of the individual subchannel mass fluxes to the average mass flux in the two subchannels i and j where the subchannel mass flux, G_m, can be defined as:

$$G_m = \frac{F_m}{A} \quad . \tag{6.8}$$

The individual equilibrium, or prefered, void distributions can be calculated as:

$$\alpha_{ieq} = \left[\frac{\bar{\alpha}}{\overline{G_m}}\right] G_{mi} \quad , \tag{6.9}$$

for subchannel i, and

$$\alpha_{j_{eq}} = \left[\frac{\bar{\alpha}}{\overline{G_m}}\right] G_{mj} \quad , \tag{6.10}$$

for subchannel j. For two subchannels i, and j, this is written as:

$$[\alpha_j - \alpha_i]_{eq} = \left[\frac{\bar{\alpha}}{\overline{G_m}}\right] \left[G_{mj} - G_{mi}\right] \quad , \tag{6.11}$$

where the average void fraction $\bar{\alpha}$ and the average mass flux $\overline{G_m}$ for the two subchannels i and j, are calculated using:

$$\bar{\alpha} = \frac{(\alpha A)_i + (\alpha A)_j}{A_i + A_j} \quad , \tag{6.12}$$

and

$$\overline{G_m} = \frac{F_{mi} + F_{mj}}{A_i + A_j} \quad . \tag{6.13}$$

The other option for the calculation of the prefered void distribution in ASSERT – 4 Version 1.5 is that α_{eq} is simply assumed to be equal in the two subchannels ie. $\alpha_{eq_i} = \alpha_{eq_j}$. Applying this assumption to the right hand side of equation 6.7 results in:

$$\nabla (\alpha - \alpha_{eq})_{ij} = \alpha_i - \alpha_j \quad . \tag{6.14}$$

When the correlation in terms of the void fraction as given by equation 6.4 is used for the void diffusivity the recommended equilibrium void distribution is the equal void option as given by equation 6.14.

6.2 ASSERT – 4 Version 2.2B Diffusion and Redistribution Models and Correlations

In ASSERT – 4 Version 2.2B the same options for the void diffusivity and the equilibrium void distribution are available as in ASSERT – 4 Version 1.5. In this

version, however, the recommended options have changed. The recommeded option for the void diffusivity, ε, in ASSERT – 4 Version 2.2B is the correlation with the Peclet number, which is a function of the Reynolds number. This correlation is given by:

$$P_e = \frac{\varepsilon}{\overline{u_m}\,\overline{D_h}} = aRe^b \quad , \tag{6.15}$$

where the recommended value of a is 0.05 and the recommended value of b is 0, $\overline{u_m}$ is the average mixture axial velocity of the adjacent subchannels i and j, and $\overline{D_h}$ is the average hydraulic diameter of the adjacent subchannels. Thus in ASSERT – 4 Version 2.2B the void diffusion coefficient is independent of the void fraction, and for that matter it is also independent of the Reynolds number as well, due to the fact that $b = 0$.

The void diffusivity, ε is:

$$\varepsilon = 0.05\overline{u_m}\,\overline{D_h} \quad . \tag{6.16}$$

In ASSERT – 4 Version 2.2B the recommended option for the void redistribution to a preferred void distribution, $\nabla(\alpha - \alpha_{eq})$ is the model proposed by Lahey and Moody [1977] using equations 6.11, 6.12, and 6.13.

6.3 Comparison of ASSERT – 4 Predictions with Experimental Results

We will now examine the results of the predictions of both versions of ASSERT – 4 in each case using the recommended option for the correlations for the void diffusivity and the recommended equilibrium void distribution model.

We will however analyze the effects of modifying the leading coefficients in both correlations for the void diffusivity. It should be noted that the void transfer mechanisms influence not only the void that is transfered but also the liquid transfer due to the fact that the void being transfered from one subchannel to another brings

with it a certain amount of liquid. The void transfer will also affect the pressure drop in a given subchannel due to the fact that the correlation for the two–phase friction multiplier $\phi_{\ell 0}^2$ is dependent on the void fraction.

We will examine the results of the predicitons of both versions of the code together with the experiments for one major parameter at a time for all of the cases shown in table 6.1. Thus all the void fraction results will be shown together, all the mass flow rates, and all the pressure drops. A brief analysis of each figure will be presented but the general conclusions will only be given at the end of the presentation for each parameter.

6.3.1 Void Fraction

Figures 6.1 through 6.16 give both the predicted void fraction profiles using ASSERT – 4 Version 1.5, ASSERT – 4 Version 2.2B and the experimental void fraction profiles. It can be seen that by adequately choosing the coefficients used it the correlations for the void diffusivity the predictions from both versions of ASSERT – 4 can be made to agree quite well with the experimental results. This suggests that physically the void diffusivity is dependent on the void fraction. Further, for ASSERT – 4 Version 1.5 which uses a correlation for the void diffusivity that is dependent on the void fraction, we can conclude that the physical dependence of the void diffusivity on the void fraction is stronger than that represented by the correlation. For the case of ASSERT – 4 Version 2.2B we can conclude that the correlation for the void diffusivity should have some dependence on the void fraction.

6.3.1.1 Run SV–1

Figures 6.1 to 6.4 show the experimental results of the void fraction profile for run SV–1, which is a case having a void fraction of $\approx$ 60% in the high void

subchannel and 0% void fraction in the low void subchannel.

Figures 6.1 and 6.2 show the comparison of the experimental results against the predicitions of ASSERT – 4 Version 1.5, which uses the correlation for the void diffusion as given by equation 6.4. The adjustable coefficient a in the correlation has been varied from $a = 0.05$ to $a = 0.6$ where the recommended default value is $a = 0.075$. The range of a examined covers more than one order of magnitude. It can be seen from figure 6.2 that the recommended value of a yields a predicted void fraction in the low void subchannel that is much smaller than that seen experimentally and overpredicted the void fraction in the high void subchannel. The higher values of a that were tried ie. $a \geq 0.25$ all yielded predicted void fractions in both subchannels that while not perfect were quite good.

Figures 6.3 and 6.4 show the comparison of the experimental results against the predicitions of ASSERT – 4 Version 2.2B, which uses the correlation for the void diffusion as given by equation 6.16. The adjustable coefficient a in the correlation has been varied from $a = 0.05$ to $a = 0.20$ where the recommended default value is $a = 0.05$. It can be seen from figure 6.3 that the recommended value of a results in a significant underprediciton of the void fraction in the low void subchannel. Again the higher values of a that were tried ie. $a \geq 0.10$ all resulted in much better results for both the high and low void subchannels.

6.3.1.2 Run SV–2

Figures 6.5 and 6.6 show the experimental results of the void fraction profile for run SV–2, which is a case having a void fraction of $\approx$ 60% in the high void subchannel and $\approx$ 20% void fraction in the low void subchannel.

Figure 6.5 shows the comparison of the experimental results against the predicitions of ASSERT – 4 Version 1.5. The adjustable coefficient a in the correlation for the void diffusion has been varied from $a = 0.075$ to $a = 0.25$. It can be seen from

figure 6.5 that the recommended value of a yields a predicted void fraction in the low void subchannel that is much smaller than that seen experimentally. Any of the higher values of a that were tried from $a = 0.15$ to $a = 0.25$ yielded predicted void profiles in both the high void subchannel and the low void subchannel that are in good agreement with the experimental results.

Figures 6.6 shows the comparison of the experimental results against the predicitions of ASSERT – 4 Version 2.2B. The adjustable coefficient a in the correlation for the void diffusion has been varied from $a = 0.05$ to $a = 0.11$. It can be seen from figure 6.6 that the recommended value of a results in a significant underprediciton of the void in the low void subchannel. The two highest values of a, $a = 0.09$ and $a = 0.11$, that were tried both resulted in very good predictions of the void fractions in both the high and low void subchannels.

6.3.1.3 Run SV–3

Figures 6.7 and 6.8 show the experimental results of the void fraction profile for run SV–3, which is a case having a void fraction of $\approx 50\%$ in the high void subchannel and 0% void fraction in the low void subchannel.

Figure 6.7 shows the comparison of the experimental results against the predicitions of ASSERT – 4 Version 1.5. The adjustable coefficient a in the correlation for the void diffusion has been varied from $a = 0.075$ to $a = 0.40$. It can be seen from figure 6.7 that the recommended value of a underpredicted void fraction in the low void subchannel and overpredicted the void fraction in the high void subchannel. The highest values of a that was tried, $a = 0.40$, yielded a predicted void fraction profile in the high void subchannel that was almost perfect. However the void fraction for the low void subchannel was slightly underpredicted. Values of a higher than $a = 0.40$ were not tested for this case due to the fact that while they might have led to improved results for predictions in the low void subchannel they would

have had detrimental effects on the predictions for the high void subchannel.

Figures 6.8 shows the comparison of the experimental results against the predicitions of ASSERT – 4 Version 2.2B. The adjustable coefficient a in the correlation for the void diffusion has been varied from $a = 0.05$ to $a = 0.15$. It can be seen from figure 6.8 that the recommended value of a results in a significant underprediciton of the void in the low void subchannel and overpredicted the void fraction in the high void subchannel. The two highest values of a, $a = 0.12$ and $a = 0.15$, that were tried both resulted in reasonably accurate predictions of the void fraction in the high void subchannel. Only the higest value of a, $a = 0.15$, yielded an accurate prediction of the void in the low void subchannel, all the other values of a that were tried resulted in underpredictions.

6.3.1.4 Run SV–4

Figures 6.9 and 6.10 show the experimental results of the void fraction profile for run SV–4, which is a case having a void fraction of $\approx 50\%$ in the high void subchannel and $\approx 30\%$ void fraction in the low void subchannel.

Figure 6.9 shows the comparison of the experimental results against the predicitions of ASSERT – 4 Version 1.5. The adjustable coefficient a in the correlation for the void diffusion has been varied from $a = 0.075$ to $a = 0.25$. It can be seen from figure 6.9 that the recommended value of a yields a predicted void fraction in the low void subchannel that is slightly smaller than that seen experimentally. The highest values of a that was tried, $a = 0.25$, yielded predicted void fraction profiles in both the high and low void subchannels that were quite good.

Figures 6.10 shows the comparison of the experimental results against the predicitions of ASSERT – 4 Version 2.2B. The adjustable coefficient a in the correlation for the void diffusion has been varied from $a = 0.05$ to $a = 0.07$. It can be seen from figure 6.10 that all values of a result in almost the same predicted void

profiles. Further, in all three cases the predictions are in very good agreement with the experimental results.

6.3.1.5 Run SV–5

Figures 6.11 and 6.12 show the experimental results of the void fraction profile for run SV–5, which is a case having a void fraction of $\approx 40\%$ in the high void subchannel and 0% void fraction in the low void subchannel.

Figure 6.11 shows the comparison of the experimental results against the predicitions of ASSERT – 4 Version 1.5. The adjustable coefficient a in the correlation for the void diffusion has been varied from $a = 0.025$ to $a = 0.25$. The smallest values of a that were tried, $a = 0.025 \rightarrow a = 0.075$, yielded predicted void fraction profiles in both the high and low void subchannels that were in reasonably good agreement with the experimental results.

Figures 6.12 shows the comparison of the experimental results against the predicitions of ASSERT – 4 Version 2.2B. The adjustable coefficient a in the correlation for the void diffusion has been varied from $a = 0.001$ to $a = 0.05$. It can be seen from figure 6.12 that the smallest value of a, $a = 0.001$, results the best predicted void fraction profile for both the high and low void subchannels.

6.3.1.6 Run SV–6

Figures 6.13 and 6.14 show the experimental results of the void fraction profile for run SV–6, which is a case having a void fraction of $\approx 40\%$ in the high void subchannel and $\approx 20\%$ void fraction in the low void subchannel.

Figure 6.13 shows the comparison of the experimental results against the predicitions of ASSERT – 4 Version 1.5. The adjustable coefficient a in the correlation for the void diffusion has been varied from $a = 0.05$ to $a = 0.15$. It can be seen from figure 6.13 that all the values of a yield a predicted void fraction profile

in both the high and low void subchannels that is quite good. In this case the value of the diffusion coefficient used had almost no effect on the predicition.

Figures 6.14 shows the comparison of the experimental results against the predicitions of ASSERT - 4 Version 2.2B. The adjustable coefficient a in the correlation for the void diffusion has been varied from $a = 0.01$ to $a = 0.05$. It can be seen from figure 6.14 that the default value of a results in an overprediction of the void fraction in the low void subchannel and an underprediction of the void fraction in the high void subchannel. The lower values of a result in reasonable predictions of the void fraction in the low void subchannel but slightly underpredict the void fraction in the high void subchannel.

6.3.1.7 Run SV–7

Figures 6.15 and 6.16 show the experimental results of the void fraction profile for run SV–7, which is a case having a void fraction of $\approx$ 15% in the high void subchannel and 0% void fraction in the low void subchannel. The scale of the graphs has been expanded in order to be able to see the void fraction profile in the low void subchannel.

Figure 6.15 shows the comparison of the experimental results against the predicitions of ASSERT - 4 Version 1.5. The adjustable coefficient a in the correlation for the void diffusion has been varied from $a = 0.075$ to $a = 0.001$. It can be seen from figure 6.15 that the all the values of a yielded a predicted void transfer that is somewhat greater than that seen experimentally, and thus overpredicted the void fraction in the low void subchannel.

Figures 6.16 shows the comparison of the experimental results against the predicitions of ASSERT - 4 Version 2.2B. The adjustable coefficient a in the correlation for the void diffusion has been varied from $a = 0.005$ to $a = 0.0005$. It can be seen from figure 6.16 that all values of a result in almost the same predicted

void fraction profile in the high void subchannel but the lowest value $a = 0.0005$ resulted in a somewhat better prediction for the low void subchannel.

6.3.1.8 General Observations on the Void Fraction Predictions

Examining figures 6.1, 6.2, 6.5, 6.7, 6.9, 6.11, 6.13, and 6.15 which show the predicted and measured void profiles for ASSERT – 4 Version 1.5, which uses the correlation for the void diffusion coefficient given by equation 6.4, we can see that for the higher void cases, SV–1 to SV–4, a higher value of the coefficient a in the void diffusion correlation is required to adequately predict the void fraction profiles. For the intermediate void fraction cases, SV–5 and SV–6, the recommended value of the diffusion coefficient, $a = 0.075$, yields good results. For the low void case, SV–7, no significant difference in the void profile is seen for any of the values of the diffusion coefficient used.

It would seem that physically the void diffusion has a greater dependence on the void fraction than that reflected in the correlation given by equation 6.4.

Examining figures 6.3, 6.4, 6.6, 6.8, 6.10, 6.12, 6.14, and 6.16 which show the predicted and measured void fraction profiles for ASSERT – 4 Version 2.2B, which uses the correlation for the void diffusion coefficient given by equation 6.6, we can see that for the higher void cases, SV–1 to SV–4, a higher value of the coefficient a in the void diffusion correlation is required to adequately predict the void profiles. For the intermediate and low void fraction cases, SV–5, SV–6, and SV–7, the value of a must be decreased from that of the recommended value, at times significantly so, to accurately predict the void transfered from the high void subchannel to the low void subchannel.

Since it was necessary to change the leading coefficient of the void diffusion correlation as given by equation 6.6 to adequatly predict the amount of void transfered in the cases from SV–1 to SV–7 which cover a range from $\approx$ 60% void to

$\approx$ 17% it would appear that the diffusion process is dependent on the void fraction. This is not physically represented by the form of the correlation for the void diffusion as given by equation 6.6.

6.3.2 Mass Flow Rate

Figures 6.17 through 6.32 give both the predicted mass flow rates using ASSERT – 4 Version 1.5 and Version 2.2B and the measured experimental mass flow rates. There are no models in ASSERT – 4 which have coefficients which impact directly on the mass flow rate predicitions. However, due to the fact that the density of the gas phase is considerably less than that of the liquid phase a change in the void diffusion coefficient does result in a change in the predicted mass flow rates in the two subchannels. An analysis of the results due to varying the transverse resistance coefficient K_{ij} from 0.5 to 100 similar to the one carried out by Tapucu et al. [1988] for COBRA showed that itthe value chosen had no significant impact on the results. Therefore all the runs were made using the recommended value of the transverse resistance coefficient $K_{ij} = 0.5$.

It should be pointed out that the mass flow rates presented are the total mass flow (ie. gas + liquid) for both versions of ASSERT – 4 and liquid only for the experimental results. However, the gas mass flow rate accounts for only 0.5% of the total mass flow rate in the experiments thus the discrepency will be negligable. In all the cases analyzed the inlet liquid mass flow rate was $\approx 3000 kg/m^2 s$ in both subchannels.

6.3.2.1 Run SV–1

Figures 6.17 to 6.20 show the experimental results of the mass flow rates for case SV–1, which is a case having a void fraction of $\approx$ 60% in the high void subchannel and 0% void fraction in the low void subchannel.

Figures 6.17 and 6.18 show the comparison of the experimental results against the predicitions of ASSERT – 4 Version 1.5. Experimentally it is observed that the mass flow rate in the high void subchannel first decreases and then increases slowly as some of the liquid lost by this subchannel is recovered. In the results of the predictions by ASSERT – 4 Version 1.5 we see that for values of the void diffusion coefficient a in the range of $a = 0.05$ to $a = 0.25$ ASSERT – 4 Version 1.5 seems to predict that an equilibrium or near equilibrium mass flow rate is reached and very little further mass transfer is seen to occur. For values of the void diffusion coefficient a in the range of $a = 0.30$ to $a = 0.60$ ASSERT – 4 Version 1.5 predicts an almost instantaneous recovery of the liquid by the high void subchannel and predicts a crossover in the liquid mass flow rates, something that is definitely not seen experimentally. Further, at the beginning of the interconnected region, experimentally we see a large rapid mass transfer from the high void subchannel to the low void subchannel, ASSERT – 4 Version 1.5 predicts that this inital transfer is much more gradual than what is observed experimentally.

Figures 6.19 and 6.20 show the comparison of the experimental results against the predicitions of ASSERT – 4 Version 2.2B. We can see that using ASSERT – 4 Version 2.2B with values of the void diffusion coefficient a that are somewhat higher than what is recommended, which is in agreement with the results of the void fraction analysis presented in the previous section, we obtain a reasonably good prediction of the mass flow rate in both the high void and the low void subchannels. Further, we can see that ASSERT – 4 Version 2.2B is capable of capturing the phenomena of the flow recovery downstream by the high void subchannel. In addition Version 2.2B does a much better job of predictiong the initial large mass transfer just after the beginning of the interconnected region. With the default value of the diffusion coefficient $a = 0.05$ the magnitude of the initial large mass transfer is captured very well but the magnitude of the recovery of the liquid

downstream is underpredicted. For higher values of a the magnitude of the initial large transfer predicted by ASSERT – 4 Version 2.2B is somewhat smaller that that seen experimentally and the recovery downstream is somewhat overpredicted.

Examining figures 6.17 and 6.18 which show the results from ASSERT – 4 Version 1.5 with respect to figures 6.19 and 6.20 which show the results from ASSERT – 4 Version 2.2B we can see the latter version of ASSERT – 4 results in better predictions of the mass flow rates. Further, Version 2.2B is capable of predicting the physical mechanisms of the initial large liquid transfer and the subsequent downstream liquid recovery much more accurately than Version 1.5.

6.3.2.2 Run SV–2

Figures 6.21 and 6.22 show the experimental results of the mass flow rate for case SV–2, which is a case having a void fraction of $\approx$ 60% in the high void subchannel and $\approx$ 20% void fraction in the low void subchannel.

Figure 6.21 shows the comparison of the experimental results against the predicitions of ASSERT – 4 Version 1.5. The initial large mass transfer from the high void subchannel to the low void subchannel is not accurately captured by the code. Further, the recovery of the liquid downstream by the high void subchannel is not seen to appear in the predicted results. Increasing the value of the coefficient a in the void diffusion correlation reduces the amount of liquid transfered from the high void to the low void subchannel. Unfortunately, in order to accurately predict the mass flow rate it would be necessary to reduce the value of the coefficient a to a value considerably under the value required to acheive an adaquate prediction of the void fraction.

Figure 6.22 shows the comparison of the experimental results against the predicitions of ASSERT – 4 Version 2.2B. The initial large mass flow from the high void subchannel to the low void subchannel is quite well predicted. The use

of the recommended void diffusion coefficient $a = 0.05$ results in an excellent prediction of the mass flow rates in both subchannels. Using a value of $a = 0.07$ the initial large mass transfer is slightly under predicted but the prediction of the recovery by the high void subchannel is improved slightly.

Examining figures 6.21 and 6.22 which show the results from ASSERT – 4 Version 1.5 and ASSERT – 4 Version 2.2B respectively it is clear that Version 2.2B results in better predictions of the mass flow rates than Version 1.5.

6.3.2.3 Run SV–3

Figures 6.23 and 6.24 show the experimental results of the mass flow rates for case SV–3, which is a case having a void fraction of $\approx 50\%$ in the high void subchannel and 0% void fraction in the low void subchannel.

Figure 6.23 shows the comparison of the experimental results against the predicitions of ASSERT – 4 Version 1.5. We can see that the default value of a leads to a prediction of the highest liquid transfer from the high void subchannel to the low void subchannel. However, it still significantly under predicts the magnitude of the large initial mass transfer from the high void subchannel to the low void subchanel. It is also interesting to note that while the experimental results show a recovery of liquid by the high void subchannel in the last third of the test section ASSERT – 4 Version 1.5 predicts that the mass transfer at this point is still from the high void subchannel to the low void subchannel.

Figures 6.24 shows the comparison of the experimental results against the predicitions of ASSERT – 4 Version 2.2B. We can see that the initial large mass transfer is quite well captured by ASSERT – 4 Version 2.2B. We can also see that all of the values of the leading coefficient still lead to a prediction of the flow recovery by the high void subchannel in the last third of the test section, albeit of varying amounts and with varying degrees of accuracy.

Examining figures 6.23 and 6.24 which show the results from ASSERT – 4 Version 1.5 and ASSERT – 4 Version 2.2B respectively it is clear that Version 2.2B results in better predictions of both the large initial crossflow and of the subsequent flow recovery by the high void subchannel in the last third of the test section.

6.3.2.4 Run SV–4

Figures 6.25 and 6.26 show the experimental results of the mass flow rate for case SV–4, which is a case having a void fraction of $\approx 50\%$ in the high void subchannel and $\approx 30\%$ void fraction in the low void subchannel.

Figure 6.25 shows the comparison of the experimental results against the predicitions of ASSERT – 4 Version 1.5. It can be seen that again ASSERT – 4 Version 1.5 underpredicts the magnitude of the crossflow at the beginning of the interconnected region. Further, it also fails to predict the recovery of the liquid by the high void subchannel in the last third of the test section.

Figure 6.26 shows the comparison of the experimental results against the predicitions of ASSERT – 4 Version 2.2B. It can be seen that the initial large crossflow at the beginning of the interconnected region is captured reasonably well by ASSERT – 4 Version 2.2B but that its magnitude is still somewhat underpredicted. It is also interesting to note that Version 2.2B predicts the position of the beginning of the flow recovery by the high void subchannel quite well.

Examining figures 6.25 and 6.26 which show the results from ASSERT – 4 Version 1.5 and ASSERT – 4 Version 2.2B respectively we see that neither version of the code did a very good job predicting the magnitude of the initial large crossflow but that Version 2.2B still performed somewhat better than Version 1.5. Further, only ASSERT – 4 Version 2.2B predicted the recovery of the liquid by the high void subchannel.

6.3.2.5 Run SV–5

Figures 6.27 and 6.28 show the experimental results of the mass flow rates for case SV–5, which is a case having a void fraction of $\approx 40\%$ in the high void subchannel and 0% void fraction in the low void subchannel.

Figure 6.27 shows the comparison of the experimental results against the predicitions of ASSERT – 4 Version 1.5. It can be seen that not only is the magnitude of the initial large crossflow underpredicted but that the continued mass transfer from the high void subchannel to the low void subchannel along the rest of the length of the interconnected region is also underpredicted.

Figures 6.28 shows the comparison of the experimental results against the predicitions of ASSERT – 4 Version 2.2B. It can be seen from figure 6.28 that the smallest value of a, $a = 0.001$, results in the best predicted mass flow rates for both the high and low void subchannels. In fact the magnitude of both the initial large crossflow as well as the continued mass transfer from the high void subchannel to the low void subchannel along the rest of the length of the interconnected region is almost perfectly predicted by ASSERT – 4 Version 2.2B. It can also be seen, by going back to the void fraction prediction for this case, shown in figure 6.12, that the same value of a results in the best prediction for both the void fraction and the mass flow rate.

Examining figures 6.27 and 6.28 which show the results from ASSERT – 4 Version 1.5 and ASSERT – 4 Version 2.2B respectively we see that Version2.2B predicted the mass flow rates in both the high and low void subchannels almost perfectly while the results of the predictions for ASSERT – 4 Version 1.5 were not nearly as accurate.

6.3.2.6 Run SV–6

Figures 6.29 and 6.30 show the experimental results of the void fraction profile for case SV–6, which is a case having a void fraction of $\approx 40\%$ in the high void subchannel and $\approx 20\%$ void fraction in the low void subchannel.

Figure 6.29 shows the comparison of the experimental results against the predicitions of ASSERT – 4 Version 1.5. Looking at the experimental results we see that the initial crossflow is much smaller than all of the cases previously analyzed. We can also see that ASSERT – 4 Version 1.5 did a better job of predicting this initial crossflow than in the previous cases. However, the total mass transfered from the high void subchannel to the low void subchannel was still underpredicted. The adjustable coefficient a in the correlation for the void diffusion has been varied from $a = 0.05$ to $a = 0.15$. It can be seen that the value of the diffusion coefficient used had almost no effect on the predicited mass flow rate.

Figures 6.30 shows the comparison of the experimental results against the predicitions of ASSERT – 4 Version 2.2B. It can be seen from figure 6.30 that ASSERT – 4 Version 2.2B does a good job of predicting the intial crossflow as well as the continued transfer from the high void subchannel to the low void subchannel. The last experimental point indicates a flow recovery by the high void subchannel. This trend is not picked up by ASSERT – 4 Version 2.2B.

Examining figures 6.29 and 6.30 which show the results from ASSERT – 4 Version 1.5 and ASSERT – 4 Version 2.2B respectively we see that the Version2.2B prediction of the mass flow rates in both the high and low void subchannels along the entire length of the interconnected region is considerably better than the prediction by ASSERT – 4 Version 1.5.

6.3.2.7 Run SV–7

Figures 6.31 and 6.32 show the experimental results of the void fraction profile for case SV–7, which is a case having a void fraction of $\approx$ 15% in the high void subchannel and 0% void fraction in the low void subchannel. The scale of the graphs has been expanded in order to be able to see the difference in the mass flow rates between the high and low void subchannels.

Figure 6.31 shows the comparison of the experimental results against the predicitions of ASSERT – 4 Version 1.5. Looking at the results shown in figure 6.31 we can see that ASSERT – 4 Version 1.5 underpredicts the magnitude of the total mass transfer from the high void to the low void subchannel.

Figures 6.32 shows the comparison of the experimental results against the predicitions of ASSERT – 4 Version 2.2B. Here we see that ASSERT – 4 Version 2.2B does a reasonably good job of predicting the mass flow rates in both subchannels along the entire length of the interconnected region.

Examining figures 6.31 and 6.32 which show the results from ASSERT – 4 Version 1.5 and ASSERT – 4 Version 2.2B respectively we see that the Version2.2B prediction is considerably better than that of ASSERT – 4 Version 1.5.

6.3.2.8 General Observations on the Mass Flow Rate Predictions

Examining figures 6.17, 6.18, 6.21, 6.23, 6.25, 6.27, 6.29, and 6.31 which show the predicted and measured mass flow rates for ASSERT – 4 Version 1.5 we see that the initial large crossflow at the beginning of the interconnected region was systematically underpredicted. Further, the recovery of the liquid by the high void subchannel which was seen experimentally for most of the cases analyzed was not predicted by ASSERT – 4 Version 1.5.

Examining figures 6.19, 6.20, 6.22, 6.24, 6.26, 6.28, 6.30, and 6.32 which show the predicted and measured mass flow rates for ASSERT – 4 Version 2.2B we

can see that while the predictions of the mass flow rates may not be perfect for all the cases analyzed they are all quite good. ASSERT – 4 Version 2.2B was able to predict, with reasonable accuracy the inital large crossflow from the high void subchannel to the low void subchannel at the beginning of the interconnected region. Version 2.2B was also able to predict the recovery the liquid by the high void subchannel in the last third of the test section, something that was completely missed by ASSERT – 4 Version 1.5.

It is interesting to note that if one examines the leading coefficients for the void diffusion correlation which lead to the best results for void fraction and the ones which lead to the best predictions for mass flow rate, the respective coefficients in ASSERT – 4 Version 1.5 are at opposite ends of the range of the values that were tested, whereas for ASSERT – 4 Version 2.2B while the two coefficients may not be identical they are at least close to one another in the range of values that were tested.

6.3.3 Pressure Drop

Figures 6.33 through 6.48 give both the predicted pressure drop profiles using ASSERT – 4 Version 1.5 and Version 2.2B and the measured experimental pressure drop profiles. The single phase friction factor used in the runs was given by a correlation with the single phase single subchannel calibration experiments as described by Tapucu et al. [1984a]. It is given by:

$$f = 0.488Re^{-0.311} \tag{6.17}$$

The process used to determine the two-phase friction multiplier is also described by Tapucu et al. [1984a]. The two-phase friction multiplier used in these runs is given by:

$$\phi_{f0}^2 = 1 + 1.8966\alpha + 2.4650\alpha^2 - 0.73214\alpha^3 - 1.3554\alpha^4 + 11.809\alpha^5 \qquad (6.18)$$

Examining figures 6.33 through 6.48 we can see that in all cases the pressure drops in both the high and low void subchannels are very accurately predicted by both ASSERT – 4 Version 1.5 and ASSERT – 4 Version 2.2B. The greatest discrepency is seen in case SV–2 where both versions of ASSERT – 4 overpredict the pressure drop by approximately 5%. In all the other cases analyzed the difference between the predicted and measured results is on the order of $\pm 2\%$, which is quite acceptable. Examining the figures quite closely we can see that varying the leading coefficient in the correlation for the void diffusion does result in minor changes in the predicted pressure drop profiles. The predicted results are in general in such good agreement with the experimental results that a run by run analysis of the comparison is not required.

Table 6.1: Inlet Conditions for the Vertical Experiments

Void Fraction α %		
RUN	High Void Channel	Low Void Channel
SV-1	58.7 %	0%
SV-2	58.2%	18.7%
SV-3	50.4%	0%
SV-4	49.8%	30.3%
SV-5	38.0%	0%
SV-6	38.3%	20.1%
SV-7	16.8%	0%
Liquid Mass Fluxes (kg/m^2s)		
SV-1	2984	2989
SV-2	2989	3009
SV-3	3012	3004
SV-4	3020	3004
SV-5	3003	2997
SV-6	2993	2997
SV-7	3000	3006
Gas Mass Fluxes (kg/m^2s)		
SV-1	21.80	0
SV-2	21.52	2.33
SV-3	12.14	0
SV-4	12.25	4.12
SV-5	5.10	0
SV-6	5.50	1.91
SV-7	1.4	0

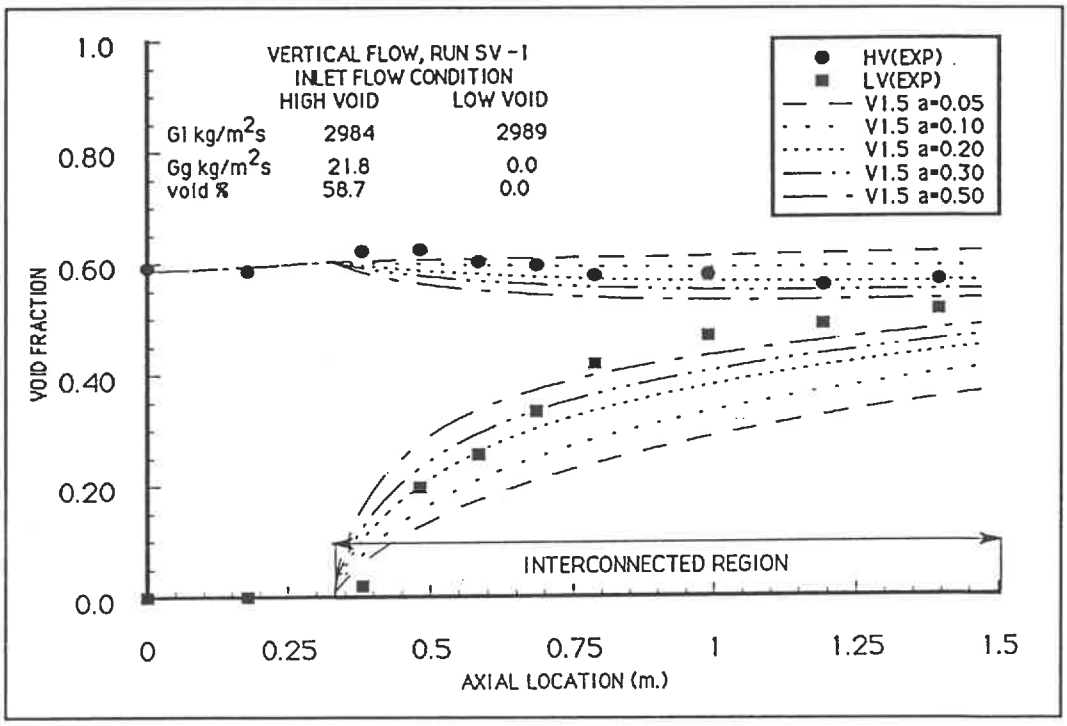

Figure 6.1: Void Fraction Profile Case SV–1 ASSERT – 4 Version 1.5 RUN–1

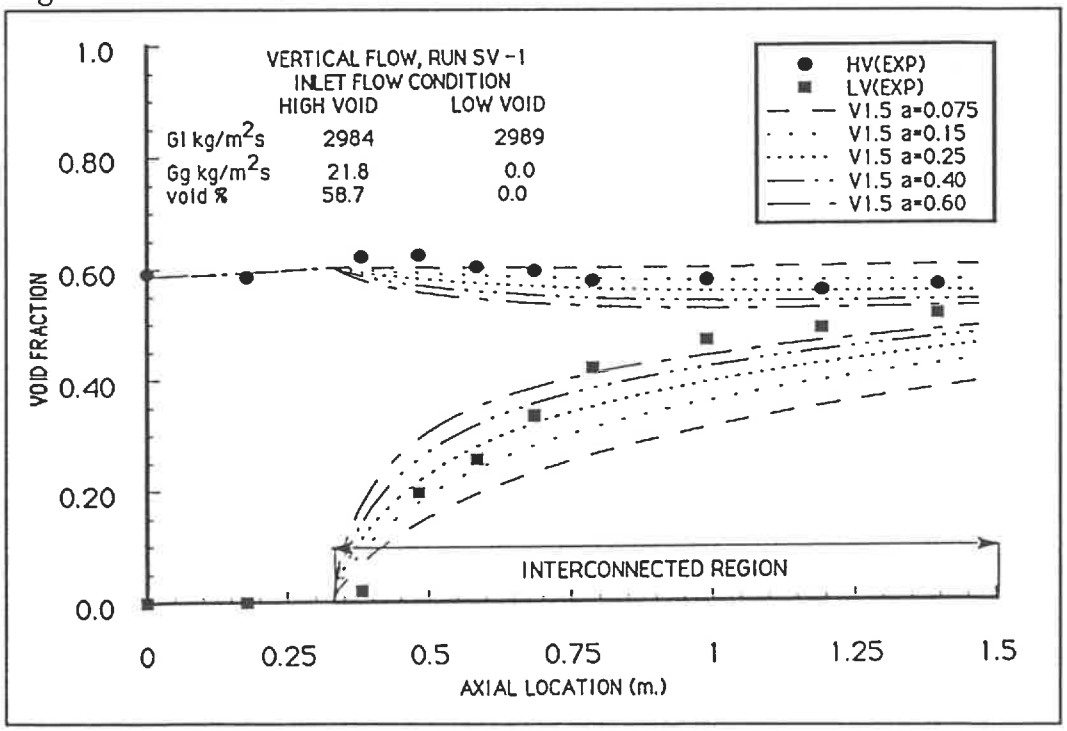

Figure 6.2: Void Fraction Profile Case SV–1 ASSERT – 4 Version 1.5 RUN–2

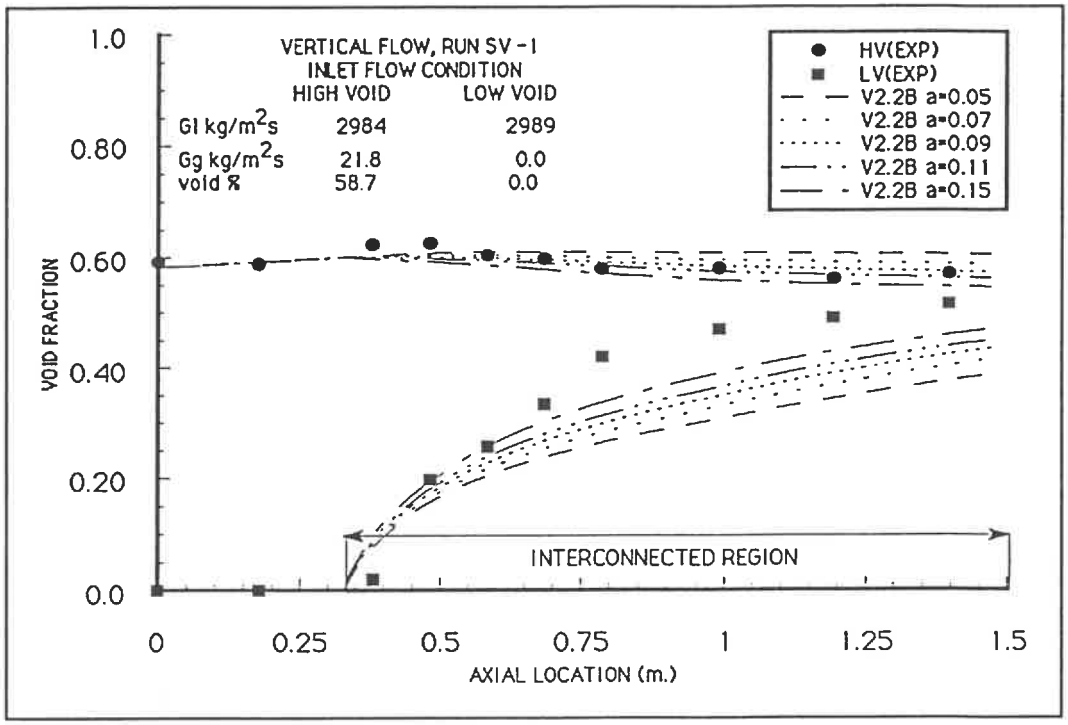

Figure 6.3: Void Fraction Profile Case SV–1 ASSERT – 4 Version 2.2B RUN–1

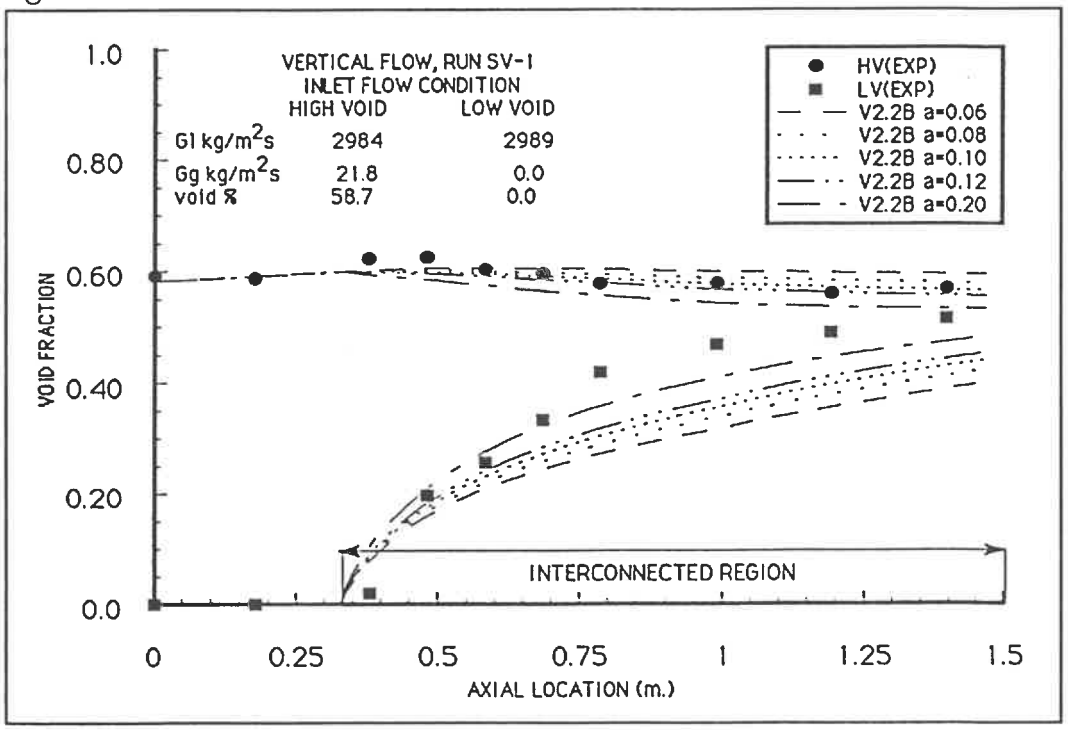

Figure 6.4: Void Fraction Profile Case SV–1 ASSERT – 4 Version 2.2B RUN–2

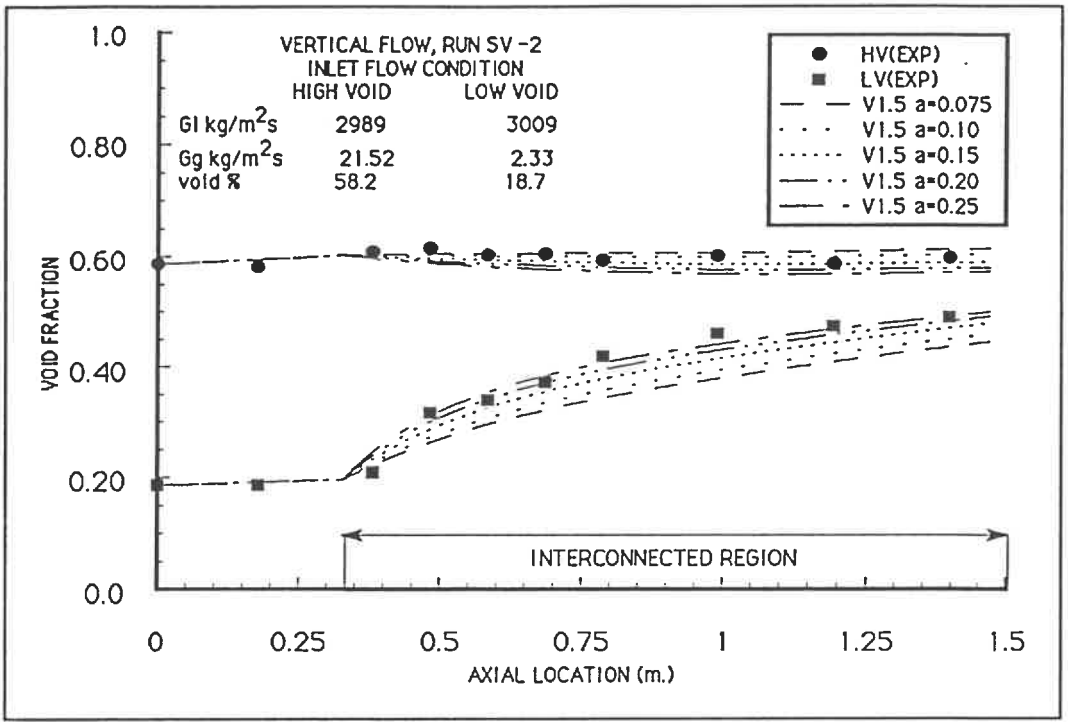

Figure 6.5: Void Fraction Profile Case SV–2 ASSERT – 4 Version 1.5

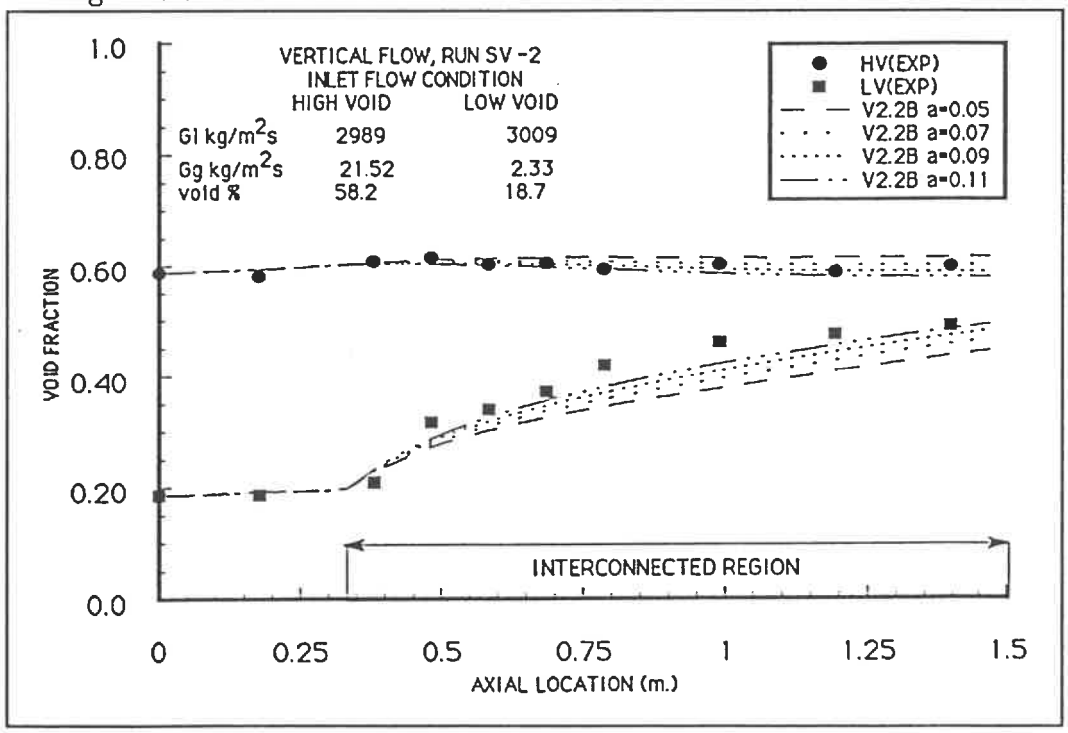

Figure 6.6: Void Fraction Profile Case SV–2 ASSERT – 4 Version 2.2B

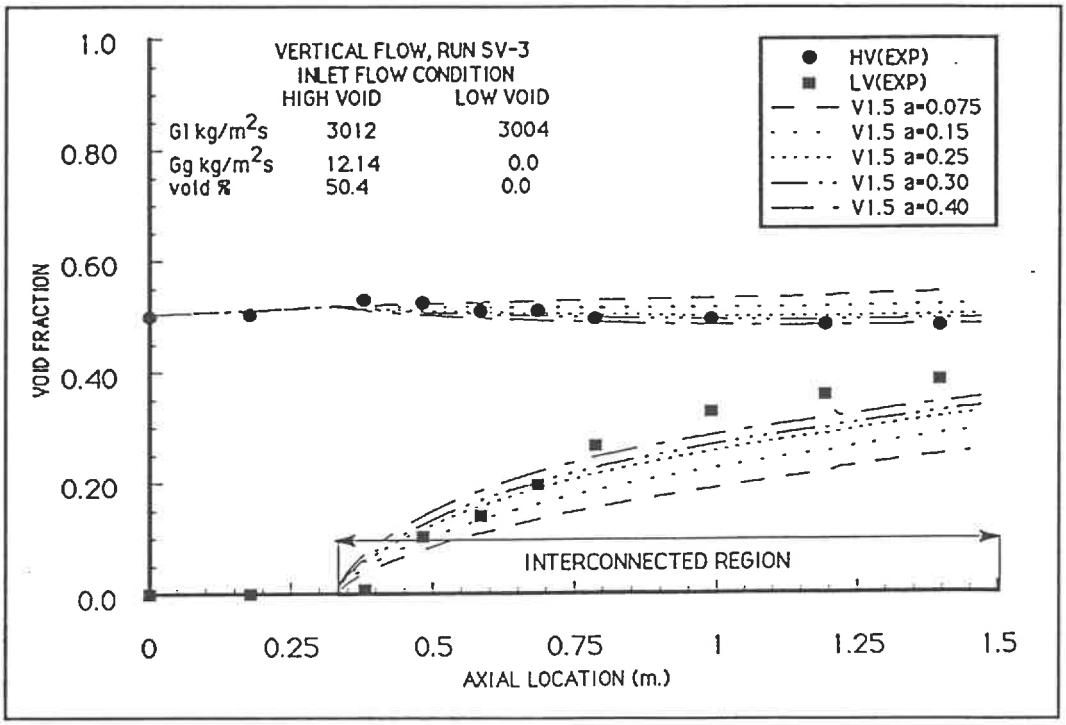

Figure 6.7: Void Fraction Profile Case SV–3 ASSERT – 4 Version 1.5

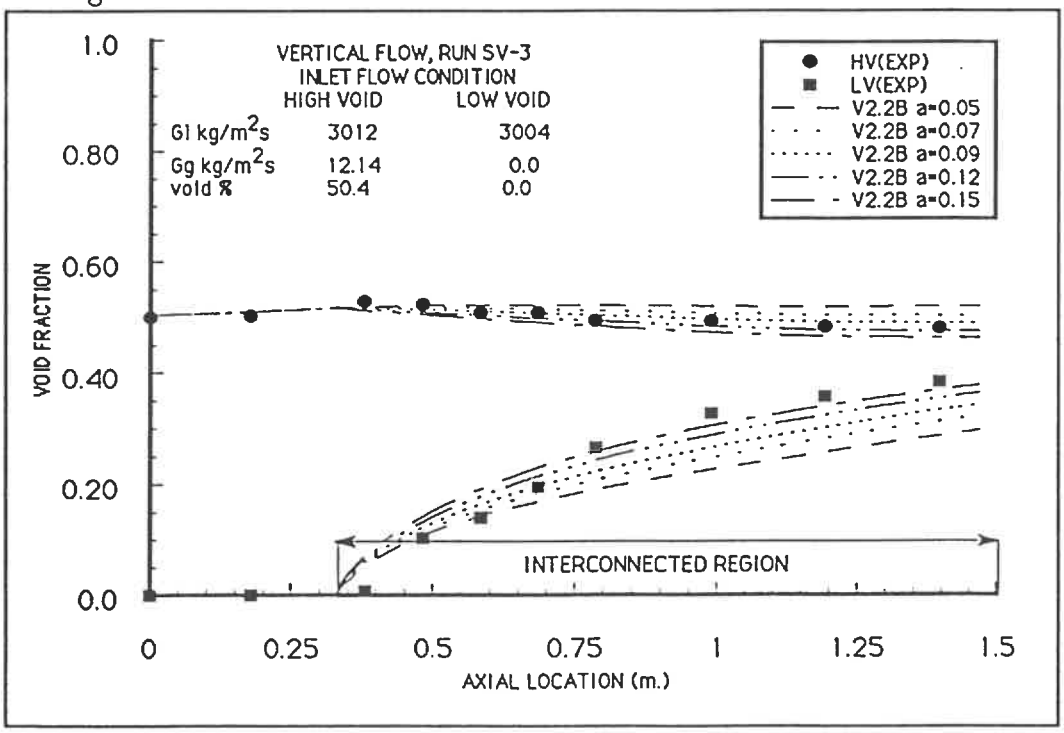

Figure 6.8: Void Fraction Profile Case SV–3 ASSERT – 4 Version 2.2B

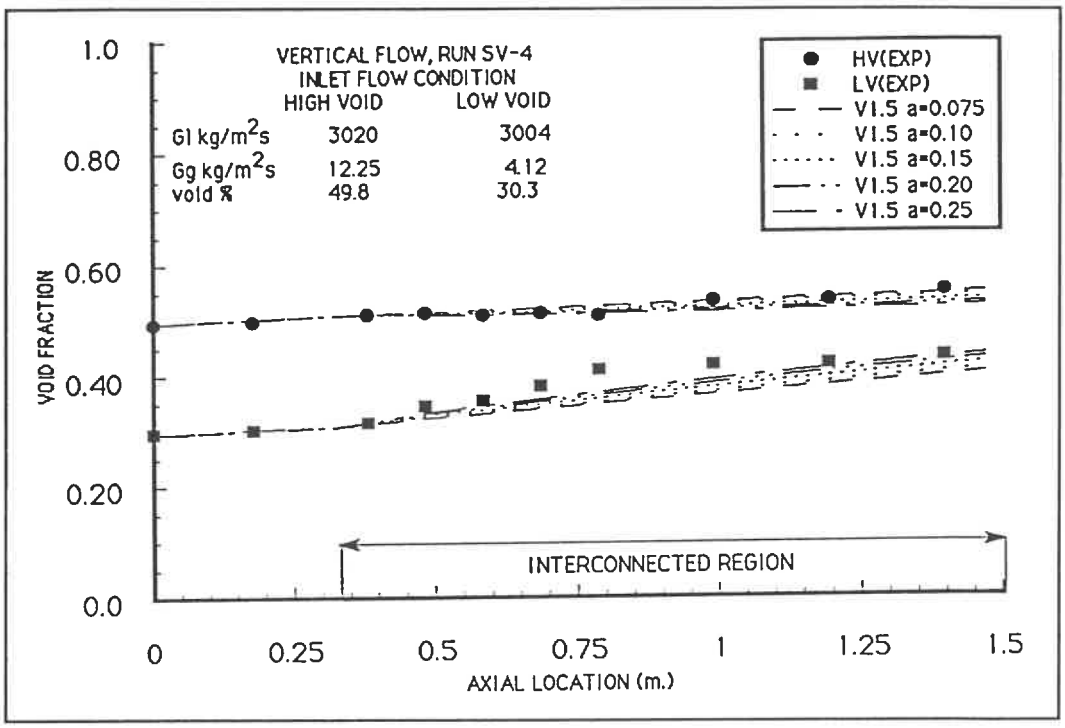

Figure 6.9: Void Fraction Profile Case SV–4 ASSERT – 4 Version 1.5

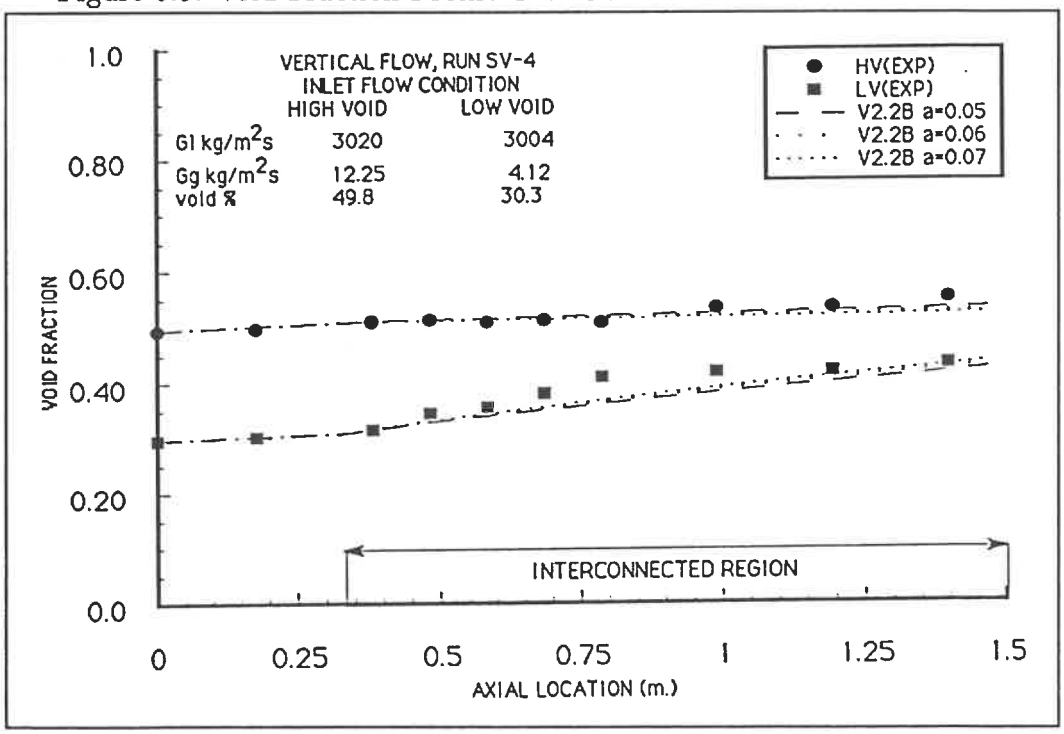

Figure 6.10: Void Fraction Profile Case SV–4 ASSERT – 4 Version 2.2B

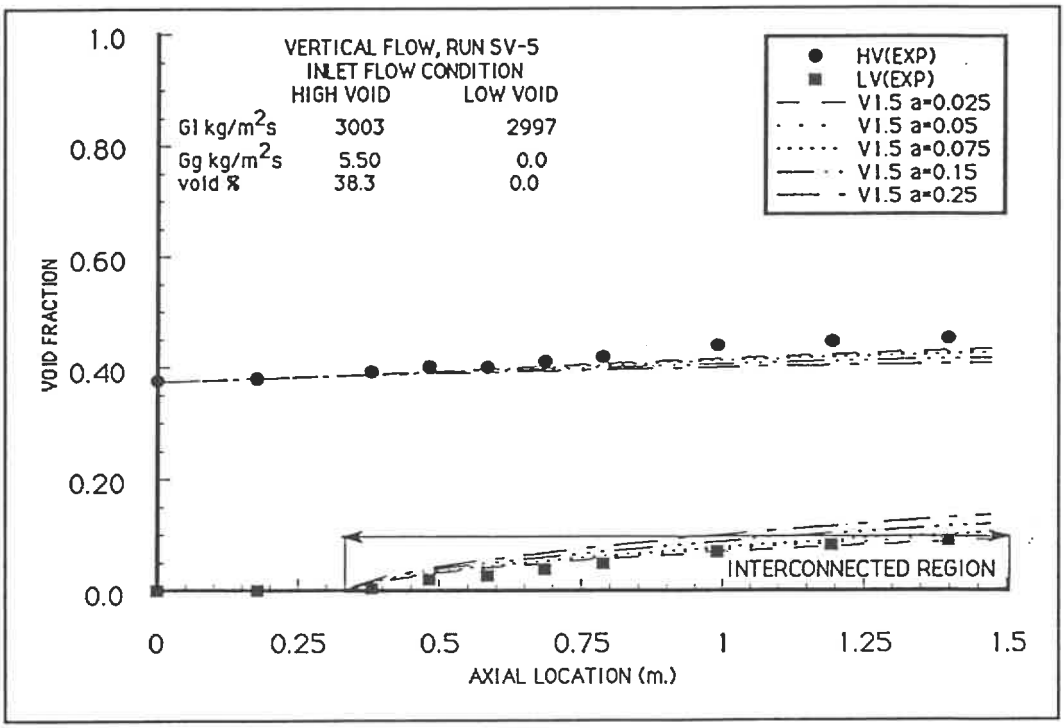

Figure 6.11: Void Fraction Profile Case SV–5 ASSERT – 4 Version 1.5

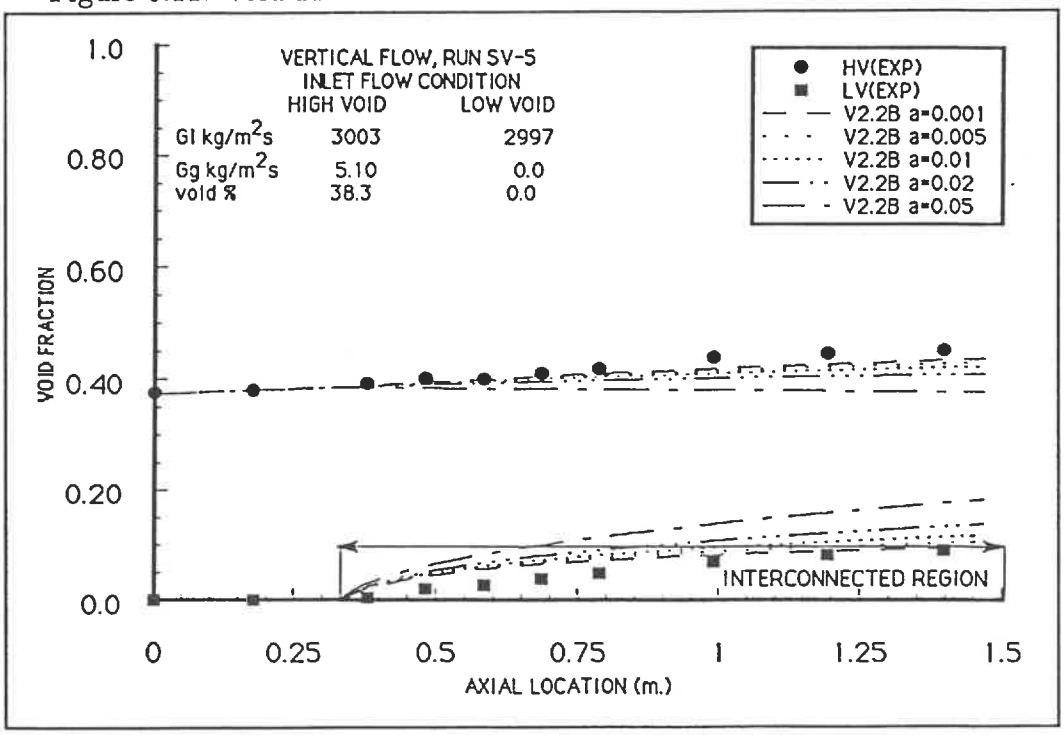

Figure 6.12: Void Fraction Profile Case SV–5 ASSERT – 4 Version 2.2B

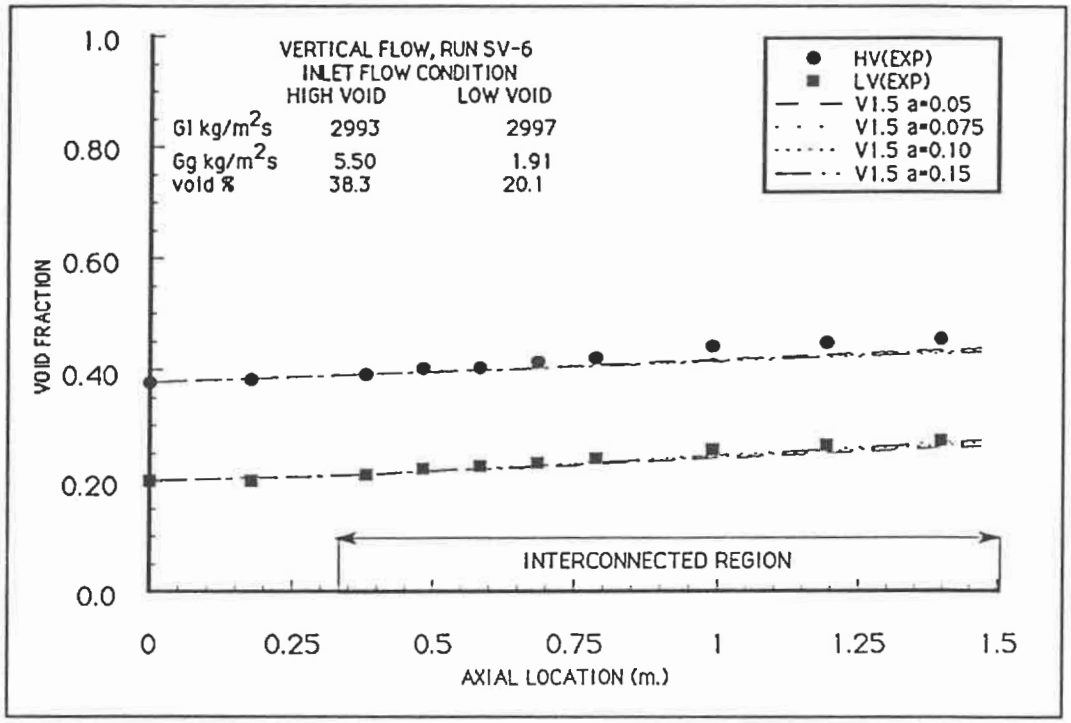

Figure 6.13: Void Fraction Profile Case SV-6 ASSERT – 4 Version 1.5

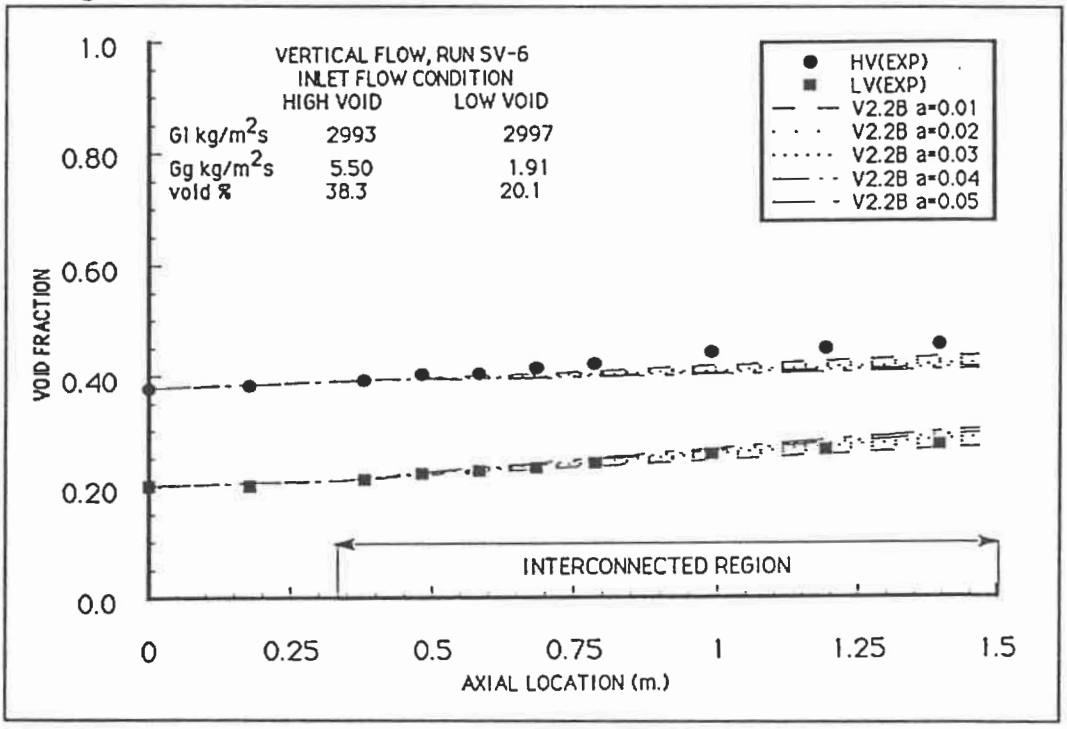

Figure 6.14: Void Fraction Profile Case SV-6 ASSERT – 4 Version 2.2B

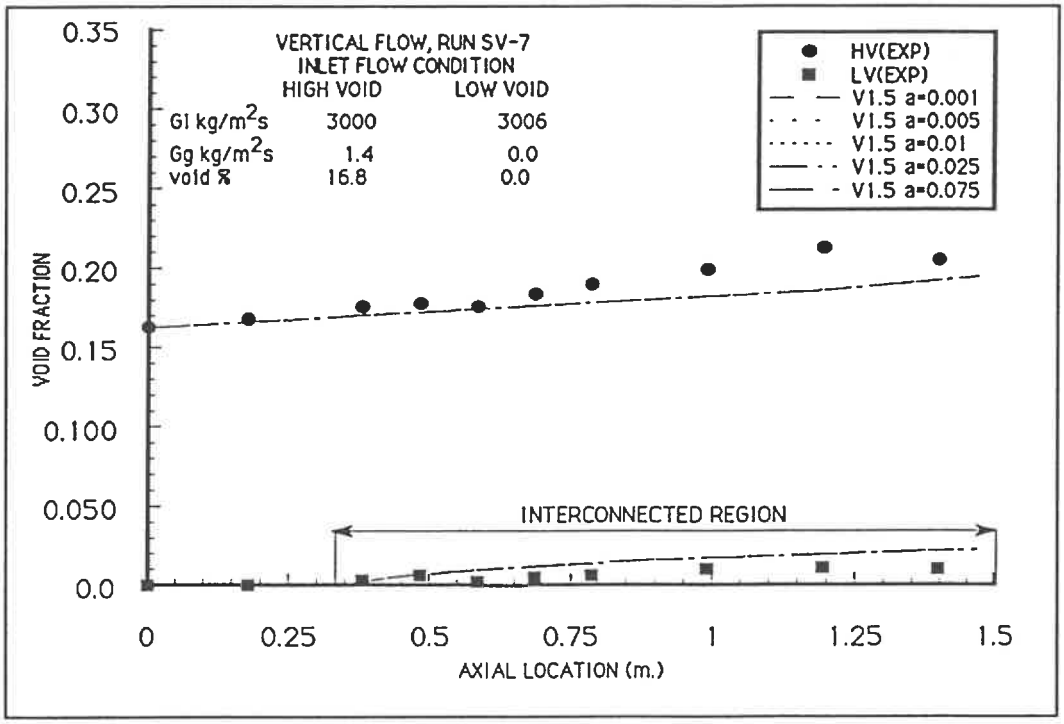

Figure 6.15: Void Fraction Profile Case SV-7 ASSERT – 4 Version 1.5

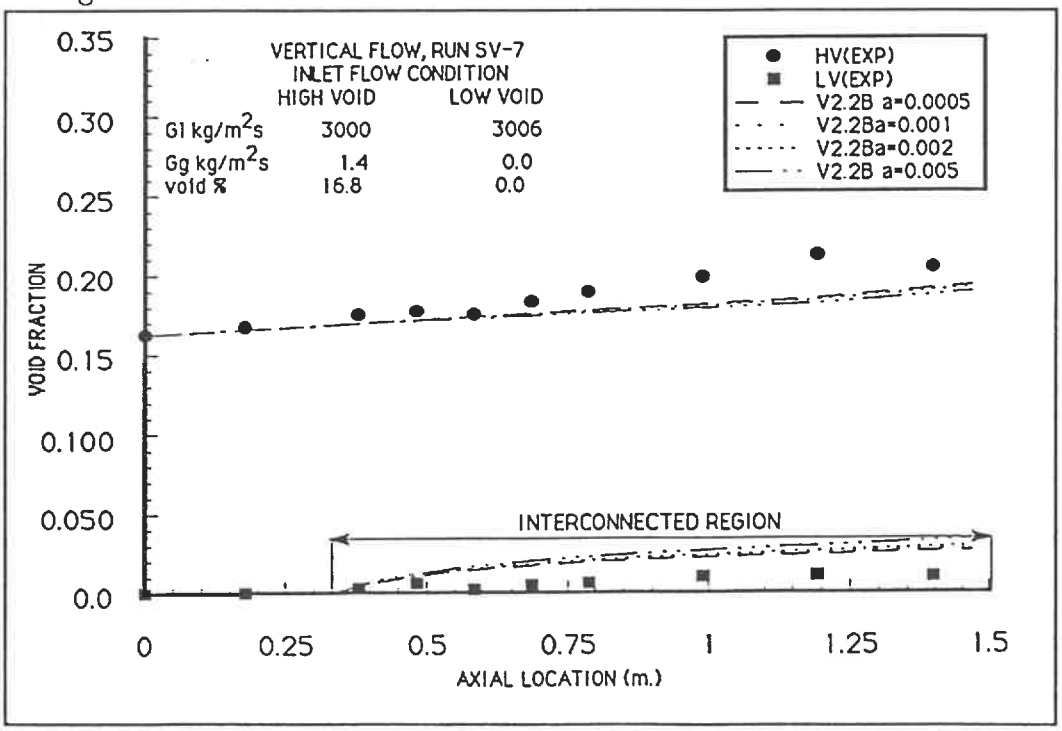

Figure 6.16: Void Fraction Profile Case SV-7 ASSERT – 4 Version 2.2B

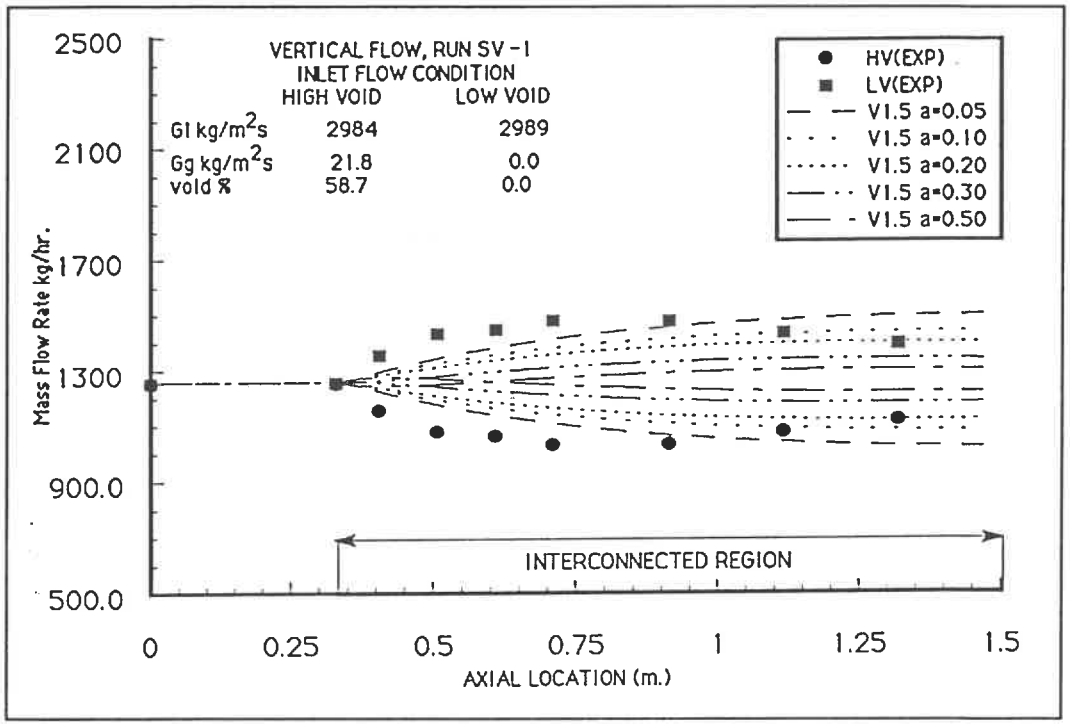

Figure 6.17: Mass Flow Rate Case SV–1 ASSERT – 4 Version 1.5 RUN–1

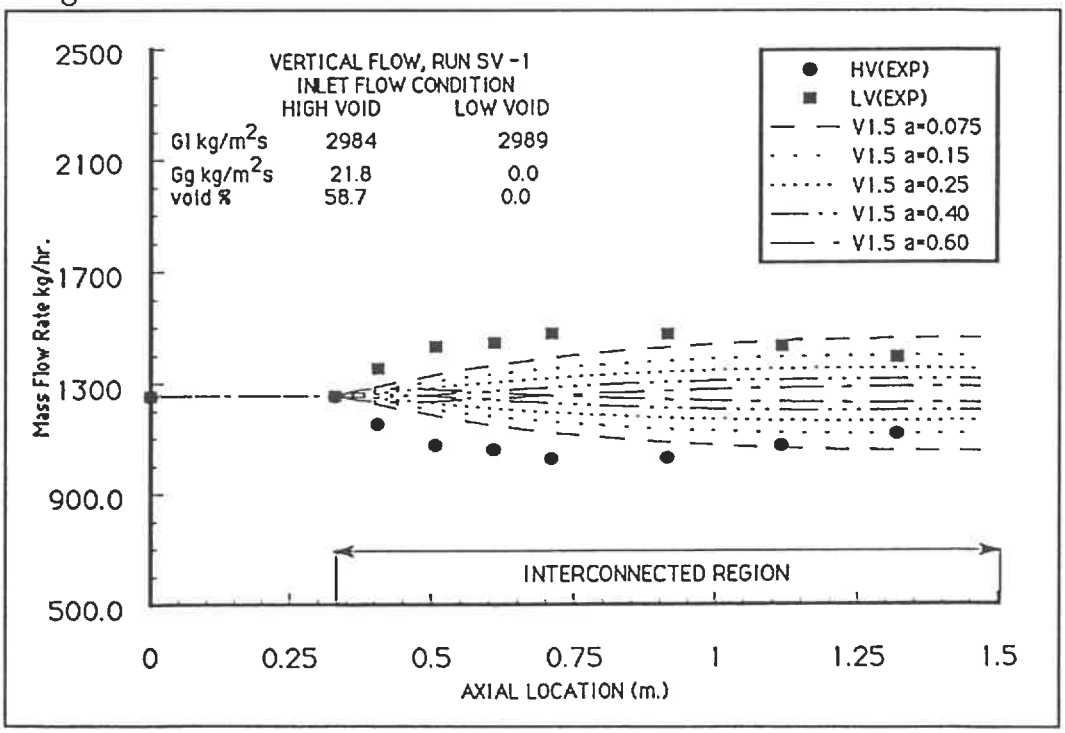

Figure 6.18: Mass Flow Rate Case SV–1 ASSERT – 4 Version 1.5 RUN–2

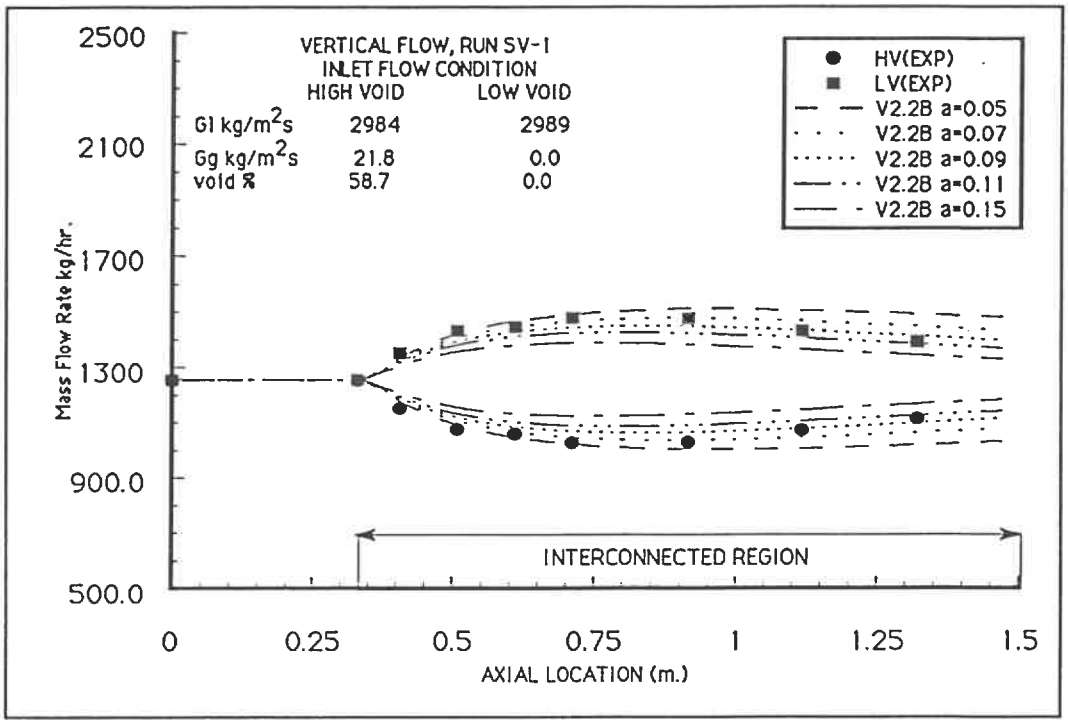

Figure 6.19: Mass Flow Rate Case SV-1 ASSERT - 4 Version 2.2B RUN-1

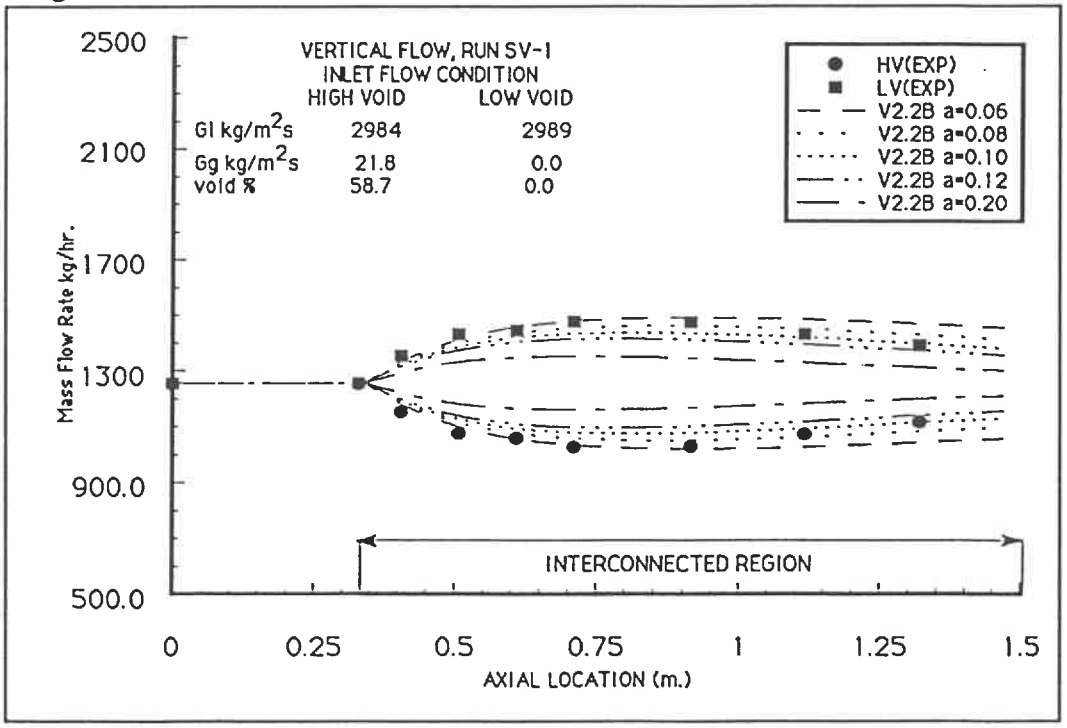

Figure 6.20: Mass Flow Rate Case SV-1 ASSERT - 4 Version 2.2B RUN-2

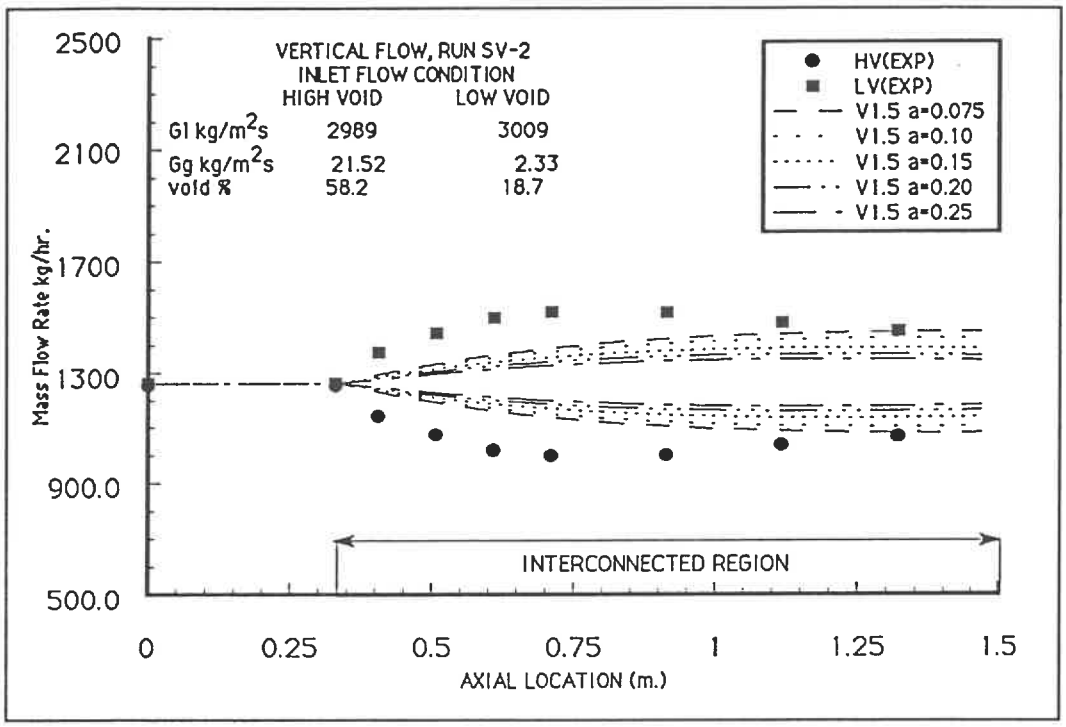

Figure 6.21: Mass Flow Rate Case SV-2 ASSERT – 4 Version 1.5

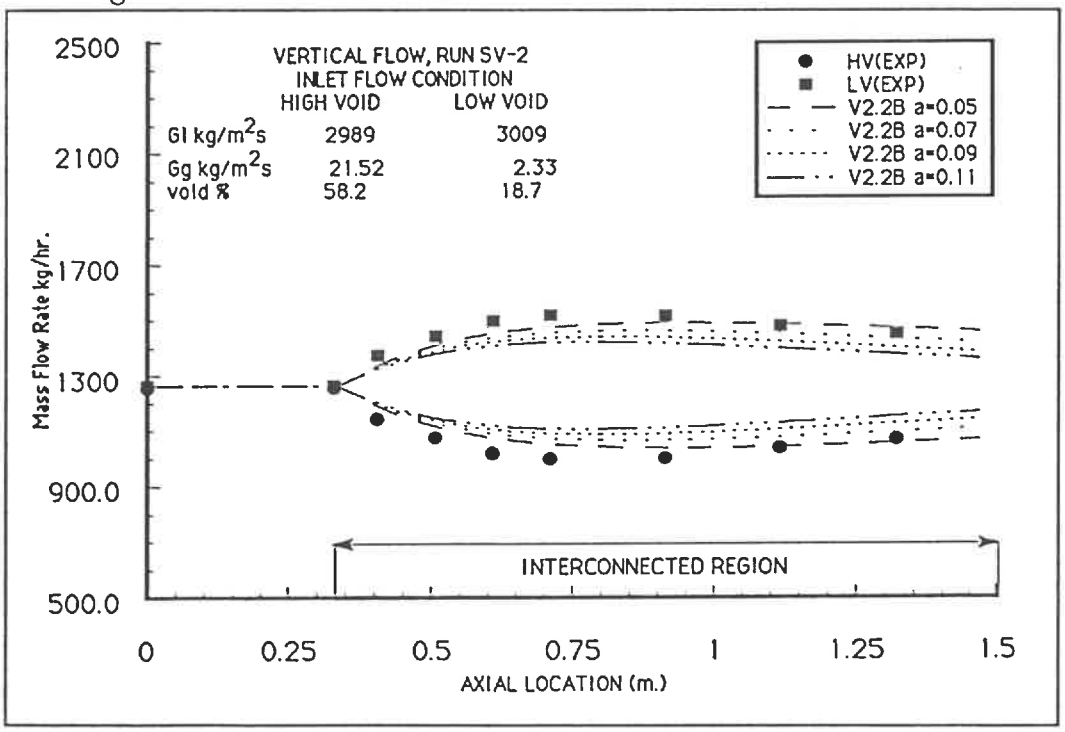

Figure 6.22: Mass Flow Rate Case SV-2 ASSERT – 4 Version 2.2B

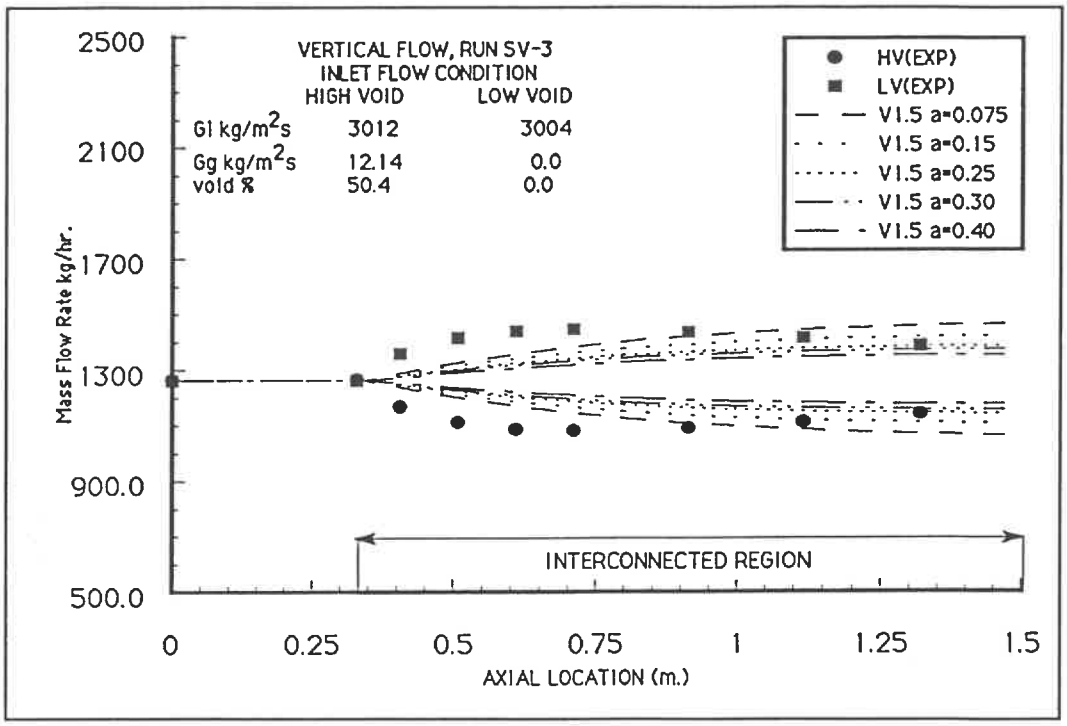

Figure 6.23: Mass Flow Rate Case SV-3 ASSERT – 4 Version 1.5

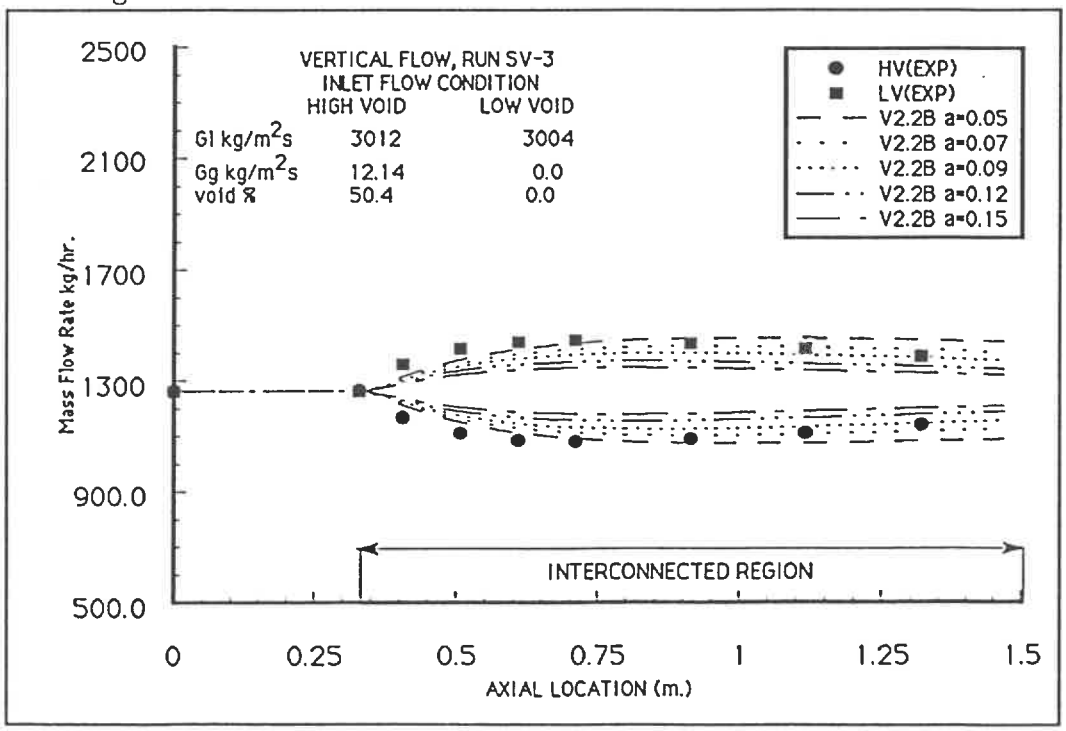

Figure 6.24: Mass Flow Rate Case SV-3 ASSERT – 4 Version 2.2B

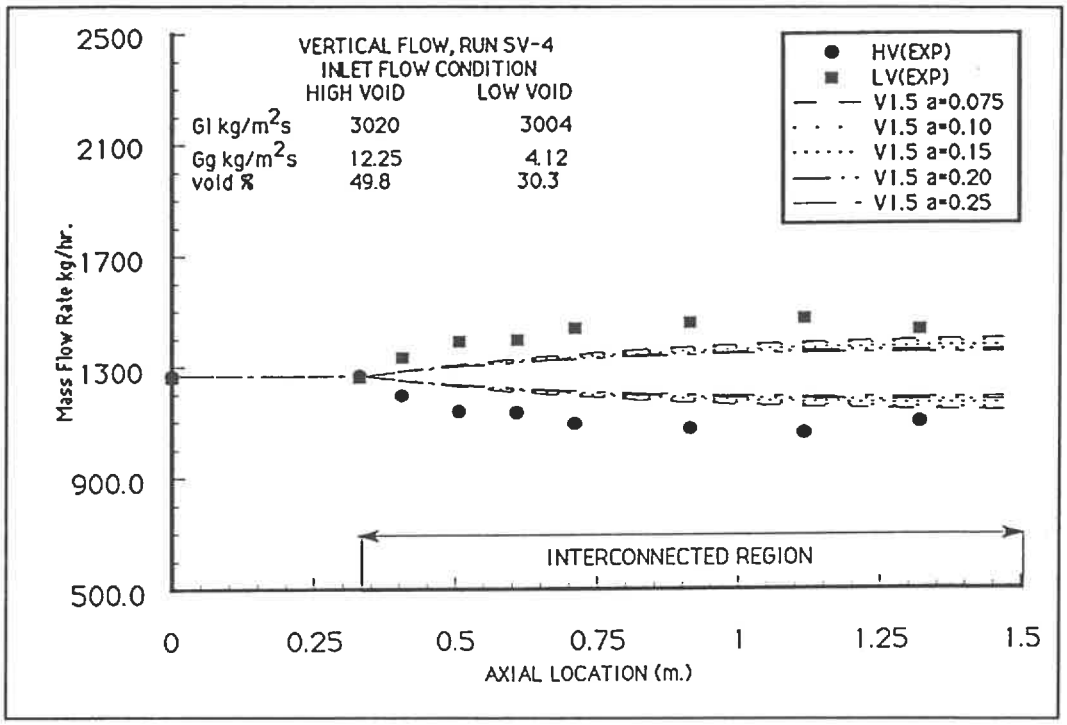

Figure 6.25: Mass Flow Rate Case SV-4 ASSERT – 4 Version 1.5

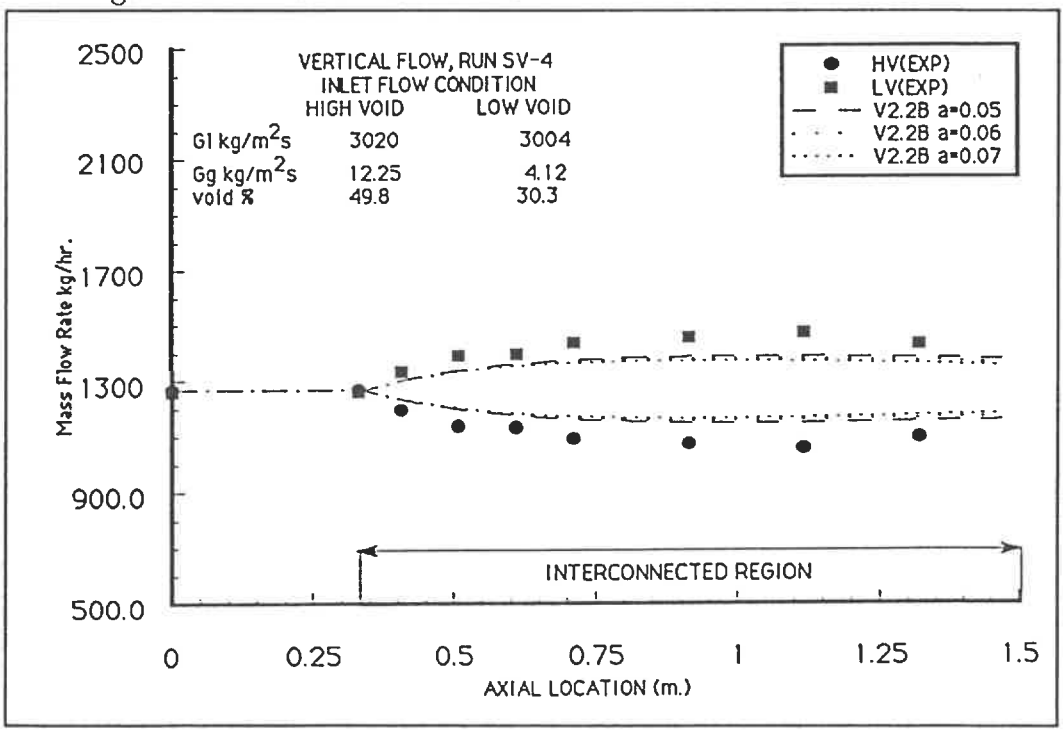

Figure 6.26: Mass Flow Rate Case SV-4 ASSERT – 4 Version 2.2B

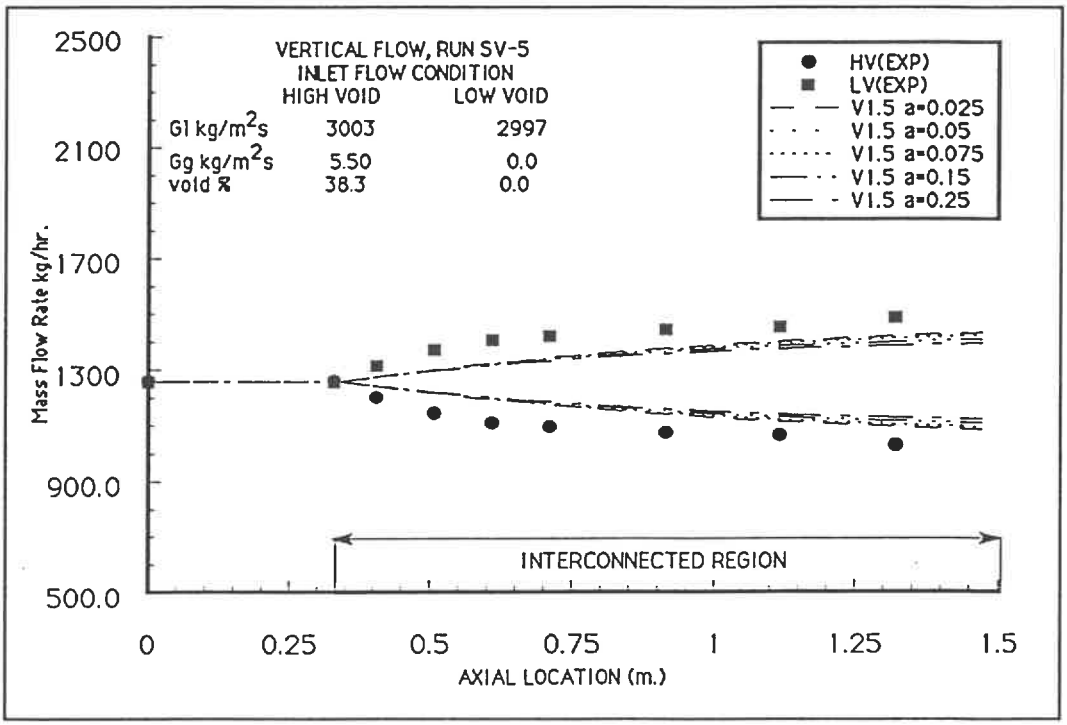

Figure 6.27: Mass Flow Rate Case SV-5 ASSERT – 4 Version 1.5

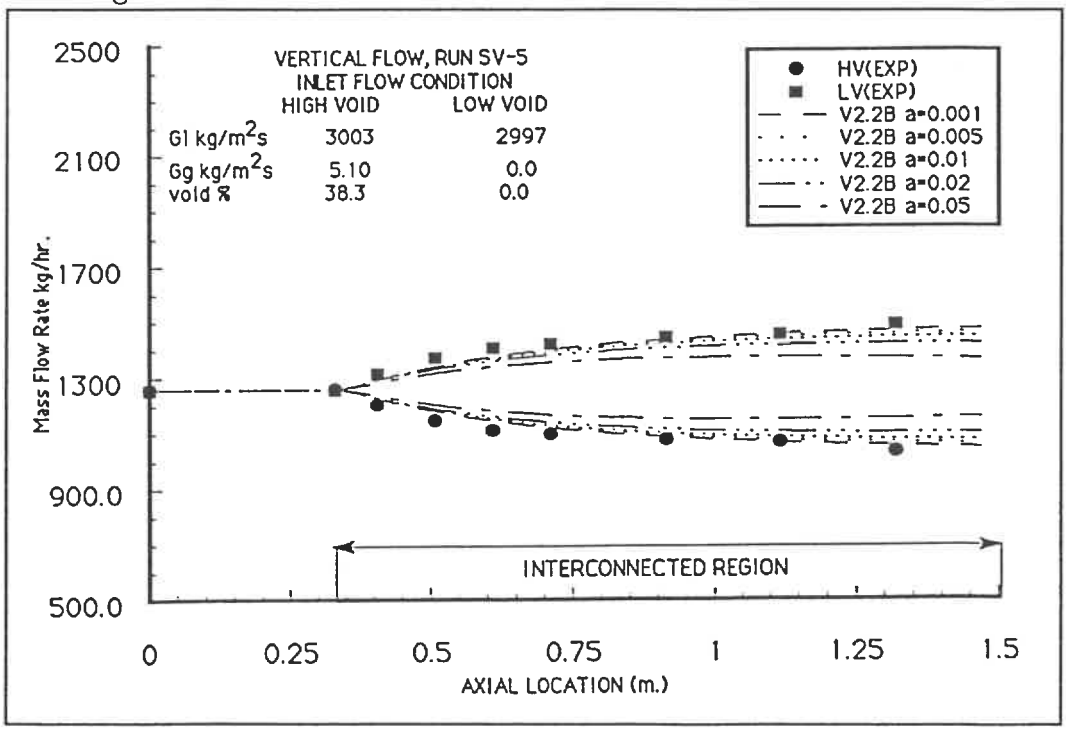

Figure 6.28: Mass Flow Rate Case SV-5 ASSERT – 4 Version 2.2B

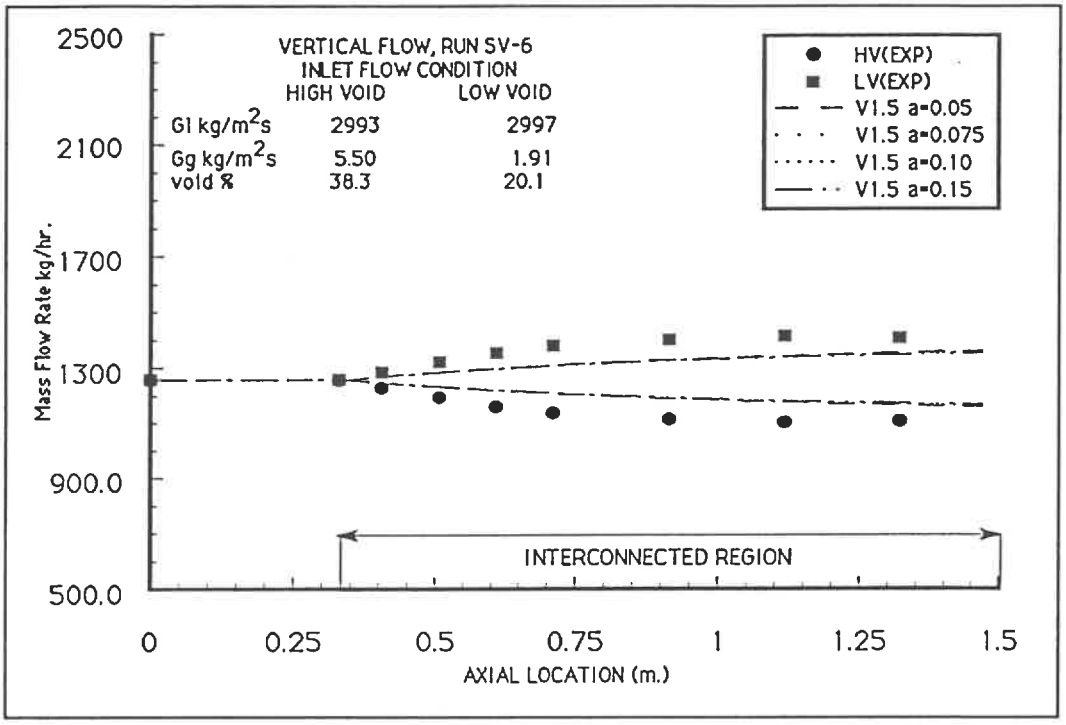

Figure 6.29: Mass Flow Rate Case SV-6 ASSERT – 4 Version 1.5

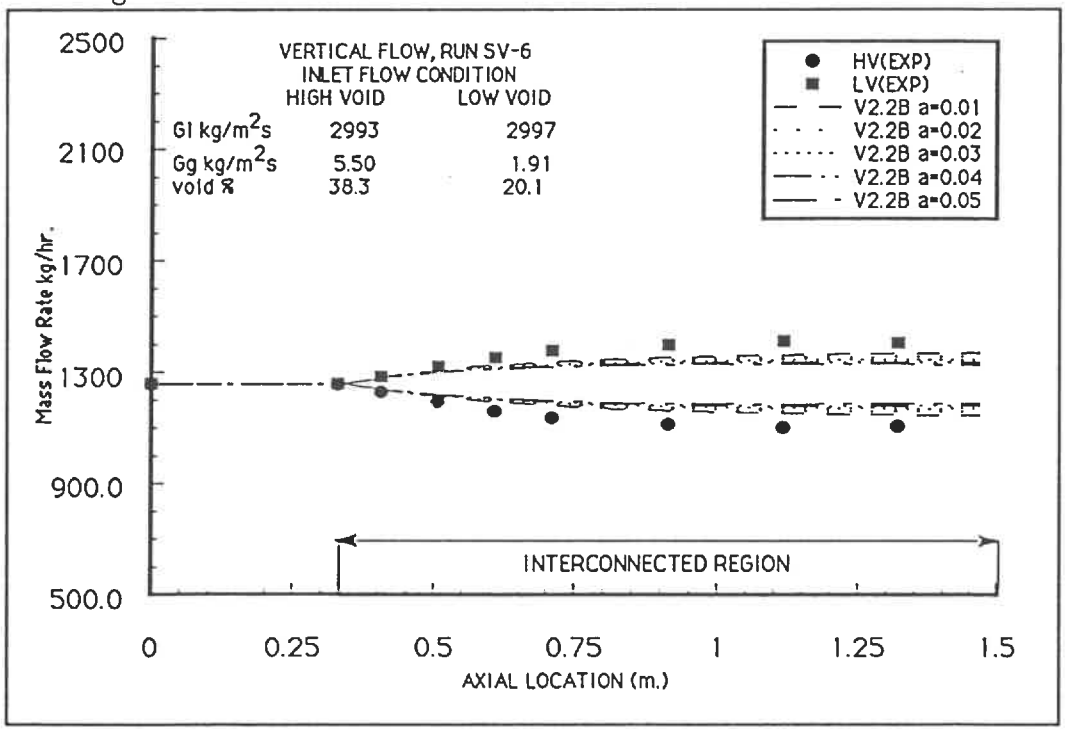

Figure 6.30: Mass Flow Rate Case SV-6 ASSERT – 4 Version 2.2B

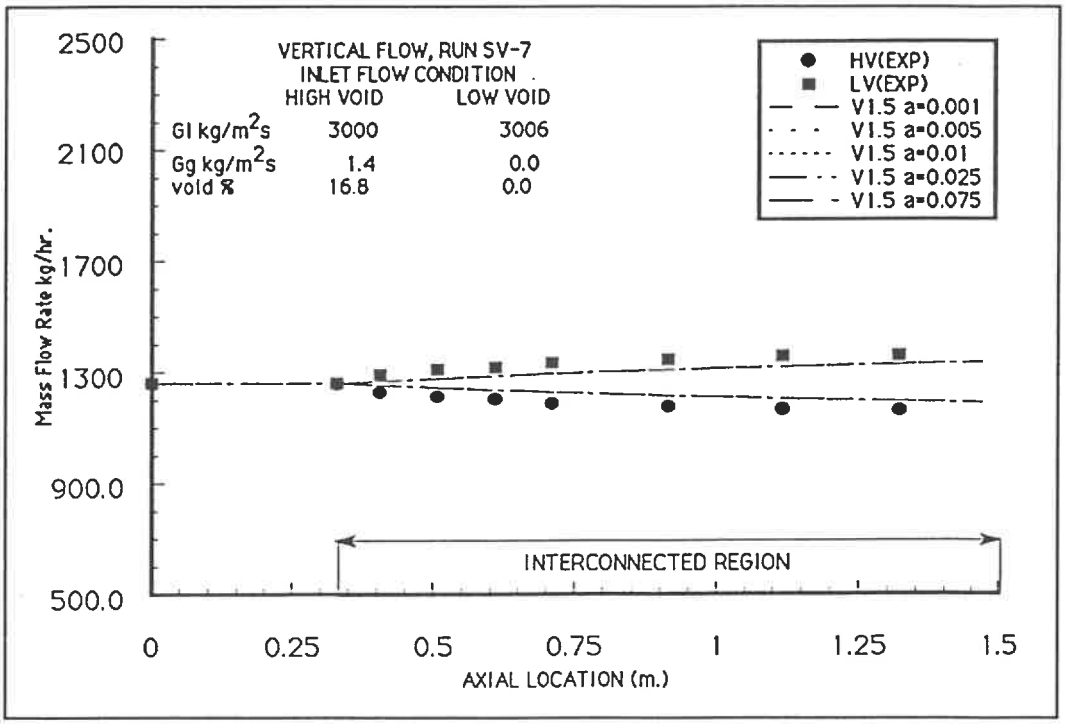

Figure 6.31: Mass Flow Rate Case SV–7 ASSERT – 4 Version 1.5

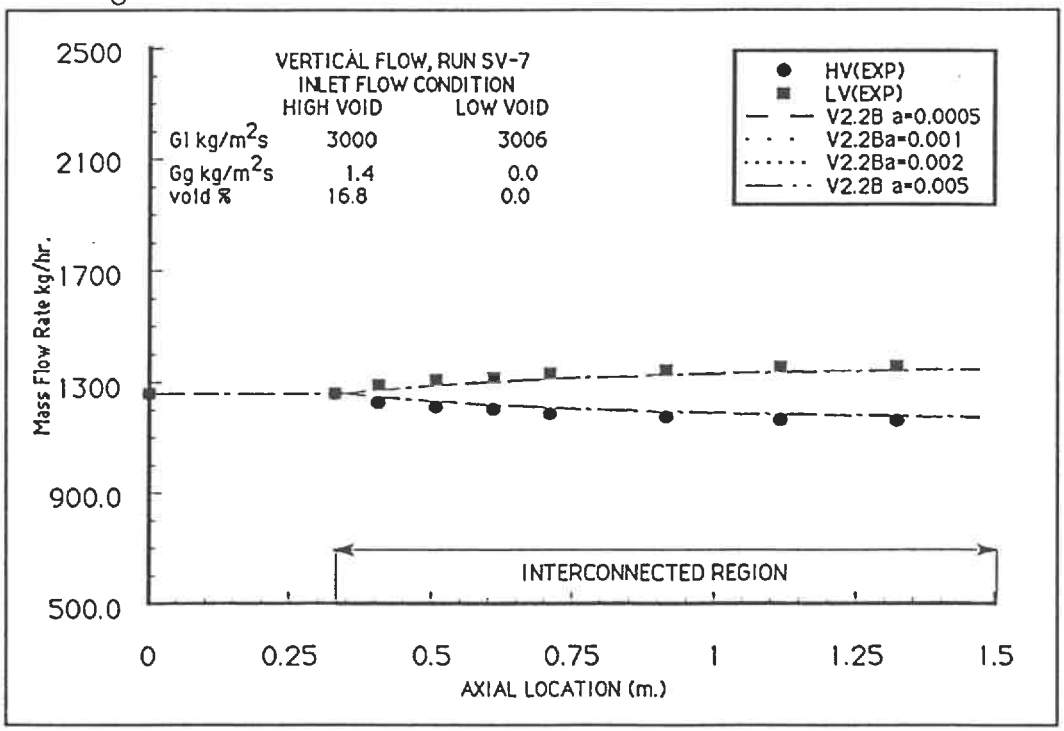

Figure 6.32: Mass Flow Rate Case SV–7 ASSERT – 4 Version 2.2B

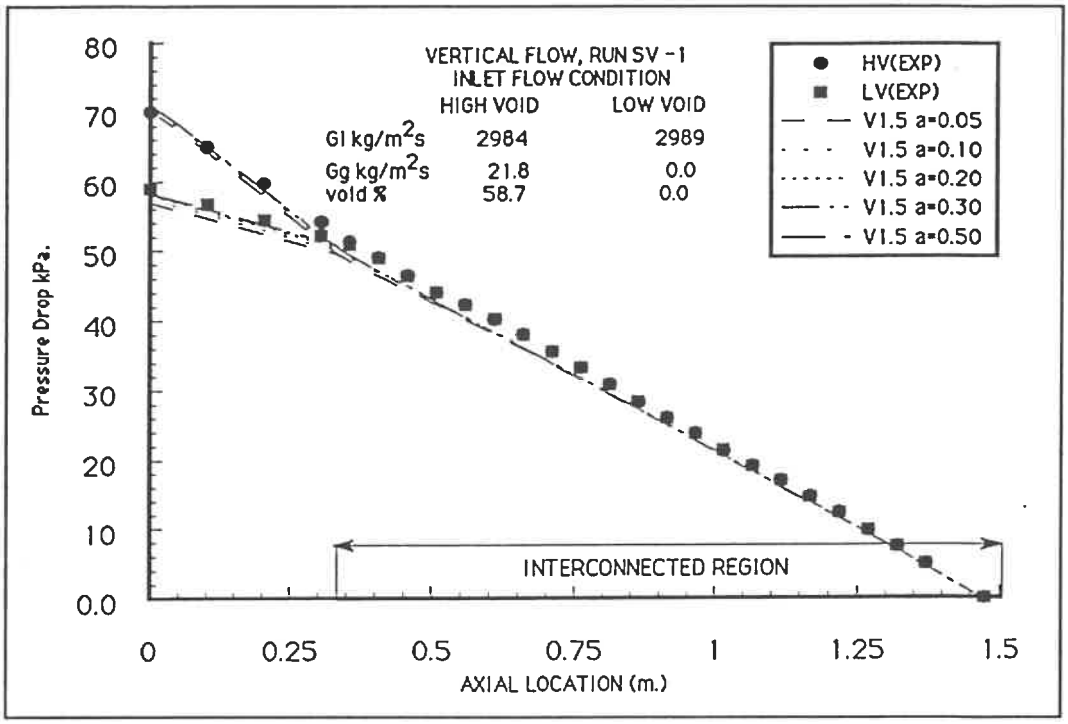

Figure 6.33: Pressure Drop Profile Case SV–1 ASSERT – 4 Version 1.5 RUN–1

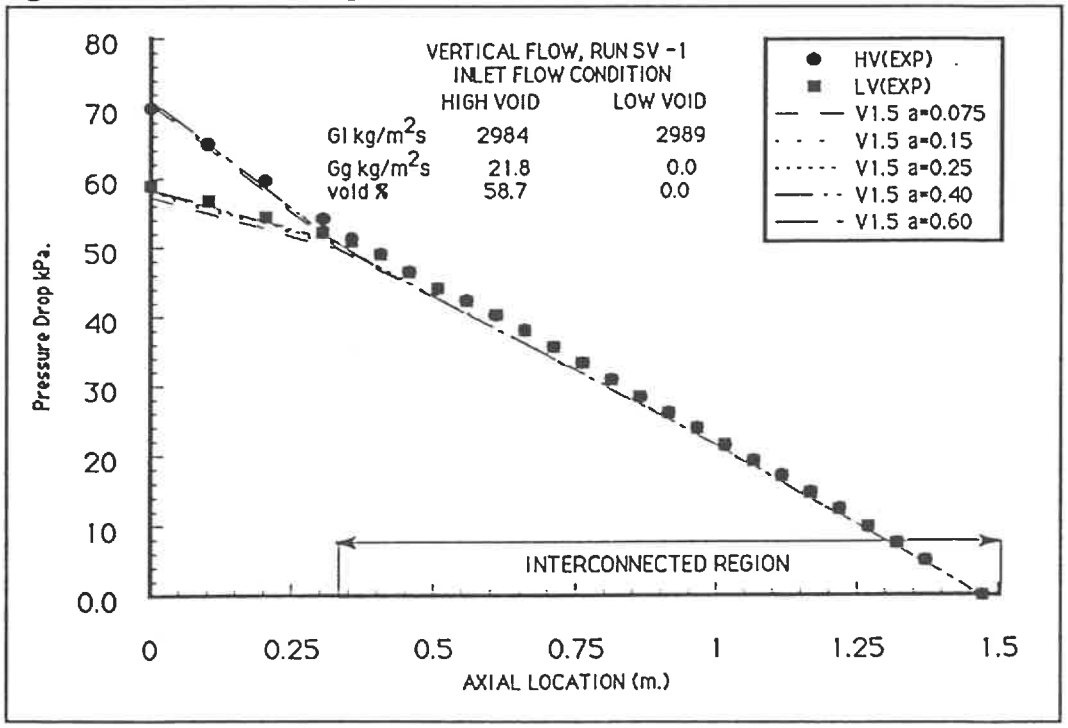

Figure 6.34: Pressure Drop Profile Case SV–1 ASSERT – 4 Version 1.5 RUN–2

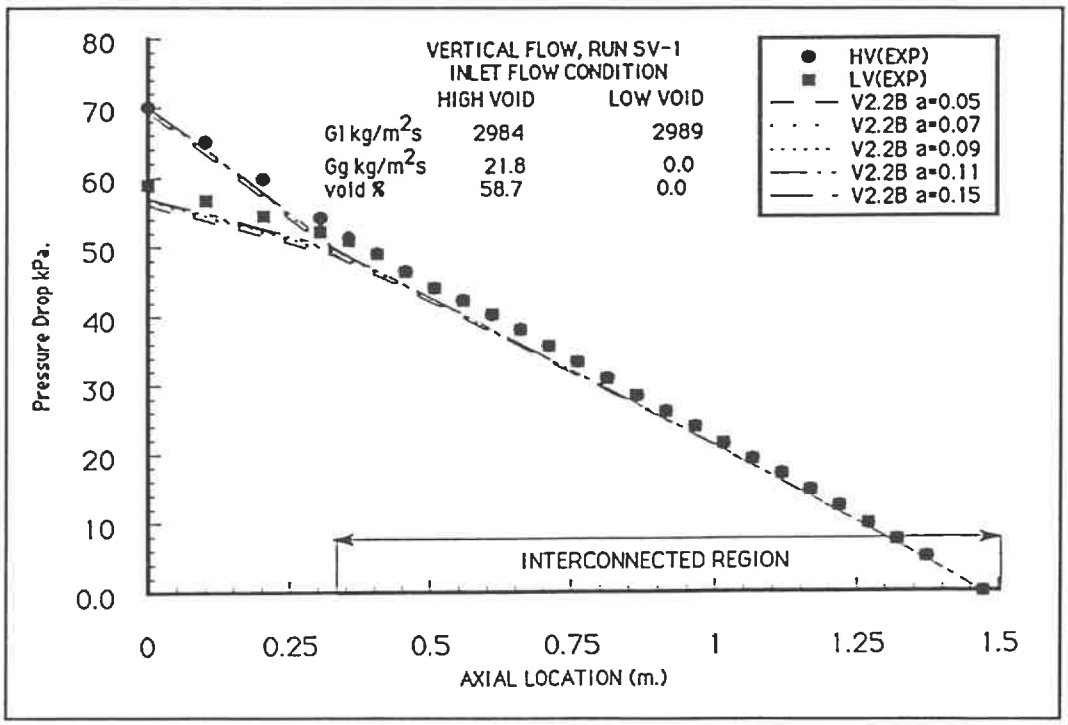

Figure 6.35: Pressure Drop Profile Case SV-1 ASSERT – 4 Version 2.2B RUN-1

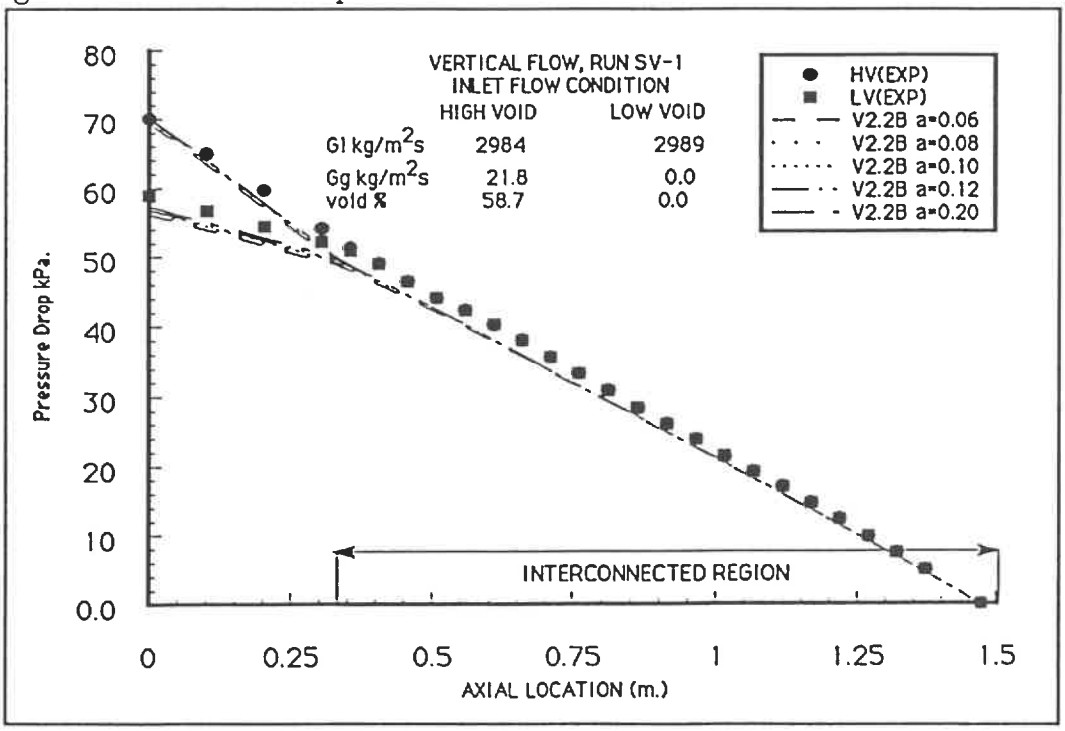

Figure 6.36: Pressure Drop Profile Case SV-1 ASSERT – 4 Version 2.2B RUN-2

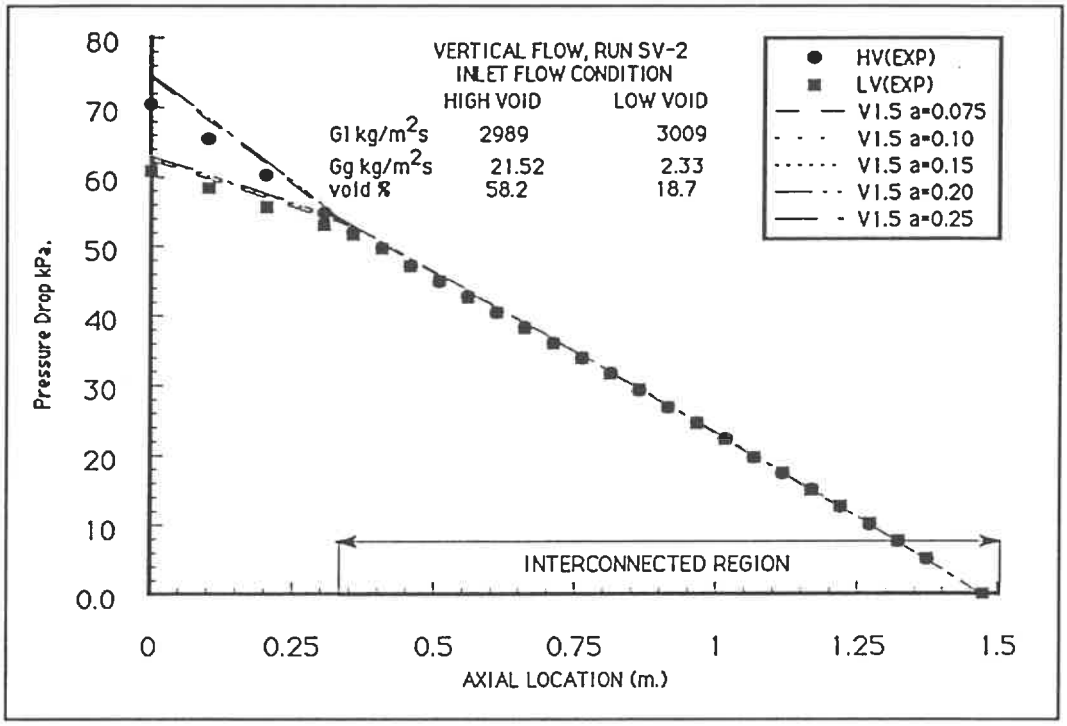

Figure 6.37: Pressure Drop Profile Case SV–2 ASSERT – 4 Version 1.5

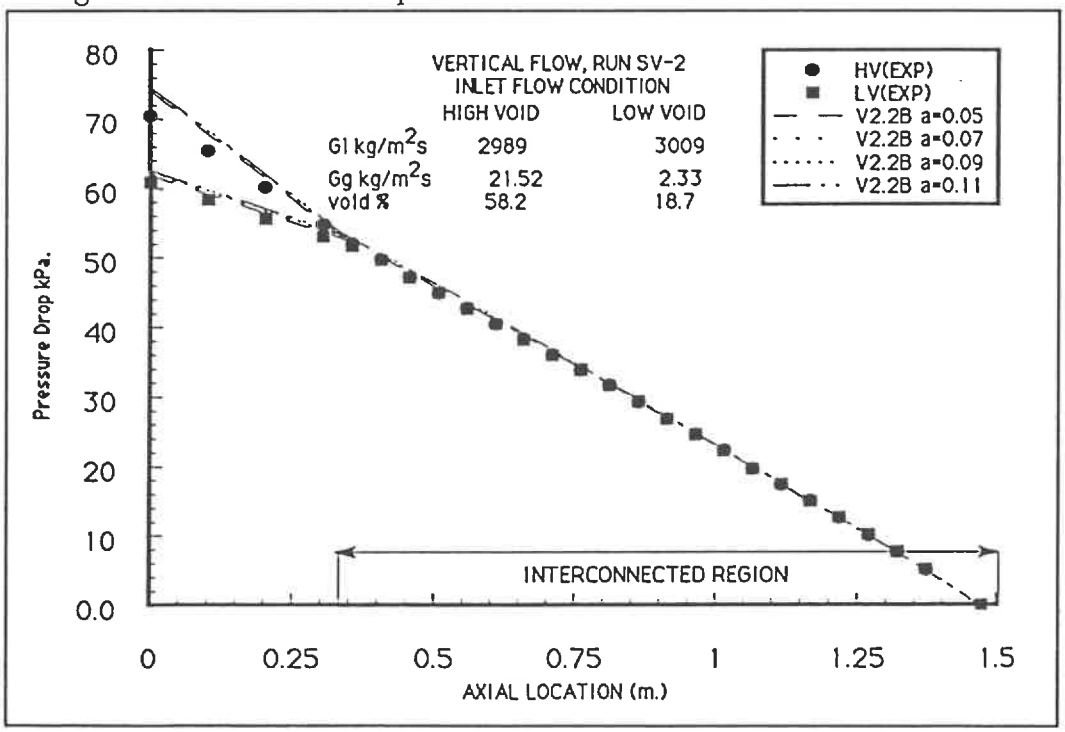

Figure 6.38: Pressure Drop Profile Case SV–2 ASSERT – 4 Version 2.2B

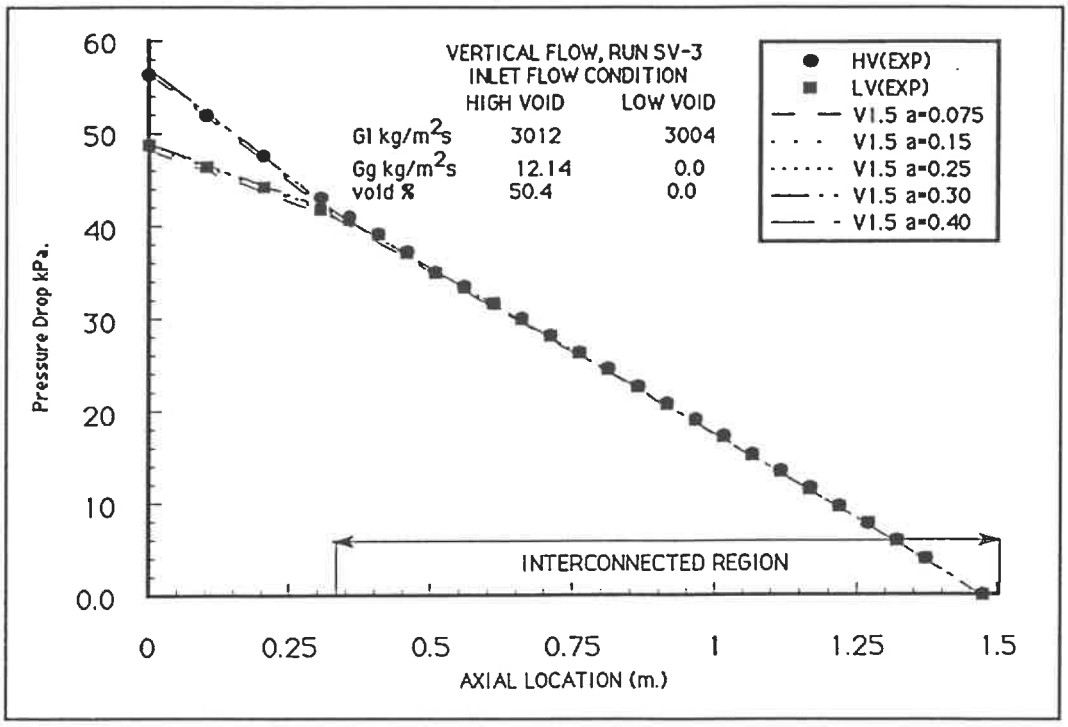

Figure 6.39: Pressure Drop Profile Case SV–3 ASSERT – 4 Version 1.5

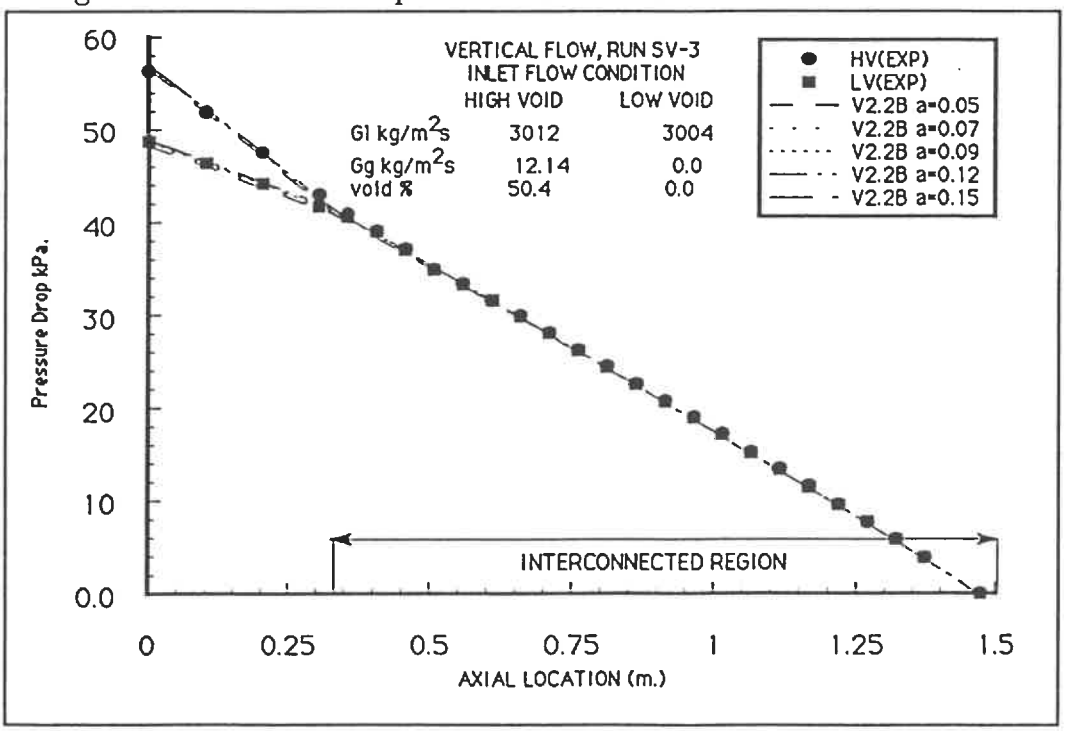

Figure 6.40: Pressure Drop Profile Case SV–3 ASSERT – 4 Version 2.2B

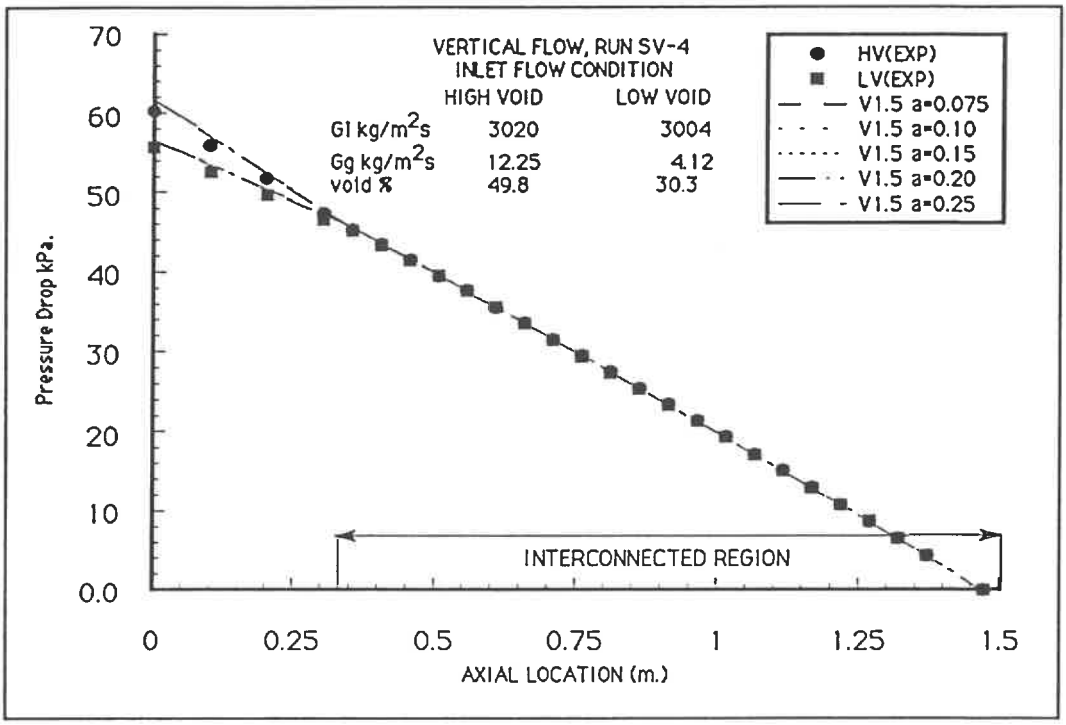

Figure 6.41: Pressure Drop Profile Case SV–4 ASSERT – 4 Version 1.5

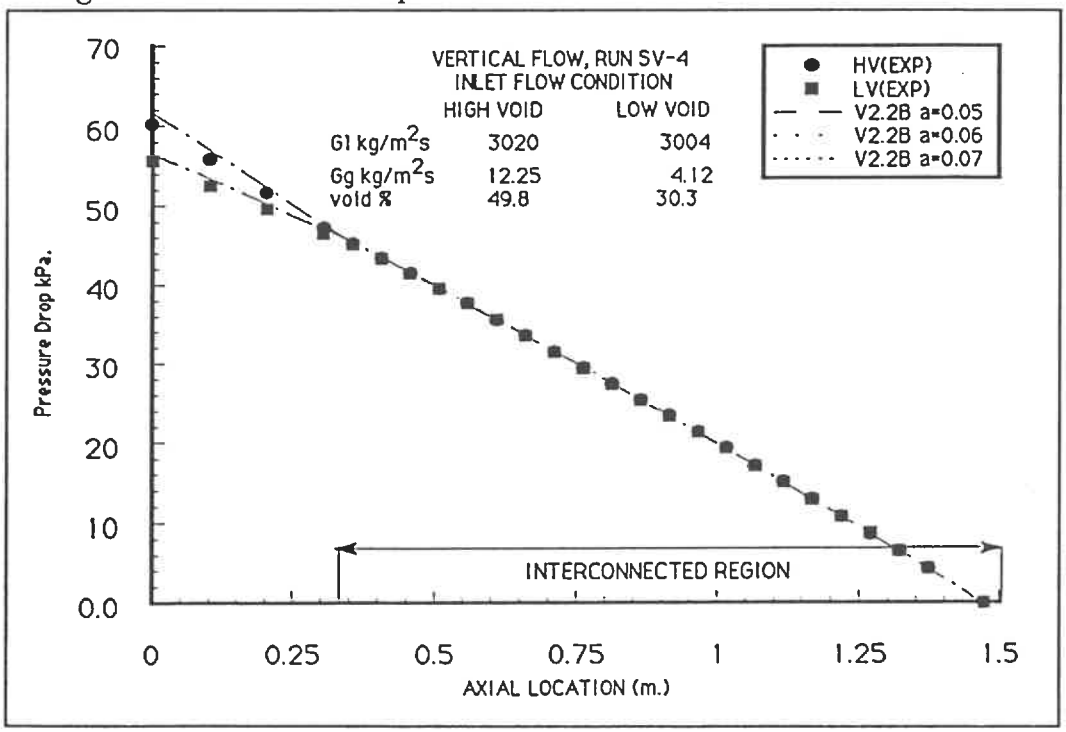

Figure 6.42: Pressure Drop Profile Case SV–4 ASSERT – 4 Version 2.2B

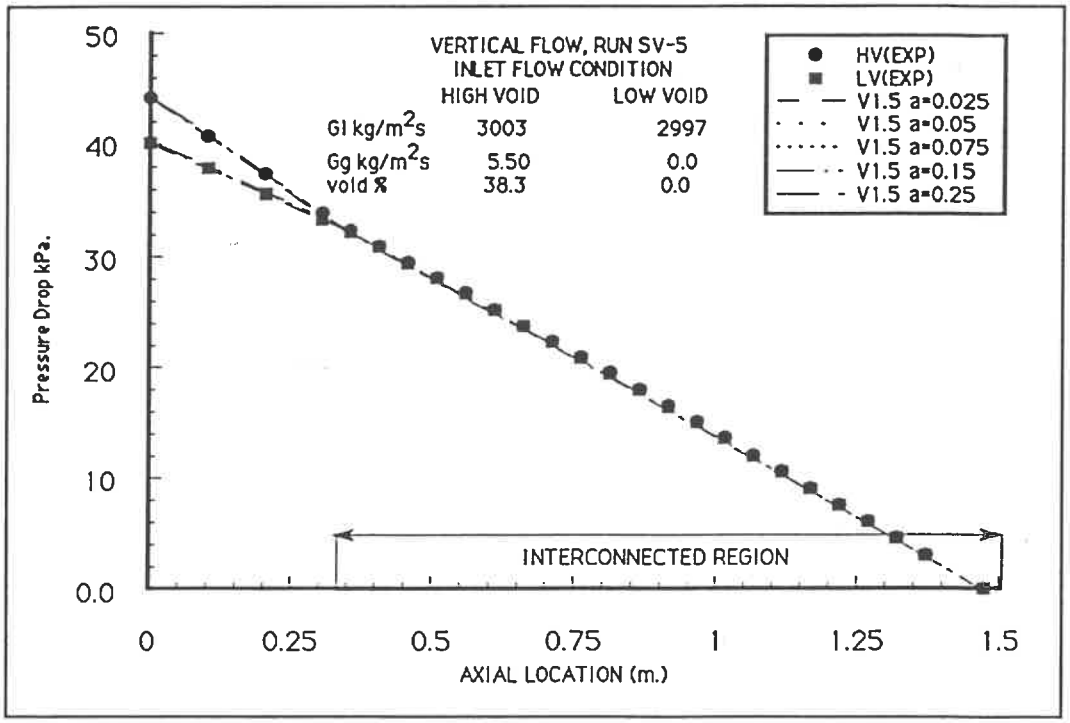

Figure 6.43: Pressure Drop Profile Case SV–5 ASSERT – 4 Version 1.5

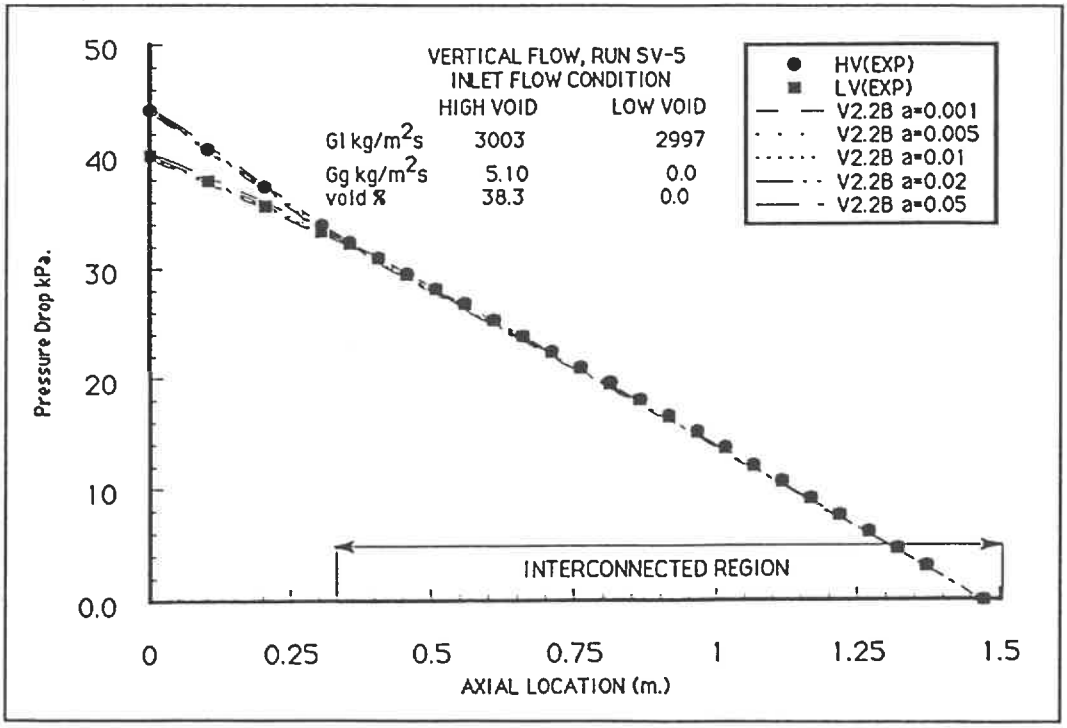

Figure 6.44: Pressure Drop Profile Case SV–5 ASSERT – 4 Version 2.2B

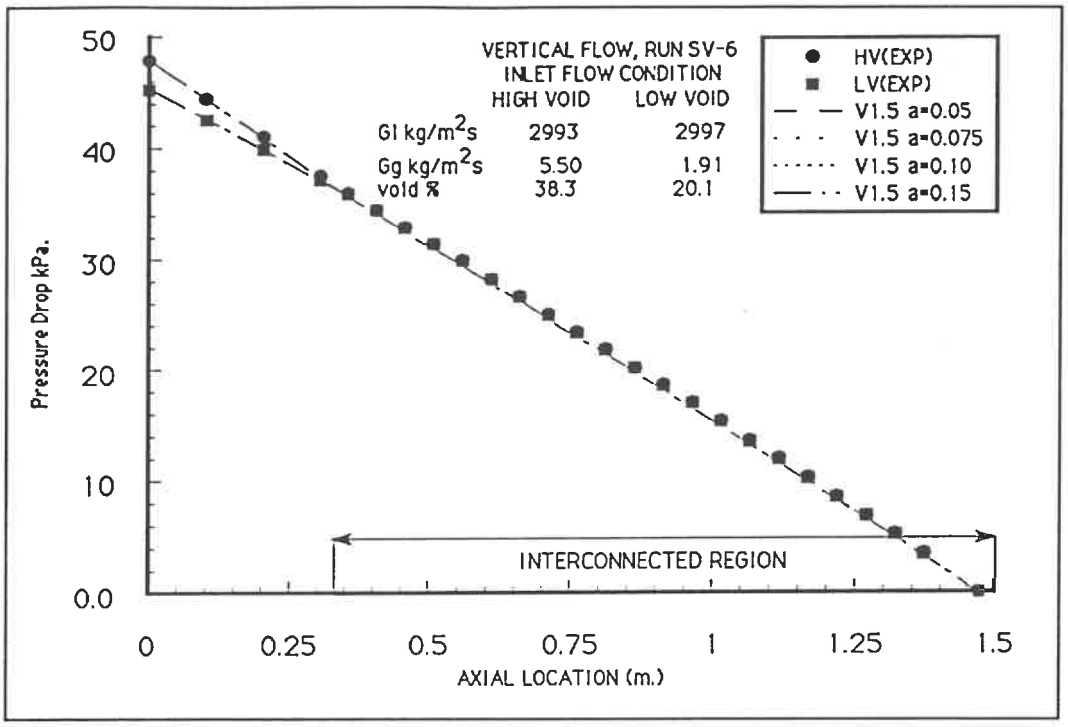

Figure 6.45: Pressure Drop Profile Case SV–6 ASSERT – 4 Version 1.5

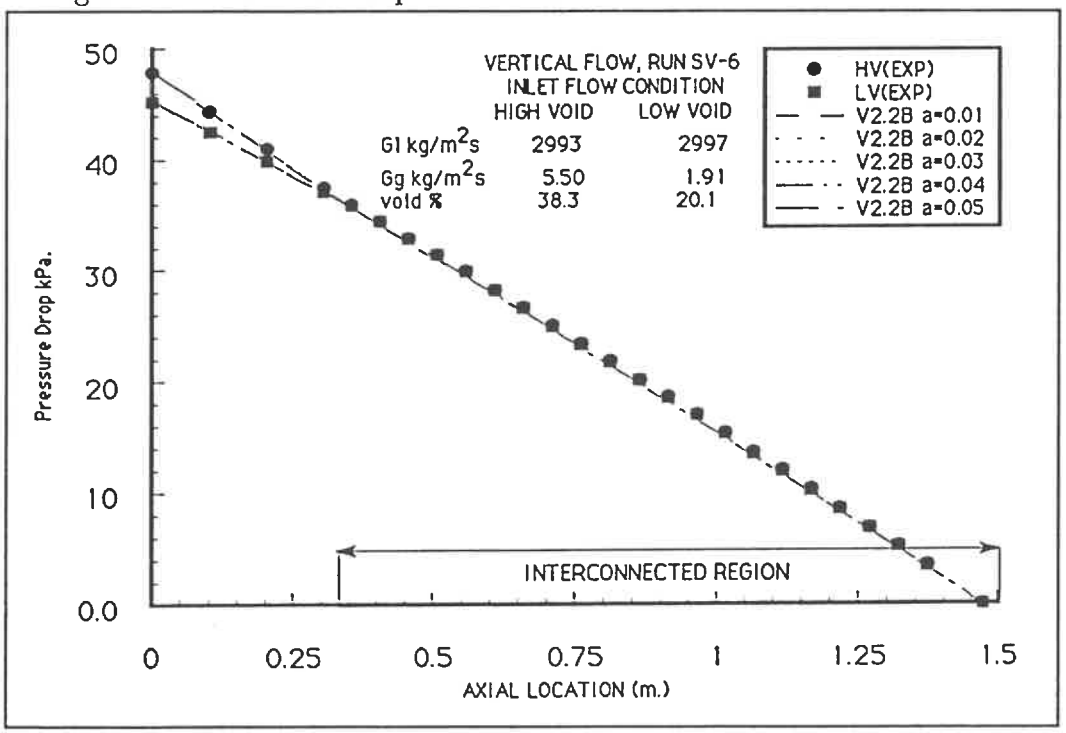

Figure 6.46: Pressure Drop Profile Case SV–6 ASSERT – 4 Version 2.2B

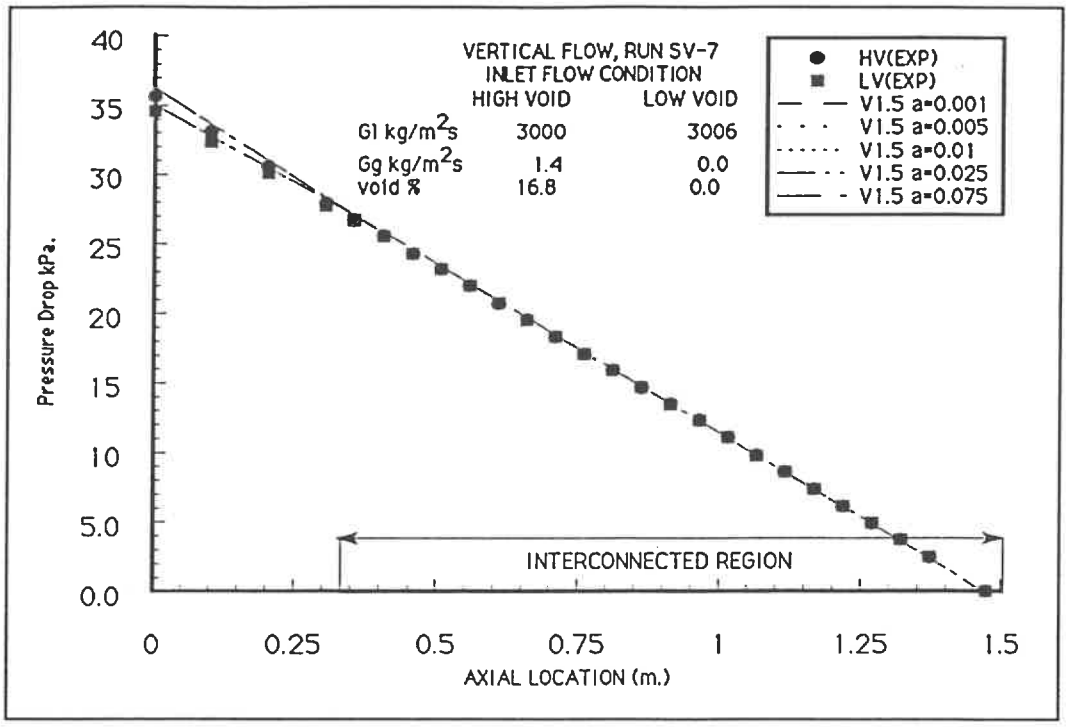

Figure 6.47: Pressure Drop Profile Case SV–7 ASSERT – 4 Version 1.5

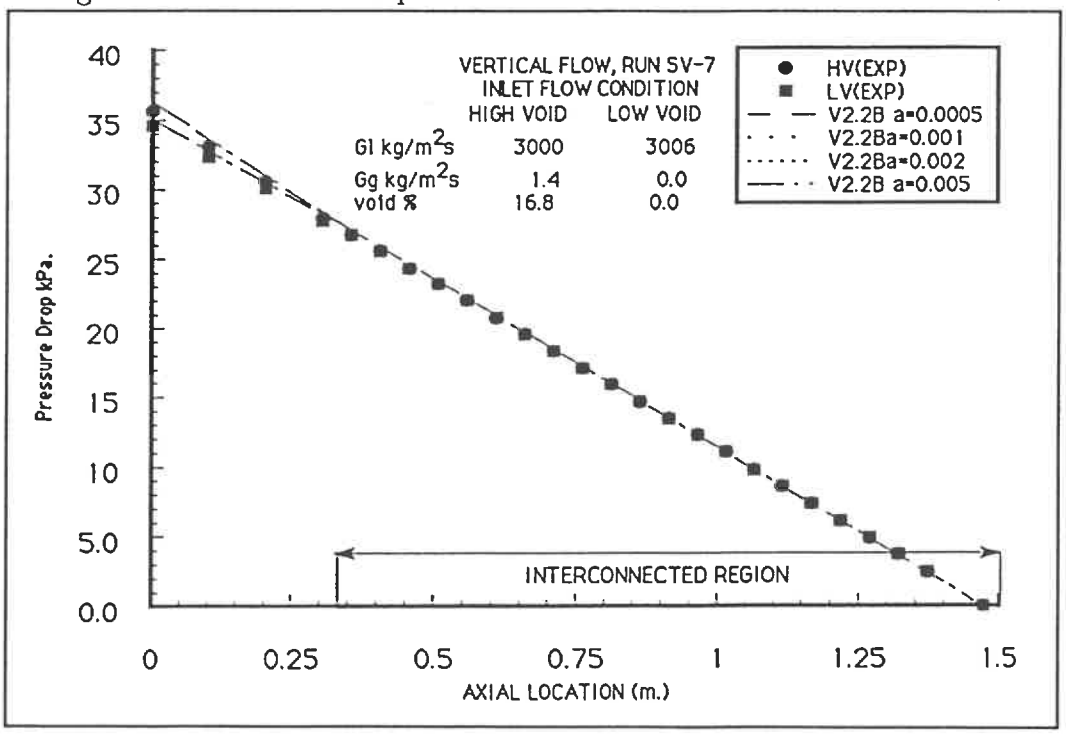

Figure 6.48: Pressure Drop Profile Case SV–7 ASSERT – 4 Version 2.2B

CHAPTER 7

COMPARISON OF COMPUTED AND MEASURED RESULTS–HORIZONTAL CASES

This chapter will present a comparison between the predictions of both ASSERT – 4 Version 1.5 and ASSERT – 4 Version 2.2B against the horizontal experiments given in Tapucu et al. [1984b]. The key to the success of these predictions lies in the ability of the code to accurately model the behaviour of the inter–subchannel transfer mechanisms which are: diversion crossflow, buoyancy drift, turbulent void diffusion, and void drift.

For the experiments under consideration the diversion crossflow is only significant in the first third of the interconnected region. In the rest of the subchannel the other lateral transfer mechanisms dominate.

In ASSERT – 4 the inter–subchannel transfer mechanisms, apart from the diversion crossflow which is due to the inter–subchannel pressure difference, are represented by various terms in the equation for the lateral relative velocity which appears in the equation of conservation of transverse momentum. The transverse relative velocity is given by:

$$v_r = \frac{v_{2j}}{1-\alpha} - \frac{\varepsilon_\alpha}{\alpha(1-\alpha)}\nabla(\alpha - \alpha_{eq}) \quad , \tag{7.1}$$

where the first term of equation 7.1 represents the effects of buoyancy drift and the second term represents the combined effects of both turbulent void diffusion and void drift. The first part of the second term represents the turbulent void diffusion and the second part represents the void drift. In the previous chapter, which dealt only with the vertical experiments, we presented a detailed look at the differences

between ASSERT – 4 Version 1.5 and Version 2.2B in the models for the void drift and the turbulent void diffusion, which are the only lateral transfer mechanisms that exist in such a subchannel orientation. In this chapter we will concentrate on the model used to represent the buoyancy drift, which is a void transfer mechanism unique to horizontal flow where one subchannel is above the other.

Due to the fact that we will be comparing the results of both ASSERT – 4 Version 1.5 and Version 2.2B predictions against the experimental results and since certain differences, although not major ones, do exist in the way the buoyancy drift is modelled in the two versions of the code we will examine the model for the buoyancy drift as it is applied in both versions of ASSERT – 4 separatly.

7.1 ASSERT – 4 Version 1.5 Buoyancy Drift Model and Correlations

In ASSERT – 4 Version 1.5 the effects of the buoyancy drift are represented by the first term of equation 7.1. The term v_{2j} is known as the drift velocity, it is this term that is used to represent the buoyancy drift mechanism. This is done by representing the term v_{2j} using Wallis's model for the terminal rise velocity of a bubble in an infinite medium v_∞.

$$v_{2j} = \bar{\alpha}(1-\bar{\alpha})^n v_\infty \quad . \tag{7.2}$$

The first part of equation 7.2, $\bar{\alpha}(1-\bar{\alpha})^n$, is used to take into account the presence of other bubbles. A point that should be made about the drift velocity is that v_{2j} should tend to zero as $\alpha \to 0$ and also as $\alpha \to 1$. In ASSERT – 4 Version 1.5 the recommended value of the coefficient n is $n = 0$, Wallis [1969] recommends a value of $n = 2$. A consequence of using $n = 0$, in the term that accounts for the presence of other bubbles, $\bar{\alpha}(1-\bar{\alpha})^n$, is that the first term in the expression for the drift velocity does not go to zero as $\alpha \to 1$ as it should. It is thus necessary to multiply the expression for the buoyancy drift, given by the first term on the right

hand side of equation 7.1 by an additional term that drives it to zero as the void fraction tends towards one. The term used for this is the Ohkawa–Lahey [1980] correction factor F, which is given by:

$$F = \left[1 - \left(\frac{\alpha - \chi}{1 - \chi}\right)\right]^m \tag{7.3}$$

where:

$$\chi = 0.588 - 1.817\Psi + 2.0\Psi^2 - 3.343\Psi^3$$

and

$$\Psi = \sqrt[2]{\frac{\rho_2}{\rho_1}}$$

for $\alpha > \chi$, otherwise $F = 1$. The recommended value of m is 1.5.

The correlation for the terminal rise velocity of a bubble in an infinite medium, v_∞, recommended by Wallis [1969] is:

$$v_\infty = K_1\left(\frac{(\rho_1 - \rho_2)}{\rho_1^2}\sigma g\right)^{0.25}\cos\phi \quad , \tag{7.4}$$

where the recommended values of the leading coefficient K_1 are in the range of $1.414 \rightarrow 1.56$ and the term $\cos\phi$ represents the orientation of the inter–subchannel gap.

In ASSERT – 4 Version 1.5 the correlation for the terminal rise velocity of a bubble in an infinite medium v_∞ is given by:

$$v_\infty = 2K_1\left(\frac{(\rho_1 - \rho_2)}{\rho_1^2}\sigma g\right)^{0.25}\cos\phi \quad , \tag{7.5}$$

where the recommended value of the leading coefficient K_1 is 2. This effectively results in the leading coefficient in the correlation for the terminal rise velocity of a bubble in an infinite medium v_∞, being 4 in ASSERT – 4 Version 1.5 while

Wallis [1969] recommends a value in the range of $1.414 \rightarrow 1.56$. This results in an expression for the drift velocity as:

$$v_{2j} = 4F\bar{\alpha}\left(\frac{(\rho_1 - \rho_2)}{\rho_1^2}\sigma g\right)^{0.25}\cos\phi \quad , \tag{7.6}$$

where $F = 1$ for $\alpha < \chi$ where χ is a function of the system pressure only. For the experimental conditions given in Tapucu et al. [1984b], $\chi \approx .53$. Therefore the Ohkawa–Lahey [1980] correction factor has no effect for void fractions below about 53 %. The combination of the use of 4 as a leading coefficient for the terminal rise velocity and $n = 0$ for the effect of the other bubbles results in a significant overprediction of the gravity effects in the buoyancy drift.

7.2 ASSERT – 4 Version 2.2B Buoyancy Drift Model and Correlations

In ASSERT – 4 Version 2.2B as in Version 1.5 the buoyancy drift is again represented using Wallis's [1969] model for the drift velocity v_{2j}. The main differences in the models are in the choices of the coefficients n for the effects of other bubbles and K_1 in the expression for the terminal rise velocity.

The term $\bar{\alpha}(1-\bar{\alpha})^n$ in equation 7.2 which is used to account for the presence of other bubbles, in ASSERT – 4 Version 2.2B the recommended value of n is 0, and the remaining α is raised to the power of 0.1, thus the effects of other bubbles is represented as $\bar{\alpha}^{0.1}$. The terminal rise velocity, v_∞, model in ASSERT – 4 Version 2.2B is also from Wallis [1969]. However ASSERT – 4 Version 2.2B is more faithfull to the original model in its implementation of the terminal rise velocity than is ASSERT – 4 Version 1.5. The terminal rise velocity is given by:

$$v_\infty = K_1\left(\frac{(\rho_1 - \rho_2)}{\rho_1^2}\sigma g\right)^{0.25}\cos\phi \quad , \tag{7.7}$$

where the recommended value of K_1 is 1.5. The fact that the coefficient n in the expression to take into account the effects of the other bubbles is again taken as

$n = 0$ makes it necessary to correct the expression for the drift velocity using the Ohkawa–Lahey correction factor, F, given by equation 7.3. The same expression is used as in ASSERT – 4 Version 1.5 but the recommended value of m is changed to $m = 3$.

Thus the drift velocity in ASSERT – 4 Version 2.2B is given by:

$$v_{2j} = 1.5F\bar{\alpha}^{0.1}\left(\frac{\rho_1 - \rho_2}{\rho_1^2}\sigma g\right)^{0.25}\cos\phi \quad . \tag{7.8}$$

7.3 Test of Wallis's Buoyancy Drift Model in ASSERT – 4 Version 2.2B

It was decided that it might be an interesting idea to implement Wallis's [1969] original model for the drift velocity in ASSERT – 4 Version 2.2B. This required a few minor modifications to the code.

The basic equation that was used was still:

$$v_{2j} = \bar{\alpha}(1 - \bar{\alpha})^n v_\infty \quad . \tag{7.9}$$

But the coefficient n used to account for the presence of other bubbles was tried using $n = 2$ and $n = 1$. As this expression automatically has the correct form as $\alpha \rightarrow 1$ the Ohkawa–Lahey correction factor F given by equation 7.3 was no longer needed.

In ASSERT – 4 Version 2.2B the expression for the terminal rise velocity of a bubble in an infinite medium v_∞ is completely in line with the one recommended by Wallis [1969] so equation 7.7 was retained. Thus the test of the full Wallis model for the drift velocity in ASSERT – 4 Version 2.2B involved simply replacing the coding for equation 7.8 by the coding for:

$$v_{2j} = 1.5\bar{\alpha}(1 - \bar{\alpha})^n\left(\frac{\rho_1 - \rho_2}{\rho_1^2}\sigma g\right)^{0.25}\cos\phi \quad , \tag{7.10}$$

where values of $n = 2$ and $n = 1$ were tried. A further, very minor modification was also required to replace the coding for the Jacobian derivative of equation 7.8 with respect to α by the coding for the Jacobian derivative of equation 7.10 with respect to α.

7.4 Comparison of ASSERT – 4 Predicitions and Experimental Results: Equal Elevation Cases

Before embarking on an analysis of the horizontal experiments having one subchannel above the other where gravity induced phase separation, " buoyancy drift", plays an important part in the void transfer we will examine the horizontal experiments having the two subchannels at the same elevation. In these experiments the void transfer, in the region where diversion crossflow is no longer significant, is only governed by the mechanisms of void diffusion and void drift. It is important to note that in this respect the horizontal experiments with the two subchannels at the same elevation are identical to the vertical experiments analyzed in the previous chapter. In view of this similarity between the horizontal equal elevation experiments and the vertical experiments it would not be unreasonable to expect that for two experiments having the same or, more correctly, at least close to the same inlet conditions that the diffusion coefficients that lead to the best overall results in both cases will be, while not necessarily identical, at least similar to one another. With this in mind we will now examine the horizontal equal elevation cases, denoted SH-$HV = LV$. In three cases we have vertical experiments which correspond to one of the horizontal equal elevation cases analyzed. The three sets of experiments that have corresponding inlet conditions are: $SV - 2$ which corresponds to $SH - HV = LV - 1$, $SV - 3$ which corresponds to $SH - HV = LV - 2$, and $SV - 5$ which corresponds to $SH - HV = LV - 3$, the inlet conditions of the vertical and horizontal experiments can be seen in tables 6.1 and 7.1 respectively.

7.4.1 $SH - HV = LV - 1$

The Tapucu et al. experiment $SH - HV = LV - 1$ is analyzed, it is a case having a void fraction of $\approx$ 60% in the high void subchannel and $\approx$ 20% void fraction in the low void subchannel. Details on the inlet conditions are shown in table 7.1.

7.4.1.1 Void Fraction

Figure 7.1 shows the results of a comparison between the experimental results and the predictions of ASSERT - 4 Version 1.5 which was run with two different values of the coefficient a that is used in the correlation for the turbulent void diffusion which is given by equation 6.3. The default value recommended in the ASSERT - 4 Version 1.5 users manual [Judd et al., 1984] is a =0.075 and the value recommended by Tye et al.[1990] is $a = 0.25$. It can be seen from figure 7.1 that the default value of the parameter a leads to an underprediction of the void fraction in the low void subchannel but still yields a good prediction of the void fraction profile in the high void subchannel. Examining figure 7.1 it can be seen that the value of a recommended by Tye et al. [1990] yields a much better prediction of the void fraction in the low void subchannel but underpredicts the void in the high void subchannel.

Figure 7.2 shows the results of a comparison between the experimental results and the predictions of ASSERT - 4 Version 2.2B which was run with three different values of the coefficient a that is used in the correlation for the turbulent void diffusion which is given by equation 6.16. The recommended value of the diffusion coefficient is $a = 0.05$. Again the default value underpredicts the void fraction in the low void subchannel. The value of the diffusion coefficient that yields the best overall result is $a = 0.10$. In the corresponding vertical case $SV - 2$ the value of the diffusion coefficient that led to the best results was $a = 0.11$ which is in excellent

agreement with the value yielding the best results in this case.

Examining figures 7.1 and 7.2 we can see that the predictions of ASSERT – 4 Version 2.2B seem to be better than the results using ASSERT – 4 Version 1.5.

7.4.1.2 Mass Flow Rate

Figure 7.3 shows the results of the comparison between the experimental results and the predictions of ASSERT – 4 Version 1.5 using both the default value of a and the value recommended by Tye et al. [1990]. We can see that for the case of the mass flow rate the default value of the diffusion coefficient yields a slightly better prediction than the value recommended by Tye et al. [1990]. It is important to note that the experimental results show a large transfer of mass from the high void subchannel to the low void subchannel occuring just after the beginning of the interconnected region which is not well represented by the predicted results which show a much more gradual mass transfer. Another interesting point in the experimental results is the recovery of mass by the high void subchannel near the end of the interconnected region, this phenomena is not captured at all by ASSERT – 4 Version 1.5.

Figure 7.4 shows the results of the comparison between the predictions of ASSERT – 4 Version 2.2B and the experimental results. The effects of varying the adjustable parameter in the calculation of the diffusion coefficient were studied. The default value of the parameter, a in ASSERT – 4 Version 2.2B is $a = 0.05$, examining figure 7.4 we can see that this leads to an excellent prediction of the mass flow rates in both the high and low void subchannels as does the use of $a = 0.06$. The use of $a = 0.10$ underpredicts the mass transfer from the high void subchannel to the low void subchannel. This is again in good agreement with the results seen in the corresponding vertical case.

It can also be seen that ASSERT – 4 Version 2.2B did a very good job of

predicting the initial large mass transfer from the high void subchannel to the low void subchannel at the beginning of the interconnected region. We can also see that ASSERT – 4 Version 2.2B is capable of predicting the flow recovery by the high void subchannel near the end of the interconnected region.

7.4.1.3 Pressure Drop

Figures 7.5 and 7.6 show the predicted and experimental pressure drop profiles using both ASSERT – 4 Version 1.5 and ASSERT – 4 Version 2.2B. All of the predicted pressure drop profiles are about 10 % lower than the experimental results.

The single phase friction factor and the two–phase friction multiplier used in the runs were the same as those used in the vertical case.

7.4.2 $SH - HV = LV - 2$

The Tapucu et al. experiment $SH - HV = LV - 2$ is analyzed, it is a case having a void fraction of $\approx 51.0\%$ in the high void subchannel and 0% void fraction in the low void subchannel. Details on the inlet conditions are shown in table 7.1.

7.4.2.1 Void Fraction

Figure 7.7 shows the results of a comparison between the experimental results and the predictions of ASSERT – 4 Version 1.5 which was run with two different values of the coefficient a that is used in the correlation for the turbulent void diffusion as given by equation 6.3. The default value recommended in the ASSERT – 4 Version 1.5 users manual [Judd et al., 1984] a =0.075. It can be seen from figure 7.7 that the default value of the parameter a leads to an underprediction of the void fraction in the low void subchannel and an overpredicition of the void fraction in the high void subchannel. Using the value recommended by Tye et al. [1990] leads to improvements in the predicted void fraction profiles in both

subchannels.

Figure 7.8 shows the results of a comparison between the experimental results and the predictions of ASSERT –4 Version 2.2B which was run with three different values of the coefficient a that is used in the correlation for the turbulent void diffusion, given by equation 6.16. We can see the default value underpredicted the void fraction in the low void subchannel and overpredicted the void fraction in the high void subchannel. Using values of $a = 0.10$ and $a = 0.14$ for the diffusion coefficient both yield excellent predictions of the void fraction profiles in both the high and low void subchannels. This is in very good agreement with the results seen in the corresponding vertical case $SV - 3$ where values of $a = 0.12$ and $a = 0.15$ both yielded quite good results.

7.4.2.2 Mass Flow Rate

Figure 7.9 shows the results of the comparison between the experimental results and the predictions of ASSERT – 4 Version 1.5 using both the default value of a and the value recommended by Tye et al. [1990]. We can see that for the case of the mass flow rate the value recommended by Tye et al. [1990] yields a better prediction than the default value. It is important to note that the experimental results show a large transfer of mass from the high void subchannel to the low void subchannel occuring just after the beginning of the interconnected region which is not well represented by the predicted results which show a much more gradual mass transfer. Another interesting point in the experimental results is the recovery of mass by the high void subchannel near the end of the interconnected region, this phenomena is not captured at all by ASSERT – 4 Version 1.5.

Figure 7.10 shows the results of the comparison between the predictions of ASSERT – 4 Version 2.2B and the experimental results. The effects of varying the adjustable parameter in the calculation of the diffusion coefficient were studied.

The default value of the parameter, a in ASSERT – 4 Version 2.2B is $a = 0.05$, examining figure 7.10 we can see that both this value and $a = 0.10$ yield an excellent prediction of the mass flow rates in both the high and low void subchannels. Using a value of $a = 0.14$ for the diffusion coefficient leads to a large underprediction of the amount of mass transfered from the high void subchannel to the low void subchannel. Examining the corresponding vertical case $SV - 3$ we see that the value of the diffusion coefficient that lead to the best result was $a = 0.09$ which is in excellent agreement with the value of $a = 0.10$ that lead to a very good prediction in this case.

It can also be seen that ASSERT – 4 Version 2.2B did a very good job of predicting the initial large mass transfer from the high void subchannel to the low void subchannel at the beginning of the interconnected region. We can also see that ASSERT – 4 Version 2.2B is capable of predicting the flow recovery by the high void subchannel near the end of the interconnected region.

7.4.2.3 Pressure Drop

Figure 7.11, shows the predicted and experimental pressure drop profiles using ASSERT – 4 Version 1.5. It can be seen that both cases significantly underpredict the pressure drop.

Figure 7.12, shows the predicted and experimental pressure drop profiles using ASSERT – 4 Version 2.2B. The results for the run using $a = 0.05$, the default, show some underprediction of the pressure drop. The other two case tried $a = 0.10$ and $a = 0.14$ show progressively better agreement with the experimental results but in both cases the pressure drop is still underpredicted.

7.4.3 $SH - HV = LV - 3$

The Tapucu et al. experiment $SH - HV = LV - 3$ is analyzed, it is a case having a void fraction of $\approx 40\%$ in the high void subchannel and 0% void fraction in the low void subchannel. Details on the inlet conditions are shown in table 7.1.

7.4.3.1 Void Fraction

Figure 7.13 shows the results of a comparison between the experimental results and the predictions of ASSERT -4 Version 1.5 which was run with two different values of the coefficient a that is used in the correlation for the turbulent void diffusion, given by equation 6.3. It can be seen from figure 7.13 that the default value of the parameter a leads to a slight underprediction of the void transfered from the high void subchannel to the low void subchannel. Consequently the void fraction in the high void subchannel is slightly overpredicted and the void fraction in the low void subchannel is slightly underpredicted. On the whole, however, the agreement between the predicted and the experimental results is quite good. Examining figure 7.13 it can be seen that the value of the parameter recommended by Tye [1990] yields a slightly better prediction of the void fraction in both subchannels.

Figure 7.14 shows the results of a comparison between the predictions of ASSERT -4 Version 2.2B which was run with three different values of the coefficient a that is used in the correlation for the turbulent void diffusion, which is given by equation 6.16. We can see the default value overpredicts the void fraction in the low void subchannel and slightly underpredicts the void fraction in the high void subchannel. The other two values of a that were tested are $a = 0.03$ and $a = 0.01$ we can see that $a = 0.01$ yields a better prediction of the void fraction profile in the low void subchannel while $a = 0.03$ yields a better prediction of the void fraction profile in the high void subchannel. In comparing this case with the corresponding vertical case we can see that the value of the diffusion coefficient that yielded the

best results for this case is slightly larger than the diffusion coefficient that led to the best results for $SV-5$. In the two cases however the same trends are evident, in both cases the values of the diffusion coefficient that lead to the best results are both smaller than the recommended default value.

7.4.3.2 Mass Flow Rate

Figure 7.15 shows the results of the comparison between the experimental results and the predictions of ASSERT - 4 Version 1.5 using both the default value a and the value recommended by Tye et al. [1990]. We can see that for this case the recommended default value of a results in a reasonably good prediction of the mass flow rates in both the high and low void subchannels. The value recommended by Tye et al. [1990] slightly underpredicts the mass mass flow rate in both subchannels.

Figure 7.16 shows the results of the comparison between the predictions of ASSERT - 4 Version 2.2B and the experimental results. The effects of varying the adjustable parameter in the calculation of the diffusion coefficient were studied. The default value of the parameter, a in ASSERT - 4 Version 2.2B is $a = 0.05$, examining figure 7.16 we can see that this leads to an underprediction of the mass transfered from the high void subchannel to the low void subchannel. Two other value of the parameter a were tried, $a = 0.03$ and $a = 0.01$, we can see that $a = 0.01$ led to an overprediction of the mass transfer and that $a = 0.03$ resulted in a very good prediction of the mass flow rate along the entire length of the interconnected region. When comparing the values of the diffusion coefficients that led to the best predictions of the mass flow rates for this case and the corresponding vertical case $SV-5$ we can see that while thet are not in perfect agreement the trends are at least the same. In both cases the diffusion coefficients are smaller than the recommended default value.

7.4.3.3 Pressure Drop

Figure 7.17 shows the predicted pressure drop using ASSERT – 4 Version 1.5 and the experimental results. It can be seen that both the default value of the parameter a and the value recommended by Tye et al. [1990] result in a prediction of the pressure drop that are in almost perfect agreement with the experimental results.

Figure 7.18 shows the predicted and experimental pressure drop profiles using ASSERT – 4 Version 2.2B. It can be seen that the use the default value for the diffusion coefficient leads to a slight overprediction of the pressure drop. The other two values of the diffusion coefficient that were tried, namely $a = 0.03$ and $a = 0.01$ both lead to an almost perfect agreement between the computed and the experimental results.

7.4.4 $SH - HV = LV - 4$

The Tapucu et al. experiment $SH - HV = LV - 4$ is analyzed, it is a case having a void fraction of $\approx 30\%$ in the high void subchannel and 0% void fraction in the low void subchannel. Details on the inlet conditions are shown in table 7.1.

7.4.4.1 Void Fraction

Figure 7.19 shows the results of a comparison between the experimental results and the predictions of ASSERT – 4 Version 1.5 which was run with two different values of the coefficient a that is used in the correlation for the turbulent void diffusion which is given by equation 6.3. The default value recommended in the ASSERT – 4 Version 1.5 users manual [Judd et al., 1984] is a =0.075. It can be seen from figure 7.19 that the default value of the parameter a leads to an overprediction of the void in the low void subchannel. The use of the value recommended by Tye et al. [1990] leads to a slightly larger overprediction of the void fraction in the low void

subchannel. The use of both the default value for a and the value recommended by Tye et al. [1990] result in excellent agreement between the predicted and the measured void fraction profiles for the high void subchannel.

Figure 7.20 shows the results of a comparison between the experimental results and the predictions of ASSERT – 4 Version 2.2B which was run with three different values of the coefficient a that is used in the correlation for the turbulent void diffusion which is given by equation 6.16. The recommended value of the diffusion coefficient is $a = 0.05$. We can see the default value yields a significant overprediction of the void fraction in the low void subchannel and a somewhat smaller underprediction of the void fraction in the highvoid subchannel. The other two values that were tried, $a = 0.02$ and $a = 0.001$ led to progressively better results with the value of $a = 0.001$ yielding a prediction for the high void subchannel that is in almost perfect agreement with the experiemtal results. For the low void subchannel the use of the value $a = 0.001$ for the diffusion coefficient results in a very slight overprediction of the void fraction in the high void subchannel.

While we have no corresponding vertical case to compare with, we may at least examine the trends in the diffusion coefficients that lead to the best results. We have seen in the previous three equal elevation cases analyzed that the diffusion coefficients that led to the best predicitions decreased with decreasing void fractions, we may therefore conclude that the diffusion coefficient that yields the best results for this case, namely $a = 0.001$ is consistent with this trend.

7.4.4.2 Mass Flow Rate

Figure 7.21 shows the results of the comparison between the experimental results and the predictions of ASSERT – 4 Version 1.5 using both the default value of a and the value recommended by Tye et al. [1990]. We can see that for this case both values of a result in a predicted mass flow rate in both subchannels that is in

almost perfect agreement with the experimental results.

Figure 7.22 shows the results of the comparison between the predictions of ASSERT – 4 Version 2.2B and the experimental results. The effects of varying the adjustable parameter in the calculation of the diffusion coefficient were studied. The default value of the parameter, a in ASSERT – 4 Version 2.2B is $a = 0.05$, examining figure 7.22 we can see that this leads to a very slight underprediction of the mass transfered from the high void subchannel to the low void subchannel. Two other values of the parameter a were tried, $a = 0.02$ and $a = 0.001$, we can see that the use of $a = 0.02$ resulted in a predicted mass flow rate for both subchannels that was in excellent agreement with the experimental results. The use of $a = 0.001$ resulted in an overprediction of the mass transfered from the high void subchannel to the low void subchannel.

7.4.4.3 Pressure Drop

Figure 7.23 shows the predicted pressure drop using ASSERT – 4 Version 1.5 and the experimental results. It can be seen that both the default value and the value recommended by Tye [1990] for the parameter a lead to a predicted pressure drop that is in almost perfect agreement with the experimental results.

Figure 7.24 shows the predicted and experimental pressure drop profiles using ASSERT – 4 Version 2.2B. It can be seen that the use the default value for the diffusion coefficient leads to an overprediction of the pressure drop. The other two values of the diffusion coefficient that were tried, namely $a = 0.02$ and $a = 0.001$ both lead to a predicted pressure drop that is in almost perfect agreement with the experimental results.

7.4.5 General Observations for $SH - HV = LV$ Cases

Looking at the comparisson between the experimental results and the predictions of ASSERT – 4 Version 1.5 for the four equal elevation cases we can see that the value of the diffusion coefficient recommended by Tye et al.[1990] resulted in better overall agreements than did the recommended value of the diffusion coefficient. Examining the mass flow rate predicitons we can see that ASSERT – 4 Version 1.5 failed to accurately predict the size of the inital large mass transfer at the beginning of the interconnected region. A further observation that can be made is that in no case did ASSERT – 4 Version 1.5 predict a recovery of liquid by the high void subchannel near the end of the interconnected region.

The results of the comparison between the experimental results and the predictions of ASSERT – 4 Version 2.2B are in general much better than the results for the comparison against the predictions of ASSERT – 4 Version 1.5. In comparing the results of the equal elevation cases with corresponding vertical cases we can see that the values of the diffusion coefficients that lead to the best results are in good agreement with each other and consistently show a trend of being directly proportional to the void fraction. We can also see that ASSERT – 4 Version 2.2B did a much better job of predicting the size of the initial large mass transfer from the high void subchannel to the low void subchannel at the begining of the interconnected region. The trend of the high void subchannel to recover some mass near the end of the interconnected region is also predicted by ASSERT – 4 Version 2.2B.

7.5 Comparison of ASSERT – 4 Predicitions and Experimental Results: Unequal Elevation Cases

Two different orientations of the two subchannels were studied these are, the high void subchannel directly above the low void subchannel denoted SH-$\frac{HV}{LV}$, the

high void subchannel directly below the low void subchannel denoted SH–$\frac{LV}{HV}$. In these two cases a number of different models for the buoyancy drift model were studied. More correctly the buoyancy drift model used in the tests was always the same model, based on the work of Wallis [1969], but the coefficient in terminal rise velocity model K_1 was varied in the ASSERT – 4 Version 1.5 runs and the coefficient used to account for the presence of other bubbles n was varied in the ASSERT – 4 Version 2.2B runs. The effect of changing the diffusion coefficient ε which appears in the second term of equation 7.1 was also studied. Details on the models for the turbulent void diffusion and the void drift for both ASSERT – 4 Version 1.5 and ASSERT – 4 Version 2.2B are given in chapter 6.

The inlet conditions for the cases having the high void subchannel directly above the low void subchannel and the high void subchannel directly below the low void subchannel are shown in tables 7.2 and 7.3 respectively.

Figure 7.25 shows a comparison of the four different leading terms in the calculation of the drift velocity, these include the terms αF used in ASSERT – 4 Version 1.5, $\alpha^{0.1} F$ used in ASSERT – 4 Version 2.2B where F is given by equation 7.3, and Wallis's original model $\alpha(1-\alpha)^n$ with both $n = 1$ and $n = 2$.

In the presentation to follow four different cases are shown for each experiment and each parameter (void fraction, mass flow rate, and pressure drop) analyzed. They are in order of appearence:

1. ASSERT – 4 Version 1.5 which is run with the default parameters for the leading coefficient in the calculation of the terminal rise velocity of a bubble in an infinite medium K_1 and the void diffusion coefficient a and another set of values recommended by Tye et al. [1990]. The default values are $K_1 = 2.0$ and $a = 0.075$ and the values recommended by Tye et al. [1990] are $K_1 = 1.4$ and $a = 0.25$.

2. ASSERT – 4 Version 2.2B which is run with the original ASSERT model

for the effects of other bubbles. Since the correlation used in ASSERT – 4 Version 2.2B for the calculation of the terminal rise velocity of a bubble in an infinite medium is in line with what is seen in the literature it was not judged appropriate to change K_1. An anlysis of the effects of varying the void diffusion coefficient is however carried out.

3. ASSERT – 4 Version 2.2B which is run with Wallis's model for the effects of other bubbles where a value of $n = 2$ is used. An anlysis of the effects of varying the void diffusion coefficient is also carried out.

4. ASSERT – 4 Version 2.2B which is run with Wallis's model for the effects of other bubbles where a value of $n = 1$ is used. An anlysis of the effects of varying the void diffusion coefficient is also carried out.

7.5.1 $SH - \frac{HV}{LV} - 1$

The Tapucu et al. experiment $SH - \frac{HV}{LV} - 1$ is analyzed, it is a case having a void fraction of $\approx 60\%$ in the high void subchannel and $\approx 20\%$ void fraction in the low void subchannel. Details on the inlet conditions are shown in table 7.2.

7.5.1.1 Void Fraction

Figure 7.26 shows the results of a comparison between the experimental results and the predictions of ASSERT – 4 Version 1.5 which was run with two different values of the coefficient K_1 that is used in equation 7.5 for the calculation of the terminal rise velocity of a bubble in an infinite medium, v_∞, and two different values of the coefficient a that is used in the correlation for the turbulent void diffusion which is given by equation 6.3. It can be seen from figure 7.26 that the default values of the parameters K_1 and a lead to an underprediction of the void fraction in the low void subchannel and an overprediction of the void fraction in

the high void subchannel.

Examining figure 7.26 it can be seen that the values of the parameters recommended by Tye [1990] yield a much better prediction of the void fraction in the low void subchannel. It is quite reasonable to suppose that lowering the value of the coefficient K_1 in the correlation for the terminal rise velocity of a bubble in an infinite medium would improve the predictions, since the value used by ASSERT – 4 Version 1.5 is $2.5 \rightarrow 3.0$ times larger than what is recommended by Wallis [1969].

Figure 7.27 shows the results of a comparison between the experimental results and the predictions of ASSERT – 4 Version 2.2B which was run with three different values of the coefficient a that is used in the correlation for the turbulent void diffusion which is given by equation 6.16. The recommended value of the diffusion coefficient is $a = 0.05$. We can see the default value underpredicts the void fraction in the low void subchannel and overpredicts the void fraction in the high void subchannel. The value of the diffusion coefficient that yields the best overall result is $a = 0.20$. Although it does somewhat underpredict the void fraction in the high void subchannel.

Figure 7.28 shows the results of a comparison between the experimental results and the predictions of ASSERT – 4 Version 2.2B which was modified so as to have Wallis's [1969] full model for taking into account the effects of the other bubbles as given by equation 7.10. The value of $n = 2$ for the coefficient in the term to account for the other bubbles was tested. The case was then run with three different values of the coefficient a that is used in the correlation for the turbulent void diffusion which is given by equation 6.16. We can see that the results are better than the cases presented in figure 7.27. The predicted void fraction profiles in both the high and low void subchannels are quite good.

Figure 7.29 shows the results of a comparison between the predictions of ASSERT – 4 Version 2.2B which was modified so as to have Wallis's [1969] full model

for taking into account the effects of the other bubbles which is given by equation 7.10. The value of $n = 1$ for the coefficient in the term to account for the other bubbles was tested. The case was then run with three different values of the coefficient a that is used in the correlation for the turbulent void diffusion which is given by equation 6.16. We can again see that the results are better than the cases presented in figure 7.27.

Examining figures 7.26, 7.27, 7.28, and 7.29 we can see that the predictions of ASSERT – 4 Version 2.2B seem to be better than the results using ASSERT – 4 Version 1.5.

Comparing the results of ASSERT – 4 Version 2.2B using the original model for the effect of other bubbles and the model proposed by Wallis, the results are shown in figures 7.28, and 7.29 we can see that for this case at least implementing Wallis's model in ASSERT – 4 Version 2.2B might prove usefull. An interesting point to note is the increase in the void fraction just after the beginning of the interconnected region in the high void subchannel, this jump is probably due to a flattening of the void fraction profile which is a three dimensional effect, that has been seen experimentally by Tapucu et al. [1988a], but that ASSERT – 4, which is essentially a one–dimensional code on the level of the individual subchannels, cannot predict.

If we compare the values of the diffusion coefficients that led to the best results for the three ASSERT – 4 Version 2.2B runs with the corresponding equal elevation or vertical cases we can see that in the case of the run using the standard ASSERT model for the effects of other bubbles the diffusion coefficient that led to the best results was quite a bit larger than the diffusion coefficients that led to the best results in the two cases where gravity played no role. In the case of the two runs using Wallis's model we can see that for the run using $n = 2$ the value of the diffusion coefficient that led to the best result was close to the values that led to

the best results for the expriments where gravity had no effect. For the run using $n = 1$ we can see that the value of the diffusion coefficient that led to the best result is closer to the values seen in the equal elevation or vertical cases than was the run using the standard ASSERT model for the effects of other bubbles but slightly larger than the run using $n = 2$.

7.5.1.2 Mass Flow Rate

Figure 7.30 shows the results of the comparison between the experimental results and the predictions of ASSERT – 4 Version 1.5 using both the default values of K_1 and a and the values recommended by Tye et al. [1990]. We can see that for the case of the mass flow rate the default values of the two parameters yield a better prediction than the values recommnded by Tye [1990]. It is important to note that the experimental results show a large transfer of mass from the high void subchannel to the low void subchannel occuring just after the beginning of the interconnected region which is not well represented by the predicted results which show a much more gradual mass transfer. Another interesting point in the experimental results is the recovery of mass by the high void subchannel near the end of the interconnected region, this phenomena is not captured at all by ASSERT – 4 Version 1.5.

Figure 7.31 shows the results of the comparison between the predictions of ASSERT – 4 Version 2.2B using the standard ASSERT – 4 model for the effects of other bubbles as given by equation 7.8 and the experimental results. The default value of the parameter a in ASSERT – 4 Version 2.2B is $a = 0.05$, examining figure 7.31 we can see that this leads to an overprediction of the mass transfered from the high void subchannel to the low void subchannel. Two other values of the parameter a where tried $a = 0.10$ and $a = 0.20$, we can see that $a = 0.20$ leads to an underprediction of the mass transfer and that $a = 0.1$ resulted in a very

good prediction of the mass flow rate along the entire length of the interconnected region.

It can also be seen that ASSERT – 4 Version 2.2B did a very good job of predicting the initial large mass transfer from the high void subchannel to the low void subchannel at the beginning of the interconnected region. We can also see that ASSERT – 4 Version 2.2B is capable of predicting the flow recovery by the high void subchannel near the end of the interconnected region.

Figure 7.32 shows the results of the comparison between ASSERT – 4 Version 2.2B using Wallis's model for the effects of other bubbles, where the value of the coefficient n used in equation 7.10 is $n = 2.0$, and the experimental results. We can see that using this model for the effect of the other bubbles the use of the default value of the parameter in the calculation of the diffusion coefficient leads to a predicted mass flow rate that is in reasonably good agreement with the experimental results although the mass transfer is slightly underpredicted.

Figure 7.33 shows the results of the comparison between ASSERT – 4 Version 2.2B using Wallis's model for the effects of other bubbles, where the value of the coefficient n used in equation 7.10 is $n = 1.0$, and the experimental results. In this case the use of the default value of the parameter in the calculation of the diffusion coefficient leads to a predicted mass flow rate that is excellent agreement with the experimental results.

Examining figures 7.30, 7.31, 7.32, and 7.33 we can see that ASSERT – 4 Version 2.2B is capable of more accurately predicting the magnitude of the large initial mass transfer from the high void subchannel to the low void subchannel at the beginning of the interconnected region than ASSERT – 4 Version 1.5. Furthermore, in all but one run, the one using the standard ASSERT model for the effects of other bubbles and the recommended value of the coefficient a, ASSERT – 4 Version 2.2B predicts the flow recovery by the high void subchannel near the end of the

interconnected region. A phenomena that is not seen in the ASSERT – 4 Version 1.5 predictions.

7.5.1.3 Pressure Drop

Figures 7.34, 7.35, 7.36, and 7.37 show the predicted and experimental pressure drop profiles using both ASSERT – 4 Version 1.5 and ASSERT – 4 Version 2.2B. All of the predicted pressure drop profiles are about 10 % lower than the experimental results. There is no good explanation for this as these runs use the same single phase friction factor and two–phase flow multiplier as was used in the comparisons presented in chapter 6 which showed much better agreement between the predicted and experimental pressure drops. Since these friction factors depend on the geometry of the test section, and the same test section is used for both the vertical and horizontal experiments it was judged inappropriate to change the friction factors used in these calculations.

7.5.2 $SH - \frac{HV}{LV} - 2$

The Tapucu et al. experiment $SH - \frac{HV}{LV} - 2$ is analyzed, it is a case having a void fraction of $\approx 51.0\%$ in the high void subchannel and 0% void fraction in the low void subchannel. Details on the inlet conditions are shown in table 7.2.

7.5.2.1 Void Fraction

Figure 7.38 shows the results of a comparison between the experimental results and the predictions of ASSERT – 4 Version 1.5 which was run with two different values of the coefficient K_1 that is used in equation 7.5 for the calculation of the terminal rise velocity of a bubble in an infinite medium, v_∞, and two different values of the coefficient a that is used in the correlation for the turbulent void diffusion which is given by equation 6.3. It can be seen from figure 7.38 that the

default values of the parameters K_1 and a lead to an underprediction of the void fraction in the low void subchannel and an overprediction of the void fraction in the high void subchannel.

Examining figure 7.38 it can be seen that the values of the parameters recommended by Tye et al. [1990] yield a much better prediction of the void fraction in both the high and low void subchannels.

Figure 7.39 shows the results of a comparison between the experimental results and the predictions of ASSERT – 4 Version 2.2B which was run with three different values of the coefficient a that is used in the correlation for the turbulent void diffusion which is given by equation 6.16. We can see the default value underpredicts the amount of the void fraction in the low void subchannel and overpredicts the void fraction in the high void subchannel. The value of the diffusion coefficient that yields the best overall result is $a = 0.20$. In ASSERT – 4 Version 2.2B the correlation for the diffusion coefficient, unlike the correlation used in ASSERT – 4 Version 1.5, has no dependence on the void fraction. Since diffusion is a process that transfers a quantity from a region of high concentration to a region of low concentration it is not unreasonable to suppose that one diffusion coefficient, namely the default value $a = 0.05$, will not be adaquate to cover the entire range of void fractions that are seen in this analysis.

Figure 7.40 shows the results of a comparison between the experimental results and the predictions of ASSERT – 4 Version 2.2B which was modified so as to have Wallis's [1969] full model for taking into account the effects of the other bubbles as given by equation 7.10, the value of $n = 2$ for the coefficient in the term to account for the other bubbles was tested. The case was then run with three different values of the coefficient a that is used in the correlation for the turbulent void diffusion which is given by equation 6.16. We can see that the results are better than the cases presented in figure 7.39. The predicted void fraction profiles in both the

high and low void subchannels are quite good. As can be seen from figure 7.25 which gives the values of the leading coefficients that are used to take into account the effects of the other bubbles, Wallis's model for this effect has a larger effect on decreasing the buoyancy drift than does the model normally implemented in ASSERT – 4 Version 2.2B. Therefore, in a case where the void transfer, which is due to turbulent void diffusion and void drift and is opposed by the buoyancy drift, is underpredicted it is not surprising that lowering the importance of the buoyancy drift mechanism will result in a better prediction of the experimental results by the code.

Figure 7.41 shows the results of a comparison between the experimental results and the predictions of ASSERT – 4 Version 2.2B which was modified so as to have Wallis's [1969] full model for taking into account the effects of the other bubbles as given by equation 7.10, the value of $n = 1$ for the coefficient in the term to account for the other bubbles was tested. The case was then run with two different values of the coefficient a that is used in the correlation for the turbulent void diffusion which is given by equation 6.16. We can again see that the results are better than the cases presented in figure 7.39 though maybe not quite as good as the results shown in figure 7.40. This is not surprising as it is evident from figure 7.25 that a value of $n = 1$ in equation 6.16 results in a larger buoyancy drift than a value of $n = 2$.

Examining figures 7.38, 7.39, 7.40, and 7.41 we can see that the predictions of ASSERT – 4 Version 2.2B seem to be better than the results using ASSERT – 4 Version 1.5. Further, comparing the results of the predictions using the standard model implemented in ASSERT – 4 Version 2.2B to take into account the effects of other bubbles, which can be seen in figure 7.39 against the results using Wallis's model, results shown in figures 7.40, and 7.41, we can see that the latter results in a better agreement between the experimental and the predicted results.

Examining the three ASSERT – 4 Version 2.2B runs in comparison to the equal elevation and vertical cases having the same inlet conditions we can see that the value of the diffusion coefficient that led to the best result for the run using the ASSERT model for the effect of other bubbles was quite a bit larger than the ones leading to the best results in the two cases where buoyancy did not play a role. In the two runs using Wallis's model for the effects of other bubbles the diffusion coefficients that led to the best results were in very good agreement with the diffusion coefficients that led to the best results in the equal elevation and vertical cases.

7.5.2.2 Mass Flow Rate

Figure 7.42 shows the results of the comparison between the experimental results and the predictions of ASSERT – 4 Version 1.5 using both the default values of K_1 and a and the values recommended by Tye et al. [1990]. We can see that for the case of the mass flow rate the values recommended by Tye et al. [1990] yield a slightly better prediction than the default values. It is important to note that the experimental results show a large transfer of mass from the high void subchannel to the low void subchannel occuring just after the beginning of the interconnected region which is not well represented by the predicted results which show a much more gradual mass transfer. Another interesting point in the experimental results is the recovery of mass by the high void subchannel near the end of the interconnected region, this phenomena is not captured at all by ASSERT – 4 Version 1.5.

Figure 7.43 shows the results of the comparison between the predictions of ASSERT – 4 Version 2.2B using the standard ASSERT – 4 model for the effects of other bubbles as given by equation 7.8 and the experimental results. The effects of varying the adjustable parameter in the calculation of the diffusion coefficient

were examined. The default value of the parameter, a in ASSERT – 4 Version 2.2B is $a = 0.05$, examining figure 7.43 we can see that this leads to a significant overprediction of the mass transfered from the high void subchannel to the low void subchannel. Two other values of the parameter a were tried $a = 0.10$ and $a = 0.20$, we can see that $a = 0.20$ led to a slight underprediction of the mass transfer and that $a = 0.1$ resulted in a slight overprediction of the mass transfer. It is interesting to note however that using the value of $a = 0.20$ led to a rather large underprediction of the initial transfer of mass from the high void subchannel to the low void subchannel as compared to the other two cases, the only reason that the value of $a = 0.20$ led to a reasonably good agreement with the experimental results at the end of the interconnected region is due to the effect of the recovery of mass by the high void subchannel.

It can also be seen that ASSERT – 4 Version 2.2B did a reasonably good job of predicting the initial large mass transfer from the high void subchannel to the low void subchannel at the beginning of the interconnected region. We can also see that ASSERT – 4 Version 2.2B is capable of predicting the flow recovery by the high void subchannel near the end of the interconnected region.

Figure 7.44 shows the results of the comparison between ASSERT – 4 Version 2.2B using Wallis's model for the effects of other bubbles, where the value of the coefficient n used in equation 7.10 is $n = 2.0$, and the experimental results. We can see that using this model for the effect of the other bubbles the use of the default value of the parameter in the calculation of the diffusion coefficient leads to a predicted mass flow rate that is in good agreement with the experimental results. In this case, the initial large mass transfer from the high void to the low void subchannel is slightly underpredicted and the mechanism of the high void subchannel recovering mass near the end of the interconnected region is captured by the code. Values of the diffusion coefficient larger than the recommended default

value lead to under predictions of the mass transfer.

Figure 7.45 shows the results of the comparison between ASSERT – 4 Version 2.2B using Wallis's model for the effects of other bubbles, where the value of the coefficient n used in equation 7.10 is $n = 1.0$, and the experimental results. In this case both the use of the default value of the parameter in the calculation of the diffusion coefficient and the other value tested $a = 0.08$ lead to predicted mass flow rates that are in excellent agreement with the experimental results.

Examining figures 7.42, 7.43, 7.44, and 7.45 we can see that ASSERT – 4 Version 2.2B is capable of more accurately predicting the magnitude of the large initial mass transfer from the high void subchannel to the low void subchannel at the beginning of the interconnected region than ASSERT – 4 Version 1.5. Furthermore, in all but one run, the one using the standard ASSERT – 4 model for the effects of other bubbles and the recommended value of the coefficient a as seen in figure 7.43, ASSERT – 4 Version 2.2B predicts the flow recovery by the high void subchannel near the end of the interconnected region. A phenomena that is not seen in the ASSERT – 4 Version 1.5 predictions.

7.5.2.3 Pressure Drop

Figure 7.46, shows the predicted and experimental pressure drop profiles using ASSERT – 4 Version 1.5. It can be seen that for the run using the default values of K_1 and a the pressure drop profile is significantly underpredicted while the case having the values of K_1 and a recommended by Tye et al. [1990] while still under the experimental results is clearly an improvement over the results using the default values.

Figure 7.47, shows the predicted and experimental pressure drop profiles using ASSERT – 4 Version 2.2B. The results for the run using $a = 0.05$, the default, show a significant underprediction of the pressure drop. The other two case tried

$a = 0.10$ and $a = 0.20$ show progressively better agreement with the experimental results.

Figure 7.48 and 7.49 show the predicted and experimental pressure drop profiles using ASSERT - 4 Version 2.2B using Wallis's model to account for the effects of other bubbles where the value of the coefficient n used are $n = 2$ and $n = 1$ respectively. The predictions are in quite good agreement with each other and with the experimentral results.

7.5.3 $SH - \frac{HV}{LV} - 3$

The Tapucu et al. experiment $SH - \frac{HV}{LV} - 3$ is analyzed, it is a case having a void fraction of $\approx 40\%$ in the high void subchannel and 0% void fraction in the low void subchannel. Details on the inlet conditions are shown in table 7.2.

7.5.3.1 Void Fraction

Figure 7.50 shows the results of a comparison between the experimental results and the predictions of ASSERT - 4 Version 1.5 which was run with two different sets values of the coefficient K_1 that is used in equation 7.5 for the calculation of the terminal rise velocity of a bubble in an infinite medium v_∞, and the coefficient a that is used in the correlation for the turbulent void diffusion which is given by equation 6.3. It can be seen from figure 7.50 that the default values of the parameters K_1 and a lead to a large underprediction of the void fraction in the low void subchannel.

Examining figure 7.50 it can be seen that the values of the parameters recommended by Tye [1990] yield a much better prediction of the void fraction in the low void subchannel and the high void subchannel. In fact the default parameters show that no void is transfered from the high void subchannel to the low void subchannel. In this case the combined effects of the void diffusion and the void drift

cannot overcome the buoyancy effects which oppose the transfer of void from the high void subchannel to the low void subchannel.

Figure 7.51 shows the results of a comparison between the experimental results and the predictions of ASSERT – 4 Version 2.2B which was run with three different values of the coefficient a that is used in the correlation for the turbulent void diffusion which is given by equation 6.16. We can see the default value underpredicts the void fraction in the low void subchannel and overpredicts the void fraction in the high void subchannel. The other two values of a that were tested are $a = 0.08$ and $a = 0.16$ we can see that $a = 0.08$ yields predicted results that are in almost perfect agreement with the experimental results.

Figure 7.52 shows the results of a comparison between the experimental results and the predictions of ASSERT – 4 Version 2.2B which was modified so as to have Wallis's [1969] full model for taking into account the effects of the other bubbles which is given by equation 7.10 where the value of $n = 2$ for the coefficient in the term to account for the other bubbles was tested. The case was then run with three different values of the coefficient a that is used in the correlation for the turbulent void diffusion which is given by equation 6.16. We can see that after having significantly decreased the effects of the buoyancy drift by the use of Wallis's model, see figure 7.25, that it was necessary to reduce the diffusion coefficient a compared to its default value. The results using $a = 0.005$ are in almost perfect agreement with the experimental results.

Figure 7.53 shows the results of a comparison between the experimental results and the predictions of ASSERT – 4 Version 2.2B which was modified so as to have Wallis's [1969] full model for taking into account the effects of the other bubbles which is given by equation 7.10 where the value of $n = 1$ for the coefficient in the term to account for the other bubbles was tested. The case was then run with three different values of the coefficient a that is used in the correlation for the turbulent

void diffusion which is given by equation 6.16. In this case the use of $n = 1$ has decreased the effects of the buoyancy drift when compared to the standard model used by ASSERT – 4 Version 2.2B, but still gives slightly more importance to this mechanism than the previous case using $n = 2$. In this case it was not necessary to decrease the diffusion coefficient as dramatically as it was in the previous case. The use of both $a = 0.01$ and $a = 0.02$ both yield very good results.

Examining figures 7.50, 7.51, 7.52, and 7.53 we can see that the predictions of ASSERT – 4 Version 2.2B seem to be better than the results using ASSERT – 4 Version 1.5. However, comparing the results of ASSERT – 4 Version 2.2B using the original model for the effect of other bubbles and the model proposed by Wallis whose results are shown in figures 7.52, and 7.53 we can see that this model has again led to very good predictions.

Examining the results of the ASSERT – 4 Version 2.2B predictions with respect to the equal elevation and vertical cases having the same inlet conditions we again see that the values of the void diffusion coefficient that lead to the best result using the standard ASSERT model for the effects of the other bubbles are much larger than the cases where gravity has no influence. The cases using Wallis's model have values of the diffusion coefficients that lead to the best results that are in good agreement with the diffusion coefficients seen in the vertical and equal elevation cases.

7.5.3.2 Mass Flow Rate

Figure 7.54 shows the results of the comparison between the experimental results and the predictions of ASSERT – 4 Version 1.5 using both the default values of K_1 and a and the values recommended by Tye et al. [1990]. We can see that for this case both sets of values for K_1 and a yield reasonably good results in comparison to the experiments. It should be noted however, that ASSERT –

4 Version 1.5 has again underpredicted the magnitude of the initial mass transfer and has also failed to predict the recovery of mass by the high void subchannel that can be seen experimentally.

Figure 7.55 shows the results of the comparison between the predictions of ASSERT – 4 Version 2.2B using the standard ASSERT – 4 model for the effects of other bubbles as given by equation 7.8 and the experimental results. The effects of varying the adjustable parameter in the calculation of the diffusion coefficient were examined. The default value of the parameter, a in ASSERT – 4 Version 2.2B is $a = 0.05$, examining figure 7.55 we can see that this leads to an overprediction of the mass transfered from the high void subchannel to the low void subchannel. Two other values of the parameter a were tried $a = 0.08$ and $a = 0.16$, we can see that $a = 0.16$ leads to an underprediction of the mass transfer and that $a = 0.08$ resulted in a very good prediction of the mass flow rate along the entire length of the interconnected region.

Figure 7.56 shows the results of the comparison between ASSERT – 4 Version 2.2B using Wallis's model for the effects of other bubbles, where the value of the coefficient n used in equation 7.10 is $n = 2.0$, and the experimental results. We can see that using this model for the effect of the other bubbles the use of the default value of the parameter in the calculation of the diffusion coefficient leads to an underprediction of the mass transfer. It is necessary to significantly reduce the value of the diffusion coefficient for the predictions to be in reasonably good agreement with the experimental results.

Figure 7.57 shows the results of the comparison between ASSERT – 4 Version 2.2B using Wallis's model for the effects of other bubbles, where the value of the coefficient n used in equation 7.10 is $n = 1.0$, and the experimental results. In this case the use of the default value of the parameter in the calculation of the diffusion coefficient leads an underprediction of the mass transfer. However, as in the case of

the void fraction the use of either $a = 0.02$ or $a = 0.01$ yield very good agreement between the computed and the measured results.

Examining figures 7.54, 7.55, 7.56, and 7.57 we can see that ASSERT – 4 Version 2.2B is capable of more accurately predicting the magnitude of the large initial mass transfer from the high void subchannel to the low void subchannel at the beginning of the interconnected region than ASSERT – 4 Version 1.5. It can also be seen that the use of Wallis' model for the effect of the other bubbles in place of the standard model used by ASSERT – 4 Version 2.2B leads to very promising results. Again we see that with the use of Wallis's model for the effects of the other bubbles the diffusion coefficients that lead to the best result for this case are in good agreement with the diffusion coefficients that led to the best results for the equal elevation and vertical cases.

7.5.3.3 Pressure Drop

Figure 7.58 shows the predicted pressure drop using ASSERT – 4 Version 1.5 and the experimental results. It can be seen that the default values of the parameters K_1 and a lead to a significant underprediction of the pressure drop. While the values recommended by Tye et al. [1990] also lead to an underprediction of the pressure drop its magnitude is much smaller.

Figure 7.59 shows the predicted and experimental pressure drop profiles using ASSERT – 4 Version 2.2B. It can be seen that the use the default value for the diffusion coefficient leads to an underprediction of the pressure drop. The other two value of the diffusion coefficient that were tried, namely $a = 0.08$ and $a = 0.16$ lead to progressively better agreement between the computed and the measured results.

Figures 7.60, and 7.61 show the predicted and experimental pressure drop profiles using ASSERT – 4 Version 2.2B with Wallis's model for the effect of other

bubbles being used in place of the standard model used in ASSERT – 4 Version 2.2B. The values of the coefficient n are $n = 2$ and $n = 1$ respectively. Both cases show excellent agreement between the predicted and the measured results.

7.5.4 $SH - \frac{HV}{LV} - 4$

The Tapucu et al. experiment $SH - \frac{HV}{LV} - 4$ is analyzed, it is a case having a void fraction of $\approx 30\%$ in the high void subchannel and 0% void fraction in the low void subchannel. Details on the inlet conditions are shown in table 7.2.

7.5.4.1 Void Fraction

Figure 7.62 shows the results of a comparison between the experimental results and the predictions of ASSERT – 4 Version 1.5 which was run with two different values of the coefficient K_1 that is used in equation 7.5 for the calculation of the terminal rise velocity of a bubble in an infinite medium v_∞, and two different values of the coefficient a that is used in the correlation for the turbulent void diffusion which is given by equation 6.3. Examining figure 7.62 it can be seen that both sets of values for the parameters K_1 and a yield very good agreement with the experimental void fraction profile for the high void subchannel but that they both fail to show any void in the low void subchannel.

Figure 7.63 shows the results of a comparison between the experimental results and the predictions of ASSERT – 4 Version 2.2B which was run with three different values of the coefficient a that is used in the correlation for the turbulent void diffusion which is given by equation 6.16. We can see the default value yields predicted results that are in almost perfect agreement with the experimental results.

Figure 7.64 shows the results of a comparison between the predictions of ASSERT – 4 Version 2.2B which was modified so as to have Wallis's [1969] full model for taking into account the effects of the other bubbles which is given by equa-

tion 7.10, where the value of $n = 2$ for the coefficient in the term to account for the other bubbles was tested, and the experimental results. The case was then run with three different values of the coefficient a that is used in the correlation for the turbulent void diffusion which is given by equation 6.16. We can see that after having significantly decreased the effects of the buoyancy drift by the use of Wallis's model, see figure 7.25, that it was necessary to reduce the diffusion coefficient a compared to its default value. In fact it can be seen that reducing the effects of the turbulent void diffusion to zero still leads to an overprediction of the void fraction in the low void subchannel. In this case the void is transfered from the high void subchannel to the low void subchannel by the diversion crossflow.

Figure 7.65 shows the results of a comparison between the predictions of ASSERT – 4 Version 2.2B which was modified so as to have Wallis's [1969] full model for taking into account the effects of the other bubbles which is given by equation 7.10, where the value of $n = 1$ for the coefficient in the term to account for the other bubbles was tested, and the experiemtal results. The case was then run with three different values of the coefficient a that is used in the correlation for the turbulent void diffusion which is given by equation 6.16. In this case the use of $n = 1$ has decreased the effects of the buoyancy drift when compared to the standard model used by ASSERT – 4 Version 2.2B, but still gives slightly more importance to this mechanism than the previous case $n = 2$. As in the previous case the use of the default value for the coefficient in the calculation of the turbulent void diffusion leads to an overprediction of the void transfer. Reducing the value of this coefficient to zero leads to an improvement in the void profile for the low void subchannel but still results in an overprediction of the void fraction in the low void subchannel. Again the void that we see in the low void subchannel is due to the diversion crossflow from the high void subchannel to the low void subchannel.

Examining figures 7.62, 7.63, 7.64, and 7.65 we can see that the predictions

of ASSERT – 4 Version 2.2B seem to be better than the results using ASSERT – 4 Version 1.5. However, comparing the results of ASSERT – 4 Version 2.2B using the original model for the effect of other bubbles and the model proposed by Wallis whose results are shown in figures 7.64, and 7.65 we can see that this time the standard model used by ASSERT – 4 Version 2.2B leads to a better prediction of the void fraction in the low void subchannel. Comparing the diffusion coefficients that yielded the best results in this case and in the corresponding equal elevation case we can see that the diffusion coefficients that gave the best results using Wallis's model for the effects of the other bubbles are more in line with the diffusion coefficients that gave the best results for the equal elevation case.

7.5.4.2 Mass Flow Rate

Figure 7.66 shows the results of the comparison between the experimental results and the predictions of ASSERT – 4 Version 1.5 using both the default values of K_1 and a and the values recommended by Tye et al. [1990]. We can see that for this case both sets of values for K_1 and a yield reasonably good results in comparison to the experiments.

Figure 7.67 shows the results of the comparison between the predictions of ASSERT – 4 Version 2.2B using the standard ASSERT – 4 model for the effects of other bubbles as given by equation 7.8 and the experimental results. Examining figure 7.67 we can see that the use of the default value of a leads to a very slight overprediction of the mass transfered from the high void subchannel to the low void subchannel. Two other values of the parameter a were tried, $a = 0.06$ and $a = 0.07$, we can see that both these values of a also lead to overpredictions of the mass transfer, but in both cases they were very small.

Figure 7.68 shows the results of the comparison between ASSERT – 4 Version 2.2B using Wallis's model for the effects of other bubbles, where the value of the

coefficient n used in equation 7.10 is $n = 2.0$, and the experimental results. We can see that using this model for the effect of the other bubbles the use of the default value of the parameter in the calculation of the diffusion coefficient leads to an underprediction of the mass transfer. Reducing the value of the coefficient to $a = 0.01$ resulted in almost perfect agreement between the predicted and the experimental results.

Figure 7.69 shows the results of the comparison between ASSERT – 4 Version 2.2B using Wallis's model for the effects of other bubbles, where the value of the coefficient n used in equation 7.10 is $n = 1.0$, and the experimental results. In this case the use of the default value of the parameter in the calculation of the diffusion coefficient leads an underprediction of the mass transfer. The two other values that were tried $a = 0.005$ and $a = 0.00$ both lead to a slight overprediction of the mass transfer.

Examining figures 7.66, 7.67, 7.68, and 7.69 we can see that ASSERT – 4 Version 2.2B is capable of more accurately predicting the magnitude of the large initial mass transfer from the high void subchannel to the low void subchannel at the beginning of the interconnected region than ASSERT – 4 Version 1.5. Examining the three runs using ASSERT – 4 Version 2.2B we can see that the values of the diffusion coefficient that led to the best results using Wallis's model for the effects of the other bubbles are more closely related to the diffusion coeffcients that gave the best results in the equal elevation case than are the values of the diffusion coefficient that gave the best results for the run using the standard ASSERT model for this effect.

7.5.4.3 Pressure Drop

Figure 7.70 shows the predicted pressure drop using ASSERT – 4 Version 1.5 and the experimental results. It can be seen that both the default values and the

values recommended by Tye [1990] for the parameters K_1 and a lead to a significant underprediction, $\approx 8\%$, of the pressure drop.

Figure 7.71 shows the predicted and experimental pressure drop profiles using ASSERT – 4 Version 2.2B. It can be seen that the use the default value for the diffusion coefficient leads to an underprediction of the pressure drop. The other two value of the diffusion coefficient that were tried, namely $a = 0.06$ and $a = 0.07$ also lead to underpredictions of the pressure drop with $a = 0.07$ being marginally better.

Figures 7.72, and 7.73 show the predicted and experimental pressure drop profiles using ASSERT – 4 Version 2.2B with Wallis's model for the effect of other bubbles being used in place of the standard model used in ASSERT – 4 Version 2.2B. The values of the coefficient n are $n = 2$ and $n = 1$ respectively. Both cases show reasonably good agreement between the predicted and the measured results.

7.5.5 General Observations for $SH - \frac{HV}{LV}$ Cases

Looking at the comparisson between the experimental results and the predictions of ASSERT – 4 Version 1.5 for the four high void over low void cases we can see that the values of the leading coefficient in the calculation of the terminal rise velocity of a bubble in an infinite medium and of the diffusion coefficient recommended by Tye et al.[1990] resulted in better overall agreements than did the recommended values of these coefficient. Examining the mass flow rate predicitons we can see that ASSERT – 4 Version 1.5 failed to accurately predict the size of the inital large mass transfer at the beginning of the interconnected region. A further observation that can be made is that in no case did ASSERT – 4 Version 1.5 predict a recovery of liquid by the high void subchannel near the end of the interconnected region.

The results of the comparison between the experimental results and the pre-

dictions of ASSERT – 4 Version 2.2B using the standard ASSERT model for the effects of the other bubbles are in general much better than the results for the comparison against the predictions of ASSERT – 4 Version 1.5. An even greater improvement on the whole ensemble of high void over low void cases analyzed can be seen when Wallis's model for the effects of other bubbles is used.

In comparing the results of the ASSERT – 4 Version 2.2B runs of the high void over low void cases against the corresponding equal elevation and vertical cases it can be seen that the values of the diffusion coefficients that led to the best results for the run which used the standard ASSERT model for the effects of the other bubbles where quite different from the values of the diffusion coefficients that led to the best results for the equal elevation and vertical cases. For the runs which used Wallis's model for the effects of the other bubbles, using both $n = 2$ and $n = 1$, it can be seen that the values of the diffusion coefficients for both the high void over low void cases and the corresponding cases where gravity did not play a role in the phase seperation were in good agreement with each other and consistently showed a trend of being directly proportional to the void fraction.

We can also see that ASSERT – 4 Version 2.2B did a much better job of predicting the size of the initial large mass transfer from the high void subchannel to the low void subchannel at the begining of the interconnected region. The trend of the high void subchannel to recover some mass near the end of the interconnected region is also predicted by ASSERT – 4 Version 2.2B.

7.5.6 $SH - \frac{LV}{HV} - 1$

The Tapucu et al. experiment $SH - \frac{LV}{HV} - 1$ is analyzed, it is a case having a void fraction of $\approx 60\%$ in the high void subchannel and $\approx 20\%$ void fraction in the low void subchannel. Details on the inlet conditions are shown in table 7.3.

7.5.6.1 Void Fraction

Figure 7.74 shows the results of a comparison between the experimental results and the predictions of ASSERT – 4 Version 1.5 which was run with two different values of the coefficient K_1 that is used in equation 7.5 for the calculation of the terminal rise velocity of a bubble in an infinite medium v_∞, and two different values of the coefficient a that is used in the correlation for the turbulent void diffusion which is given by equation 6.3. It can be seen from figure 7.74 that the default values of the parameters K_1 and a lead to an overprediction of the void fraction in the low void subchannel and an underprediction of the void fraction in the high void subchannel.

Examining figure 7.74 a number of important physical mechanisms can be seen to have an effect on the void fraction profile. The first is the jump in the void fraction in the high void subchannel just after the beginning of the interconnected region. This is a three dimensional effect linked to a flattening of the void fraction profile, it has been observed experimentally by Tapucu et al. [1988a]. Another important fact is that from the beginning of the interconnected region to the point where the voids cross, that is to say the point at which the initially high void subchannel becomes the low void subchannel and vice versa, the net effects of the void transfer mechanisms of turbulent void diffusion, void drift and buoyancy drift all act in the same direction, ie. to transfer void from the initially high void subchannel, (physically the lower subchannel), to the initially low void subchannel, (physically the upper subchannel), at the crossing point the turbulent void diffusion and void drift effects dissappear and the continued transfer is due to the buoyancy drift alone. A little bit farther along the subchannel, the initially high void subchannel has become the low void subchannel due to the effects of the buoyancy drift mechanism, from the point at which a difference in the voids in the two subchannels again exists the turbulent void diffusion and the void drift re–establish

themselves, however their net effect now acts in opposition to the buoyancy drift which always acts physically upwards.

Looking at figure 7.74 we can see that ASSERT – 4 Version 1.5 with both sets of parameters lead to a reasonably good prediction of the void profile up to the point where the voids cross. From this point on, the effect of the buoyancy drift overcomes the combined effects of turbulent void diffusion and void drift and void fraction in the initially high void subchannel is underpredicted. The set of parameters recommended by Tye et al. [1990] lead to a slightly smaller underprediction but the void fraction is none the less underpredicted.

Figure 7.75 shows the results of a comparison between the experimental results and the predictions of ASSERT – 4 Version 2.2B which was run with three different values of the coefficient a that is used in the correlation for the turbulent void diffusion given by equation 6.16. The recommended value of the diffusion coefficient is $a = 0.05$. We can see the default value predicts that the voids will cross sooner than what is seen experimentally and also underpredicts the void fraction in the initially high void subchannel. Two other values of the diffusion coefficient were tried, these were $a = 0.01$ and $a = 0.0$, it can be seen from figure 7.75 that with the diffusion coefficient set to zero the crossing point is more accuratly predicted but that after the point where the voids cross there is no mechanism to act against the buoyancy drift mechanism and the void fraction in the initially high void subchannel is again underpredicted.

Figure 7.76 shows the results of a comparison between the predictions of ASSERT – 4 Version 2.2B which was modified so as to have Wallis's [1969] full model for taking into account the effects of the other bubbles which is given by equation 7.10, where the value of $n = 2$ for the coefficient in the term to account for the other bubbles was tested, and the experimental results. The case was then run with three different values of the coefficient a that is used in the correlation for

the turbulent void diffusion which is given by equation 6.16. The use of $n = 2$ in equation 7.10 has reduced the effects of the buoyancy drift mechanism to the point where the voids are not predicted to cross. Examining figure 7.25 which shows the leading terms for calculating the effects of other bubbles as shown in equations 7.8 and 7.10 we can suppose that we have reduced the effect of the gravity driven phase seperation too much.

Figure 7.77 shows the results of a comparison between the experimental results and the predictions of ASSERT – 4 Version 2.2B which was modified so as to have Wallis's [1969] full model for taking into account the effects of the other bubbles which is given by equation 7.10 the value of $n = 1$ for the coefficient in the term to account for the other bubbles was tested. The case was then run with three different values of the coefficient a that is used in the correlation for the turbulent void diffusion which is given by equation 6.16. We can see that the use of both $a = 0.05$, the default, and $a = 0.11$ lead to an underprediction of the amount of void transfered and the void fractions in the high and low void subchannels are not seen to cross. Looking at the results using $a = 0.20$ we see a reasonably good prediction of the void profile in the low void subchannel. Unfortunately, the void fraction in the high void subchannel is seen to drop too rapidly, this is in part due to the fact that the initial jump in the void fraction in the high void subchannel was not predicted by ASSERT – 4 Version 2.2B and in part because too much void is transfered. We see that the crossing point is reasonably well predicted but the amount of total void is slightly underestimated.

Examining figures 7.74, 7.75, 7.76, and 7.77 we can see that the predictions of ASSERT – 4 Version 2.2B seem to be better than the results using ASSERT – 4 Version 1.5. However, comparing the results of ASSERT – 4 Version 2.2B using the original model for the effect of other bubbles and the model proposed by Wallis whose results are shown in figures 7.76, and 7.77 we can see that the best

predictions result for the case where $n = 1$ is used in Wallis's model.

Comparing the diffusion coefficients that led to the best predictions in the ASSERT – 4 Version 2.2B runs with the diffusion coefficients that led to the best predictions in the corresponding equal elevation and vertical cases it can be seen that only the values for the runs using Wallis's model for the effects of other bubbles correspond to the values of the diffusion coefficients that gave the best results for the cases where gravity had no effect on the void transfer. In the case of the run using the standard ASSERT model for the effects of the other bubbles the diffusion coefficient that led to the best result was considerably smaller than the values seen in the corresponding equal elevation and vertical cases.

7.5.6.2 Mass Flow Rate

Figure 7.78 shows the results of the comparison between the experimental results and the predictions of ASSERT – 4 Version 1.5 using both the default values of K_1 and a and the values recommended by Tye et al. [1990]. We can see that for the case of the mass flow rate the default values of the two parameters yield a slightly better prediction than the values recommnded by Tye et al. [1990]. It is important to note that the experimental results show a large transfer of mass from the high void subchannel to the low void subchannel occuring just after the beginning of the interconnected region which is not well represented by the predicted results which show very little mass transfer occuring. The predicted results show a crossing of the mass flow rates, something that is not seen experimentally in the length of the interconnceted region.

Figure 7.79 shows the results of the comparison between the predictions of ASSERT – 4 Version 2.2B using the standard ASSERT – 4 model for the effects of other bubbles as given by equation 7.8 and the experimental results. The effects of varying the adjustable parameter in the calculation of the diffusion coefficient

were examined. Examining figure 7.79 we can see while ASSERT – 4 Version 2.2B does a very good job of predicting the inital large mass transfer at the beginning of the interconnected region it considerably overpredicts the recovery of mass by the high void subchannel and predicts a crossing of the mass flow rates near the end of the interconnected region that is not seen experimentally.

Figure 7.80 shows the results of the comparison between ASSERT – 4 Version 2.2B using Wallis's model for the effects of other bubbles, where the value of the coefficient n used in equation 7.10 is $n = 2.0$, and the experimental results. We can see that using this model for the effect of the other bubbles the use of the default value of the parameter in the calculation of the diffusion coefficient leads to a prediction that the mass flow rates in the high and low void subchannels will cross. The other two values of the diffusion coefficient that were tried, namely $a = 0.09$ and $a = 0.15$ both predict the trends in the mass flow rates quite well, with the value of $a = 0.09$ leading to a slightly better result.

Figure 7.81 shows the results of the comparison between ASSERT – 4 Version 2.2B using Wallis's model for the effects of other bubbles, where the value of the coefficient n used in equation 7.10 is $n = 1.0$, and the experimental results. In this case the use of the default value of the parameter $a = 0.05$ and one of the other values tested, $a = 0.11$, both lead to a good prediction of the trends in the mass flow rate, with the value of $a = 0.11$ leading to a very good prediction of the mass flow rates in both subchannels for the entire length of the interconnected region. The use of $a = 0.20$ leads to an overprediction of the recovery of the mass by the high void subchannel.

Examining figures 7.78, 7.79, 7.80, and 7.81 we can see that ASSERT – 4 Version 2.2B is capable of more accurately predicting the magnitude of the large initial mass transfer from the high void subchannel to the low void subchannel at the beginning of the interconnected region than ASSERT – 4 Version 1.5. We can

also see that the only cases that did not lead to a prediction of the mass flow rates in the high and low void subchannels crossing was when Wallis's model was used.

Another important point is that only the diffusion coefficients that yielded the best results with the use of Wallis's model for the effects of the other bubbles are in agreement with the diffusion coefficients that gave the best results in the corresponding vertical and equal elevation cases.

7.5.6.3 Pressure Drop

Figure 7.82 shows the predicted and experimental pressure drop profiles using ASSERT – 4 Version 1.5. We can see that both sets of parameters lead to a slight underprediction of the pressure drop.

Figure 7.83 shows the predicted and experimental pressure drop profiles using ASSERT – 4 Version 2.2B. We can see that all three runs predicted the pressure drop reasonably well.

Figure 7.84 shows the predicted and experimental pressure drop profiles using ASSERT – 4 Version 2.2B with Wallis's model for the effects of other bubbles where $n = 2$ was used. We can see that the use of the default value for the diffusion coefficient $a = 0.05$ leads to an underprediction of the pressure drop, while the other two values of a that were tried, namely $a = 0.09$ and $a = 0.15$ both lead to a very good prediction of the pressure drop.

Figure 7.85 shows the predicted and experimental pressure drop profiles using ASSERT – 4 Version 2.2B with Wallis's model for the effects of other bubbles where $n = 1$ was used. We can see that all the values of the diffusion coefficient that were tried led to a very good prediction of the pressure drop.

7.5.7 $SH - \frac{LV}{HV} - 2$

The Tapucu et al. experiment $SH-\frac{LV}{HV}-2$ is analyzed, it is a case having a void fraction of $\approx 50.0\%$ in the high void subchannel, physically the lower subchannel, and 0% void fraction in the low void subchannel, physically the upper subchannel. Details on the inlet conditions are shown in table 7.3.

7.5.7.1 Void Fraction

Figure 7.86 shows the results of a comparison between the experimental results and the predictions of ASSERT –4 Version 1.5 which was run with two different values of the coefficient K_1 that is used in equation 7.5 for the calculation of the terminal rise velocity of a bubble in an infinite medium v_∞, and two different values of the coefficient a that is used in the correlation for the turbulent void diffusion which is given by equation 6.3. It can be seen from figure 7.86 that the default values of the parameters K_1 and a lead to a slight overprediction of the void fraction in the low void subchannel and a slight underprediction of the void fraction in the high void subchannel. Examining figure 7.86 it can be seen that the both sets of values of the parameters K_1 and a lead to good predictions of the void fraction profiles. The default values however, slightly overpredict the amount of void transfered after the point that the void fraction in the two subchannels cross.

Figure 7.87 shows the results of a comparison between the experimental results and the predictions of ASSERT –4 Version 2.2B which was run with three different values of the coefficient a that is used in the correlation for the turbulent void diffusion which is given by equation 6.16. We can see the default value slightly overpredicts the void fraction in the low void subchannel and underpredicts the void fraction in the hgh void subchannel. However the overall prediction is excellent. The other two values that were tried, $a = 0.02$ and $a = 0.001$, predicted the point where the voids cross to be farther downstream than that seen experimentally.

Figure 7.88 shows the results of a comparison between the experimental results and the predictions of ASSERT – 4 Version 2.2B which was modified so as to have Wallis's [1969] full model for taking into account the effects of the other bubbles which is given by equation 7.10 the value of $n = 2$ for the coefficient in the term to account for the other bubbles was tested. The case was then run with three different values of the coefficient a that is used in the correlation for the turbulent void diffusion which is given by equation 6.16. We can see that none of the values of the diffusion coefficient tried lead to a prediction of the voids crossing although the run with, $a = 0.20$ being used for the diffusion coefficient did do a very good job predicting the profile over the first half of the interconnected region.

Figure 7.89 shows the results of a comparison between the experimental results and the predictions of ASSERT – 4 Version 2.2B which was modified so as to have Wallis's [1969] full model for taking into account the effects of the other bubbles which is given by equation 7.10 where the value of $n = 1$ for the coefficient in the term to account for the other bubbles was tested. The case was then run with three different values of the coefficient a that is used in the correlation for the turbulent void diffusion which is given by equation 6.16. We can again see that only the use of a very large diffusion coefficient $a = 0.50$, an order of magnitude larger than the recommended value, leads to a prediction that the voids would cross, even then however, the overall profile was not well predicted.

The best overall prediction was by ASSERT – 4 Version 2.2B with the standard ASSERT model for the effects of the other bubbles. The diffusion coefficient used for this prediction is considerably smaller than the diffusion coefficients seen in the corresponding equal elevation and vertical cases. The runs using Wallis's model and a value of $n = 1$ led to a fairly good prediction while using a value of the diffusion coefficient that was in much better agreement with the corresponding equal elevation and vertical cases.

7.5.7.2 Mass Flow Rate

Figure 7.90 shows the results of the comparison between the experimental results and the predictions of ASSERT – 4 Version 1.5 using both the default values of K_1 and a and the values recommended by Tye et al. [1990]. We can see that for the case of the mass flow rate that both the default values of K_1 and a and the values recommended by Tye et al. [1990] yield similar results. In both cases the crossing of the mass flow rates is predicted to occur. However, in both cases it is predicted to occur much further downstream than what is seen experimentally.

Figure 7.91 shows the results of the comparison between the predictions of ASSERT – 4 Version 2.2B using the standard ASSERT – 4 model for the effects of other bubbles as given by equation 7.8 and the experimental results. Examining figure 7.91 we can see that the use of the default value of the parameter a leads to a reasonably good prediction of the mass flow rates in both the high and low void subchannels. Two other values of the parameter a were tried $a = 0.02$ and $a = 0.001$, we can see that they both lead to a better prediction of the initial mass transfer from the high void subchannel to the low void subchannel, but that in both cases the crossing point was predicted to occur much farther downstream than what was seen experimentally.

Figure 7.92 shows the results of the comparison between ASSERT – 4 Version 2.2B using Wallis's model for the effects of other bubbles, where the value of the coefficient n used in equation 7.10 is $n = 2.0$, and the experimental results. We can see that using this model for the effect of the other bubbles the mass flow rates in the two subchannels are not predicted to cross, which is in error as compared to the experiments.

Figure 7.93 shows the results of the comparison between ASSERT – 4 Version 2.2B using Wallis's model for the effects of other bubbles, where the value of the coefficient n used in equation 7.10 is $n = 1.0$, and the experimental results. In this

case only the use of a diffusion coefficient that was an order of magnitude larger than the recommended default value lead to a prediction of the mass flow rates crossing and the prediction of the crossing point was much further downstream than the point at which they were seen to cross experimentally.

7.5.7.3 Pressure Drop

Figures 7.94, 7.95, 7.96 and 7.97 show the predicted and experimental pressure drop profiles using ASSERT – 4 Version 1.5, ASSERT – 4 Version 2.2B and ASSERT – 4 Version 2.2B with Wallis's model for the effects of the other bubbles with $n = 2$ and $n = 1$ respectively. In all cases the predictions are in excellent agreement with each other and with the experimentral results.

7.5.8 $SH - \frac{LV}{HV} - 3$

The Tapucu et al. experiment $SH - \frac{LV}{HV} - 3$ is analyzed, it is a case having a void fraction of $\approx 40\%$ in the high void subchannel, physically the lower subchannel, and 0% void fraction in the low void subchannel, physically the upper subchannel. Details on the inlet conditions are shown in table 7.3.

7.5.8.1 Void Fraction

Figure 7.98 shows the results of a comparison between the experimental results and the predictions of ASSERT –4 Version 1.5 which was run with two different values of the coefficient K_1 that is used in equation 7.5 for the calculation of the terminal rise velocity of a bubble in an infinite medium, v_∞, and two different values of the coefficient a that is used in the correlation for the turbulent void diffusion which is given by equation 6.3. It can be seen from figure 7.98 that the default values of the parameters K_1 and a lead to an overprediction of the void fraction in the low void subchannel and an underprediction of the void fraction in

the high void subchannel. Examining figure 7.98 it can be seen that the values of the parameters recommended by Tye [1990] yield a better prediction of the void fractions in both the high and low void subchannels. In fact the default parameters show that void fractions in the two subchannels cross something that is not seen experimentally.

Figure 7.99 shows the results of a comparison between the predictions of ASSERT –4 Version 2.2B which was run with three different values of the coefficient a that is used in the correlation for the turbulent void diffusion which is given by equation 6.16. We can see all the values that were tried for the diffusion coefficient, even $a = 0.0$ predicted that the void fractions in the high and low void subchannels would cross which is not seen in the experimental results.

Figure 7.100 shows the results of a comparison between the predictions of ASSERT –4 Version 2.2B which was modified so as to have Wallis's [1969] full model for taking into account the effects of the other bubbles which is given by equation 7.10, where the value of $n = 2$ for the coefficient in the term to account for the other bubbles was tested, and the experimental results. The case was then run with three different values of the coefficient a that is used in the correlation for the turbulent void diffusion which is given by equation 6.16. We can see that the trends in the void profiles for both the high and low void subchannels are accurately predicted. Both the default value $a = 0.05$ for the diffusion coefficient and the value of $a = 0.07$ lead to reasonably good predictions of the void fraction profiles.

Figure 7.101 shows the results of a comparison between the predictions of ASSERT –4 Version 2.2B which was modified so as to have Wallis's [1969] full model for taking into account the effects of the other bubbles which is given by equation 7.10, where the value of $n = 1$ for the coefficient in the term to account for the other bubbles was tested, and the experimental results. The prediction of

the void fraction profile with the use of the default value for the diffusion coefficient was perfect for the low void subchannel and lead to a slight overprediction for the high void subchannel. Only one value of the diffusion coefficient was tested as the results of increasing the diffusion coefficient to improve the prediction in the high void subchannel would only lead to a worse prediction for the low void subchannel, in any case the aim of this work is not to fit a bunch of curves using ASSERT – 4 but to examine the effects of the various inter–subchannel transfer mechanisms and test the various models that exist for these mechanisms.

Examining figures 7.98, 7.99, 7.100, and 7.101 we can see that the predictions of ASSERT – 4 Version 2.2B using the model proposed by Wallis whose results are shown in figures 7.100, and 7.101 are the only cases other than the ASSERT – 4 Version 1.5 run with the parameters recommended by Tye et al. [1990], that produce the correct trends for the void fraction profile.

The values of the diffusion coefficients that led to reasonably good predictions for the runs using Wallis's model for the effects of the other bubbles were a bit larger tha the values of the diffusion coefficient seen in the corresponding equal elevation and vertical cases.

7.5.8.2 Mass Flow Rate

Figure 7.102 shows the results of the comparison between the experimental results and the predictions of ASSERT – 4 Version 1.5 using both the default values of K_1 and a and the values recommended by Tye et al. [1990]. We can see that for this case the default values of K_1 and a lead to a prediction that the mass flow rates in the two subchannels will cross, something that is not seen experimentally. Using the values recommended by Tye et al. [1990], the correct trend in the mass flow rates is predicted but the magnitude of the initial large mass transfer at the begining of the interconnected region is underpredicted.

Figure 7.103 shows the results of the comparison between the predictions of ASSERT – 4 Version 2.2B using the standard ASSERT – 4 model for the effects of other bubbles as given by equation 7.8 and the experimental results. Examining figure 7.103 we can see that the mass flow rate is predicted to cross, something that is not seen in the experiments, regardless of the value used for the diffusion coefficient.

Figure 7.104 shows the results of the comparison between ASSERT – 4 Version 2.2B using Wallis's model for the effects of other bubbles, where the value of the coefficient n used in equation 7.10 is $n = 2.0$, and the experimental results. We can see that using this model for the effect of the other bubbles the use of both the default value of the parameter in the calculation of the diffusion coefficient, $a = 0.05$ and a value of $a = 0.07$ both lead to an excellent prediction of the mass flow rates in both the high and low void subchannels.

Figure 7.105 shows the results of the comparison between ASSERT – 4 Version 2.2B using Wallis's model for the effects of other bubbles, where the value of the coefficient n used in equation 7.10 is $n = 1.0$, and the experimental results. In this case the use of the default value of the parameter in the calculation of the diffusion coefficient leads an almost perfect prediction of the mass flow rates in both subchannels.

Examining figures 7.102, 7.103, 7.104, and 7.105 we can see that the use of Wallis's model for the effect of the other bubbles in place of the standard model used by ASSERT – 4 Version 2.2B leads to the best results for the prediction of the mass flow rates for this case.

7.5.8.3 Pressure Drop

Figures 7.106, 7.107, 7.108, and 7.109 show the predicted pressure drop using ASSERT – 4 Version 1.5, ASSERT – 4 Version 2.2B, and ASSERT – 4 Version

2.2B with Wallis's model for the effect of other bubbles where the values of the coefficient n are $n = 2$ and $n = 1$ respectively. In all cases the pressure drop was overpredicted by $\approx 3\%$.

7.5.9 $SH - \frac{LV}{HV} - 4$

The Tapucu et al. experiment $SH - \frac{LV}{HV} - 4$ is analyzed, it is a case having a void fraction of $\approx 30\%$ in the high void subchannel, which is physically the lower subchannel, and 0% void fraction in the low void subchannel, physically the upper subchannel. Details on the inlet conditions are shown in table 7.3.

7.5.9.1 Void Fraction

Figure 7.110 shows the results of a comparison between the experimental results and the predictions of ASSERT –4 Version 1.5 which was run with two different values of the coefficient K_1 that is used in equation 7.5 for the calculation of the terminal rise velocity of a bubble in an infinite medium v_∞, and two different values of the coefficient a that is used in the correlation for the turbulent void diffusion which is given by equation 6.3. It can be seen from figure 7.110 that the default values of the parameters K_1 and a lead to an overprediction of the void fraction in low void subchannel and an underprediction of the void fraction in the high void subchannel. The set of parameters recommended by Tye et al. [1990] leads to an improvement in the predictions but the void fraction in the low void subchannel is still overpredicted and the void fraction in the high void subchannel is still underpredicted.

Figure 7.111 shows the results of a comparison between the predictions of ASSERT –4 Version 2.2B, which was run with three different values of the coefficient a that is used in the correlation for the turbulent void diffusion which is given by equation 6.16, and the experimental results. We can see that regardless of the value

of the diffusion coefficient used, ASSERT – 4 Version 2.2B always predicts that the void fraction in the two subchannels will cross, which is not in agreement with the experimental results.

Figure 7.112 shows the results of a comparison between the predictions of ASSERT – 4 Version 2.2B which was modified so as to have Wallis's [1969] full model for taking into account the effects of the other bubbles which is given by equation 7.10, where the value of $n = 2$ for the coefficient in the term to account for the other bubbles was tested, and the experimental results. The case was then run with three different values of the coefficient a that is used in the correlation for the turbulent void diffusion which is given by equation 6.16. We can see that after having significantly decreased the effects of the buoyancy drift by the use of Wallis's model, see figure 7.25, that ASSERT – 4 Version 2.2B no longer predicts that the voids will cross. The use of the default value, $a = 0.05$, in the correlation for the turbulent void diffusion leads to an overprediction of the void transfer. The other two runs using $a = 0.01$ and $a = 0.00$ for the turbulent void diffusion both lead to a very good prediction of the void profile in both subchannels.

Figure 7.113 shows the results of a comparison between the predictions of ASSERT –4 Version 2.2B which was modified so as to have Wallis's [1969] full model for taking into account the effects of the other bubbles which is given by equation 7.10, where the value of $n = 1$ for the coefficient in the term to account for the other bubbles was tested, and the experimental results. The case was then run with two different values of the coefficient a that is used in the correlation for the turbulent void diffusion which is given by equation 6.16. In this case the use of $n = 1$ has decreased the effects of the buoyancy drift when compared to the standard model used by ASSERT – 4 Version 2.2B, but still gives slightly more importance to this mechanism than the previous case $n = 2$. As in the previous case the use of the default value for the coefficient in the calculation of the turbulent void

diffusion leads to an overprediction of the void fraction in the low void subchannel and an underprediction of the void fraction in the high void subchannel. Reducing the value of this coefficient to zero leads to an improvement in the void profile for both subchannels, the amount of void in the low void subchannel in still somewhat overpredicted.

Comparing this case with the corresponding equal elevation case we can see that the values of the diffusion coefficient that yielded the best results for the runs using Wallis's model for the effects of the other bubbles are in reasonably good agreement with the diffusion coefficient that yielded the best results in the equal elevation case.

7.5.9.2 Mass Flow Rate

Figure 7.114 shows the results of the comparison between the experimental results and the predictions of ASSERT – 4 Version 1.5 using both the default values of K_1 and a and the values recommended by Tye et al. [1990]. We can see that for this case both sets of values for K_1 and a yield reasonably good results in comparison to the experiments, but that the default values lead to a larger underprediction of the mass transfered from the high void subchannel to the low void subchannel than do the set of parameters recommended by Tye et al. [1990].

Figure 7.115 shows the results of the comparison between the predictions of ASSERT – 4 Version 2.2B using the standard ASSERT – 4 model for the effects of other bubbles as given by equation 7.8 and the experimental results. Examining figure 7.115 we can see that regardless of the value used for the coefficient in the correlation for the turbulent void diffusion ASSERT – 4 Version 2.2B always leads to a prediction of the mass flow rates crossing, a phenomena not in agreement with the experimental results.

Figure 7.116 shows the results of the comparison between ASSERT – 4 Version

2.2B using Wallis's model for the effects of other bubbles, where the value of the coefficient n used in equation 7.10 is $n = 2.0$, and the experimental results. We can see that using this model for the effects of the other bubbles the use of the default value of the parameter in the calculation of the diffusion coefficient leads to a very slight underprediction of the mass transfer. Reducing the value of the coefficient to $a = 0.01$ resulted in very good agreement between the predicted and the experimental results.

Figure 7.117 shows the results of the comparison between ASSERT – 4 Version 2.2B using Wallis's model for the effects of other bubbles, where the value of the coefficient n used in equation 7.10 is $n = 1.0$, and the experimental results. In this case the use of the default value of the parameter in the calculation of the diffusion coefficient leads an underprediction of the mass transfer. The other value that was tried $a = 0.00$ leads to a very slight overprediction of the mass transfer.

7.5.9.3 Pressure Drop

Figure 7.118 shows the predicted pressure drop using ASSERT – 4 Version 1.5 and the experimental results. It can be seen that both the default values and the values recommended by Tye [1990] for the parameters K_1 and a lead to an overprediction, $\approx 4\%$, of the pressure drop.

Figure 7.119 shows the predicted and experimental pressure drop profiles using ASSERT – 4 Version 2.2B. It can be seen that all the runs lead to an overprediction, $\approx 4\%$, of the pressure drop.

Figures 7.120, and 7.121 show the predicted and experimental pressure drop profiles using ASSERT – 4 Version 2.2B with Wallis's model for the effect of other bubbles being used in place of the standard model used in ASSERT – 4 Version 2.2B. The values of the coefficient n are $n = 2$ and $n = 1$ respectively. In both cases the use of the default value for the diffusion coefficient leads to an overprediction

of $\approx 4\%$ in the pressure drop as compared to the experimental results. The other values of the diffusion coefficient that were tried reduced this overprediction to about 1.5%.

7.5.10 General Observations for $SH - \frac{LV}{HV}$ Cases

Looking at the comparisson between the experimental results and the predictions of ASSERT – 4 Version 1.5 for the four low void over high void cases we can see that the value of the diffusion coefficient recommended by Tye et al.[1990] resulted in better overall agreements than did the recommended value of the diffusion coefficient. Examining the mass flow rate predicitons we can see that ASSERT – 4 Version 1.5 failed to accurately predict the size of the inital large mass transfer at the beginning of the interconnected region.

The results of the comparison between the experimental results and the predictions of ASSERT – 4 Version 2.2B using the standard ASSERT model for the effects of the other bubbles predicted that the void fractions and the mass flow rates would cross in a number of cases that this was not seen in the experiments. The use of Wallis's model for the effects of the other bubbles in ASSERT – 4 Version 2.2B improved the predicted results somewhat compared to the use of the standard ASSERT model for this effect.

In comparing the results of the ASSERT – 4 Version 2.2B runs of the low void over high void cases against the corresponding equal elevation and vertical cases it can be seen that the values of the diffusion coefficients that led to the best results for the run which used the standard ASSERT model for the effects of the other bubbles where quite different from the values of the diffusion coefficients that led to the best results for the equal elevation and vertical cases. For the runs which used Wallis's model for the effects of the other bubbles it can be seen that the values of the diffusion coefficients for both the low void over high void cases and

the corresponding equal elevation and vertical cases were in reasonable agreement with each other.

Table 7.1: Inlet Conditions for the Horizontal SH-$LV = HV$ Experiments

Void Fraction α %		
RUN	High Void Channel	Low Void Channel
SH-$LV = HV$-1	59.3 %	19.6%
SH-$LV = HV$-2	52.2%	0.0%
SH-$LV = HV$-3	42.6%	0.0%
SH-$LV = HV$-4	31.1%	0.0%
Liquid Mass Fluxes (kg/m^2s)		
SH-$LV = HV$-1	2926	2905
SH-$LV = HV$-2	2981	2983
SH-$LV = HV$-3	3005	2985
SH-$LV = HV$-4	2995	2997
Gas Mass Fluxes (kg/m^2s)		
SH-$LV = HV$-1	22.62	2.13
SH-$LV = HV$-2	11.85	0.0
SH-$LV = HV$-3	5.64	0.0
SH-$LV = HV$-4	2.81	0.0

Table 7.2: Inlet Conditions for the Horizontal SH-$\frac{HV}{LV}$ Experiments

Void Fraction α %		
RUN	High Void Channel	Low Void Channel
SH-$\frac{HV}{LV}$-1	59.0 %	19.8%
SH-$\frac{HV}{LV}$-2	51.0%	0.0%
SH-$\frac{HV}{LV}$-3	41.6%	0.0%
SH-$\frac{HV}{LV}$-4	30.0%	0.0%
Liquid Mass Fluxes (kg/m^2s)		
SH-$\frac{HV}{LV}$-1	3010	3005
SH-$\frac{HV}{LV}$-2	3014	2989
SH-$\frac{HV}{LV}$-3	3006	2982
SH-$\frac{HV}{LV}$-4	3002	3001
Gas Mass Fluxes (kg/m^2s)		
SH-$\frac{HV}{LV}$-1	23.23	2.05
SH-$\frac{HV}{LV}$-2	11.85	0.0
SH-$\frac{HV}{LV}$-3	5.61	0.0
SH-$\frac{HV}{LV}$-4	2.73	0.0

Table 7.3: Inlet Conditions for the Horizontal SH-$\frac{LV}{HV}$ Experiments

Void Fraction α %		
RUN	High Void Channel	Low Void Channel
SH-$\frac{LV}{HV}$-1	59.8 %	17.0%
SH-$\frac{LV}{HV}$-2	52.2%	0.0%
SH-$\frac{LV}{HV}$-3	42.6%	0.0%
SH-$\frac{LV}{HV}$-4	31.1%	0.0%
Liquid Mass Fluxes (kg/m^2s)		
SH-$\frac{LV}{HV}$-1	2967	2985
SH-$\frac{LV}{HV}$-2	2977	2974
SH-$\frac{LV}{HV}$-3	2995	2988
SH-$\frac{LV}{HV}$-4	2987	2992
Gas Mass Fluxes (kg/m^2s)		
SH-$\frac{LV}{HV}$-1	22.31	2.08
SH-$\frac{LV}{HV}$-2	11.61	0.0
SH-$\frac{LV}{HV}$-3	5.61	0.0
SH-$\frac{LV}{HV}$-4	2.76	0.0

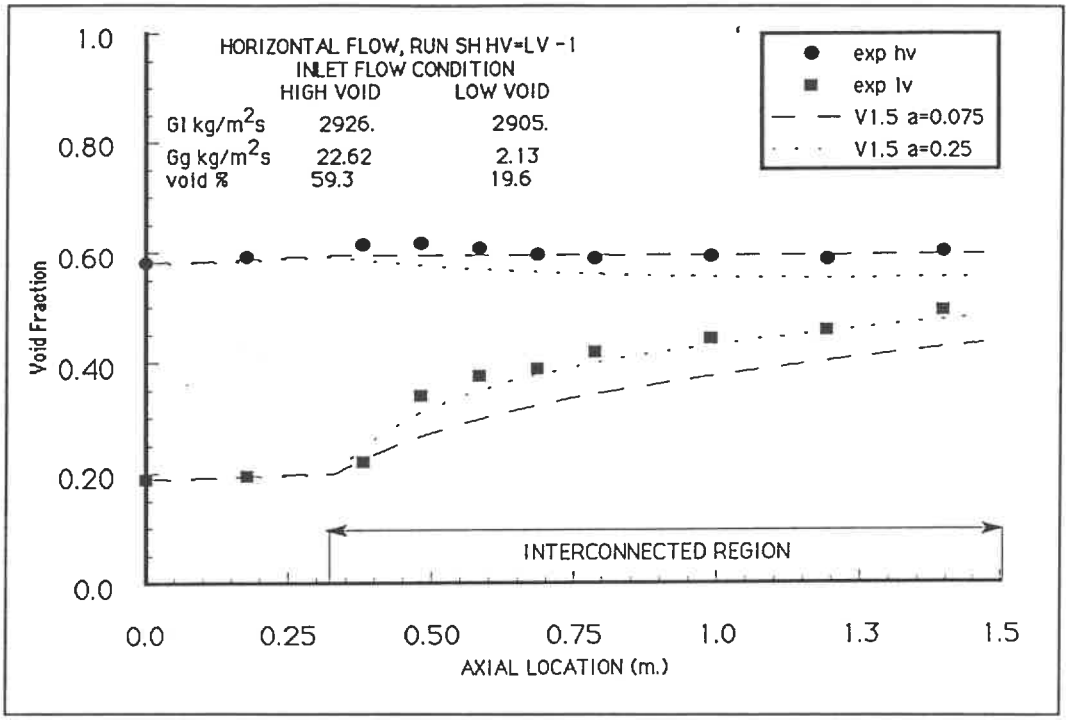

Figure 7.1: Void Fraction $SH - HV = LV - 1$ ASSERT-4 Version 1.5

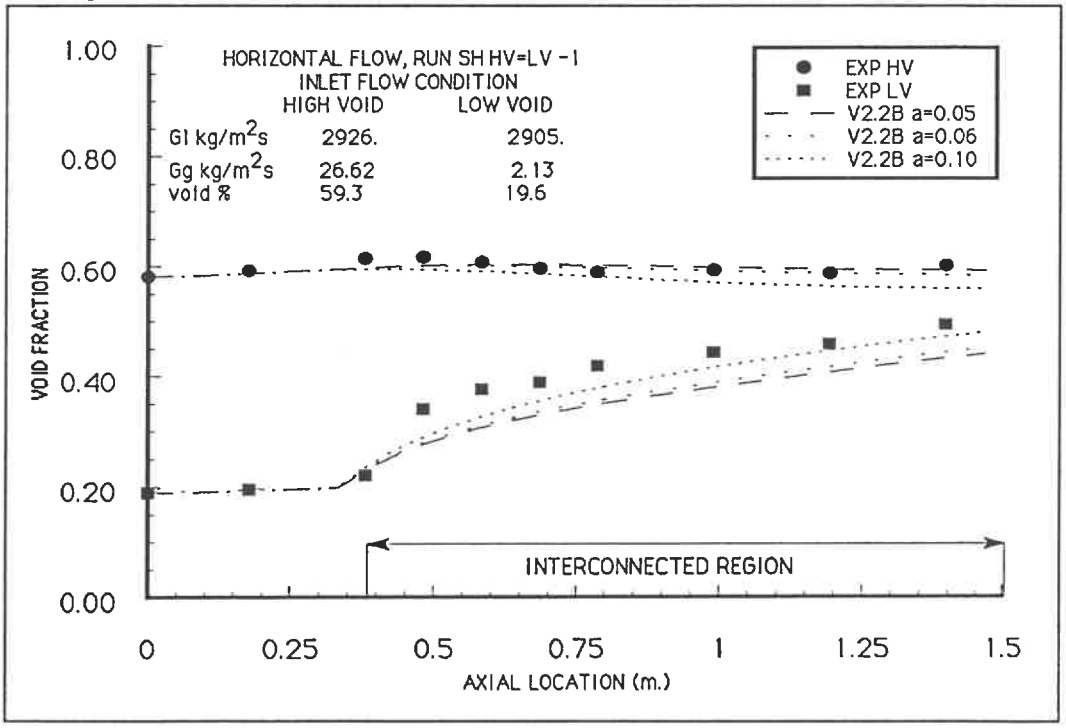

Figure 7.2: Void Fraction $SH - HV = LV - 1$ ASSERT-4 Version 2.2B

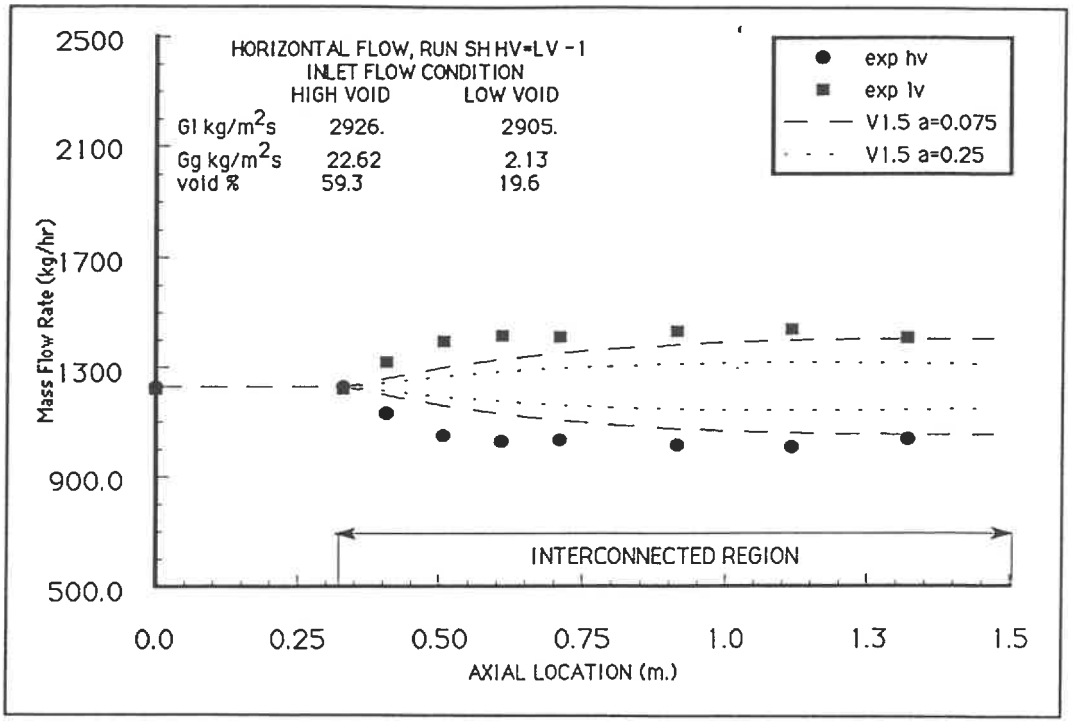

Figure 7.3: Mass Flow $SH - HV = LV - 1$ ASSERT–4 Version 1.5

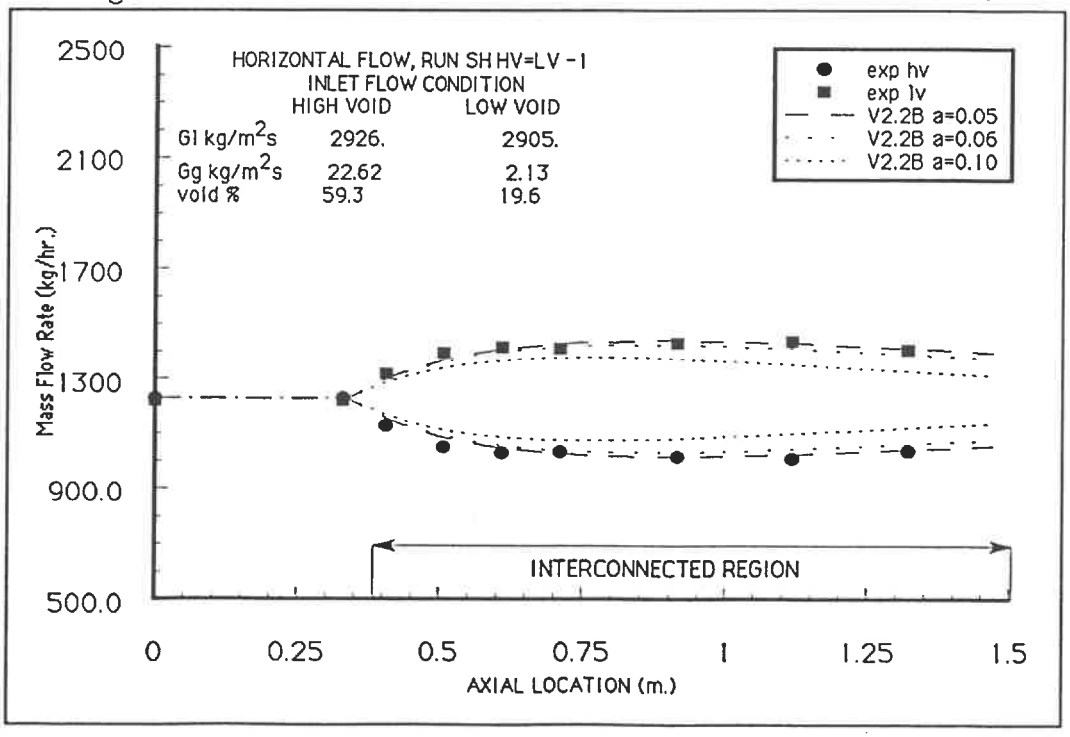

Figure 7.4: Mass Flow $SH - HV = LV - 1$ ASSERT–4 Version 2.2B

Page 313 manquante

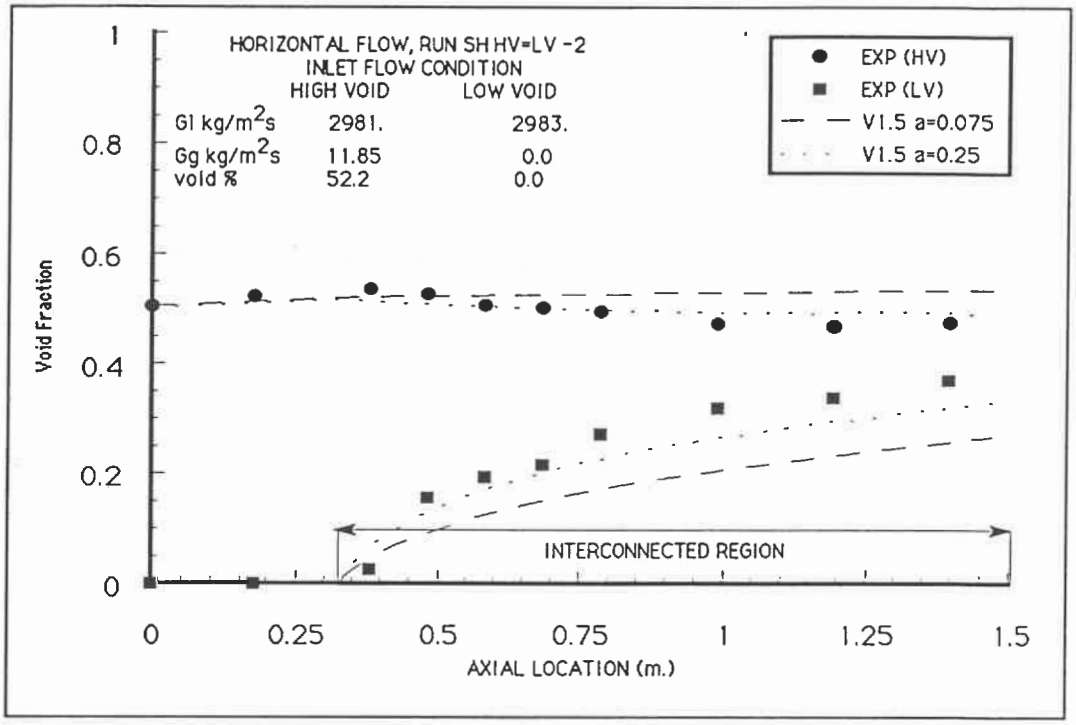

Figure 7.7: Void Fraction $SH - HV = LV - 2$ ASSERT-4 Version 1.5

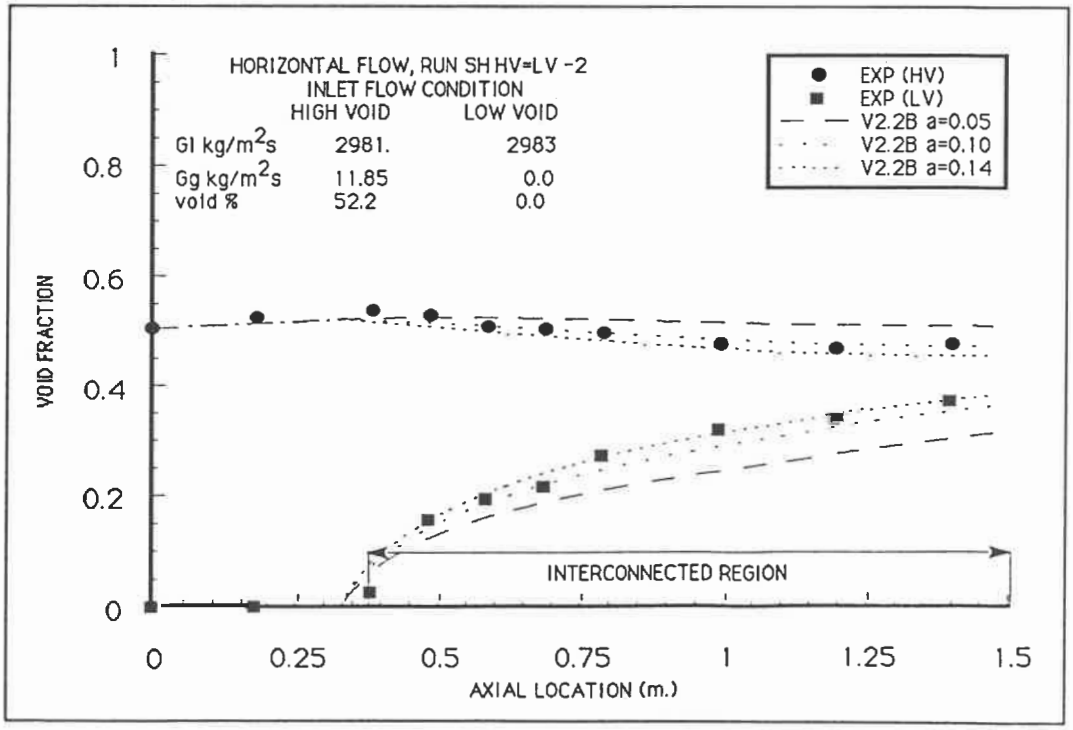

Figure 7.8: Void Fraction $SH - HV = LV - 2$ ASSERT-4 Version 2.2B

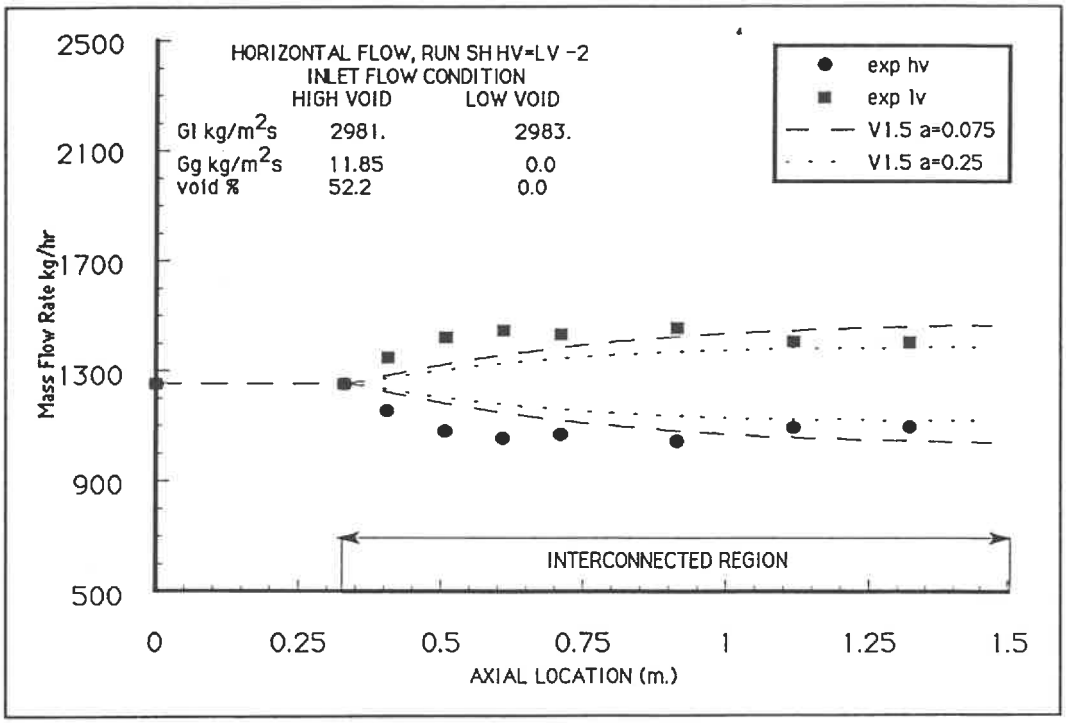

Figure 7.9: Mass Flow $SH - HV = LV - 2$ ASSERT-4 Version 1.5

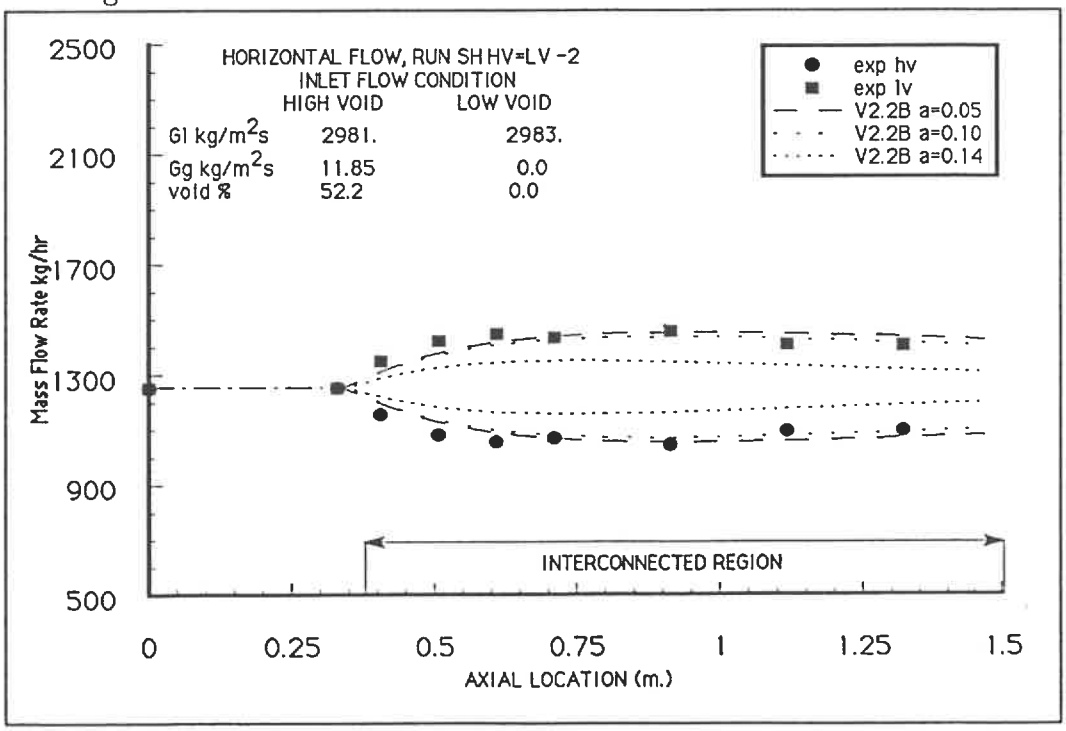

Figure 7.10: Mass Flow $SH - HV = LV - 2$ ASSERT-4 Version 2.2B

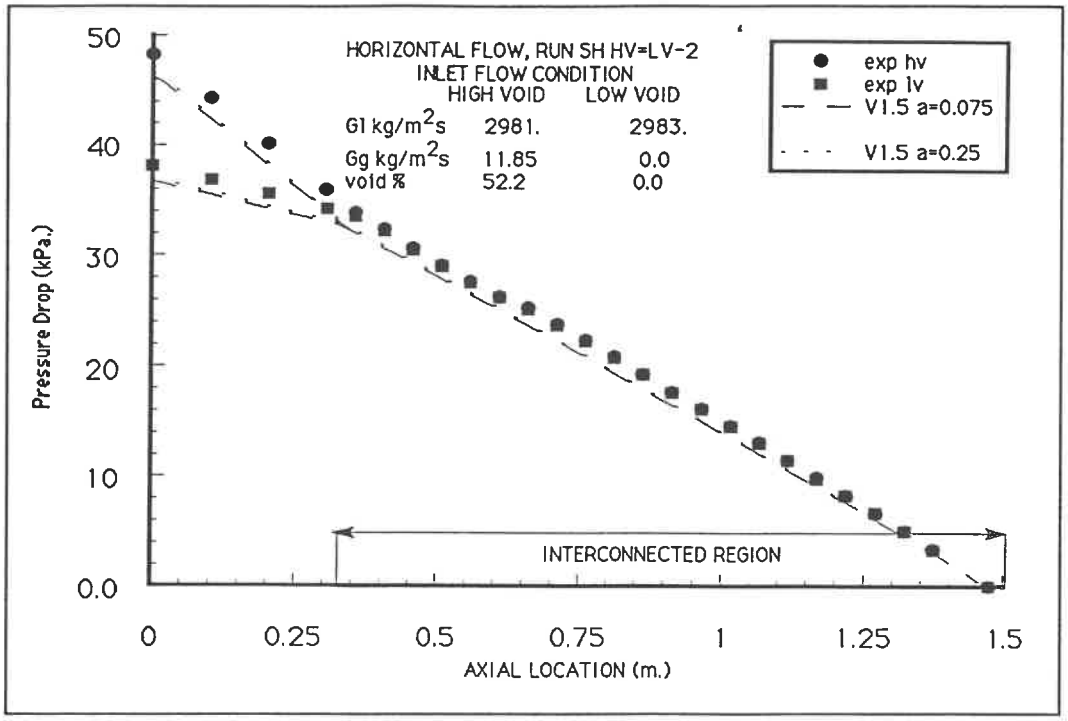

Figure 7.11: Pressure Drop $SH - HV = LV - 2$ ASSERT-4 Version 1.5

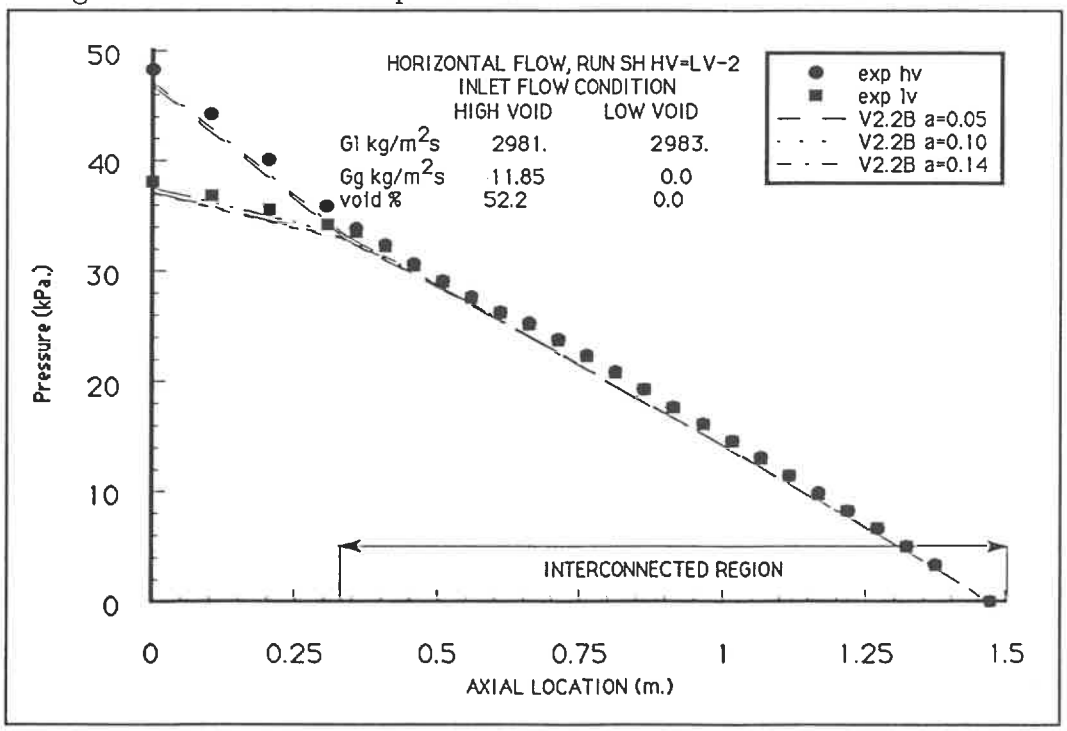

Figure 7.12: Pressure Drop $SH - HV = LV - 2$ ASSERT-4 Version 2.2B

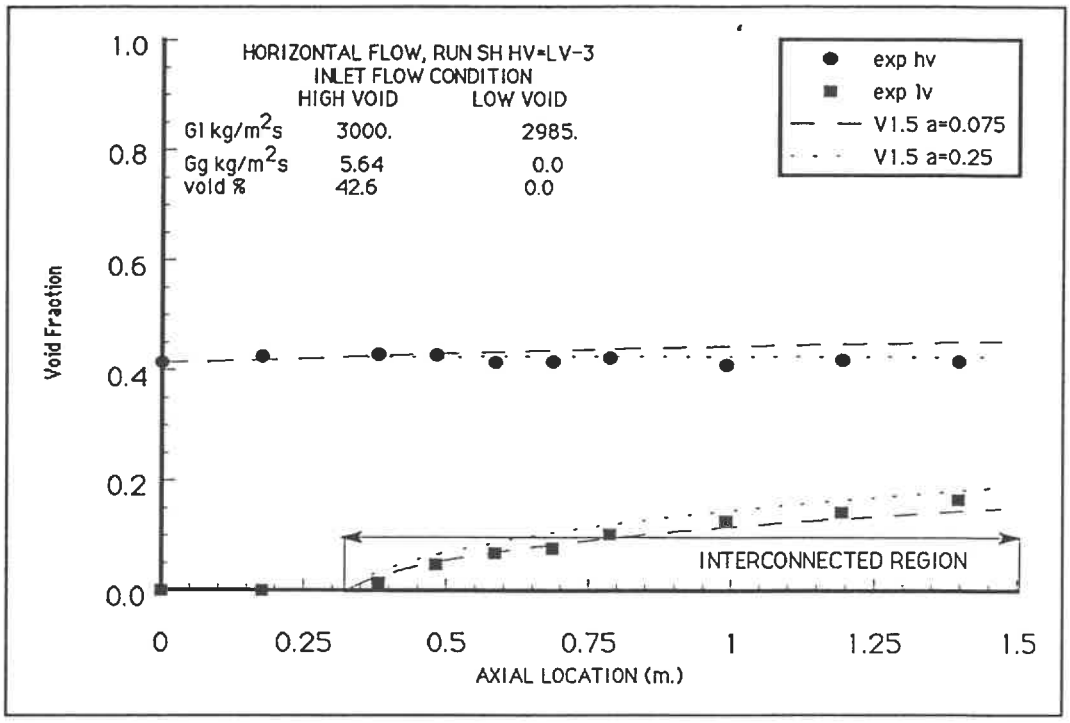

Figure 7.13: Void Fraction $SH - HV = LV - 3$ ASSERT-4 Version 1.5

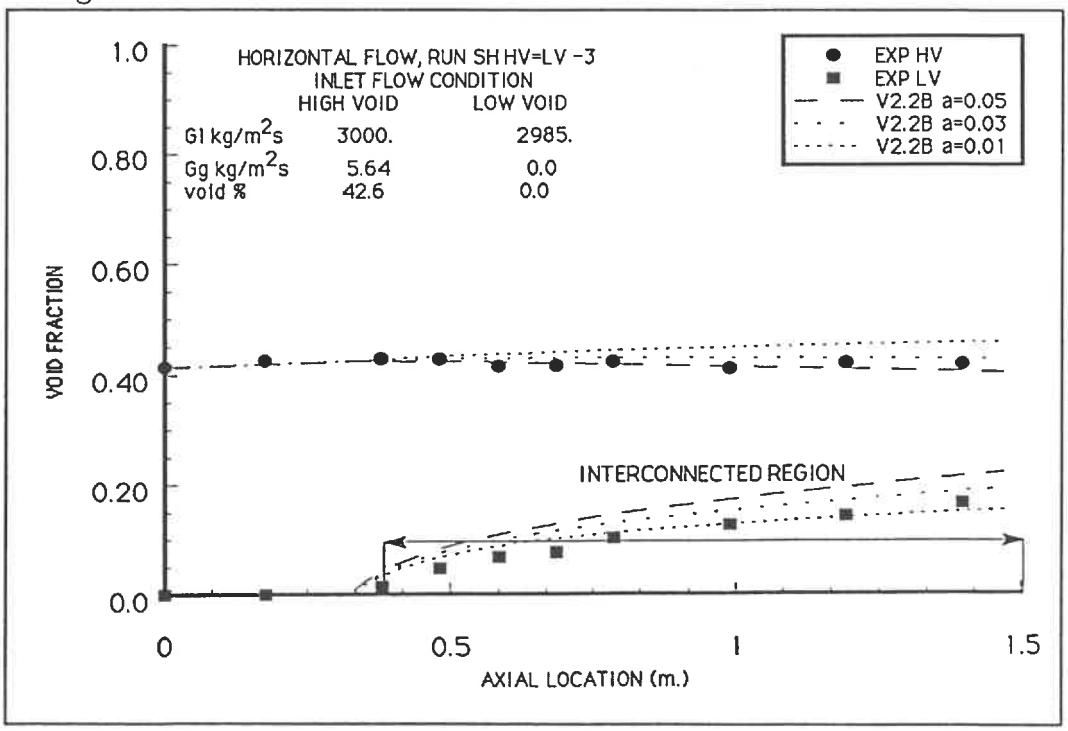

Figure 7.14: Void Fraction $SH - HV = LV - 3$ ASSERT-4 Version 2.2B

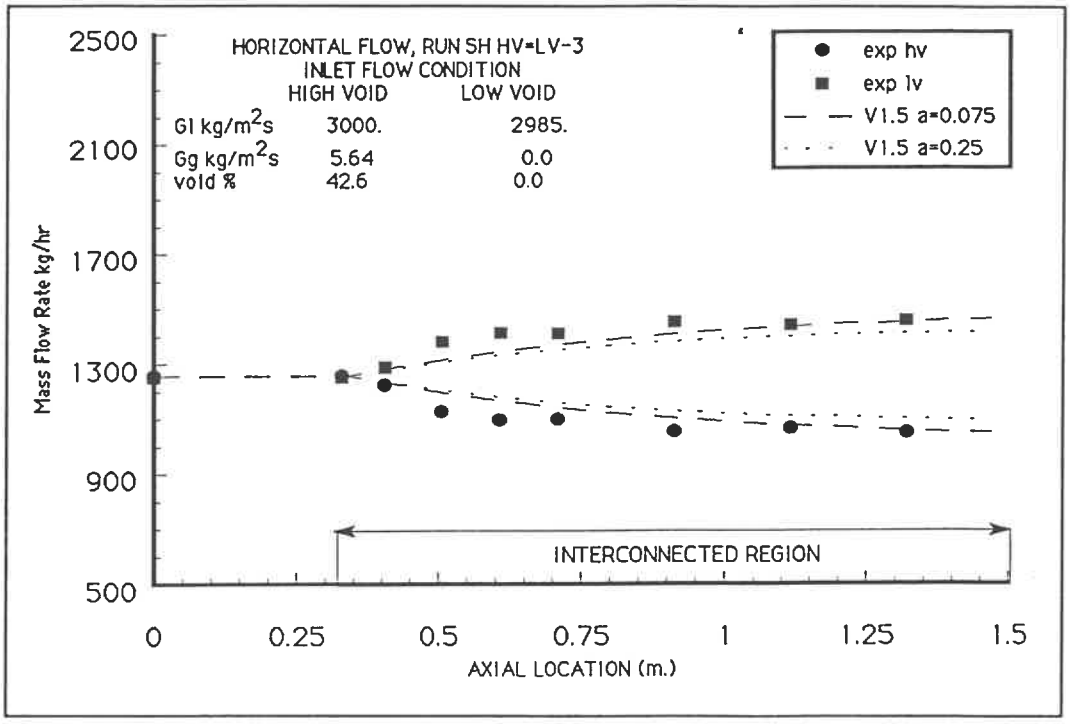

Figure 7.15: Mass Flow $SH - HV = LV - 3$ ASSERT-4 Version 1.5

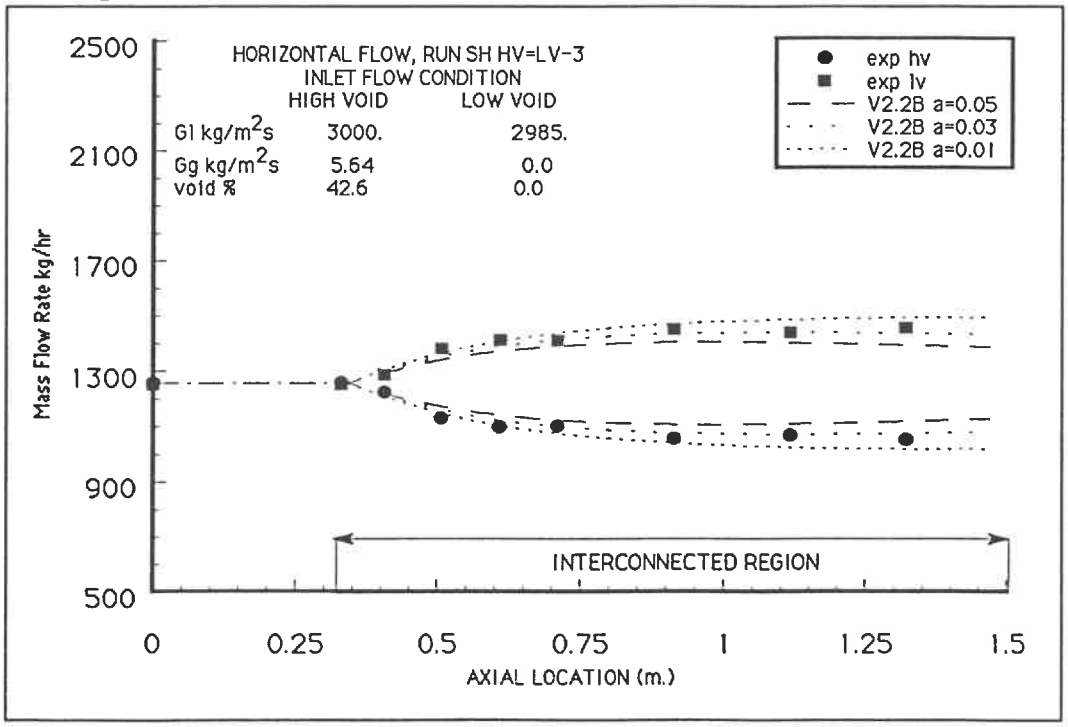

Figure 7.16: Mass Flow $SH - HV = LV - 3$ ASSERT-4 Version 2.2B

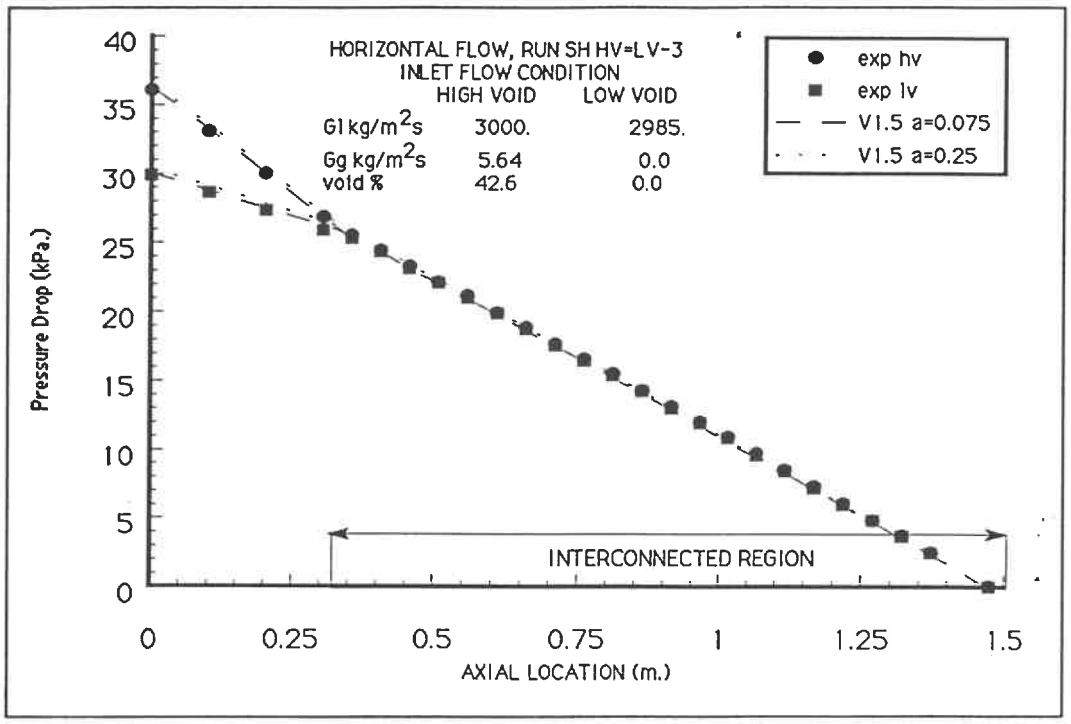

Figure 7.17: Pressure Drop $SH - HV = LV - 3$ ASSERT-4 Version 1.5

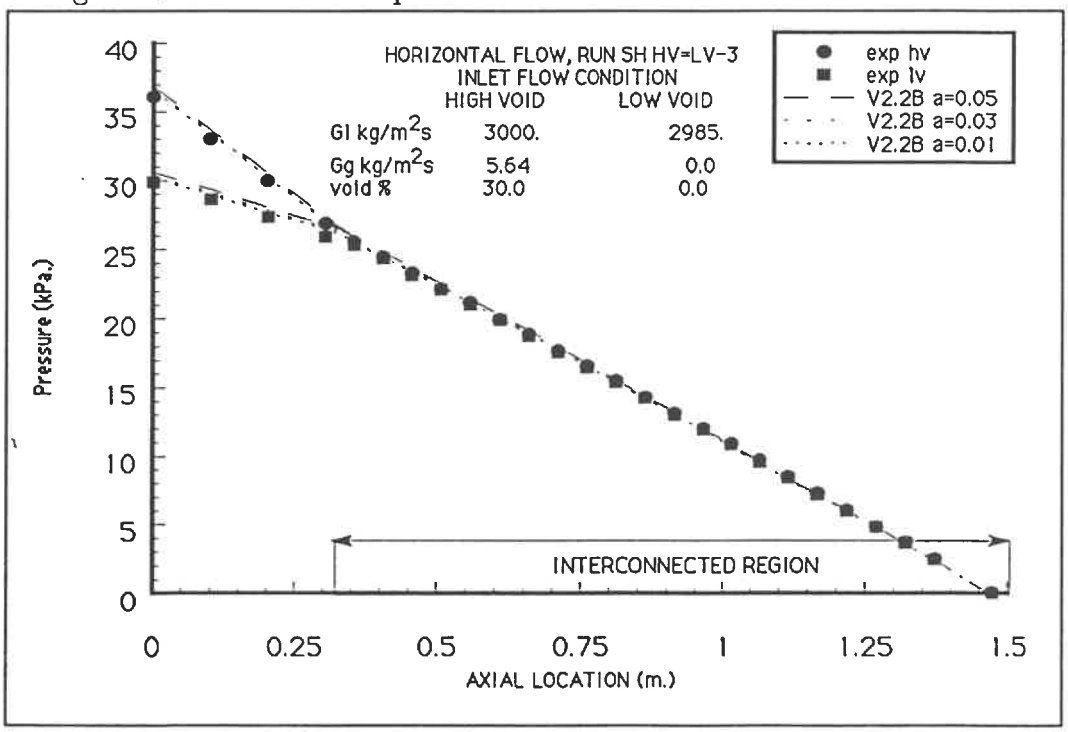

Figure 7.18: Pressure Drop $SH - HV = LV - 3$ ASSERT-4 Version 2.2B

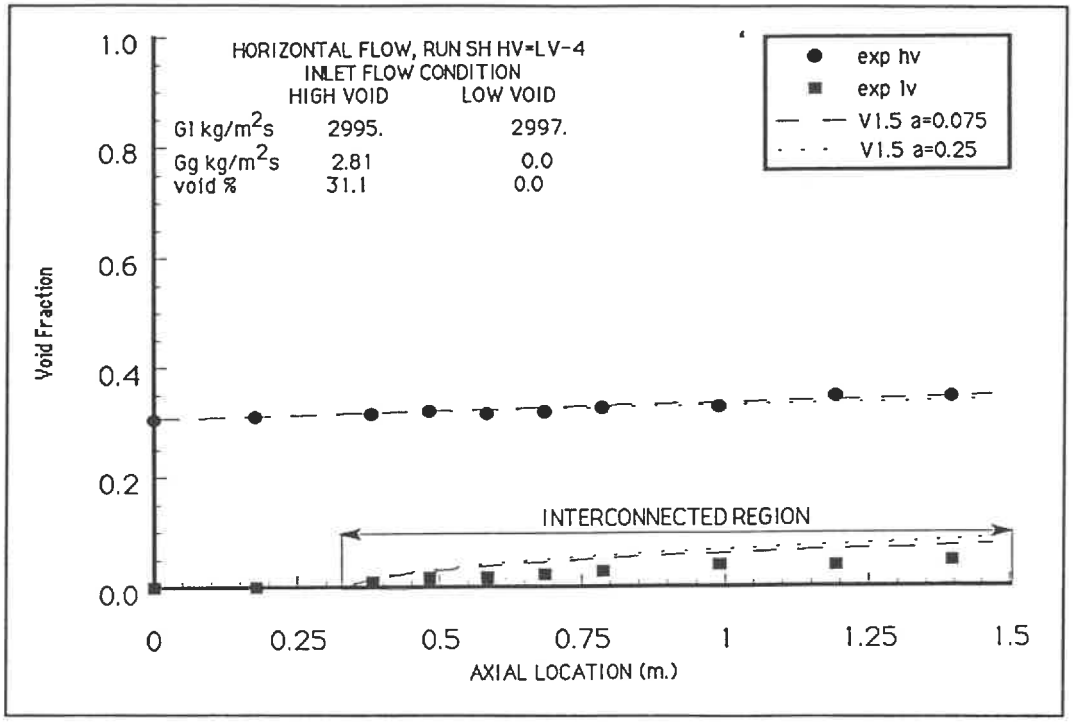

Figure 7.19: Void Fraction $SH - HV = LV - 4$ ASSERT-4 Version 1.5

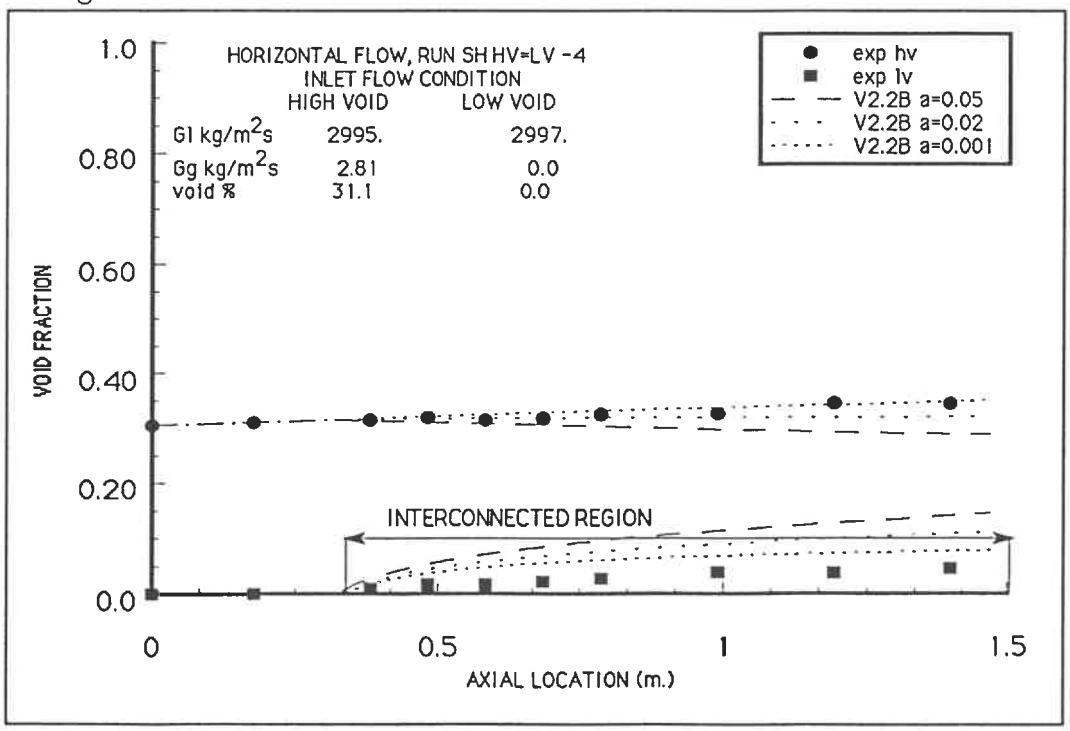

Figure 7.20: Void Fraction $SH - HV = LV - 4$ ASSERT-4 Version 2.2B

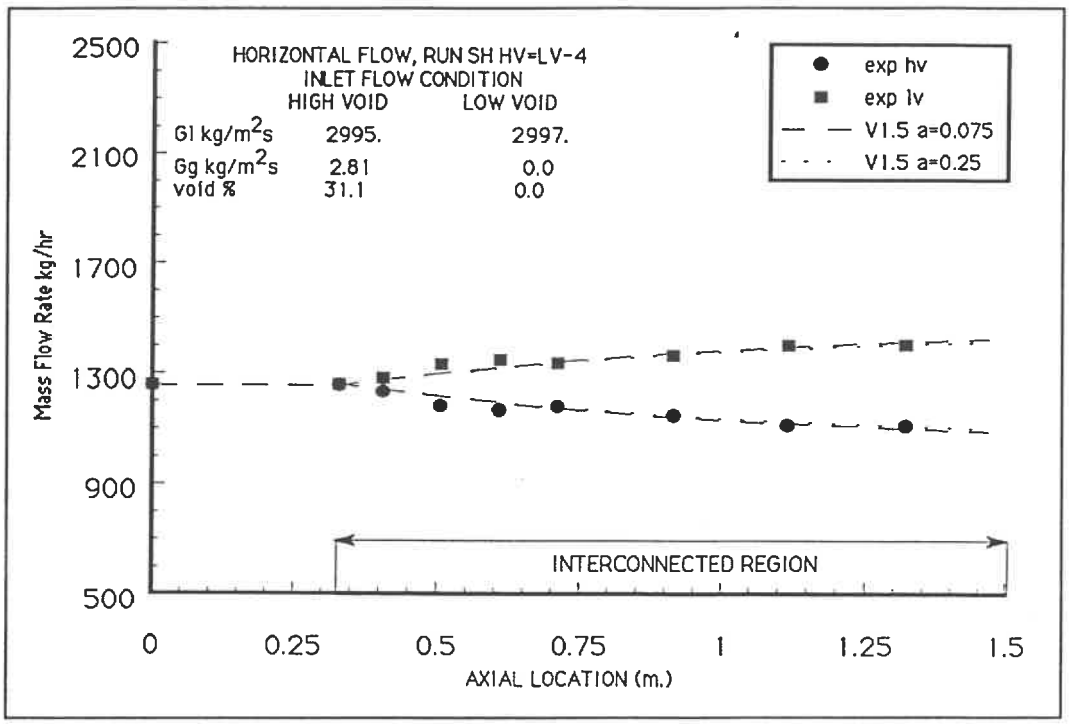

Figure 7.21: Mass Flow $SH - HV = LV - 4$ ASSERT-4 Version 1.5

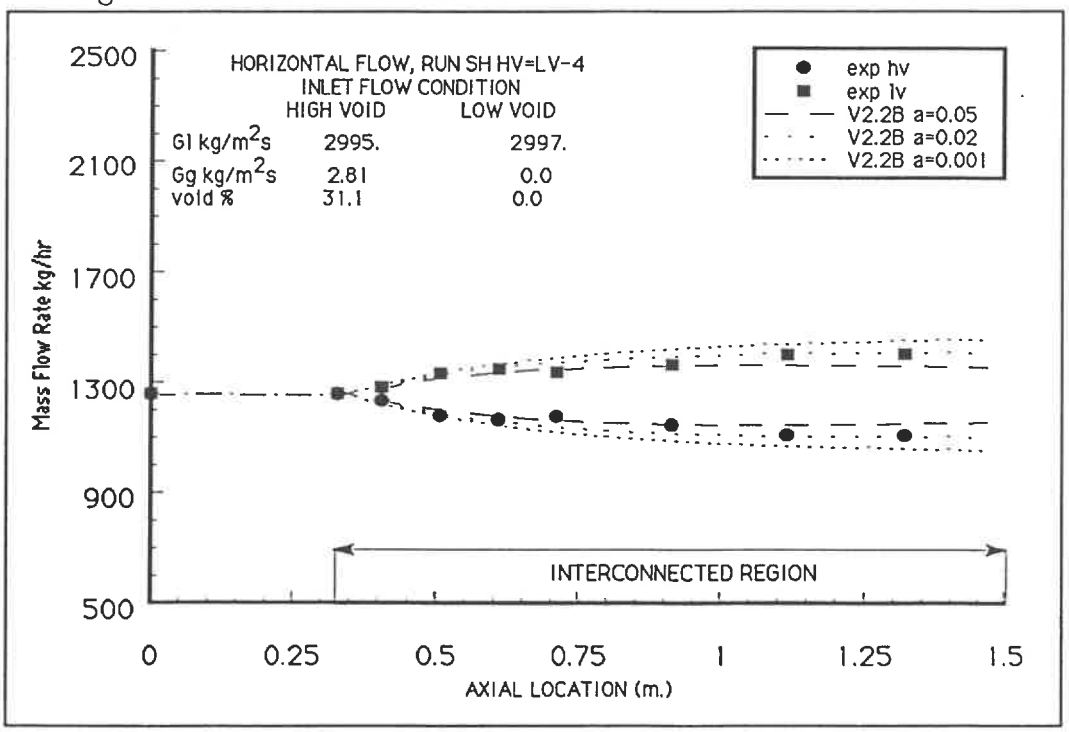

Figure 7.22: Mass Flow $SH - HV = LV - 4$ ASSERT-4 Version 2.2B

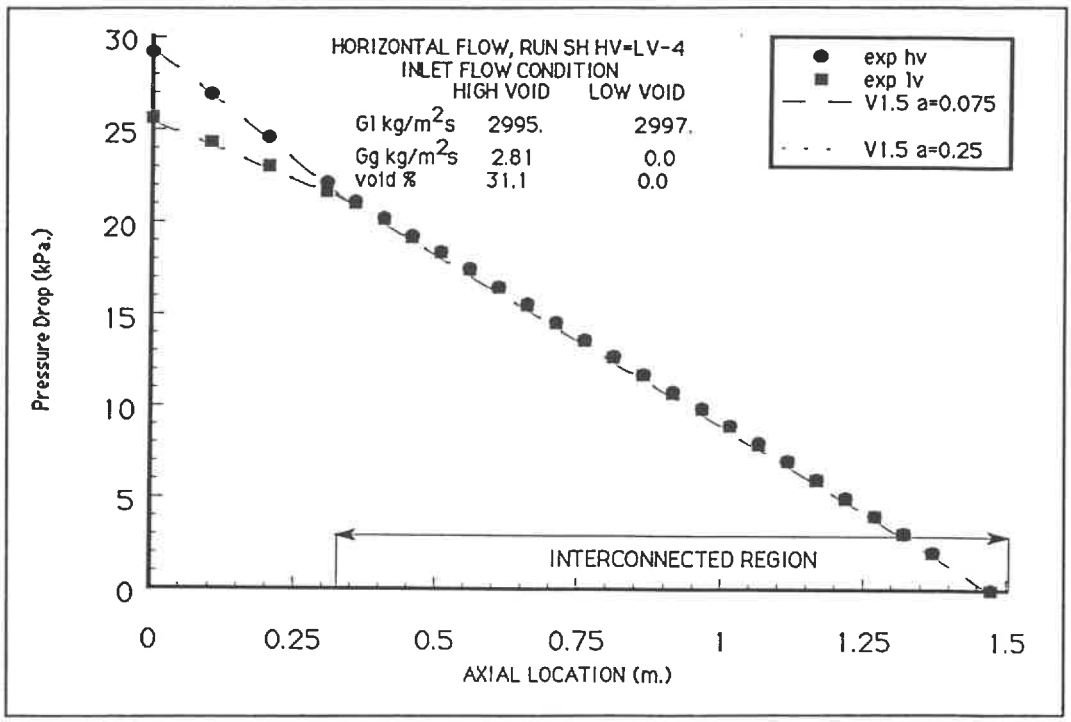

Figure 7.23: Pressure Drop $SH - HV = LV - 4$ ASSERT-4 Version 1.5

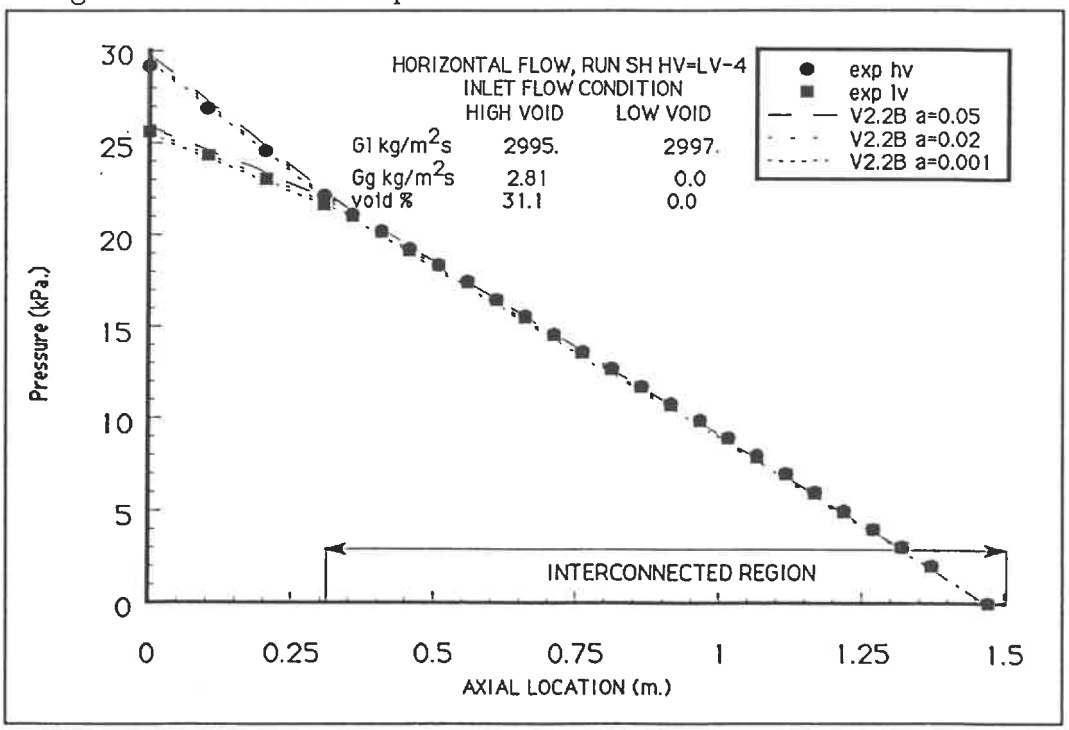

Figure 7.24: Pressure Drop $SH - HV = LV - 4$ ASSERT-4 Version 2.2B

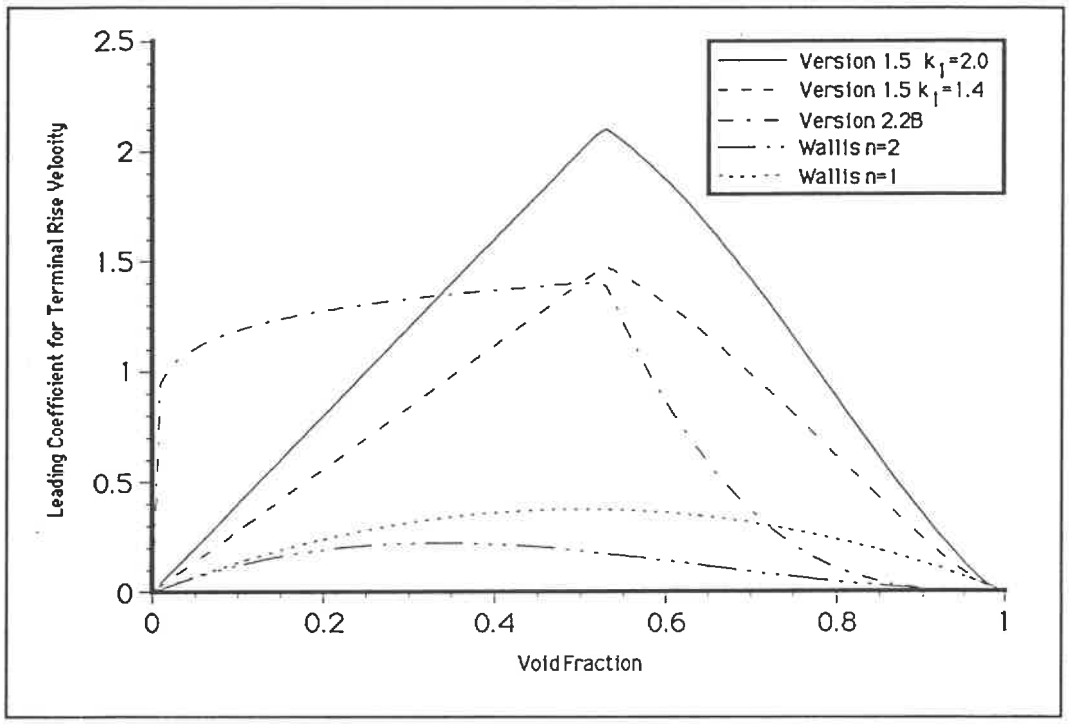

Figure 7.25: Leading Terms in the Calculation of the Drift Velocity

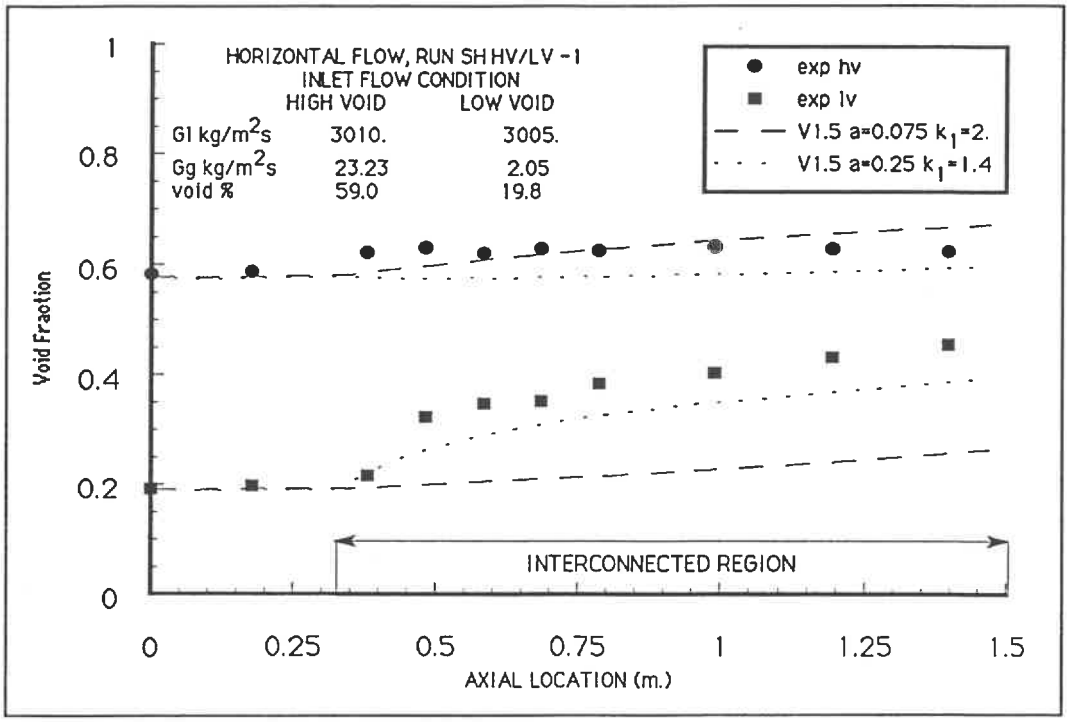

Figure 7.26: Void Fraction $SH - \frac{HV}{LV} - 1$ ASSERT–4 Version 1.5

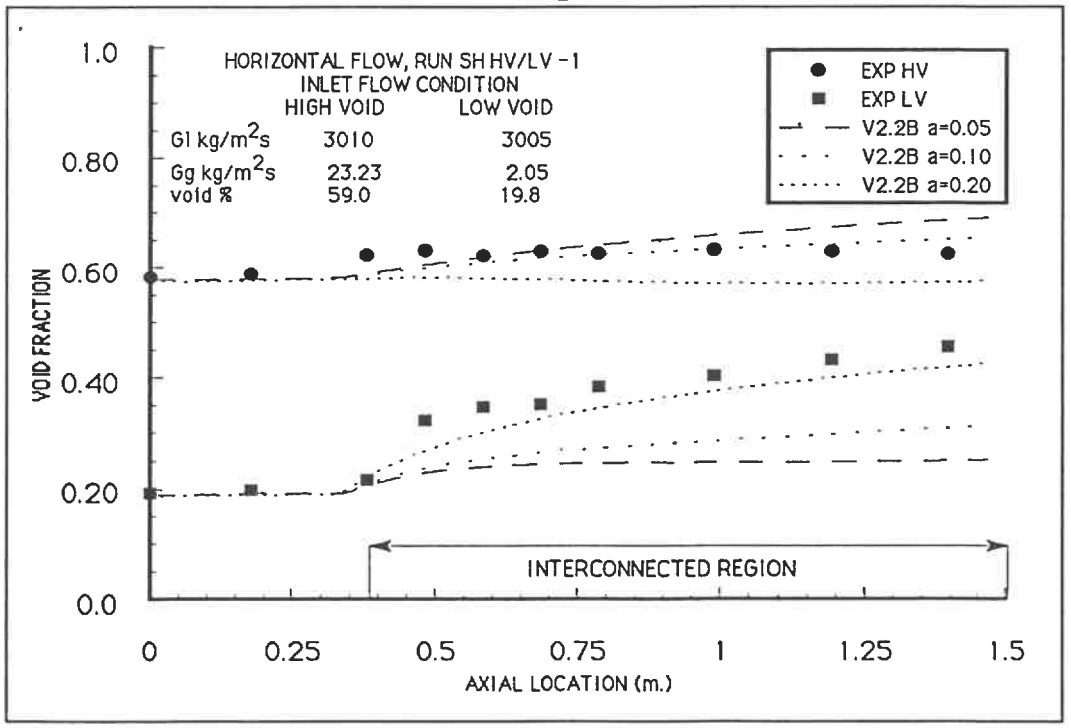

Figure 7.27: Void Fraction $SH - \frac{HV}{LV} - 1$ ASSERT–4 Version 2.2B

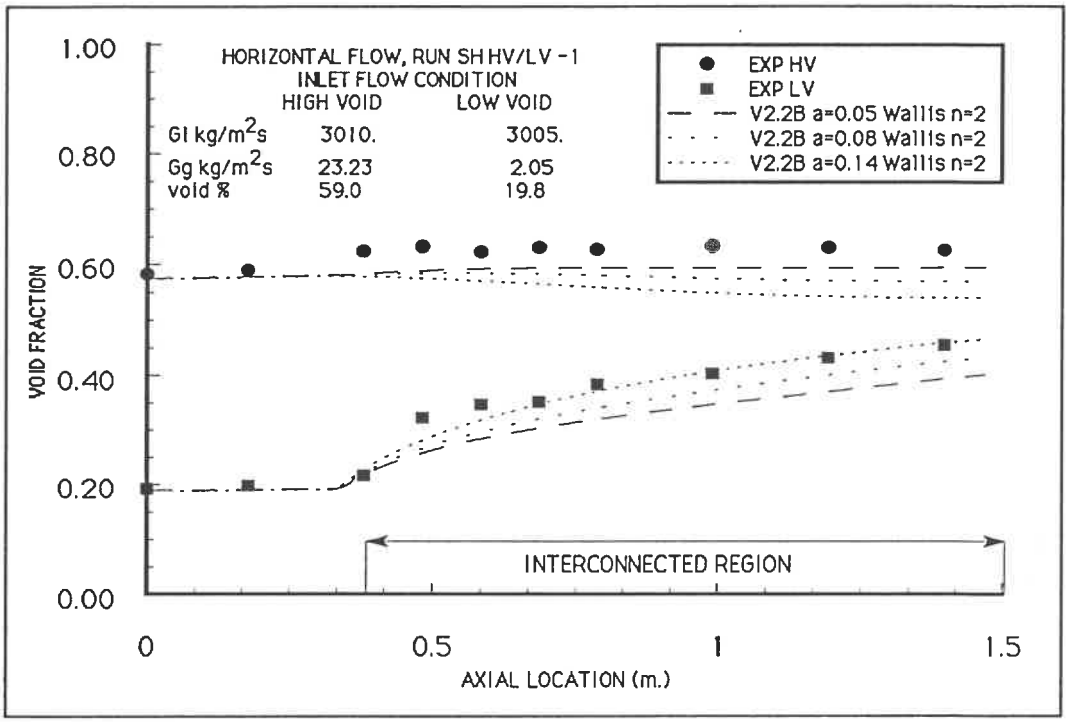

Figure 7.28: Void Fraction $SH - \frac{HV}{LV} - 1$ ASSERT-4 Version 2.2B Wallis n=2

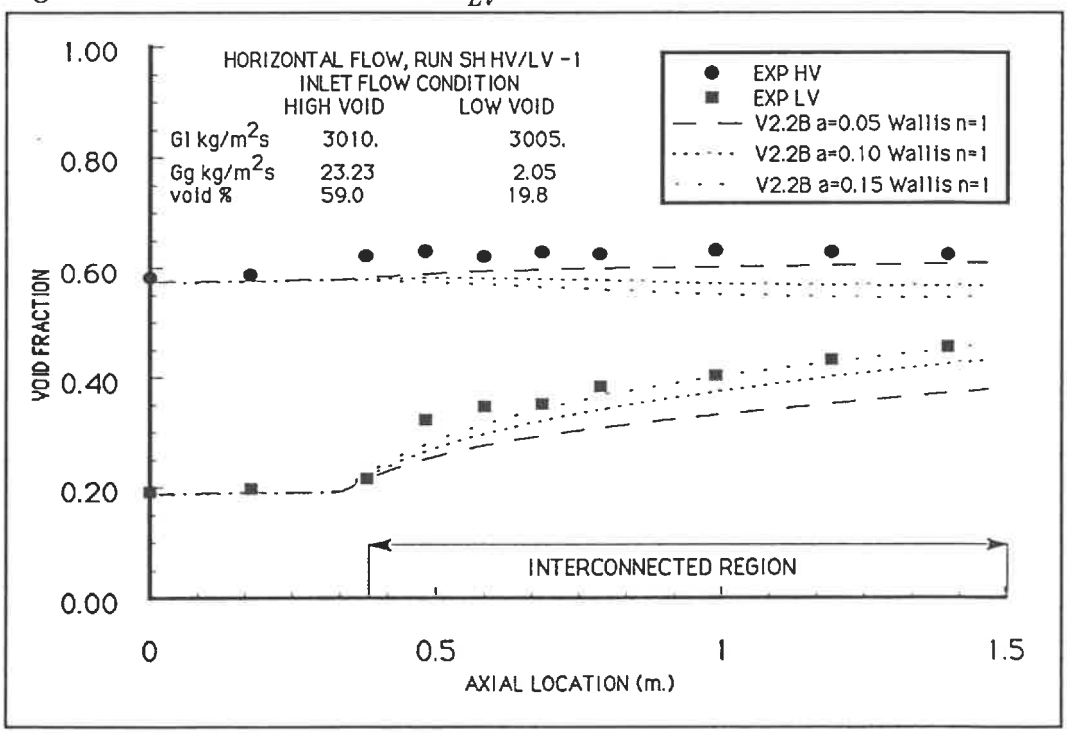

Figure 7.29: Void Fraction $SH - \frac{HV}{LV} - 1$ ASSERT-4 Version 2.2B Wallis n=1

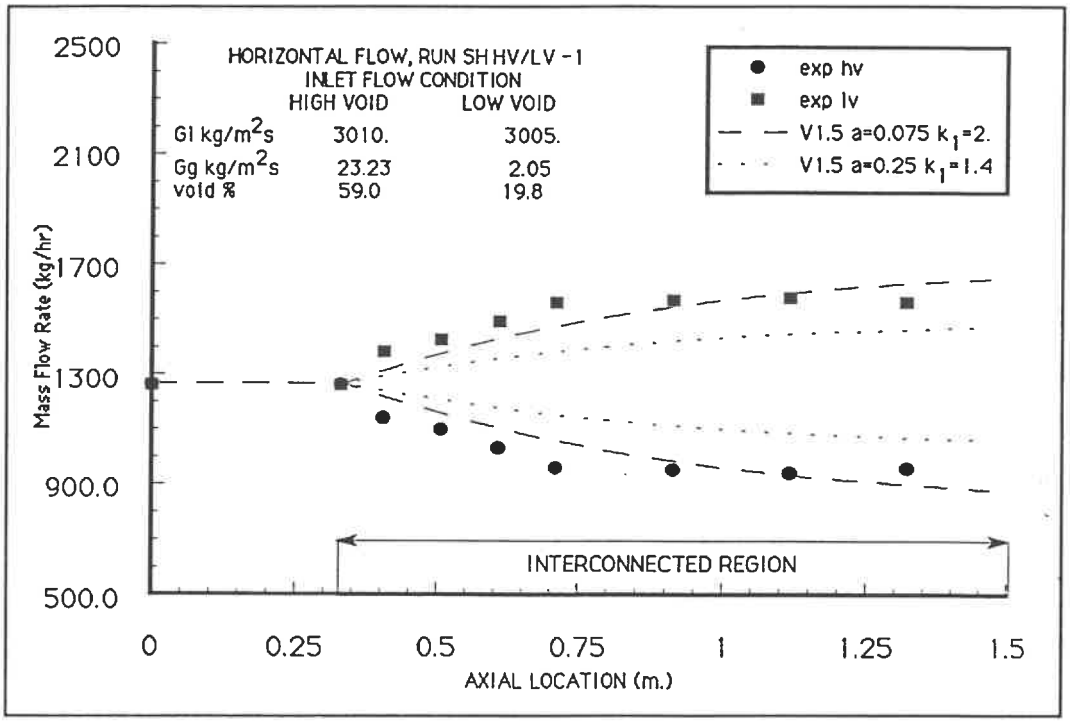

Figure 7.30: Mass Flow $SH - \frac{HV}{LV} - 1$ ASSERT–4 Version 1.5

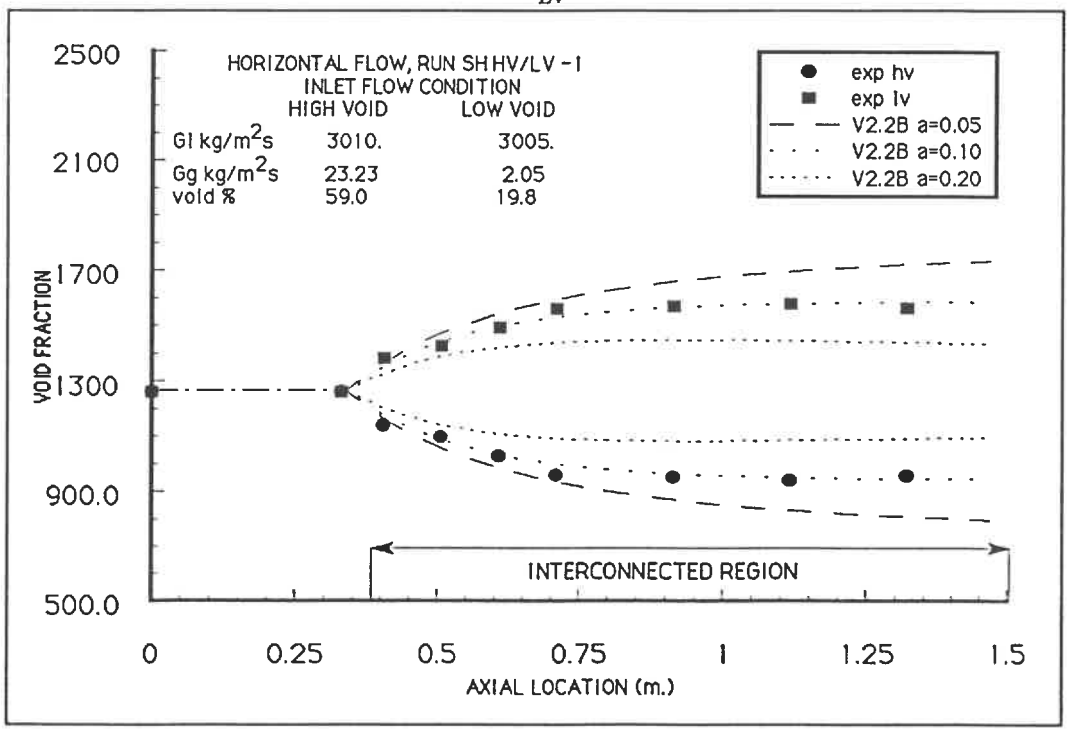

Figure 7.31: Mass Flow $SH - \frac{HV}{LV} - 1$ ASSERT–4 Version 2.2B

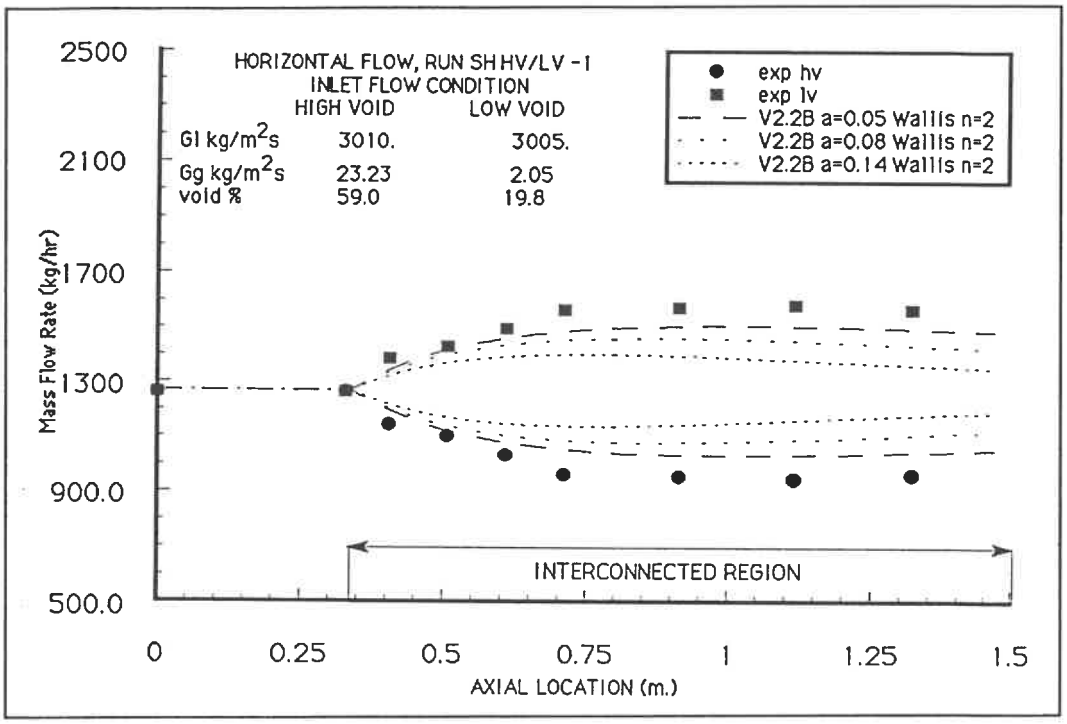

Figure 7.32: Mass Flow $SH - \frac{HV}{LV} - 1$ ASSERT-4 Version 2.2B Wallis n=2

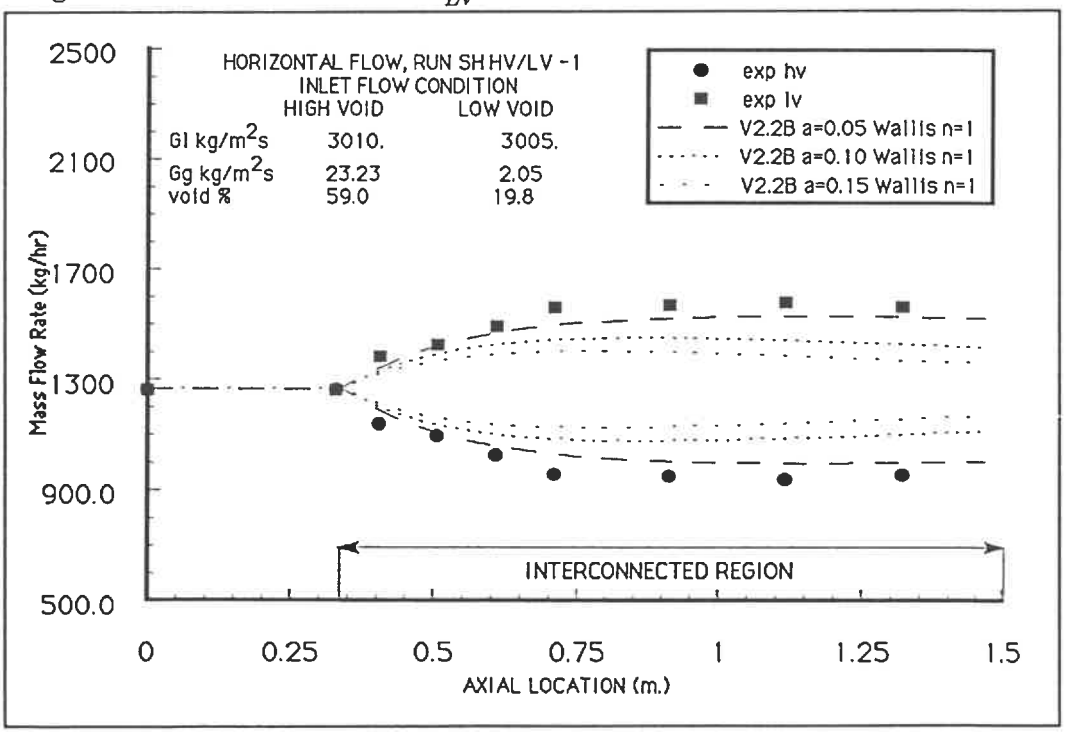

Figure 7.33: Mass Flow $SH - \frac{HV}{LV} - 1$ ASSERT-4 Version 2.2B Wallis n=1

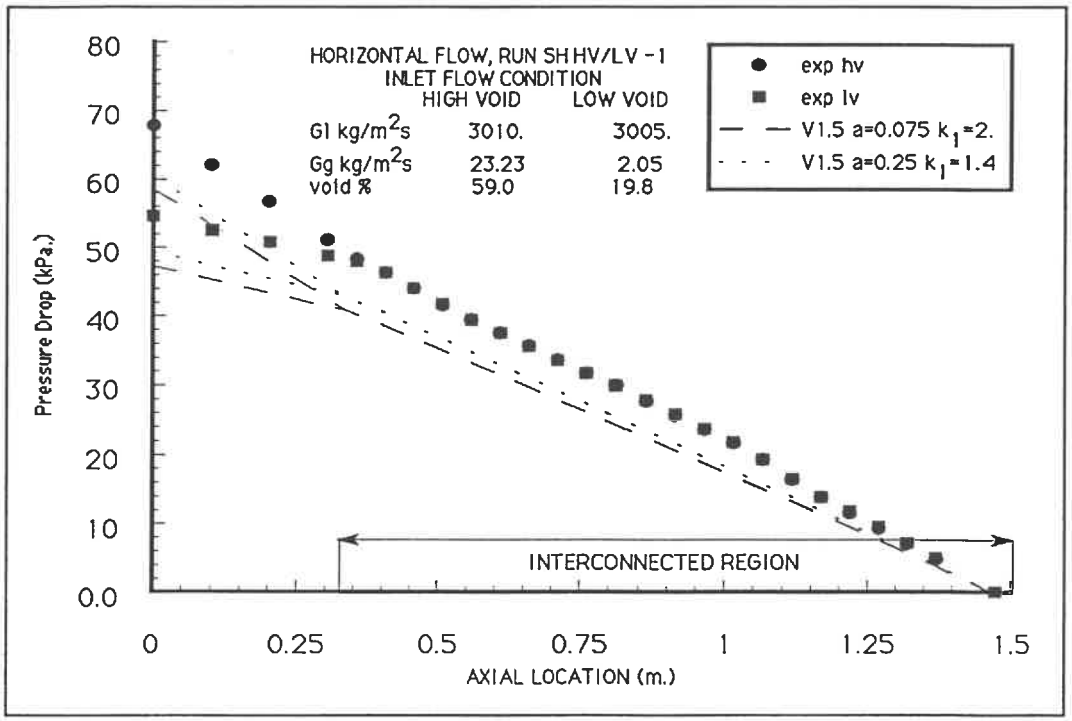

Figure 7.34: Pressure Drop $SH - \frac{HV}{LV} - 1$ ASSERT-4 Version 1.5

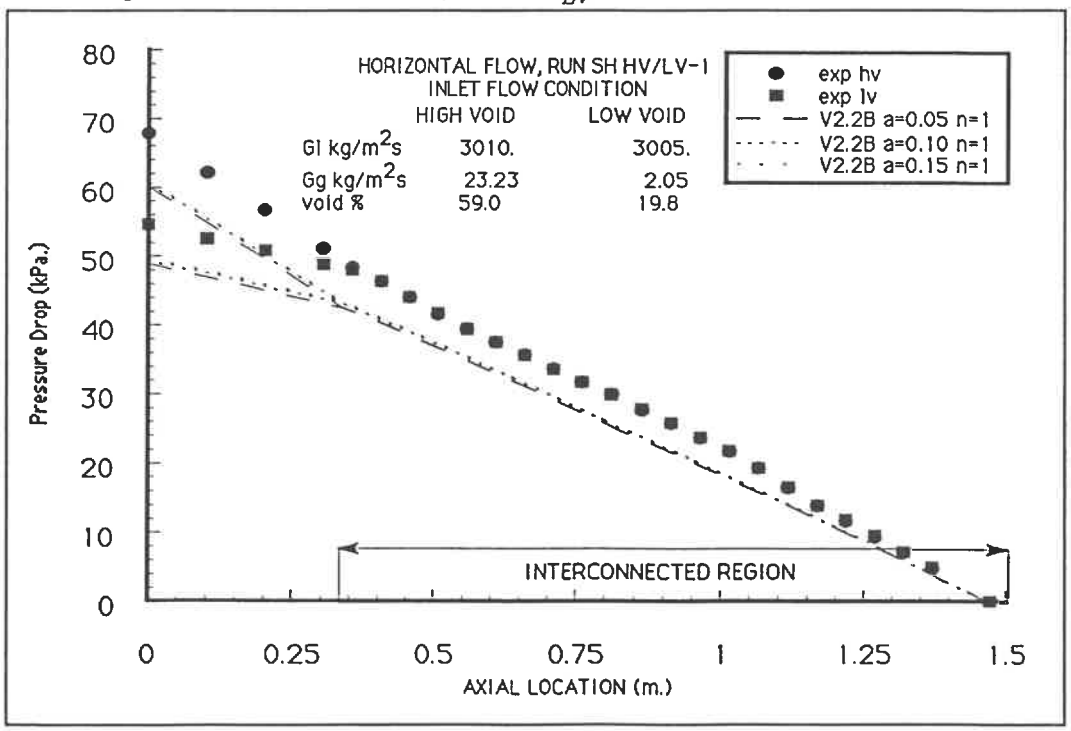

Figure 7.35: Pressure Drop $SH - \frac{HV}{LV} - 1$ ASSERT-4 Version 2.2B

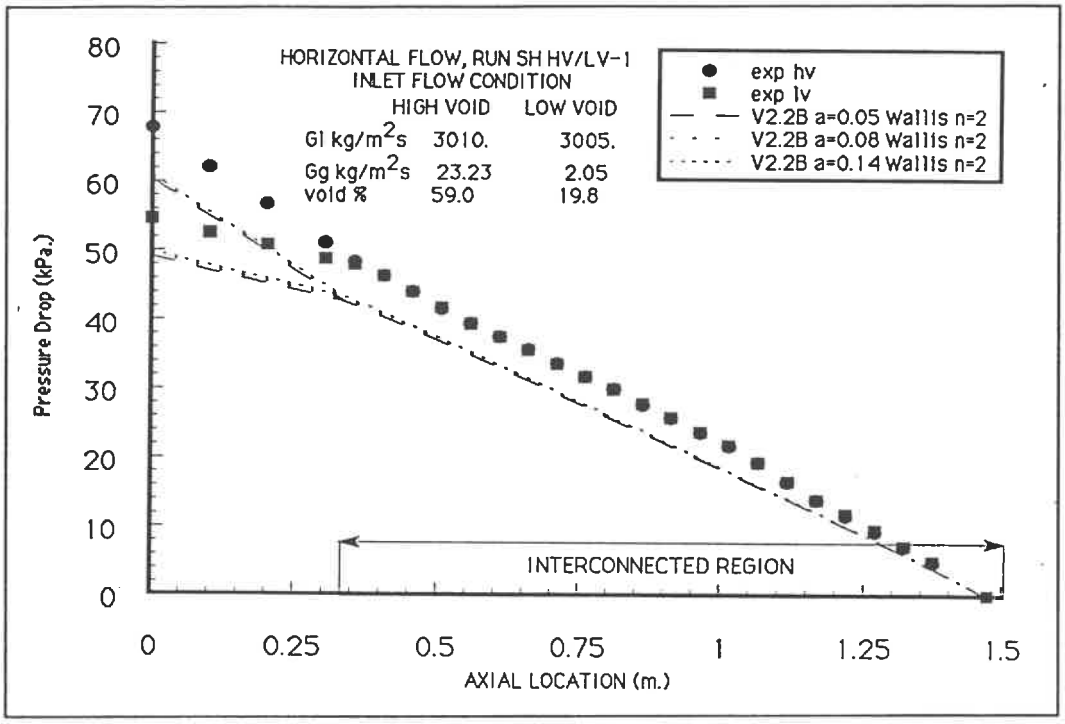

Figure 7.36: Pressure Drop $SH - \frac{HV}{LV} - 1$ ASSERT-4 Version 2.2B Wallis n=2

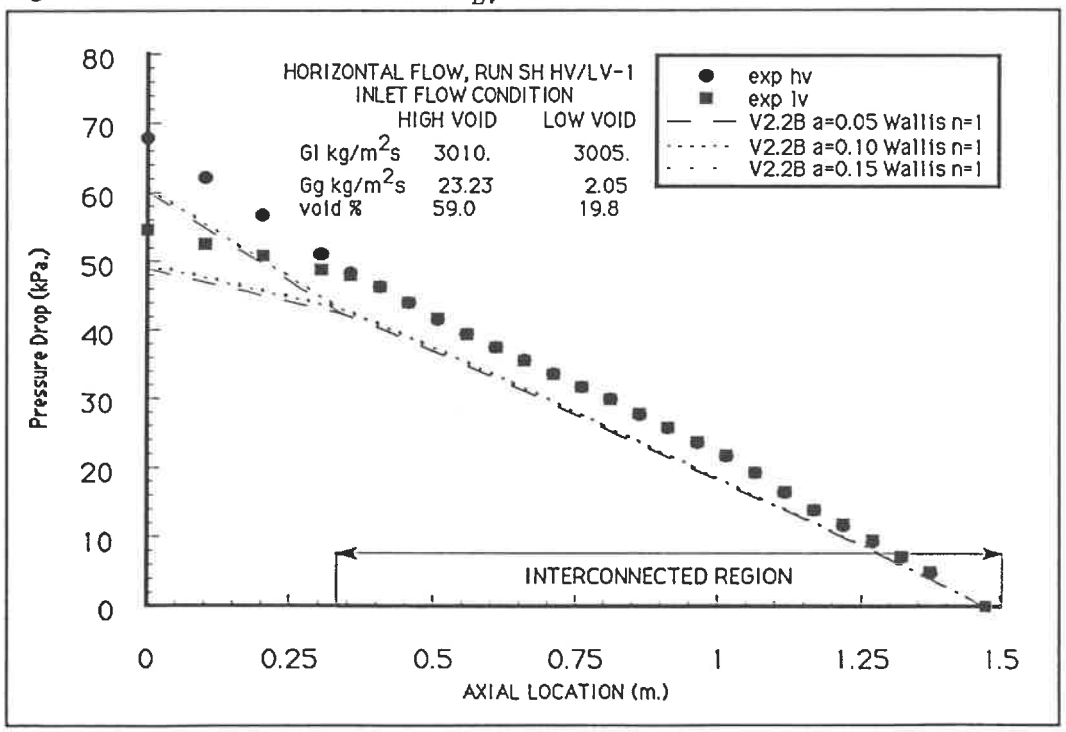

Figure 7.37: Pressure Drop $SH - \frac{HV}{LV} - 1$ ASSERT-4 Version 2.2B Wallis n=1

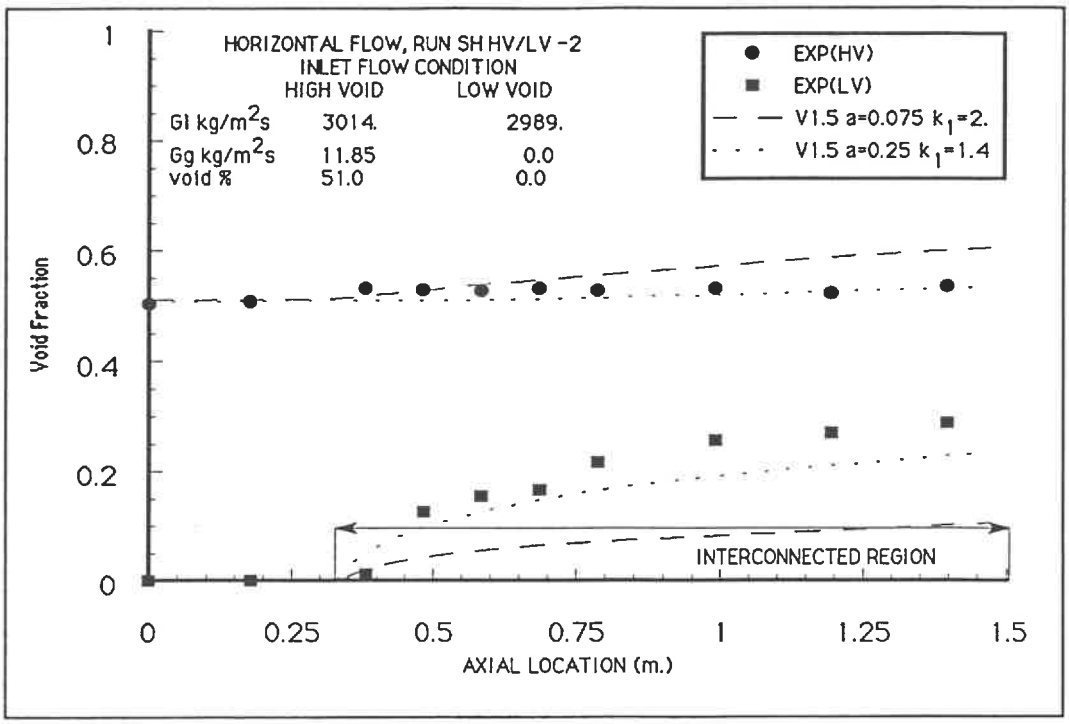

Figure 7.38: Void Fraction $SH - \frac{HV}{LV} - 2$ ASSERT-4 Version 1.5

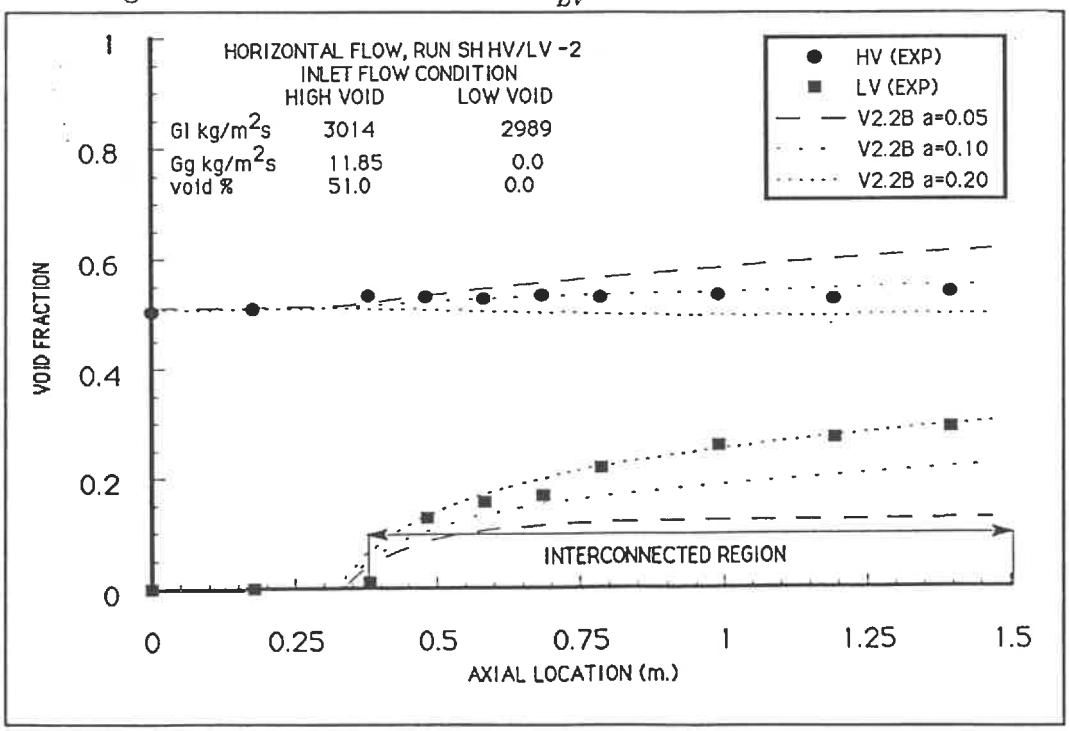

Figure 7.39: Void Fraction $SH - \frac{HV}{LV} - 2$ ASSERT-4 Version 2.2B

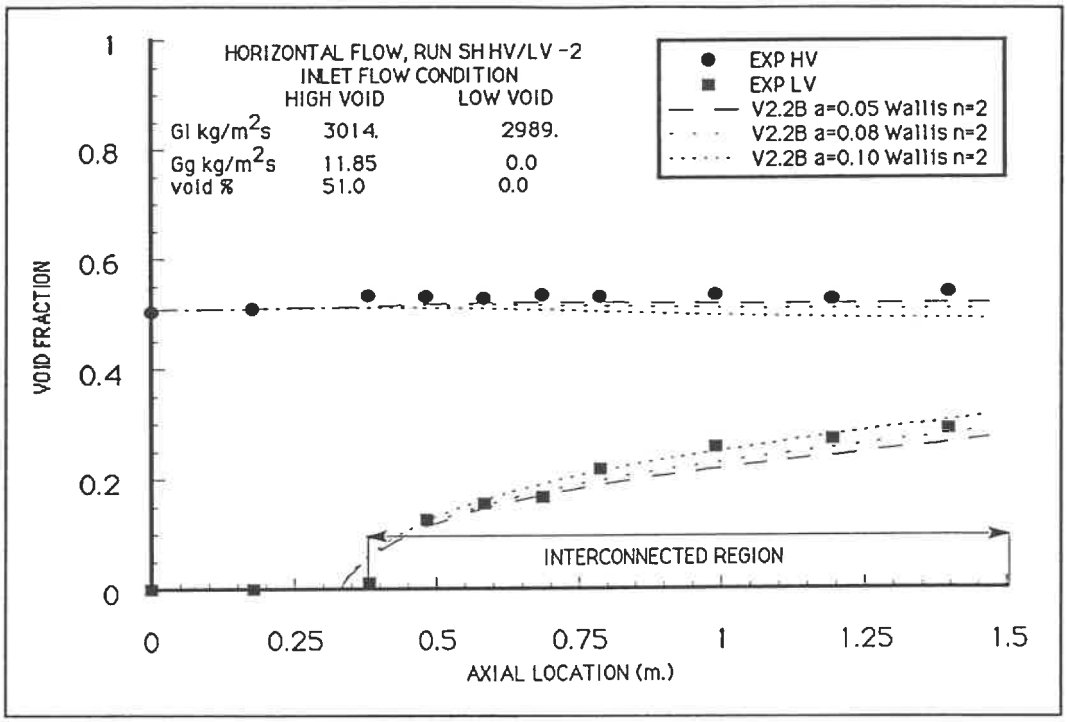

Figure 7.40: Void Fraction $SH - \frac{HV}{LV} - 2$ ASSERT-4 Version 2.2B Wallis n=2

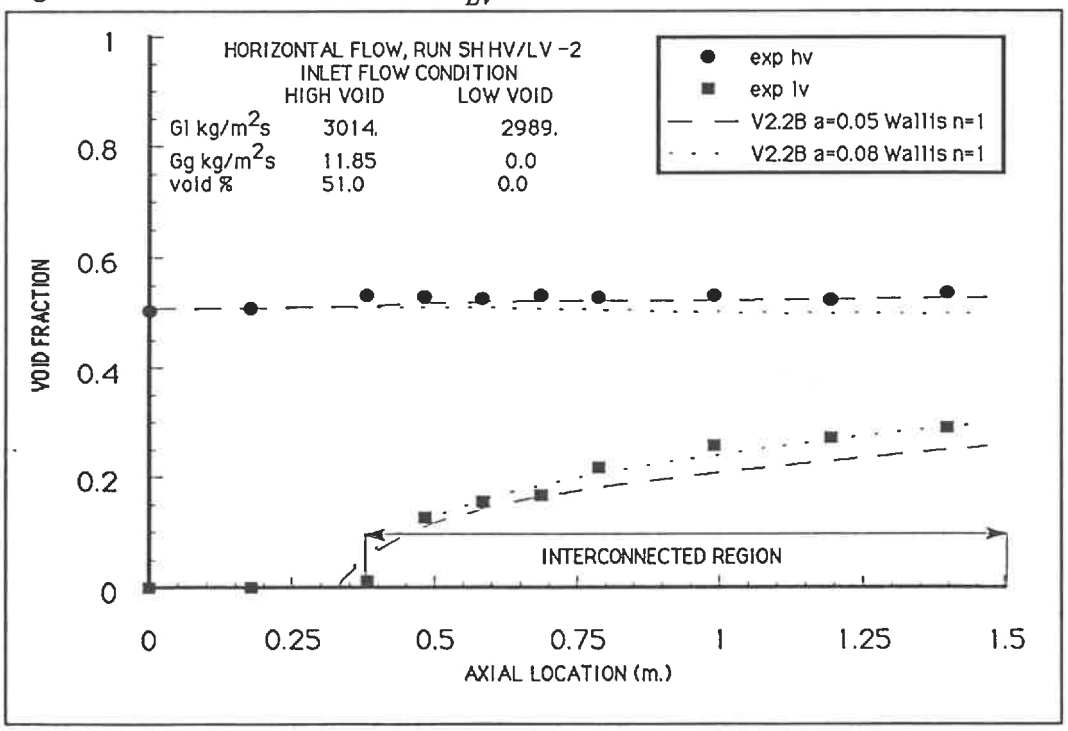

Figure 7.41: Void Fraction $SH - \frac{HV}{LV} - 2$ ASSERT-4 Version 2.2B Wallis n=1

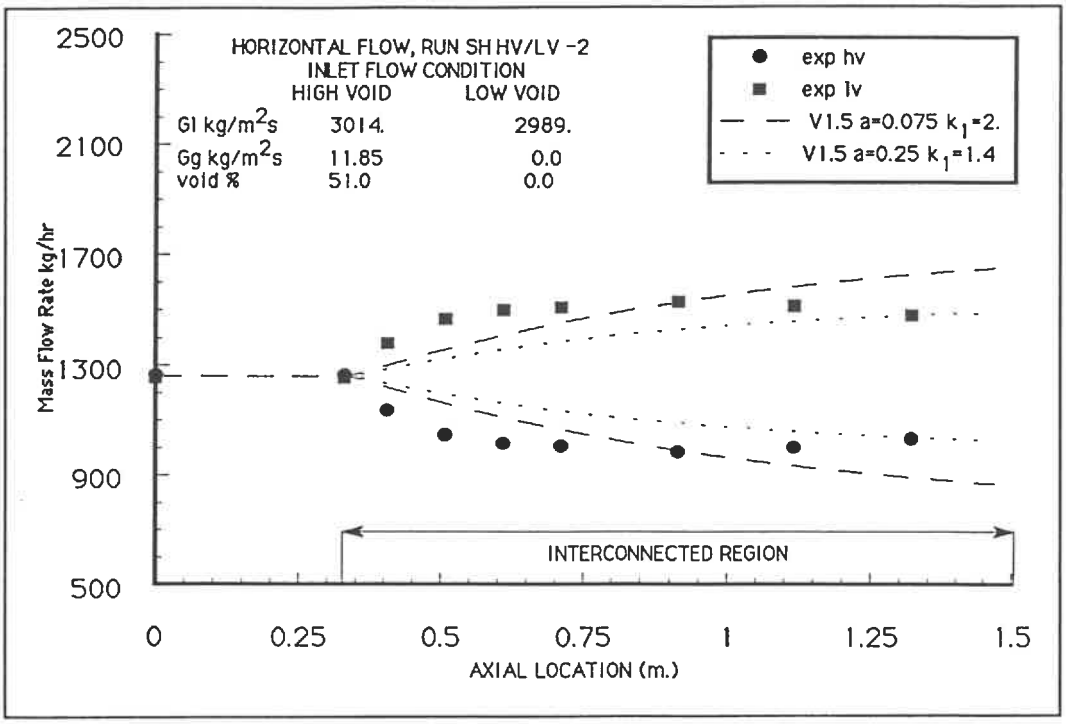

Figure 7.42: Mass Flow $SH - \frac{HV}{LV} - 2$ ASSERT-4 Version 1.5

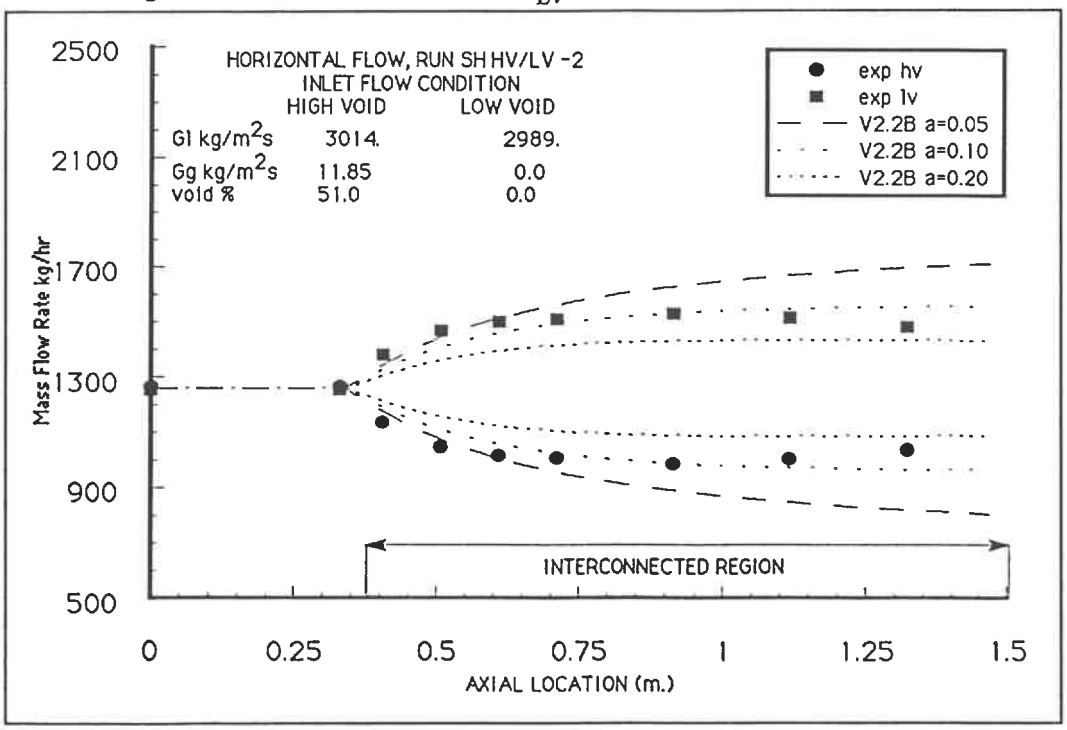

Figure 7.43: Mass Flow $SH - \frac{HV}{LV} - 2$ ASSERT-4 Version 2.2B

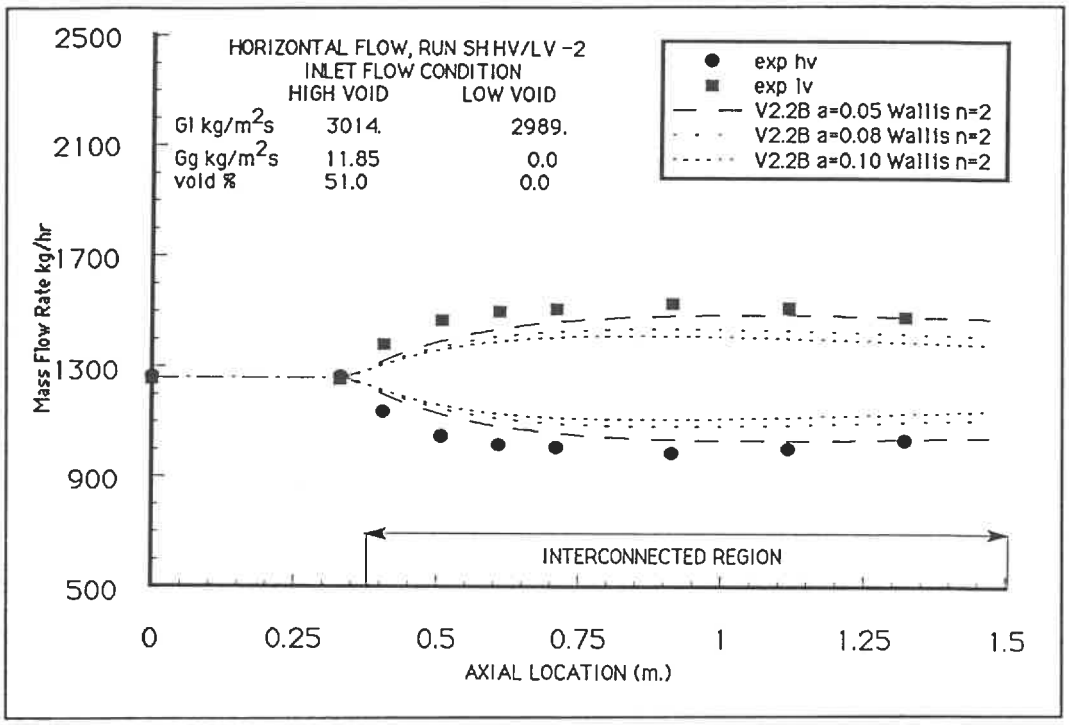

Figure 7.44: Mass Flow $SH - \frac{HV}{LV} - 2$ ASSERT-4 Version 2.2B Wallis n=2

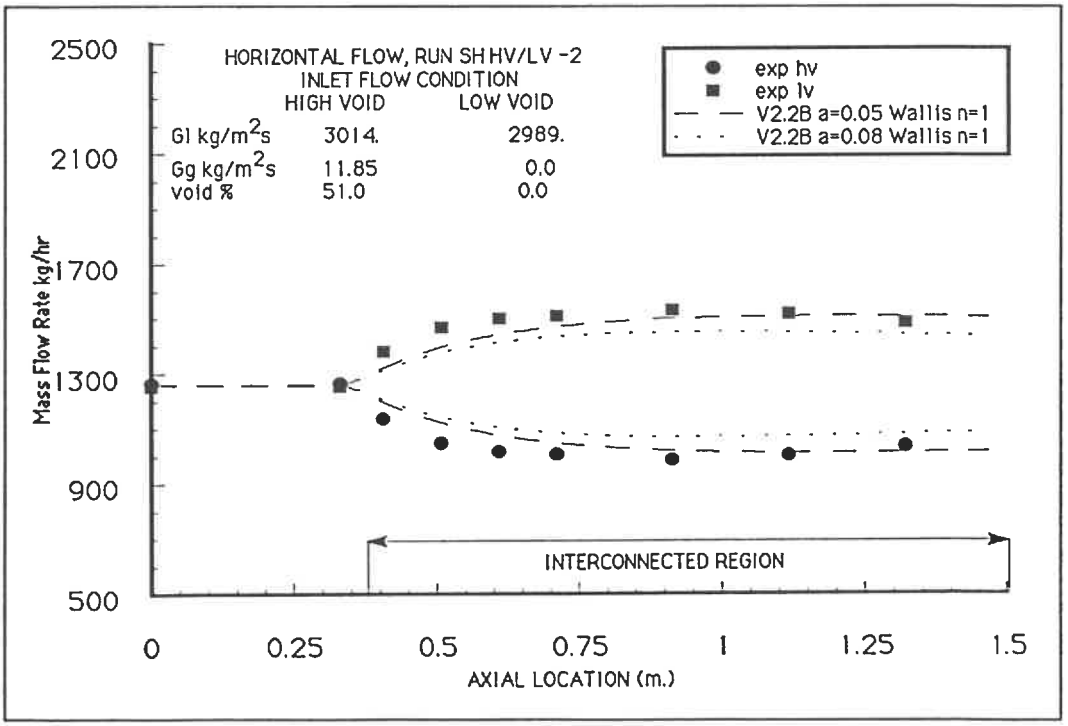

Figure 7.45: Mass Flow $SH - \frac{HV}{LV} - 2$ ASSERT-4 Version 2.2B Wallis n=1

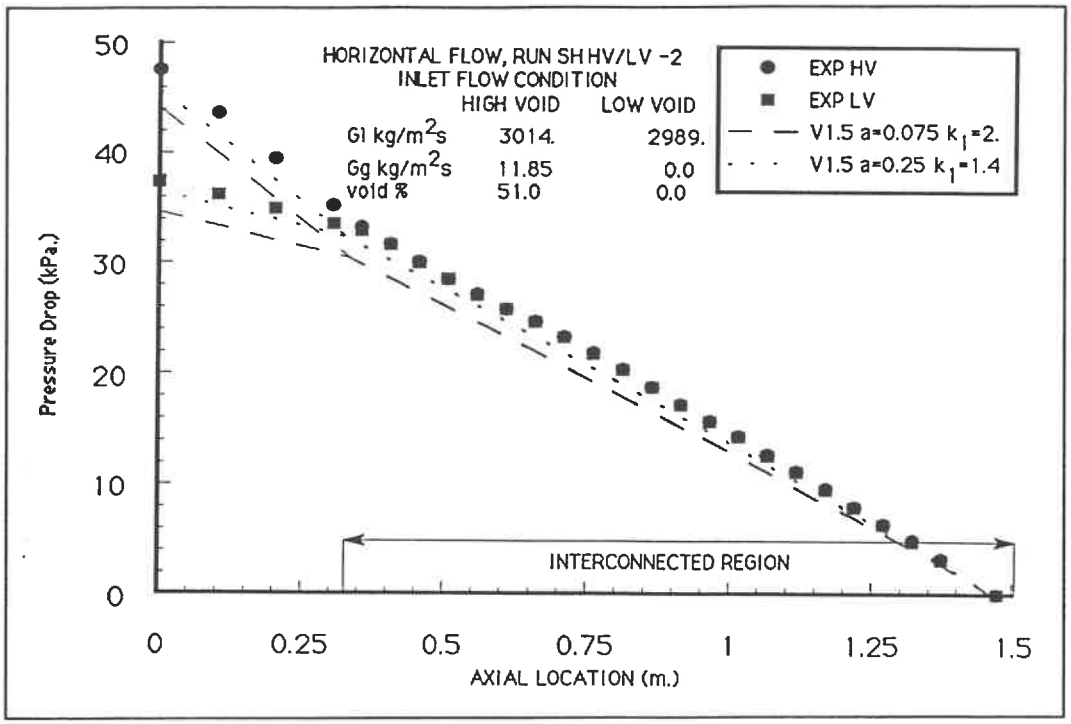

Figure 7.46: Pressure Drop $SH - \frac{HV}{LV} - 2$ ASSERT-4 Version 1.5

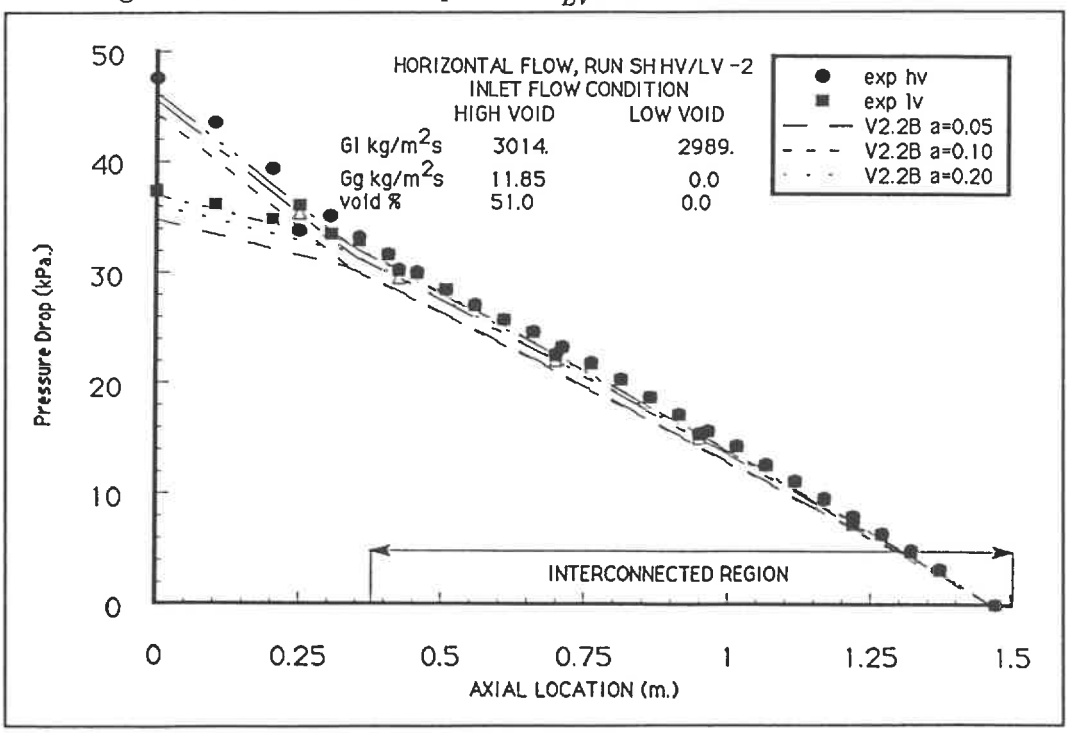

Figure 7.47: Pressure Drop $SH - \frac{HV}{LV} - 2$ ASSERT-4 Version 2.2B

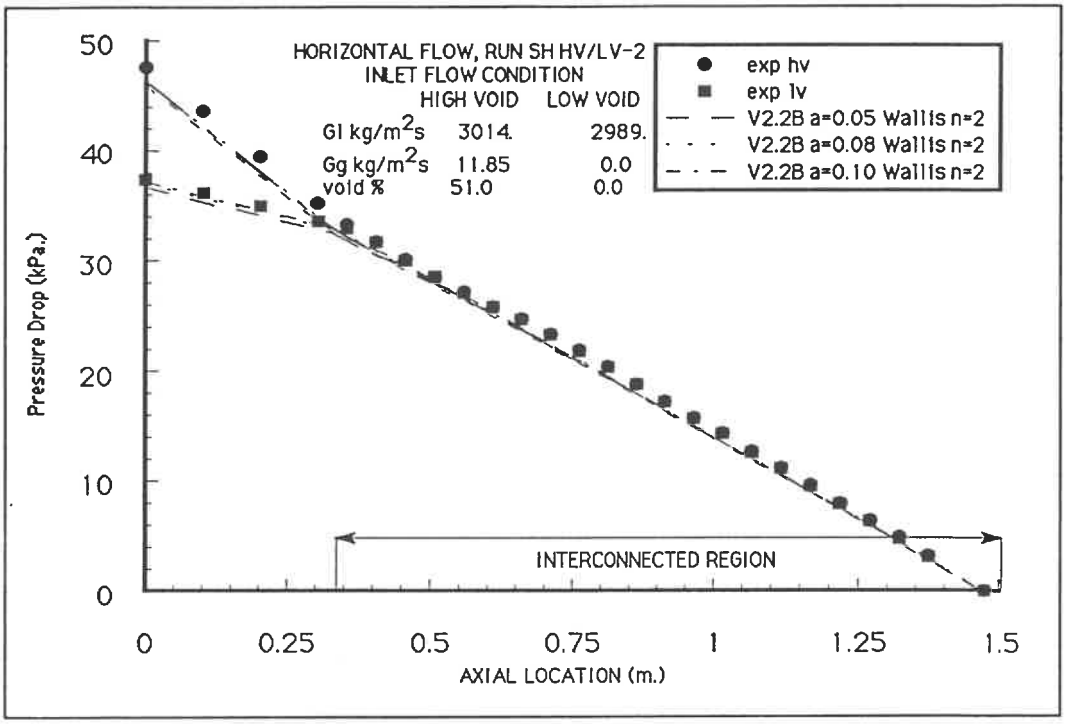

Figure 7.48: Pressure Drop $SH - \frac{HV}{LV} - 2$ ASSERT-4 Version 2.2B Wallis n=2

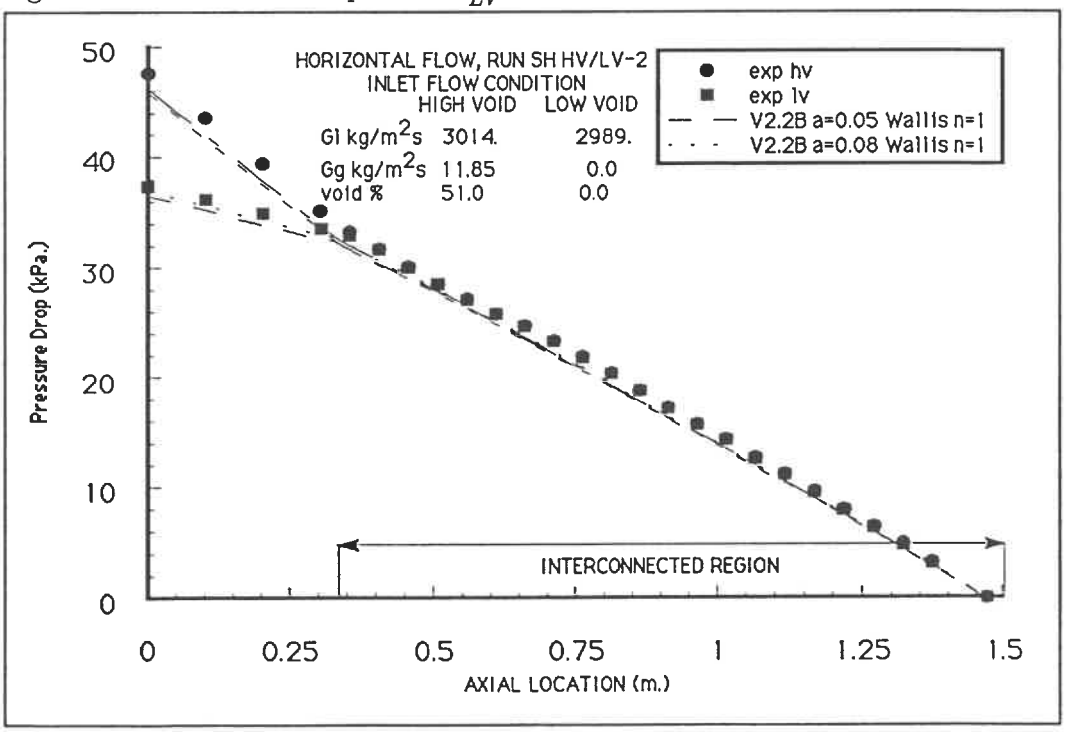

Figure 7.49: Pressure Drop $SH - \frac{HV}{LV} - 2$ ASSERT-4 Version 2.2B Wallis n=1

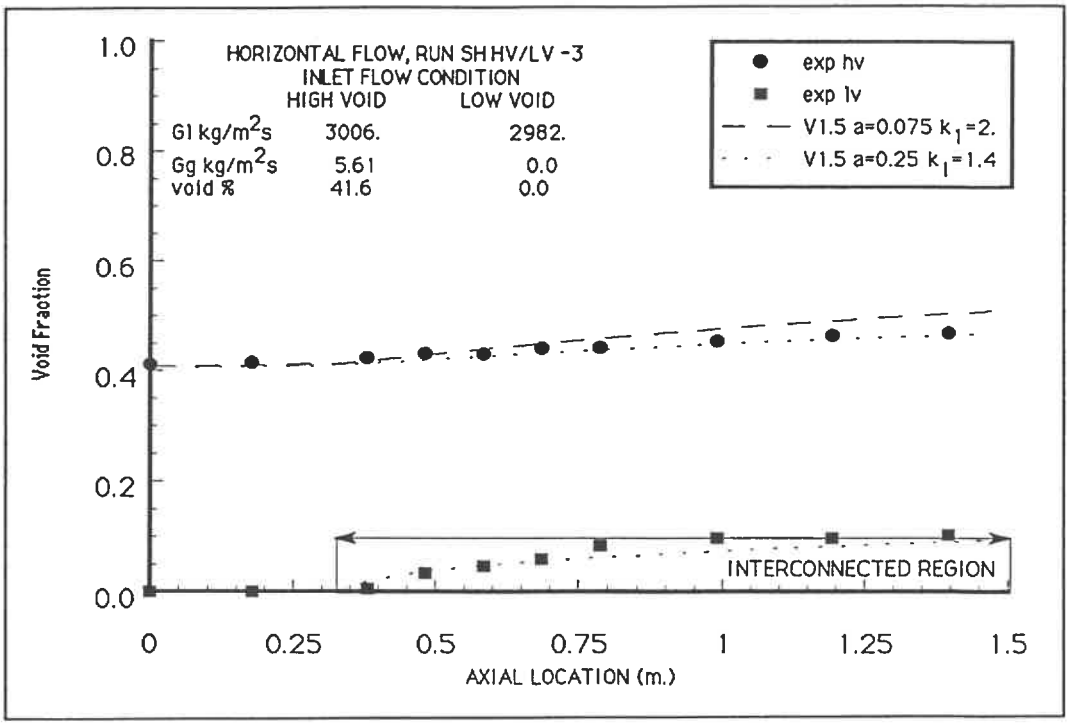

Figure 7.50: Void Fraction $SH - \frac{HV}{LV} - 3$ ASSERT-4 Version 1.5

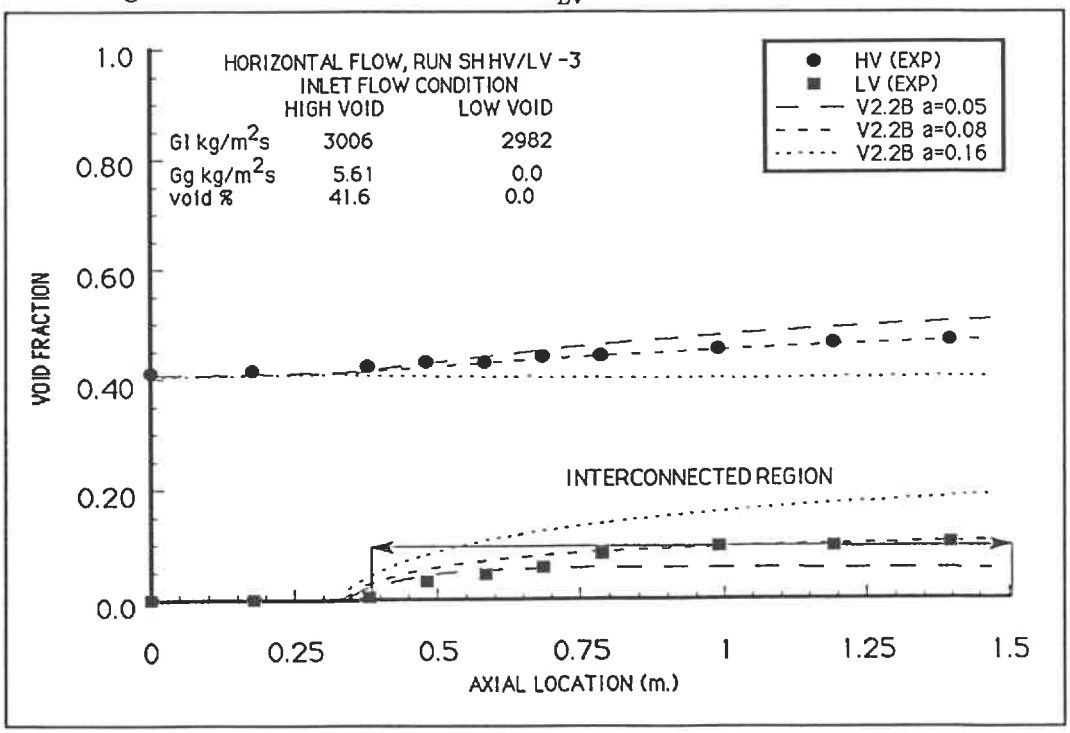

Figure 7.51: Void Fraction $SH - \frac{HV}{LV} - 3$ ASSERT-4 Version 2.2B

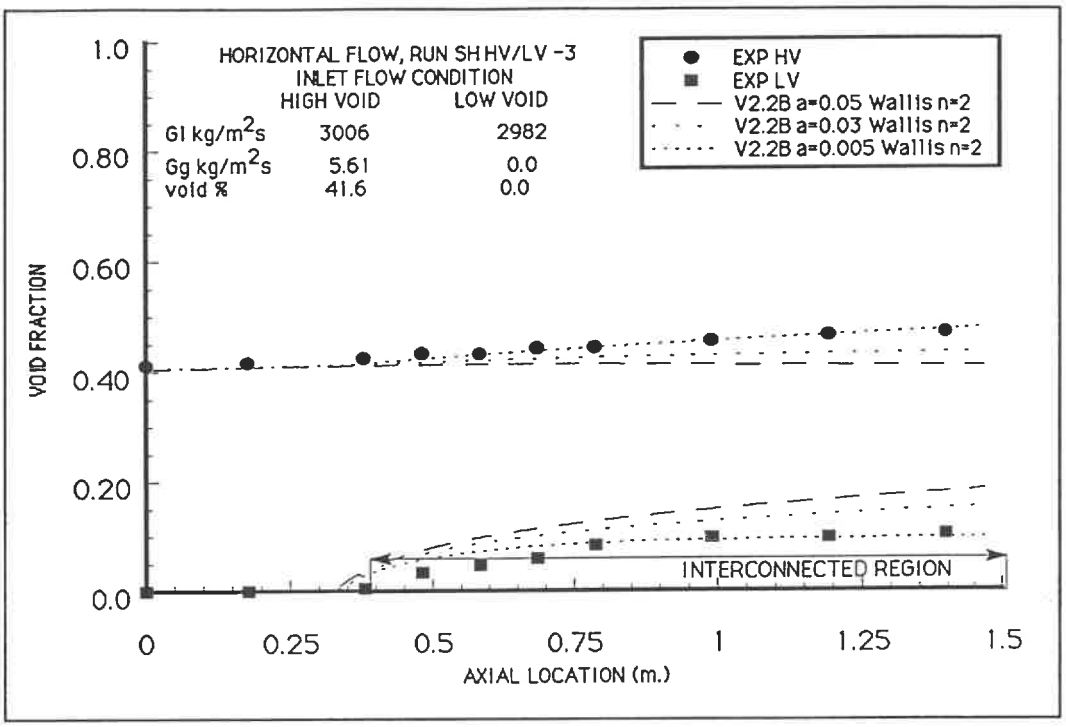

Figure 7.52: Void Fraction $SH - \frac{HV}{LV} - 3$ ASSERT-4 Version 2.2B Wallis n=2

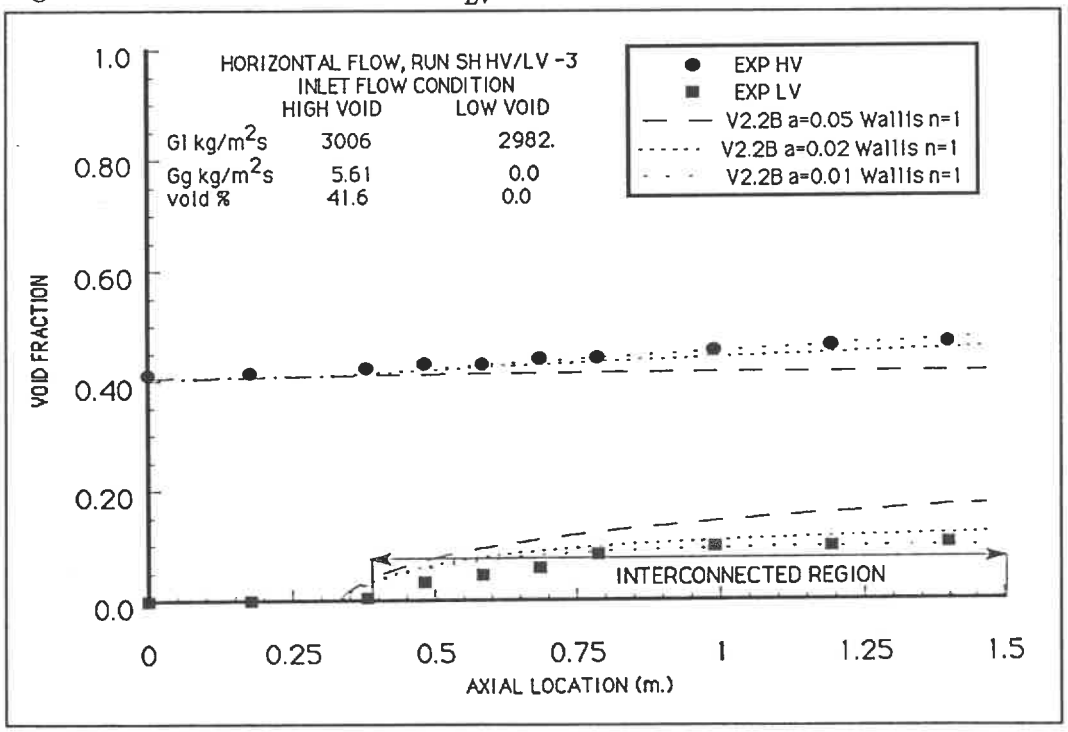

Figure 7.53: Void Fraction $SH - \frac{HV}{LV} - 3$ ASSERT-4 Version 2.2B Wallis n=1

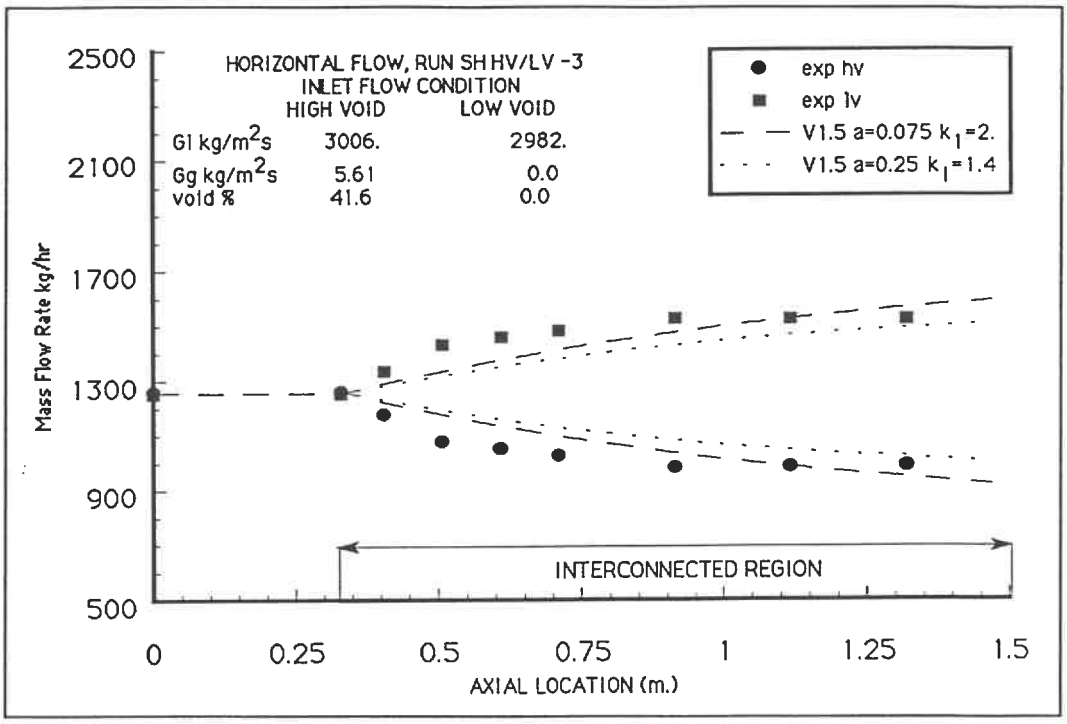

Figure 7.54: Mass Flow $SH - \frac{HV}{LV} - 3$ ASSERT–4 Version 1.5

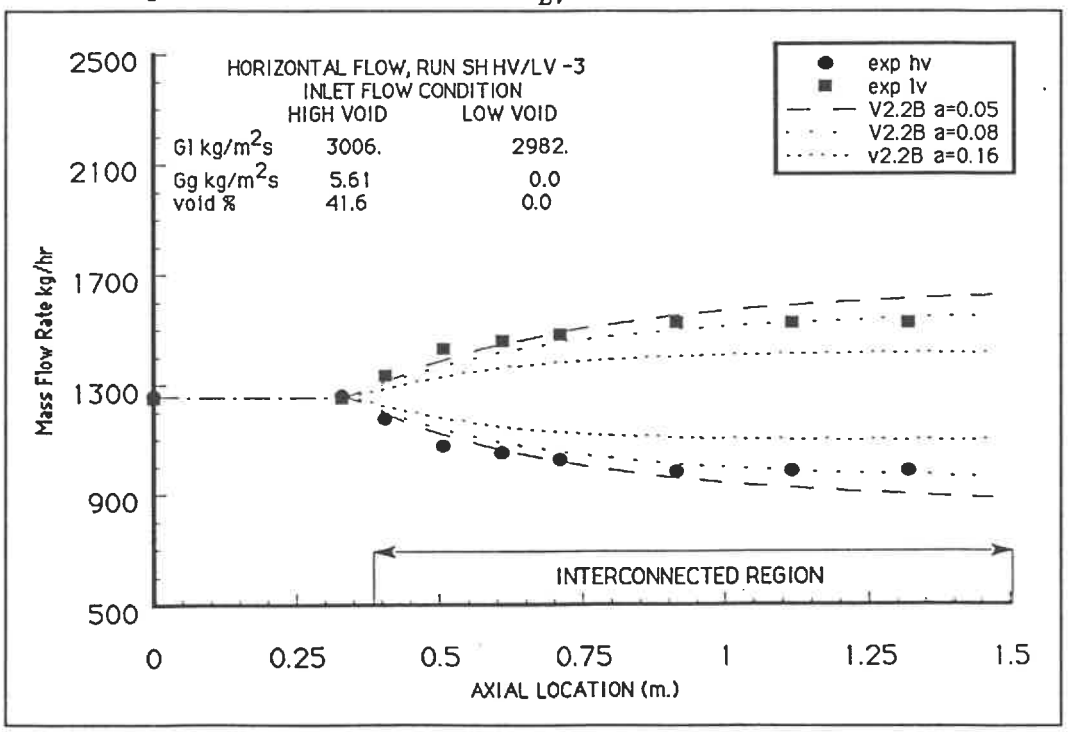

Figure 7.55: Mass Flow $SH - \frac{HV}{LV} - 3$ ASSERT–4 Version 2.2B

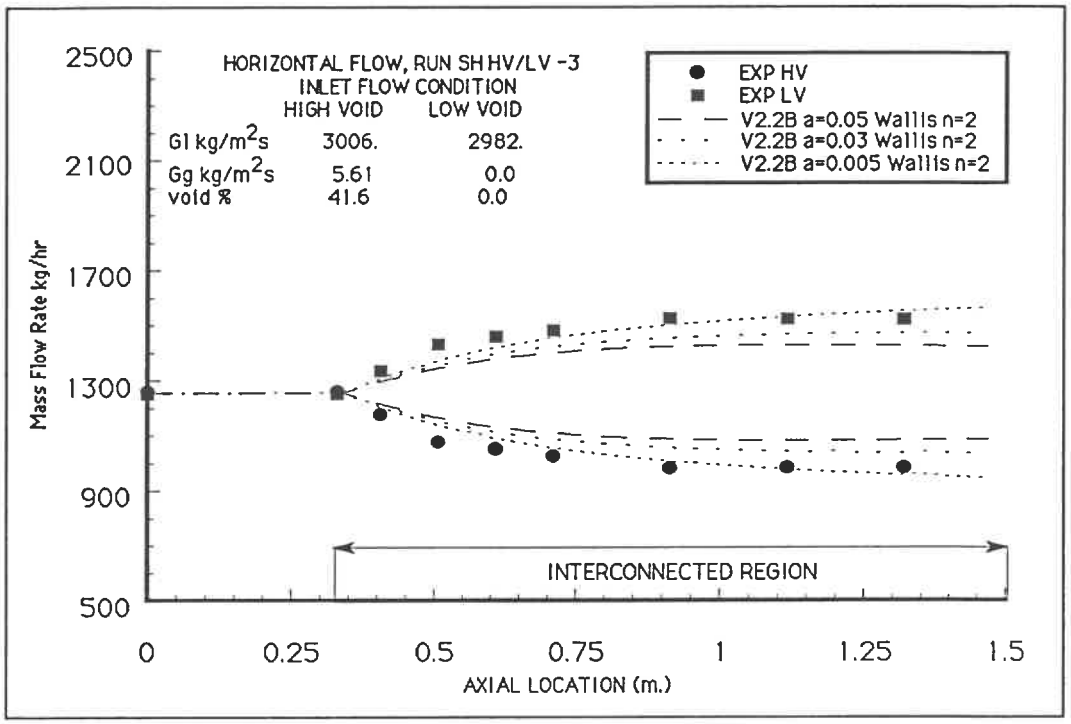

Figure 7.56: Mass Flow $SH - \frac{HV}{LV} - 3$ ASSERT-4 Version 2.2B Wallis n=2

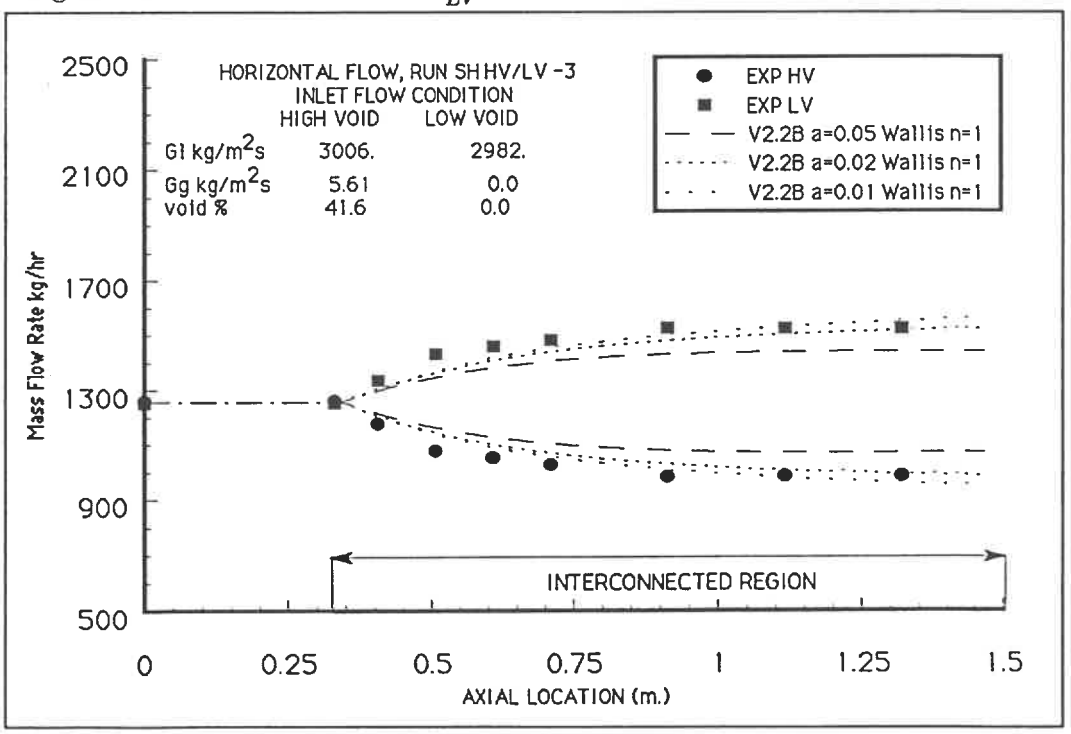

Figure 7.57: Mass Flow $SH - \frac{HV}{LV} - 3$ ASSERT-4 Version 2.2B Wallis n=1

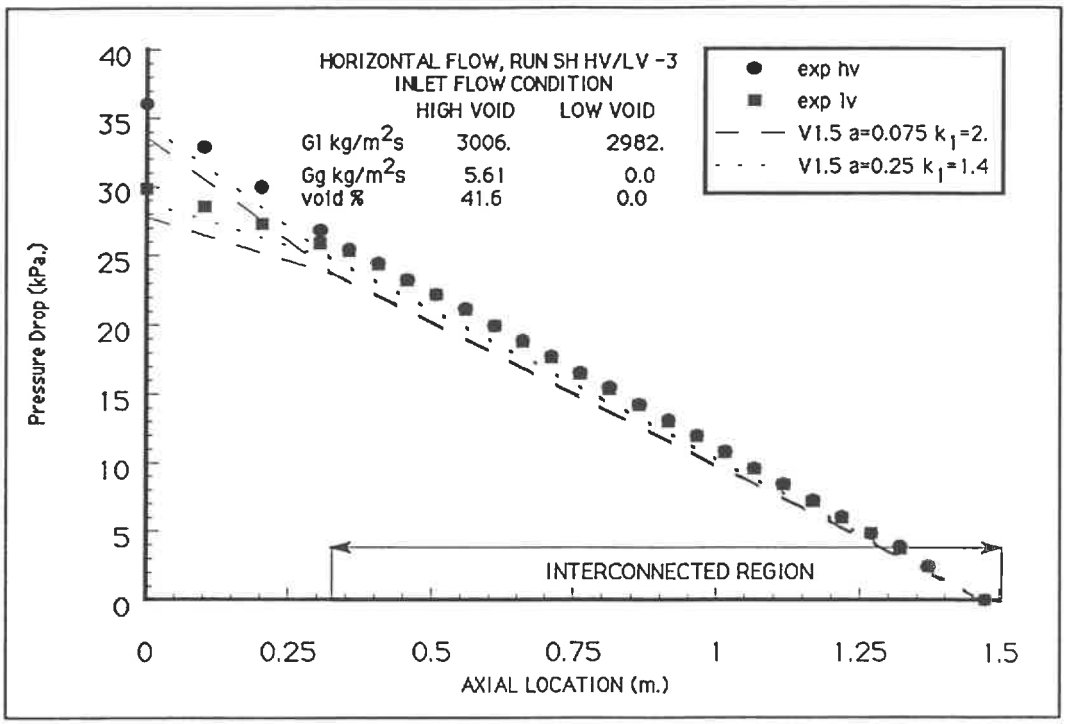

Figure 7.58: Pressure Drop $SH - \frac{HV}{LV} - 3$ ASSERT–4 Version 1.5

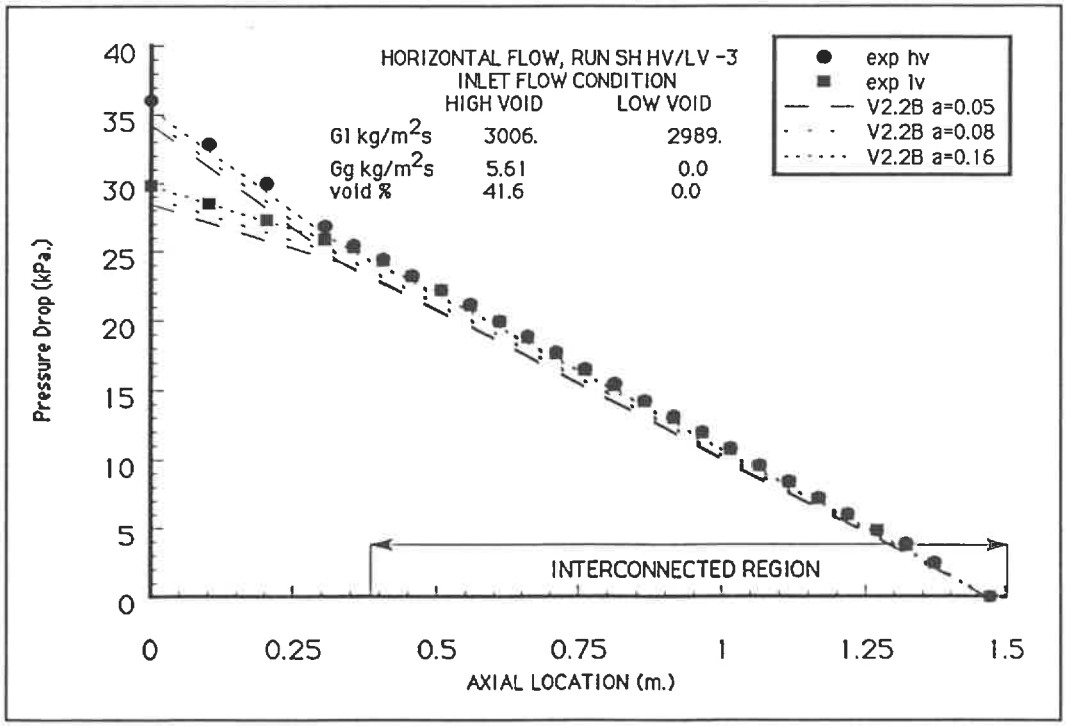

Figure 7.59: Pressure Drop $SH - \frac{HV}{LV} - 3$ ASSERT–4 Version 2.2B

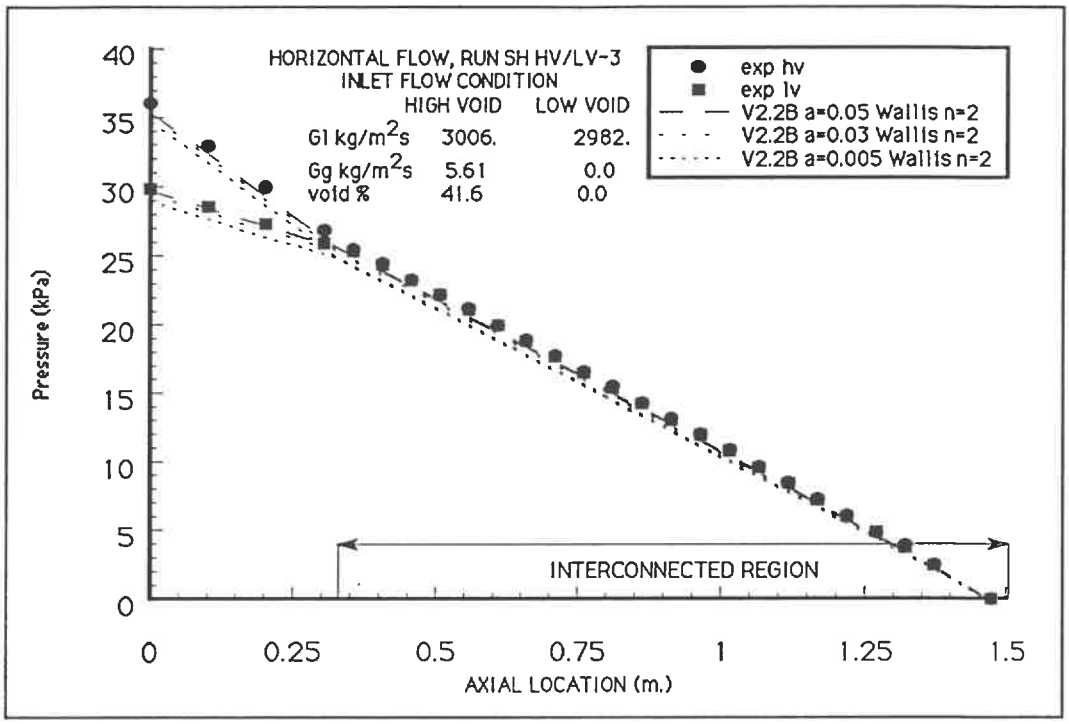

Figure 7.60: Pressure Drop $SH - \frac{HV}{LV} - 3$ ASSERT-4 Version 2.2B Wallis n=2

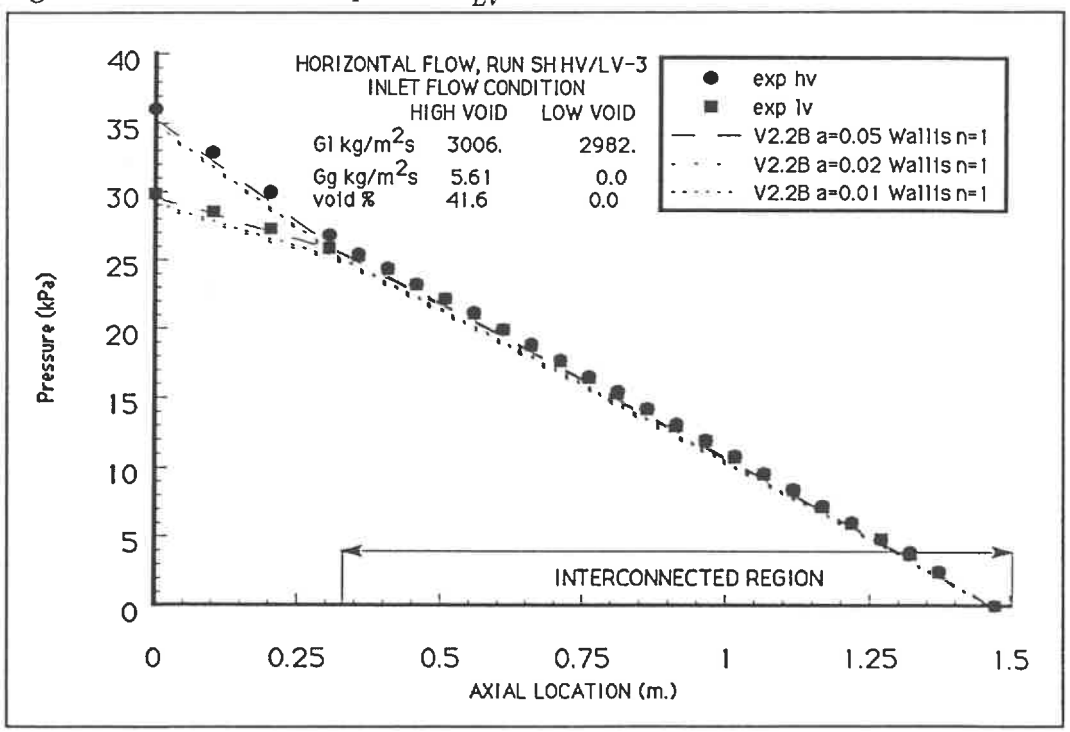

Figure 7.61: Pressure Drop $SH - \frac{HV}{LV} - 3$ ASSERT-4 Version 2.2B Wallis n=1

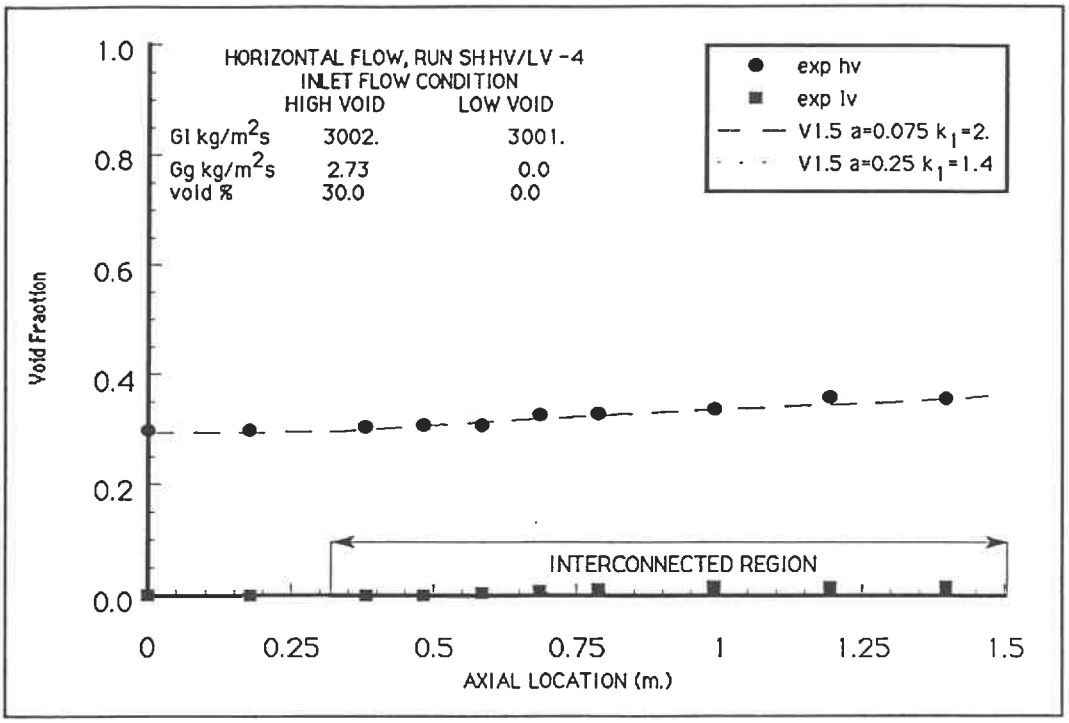

Figure 7.62: Void Fraction $SH - \frac{HV}{LV} - 4$ ASSERT-4 Version 1.5

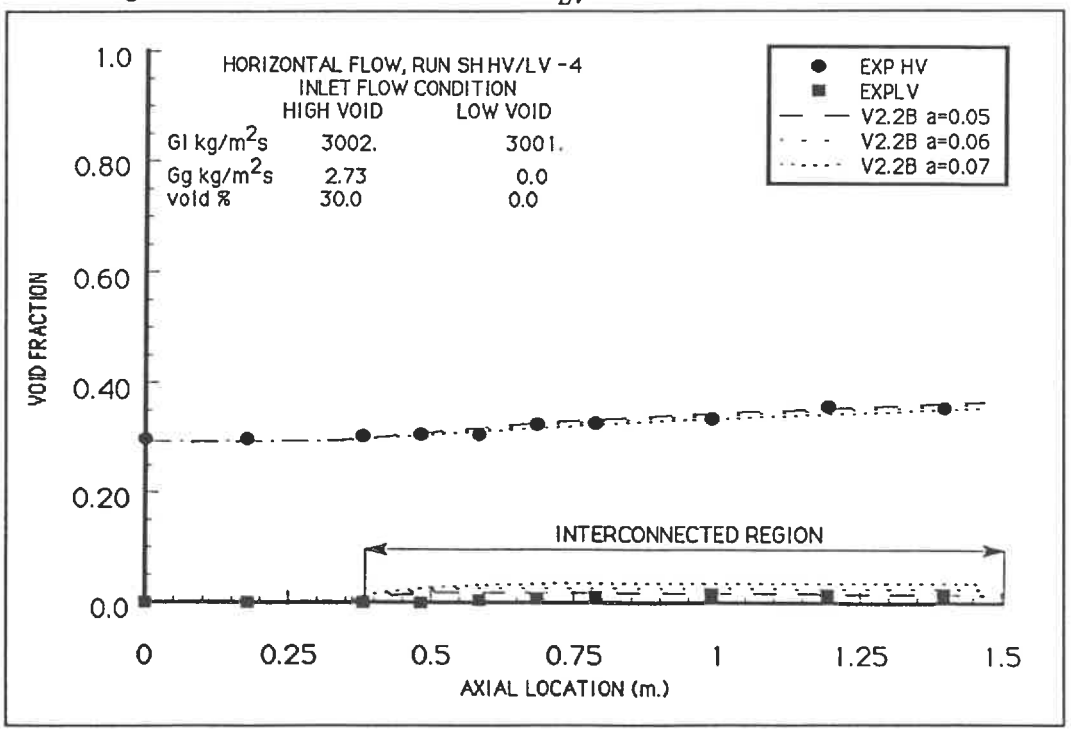

Figure 7.63: Void Fraction $SH - \frac{HV}{LV} - 4$ ASSERT-4 Version 2.2B

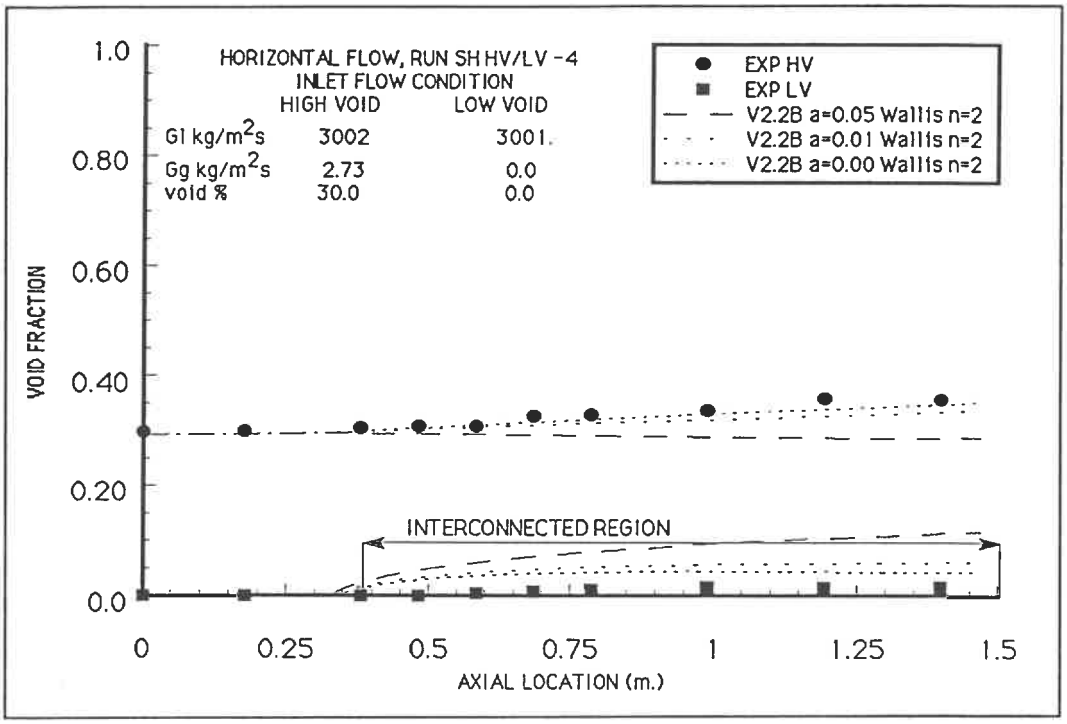

Figure 7.64: Void Fraction $SH - \frac{HV}{LV} - 4$ ASSERT-4 Version 2.2B Wallis n=2

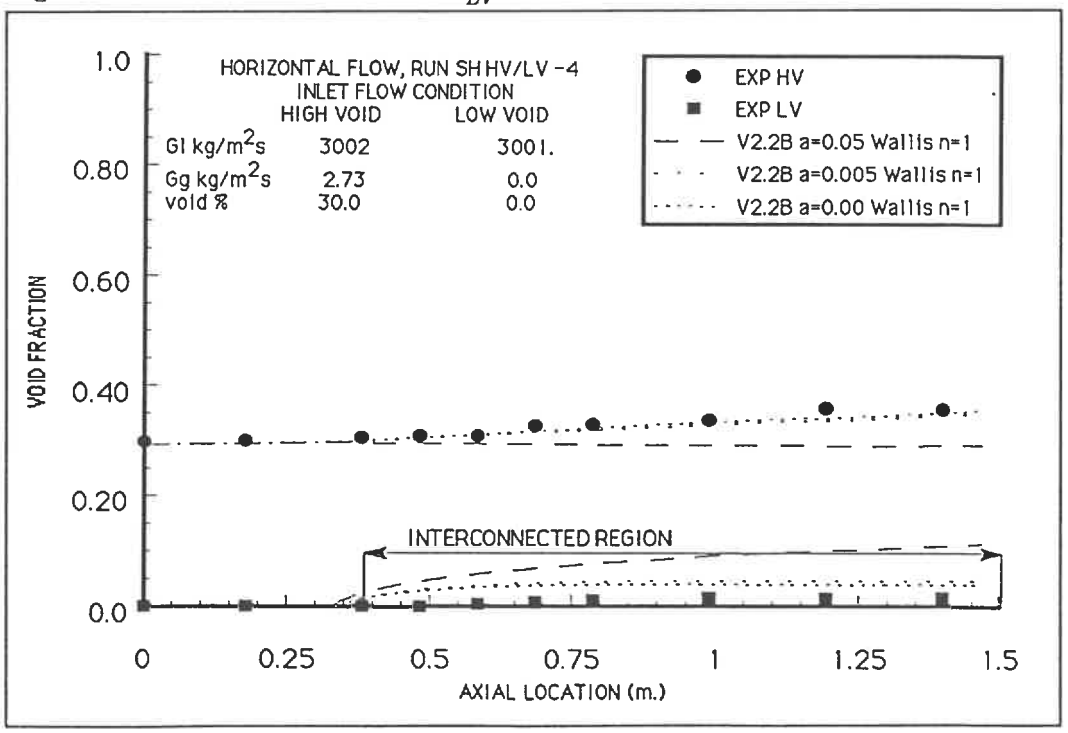

Figure 7.65: Void Fraction $SH - \frac{HV}{LV} - 4$ ASSERT-4 Version 2.2B Wallis n=1

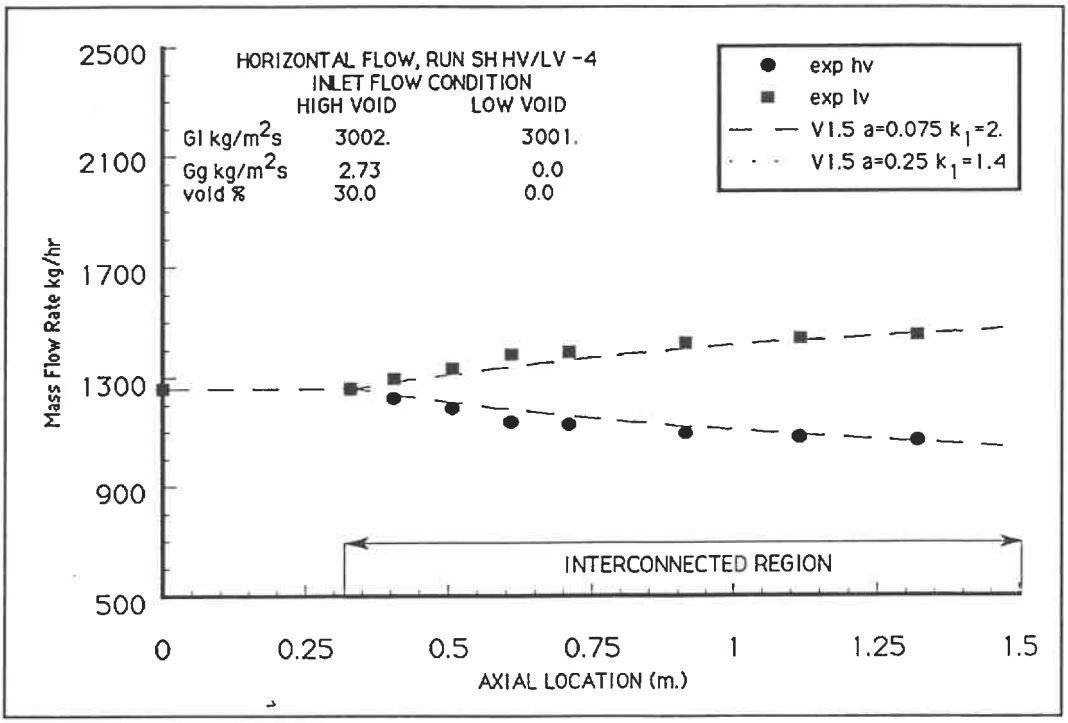

Figure 7.66: Mass Flow $SH - \frac{HV}{LV} - 4$ ASSERT-4 Version 1.5

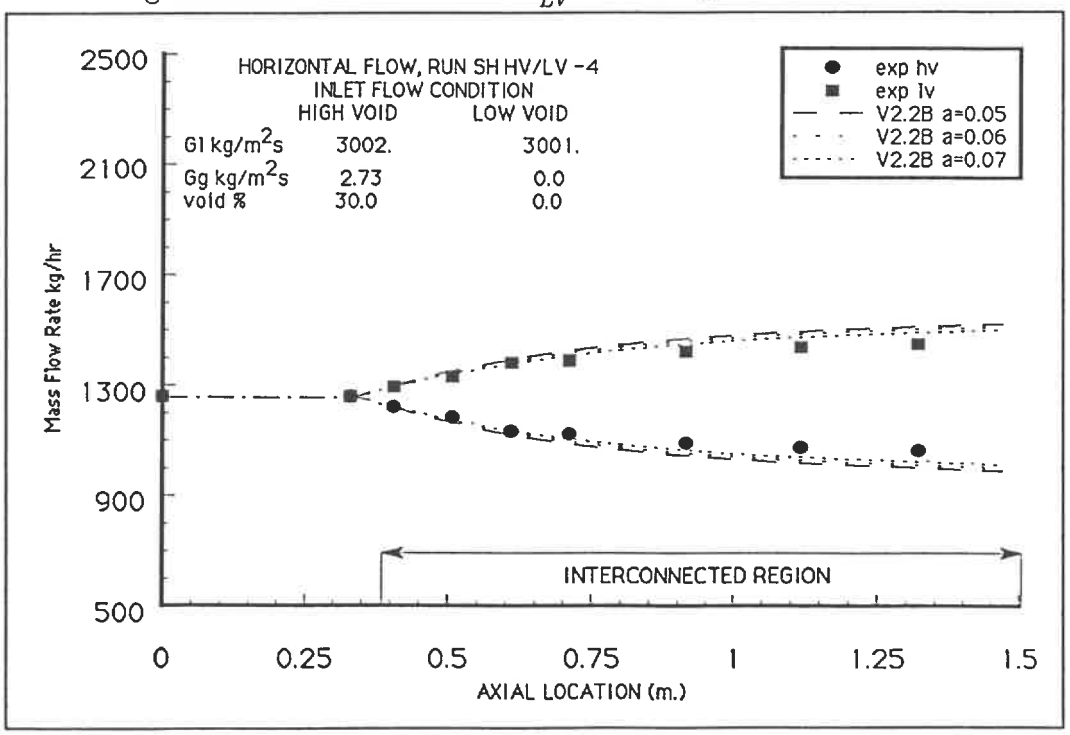

Figure 7.67: Mass Flow $SH - \frac{HV}{LV} - 4$ ASSERT-4 Version 2.2B

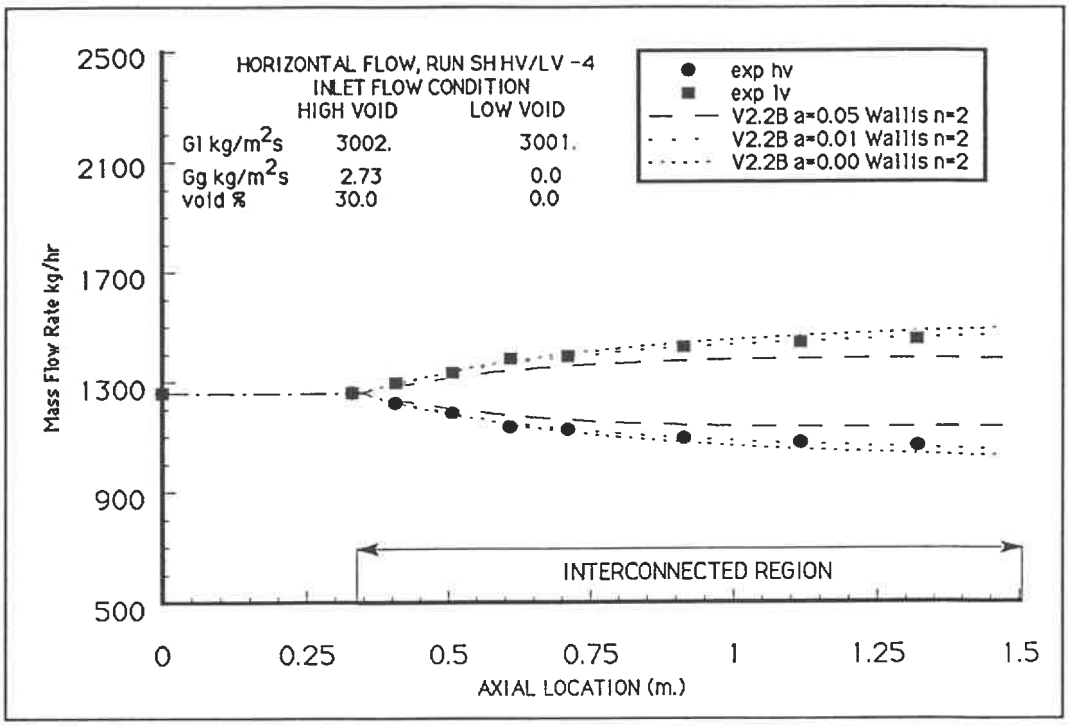

Figure 7.68: Mass Flow $SH - \frac{HV}{LV} - 4$ ASSERT-4 Version 2.2B Wallis n=2

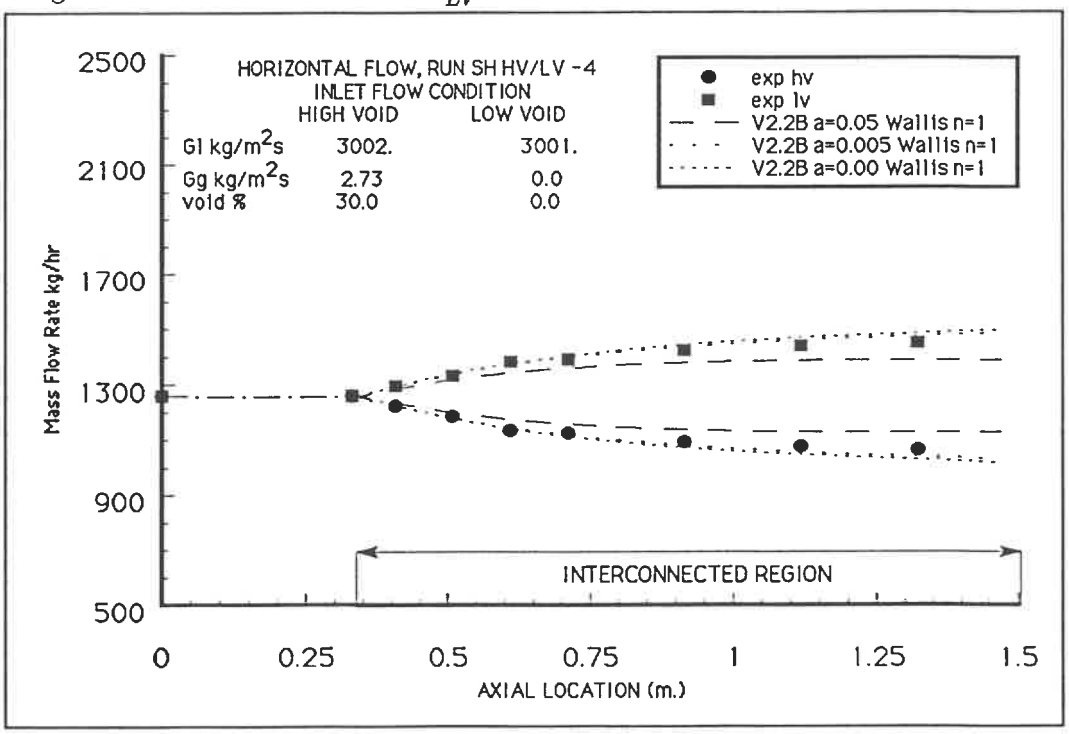

Figure 7.69: Mass Flow $SH - \frac{HV}{LV} - 4$ ASSERT-4 Version 2.2B Wallis n=1

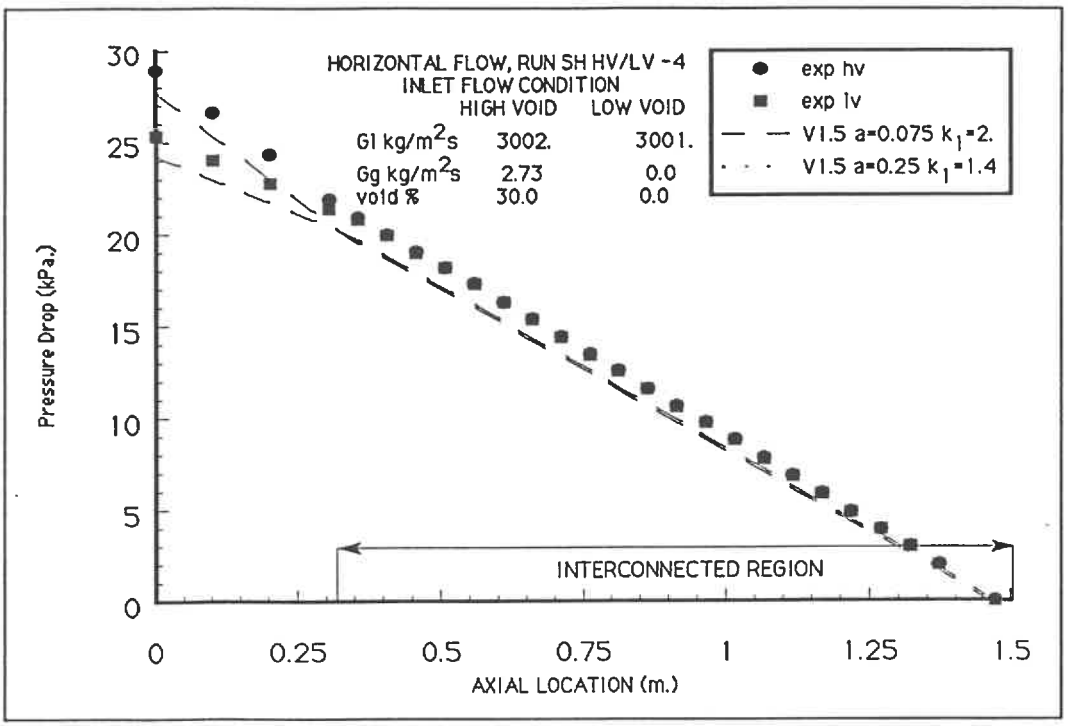

Figure 7.70: Pressure Drop $SH - \frac{HV}{LV} - 4$ ASSERT-4 Version 1.5

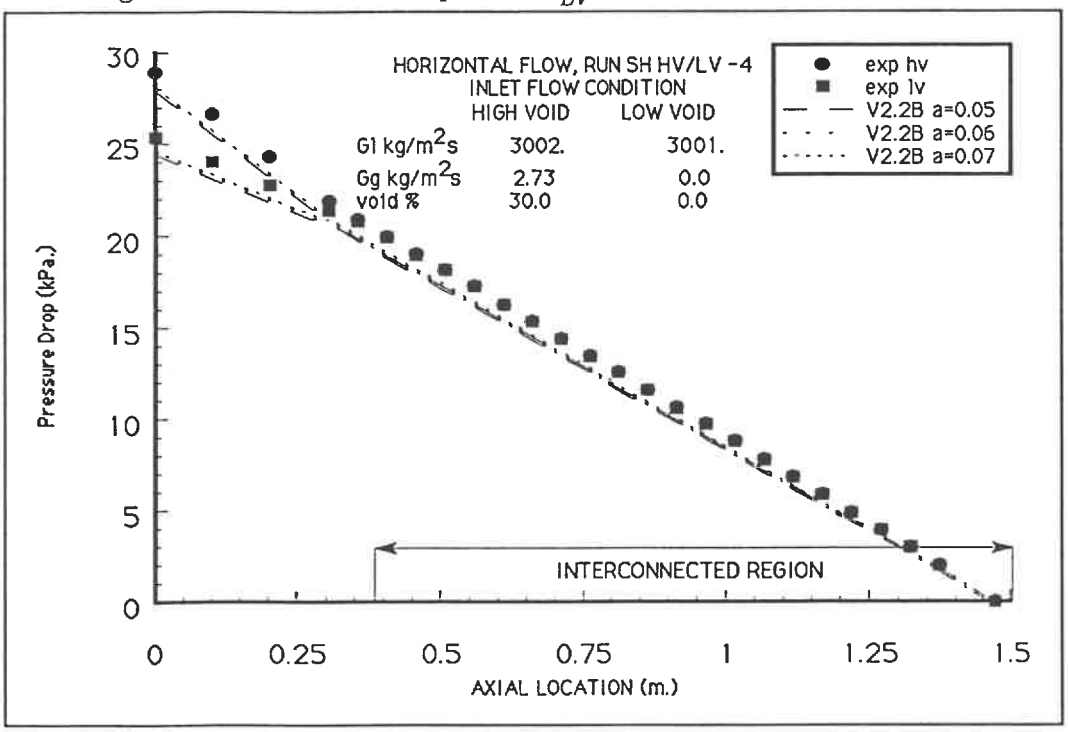

Figure 7.71: Pressure Drop $SH - \frac{HV}{LV} - 4$ ASSERT-4 Version 2.2B

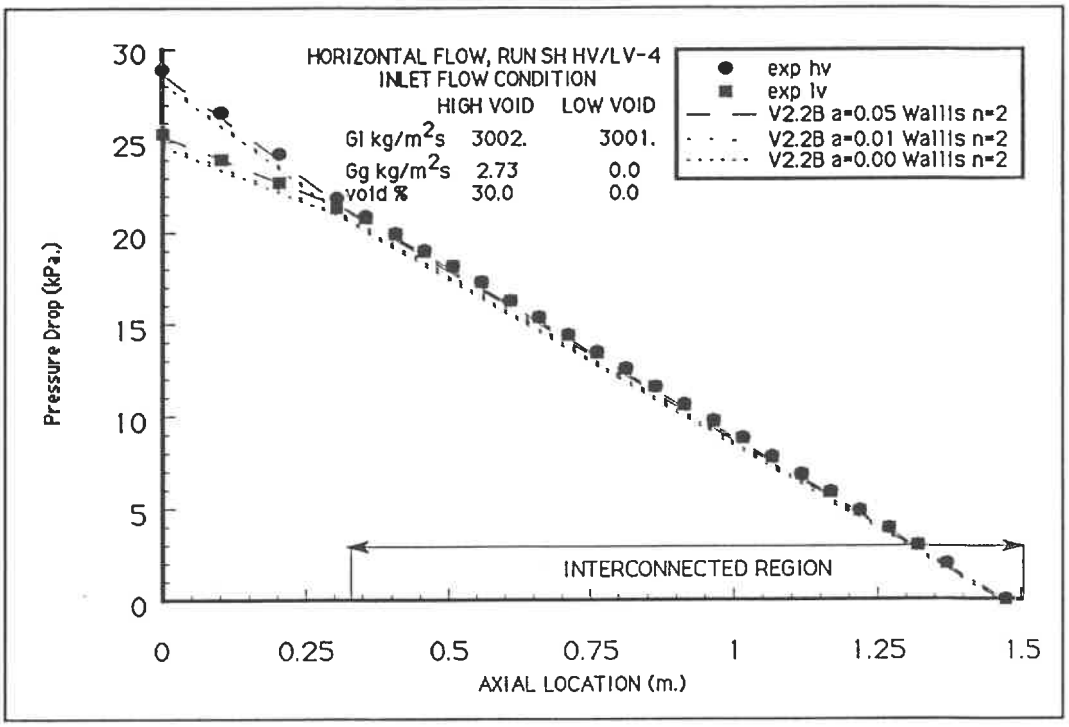

Figure 7.72: Pressure Drop $SH - \frac{HV}{LV} - 4$ ASSERT–4 Version 2.2B Wallis n=2

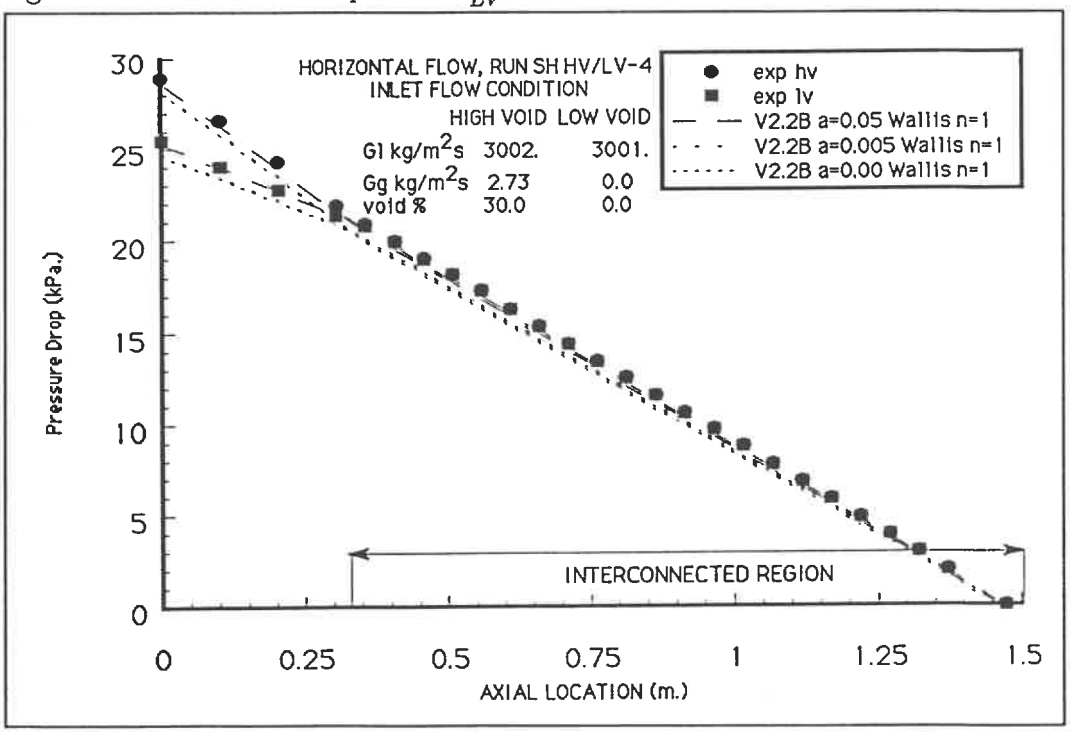

Figure 7.73: Pressure Drop $SH - \frac{HV}{LV} - 4$ ASSERT–4 Version 2.2B Wallis n=1

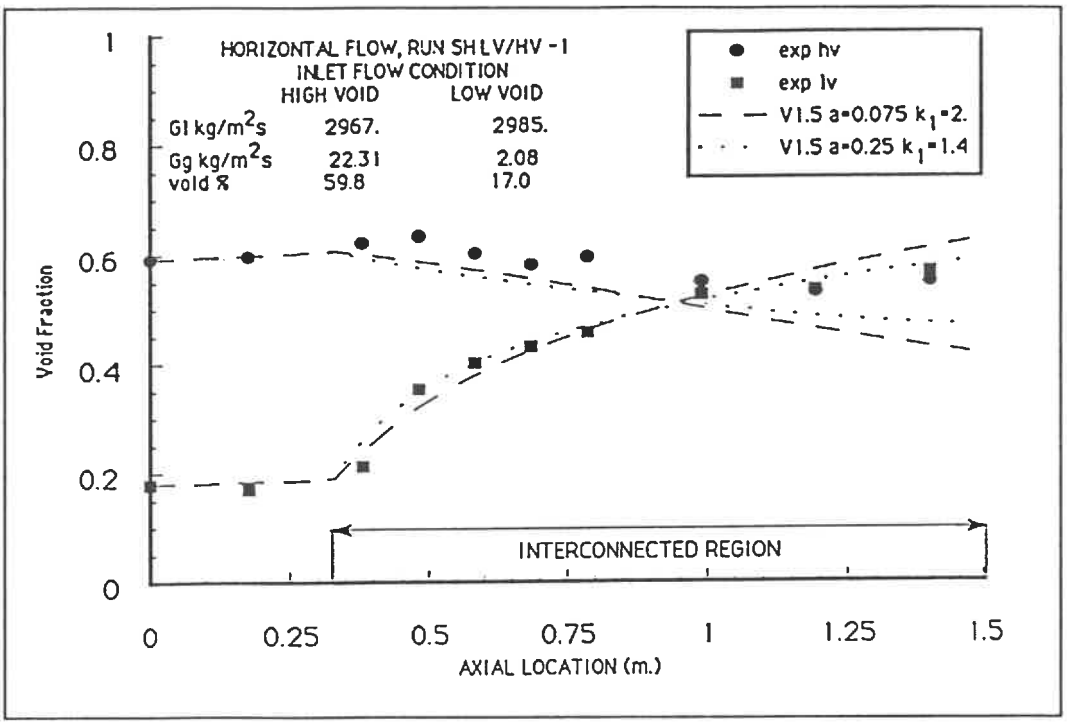

Figure 7.74: Void Fraction $SH - \frac{LV}{HV} - 1$ ASSERT–4 Version 1.5

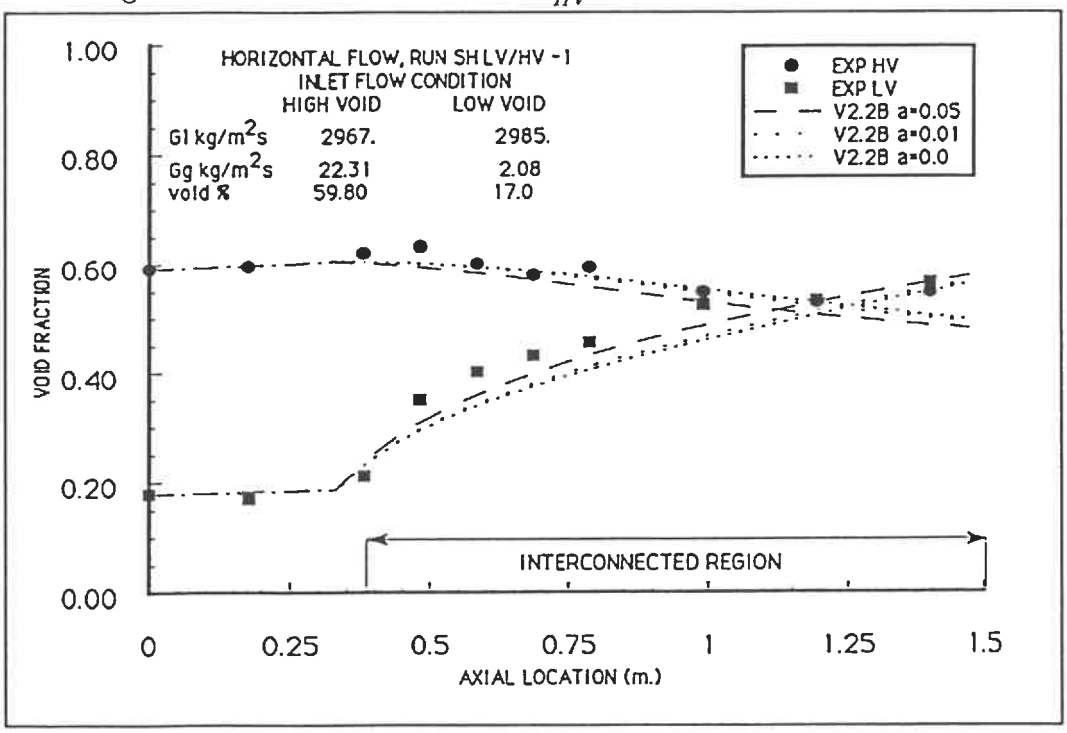

Figure 7.75: Void Fraction $SH - \frac{LV}{HV} - 1$ ASSERT–4 Version 2.2B

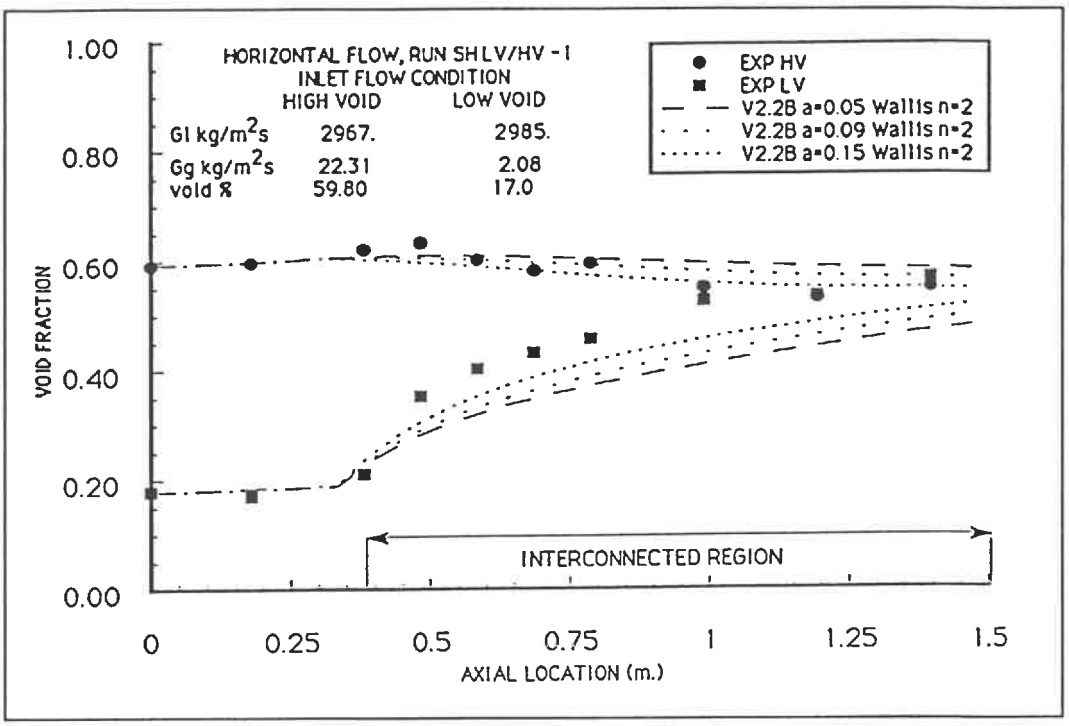

Figure 7.76: Void Fraction $SH - \frac{LV}{HV} - 1$ ASSERT–4 Version 2.2B Wallis n=2

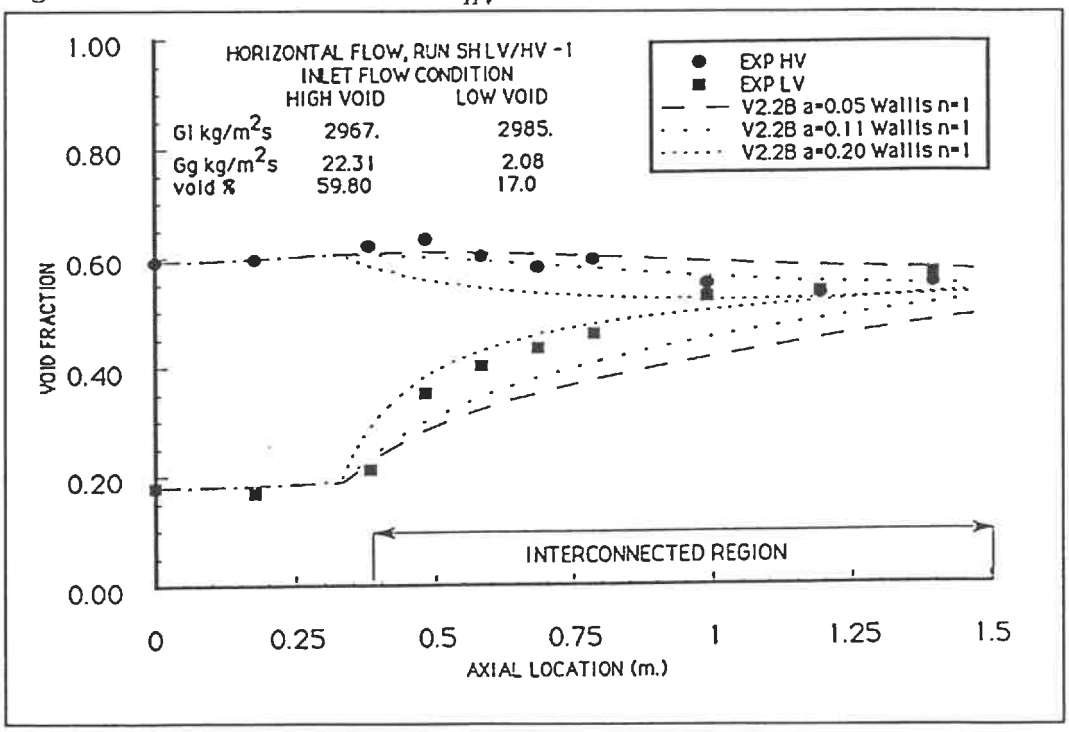

Figure 7.77: Void Fraction $SH - \frac{LV}{HV} - 1$ ASSERT–4 Version 2.2B Wallis n=1

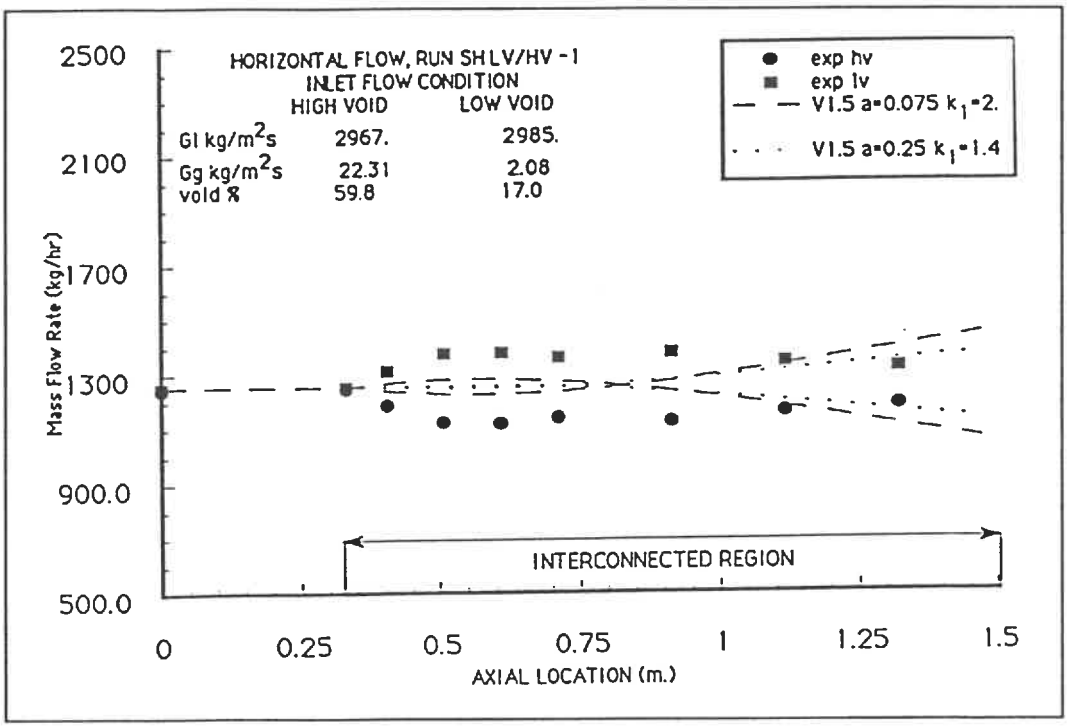

Figure 7.78: Mass Flow $SH - \frac{LV}{HV} - 1$ ASSERT-4 Version 1.5

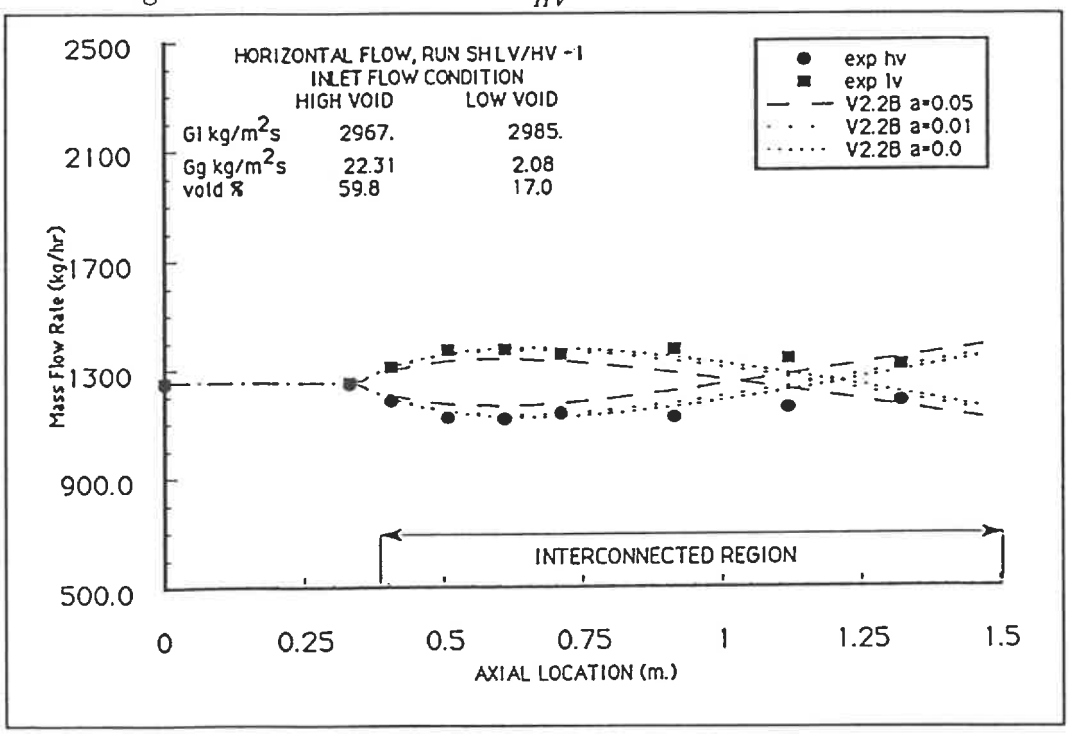

Figure 7.79: Mass Flow $SH - \frac{LV}{HV} - 1$ ASSERT-4 Version 2.2B

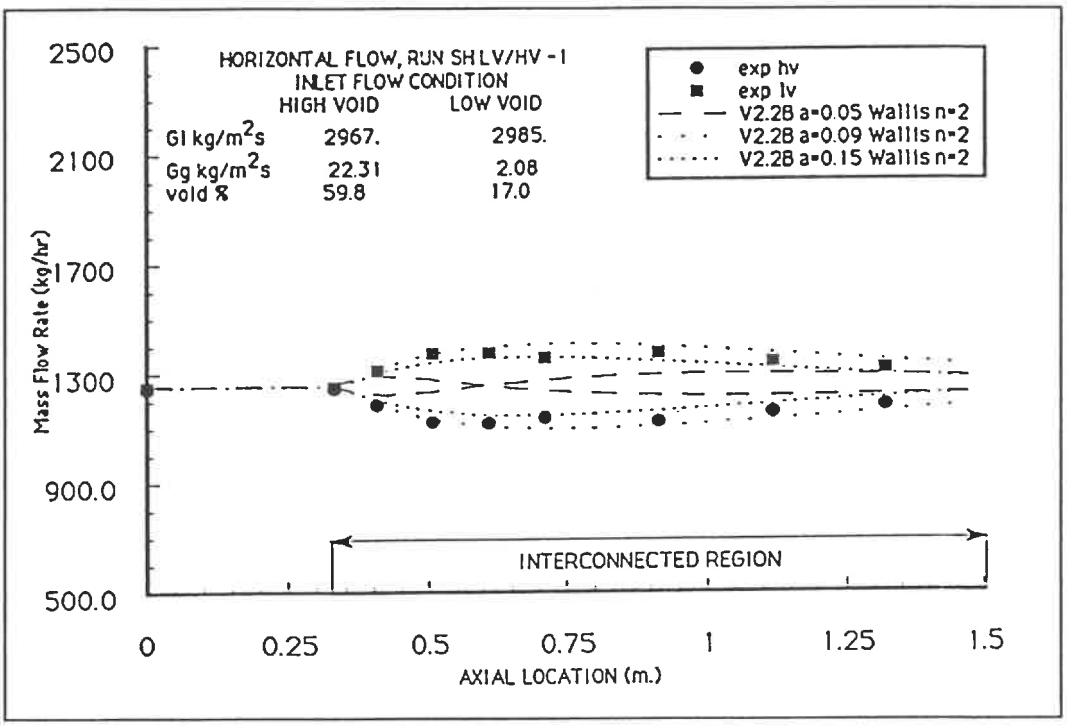

Figure 7.80: Mass Flow $SH - \frac{LV}{HV} - 1$ ASSERT-4 Version 2.2B Wallis n=2

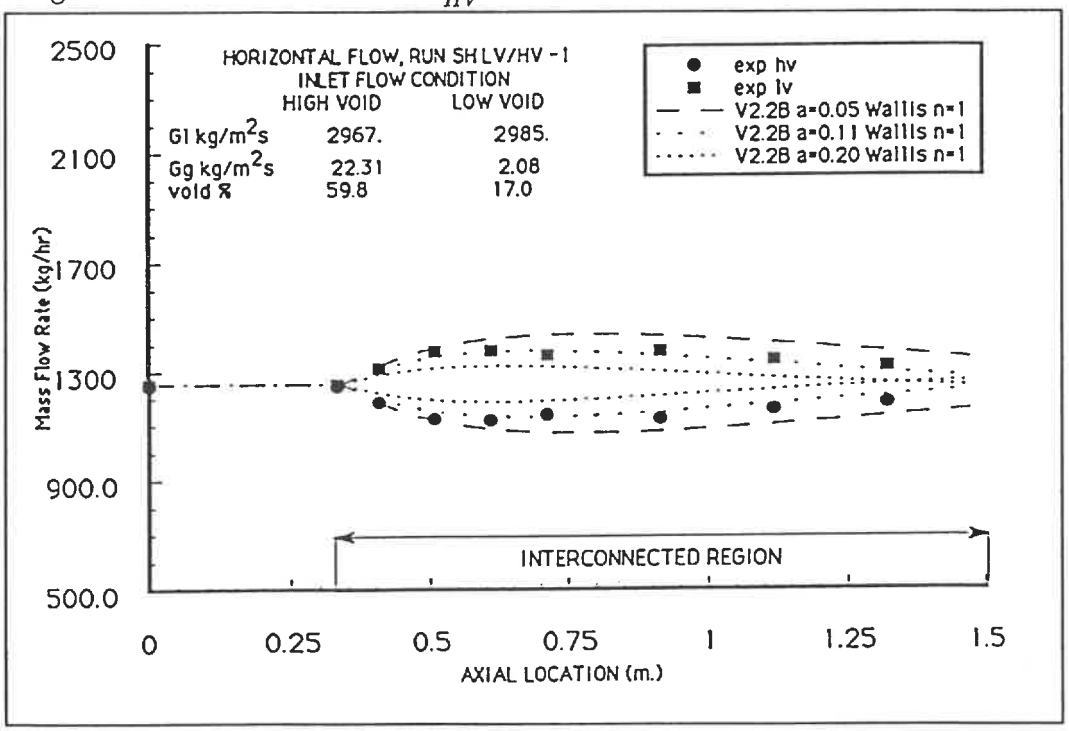

Figure 7.81: Mass Flow $SH - \frac{LV}{HV} - 1$ ASSERT-4 Version 2.2B Wallis n=1

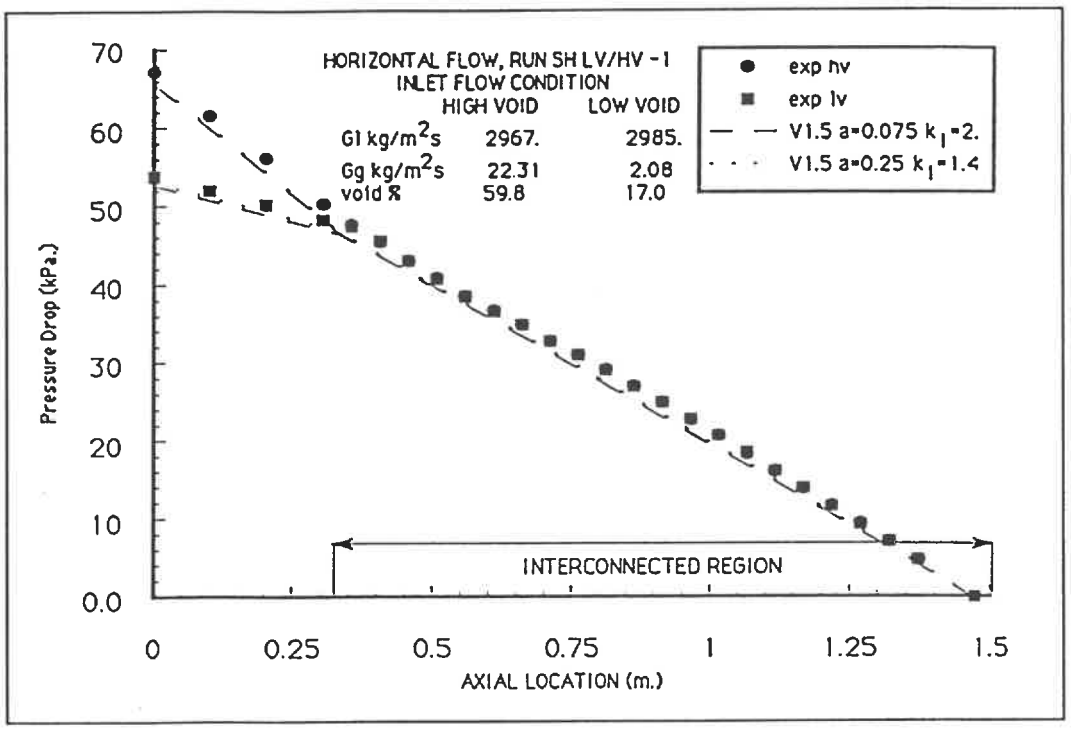

Figure 7.82: Pressure Drop $SH - \frac{LV}{HV} - 1$ ASSERT-4 Version 1.5

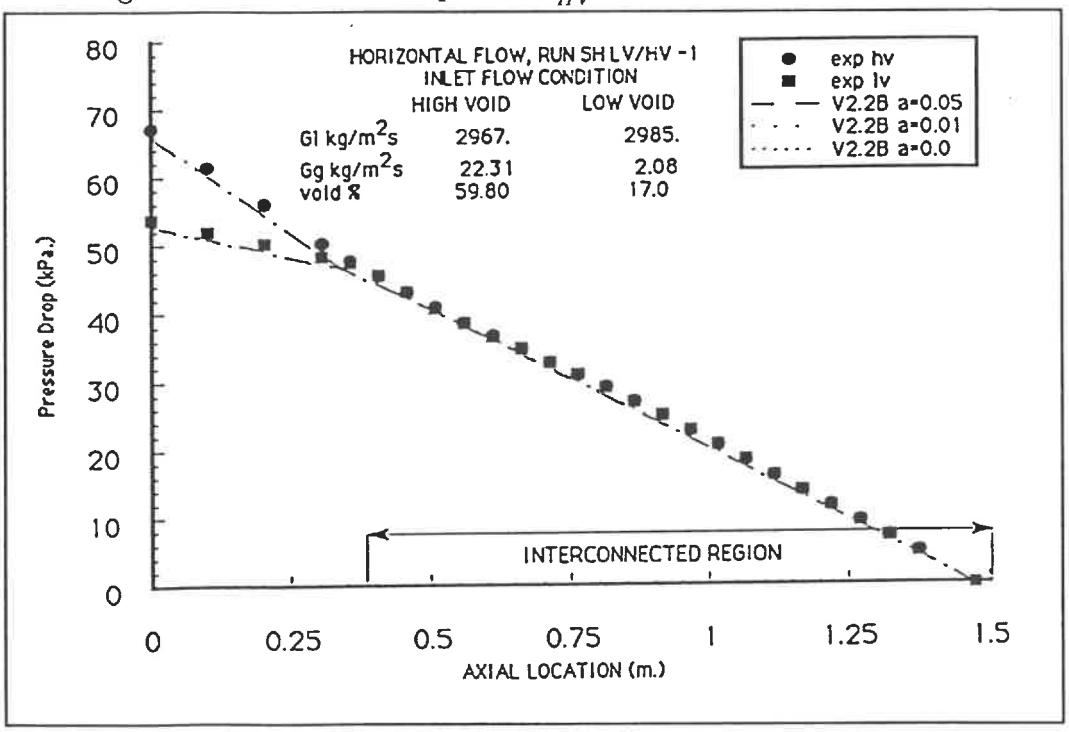

Figure 7.83: Pressure Drop $SH - \frac{LV}{HV} - 1$ ASSERT-4 Version 2.2B

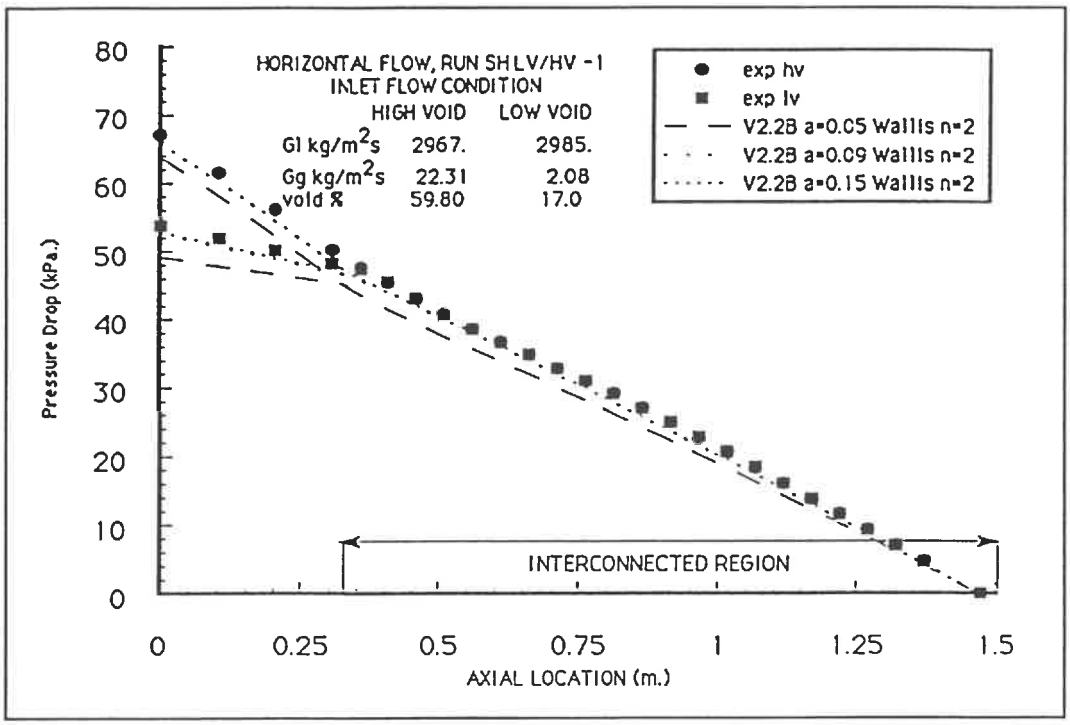

Figure 7.84: Pressure Drop $SH - \frac{LV}{HV} - 1$ ASSERT–4 Version 2.2B Wallis n=2

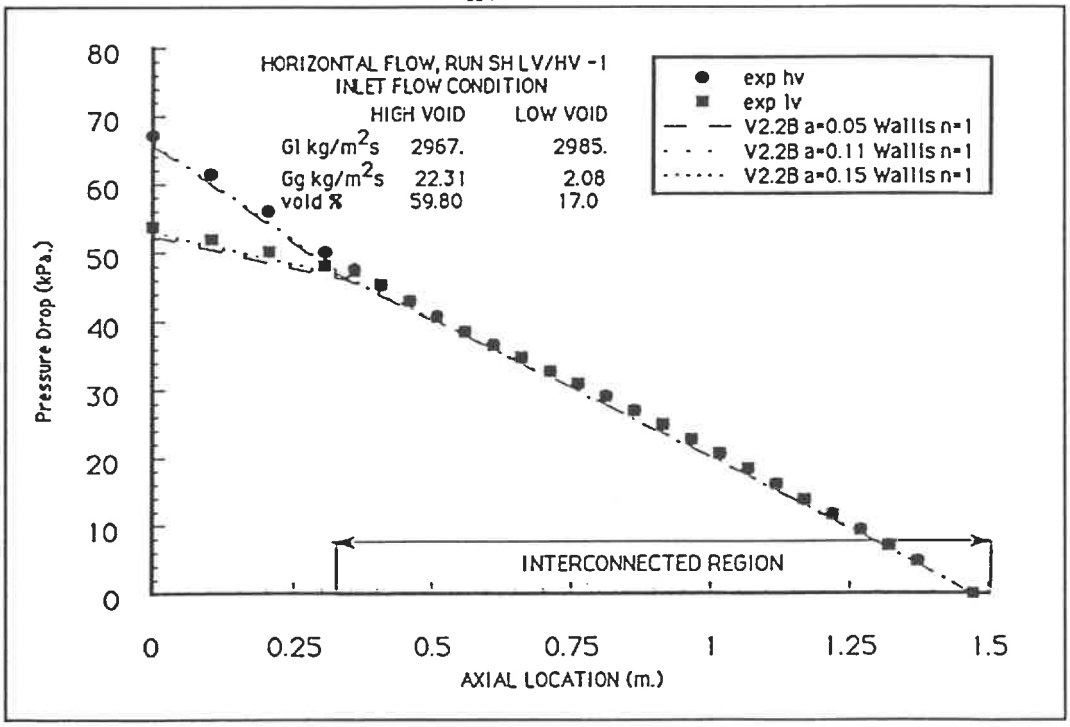

Figure 7.85: Pressure Drop $SH - \frac{LV}{HV} - 1$ ASSERT–4 Version 2.2B Wallis n=1

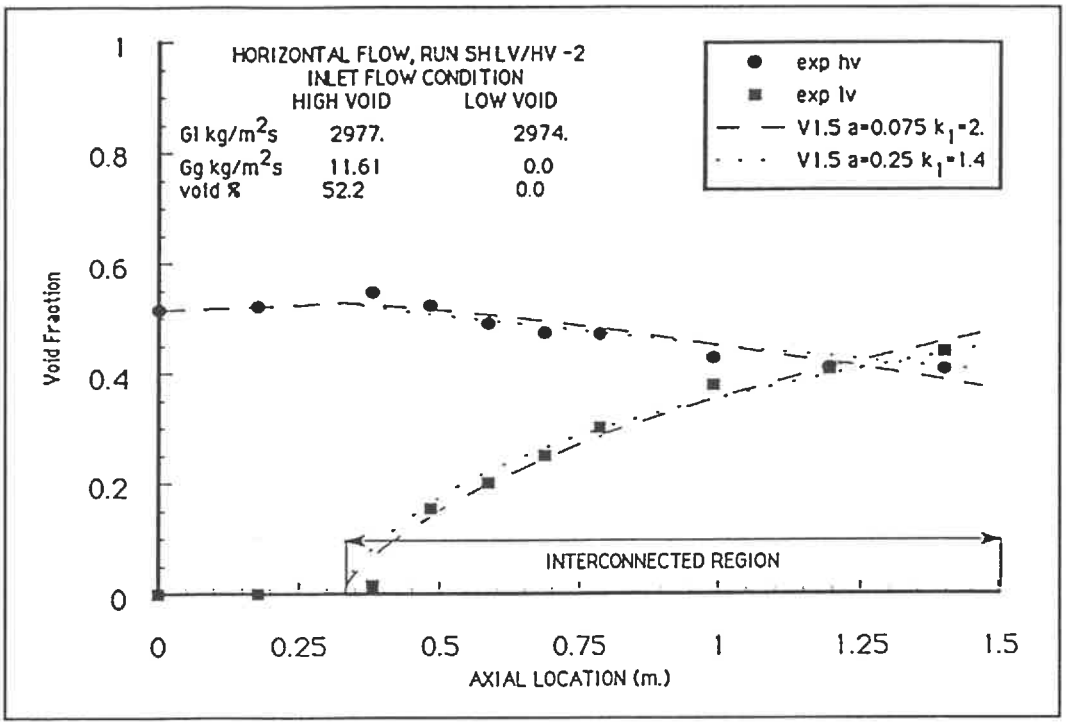

Figure 7.86: Void Fraction $SH - \frac{LV}{HV} - 2$ ASSERT-4 Version 1.5

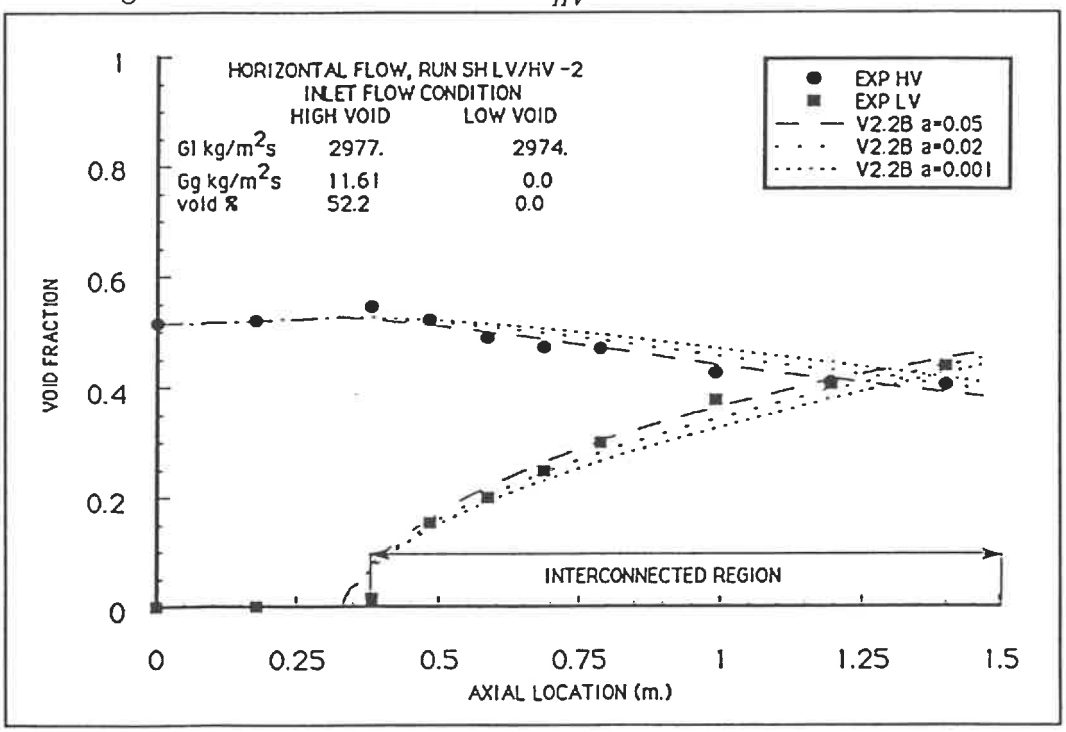

Figure 7.87: Void Fraction $SH - \frac{LV}{HV} - 2$ ASSERT-4 Version 2.2B

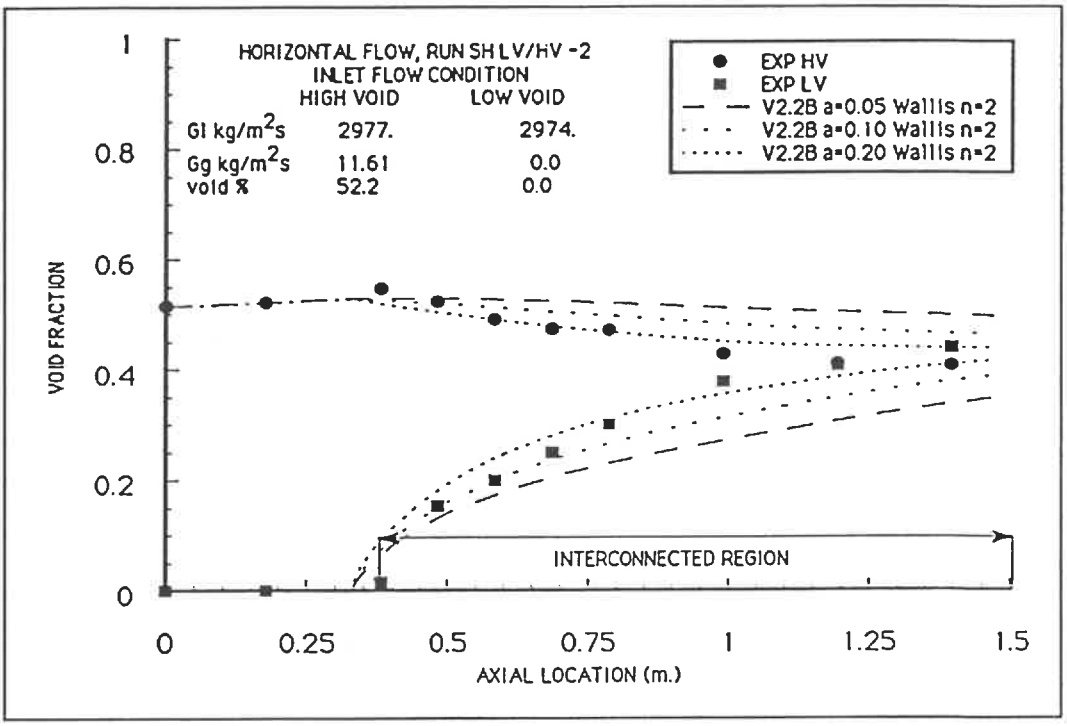

Figure 7.88: Void Fraction $SH - \frac{LV}{HV} - 2$ ASSERT–4 Version 2.2B Wallis n=2

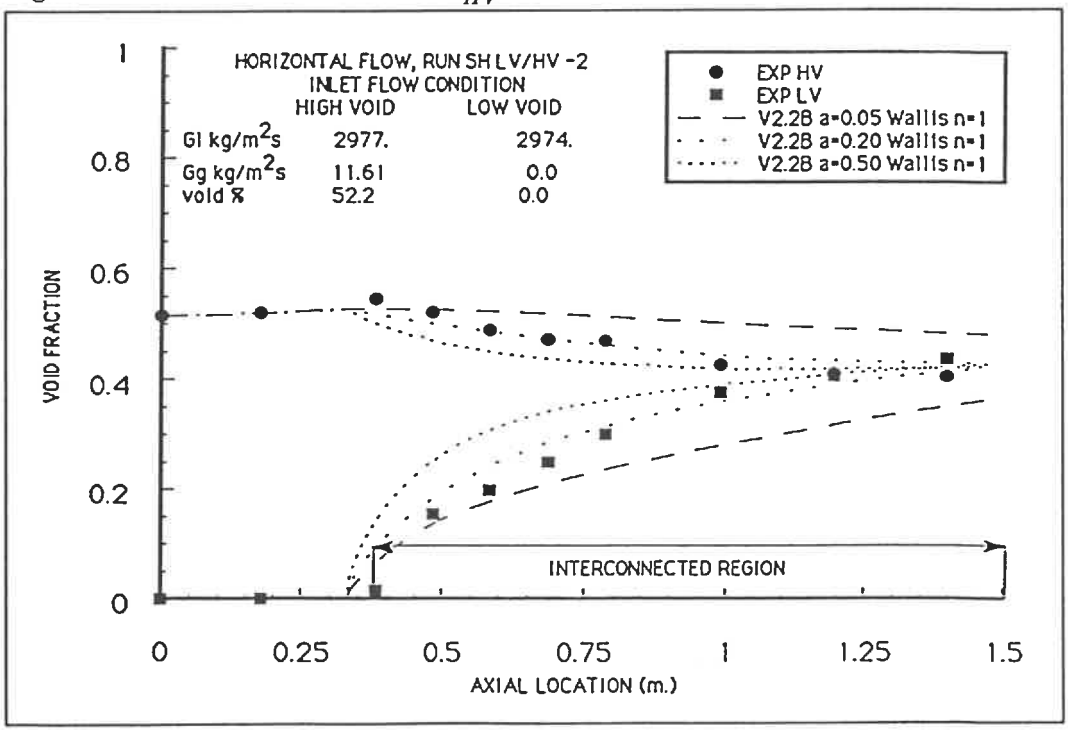

Figure 7.89: Void Fraction $SH - \frac{LV}{HV} - 2$ ASSERT–4 Version 2.2B Wallis n=1

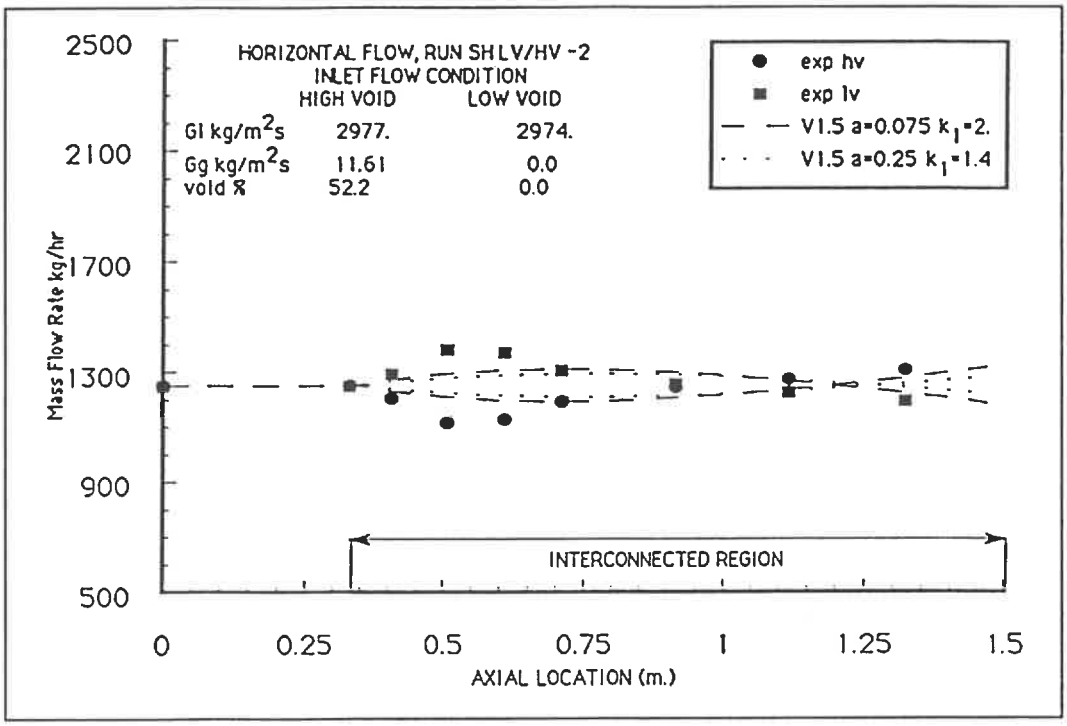

Figure 7.90: Mass Flow $SH - \frac{LV}{HV} - 2$ ASSERT-4 Version 1.5

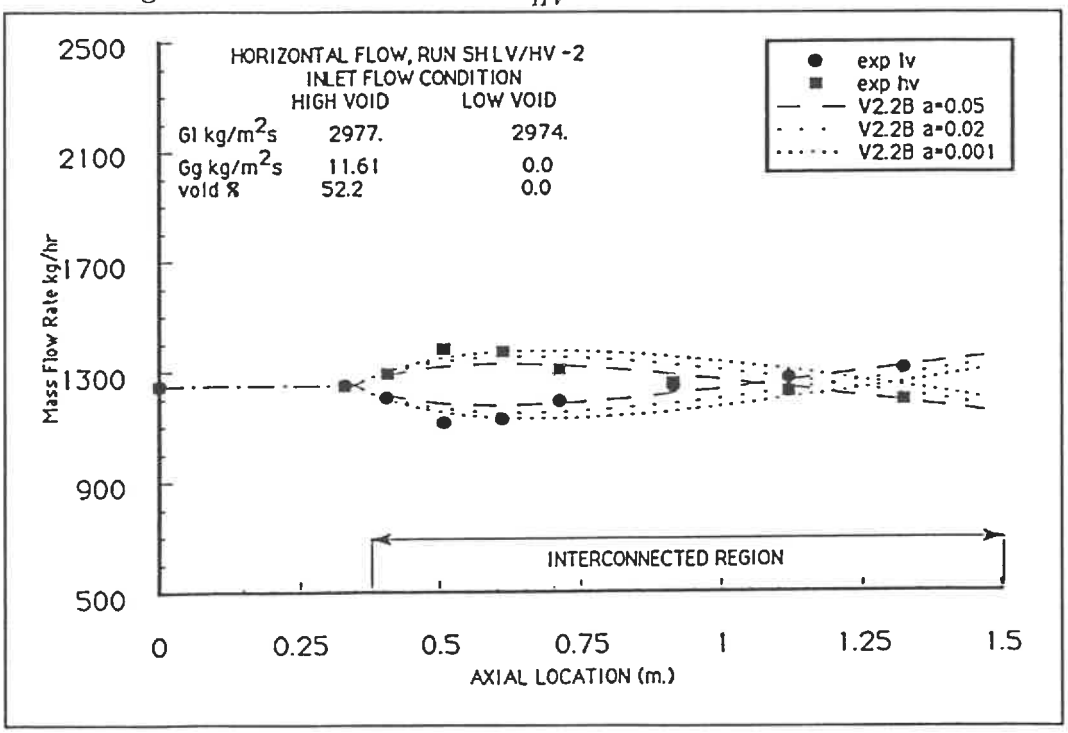

Figure 7.91: Mass Flow $SH - \frac{LV}{HV} - 2$ ASSERT-4 Version 2.2B

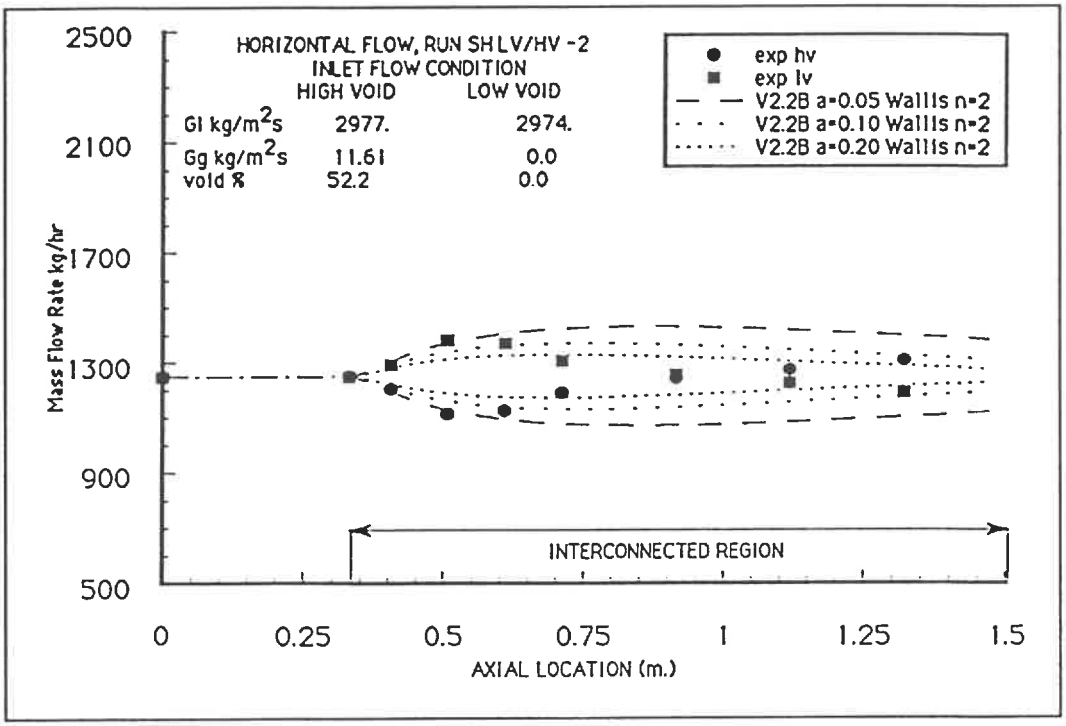

Figure 7.92: Mass Flow $SH - \frac{LV}{HV} - 2$ ASSERT–4 Version 2.2B Wallis n=2

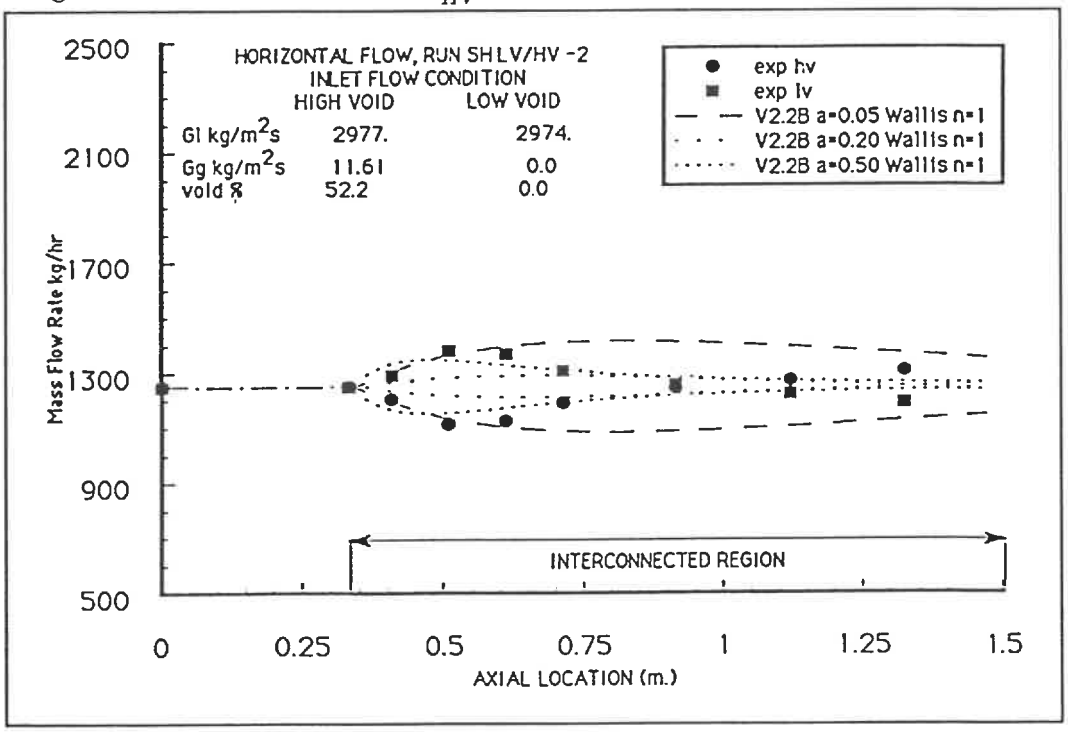

Figure 7.93: Mass Flow $SH - \frac{LV}{HV} - 2$ ASSERT–4 Version 2.2B Wallis n=1

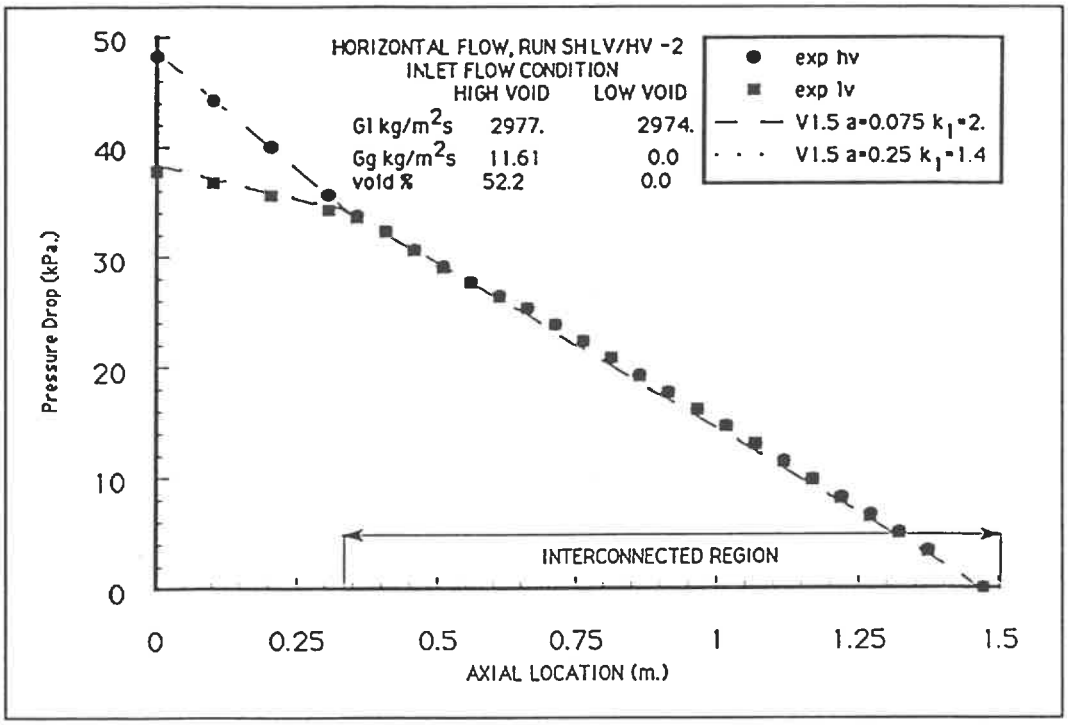

Figure 7.94: Pressure Drop $SH - \frac{LV}{HV} - 2$ ASSERT-4 Version 1.5

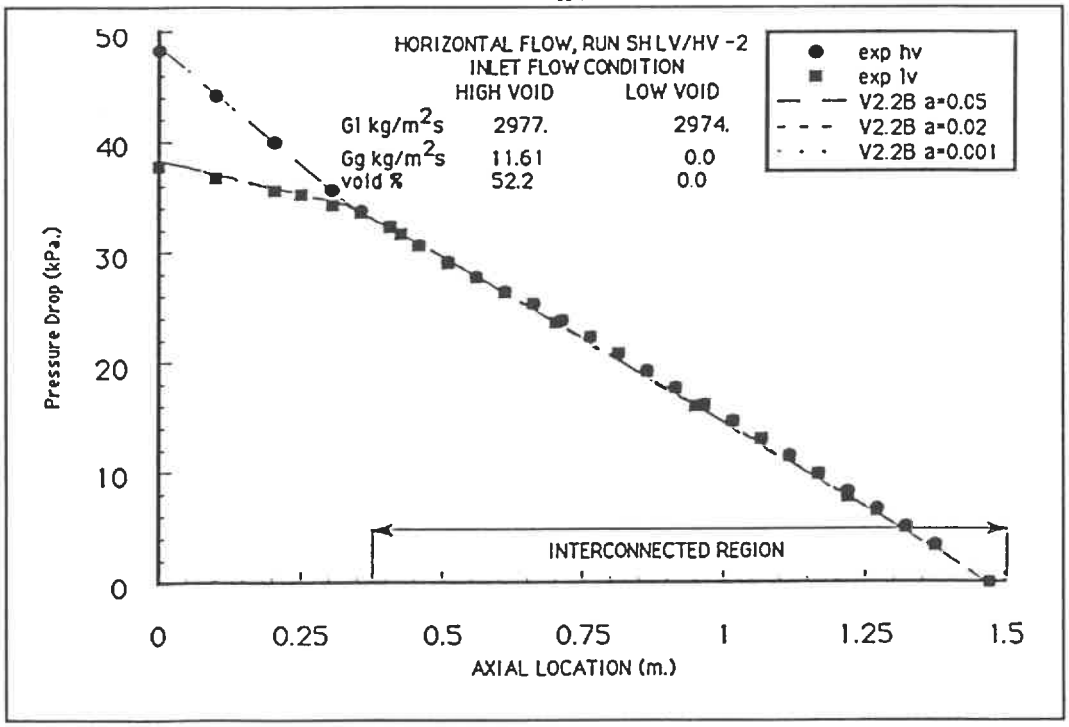

Figure 7.95: Pressure Drop $SH - \frac{LV}{HV} - 2$ ASSERT-4 Version 2.2B

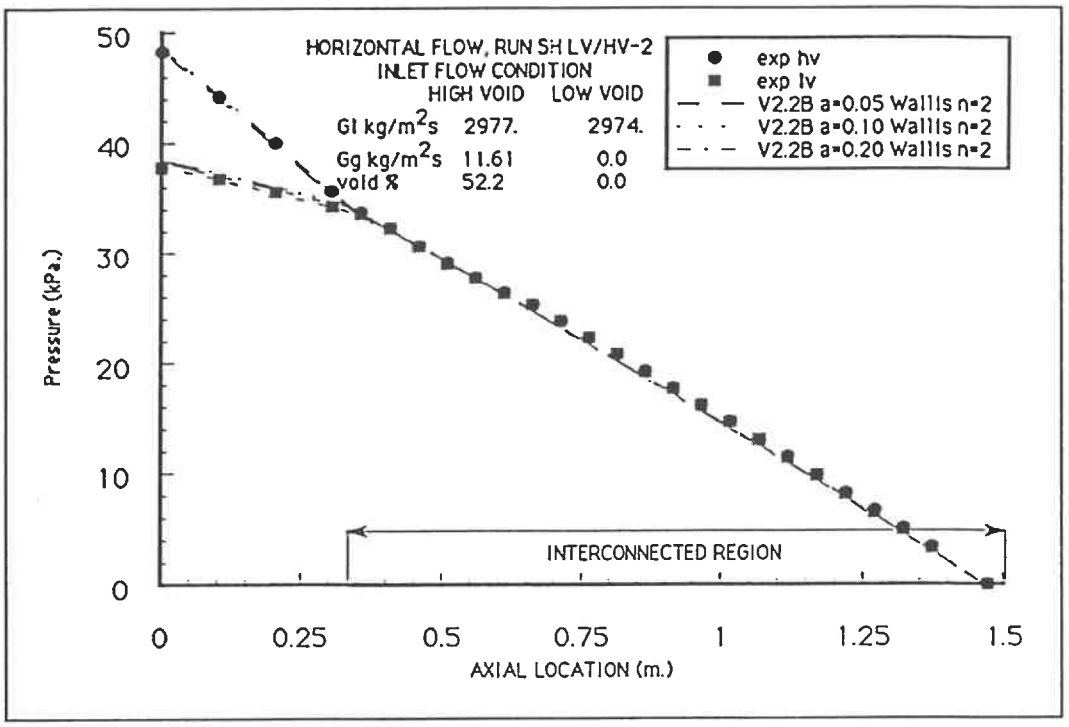

Figure 7.96: Pressure Drop $SH - \frac{LV}{HV} - 2$ ASSERT-4 Version 2.2B Wallis n=2

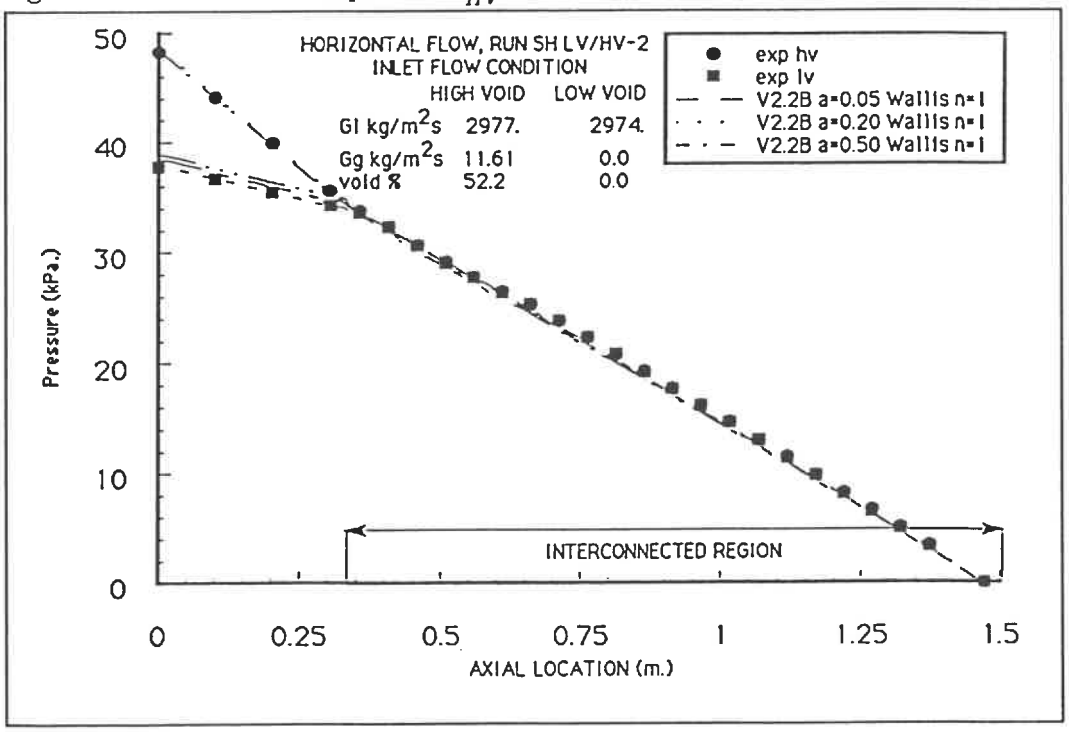

Figure 7.97: Pressure Drop $SH - \frac{LV}{HV} - 2$ ASSERT-4 Version 2.2B Wallis n=1

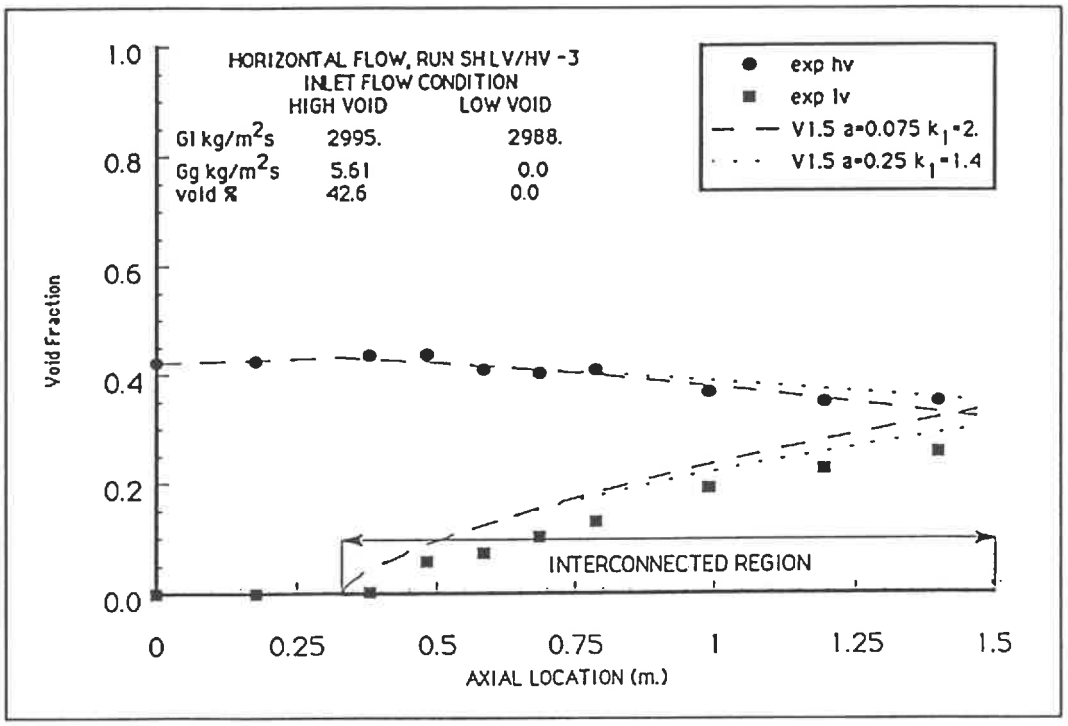

Figure 7.98: Void Fraction $SH - \frac{LV}{HV} - 3$ ASSERT-4 Version 1.5

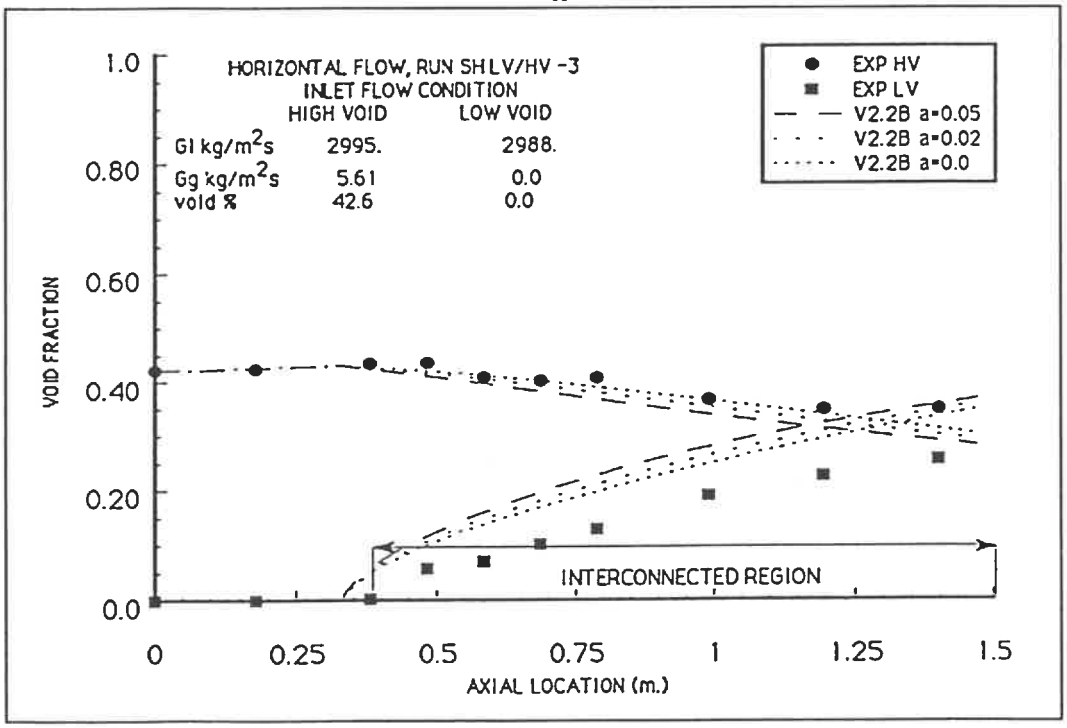

Figure 7.99: Void Fraction $SH - \frac{LV}{HV} - 3$ ASSERT-4 Version 2.2B

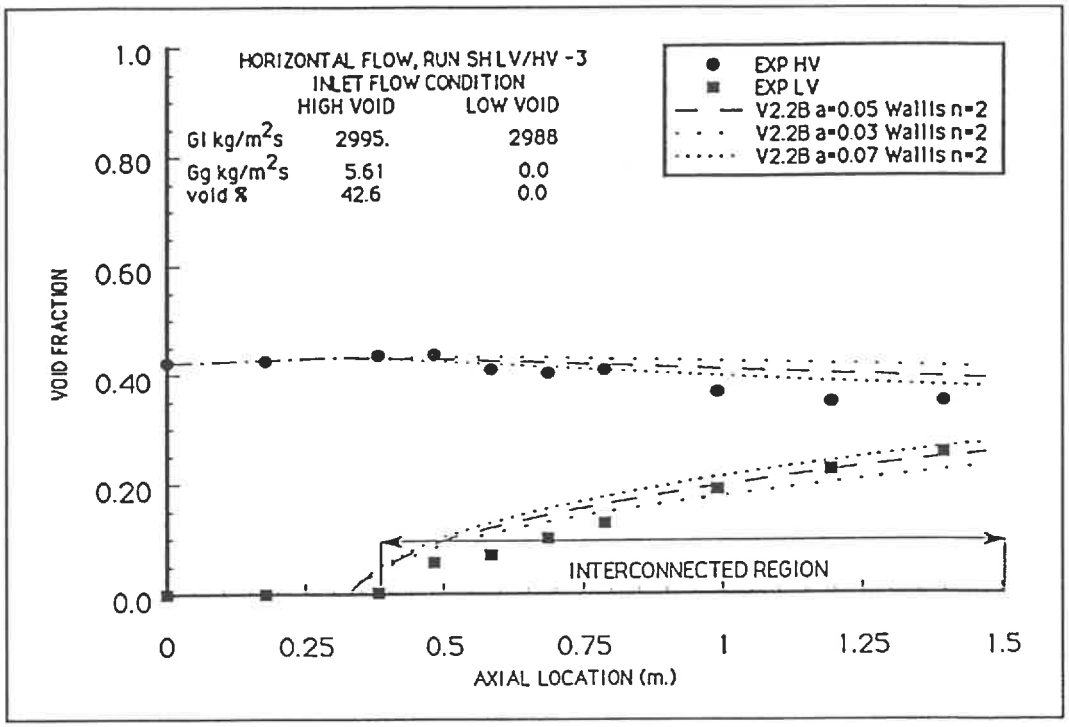

Figure 7.100: Void Fraction $SH - \frac{LV}{HV} - 3$ ASSERT-4 Version 2.2B Wallis n=2

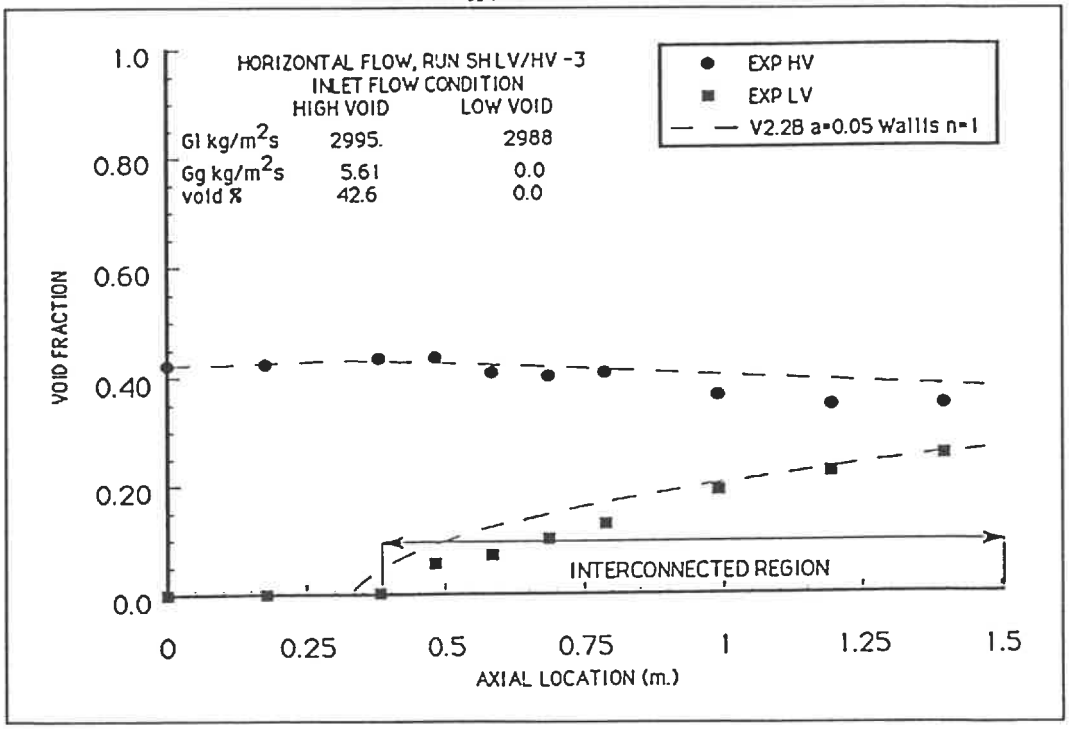

Figure 7.101: Void Fraction $SH - \frac{LV}{HV} - 3$ ASSERT-4 Version 2.2B Wallis n=1

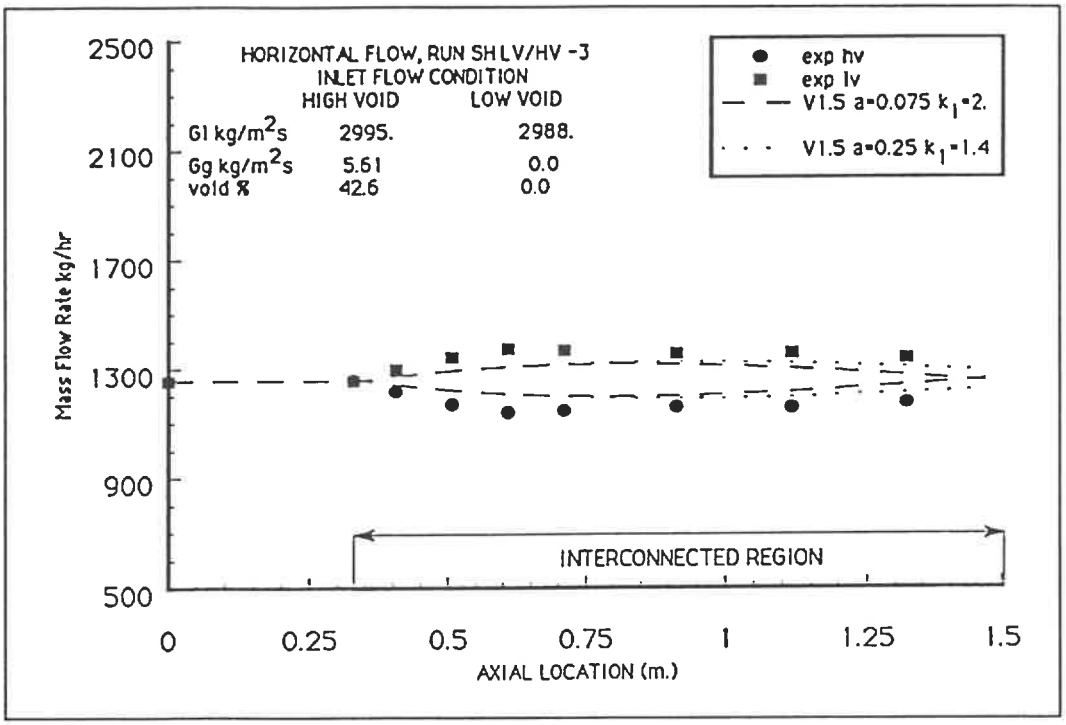

Figure 7.102: Mass Flow $SH - \frac{LV}{HV} - 3$ ASSERT-4 Version 1.5

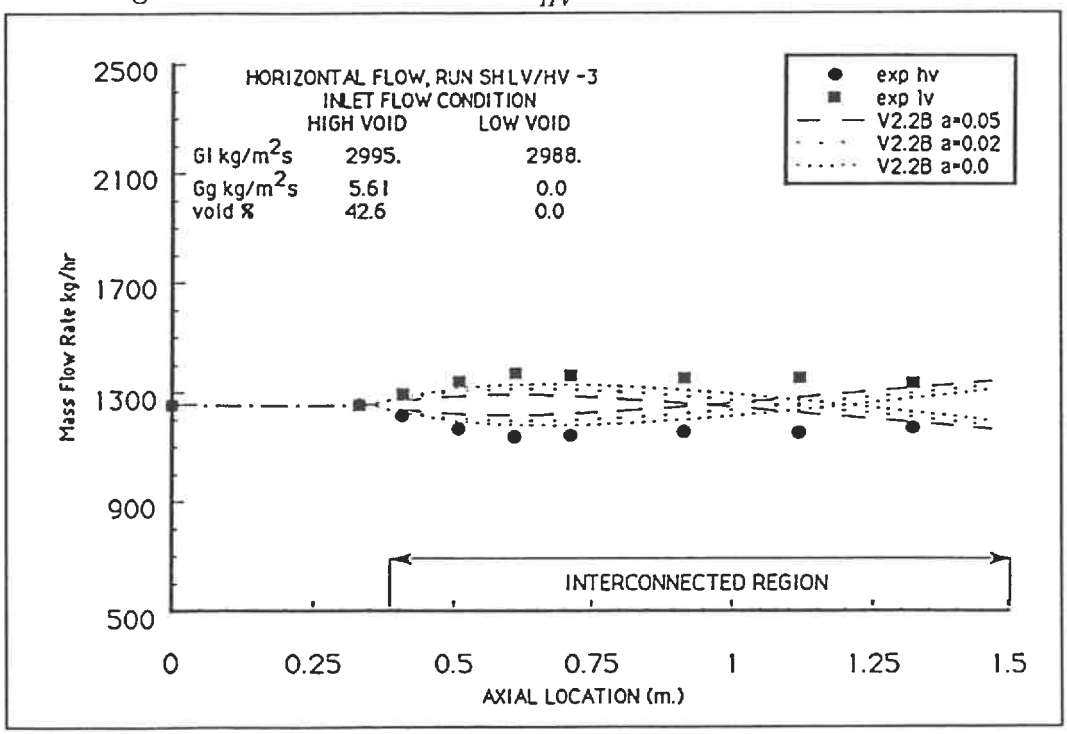

Figure 7.103: Mass Flow $SH - \frac{LV}{HV} - 3$ ASSERT-4 Version 2.2B

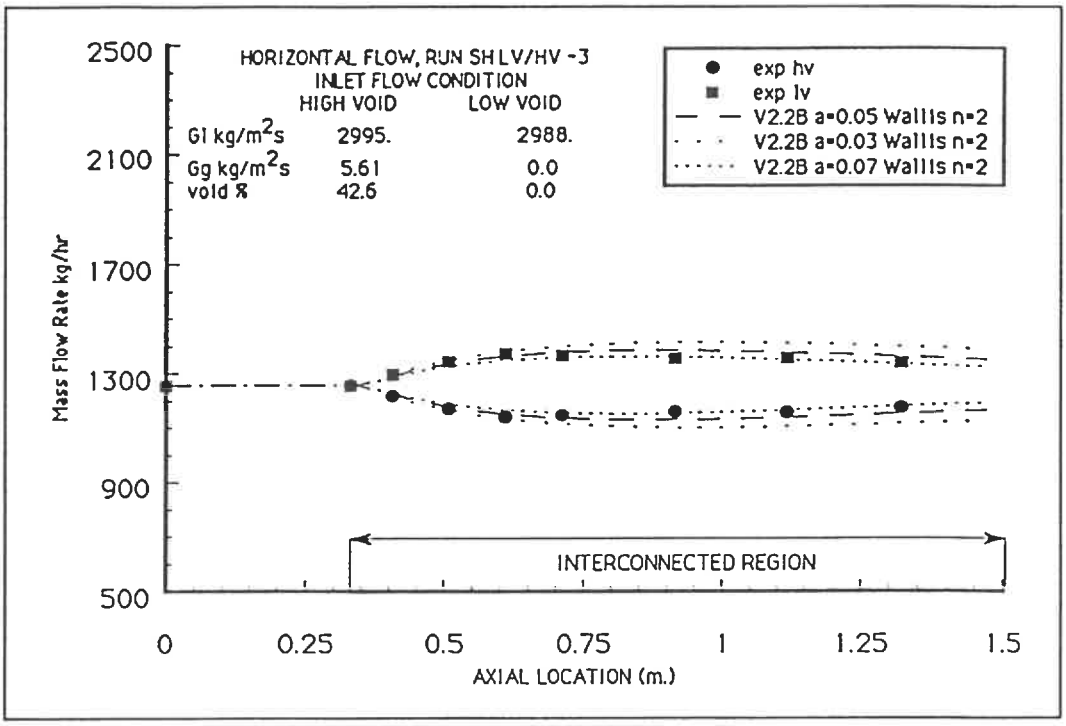

Figure 7.104: Mass Flow $SH - \frac{LV}{HV} - 3$ ASSERT-4 Version 2.2B Wallis n=2

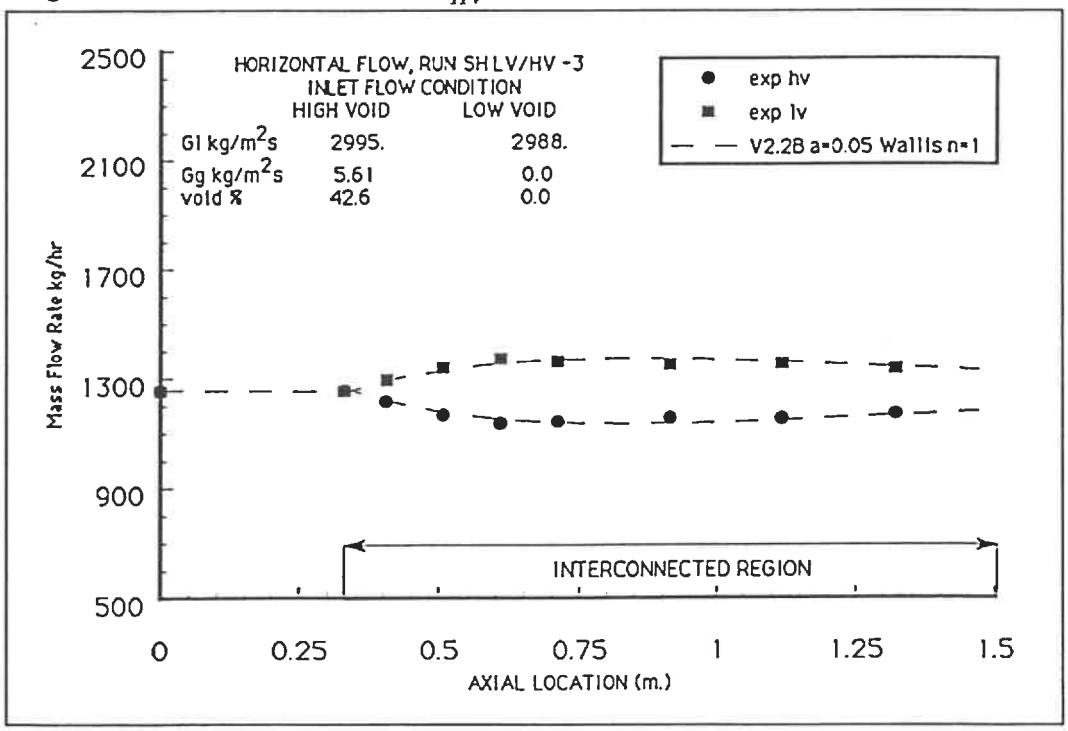

Figure 7.105: Mass Flow $SH - \frac{LV}{HV} - 3$ ASSERT-4 Version 2.2B Wallis n=1

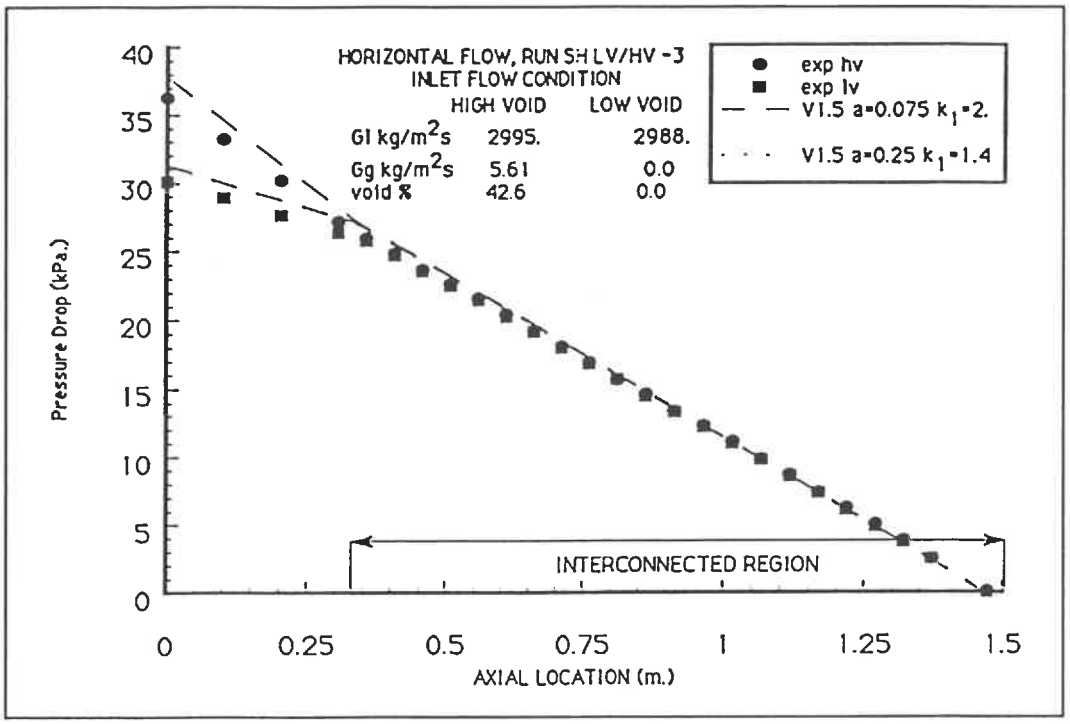

Figure 7.106: Pressure Drop $SH - \frac{LV}{HV} - 3$ ASSERT-4 Version 1.5

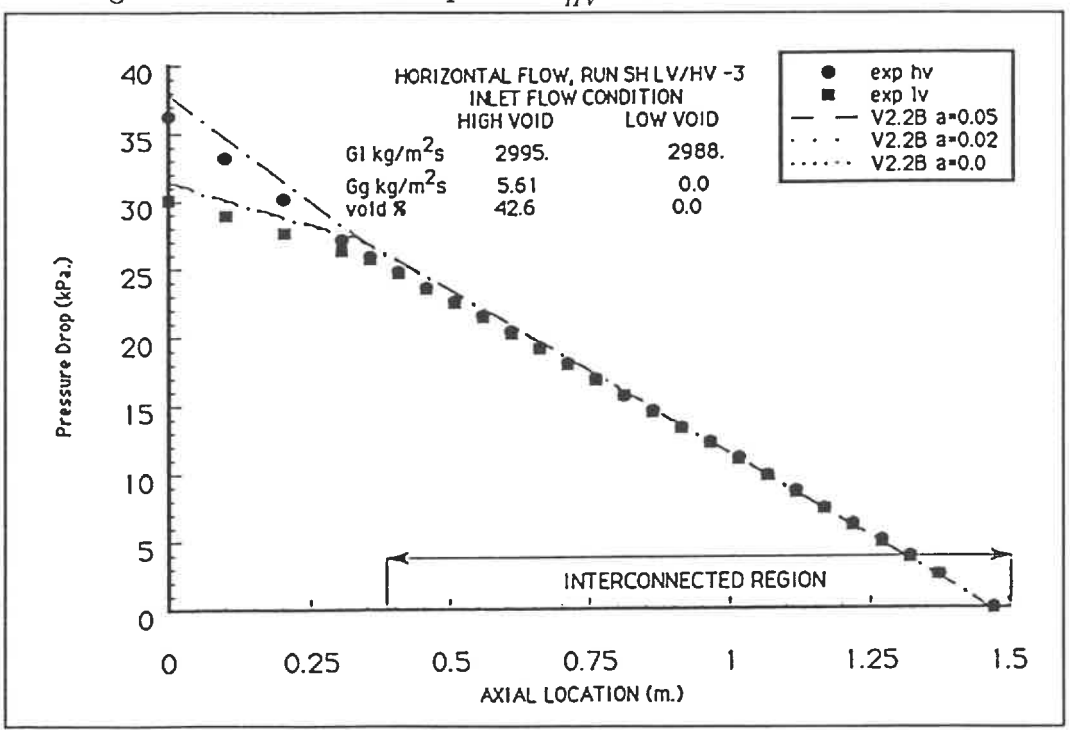

Figure 7.107: Pressure Drop $SH - \frac{LV}{HV} - 3$ ASSERT-4 Version 2.2B

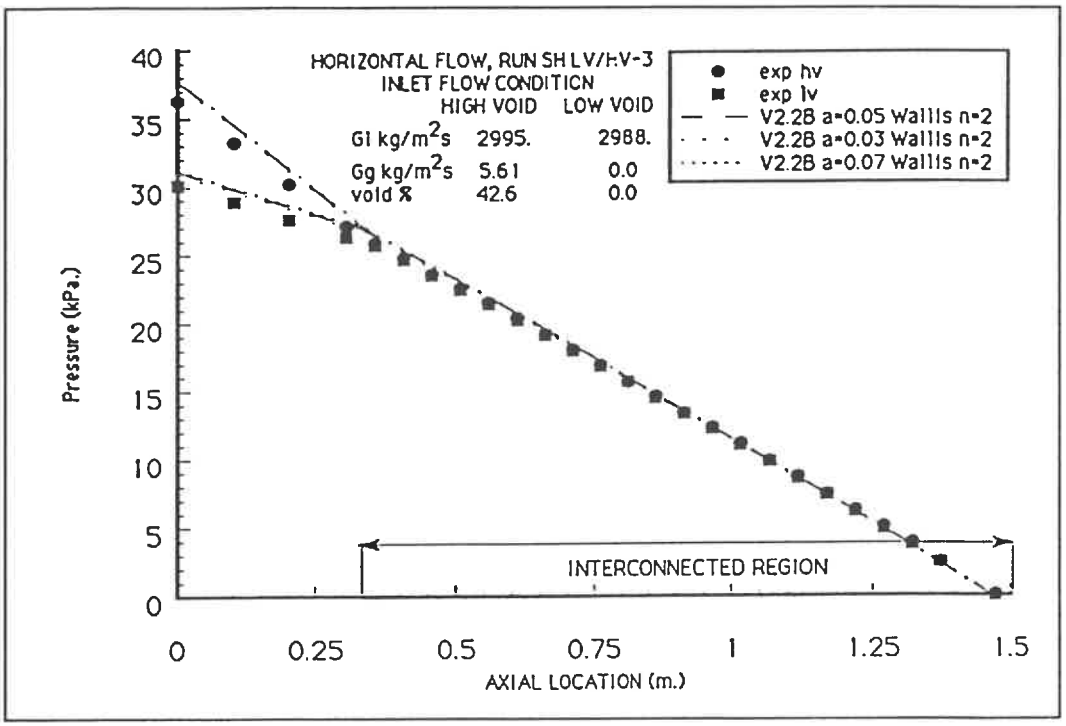

Figure 7.108: Pressure Drop $SH - \frac{LV}{HV} - 3$ ASSERT-4 Version 2.2B Wallis n=2

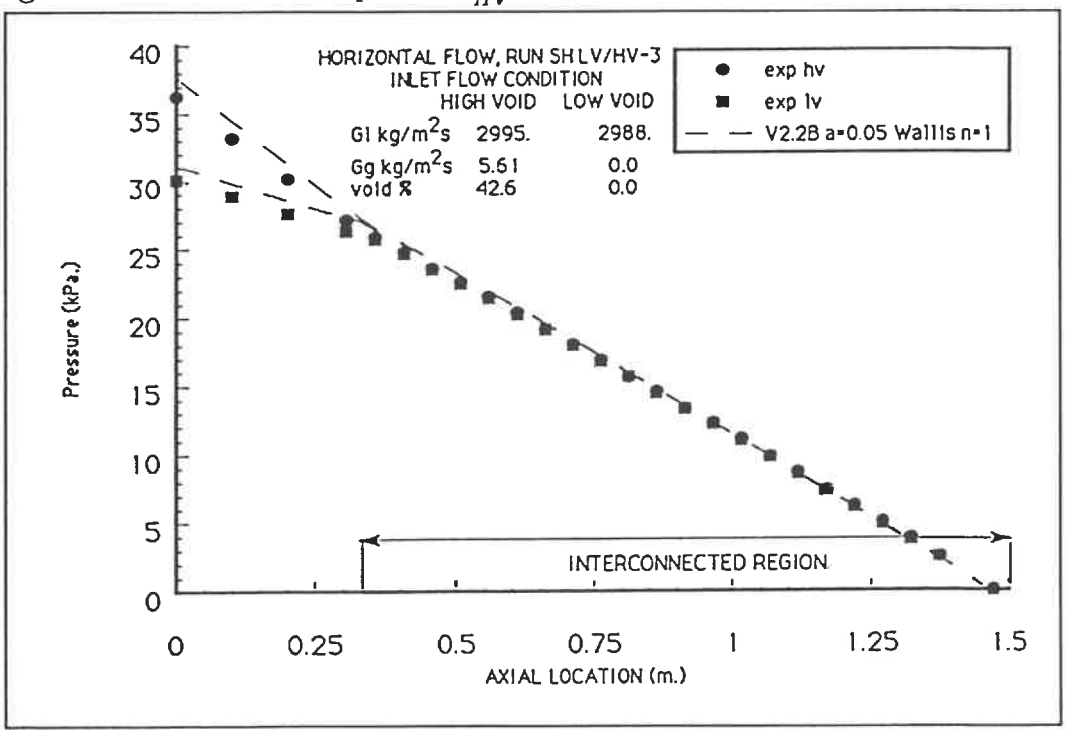

Figure 7.109: Pressure Drop $SH - \frac{LV}{HV} - 3$ ASSERT-4 Version 2.2B Wallis n=1

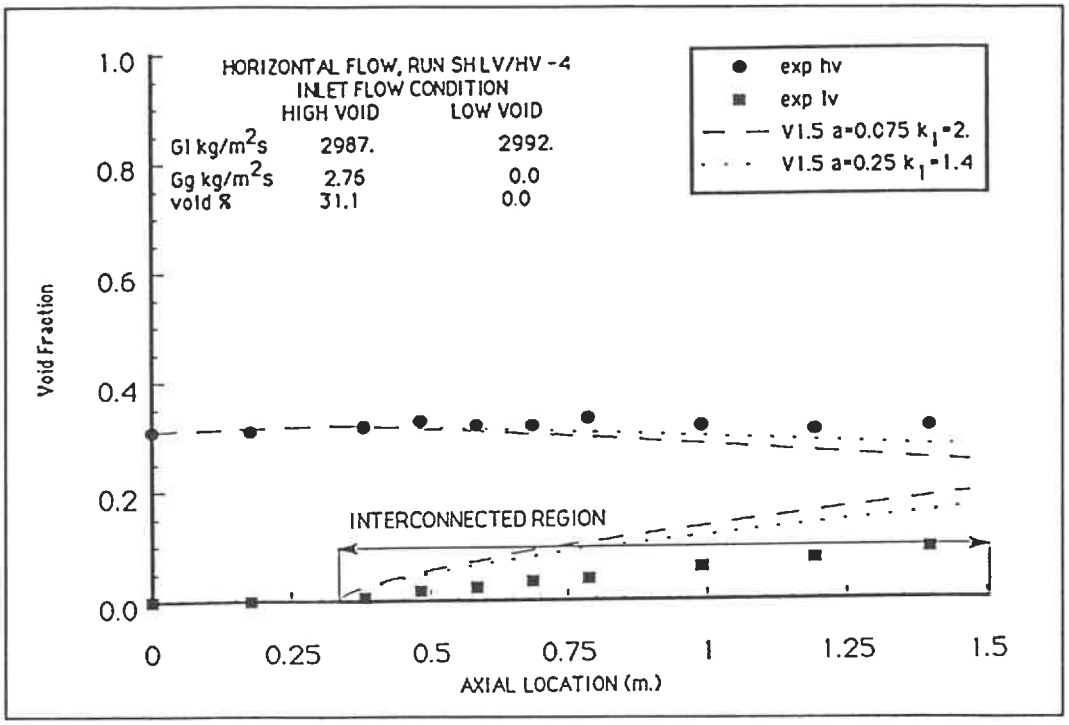

Figure 7.110: Void Fraction $SH - \frac{LV}{HV} - 4$ ASSERT-4 Version 1.5

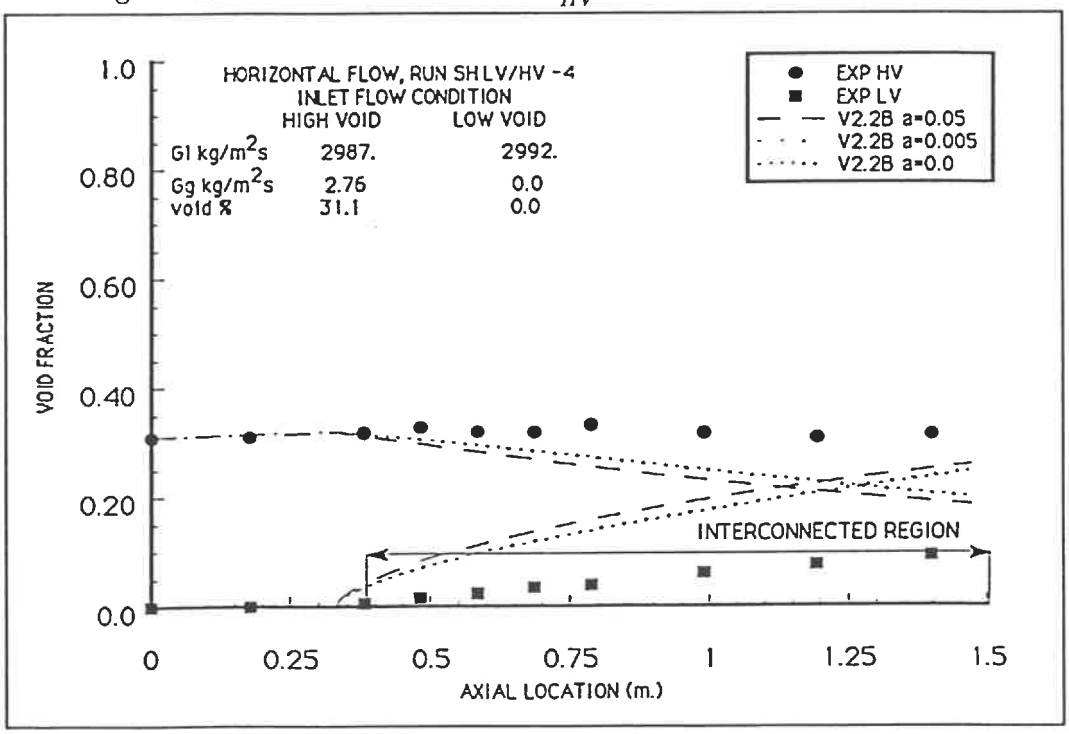

Figure 7.111: Void Fraction $SH - \frac{LV}{HV} - 4$ ASSERT-4 Version 2.2B

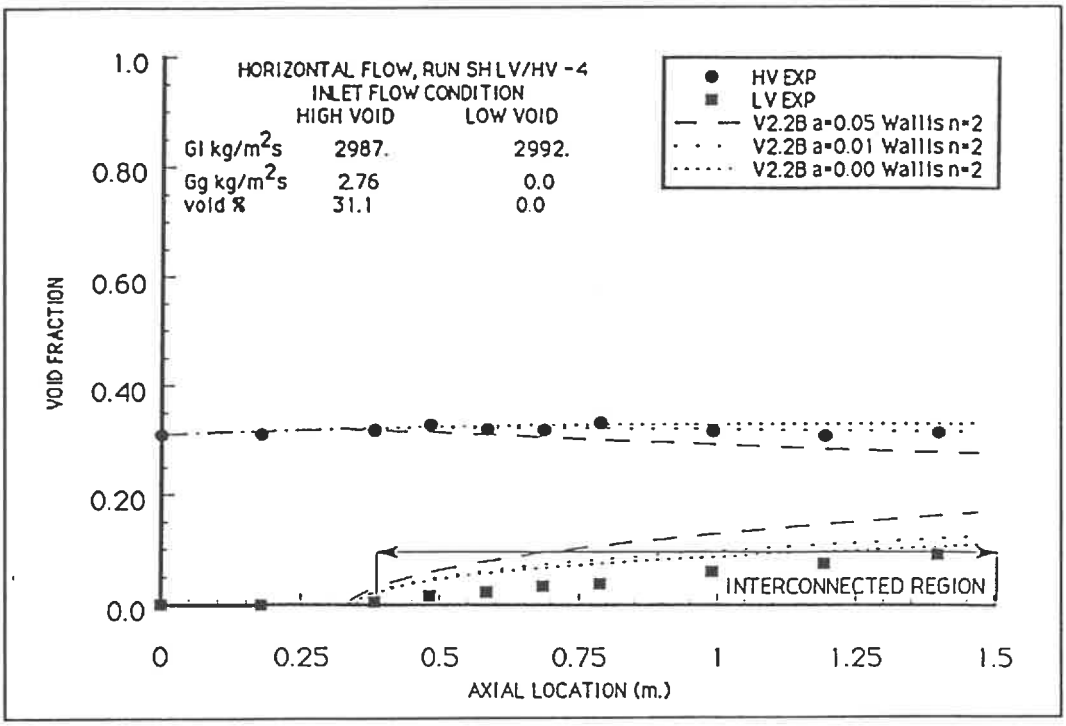

Figure 7.112: Void Fraction $SH - \frac{LV}{HV} - 4$ ASSERT-4 Version 2.2B Wallis n=2

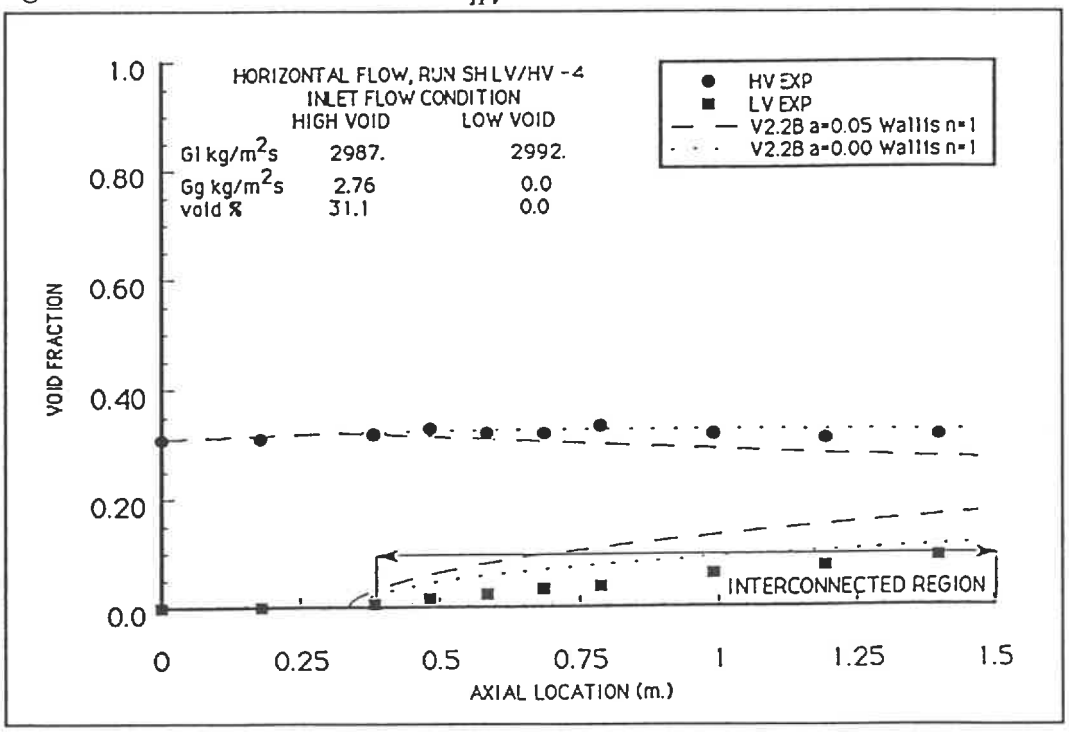

Figure 7.113: Void Fraction $SH - \frac{LV}{HV} - 4$ ASSERT-4 Version 2.2B Wallis n=1

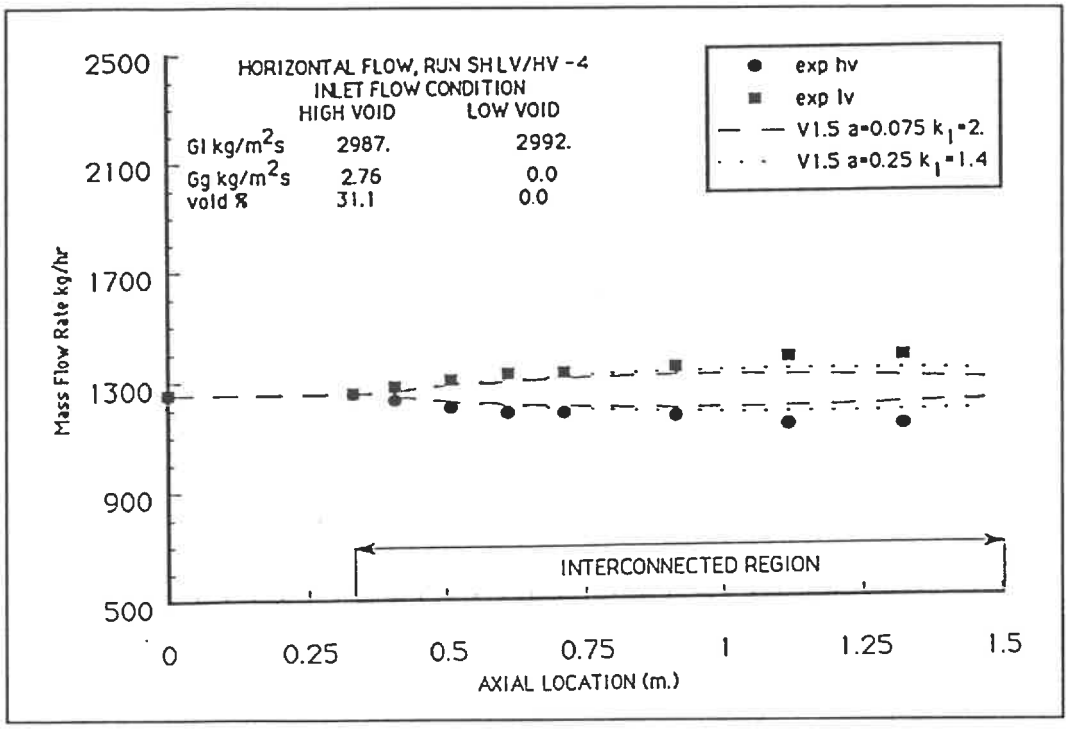

Figure 7.114: Mass Flow $SH - \frac{LV}{HV} - 4$ ASSERT–4 Version 1.5

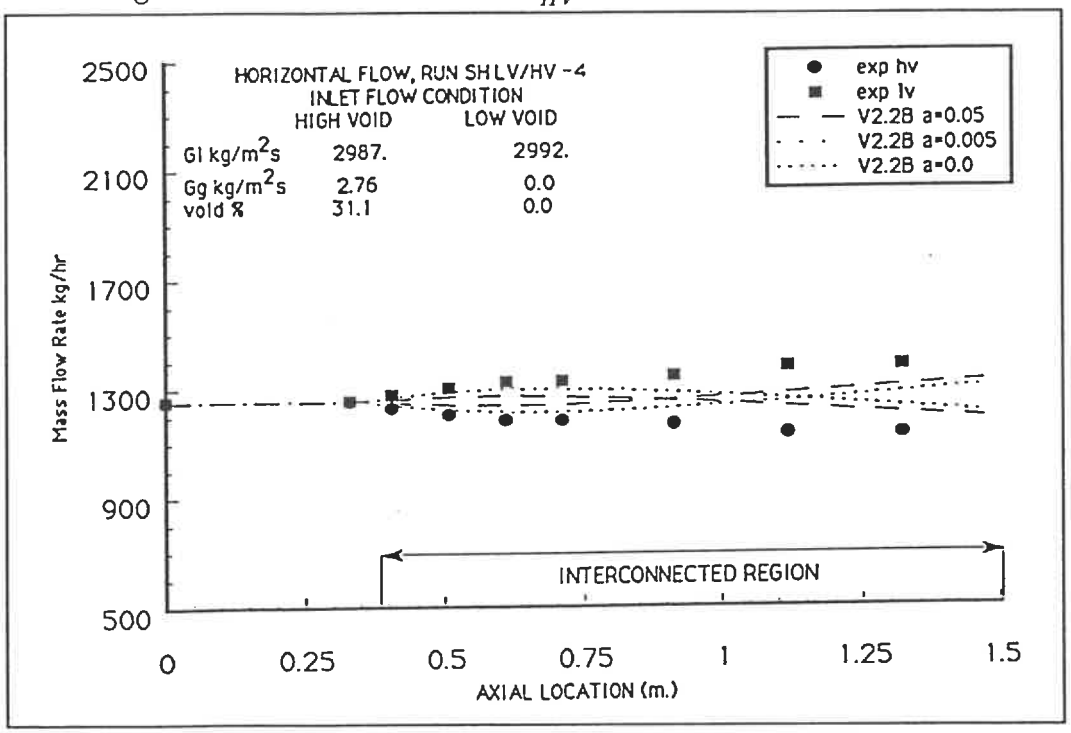

Figure 7.115: Mass Flow $SH - \frac{LV}{HV} - 4$ ASSERT–4 Version 2.2B

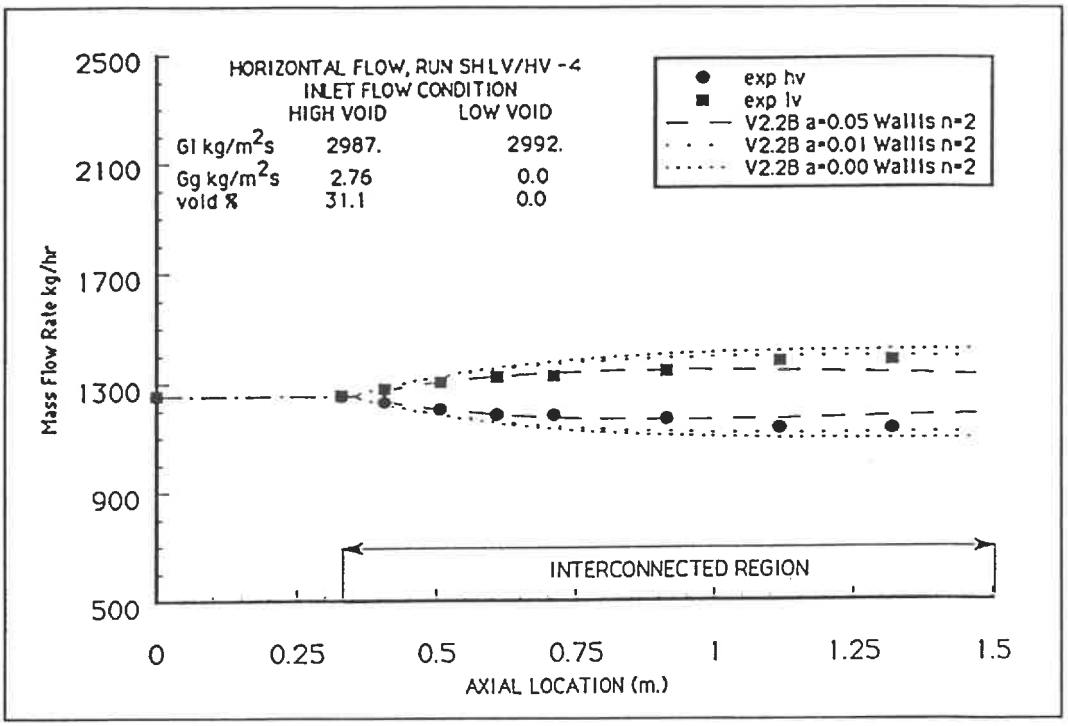

Figure 7.116: Mass Flow $SH - \frac{LV}{HV} - 4$ ASSERT–4 Version 2.2B Wallis n=2

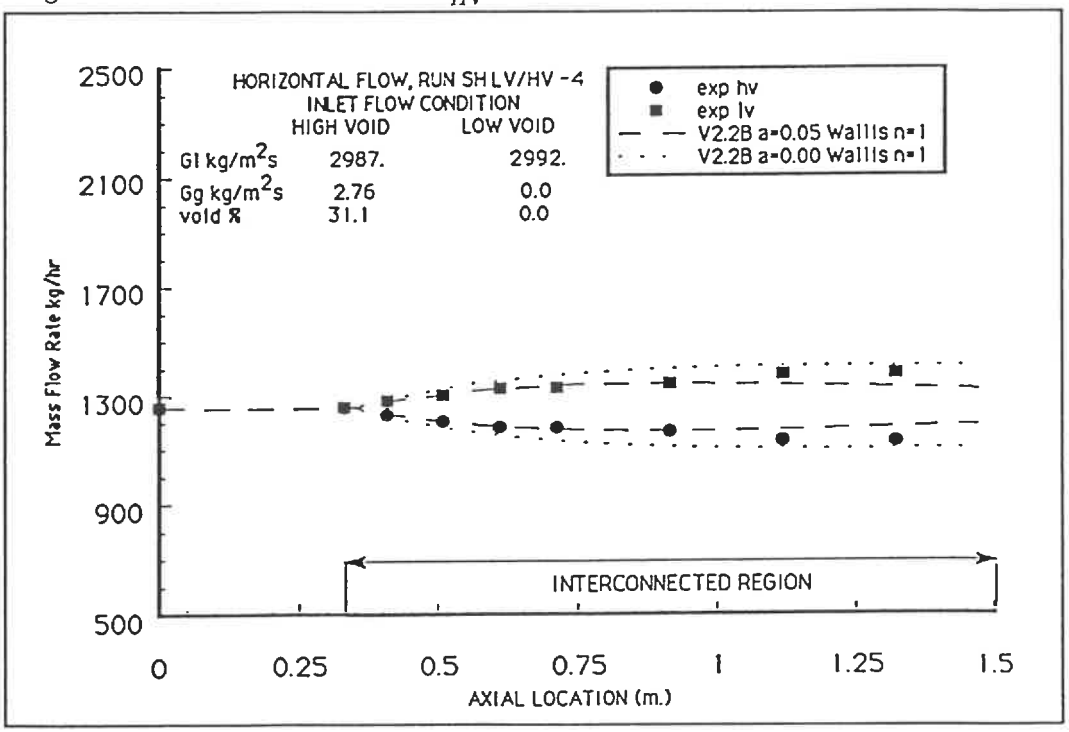

Figure 7.117: Mass Flow $SH - \frac{LV}{HV} - 4$ ASSERT–4 Version 2.2B Wallis n=1

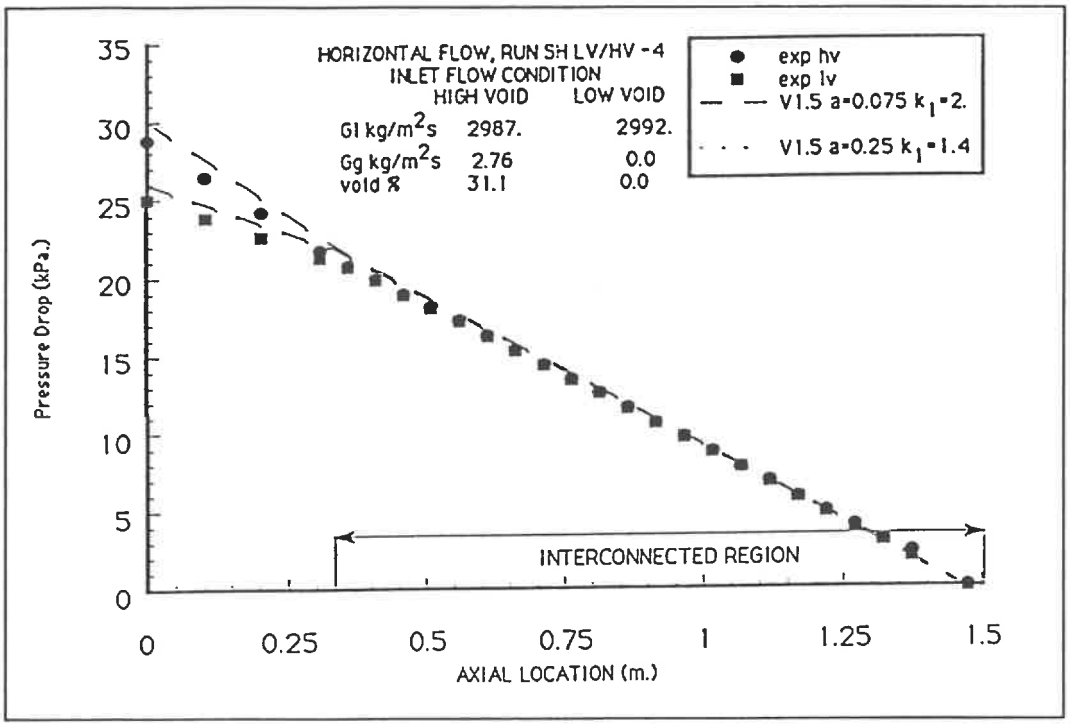

Figure 7.118: Pressure Drop $SH - \frac{LV}{HV} - 4$ ASSERT-4 Version 1.5

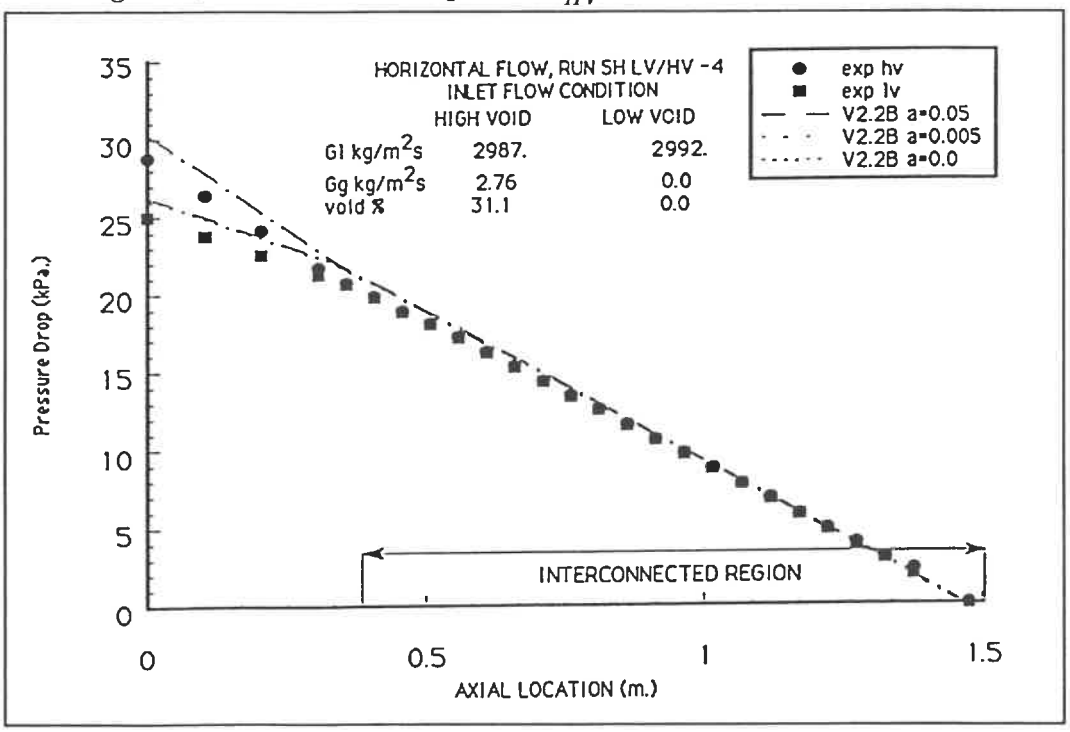

Figure 7.119: Pressure Drop $SH - \frac{LV}{HV} - 4$ ASSERT-4 Version 2.2B

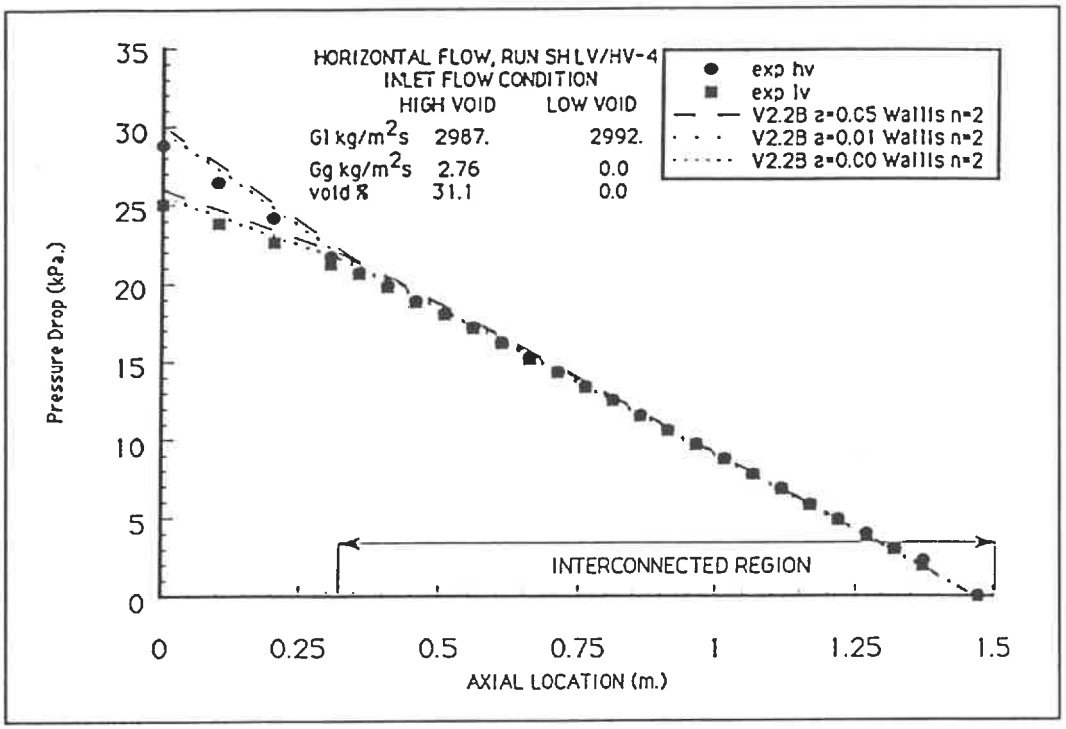

Figure 7.120: Pressure Drop $SH - \frac{LV}{HV} - 4$ ASSERT-4 Version 2.2B Wallis n=2

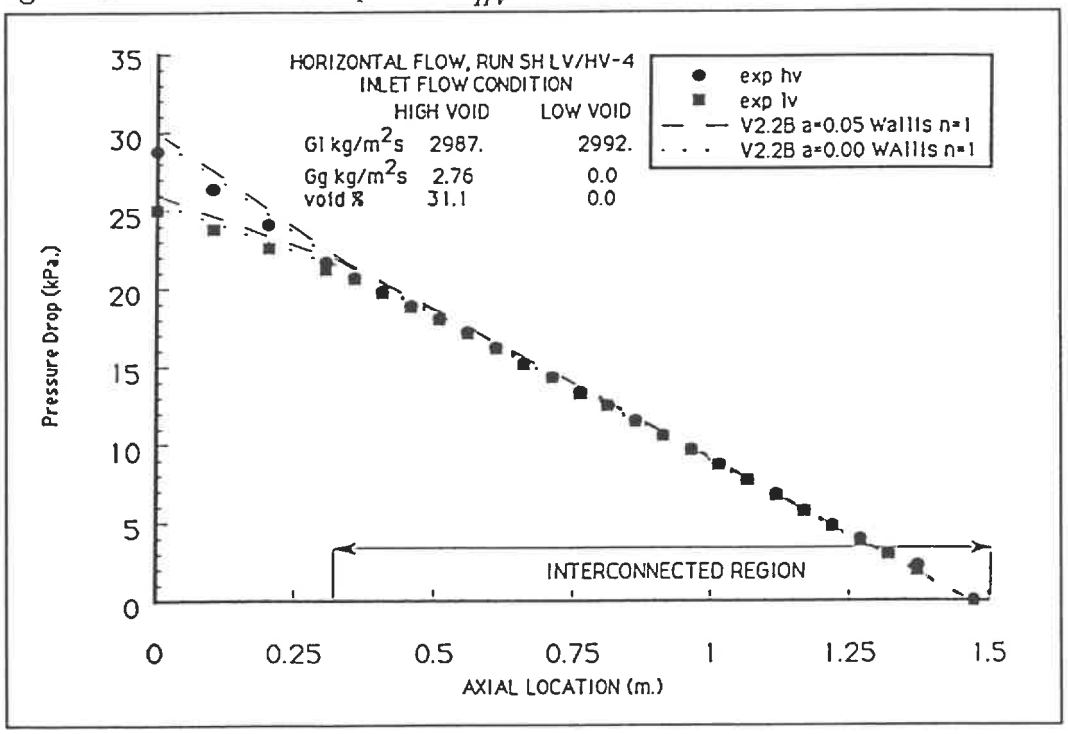

Figure 7.121: Pressure Drop $SH - \frac{LV}{HV} - 4$ ASSERT-4 Version 2.2B Wallis n=1

Chapter 8

CONCLUSIONS AND RECOMMENDATIONS

This chapter presents the conclusions that can be drawn from the work done in this research project and also proposes some recommendations for future work in the areas of both theoretical and experimental subchannels analysis. The objective of this research project was to compare the predictions of the ASSERT–4 subchannel code developed by Atomic Energy of Canada Limited against the experimental results on two–interconnected subchannels obtained at the Institut de Génie Énergétique.

The work described in this thesis can be broken down into two major categories, a theoretical analysis of the basic equations used to mathematically describe two–phase flows and the comparison of the predictions of ASSERT–4 Version 1.5 and ASSERT–4 Version 2.2B against the experimental results. The conclusions for each part of this work will be presented seperately.

8.1 Conclusions From The Theoretical Work

An integral part of any rigorous comparison between the predictions of a computer code and a set of experimental results must, by neccessity, involve an analysis of the underlying physics of the phenomena being studied. To this end, an analysis of the basic equations of two–phase flow was carried out. This involved the formal derivation of a three dimensional composite space–time averaged set of conservation equations for mass, momentum, and energy. From this general model, the equations actually used in the ASSERT–4 subchannel code were derived. To do this, a number of simplifying assumptions were introduced and the physical

implications of these simplifications are assessed.

The numerical solution scheme employed to solve the set of equations used in the ASSERT–4 subchannel code was then analyzed. The limitations placed on the code by the choice of the particular solution scheme were then discussed.

The correlations and constitutive equations used to supply the information required to model the intersubchannel transfer mechanisms and the impact of the choices made for these models on the code predictions were also analyzed.

One of the basic choices made in the development of the ASSERT–4 subchannel code was to describe the flow in terms of a mixture momentum equation and the relative velocities of the two phases by the use of a drift flux model. There are a number of very good reasons to do this; such as to simplify the numerical considerations. This approach might present problems in the future due to the fact that one of the basic assumptions of the drift flux model is that there must be a strong coupling between the phases. At low flows this strong coupling between the phases is lost, thus it is possible that this might impose a lower limit on the flow rates for which ASSERT–4 could be used.

Another very important assumption that was made in the development of the transverse momentum equation was that the transverse flow was small compared to the axial flow, an assumption that is completely justified under normal conditions. This assumption was then used to eliminate a number of terms in the transverse momentum equation. Under low flow conditions or in cases involving a large transverse flow due to a partial subchannel blockage this assumption might no longer be justified and may cause problems regarding the ability of the code to accurately describe these types of flows.

8.2 Conclusions From The Comparison Between The Code Predictions And The Experimental Results

Two versions of the ASSERT – 4 subchannel code, ASSERT – 4 Version 1.5 and ASSERT – 4 Version 2.2B were used to simulate a large number of experiments carried out on two interconnected subchannels at I.G.E. for both vertical and horizontal flows. For the horizontal flows a number of different subchannel arrangments were studied, these were: the two subchannels at the same elevation, the high void subchannel above the low void subchannel and the high void subchannel below the low void subchannel. For all these simulations the effects of varying certain parameters in the correlations and constitutive equations for the intersubchannel transfer mechanisms were examined.

8.2.1 Conclusions for Vertical Comparisons

An analysis of the predicted and measured void profiles for ASSERT – 4 Version 1.5, which used the correlation for the void diffusion coefficient given by equation 6.4, has shown that for the higher void cases, SV–1 to SV–4, a higher value of the coefficient a in the void diffusion correlation was required to adequately predict the void fraction profiles. For the intermediate void fraction cases, SV–5 and SV–6, the recommended value of the diffusion coefficient, $a = 0.075$, yielded good results. For the low void case, SV–7, no significant difference in the void profile was seen for any of the values of the diffusion coefficient used. It seems that physically the void diffusion shows a greater dependence on the void fraction than that reflected by equation 6.4.

An analysis of the predicted and measured void fraction profiles for ASSERT – 4 Version 2.2B, which used the correlation for the void diffusion coefficient given by equation 6.6, has shown that for the higher void fraction cases, SV–1 to SV–4, a higher value of the coefficient a, as compared to the default value, in the void

diffusion correlation was required to adequately predict the void profiles. For the intermediate and low void fraction cases, SV–5, SV–6, and SV–7, it was neccessary to decrease the value of the diffusion coefficient a, at times significantly so, to accurately predict the void transfered from the high void subchannel to the low void subchannel.

Since it was necessary to change the leading coefficient of the void diffusion correlation as given by equation 6.6 to adequatly predict the void transfered in the cases from SV–1 to SV–7 which covered a range from $\approx$ 60% void to $\approx$ 17% it would appear that the diffusion process is dependent on the void fraction. This is not physically represented by the form of the correlation for the void diffusion as given by equation 6.6.

An analysis of the predicted and measured mass flow rates for ASSERT – 4 Version 1.5 showed that the initial large crossflow at the beginning of the interconnected region was systematically underpredicted. Further, the recovery of the liquid by the high void subchannel which was seen experimentally for most of the cases analyzed was not predicted by ASSERT – 4 Version 1.5.

An analysis of the predicted and measured mass flow rates for ASSERT – 4 Version 2.2B showed that the predictions of the mass flow rates were in general quite good. ASSERT – 4 Version 2.2B was able to predict, with reasonable accuracy the inital large crossflow from the high void subchannel to the low void subchannel at the beginning of the interconnected region. ASSERT – 4 Version 2.2B was also able to predict the recovery the liquid by the high void subchannel in the last third of the test section, something that was completely missed by ASSERT – 4 Version 1.5.

An interesting point to note was that the leading coefficients for the void diffusion correlation which led to the best results for void fraction and the ones which led to the best predictions for mass flow rate using ASSERT – 4 Version 1.5

were at opposite ends of the range of the values that were tested. For ASSERT – 4 Version 2.2B while the two coefficients may not have been identical they were at least close to one another in the range of values that were tested.

8.2.2 Conclusions for Horizontal Comparisons

Conclusions for $SH - HV = LV$ Cases

Looking at the comparison between the experimental results and the predictions of ASSERT – 4 Version 1.5 for the four equal elevation cases it was clear that the value of the diffusion coefficient recommended by Tye et al.[1990] resulted in better overall agreements than did the recommended value of the diffusion coefficient. Examining the mass flow rate predicitons it was seen that ASSERT – 4 Version 1.5 failed to accurately predict the size of the inital large mass transfer at the beginning of the interconnected region. A further observation that can be made was that in no case did ASSERT – 4 Version 1.5 predict a recovery of liquid by the high void subchannel near the end of the interconnected region.

The results of the comparison between the experimental results and the predictions of ASSERT – 4 Version 2.2B were in general much better than the results for the comparison against the predictions of ASSERT – 4 Version 1.5. In comparing the results of the equal elevation cases with corresponding vertical cases it could be seen that the values of the diffusion coefficients that led to the best results were in good agreement with each other and consistently show a trend of being proportional to the void fraction. It was also shown that ASSERT – 4 Version 2.2B did a much better job of predicting the size of the initial large mass transfer from the high void subchannel to the low void subchannel at the begining of the interconnected region. The trend of the high void subchannel to recover some mass near the end of the interconnected region was also predicted by ASSERT – 4 Version 2.2B.

Conclusions for SH-$\frac{HV}{LV}$ Cases

Looking at the comparisson between the experimental results and the predictions of ASSERT – 4 Version 1.5 for the four high void over low void cases it could be seen that the values of the leading coefficient in the calculation of the terminal rise velocity of a bubble in an infinite medium and of the diffusion coefficient recommended by Tye et al.[1990] resulted in better overall agreements than did the default values of these coefficient. Examining the mass flow rate predicitons it could be seen that ASSERT – 4 Version 1.5 failed to accurately predict the size of the inital large mass transfer at the beginning of the interconnected region. A further observation that can be made was that in no case did ASSERT – 4 Version 1.5 predict a recovery of liquid by the high void subchannel near the end of the interconnected region.

The results of the comparison between the experimental results and the predictions of ASSERT – 4 Version 2.2B using the standard ASSERT model for the effects of the other bubbles were in general much better than the results for the comparison against the predictions of ASSERT – 4 Version 1.5. An even greater improvement on the whole ensemble of high void over low void cases analyzed was seen when Wallis's model for the effects of other bubbles was used.

In comparing the results of the ASSERT – 4 Version 2.2B runs of the high void over low void cases against the corresponding equal elevation and vertical cases it was seen that the values of the diffusion coefficients that led to the best results for the run which used the standard ASSERT model for the effects of the other bubbles were quite different from the values of the diffusion coefficients that led to the best results for the equal elevation and vertical cases. For the runs which used Wallis's model for the effects of the other bubbles, using both $n = 2$ and $n = 1$, it was seen that the values of the diffusion coefficients for both the high void over low void cases and the corresponding cases where gravity did not play a role in the

phase seperation were in good agreement with each other and consistently showed a trend of being directly proportional to the void fraction.

It was also shown that ASSERT – 4 Version 2.2B did a much better job of predicting the size of the initial large mass transfer from the high void subchannel to the low void subchannel at the begining of the interconnected region. The trend of the high void subchannel to recover some mass near the end of the interconnected region was also predicted by ASSERT – 4 Version 2.2B.

Conclusions for SH–$\frac{LV}{HV}$ Cases

An analysis of the experimental results and the predictions of ASSERT – 4 Version 1.5 for the four low void over high void cases showed that the values of coefficient for the calculation of the terminal rise velocity of a bubble in an infinite medium and the diffusion coefficient recommended by Tye et al.[1990] resulted in better overall agreements than did the recommended values of these coefficient. An analysis of the mass flow rate predicitons showed that ASSERT – 4 Version 1.5 failed to accurately predict the size of the inital large mass transfer at the beginning of the interconnected region.

The results of the comparison between the experimental results and the predictions of ASSERT – 4 Version 2.2B using the standard ASSERT model for the effects of the other bubbles predicted that the void fractions and the mass flow rates would cross in all four of the low void over high void cases. This phenomenon was only observed in two of the four expermients. The use of Wallis's model for the effects of the other bubbles in ASSERT – 4 Version 2.2B improved the predicted results somewhat compared to the use of the standard ASSERT model for this effect.

In comparing the results of the ASSERT – 4 Version 2.2B runs of the low void over high void cases against the corresponding equal elevation and vertical cases it was seen that the values of the diffusion coefficients that led to the best results

for the runs which used the standard ASSERT model for the effects of the other bubbles were quite different from the values of the diffusion coefficients that led to the best results for the equal elevation and vertical cases. For the runs which used Wallis's model for the effects of the other bubbles it was seen that the values of the diffusion coefficients for both the low void over high void cases and the corresponding equal elevation and vertical cases were in reasonable agreement with each other.

8.2.3 General Conclusions

An analysis of all the predicted and experimental results has shown that by properly choosing the values of the coefficients used in the constitutive equations for the terminal rise velocity of a bubble in an infinite medium and for the void diffusivity that both versions of ASSERT – 4 can quite accurately predict the behaviour of the flow in the two interconnected subchannel experiments carried out at I.G.E.. ASSERT – 4 Version 2.2B did however prove to be quite a bit better than the earlier version. ASSERT – 4 Version 1.5 was, in all the cases analyzed, incapable of accurately predicting the magnitude of the initial crossflow at the beginning of the interconnected region. Further, in no case did ASSERT – 4 Version 1.5 predict a recovery of the liquid by the high void subchannel. ASSERT – 4 Version 2.2B was capable of much more accurately predicting both the magnitude of the initial crossflow and the existance of the flow recovery.

8.3 Recommendations

It was pointed out earlier that for ASSERT – 4 Version 2.2B the diffusion coefficients that led to the best results for both the void fraction predicitons and the mass flow rate predicitons were quite similar to each other. It was thought that it might be a worthwhile excercise to generate a correlation for the coefficient

a in the void diffusion correlation based on these results. This was tried using the diffusion coefficients from our analysis that gave the best result and correlating it with both the void fraction in the subchannel having the maximum void fraction of the two subchannels under study and the average void in the two subchannels. While some trends could be seen in the analysis this attempt did not bear fruit due to the limited range covered by the available data. The first recommendation is therefore to preform a series of experiments covering a wider range of void fractions and of void fraction differences between the subchannel and repeat the attempt to correlate the diffusion coefficients to the void fraction as it was quite clear for the work presented in this thesis that they are related.

Another important point is that all the experiments were preformed using the same mass flux $\approx 3000 kg/m^2 s$ for both subchannels. It would be very usefull to have the same type of data as was used to test the code in this thesis for a wider range of mass fluxes and also for cases having a different mass flux in each subchannel. This would permit a more in depth analysis of the capabilities of the code to be preformed.

The tests involving the use of the model for the effects of the other bubbles due to Wallis proved to be reasonably beneficial, in fact in only two cases did the model not improve the results. Thus two recommendations for future work can be made with regards to this model. The first recommendation is that the possibility of adding this model to the code with the coefficient n as an input variable should be investigated. The experiments analyzed in this thesis were all conducted a low pressures using an air water mixture as the working fluid. While they are very usefull for benchmarking the code, the aim of the ASSERT - 4 subchannel code is not per say to model low pressure air water flows but to model the behaviour of the flow in the channel of a nuclear reactor. Thus the second recommendation is that this new model for the effects of the other bubbles should therefore be tested

against high temperature steam water data.

BIBLIOGRAPHY

ALY, A.M., and AHMAD, S.Y.,1980 "SAGA-III: A Computer Program for Subchannel Analysis of Two-Phase Flow in Two Interconnected Channels." ASME, 79-QA/HT-64.

ARIS, R.,1962 "Vectors, Tensors, and the Basic Equations of Fluid Mechanics" Prentice – Hall, Inc..

BANERGEE,S. and CHAN, A.M.C., 1980 "Seperated Flow Models–1 Analysis of the Averaged and Local Instantaneous Formulations," Int. J. of Multiphase Flow, Vol. 6, pp. 1–24.

BERGLES, A.E., COLLIER, J.G., DELHAYE, J.M., HEWITT, G.F. and F. MAYINGER, 1981, "Two–Phase Flow and Heat Transfer in the Power and Process Industries", McGraw–Hill Book Company.

BIRD, R.B., STEWART, W.E., and LIGHTFOOT,E.N., 1960, "Transport Phenomena" John Wiley & Sons.

BOSIO, J. and IMSET, O.R.; "Experimental Two-Phase Flow Investigating in a 7-rod Bundle,", 1970, Inst. Atomenergi report SD-136/SDS-70.

CARVER, M.B. "Development and Application of a Three–Dimensional Two–Fluid Numerical Algorithm for Simulation of Phase Redistribution by Bends and Elbows," 1987, Ph.D. Thesis, University of Ottawa.

CARVER, M.B., TAHIR, A., ROWE, D.S., TAPUCU, A. and AHMAD, S.Y. "Computational Analysis of Two-Phase Flow in Horizontal Bundles,", 1983, Nucl. Eng. and Design, V82, P12.

CHANG, Y.F., and J. SKEARS, 1977, "SOPHT– A Computer Model for CANDU–PHWR Heat Transport Networks and their Control," Nucl Tech., 35, pp381–395.

CHEXAL,B. & G. LELLOUCHE, 1986 "EPRI Full Range Drift–Flux Model," EPRI–NP–3989–SR–R1.

DELHAYE, J.M., GIOT, M., and M.L. REITHMULLER, 1981, "Thermohydraulics of Two–Phase Systems for Industrial Design and Nuclear Engineering", McGraw–Hill Book Company.

DORBRAN, F., 1984, "Constitutive Equations for Multiphase Mixtures of Fluids," Int. J. of Multiphase Flow, Vol. 10, No. 3 pp. 273–305.

DORBRAN, F., 1985, "Theory of Multiphase Mixtures A Thermomechanical Formulation," Int. J. of Multiphase Flow, Vol. 11, No. 1 pp. 1–30.

DREW, D.A., 1971, "Averaged Field Equations for Two–Phase Media," Studies in Applied Mathematics, Vol. L, No. 2.

HARLOW, F.H., and A.A. AMSDEN, 1971, "A Numerical Fluid Dynamics Calculation Method for All Flow Speeds," Journal of Computational Physics, Vol. 8, No. 2.

ISHII, M., 1975, "Thermo–Fluid Dynamic Theory of Two–Phase Flow." Eyrolles, France.

ISHII,M., 1977, "One–Dimensional Drift–Flux Model and Constitutive Equations for Relative Motion Between Phases in Various Two–Phase Flow Regimes," ANL–77–47.

JUDD,R.A., TAHIR,A., CARVER,M.B., KITELEY,J.C., ROWE,D.S., STEWART,D.G. and THIBEAULT P.R., 1984, "Two-Phase Flow and Heat Transfer in Rod Bundles." ASSERT-4 User's Manuel. AECL-8573.

KOCAMUSTAFAOGULLARI, G., 1971, "Thermo–Fluid Dynamics of Seperated Two–Phase Flow," Ph.D. Thesis, Georgia Institute of Technology.

LAHEY, Jr., R.T. and D.A. DREW, 1988, "The Three–Dimensional Time and Volume Averaged Conservation Equations of Two–Phase Flow," in Advances in Nuclear Science and Technology Volume 20, Lewins and Backer Eds. Plenum Press, N.Y..

LAHEY Jr., R.T., and F.J. MOODY, 1977, "The Thermal–Hydraulics of a Boiling Water Nuclear Reactor," American Nuclear Society.

MALLORY, J.P. and P. INGHAM, 1986, "CATHENA Simulation of Thermosiphoning in a Pressurized–Water Test Facility," 2^{nd} Int. Conf. on Sim. Meth. in Nucl. Eng. Montréal.

NIGMATULIN, R.I., 1979, "Spatial Averaging in the Mechanics of Heterogeneous and Dispersed Systems", Int. J. of Multiphase Flow, Vol. 5, pp. 353-385.

OHKAWA,K. and LAHEY Jr.,R.T., 1980, "The Analysis of CCFL Using Drift-Flux Models," Nuclear Engineering and Design,Vol. 61.

PATANKAR, S.V., 1980, "Numerical Heat Transfer and Fluid Flow," McGraw–Hill Book Company.

REDDY, J.N., 1984, "An Introduction to the Finite Element Method," McGraw–Hill Book Company.

ROWE, D.S., 1970, "COBRA–II: A Digital Computer Program for Thermal–Hydraulic Subchannel Analysis of Rod Bundle Nuclear Fuel Elements," BNWL–1229.

ROWE, D.S., 1973, "COBRA-III-C: A Digital Computer Program for Steady State and Transient Thermal Analysis of Rod Bundle Nuclear Fuel Elements." BNWL-1695, Pacific Northwest Laboratory.

SHA, W.T., SCHMITT, R. and LIN, E., 1977, "THI3D-1: A Computer Program for Steady-State Thermal-Hydraulic Multichannel Analysis." ANL-77-15.

SHA, W.T., 1980, "An Overview of Rod Bundle Thermal–Hydraulics Analysis," Nucl. Eng. And Desg, Vol. 62., pp 1–24.

SHOUKRI, M., TAWFIK, H., and CHAN, A.M.C., 1984, "Two-Phase Redistribution in Horizontal Subchannel Flow - Turbulent Mixing and Gravity Seperation," Int. J. of Multiphase Flow, Vol. 10, No. 3 pp. 357-369.

STEWART, C., WHEELER, C., CENA, R., McMONAGLE,C., CUTA,J., and TRENT,D., 1977, "COBRA-IV: The Model and the Method." BNWL-2214, NRC-4.

TAHIR, A., and CARVER, M.B., 1982, "Numerical Analysis of Two-Phase Flow in Horizontal Channels." SAGA-III User's Guide. AECL-7613.

TAHIR, A., and CARVER, M.B., 1984a, "Comparison of ASSERT Subchannel Code with Marviken Bundle Data," AECL-8352.

TAHIR, A., and CARVER, M.B., 1984b, "ASSERT and COBRA Predictions of Flow Distribution on Vertical Bundles," CNS Conference on Numerical Methods in Engineering, Montréal.

TAPUCU A., AHMAD, S.Y., and GENCEY, S., 1982, "Behaviour of Two-Phase Flow in Two-Laterally Interconnected Subchannels", Proceedings of 7th International Heat Transfer Conference, Munich, Vol. 5, pp. 361-366.

TAPUCU, A., GECKINLI, M., TROCHE, N., 1984a, "Experimental Investigation of Mass Exchanges Between Two Laterally Interconnected Two-Phase Flows," "Part-I: Subchannel Geometry–Vertical Flow," École Polytechnique de Montréal, Report IGN-556.

TAPUCU, A., GECKINLI, M., TROCHE, N., 1984b, "Experimental Investigation of Mass Exchanges Between Two Laterally Interconnected Two-Phase Flows," "Part-II: Subchannel Geometry–Horizontal Flow," École Polytechnique de Montréal, Report IGN-557.

TAPUCU, A., GECKINLI, M., TROCHE, N., and GIRARD, R., 1988a, "Experimental Investigation of Mass Exchanges Between Two Laterally Interconnected Two-Phase Flows", Nuclear Engineering and Design Vol. 105, pp. 295-312.

TAPUCU, A., PARENT, M., TROCHE, N., 1988b, "Experimental Investigation of Mass Exchanges Caused by Blockages," "Horizontal Two-Phase Flows" École Polytechnique de Montréal, Report IGE-73.

TAPUCU, A., TEYSSEDOU, A.J., DAVIDSON, M. and JOUHRI, H., 1990, "Experimental Study of Mass Exchanges Between Two Laterally Interconnected Two-Phase Flows:" "Effect of Gap Clearence" École Polytechnique de Montréal, Report IGE-85.

TEYSSEDOU, A.J., 1987, "Thermo-Hydraulic Behavior of Interconnected Subchannels with Blockages" Ph.D. Thesis, University of Montreal, École Polytechnique de Montréal.

TODREAS, N.E. and M.S. KAZIMI, 1989, "Nuclear Systems I, Thermal Hydraulic Fundamentals" Hemisphere Publishing Corporation.

TRUESDELL, C. and R. TOUPIN, 1960 "Handbuch der Physik," Vol,3/I, Springer Verlag.

TSUGE, A., SAKATA,K., and HIRAO,Y., 1979, "Abnormal Characteristics of Two-Phase Flow in Vertical Tube Banks," Fluid Flow and Heat Transfer Over Rod or Tube Bundles, pp. 139-142, ASME, New York.

TYE P., TAPUCU A., and S. GENCAY, 1990, "An Analysis of the Lateral Void Transfer Mechanisms in the ASSERT Subchannel Code", 3^{rd} International Conference on Simulation Methods in Nuclear Engineering, Montréal, Vol. 1, pp. 115–139, April 1990.

VAN DOORMAL, J.P., 1980, "A Review of Pertinent Methods Used in Multi–Dimensional Rod Bundle Thermal–Hydraulics Analysis," W.N.R.E. Report 907–16.

VANKA. S.P., et al., 1980, "A Semi–Implicit Calculation Procedure for Flows Described in Boundary–Fitted Coordinate Systems," Numerical Heat Transfer, Vol. 3, pp. 1–19.

VERNIER, P. and J.M. DELHAYE, 1968, "Équation général des écoulements diphasiques appliquées à la thermohydrodynamique des réacteur nucléaires à eau bouillante" Extrait de la revue EPE, Vol. IV, no 1-2.

WALLIS, G.B., 1969, "One-Dimensional Two-Phase Flow" McGraw-Hill.

WEBB, S.W., and D.S. ROWE, 1986, "Modeling Techniques For Dispersed Multiphase Flows," Encyclopedia of Fluid Mechanics, Gulf Publishing Company.

WHITAKER, S., 1960, "Introduction to Fluid Mechanics" Prentice–Hall, Inc.

ZUBER, N. and J.A. FINDLAY., 1965, "Journal of Heat Transfer," A.S.M.E..

APPENDIX A

USING ASSERT–4 TO MODEL THE TWO INTERCONNECTED SUBCHANNEL EXPERIMENTS OF TAPUCU

In order to model the two incterconnected subchannel experiments of Tapucu et al. [1984a, 1984b] it was necessary to make a few minor modifications to the ASSERT–4 subchannel code. It is important to point out that all of these modifications deal strictly with the specific geometry of the experiments and in no way touch the basic thermalhydraulic models in the code or the solution scheme used. In the two subchannel test facility at the I.G.E. the two subchannels do not communicate with each other until a point 32.5 *cm*. downstream of the inlet. This makes it necessary to:

1. Ensure that the begining of a node corresponds to the begining of the the interconnected region. This is done by using the variable noding option available in ASSERT–4 and specifying the location of all the nodes manually.

2. Prevent the crossflow and all the intersubchannel transfer mechanisms until the interconnected region. This requires a few minor modifications to the code, but as has already been stated the basic model used by ASSERT–4 is not touched. To prevent the crossflow and the other intersubchannel transfer mechanisms the following steps are taken. At each axial node from the inlet until the node corresponding to the begining of the interconnected region is reached the crossflow, the transverse relative velocity and the void diffusion are set to zero in the code.

Initially it was believed that an additional change was required in the code due to significant differences in the predicted pressure drops between high void over low void and low void over high void cases having the same inlet conditions, something that was not observed experimentally. Further tests proved that these differences were simply due to the fact that the convergence criteria were not being set small enough. In the ASSERT–4 users manual [Judd et al., 1984] the recommended convergence criteria for the flow solution was:

$$\frac{\Delta F}{F} = 0.01$$

where ΔF was the incremental correction for a given iteration and F was the flow. To correct the problem it was simply necessary to change the convergence for the flow solution to:

$$\frac{\Delta F}{F} = 0.00001$$

which was the minimum that could be used without changing the input format. It should be noted that since modelling the two subchannel experiments of Tapucu et al. with ASSERT–4 only requires 2 seconds of computer time on the machine used no attempt was made to optimize the convergence criteria, they were simply set as small as possible.

A.1 Values of Important Parameters for the ASSERT-4 Version 1.5 Runs

Single Phase Friction Factor: $f = .488Re^{-0.311}$

Two-Phase Flow Multiplier: $\phi_{fo}^2 = 1+1.8066\alpha+2.4650\alpha^2-0.73214\alpha^3-1.3554\alpha^4+11.809\alpha^5$

Number of Nodes: 64

K_1 Leading Coefficient for V_∞: 2 (default) and 1.4 (our recommended value)

Crossflow loss coeffiecient K_{ij}: 0.5 (default)

Bare Rod Void Diffusion Mixing Option: $P_e = \frac{\epsilon}{UDh} = a\left(\frac{\alpha_m}{0.6}\right)^6$

with a being 0.075 (default) and 0.25 (our recommended value)

Bare Rod Equilibrium Void Distribution: $\alpha_{0_i} = \alpha_{0_j}$

A.2 Values of Important Parameters for the ASSERT-4 Version 2.2B Runs

Single Phase Friction Factor: $f = .488Re^{-0.311}$

Two-Phase Flow Multiplier: $\phi^2_{fo} = 1 + 1.8066\alpha + 2.4650\alpha^2 - 0.73214\alpha^3 - 1.3554\alpha^4 + 11.809\alpha^5$

Number of Nodes: 64

K_1 Leading Coefficient for V_∞: 1.5 (default)

Crossflow loss coeffiecient K_{ij}: 0.5 (default)

Bare Rod Void Diffusion Mixing Option: $P_e = \frac{\epsilon}{UDh} = aRe^b$

with a being 0.05 (default) and b being 0

Bare Rod Equilibrium Void Distribution: $\alpha_{0_i} = \left(\frac{\bar{\alpha}}{\bar{G}}\right) G_i$